2002

Hydrodynamics of mine impact burial

Evans, Ashley D.

Monterey, California. Naval Postgraduate School

NAVAL POSTGRADUATE SCHOOL
Monterey, California

THESIS

HYDRODYNAMICS OF MINE IMPACT BURIAL

by

Ashley D. Evans

September 2002

Thesis Advisor: Peter Chu
Second Reader: Peter Fleischer

Approved for public release; distribution is unlimited

THIS PAGE INTENTIONALLY LEFT BLANK

REPORT DOCUMENTATION PAGE

Form Approved OMB No. 0704-0188

1. AGENCY USE ONLY *(Leave blank)*	2. REPORT DATE	3. REPORT TYPE AND DATES COVERED
	September 2002	Master's Thesis

4. TITLE AND SUBTITLE
Hydrodynamics of Mine Impact Burial

5. FUNDING NUMBERS
N0001402WR20174

6. AUTHOR (S) Evans, Ashley Drew

7. PERFORMING ORGANIZATION NAME(S) AND ADDRESS(ES)
Naval Postgraduate School
Monterey, CA 93943-5000

8. PERFORMING ORGANIZATION REPORT NUMBER

9. SPONSORING / MONITORING AGENCY NAME(S) AND ADDRESS(ES)
NAVOCEANO, Stennis Space Center, MS 39522-5001
Institute of Joint Warfare Analysis, NPS, Monterey, CA, 93943

10. SPONSORING/MONITORING AGENCY REPORT NUMBER

11. SUPPLEMENTARY NOTES The views expressed in this thesis are those of the author and do not reflect the official policy or position of the U.S. Department of Defense or the U.S. Government.

12a. DISTRIBUTION / AVAILABILITY STATEMENT
Approved for public release, distribution is unlimited

12b. DISTRIBUTION CODE

13. ABSTRACT: A general physics based hydrodynamic flow model is developed that predicts the three-dimensional six degrees of freedom free fall time history of a circular cylinder through the water column to impact with an unspecified bottom. Accurate vertical impact velocity and impact angle parameters are required inputs to subsequent portions of any Impact Mine Burial Model. The model vertical impact velocity and impact angle are compared with experimental data, vertical impact velocities and impact angle to validate the model mechanics and accuracy. The three dimensional model results are compared through the experimental data with IMPACT28 vertical impact velocities and impact angle. Results indicate the three dimensional model mechanics are sound and marginal improvements are obtained in predicted vertical velocities. No improvement is gained using the three-dimensional model over IMPACT28 to predict impact angle. The observed stochastic nature of mine movement in experimental data suggests this three dimensional model be used to model the hydrodynamic flow phase in a statistical mine burial model that provides distributions for input parameters, and domain characteristics and present a probabilistic output for development of a relevant navy tactical decision aid.

14. SUBJECT TERMS: Mine Impact Burial, Hydrodynamics, IMPACT28, Bottom Mine, Mine Countermeasures, Mine Warfare, Numerical Modeling

15. NUMBER OF PAGES 470

16. PRICE CODE

17. SECURITY CLASSIFICATION OF REPORT	18. SECURITY CLASSIFICATION OF THIS PAGE	19. SECURITY CLASSIFICATION OF ABSTRACT	20. LIMITATION OF ABSTRACT
Unclassified	Unclassified	Unclassified	UL

NSN 7540-01-280-5500

Standard Form 298 (Rev. 2-89)
Prescribed by ANSI Std. 239-18

THIS PAGE INTENTIONALLY LEFT BLANK

Approved for public release; distribution is unlimited

HYDRODYNAMICS OF MINE IMPACT BURIAL

Ashley D. Evans
Lieutenant Commander, United States Navy
B.S., Pennsylvania State University, 1988

Submitted in partial fulfillment of the
requirements for the degree of

**MASTER OF SCIENCE IN
METEOROLOGY AND PHYSICAL OCEANOGRAPHY**

from the

**NAVAL POSTGRADUATE SCHOOL
September 2002**

Author: Ashley D. Evans

Approved by: Peter Chu
Thesis Advisor

Peter Fleischer
Second Reader

Mary L. Batteen
Chairman, Department of Oceanography

THIS PAGE INTENTIONALLY LEFT BLANK

ABSTRACT

A general physics based hydrodynamic flow model is developed that predicts the three-dimensional six degrees of freedom free fall time history of a circular cylinder through the water column to impact with an unspecified bottom. Accurate vertical impact velocity and impact angle parameters are required inputs to subsequent portions of any Impact Mine Burial Model. The model vertical impact velocity and impact angle are compared with experimental data, vertical impact velocities and impact angle to validate the model mechanics and accuracy. The three dimensional model results are compared through the experimental data with IMPACT28 vertical impact velocities and impact angle. Results indicate the three dimensional model mechanics are sound and marginal improvements are obtained in predicted vertical velocities. No improvement is gained using the three-dimensional model over the IMPACT28 model to predict impact angle. The three dimensional model produces dispersed results for impact angle The observed stochastic nature of mine movement in experimental data suggests this three dimensional model be used to model the hydrodynamic flow phase in a statistical mine burial model that provides distributions for input parameters, and domain characteristics and present a probabilistic output for development of a relevant navy tactical decision aid.

THIS PAGE INTENTIONALLY LEFT BLANK

TABLE OF CONTENTS

THIS PAGE INTENTIONALLY LEFT BLANK

LIST OF FIGURES

THIS PAGE INTENTIONALLY LEFT BLANK

LIST OF TABLES

THIS PAGE INTENTIONALLY LEFT BLANK

TABLE OF SYMBOLS

Symbols are presented as they are encountered for the first time in the document.

V_x	=	X Component of Velocity in Earth Fixed Coordinates
V_z	=	Z Component of Velocity in Earth Fixed Coordinates
V_a	=	Axial Velocity in Mine Coordinates
V_c	=	Cross Velocity in Mine Coordinates
θ	=	Angle the Long Mine Axis Makes with the Vertical Earth Fixed Coordinate
V_t	=	Total Velocity for Point Along the Long Axis of the Mine
$\vec{\omega}$	=	Angular Velocity Vector
l	=	Distance from the Center of Mass to Point on the Long Axis of the Mine
d	=	Diameter of the Mine Shape
T	=	Mine Body Torque
$\frac{dT}{dt}$	=	Differential Torque about the Center of Mass
C_d	=	Drag Coefficient for Cross Motion
ρ_w	=	Fluid Density
$\vec{V}$	=	Mine Velocity Vector

t	=	Time
m	=	Mass
$\vec{F}$	=	Force Vector
$\vec{r}$	=	Position Vector
$\vec{M}$	=	Resultant Moment Vector
$F_E\left(o,\vec{i},\vec{j},\vec{k}\right)$	=	Earth Fixed Coordinate System and Directors
(x, y, z)	=	Position Vector Components in Earth Fixed Coordinates
(u, v, w)	=	Velocity Vector Components in Earth Fixed Coordinates
M	=	Center of Mass
$F_M\left(M, \vec{i}_M, \vec{j}_M, \vec{k}_M\right)$	=	Body Fixed Coordinate System and Directors
$F_F\left(M, \vec{i}_F, \vec{j}_F, \vec{k}_F\right)$	=	Drag-lift Force Coordinate System and Directors
$(\Omega_1, \psi_2, \psi_3)$	=	Euler Angles
$\vec{V}_w$	=	Fluid Velocity
$\vec{V}_r$	=	Relative Flow Velocity
$\vec{V}_1$	=	Axial Flow Velocity in Body Fixed Coordinates
$\vec{V}_2$	=	Cross Flow Velocity in Body Fixed Coordinates
$[e]$	=	Rotation Component Matrix in Earth Fixed Coordinates
$[d]$	=	Rotation Component Matrix in Body Fixed Coordinates
${}^E\vec{P}$	=	Position Matrix in Earth Fixed Coordinates

${}^{M}\vec{P}$	=	Position Matrix in Body Fixed Coordinates
${}^{E}_{M}R$	=	Earth Fixed Coordinate to Body Fixed Coordinate Rotation Matrix.
${}^{F}\vec{P}$	=	Position Matrix in Drag-lift Force Coordinates
${}^{E}_{F}R$	=	Earth Fixed Coordinate to Drag-lift Force Coordinate Rotation Matrix
$(\omega_2\ \omega_3)$	=	Angular Velocities in Body Fixed Coordinates
$(\omega'_2\ \omega'_3)$	=	Angular Velocities in Drag-lift Force Coordinates
m_a	=	Hydrodynamic Mass
$\vec{a}$	=	Acceleration Vector
e	=	Eccentricity
(k_1, k_2, k_r)	=	Inertial Coefficients for an Ellipsoid of Rotation
(α_o, β_o)	=	Sub-coefficients used to Calculate Inertial Coefficients for an Ellipsoid of Rotation
Π	=	Mine Volume
$(f_{k1,k2,kr})$	=	Hydrodynamic Mass Correction Factors
$\vec{F}_r$	=	Force Vector Corrected for Hydrodynamic Mass
m_t	=	Total Inertial Mass Including Mine Mass and Hydrodynamic Mass
$\bar{\rho}$	=	Average Mine Density
$\vec{F}_b$	=	Body Force Vector
$\vec{F}_s = (F_{sx}, F_{sy}, F_{sz})$	=	Surface Force Vector and Components

g	=	Gravitation Constant
$\vec{F}_{(d1,d2,d3,l)}$	=	Force Vector in Drag and Lift Component Form
$\vec{\omega}_m$	=	Angular Velocity Around the Long Axis of the Mine
$\vec{\omega}_f$	=	Angular Velocities around the Mine Cross Flow Axes
$[J]$	=	Inertia Tensor
$\vec{M}_b$	=	Body Force Moment
$\vec{M}_s$	=	Surface Force Moment
$\vec{M}_r$	=	Surface Force Moment Corrected for Hydrodynamic Mass
B	=	Center of Volume
χ	=	Center of Mass to Center of Volume Offset
ς	=	Center of Mass to Center of Volume Moment Offset
$f_{(d1,d2,d3,l)}$	=	Force Magnitude Coefficients
ν	=	Kinematic Viscosity
$C_{(d,l)}$	=	Drag and Lift coefficients
A_w	=	Solid Body Characteristic Area
R_e	=	Reynolds Number
T	=	Temperature
AR	=	Aspect Ratio
ε	=	Drag-lift Force Moment Center Adjustment
$M_{(sl,sd3,sd2)}$	=	Drag-lift Force Torque Vector
$m_{(cm3,\ cm2,\ cml)}$	=	Drag-lift Force Torque Vector Magnitude Coefficients
q	=	Model Output Parameters Vector

ACKNOWLEDGEMENTS

The author gratefully acknowledges the financial support of the Naval Oceanographic Office, Office of Naval Research and Institute of Joint Warfare Analysis. This thesis work was performed under Office of Naval Research contract number N0001402WR20174. I would like to acknowledge and thank Professor Peter Chu for his imparted knowledge, mentoring, patience and guidance. I thank ONR, NAVOCEANO, and Naval Research Laboratory, Stennis Space Center for the research support provided to complete this thesis. I thank Dr. Peter Fleischer who provided great insight as my second reader. I want to thank the “Mine Drop Gang” of NRL-SSC and specifically Dr. Philip Valent for the experience gained participating in the NSWC-Carderock Model Mine Hydrodynamics Experiment in September 2001. The experiment provided an outstanding data set. I truly appreciate Dr. Valent’s continued friendship and mentoring since that time. Additionally, special thanks to Mr. Chenwu Fan, NPS Oceanographer, who provided extensive effort producing a viable numerical model and mentored my efforts and struggles throughout the thesis process. This group of people made this thesis effort successful, yet personally challenging and memorable. I remain ever in their debt.

Lastly, thanks, gratitude and eternal love go to my best friend and spouse Edie and my twins, Eva and Katie, who always provided the optimistic perspective of cheery hellos, hugs, and kisses at the end of many long days.

“Keep Chargin’”

THIS PAGE INTENTIONALLY LEFT BLANK

I. INTRODUCTION

The conclusion of the cold war culminated with the Union of Soviet Socialist Republics (USSR) effectively ceasing to exist under international law on December 31, 1991. This historical event caused the U.S. military and specifically the Navy and Marine Corp Team to shift tactical emphasis from blue water, deep ocean doctrine to littoral warfare doctrine. This shift predicated military responses dealing with a wide range of worldwide regional crises requiring forward sea basing, and expeditionary force landing support.

The Navy Marine Corp team developed a doctrine concept white paper, "… From the Sea, 1992", to support joint warfare doctrine concepts of forward presence and engagement developed as National Defense Strategy in "Joint Vision 2010, 1996", (Rhodes and Holder 1998). The document provided guiding tenets for naval operations of the 21st century. A subsequent Naval Department revision, "Forward …From the Sea, 1994", and its Marine Corp counterparts "Operational Maneuver from the Sea, 1996", and "Ship to Objective Maneuver, 1997" all focus on sea based power projection into littoral regions and guiding naval operations in those areas in the new millennium. "Joint Vision 2020, 2000" and "Sea Strike, Sea Shield, Sea Basing, 2002" are the current National Defense Strategy and Naval Department concept papers providing guiding tenets for naval and joint operations well into the 21st century. Both papers incorporate emerging technology, processes, people and organizations synergized via the netcentric warfare

concept to provide total power projection and dominance across littoral regions during any crises requiring U.S. response.

> ...the very shallow water (VSW) region is a critical point for our offensive forces and can easily, quickly and cheaply be exploited by the enemy. The magnitude of the current deficiency in reconnaissance and neutralization in these regions and the impact on amphibious assault operations were demonstrated during Operation Desert Storm. Maj. Gen. Edward J. Hanlon Jr. “From (Rhodes and Holder 1998).”

Any military operation that occurs in the littoral regions also occurs in mine country. The increasing pace of shallow-water naval operations (i.e. Persian Gulf, Adriatic Sea, Yellow Sea, and Gulf of Aden) translates into a high probability of encountering mines. The required shift in focus of naval operations from the open ocean to the regional littoral areas increases the importance of mine warfare as a navy core competency. The proliferation of inexpensive, bottom type mines make shallow water and very shallow water MCM a critical and expensive challenge. In times of conflict domination of coastal operating areas will largely depend on the ability to remove or neutralize any emplaced littoral mine threat, figure 1, and prepare the battle space for follow-on action in a timely fashion

Naval mines may be found throughout the water column and on or within the seafloor Figure 1. Ask anyone to describe a typical naval mine to you and the response will be a description of the spherical, hertz-horn World War II vintage drifting mine shape common in Hollywood films. But, it is the buried naval mine that poses the most severe

threat to naval assets since naval forces possess very limited resources and capabilities for detecting, identifying, and neutralizing them, and the mine itself remains fully effective when buried, (Lott, 2001). An important factor in mine hunting and clearance is the amount of initial impact and subsequent sediment burial a mine undergoes with time because buried mines are substantially more difficult to detect and classify. The amount of burial becomes a critical parameter and crossroad in the naval MCM mission planning process because the mine countermeasures effort transitions from mine hunting to mine sweeping, (Rennie 2002.)

Figure 1. Littoral Mine Threat. "From Rhodes (1998)."

> Mine warfare, perhaps more than any other single littoral warfare mission area is the "key" that will unlock the "door" to the littoral battle space. In the most fundamental way, then, mine warfare and the need for effective mine countermeasures must be an "all-hands" concern for the Navy and the Marine Corps. (Boorda 1995)

The Office of Naval Research (ONR) in 1999 created the Mine Burial Program (MBP), an applied (6.2) research program to develop decision aids and mine burial prediction tools. The program mission is to predict the behavior of mines in different environments, (Bennett 2000). The Impact Mine Burial Prediction model development falls under the MBP program.

The Impact Mine Burial Prediction model developed in 1980 was developed to semi-empirically model the mine burial process. Several revisions have occurred in the last two decades but there have been limitations noted in the model performance, as well as little scientific advancement in mine burial prediction, (Dolan et al 1999), (Taber 1999), (Smith 2000), and (Gilless 2001).

The model is currently limited to three degrees of freedom that include two dimensional momentum equations and artificial rotation around the aerodynamically defined pitch axis. The model also makes assumptions on shape density and assignment of constants to certain mine characteristics and environment parameters that limit performance. Experimental test data reveals that mine shape dynamics are extremely chaotic (stochastic) during free-fall through the water column, (hydrodynamic phase) (Richardson et al 2001b) and (Valent et al 2002). These major weaknesses in the current model are well accepted in the mine warfare community, (Chu 2001).

The goals of this investigation include development of a new mine impact burial model for implementation as the hydrodynamic phase in the short-term into a probabilistic prediction model for navy tactical decision aids. The long-

term goal is for model inclusion as the hydrodynamic phase in a full spectrum deterministic model for mine burial in a comprehensive navy tactical decision aid.

The current modeling approach is development of a model that lifts the assumption of uniform density, uses the three dimensional momentum equations, and the three dimensional moment of momentum equations for rotation about the mine shape axes to generate a mine shape’s position during freefall through the water column. The external hydrodynamic forces and torques are modeled using empirical drag and lift coefficient data. A system of first order differential equations with approximate solutions is generated for linear velocity and angular velocity that are integrated to generate (x, y, z) positions and the Euler orientation angles for the center of mass of the mine shape.

Two data sets will be used to validate model performance based on two critical parameters at impact; fall velocity and impact orientation. The first data set was generated at Naval Postgraduate School in July 2001. The second data set was generated at Naval Surface Warfare Command, Carderock, MD in September 2001 under the direction of principle investigators Dr. Philip Valent and Mr. Todd Holland.

THIS PAGE INTENTIONALLY LEFT BLANK

II. MINE COUNTERMEASURE WARFARE OVERVIEW

The single greatest threat to U.S. sea-based power projection in littoral areas is the naval mine. There are over 300 variations of mines available worldwide, a 75% increase in the last decade, (Lehr 2000). Each mine type is listed with a multitude of triggering devices listed in (NMWP 2000).

In terms of simplicity, effectiveness, availability, cost efficiency, ease of deployment and potential battle space impact, naval mines are most appealing to third world countries, political insurgents and even stateless actors such as terrorist groups, Figure 2, determined to prevent U.S. naval forces from achieving sea control and power projection ashore from sea basing, (NMWP 2000).

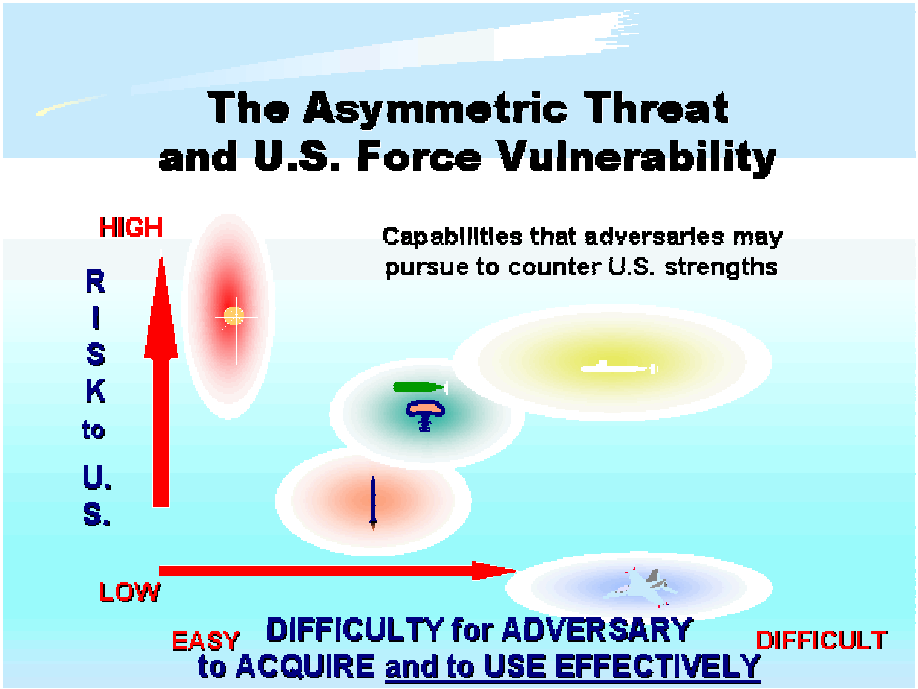

Figure 2. The Risk to U.S. Forces Versus the Ease with Which an Asymmetric Threat can Acquire a Specific Capability. “From Garrold (1998).”

The ancestry of naval mines can be traced to the fourth century B.C. and Alexander the Great's siege of Tyre in the eastern Mediterranean Sea. The Phoenicians frustrated Alexander's attempts to land and take the city by strewing the surrounding shallows with large boulders. The next attempt occurred in 1585, when the Dutch floated explosives down the Scheldt River to disrupt a blockade of Antwerp, Belgium by the Spanish fleet.

But an American inventor, David Bushnell, is credited as the father of naval mine warfare, (Lluy 1995). He developed the first true naval mine in 1776 under direction from the insurgent Continental Army for use against the English blockade of Philadelphia, using gunpowder, fuse, a fishing float and a wooden powder keg.

Naval mines were used in the War of 1812 and successfully by the Confederacy during the Civil War in attempts to thwart the union blockade of southern ports; of notable fame is Admiral Farragut at Mobile Bay where eight ships fell prey to naval mines. The full impact of mine warfare was realized when the Japanese mined Port Arthur then lured the Russian fleet into the minefield, and defeated the Russian fleet during the Russo-Japanese War in 1905. Mines were used extensively during both World War I and World War II. In the early hours of 6 June 1944 leading up to the Normandy Invasion, 300 allied ships moved along the French coastal waters attempting to locate and neutralize the extensive minefield in place there, (Lluy 1995).

The Wonsan Bay Korea Mine Crisis provides an excellent example of the value of the naval mine as a defensive

weapon by a third world country against a world superpower. 3000 Russian made, World War I vintage mines caused 250 ships to wait off the Korean Coast for 8 days doing circles, “Operation Yo-Yo”, as mine sweepers attempted to clear sea-lanes to shore landing zones, Figure 3.

Figure 3. Republic of Korea Minesweeper *YMS-516* Blown Up by a Magnetic Mine, During Sweeping Operations, Wonsan Harbor, on 18 October 1950. “From http://www.history.navy.mil/ (2002).”

Shortly after the October 1950 Wonsan, Korea mine crisis, then Rear Admiral Allen "Hoke" Smith, Commander, Amphibious Task Force, Wonson, Korea exclaimed,

> We have lost control of the seas to a country without a navy, using pre-WWI weapons, laid by vessels that were utilized at the time of the birth of Christ.

More recently, in August 1984, Libya’s General Muammar Gadaffi ordered a commercial roll-on, roll-off ship to lay mines in the Suez Canal and Red Sea during peacetime. It

took coalition forces months to verify the Suez Canal and Red Sea free of mines, (Wettern 1991).

Within the past 15 years while conducting operations in the Persian Gulf, three U.S. ships have fallen victim to mines, the USS Samuel B. Roberts (FFG-58); hit an Iraqi SADAF-02 contact mine, USS Tripoli (LPH-10); hit a LUGM-145 moored contact mine, and USS Princeton (CG-59); activated an Italian Manta bottom mine. Total ship damages were $125 million, (Boorda 1999), while the mines cost approximately $15 thousand, (Lluy 1995). Since Operation Desert Storm, 1400 mines have been removed from the Persian Gulf. More recently, strategic planning for possible ground force operations in Kosovo included plans to deal with possible mining of Kotar Bay and Durres harbor by Yugoslavian forces. Since 1980, 38 vessels have been lost or severely damaged by mines worldwide, (NMCF 1991). In fact 80% of U.S. ship damage in the last 50 years is a direct result of mines, (Avery 1998, as cited in Oceanography and Mine Warfare 2000).

Today, an estimated 50 countries, including those in politically sensitive regions possess some sort of mining capability, an increase of 40% in the last decade. Thirty-two countries have demonstrated mine production capability, a 60% increase since 1988 and 24 countries have attempted to export the systems, a 60% increase since 1992, (Lehr 2000). Mines can be used in both offensive and defensive roles. Offensively, they can be placed in enemy waters or nearby sea-lanes in order to harass military and commercial shipping. Defensively, they can be used to delay or prevent

amphibious assaults limit harbor use or deny command of the sea.

Mines have evolved over the years from the dumb “horned” contact mines similar to those that damaged the “Tripoli” and “Roberts” to relatively sophisticated mines with; non-magnetic materials, irregular shapes, anechoic coatings, multiple sensors and ship count routines such as the Manta mine the “Princeton” activated. Despite their increased sophistication, mines remain a relatively inexpensive weapon and are relatively easy to manufacture, maintain and deploy.

Mines provide a small country with an inferior defense infrastructure and/or no navy with a highly efficient and potent force multiplier and defensive system with minimal expense, one that is readily available on the arms market today; the poor man’s navy. Mine’s are particularly valuable to asymmetric forces that cannot or will not engage U.S. forces directly, (NMWP 2000). Any political insurgent or terrorist group with money can buy quantities of mines on the black arms market to use in sea-lanes and/or ports around the world.

Intelligence estimates the former Soviet Union mine stockpile exceeds half a million mines, and an increase in sales from the independent states of the region to third world countries, stateless factions and others is expected to increase as economic and political conditions continue to languish in the region, (Wettern 1991). The growing threat comes from small craft from hostile nations easily concealing mining operations from intelligence gathering

initiatives, and the isolated acts of terrorism on the high seas, (NMWP 2000.).

Through history to modern day the naval mine has proven again and again to be a cost effective weapon that causes physical damage, creates psychological uncertainty and requires a countermeasures effort far out of proportion to the initial mining effort costs (Lluy 1995). The mine itself need not be laid: the threat itself will change the focus of operations within any battle space.

Naval mines are characterized by three factors: position in water (bottom, moored, rising, floating), method of delivery (aircraft, surface, subsurface) and

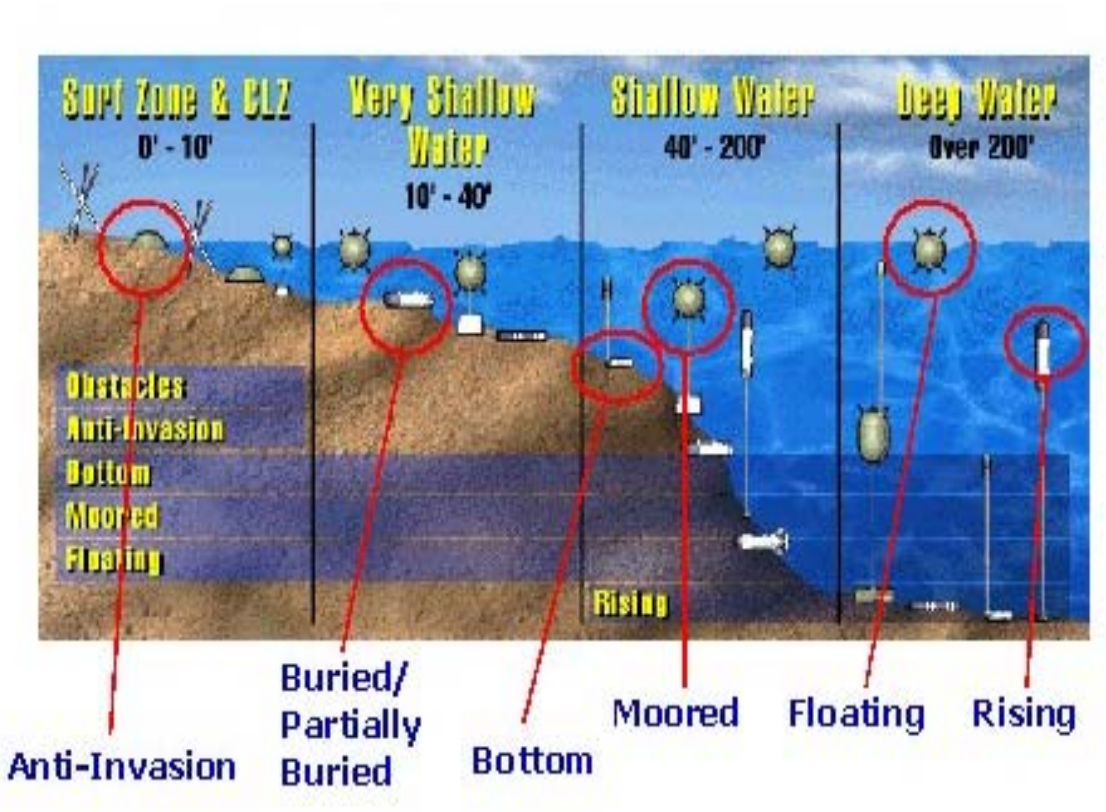

Figure 4. The Littoral Battle Space Mine Regions and the Types of Mines That Could be Encountered in Each Region. “From NMWP (2000).”

method of actuation (acoustic and/or magnetic influence, pressure, contact, controlled), (Oceanography and Mine Warfare 2000). The littoral battle space is divided into five regions based upon water depth. Within each of these regions naval forces can encounter multiple types of threats, Figure 4. The littoral regions are defined, (NMWP 2000):

- Deep Water (DW). Water depths: >300 ft. Threat: mainly moored and rising mines, although a few large bottom mines exist.
- Shallow Water (SW). Water depths: from 40 to 300 ft. Threat: bottom, moored and rising.
- Very Shallow Water (VSW). Water depths: from 10 to 40 ft. Threat: bottom, moored, rising and controlled.
- Surf Zone (SZ). Water depths: < 10 ft. to the beach itself. Threat: same as VSW but land mines and obstacles can also be encountered.
- Craft Landing Zone (CLZ). Water depths: the beach itself. Threat: conventional land mines and obstacles.

The most challenging mine countermeasures (MCM) scenario in Figure 4 involves the bottom mine. Bottom mines are inherently hard to detect in the complex littoral environment due to their small size compared to the surrounding environmental spatial scale. Common bottom mine seeding areas include shipping channels, harbors, anchorages, rivers, and estuaries. Aircraft, surface ships or submarines can deploy mines. Although bottom mines are designed to deploy from specific platforms, most mines are easily adapted to deploy from any size seaworthy vessel.

Bottom mines rest on the ocean floor and are generally deployed in the littoral areas from the Shallow Water region into the Craft Landing Zone region, (NMCF 1991). Bottom mines are seldom seen as a viable threat beyond a depth of 70m, (Lluy 1995). The most influential environmental parameter to successful MCM operations is the character of the bottom. This primary planning parameter often determines whether an area should be swept or hunted. Bottom clutter in the form of rock outcroppings, coral reefs, man-made debris and slope irregularities provide false sonar contacts and reverberation that increase overall clearance times. In addition, in areas where the sea floor is rough with Non-mine, mine-like bottom objects (NOMBOs), adversaries can create an effective minefield with a few mines, dummy mines or even no mines; the threat is enough, (NMWP 2000).

Bottom Composition	Predicted Mine Case Burial %	Bottom Roughness	Bottom Category
Rock	0	Smooth Moderate Rough	B C C
MUD OR SAND	0 TO 10	Smooth Moderate Rough	A B C
	10 TO 20	Smooth Moderate Rough	A B C
	25 TO 75	Smooth Moderate Rough	A B C
	75 TO 100	All	C

Table 1. MCM Doctrine Bottom Definitions For Impact Burial. “From Oceanography and Mine Warfare (2000).”

Soft bottom sediments such as marine clays and silts can cause a high degree of mine burial upon impact. Buried or partially buried bottom mines are of greatest concern to the MCM planner, (Gilless 2001). Bottom mines normally undergo some percentage of burial into the bottom sediment.

The Navy currently uses only anecdotal information to characterize burial into general categories 0-10%, 10-20%, 20-75%, and 75-100%. The prediction only centers on the initial bottom impact burial. Any subsequent burial is ignored for planning purposes. These subsequent burial processes include but are not limited to: scour, bed-form migration, and the unknown contributions by liquefaction, gravity shakedown, and biological modification of the sediment, (Lott 2001). The complexity of the subsequent burial processes rely on a wide array of oceanographic and atmospheric factors with varying spatial and temporal scales.

The “initial” burial depth percentage is the second critical environmental parameter currently required by mine warfare decision makers as part of developing any operational mine countermeasures strategy in a given operating area. This burial depth parameter is influenced by a wide array of other complex near-shore atmospheric and oceanographic processes, (i.e. bathymetry, currents, temperature and density.), (NMWP 2000). The combination of burial percentage and bottom character are used to empirically categorize mining areas and determine whether mine countermeasures operations are conducted via hunting or sweeping. A transition occurs from hunting for bottom mines to sweeping for bottom mines when more than 80%

burial has occurred or Bottom Type C is empirically derived, Table 1, (NMCP 1991). Operators and planners alike prefer to hunt for mines vice sweep for mines as the later is much more dangerous. The discouraging factor is that mines remain effective when buried and much harder to detect and neutralize, (Lott 2001).

Mine Countermeasures doctrine has changed little since the end of World War II. Bottom mines cannot feasibly be searched for visually within time limits of naval operations, and if even partially buried difficult to hard to locate with acoustic sensors. SACLANTCEN MCM sonar performance models predicts the SNR of a buried mine will be approximately 20 dB lower than that of a mine resting on top of a bottom sediment, (NATO SG31 1999).

In conducting minesweeping operations, mission success hinges on knowing as much intelligence as possible about the mines that have placed in the area and the effects the environment has had on that placement. Any estimate of the area or height protruding above the bottom sediment, or complete mine burial is a crucial parameter in the MCM decision making process and subsequent execution of mine counter measure operations in an area, (Taber 1999).

III. MINE IMPACT BURIAL PROGRAM HISTORY

A. MODEL DEVELOPMENT

The essential output parameters required from Mine Impact Burial Prediction models evolve from a fundamental understanding of physics, engineering and hydrodynamic theory associated with a solid body free falling through a fluid medium and imbedding into a semi-porous surface and dissipating its acquired kinetic energy. The modeling process involves nonlinear behavior across a wide range of complex, coupled environmental, sediment transport and seabed properties that occur in shallow water coastal zones, (Bennett 2000). Modeling solid body behavior is still an inexact science. Empirical relationships and linear expressions have provided the most feasible and accurate deterministic solutions to describe mine behavior in the past.

Arnone and Bowen (1980) of Naval Coastal Systems Center developed the first dynamic based model to predict the amount of burial a mine undergoes when it impacts the bottom marine sediments in 1980. The model is based on simple cylindrical shapes and the associated theoretical equations and experimental data that exist in current literature for cylinders. Some of the data is more than 75 years old. The model was written in Basic language. This model created an alphanumeric read-out of the two-dimensional time history of a right circular cylinder as it free falls through three possible phases, (air, water, sediment) and two sub-phases (air-water cavity and water-sediment cavity), Figure 5.

A summation of the forces acting on the cylinder is calculated at discrete time steps, and the resulting acceleration computed. The acceleration is integrated in time to determine the velocity and transverse x-axis excursion by the cylinder during free-fall. It calculates the burial depth of the mine after it initially comes to rest in the modeled bottom marine sediment. Arnone and Bowen point out that both impact velocity and orientation at the sediment interface are important parameters to determining final mine burial depth.

The Arnone and Bowen model became the standard to predict mine burial, known as Impact Mine Burial Prediction (IMBP). The model since that time has been evaluated extensively both parametrically by the authors and by a variety of sources (Satkowiak 1988), (Rumbell and Kitchings 1989), (Hurst and Murdoch 1991), (Mulhearn 1993), (Taber

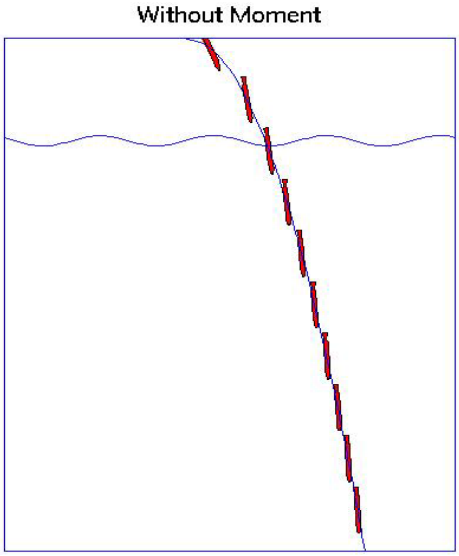

Figure 5. Arnone and Bowen IBPM Mine Motion Depicting Constant Angle in the Water Without Rotation. “From Gilless (2001).”

1999), (Smith 2000), (Richardson et al 2001a), (Gilless 2001), and (Valent et al 2002) using experimental data. The major contributors to model improvements since Arnone and Bowen are (Satkowiak 1987), and (Hurst 1992).

The initial model was conceptually sound, but the code did contain flaws. (Satkowiak 1987) recognized there were problems with the certain routines in the model and made a number of substantial modifications. These include:

- Correcting the reference flow area used in the drag calculations
- Correcting the calculation of the added mass term
- Including a term to calculate the drag due to the front nose of the cylinder
- Allowing for non-blunt noses (i.e., front end) of mines
- Including an option to input water temperature (impacts both density and kinematic viscosity calculations)
- Including the retarding forces in the sediment due to its semi-solid nature
- Redefining the method of determining the viscosity and density of the water/sediment mixture during the sediment/cavity regime.

(Satkowiak 1987) points out the improvements greatly improved the predictive capability of the model as assessed in (Satkowiak 1987, and 1988). Satkowiak stresses that the orientation and impact velocity of the mine at the water sediment interface are two critical parameters to determining the final burial depth of a particular mine shape into the bottom sediments. (Satkowiak 1988) also

points out that the final burial depth and impact parameters are highly dependent on accurately initializing model inputs. It is discussed that if some degree of uncertainty exists in the initial parameters the model should be used in a probabilistic manner vice deterministic manner.

(Rumball and Kitchings 1988) translated the code to HP-UX Technical Basic to run on a HP 9000 computer with a UNIX operating system. They subsequently tested the model and acquired results similar to Satkowiak's results. In 1990, S Murdock, (Hurst 1992), converted the code to QuickBasic to run on an IBM compatible PC and converted all units from English to metric.

(Hurst 1992) provided the next generation of substantial improvements to IMBP. He recognized that to this point the model treated the falling shape as a one-dimensional dynamic system, a simplifying feature recognized as limiting the overall accuracy of impact burial predictions, (Lott 2001).

The modifications involved developing new methods for deriving the forces acting on the mine as it passes through the air-water interface and sediment. Specifically a new reference frame was developed to simplify computation of external drag forces acting on the mine. Additionally the model was extended to allow rotational movement of the mine in addition to the normal lateral and vertical movement covered in the original IBPM model, Figure 6.

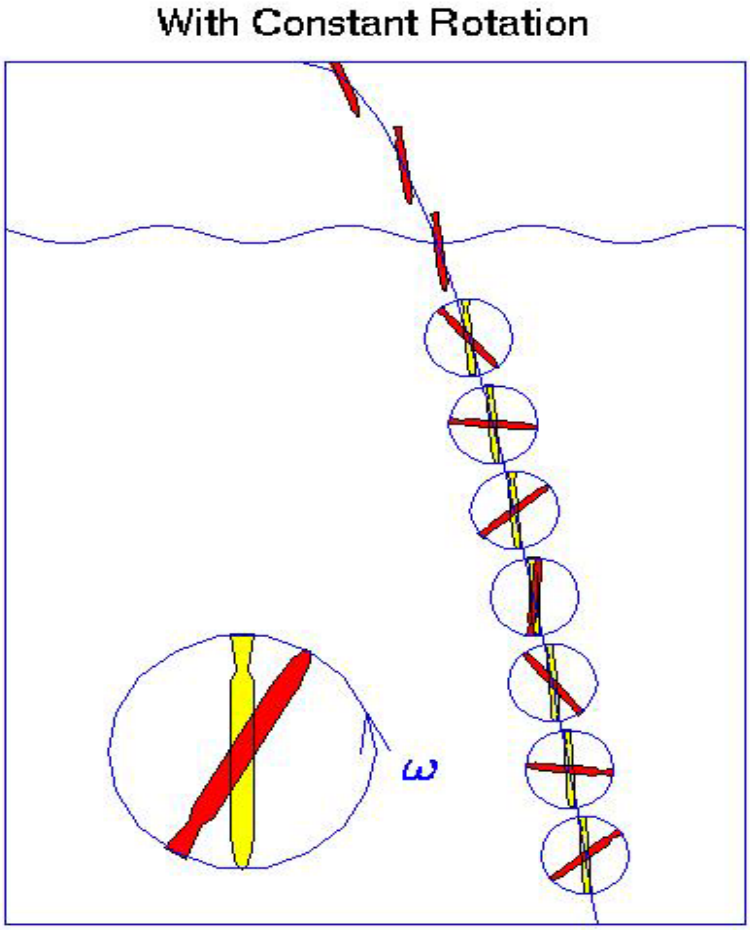

Figure 6. Hurst IBPM Mine Motion with Rotation. "From Gilless (2001)."

The modified model differed from the original version in seven primary areas:

- Calculation of fluid drag
- Calculation of forces at the air-water interface
- Calculation of forces during impact in the sediment
- Improved Treatment of multi-layered sediments.
- Allowing for rotational movement of mine as it falls

- Calculation of the fall angle from solid body dynamics.
- Treatment and calculation of water density and viscosity.

The discussion that follows expands the explanation of those improvements significant to the water phase hydrodynamics and important precursors to current modeling efforts. Allowing the cylinder the move in multiple directions and experience rotational motion requires that two coordinate systems be used. This is a novel approach to numerical modeling to find solutions to the solid body dynamics system. The two systems used by (Hurst 1992) are shown in Figure 7. The coordinate systems are related by:

$$V_a = V_z \sin\theta + V_x \cos\theta \quad (1)$$

$$V_c = V_z \cos\theta + V_x \sin\theta \quad (2)$$

As seen, the cylinder rotates with respect to the (x,z) system as it falls. The addition of the mine-oriented coordinate system is important because the total mass of the mine differs in axial and cross axis flow directions due to inclusion of hydrodynamic mass, (Lamb, 1932. Without the reference frame transformation the mass would have to be treated as a tensor quantity.

Additionally, calculation of fluid drag forces is simplified in the new coordinate system. Hurst recognized that the mine motion is neither purely cross nor axial but rather oblique. He made a calculated hypothesis that the drag can be estimated by calculating cross and axial drag

from the cross and axial velocities as if they were independent. (Sumer and Fredsoe 1997) provide a similar and complimentary assessment to determining the axial and cross

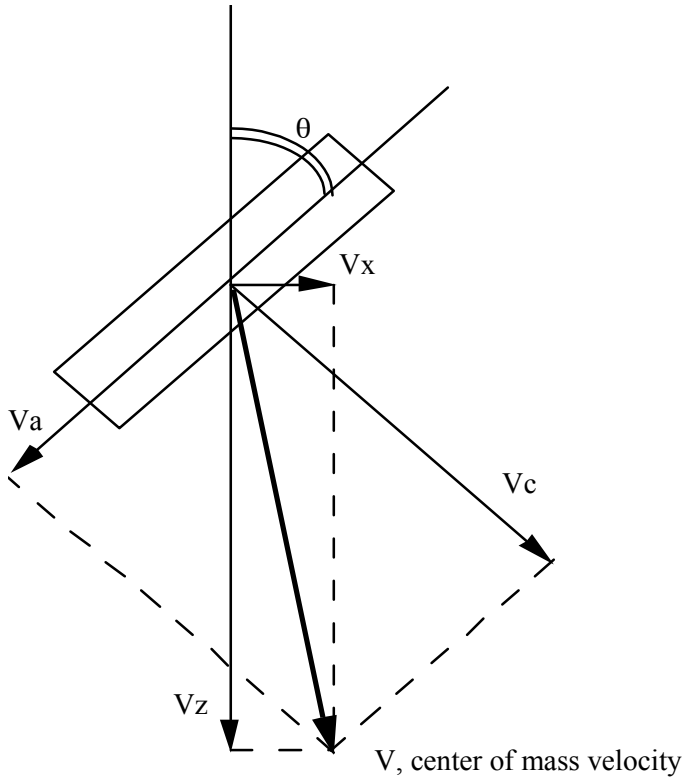

Figure 7. The Fixed (x,z) and Mine-orientated Coordinate Systems Developed by Hurst. “From Hurst (1992).”

flow drag and lift forces. Hurst performed analysis of different methods for calculating the drag forces with at most a 10% increase in drag force. Thus this effect is deemed second order and the approximation adequate.

Hurst also determined that if a mine is both rotating and falling, the cross drag force would act unevenly along the length of the mine. This dampens any rotating motion of the mine about the cross flow axis and is called braking

torque. Using the notation of Figure 8, Hurst developed and incorporated a braking torque calculation where the total cross-velocity of a point on the mine is:

$$V_t = V_c + \omega l \qquad (3)$$

V_c = cross velocity

V_t = total cross velocity for point along the long axis of the mine

ω = angular velocity

l = distance from the center of a point

d = diameter of the cylinder

Adding the contributions from the movement of the center of mass and rotation for an element, dl, the torque about the center of mass due to drag forces becomes:

$$\frac{\delta T}{\delta t} = -C_d d \times (dl) \rho_w (V_c + \omega l)^2 / 2 \qquad (4)$$

$\frac{\delta \Gamma}{\delta t}$ = differential torque about the center of mass

C_d = drag coefficient for cross motion

ρ_w = fluid density

d = diameter of the mine

The total torque is determined by integrating along the

entire length of the mine, (i.e., -L/2 to L/2) according to the equation:

$$T = - C_d d \rho_w V_c L^3/12 \qquad (5)$$

Hurst performed analysis on the time step stability in the model and found that doubling or halving the time step from the established 0.01 seconds produced less than 0.5% change in final burial depth calculations. This version of IMBP was designated IMPACT25 and further model improvements have been based on this baseline model code.

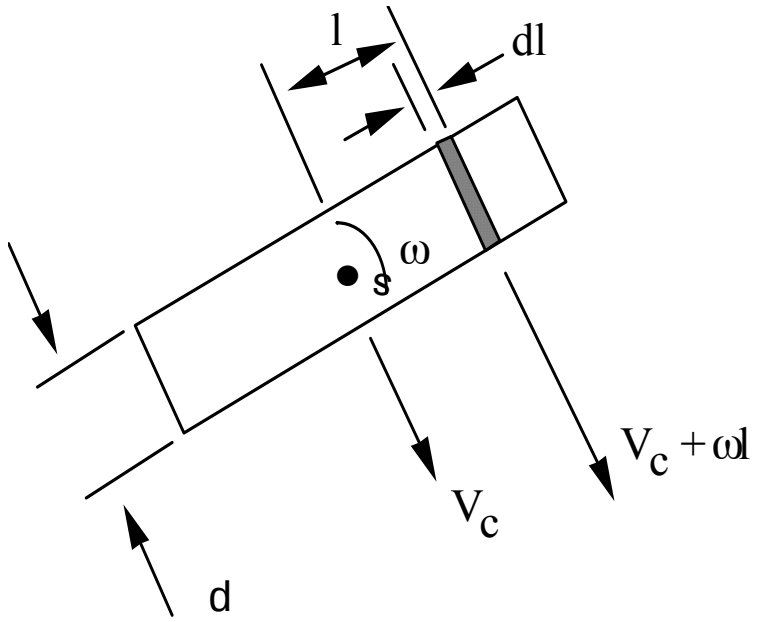

Figure 8. Braking Torque: Notation Used by Hurst. "After Hurst (1992)."

The last major documented changes to occur to the model code occurred in (Mulhearn 1993). Mulhearn developed a formulation for sediment bearing strength that includes sediment shear strength as well as the object mass and

center of geometry to compute bearing strength. He also modified the code to allow for a mine center of mass displaced from the center of volume.

B. MODEL SENSITIVITY STUDIES

Model Sensitivity studies by (Hurst and Murdoch 1991) (Taber 1999), (Richardson et al 2001a) and (Smith 2000) shows that the sediment density and shear strength are the two most important environmental factors influencing mine burial. Satkowiak (1987) shows that in different initial conditions and bottom characterizations either shear strength of density can dominate the sediment penetration but in most case the shear strength is the dominating factor in the sediment phase. (Gilless 2001) and (Valent et al 2002) both observe that the current model solid body dynamics tend to incorrectly predict both sediment impact velocity and impact angle. These two parameters are viewed as the most important parameters from the hydrodynamic phase of the model required to produce accurate kinetic energy dissipation predictions in the sediment phase of the model. (Smith 2000) provide evidence that IMPACT overestimates penetration in some sediment types by an order of magnitude. It was observed by (Valent et al 2002) that the hydrodynamic section of the current impact burial program was contributing significantly to orientation and penetration errors. The errors at times approach 150%.

There are currently more than 10 versions of IBPM available. They all operate using the same physics, and solid body dynamics with three degrees of freedom. The

models predict the vertical free-fall time history of a variety of mine shapes as the shape passes through the air, air-water cavity, water, water-sediment cavity, and sediment phases. The defining output is sediment mine burial depth. Environmental parameters are considered constants in all these model versions.

In an inexact science containing complex nonlinear processes, limiting the degrees of freedom of the solid body and assuming uniform shape density limits the usefulness of output for both probabilistic and deterministic prediction models and tactical decision aids in the fleet. This investigation develops a three dimensional model that involves all six independent degrees of freedom. Solutions are obtained for the linear system of ordinary differential equation approximations to for the momentum and moment of momentum equations. This model is then compared to two independently obtained data sets for mine shape’s positions obtained at defined increments during free fall through the water column.

THIS PAGE INTENTIONALLY LEFT BLANK

IV. MINE DROP EXPERIMENTAL DATA

Two independent data sets are used to validate the Three Dimensional Mine Impact Hydrodynamic Flow model. The first data set was collected during a Mine Drop Experiment (MIDEX) that took place at Naval Postgraduate School (NPS) in July 2001, (Gilless 2001).

The second data set originates from the Carderock Mine Drop Experiment designed principally by Dr. Philip Valent and Todd Holland of the Naval Research Laboratory, Stennis Space Center, (Valent and Holland 2001). The experimental work was conducted 10-14 September 2001 at the Naval Surface Warfare Center, Carderock Division, Explosion Test Pond, (Valent and Holland 2001) and funded by the Office of Naval Research.

The experiments are summarized briefly. The details of each experiment can be found in (Gilless 2001), (Chu et al 2002), (Valent and Holland 2001), and (Valent et al 2002).

A. MINE DROP EXPERIMENT

MIDEX took place at the Naval Postgraduate School swimming pool. It consisted of dropping cylindrical mine shapes, Figure 9, into the water and recording the position as a function of time using two digital cameras at (30 Hz) as the mine shapes fell 2.4 meters to the pool bottom. The scale of the mine used was tailored to be representative of dropping a full-scale bottom mine into 45 meters of water. A 15:1 ratio provided a safety factor on weight forcing so as to not damage the bottom of the concrete swimming pool.

Figure 9. Exterior Façade and Iterior Components of the Mine Shape. “From Gilless (2001).”

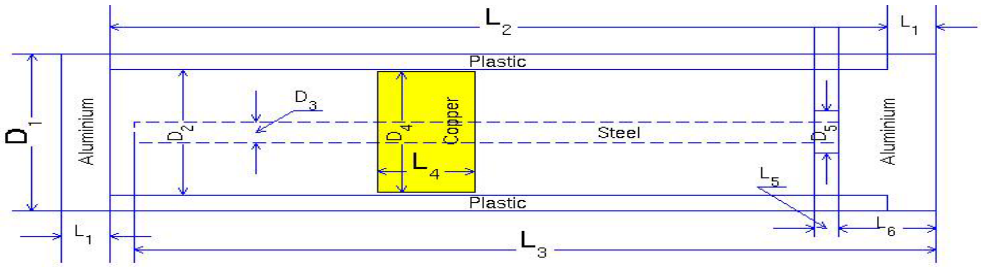

units: mm

mine#	D1	D2	D3	D4	D5	L1	L2	L3	L4	L5	L6
1	40	25	6	24	11.5	7	138	136	26.94	0	25
2	40	25	6	24	11.5	7	107	108	17.00	6	24.5
3	40	25	6	24	11.5	7	77.2	77.3	15.31	6	25

Material	Aluminium	Plastic	Steel	Copper
Specific-gravity(g/cm^3)	2.7	1.155	7.8	8.93

mine#	mass(kg	J1(kg*m^2)	J2(J3)	chl(m)	L(m)	vol(m^3)	rmean
1	0.3225	3.3046e-05	0.00060879	4.6e-05	0.152	0.00019101	1.6885
			0.0005783	0.007411			
			0.00062338	0.014772			
2	0.2542	2.7132e-05	0.00034262	0.000644	0.121	0.00015205	1.6717
			0.00032065	0.005307			
			0.00033126	0.00997			
3	0.2153	2.3503e-05	0.00016952	2.9e-05	0.0912	0.00011461	1.8785
			0.00015775	0.002911			
			0.00015568	0.005796			

Table 2. MIDEX Mine Shape Characteristics. Left Column Indicates COM position 0, and Right Column Indicates COM Position 2. “After Gilless (2001).”

The control parameters for the drops were: center of mass position (COM), initial velocity (V_i), drop angle and mine aspect ratio, $\left(L/d\right)$. Three mine aspect ratios were used. All mines had a diameter of 4 cm, and lengths of (15,12,9) cm. The range of lengths accounts for the variety of mine in use today worldwide. The characteristics of each mine are shown in Table 2. An internal threaded weight was used to vary the center of mass (COM) between 5 different positions (2,1,0,-1,-2), as shown in Table 3, for each of the three mine shapes. Initial velocity was obtained using an infrared photo detector and backing out a near instantaneous velocity as the shape past the unit.

Mine Length →	15	12	9
COM Position			
2	0.1939	0.1594	0.1198
1	0.0969	0.0797	0.0599
0	0	0	0
-1	-0.0969	-0.0797	-0.0599
-2	-0.1939	-0.1594	-0.1198

Table 3. Non-dimensional COM Positions. Non-dimensional COM Positions Determined Using $2M/L$. "From Gilless (2001)."

The drop angle was measured with the pool walkway serving as the x-y plane and the drop injector angle (pitch angle) was varied from 15° to 75° in 15° increments. The range of drop angles represents conservative limits of mine entry angles into the water from air borne and waterborne craft. The COM position on the mine shape was set based on positions (0,1,2) and loaded into the drop injector nose first. The negative COM positions were achieved by loading the mine shape into the injector with the COM behind and

above the center of buoyancy. Two grids were constructed on the pool walls to measure the cylinder position relative to the wall as the shape fell through the water column. The two dimensional measurements were then combined to create a three-dimensional data set. The spacing between grid divisions was 10 cm. The number of drops conducted, for each COM and drop angle, is shown in Table 4. A total of 230 mine shape drops were analyzed and results compiled in (Gilless 2001).

Drop Angle ⟶	15°	30°	45°	60°	75°
COM Position					
2	13	15	15	15	12
1	9	15	15	15	9
0	12	15	14	18	6
-1	0	6	6	6	0
-2	2	6	6	0	0

Table 4. Number of Drops Conducted by Drop Angle and COM Position. “From Gilless (2001).”

B. CARDEROCK MINE DROP EXPERIMENT

The model mine drop experiment at Carderock was a direct result of impact burial tests using NRL's first generation mine-like instrumented cylinder in September and November 2000. The results from at sea testing off of the Mississippi Sound and East Bay, LA were a strong indication of deficiencies in the hydrodynamic (water) portion of the Impact Burial Prediction Model currently in use, (Valent 2002). The Mine Burial Project Team, lead by principal investigator; NRL’s Dr. Philip Valent, and Mr. Todd Holland designed the Carderock Experiment to gather a statistically representative data sample from many test drops of scaled models.

Concerns over “dynamic similarity” (Panton 1996) via Reynolds number differences between scaled models and full size prototypes led the Mine Burial Project Team to determine 1/3-rd scale models, with diameter of 0.168 m, length to diameter ratio of 3 and 6, and mass up to 45 kg,

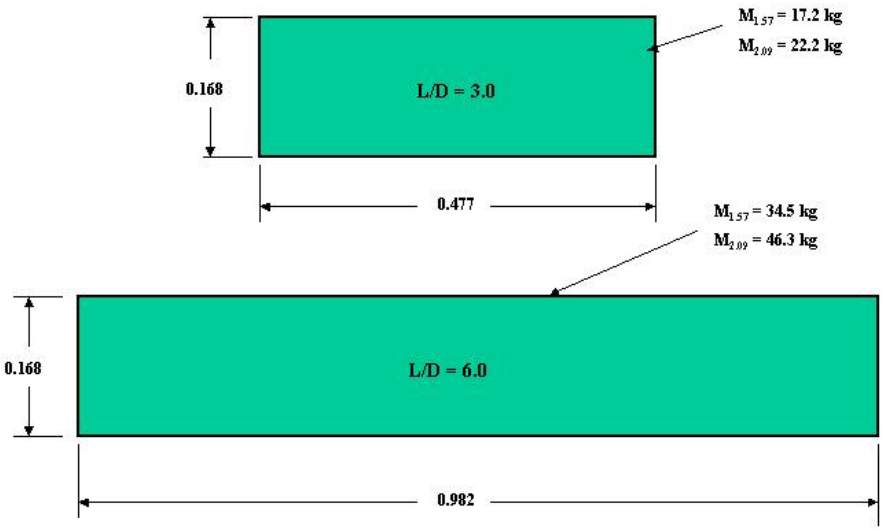

Figure 10. 1/3rd Scale Blunt Nosed Models Used for Carderock Mine Drop Experiment. Dimensions in Meters, “After Valent et al (2002).”

were the smallest acceptable model size. Cross sections of the models are shown in Figure 10 with complete mine shape characteristics include in Table 5.

The mine shapes are fabricated from aluminum pipe with a urethane covered aluminum front plate. The center of mass was coincident with the center of volume for four models and placed 5.5 cm forward of center of volume in model five and 8.7 cm forward of center of volume in model six. The void area was ballasted with aluminum and steel plates and water to adjust bulk densities to 1.60 and 2.10 Mg/m^3, see

Table 5. Figure 11 shows all six blunt nosed model mine shapes on deck at the experiment site awaiting a drop cycle.

The mine drops of interest for model validation, 44 drops total, consisted of all in water drops of blunt nosed mines from three initial target drop orientations; horizontal, vertical, and 45° nose down. Due to the buoyancy moment acting on the mines during initial water insertion the target drop orientations were not achieved

CHARACTERISTICS OF MINE MODELS USED IN TEST POND, NSWC CARDEROCK, MD, 10-14 Sept 2001 (Revised 28 Feb 2002)						
Model number	**1**	**2**	**3**	**4**	**5**	**6**
Blunt Mine Parameters						
Diameter, m(in.)	0.168 (6.63)	0.168 (6.63)	0.168 (6.63)	0.168 (6.63)	0.168 (6.63)	0.168 (6.63)
Length, blunt, m(in.)	0.477 (18.78)	0.477 (18.78)	0.982 (38.65)	0.982 (38.65)	0.982 (38.65)	0.982 (38.65)
L/D for blunt nose	2.8	2.8	5.8	5.8	5.8	5.8
Volume, cu m (cu ft) (blunt)	0.0106 (0.374)	0.0106 (0.374)	0.0218 (0.771)	0.0218 (0.771)	0.0218 (0.771)	0.0218 (0.771)
Weight (lbs)	38	49	76	102	100	98.5
Mass, kg	17.2	22.2	34.5	46.3	45.4	44.7
Mass Wet kg (4) (blunt)	6.33	11.33	12.13	23.93	23.04	22.34
Bulk density, pcf (Mg/cu m)	101.6 (1.63)	131.0 (2.10)	98.6 (1.58)	132.3 (2.12)	129.7 (2.08)	127.8 (2.05)
χ=(CM - CV) (m)	-0.0002385	-0.001908	-0.001964	-0.008838	0.045172	0.076596
(CM - CV) / (mine length)	-0.0005	-0.004	-0.002	-0.009	0.046	0.078
Moment of Inertia about CM						
I_{xx}[1], kg-m^2 (lb-in^2)	0.0647 (221)	0.0806 (275)	0.1362 (465)	0.1696 (579)	0.1693 (578)	0.1692 (578)
I_{yy}[2], kg-m^2 (lb-in^2)	0.356 (1216)	0.477 (1627)	2.90 (9910)	3.82 (13,050)	3.94 (13,440)	4.57 (15,600)
I_{zz}[3], kg-m^2 (lb-in^2)	0.356 (1214)	0.476 (1625)	2.90 (9910)	3.82 (13,050)	3.94 (13,430)	4.57 (15,600)
Note:						
1. I_{xx} about long axis (Roll)						
2. I_{yy} about transverse vertical axis (Yaw)						
3. I_{zz} about transverse horizontal axis (Pitch)						
4. Wet mass calculations required for IMPACT28						
Wet mass calculation based on water density 1025.8 kg/m^3						

Table 5. Physical Characteristics of Cylindrical Blunt Nosed Model Mines Used in 1/3rd Scale Tests, NSWCCD Explosion Test Pond. “After Valent et al (2002).”

Figure 11. Six Blunt Nosed Models. “From Valent and Holland (2001).”

for all orientations, especially significant for models five and six. Table 6 shows the water borne initial drop angles measured in at NRL after the experiment.

Mine Shape	Target Angle	Actual Drop Angle
1	+45	+35
2	+45	+37
3	+45	+38
4	+45	+38
5	0	+30
	+45	+30
6	0	-8
	+45	+50

Table 6. Model Mine Shape In-Water Initial Drop Angles. “From Valent and Holland (2001).”

A design change in the lifting lugs on the mine caused additional drop angle changes for the remainder of the models when hung at the target 45° down angle, see Table 6.

Naval Surface Warfare Center, Carderock Division, West Bethesda, Maryland, agreed to let the Mine Burial Prediction Group drop the 45 kg mine shape models and associated impact force approximately 26 ft into their concrete-floored pond, shown in Figure 12.

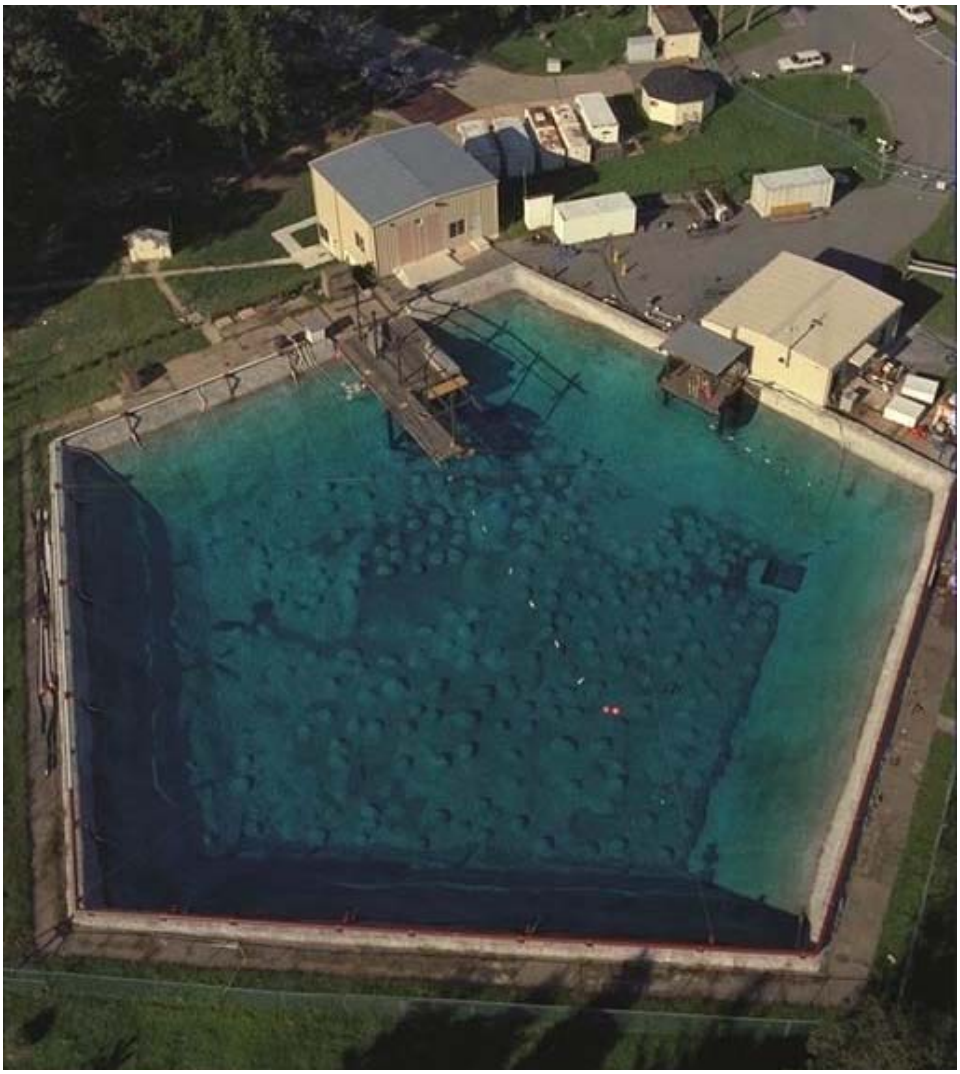

Figure 12. Explosion Test Pond, NSWCCD, West Bethesda, MD. “Photo courtesy of NSWCCD, William Lewis.”

This facility is the only facility in the United States capable of delivering high-speed, high-resolution underwater photography. NRL and NSWC Technical Media Lab designed a submerged three camera digital high speed recording analyzer, Figure 14, that captured the entire fall of the mine shapes through the water column in high resolution, color recordings at 125 fps on all three cameras.

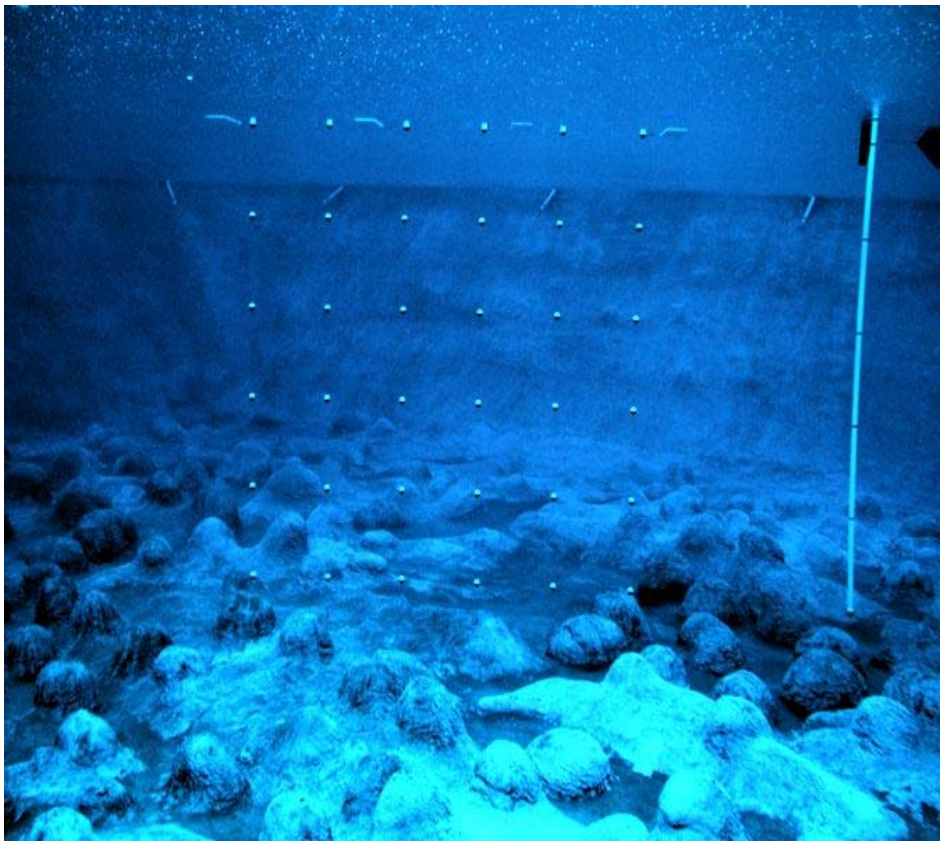

Figure 13. The Underwater Calibration Target for the Digital Camera Tracking System.

The cameras were calibrated each day using a geo-referenced calibration target consisting of white balls

strung uniformly across the plane of the camera on aircraft cabling, Figure 13. The z-axis was acquired and fixed through use of a weighted pole tied off to a bottomed weight that hung freely from the overhead crane ball hook. This allowed the cameras to initialize their position in the pond each day so the digital camera analyzer and motion analysis software could compute positions to the mine shapes.

A Pelican hook was attached to the mine shape release cable and activated through an electrical powered solenoid. The video analyzer was synchronized with the solenoid activation to start the three-camera high-speed recording. The data was transmitted through an ethernet cable to a commercially leased, high powered, image-processing computer Figure 14 that contained an advanced motion

Figure 14. The Digital Camera Analyzer Network and the Digital Imaging Processing Computer at NSWCCD.

analysis “Redlake” software, typical of those used in the automotive industry to measure impact accelerations, in crash tests The image processor tracked multiple positions on the mine shapes to derive (x, y, z) positions. NRL reduced the data to positions, yaw and pitch angles, linear velocities and instantaneous accelerations for each mine drop.

The mine shapes were brought into place by a commercial heavy overhead crane and lowered into the water.

The external forcing due to cable sway were allowed to dampen to bring the resultant mine velocities to near zero.

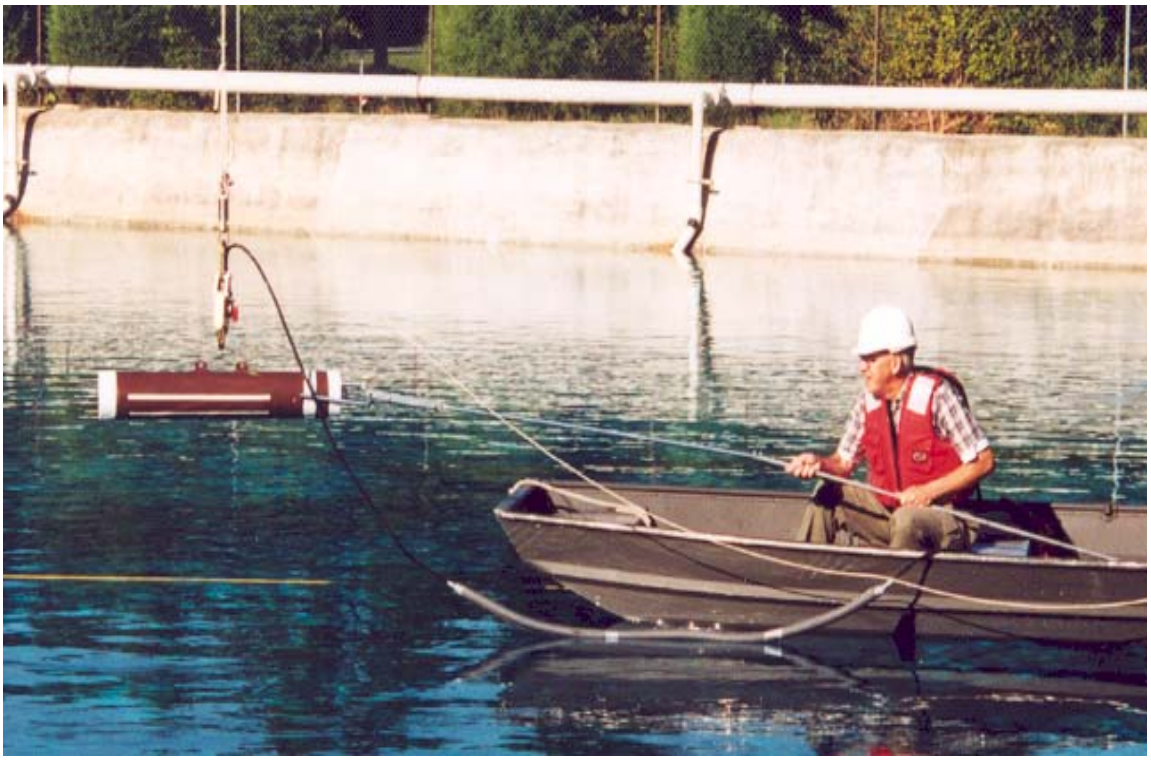

Figure 15. Blunt Nose Model Mine Shape Four Being Lowered Into Place by the Crane and Aligned for Release. Dr. Philip Valent Steadies the Mine Shape as it is Lowered into the Water.

The mine was aligned with the head of the mine away from the cantilever pier that hung out over the pond, as shown in Figure 15 and released. The digital cameras tracked the free fall of the mine recording the (x, y, z) position at 125 fps, for example in Figure 16. While not a clean image the analyzer software tracked the digital images frame by frame to calculate incremental position parameters.

Figure 16. Digital Camera Shot of Mine Shape Six During Free-fall from an Initial Horizontal Position Towards the Pond Floor. “Photo courtesy of NRL-SSC, Mr. Todd Holland.”

V. MINE IMPACT THREE DIMENSIONAL MODEL

A. DYNAMICS EQUATIONS

Any solid object (such as a mine) falling freely through the water column should obey two essential laws of the motion: momentum balance and the moment of momentum balance. They are usually represented by six equations fully describing the position and orientation of the object at any time along its path.

Let (x, y, z) represent the Earth coordinates and (u, v, w) be the velocity components of the mine's center of mass point (M) in the (x, y, z) directions. Let (B, L, d, g) represent the mine center of volume, mine length, mine diameter, and the gravitational acceleration. The momentum equation of the falling object is written:

$$\int(d\vec{V}/dt)\,dm = \sum\vec{F} \qquad (6)$$

In this case $\vec{V}$=(u, v, w) is the mine velocity, m is the mass of the mine and ($\vec{F}$) is the resultant force acting on the mine. The moment of momentum equations describing the angular velocities of the mine around COM is given by:

$$\int[\vec{r}\times(d\vec{V}/dt)]\,dm = \sum\vec{M} \qquad (7)$$

Here ($\vec{r}$) is the position vector, and ($\vec{M}$) the resultant moment.

The momentum equation (6) and the moment of momentum equation (7) comprise the core hydrodynamic system of mine movement in the water column. All the Newtonian dynamic equations (momentum and moment of momentum equations) are originally based on the earth fixed reference frame as shown in Figure 17(a). To simplify the computation, the moment of momentum equations are solved using the mine body coordinate reference frame, with the external forcing being transferred from the drag-lift force reference frame to the appropriate reference frame to include in the momentum and the moment of momentum calculations (Boiffier 1998). In this study, the mine is assumed cylindrical and axially symmetric.

B. THREE COORDINATE SYSTEMS

The coordinate systems used in the model are all three-dimensional, orthogonal and right-handed. The associated transformation matrices between coordinate systems only require a rotation component about the origin. No translation component of the axes is required

1. Earth Fixed Coordinate System $F_E\left(o,\vec{i},\vec{j},\vec{k}\right)$

In the earth fixed coordinate system Figure 17(a), the position of the cylinder's center of mass (M) is represented by (x,y,z), the velocity of (M) is represented by (u,v,w). The vector $\vec{i}_M$ is along the mine cylinder's long axis with the direction from center of volume (B) to (M). The angle between two vectors ($\vec{i}_M$) and ($\vec{k}$) are denoted by $\psi_2+\pi/2$. The projection of the vector ($\vec{i}_M$) onto the (x, y)

plane creates angle (ψ_3) between the projection and the x-axis.

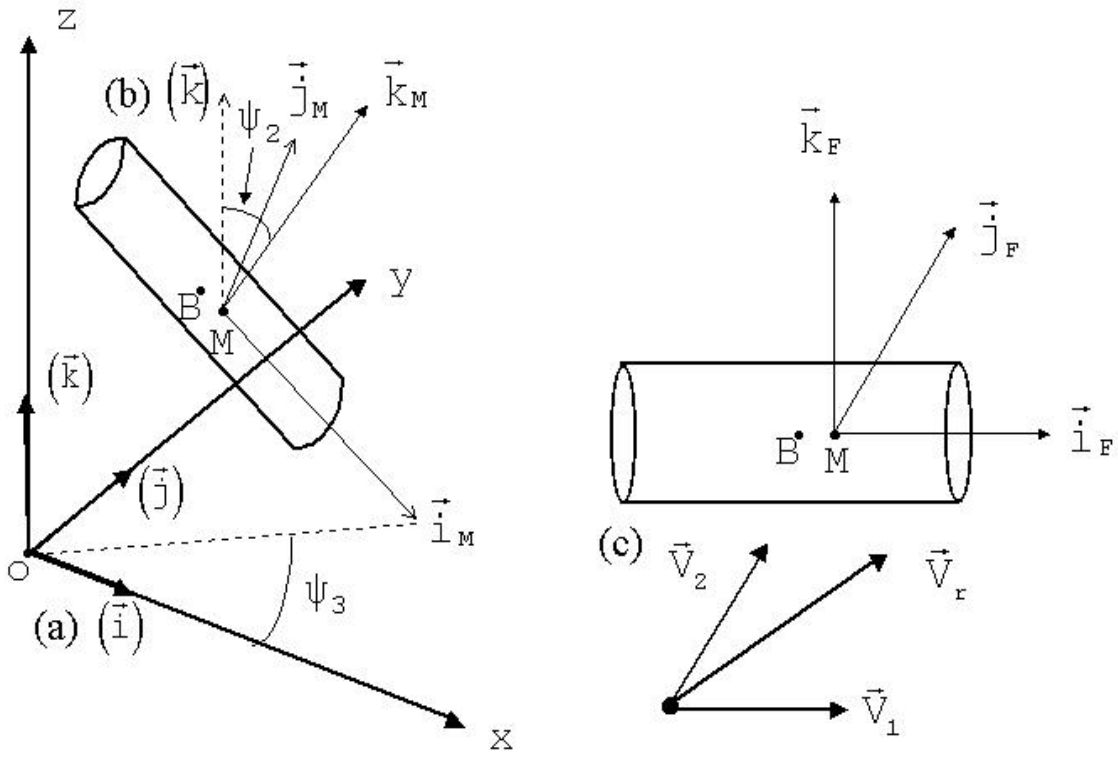

Figure 17. The Three Coordinate Reference Frames Used to Perform Transformation in the Three Dimensional Model; (a) Earth Fixed Coordinates, (b) Body Fixed Coordinates, (c) Drag Lift Force Coordinates.

2. Body-Fixed Coordinate System $F_M\left(M, \vec{i}_M, \vec{j}_M, \vec{k}_M\right)$

The body-fixed coordinate is used for effectively computing the moment of momentum. The origin of this coordinate system is at the COM of the cylinder (point M in Figure 17(b). In the plane (consisting of vectors $\vec{i}_M$ and $\vec{k}$ (passing through the point M, called the IMK plane), two new unit vectors ($\vec{j}_M$, $\vec{k}_M$) are defined with ($\vec{j}_M$) perpendicular

to the IMK plane, and ($\vec{k}_M$) perpendicular to ($\vec{i}_M$) in the IMK plane. The body-fixed coordinate system directors are expressed:

$$\vec{j}_M = \frac{\vec{k} \times \vec{i}_M}{\left| \vec{k} \times \vec{i}_M \right|} \tag{8}$$

$$\vec{k}_M = \vec{i}_M \times \vec{j}_M \tag{9}$$

Use of the body-fixed coordinate system simplifies the calculations for the moments of inertia as well as the resultant action of individual external forcing torques on the cylinder. The Earth-fixed and body-fixed coordinate systems are connected by the transformation,

$$\vec{i}_M = e_{11}\vec{i} + e_{21}\vec{j} + e_{31}\vec{k} \tag{10}$$

$$\vec{j}_M = e_{12}\vec{i} + e_{22}\vec{j} + e_{32}\vec{k} \tag{11}$$

$$\vec{k}_M = e_{13}\vec{i} + e_{23}\vec{j} + e_{33}\vec{k} \tag{12}$$

3. Drag-Lift Force Coordinate System

$F_F\left(M, \vec{i}_F, \vec{j}_F, \vec{k}_F\right)$

The drag and lift forces and moments of a moving cylinder are determined not only by the position of the cylinder, but also by the relative water velocity flowing past the cylinder, Figure 17(c). To simplify the calculation of the lift and drag forces and torques acting on the cylinder, we propose to use the drag-lift force coordinate system. Let ($\vec{V}_w$) be the fluid velocity. The relative velocity the fluid to the cylinder is represented

by $\vec{V}_r = \vec{V}_w - \vec{V}$, and decomposed into two parts: ($\vec{V}_1$) is parallel to the cylinder's axial direction ($\vec{i}_M$), and perpendicular to the cylinder's axial direction, $\vec{V}_2 = \vec{V}_r - \vec{V}_1$. Two unit vectors for the drag-lift force coordinate reference frame can be defined:

$$\vec{i}_F = \vec{i}_M \tag{13}$$

$$\vec{j}_F = \vec{V}_2 / \left|\vec{V}_2\right| \tag{14}$$

The third unit vector for the drag-lift force coordinate system is defined:

$$\vec{k}_F = \vec{i}_F \times \vec{j}_F \tag{15}$$

The Earth-fixed and drag-lift force coordinate systems are connected by the transformation:

$$\vec{i}_F = e_{11}\vec{i} + e_{21}\vec{j} + e_{31}\vec{k} \tag{16}$$

$$\vec{j}_F = e'_{12}\vec{i} + e'_{22}\vec{j} + e'_{32}\vec{k} \tag{17}$$

$$k_F = e'_{13}\vec{i} + e'_{23}\vec{j} + e'_{33}\vec{k} \tag{18}$$

C. COORDINATE TRANSFORMATION MATRICES

Rotational matrices connect the three coordinate systems. Let E, M, F indicate the Earth fixed, body-fixed, and drag-lift force coordinate systems. The position vector

represented in the body-fixed coordinate system ($^{M}\vec{P}$) are transferred to the earth coordinate system ($^{E}\vec{P}$) through the rotation matrix ($^{E}_{M}R$) as:

$$^{E}\vec{P} = {}^{E}_{M}R \cdot {}^{M}\vec{P} \tag{19}$$

The rotation matrix is computed by:

$$^{E}_{M}R \equiv \begin{bmatrix} e_{11} & e_{12} & e_{13} \\ e_{21} & e_{22} & e_{23} \\ e_{31} & e_{32} & e_{33} \end{bmatrix} = \begin{bmatrix} \cos\psi_3 & -\sin\psi_3 & 0 \\ \sin\psi_3 & \cos\psi_3 & 0 \\ 0 & 0 & 1 \end{bmatrix} \cdot \begin{bmatrix} \cos\psi_2 & 0 & \sin\psi_2 \\ 0 & 1 & 0 \\ -\sin\psi_2 & 0 & \cos\psi_2 \end{bmatrix} \tag{20}$$

The reverse rotation process is given by:

$$^{M}\vec{P} = {}^{M}_{E}R \cdot {}^{E}\vec{P} \tag{21}$$

$$^{M}_{E}R = {}^{E}_{M}R^{-1} \tag{22}$$

The rotation matrix to transfer between the earth-fixed coordinates and drag-lift force coordinate systems:

$$^{E}\vec{P} = {}^{E}_{F}R \cdot {}^{F}\vec{P} \tag{23}$$

$$^{E}_{F}R = \begin{bmatrix} e_{11} & e'_{12} & e'_{13} \\ e_{21} & e'_{22} & e'_{23} \\ e_{31} & e'_{32} & e'_{33} \end{bmatrix} \tag{24}$$

$$^{F}\vec{P} = {}^{F}_{E}R \cdot {}^{E}\vec{P} \tag{25}$$

$$^{F}_{E}R = {}^{E}_{F}R^{-1} = \begin{bmatrix} e_{11} & e_{21} & e_{31} \\ e'_{12} & e'_{22} & e'_{32} \\ e'_{13} & e'_{23} & e'_{33} \end{bmatrix} \tag{26}$$

The rotation matrix between the body-fixed coordinate and drag-lift force coordinate systems:

$$ {}^{M}\vec{P} = {}^{M}_{F}R \cdot {}^{F}\vec{P} \tag{27} $$

$$ {}^{F}\vec{P} = {}^{F}_{M}R \cdot {}^{M}\vec{P} \tag{28} $$

This relationship can be expressed in terms of the respective angular velocity components in body fixed coordinates and drag-lift force coordinates:

$$ \begin{bmatrix} 0 \\ \omega_2 \\ \omega_3 \end{bmatrix} = {}^{M}_{F}R \cdot \begin{bmatrix} 0 \\ \omega'_2 \\ \omega'_3 \end{bmatrix} \tag{29} $$

$$ \begin{bmatrix} 0 \\ \omega'_2 \\ \omega'_3 \end{bmatrix} = {}^{F}_{M}R \cdot \begin{bmatrix} 0 \\ \omega_2 \\ \omega_3 \end{bmatrix} \tag{30} $$

Equations 29 and 30 can be expanded and expressed:

$$ \begin{bmatrix} \omega_2 \\ \omega_3 \end{bmatrix} = \begin{bmatrix} d_{22} & d_{23} \\ d_{32} & d_{33} \end{bmatrix} \cdot \begin{bmatrix} \omega'_2 \\ \omega'_3 \end{bmatrix} \tag{31} $$

$$ \begin{bmatrix} \omega'_2 \\ \omega'_3 \end{bmatrix} = \begin{bmatrix} d_{22} & d_{32} \\ d_{23} & d_{33} \end{bmatrix} \cdot \begin{bmatrix} \omega_2 \\ \omega_3 \end{bmatrix} \tag{32} $$

This results in the transformation matrices:

$$ {}^{M}_{F}R \equiv \begin{bmatrix} 1 & 0 & 0 \\ 0 & d_{22} & d_{23} \\ 0 & d_{32} & d_{33} \end{bmatrix} = {}^{M}_{E}R \cdot {}^{E}_{F}R \tag{33} $$

D. HYDRODYNAMIC MASS

Hydrodynamic mass is defined as the as the mass of the fluid around a solid body that is accelerated with the movement of the body due to the action of pressure forcing, (Sumer and Fredsoe 1997).

When a solid body is accelerated through a near still fluid at some velocity ($\vec{V}$), a kinetic energy balance between the end states reveals that when the body is accelerated from $\vec{V}(t_1)$ to $\vec{V}(t_2)$ the flow field at the second speed has more kinetic energy than at the first speed, (Panton 1996). The difference in kinetic energy between the end-states results from not only accelerating the mine shape but also the fluid medium (water or seawater) in the immediate neighborhood of the mine shape. The hydrodynamic mass (m_a) can be included in Newton's equations in general terms as:

$$\vec{F} = (m + m_a) \cdot \vec{a} \tag{34}$$

Lamb (1932) outlines the steps to calculate the hydrodynamic mass based on inertial coefficients associated with the axial, cross, and rotational flow properties. These coefficients are adapted from (Lamb 1932) and (Arnone and Bowen 1980). The mine shape is treated as an ellipsoid of rotation, where the maximum mine diameter and the maximum mine length equate to the axes of the ellipse, (Hurst 1992).

The inertial coefficients are based on the eccentricity of the mine shape:

$$e = \left(1 - \left(\frac{d}{L}\right)^2\right)^{1/2} \tag{35}$$

(L) is maximum length and (d) is maximum diameter of the mine shape. The inertial coefficient for the mine shape axial flow component is defined as:

$$k_1 = \frac{\alpha_o}{2 - \alpha_o} \tag{36}$$

$$\alpha_0 = \left(\frac{2\left(1 - e^2\right)}{e^3}\right) \cdot \left(1/2 \ln\left[\frac{1+e}{1-e}\right] - e\right) \tag{37}$$

The inertial coefficient for the mine shape cross flow component is defined as:

$$k_2 = \frac{\beta_o}{2 - \beta_o} \tag{38}$$

$$\beta_o = 1/e^2 - \left(\frac{1 - e^2}{2e^2}\right) \cdot \ln\left[\frac{1+e}{1-e}\right] \tag{39}$$

The inertial coefficient for rotation about the cross flow axes of the mine shape is defined as:

$$k_r = \frac{1}{\left(\frac{2}{e^2 - 1}\right) \cdot \left(\frac{2}{(\beta_0 - \alpha_0)} - \left(\frac{2}{e^2 - 1}\right)\right)} \tag{40}$$

The hydrodynamic mass correction along either the axial or cross flow axis is the product of the appropriate inertial coefficient and the displaced mass of the mine shape:

$$m_a = (k_{(1,2,r)})(\rho_w)(\Pi) \tag{41}$$

Here the variable set $k_{(1,2,r)}$ denotes the appropriate inertial coefficient, (ρ_w) the fluid medium density, and (Π) the volume of the mine.

The hydrodynamic mass is added to the external forcing in the momentum equations:

$$\frac{d\vec{V}}{dt} = \vec{F}_r / m \tag{42}$$

$$\vec{F}_r = \vec{F} / f_{(k1,k2)} \tag{43}$$

A correction factor is used. Here $f_{(k1,k2)}$ denotes the appropriate correction factor based on whether the forcing is along the axial or cross flow direction.

$$m_t = m + m_a \tag{44}$$

$$m_t = \bar{\rho}\Pi + k_{(1,2)}\rho_w\Pi \tag{45}$$

$$m_t = m\left(1 + k_{(1,2,r)} \times \frac{\rho_w}{\bar{\rho}}\right) \tag{46}$$

$$f_{(k1,k2)} = \left(1 + k_{(1,2)} \times \frac{\rho_w}{\bar{\rho}}\right) \tag{47}$$

Similarly the hydrodynamic mass is accounted for and added to the external torque forcing in the moment of momentum equations:

$$\frac{d\vec{\omega}}{dt} = \vec{M}_r / [J] \tag{48}$$

$$\vec{M}_r = \vec{M} / f_{(kr)} \tag{49}$$

The correction factor used, ($f_{(kr)}$), denotes the appropriate correction factor for rotation about any of the body fixed axes axis.

$$m_t = \bar{\rho}\Pi + k_{(r)}\rho_w\Pi \tag{50}$$

$$m_t = m\left(1 + k_{(r)} \times \frac{\rho_w}{\bar{\rho}}\right) \tag{51}$$

$$f_{(r)} = \left(1 + k_{(r)} \times \frac{\rho_w}{\bar{\rho}}\right) \tag{52}$$

E. MOMENTUM EQUATIONS:

The momentum equations in a general format are written, (Von Mises 1959):

$$\vec{F} - m\frac{d\vec{V}}{dt} = 0 \tag{53}$$

$$\vec{F} = \vec{F}_b + \vec{F}_s \tag{54}$$

For these equations, (m) is the mine mass, and ($\bar{\rho}$) is the average mine density, then $m = \bar{\rho} \cdot \Pi$, where (Π) is the mine volume. The force vector $\vec{F}_s = (F_{sx}, F_{sy}, F_{sz})$ comprises the resultant surface forces, (drag and lift forces) where added mass has been taken into account. ($\vec{F}_b$) is the volume force including both the buoyancy force and gravitation force. The body force is written:

$$\vec{F}_b = -\Pi(\bar{\rho} - \rho_w)g\vec{k} \tag{55}$$

Here (ρ_w) is seawater density. The seawater density can be calculated based on empirically fitting an equation to tabular data found in (CRC Handbook 1981, as cited in Hurst, 1992).

$$\rho_w = 1028.17 - 0.0742 \times T - 0.0048 \times T^2 \tag{56}$$

The surface force is the resultant force from both the drag and lift force on the rotating, moving cylinder as expressed below:

$$\vec{F}_s = \vec{F}_{d1} + \vec{F}_{d2} + \vec{F}_{d3} + \vec{F}_l \tag{57}$$

The dimensional momentum equation describes the movement of the center of mass (M) for the cylinder as expressed below:

$$\frac{d\vec{V}}{dt} = -\left(1 - \frac{\rho_w}{\overline{\rho}}\right) \cdot g \cdot \vec{k} + \frac{\vec{F}_s}{\overline{\rho} \cdot \Pi} \tag{58}$$

The component momentum equations are expressed:

$$\frac{du}{dt} = \frac{F_{sx}}{\overline{\rho} \times \Pi} \tag{59}$$

$$\frac{dv}{dt} = \frac{F_{sy}}{\overline{\rho} \times \Pi} \tag{60}$$

$$\frac{dw}{dt} = -\left(1 - \frac{\rho_w}{\overline{\rho}}\right) g + \frac{F_{sz}}{\overline{\rho} \cdot \Pi} \tag{61}$$

F. MOMENT OF MOMENTUM EQUATIONS:

The moment of momentum equations are written in the body-fixed coordinate reference frame, the mine angular velocity is decomposed into components:

$$\vec{\omega} = \vec{\omega}_M + \vec{\omega}_F \tag{62}$$

In this case, $\vec{\omega}_m = \Omega \cdot \vec{i}_M$, is the angular velocity around the fixed- body axis director ($\vec{i}_M$) and angular velocities around

The ($\vec{j}_M$ and $\vec{k}_M$) mine body axis directors are:

$$\vec{\omega}_f = \omega_2 \vec{j}_M + \omega_3 \vec{k}_M \tag{63}$$

The moment of momentum equations can be expressed in terms of the component angular velocities, (Von Mises 1959):

$$J \cdot \frac{d\vec{\omega}_M}{dt} = \vec{M} - J \cdot \frac{d\vec{\omega}_F}{dt} \tag{64}$$

The components of angular velocity can also be expressed:

$$J \cdot \frac{d\vec{\omega}}{dt} = \vec{M}_b + \vec{M}_s \tag{65}$$

$$\vec{\omega} = \Omega \vec{i}_M + \omega_2 \vec{j}_M + \omega_3 \vec{k}_M \tag{66}$$

$$\vec{M} = \vec{M}_b + \vec{M}_s \tag{67}$$

($\vec{M}_b$) is the body force moment and ($\vec{M}_s$) is the resultant surface force moment where added mass ahs been taken into account. The gravitation force must pass the mine shape’s mass center, so its relative moment is zero. The float

force moment of momentum reduces to only buoyancy force moment, where $\chi = (M)-(B)$:

$$\vec{M}_b = \Pi \chi \rho_w g \cdot \cos\psi_2 \cdot \vec{j}_M \tag{68}$$

1. Moment of Inertia Tensor

The matrix [J] constitutes the mass moments of inertia (gyration) and mass moments of deviation, (products of inertia) for the mine shape, (Von Mises 1959) and (White 1979). The square matrix $[J]$ is commonly called the inertia tensor for an arbitrary solid body, (Cannon, 1967).

$$J = \begin{bmatrix} J_1 & J_{12} & J_{13} \\ J_{21} & J_2 & J_{23} \\ J_{31} & J_{32} & J_3 \end{bmatrix} \tag{69}$$

J_1, J_2, and J_3 are the three moments of inertia around the principal body fixed coordinate axes and are expressed:

$$J_1 = \int (r_2^2 + r_3^2) dm \tag{70}$$

$$J_2 = \int (r_3^2 + r_1^2) dm \tag{71}$$

$$J_3 = \int (r_1^2 + r_2^2) dm \tag{72}$$

The moments of deviation (or inertia products of second order) are for example expressed:

$$J_{31} = \int r_3 r_1 dm \tag{73}$$

For a symmetrically shaped cylinder the principal axes are aligned such that the moment of deviations are, $J_{12} = J_{21} = J_{13} = J_{31} = J_{23} = J_{32} = 0$, (Von Mises 1959) and (White 1979). The component moment of momentum equations simplify in this case to:

$$\frac{d\Omega}{dt} = \frac{M_{s1}}{J_1} \tag{74}$$

$$\frac{d\omega_2}{dt} = \frac{\Pi \chi g \rho_w}{J_2} \cdot \cos\psi_2 + \frac{M_{s2}}{J_2} \tag{75}$$

$$\frac{d\omega_3}{dt} = \frac{M_{s3}}{J_3} \tag{76}$$

2. Mass Moment of Inertia

Calculations of the moments of inertia for the mine shapes include allowances for non-uniform mine density along the length of the mine shape, Figure 18. Here the offset between the center of mass (M) and center of volume is given by χ:

$$\chi = \frac{\int_{-\frac{L}{2}}^{\frac{L}{2}} \rho \cdot x \cdot dx}{\int_{-\frac{L}{2}}^{\frac{L}{2}} \rho \cdot dx} = \int_{-\frac{L}{2}}^{\frac{L}{2}} \frac{\rho}{\overline{\rho}} \cdot \frac{x}{L} \cdot dx \tag{77}$$

The variable density of a mine shape is expressed as: $\rho = \rho(x)$. The mass moment of inertia around body-fixed coordinate reference frame director ($\vec{i}_M$) (cylinder axis director) will be:

$$J_1 = \frac{1}{8} m \cdot d^2 \tag{78}$$

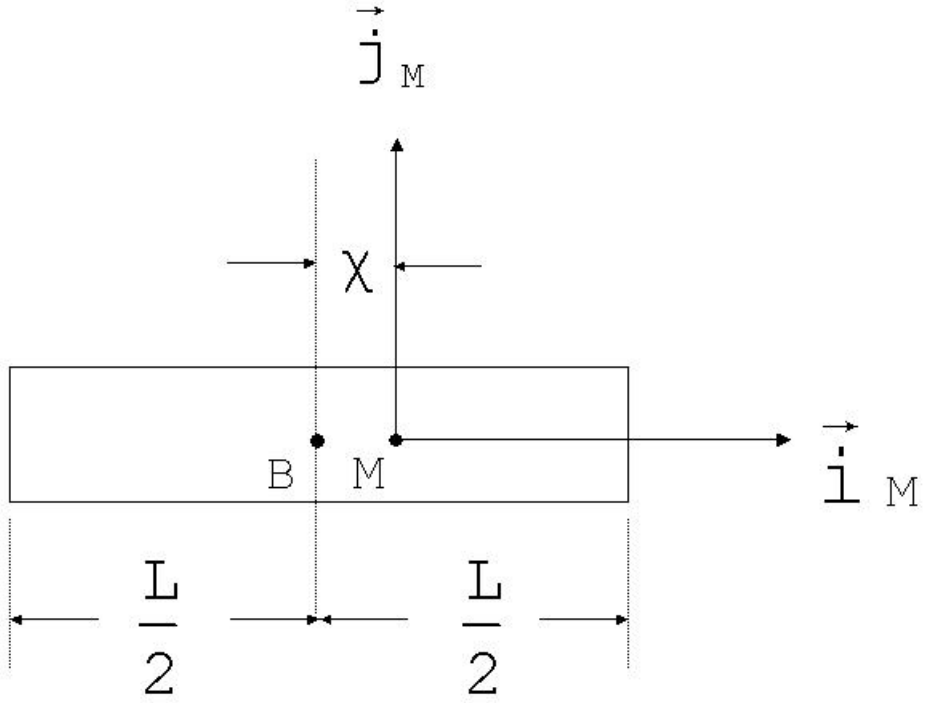

Figure 18. The Mine Shape Body Fixed Coordinate System with the Center of Mass (M) to Center of Volume (B) Offset - (χ) Shown.

The mass of the mine is determined from the expression:

$$m = \frac{\bar{\rho}}{4} \pi \cdot d^2 \cdot L \tag{79}$$

The mass moments of inertia around mine body-fixed frame axes principal directors, ($\vec{j}_M$ and $\vec{k}_M$) will be equal, due to mine shape's symmetry, as follows:

$$J_2 = J_3 = \frac{m}{4}\cdot\left(\frac{d}{2}\right)^2 + \frac{m}{12}\cdot L^2 + \left(\chi^2 + \varsigma\right)\cdot m\cdot L^2 \tag{80}$$

$$\varsigma = \int_{-\frac{1}{2}-\chi}^{\frac{1}{2}-\chi}\left(\frac{\rho(\eta)}{\bar{\rho}} - 1\right)\cdot\eta^2\cdot d\eta \tag{81}$$

The first and second terms evaluate the moment of inertia for the uniform cylinder. The last term computes the differences encountered along the length of a non-uniform density mine shape cylinder where $\eta = \frac{x}{L}$ defines a non-dimensional position along the length of the cylinder.

G. DRAG AND LIFT FORCES ON MOVING ROTATIONAL CYLINDERS

The circular cylinder body has been studied widely in fluid dynamics, from both a theoretical and experimental standpoint. Drag data for cylinders are known for the wide range of Reynolds numbers and flow orientations encountered in modeling a mine shape free fall through the water column. The relative flow velocity around the mine shape cylinder is expressed:

$$\vec{V}_r = \vec{V}_w - \vec{V} = \vec{V}_1 + \vec{V}_2 = V_1\cdot\vec{i}_F + V_2\cdot\vec{j}_F \tag{82}$$

Here ($\vec{V}_r$) represents the relative flow velocity across the solid body, ($\vec{V}_w$) is the water velocity (currents) and ($\vec{V}$) represents the mine shape's velocity.

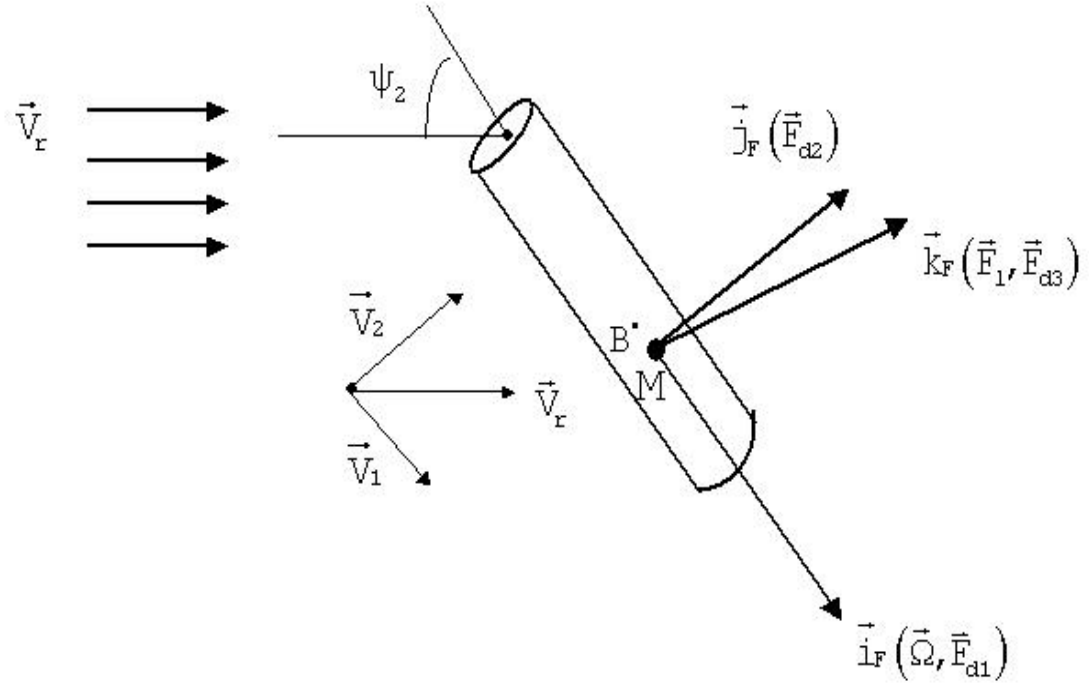

Figure 19. The Drag-lift Force Coordinate Reference Frame Under Oblique Relative Flow Conditions Across the Mine Shape Solid Body.

When a cylinder is placed at an angle to the flow as in Figure 19, the so-called independence or cross-flow principle is applicable, for calculation of the cross and axial flow drag forces, (Hoerner 1965, as cited in Fomer and Bredsoe 1997). Hurst (1992) used the same approach for model improvements, and although the technique follows sound engineering practice it may be an oversimplification of the nonlinear effects oblique flow produces on the solid body dynamics.

Essentially the model works on the assumption the drag-lift frame coordinate velocity components act to produce independent axial and cross flow drag and lift forces that act on the cylinder. The along cylinder axial velocity component is written:

$$\vec{V}_1 = \vec{V}_r \cdot \cos(\psi_2) = \vec{V}_r \cdot \vec{i}_F = (u_w - u)e_{11} + (v_w - v)e_{21} + (w_w - w)e_{31} \qquad (83)$$

The cross-flow velocity component is written:

$$\vec{V}_2 = \vec{V}_r - \vec{V}_1 \qquad (84)$$

The cross flow axis director is expressed:

$$\vec{j}_F = e'_{12} \times \vec{i} + e'_{22} \times \vec{j} + e'_{32} \times \vec{k} = \vec{V}_2 \Big/ \left|\vec{V}_2\right| \qquad (85)$$

The determination of the velocity components relative to the drag-lift force coordinates allows for calculation of component drag and lift forces. The axial drag force along the cylinder is given by:

$$\vec{F}_{d1} = f_{d1} \cdot \vec{i}_F = f_{d1}\left(e_{11}\vec{i} + e_{21}\vec{j} + e_{31}\vec{k}\right) \qquad (86)$$

The cross-flow drag force:

$$\vec{F}_{d2} = f_{d2} \cdot \vec{j}_F = f_{d2}\left(e'_{12}\vec{i} + e'_{22}\vec{j} + e'_{32}\vec{k}\right) \qquad (87)$$

The lift director, ($\vec{k}_F = \vec{i}_F \times \vec{j}_F$), induced drag force is produced as a direct result of the lift force acting on the

solid body of uneven density causing a rotational response. The solid body lift force is tied directly to rotation of the solid body (Ω_1) around the drag-lift force coordinate director ($\vec{i}_F$), (Crowe et al 2001). The resultant lift is expressed:

$$\vec{F}_l = f_l \cdot \vec{k}_F \tag{88}$$

The solid body drag force due to the lift force is tied directly to rotation of the solid body (ω_2) around the drag-lift force coordinate director ($\vec{j}_F$), (Von Mises 1959). The resultant drag force due to lift is expressed:

$$\vec{F}_{d3} = f_{d3} \cdot \vec{k}_F \tag{89}$$

The lift force and induced drag force act along the same lift-drag force director expressed as:

$$\vec{F}_l + \vec{F}_{d3} = \left(f_l + f_{d3}\right) \cdot \left(e'_{13}\vec{i} + e'_{23}\vec{j} + e'_{33}\vec{k}\right) \tag{90}$$

The total surface forces acting on the solid body will be:

$$\vec{F}_s = \vec{F}_{d1} + \vec{F}_{d2} + \vec{F}_{d3} + \vec{F}_l = f_{d1}\vec{i}_F + f_{d2}\vec{j}_F + \left(f_{d3} + f_l\right)\vec{k}_F \tag{91}$$

In general, a mines velocity during free fall is on the order of magnitude, 1 m/s, the seawater kinematic

viscosity is $\nu = 1.4 \times 10^{-6} \, m^2/s$, and the radius of the mine $r \cong 0.2\text{-}0.4m$. The average Reynolds number for the flow regime to calculate drag and lift forces is $Re \approx 10^5$. The flow is assumed to remain laminar around the mine shape with turbulent vortex shedding occurring in the wake region for this Reynolds number flow regime as discussed (Purday 1951) and (Sumer and Fredsoe 1997).

The flow around the cylindrical mine shape transitions rapidly through the low and mid Reynolds number flow regimes once the shape is released and begins a trajectory. It rapidly accelerates into the high Reynolds number sub-critical flow regime where pressure effects and boundary layer effects dominate the momentum and moment of momentum external lift and drag forces, (Panton 1996).

Drag forces are composed of both form drag and skin friction drag. The skin friction drag is a result of the viscous forces acting on the body as it moves through the water usually making up no more than 2-3% of the total drag force, (Somer and Fredsoe 1997). The form drag is due to the unbalanced pressure forces acting on the body. The sum of the two independent drag forces is called the total or profile drag. Drag coefficients are empirically obtained for common bodies (like right symmetric cylinders) based on calculation of the profile drag force through the collection of experimental data using the following relationship.

$$C_d = \frac{\vec{F_d}}{\frac{1}{2}\rho \vec{U}^2 A_w} \qquad (92)$$

where (A_w) represents the bodies characteristic area, and (L) in this case is some characteristic size scale for the considered body shape. It is common in hydrodynamic drag calculations to use the shape diameter (d) and projected area as the characteristic length and area scales, (Purday 1949).

The drag-lift force coordinate reference frame selection simplifies the projected area calculations. The reference area for axial flow is ($A_w = \pi/4\, d^2$), and the reference area for cross flow is ($A_w = d \cdot L$).

A factor of 1.1 is nominally added to the profile drag force to account for surface roughness and body imperfections in both the axial and cross flow drag coefficients, (Hurst 1992). The empirical equations used to formulate axial and cross flow drag coefficients used in model computations encompass both form and skin friction drag, or comprise the profile/total drag coefficient.

1. Cylinder Axial Drag Force

The axial drag force is expressed as:

$$\vec{F}_{d1} = \frac{\left(\frac{1}{2} C_{d1} \cdot \frac{\pi d^2}{4} \cdot \rho_w \cdot \left|\vec{V}_1\right| \cdot \vec{V}_1\right)}{f_{k1}} = C_{f1} \cdot \left|\vec{V}_1\right| \cdot \left(e_{11}\vec{i} + e_{21}\vec{j} + e_{31}\vec{k}\right) \qquad (93)$$

$$C_{f1} = \frac{\frac{1}{2} C_{d1} \cdot \frac{\pi d^2}{4} \cdot \rho_w \cdot \left|\vec{V}_1\right|}{f_{k1}} \tag{94}$$

The axial flow velocity component in the drag-lift force coordinates can be expressed:

$$\begin{aligned} \vec{V}_1 &= \left(\vec{V}_w - \vec{V}_o\right) \cdot \left(e_{11}\vec{i} + e_{21}\vec{j} + e_{31}\vec{k}\right) \\ &= u_w e_{11} - u_o e_{11} + v_w e_{21} - v_o e_{21} + w_w e_{31} - w_o e_{31} \end{aligned} \tag{95}$$

This allows the axial drag force to be expressed:

$$\begin{aligned} \vec{F}_{d1} &= C_{f1}\left(u_w e_{11} + v_w e_{21} + w_w e_{31}\right)\begin{bmatrix} e_{11} \\ e_{21} \\ e_{31} \end{bmatrix} - C_{f1}\left(u_o e_{11} + v_o e_{21} + w_o e_{31}\right)\begin{bmatrix} e_{11} \\ e_{21} \\ e_{31} \end{bmatrix} \\ &= -C_{f1} \times \begin{bmatrix} e_{11}^2 & 0 & 0 \\ 0 & e_{21}^2 & 0 \\ 0 & 0 & e_{31}^2 \end{bmatrix}\begin{bmatrix} u_o \\ v_o \\ w_o \end{bmatrix} - C_{f1} \times \begin{bmatrix} 0 & e_{11} \cdot e_{21} & e_{11} \cdot e_{31} \\ e_{21} \cdot e_{11} & 0 & e_{21} \cdot e_{31} \\ e_{31} \cdot e_{11} & e_{31} \cdot e_{21} & 0 \end{bmatrix}\begin{bmatrix} u_o \\ v_o \\ w_o \end{bmatrix} \\ &\quad + C_{f1} \times \begin{bmatrix} e_{11}^2 & e_{11} \cdot e_{21} & e_{11} \cdot e_{31} \\ e_{21} \cdot e_{11} & e_{21}^2 & e_{21} \cdot e_{31} \\ e_{31} \cdot e_{11} & e_{31} \cdot e_{21} & e_{31}^2 \end{bmatrix}\begin{bmatrix} u_w \\ v_w \\ w_w \end{bmatrix} \end{aligned} \tag{96}$$

To calculate the drag coefficients as well as later calculate the lift coefficients requires the calculation of axial flow Reynolds number,(R_a):

$$R_a = \left|\frac{V_1 d}{\nu}\right| \tag{97}$$

The kinematic viscosity of pure water (ν) that is used to calculate the Reynolds number is empirically derived

from tabular data, (Crowe et al, 2001) for the temperature range of concern:

$$(T)\ ^{\circ}C \leq 10^{\circ}$$
$$n = -5.7471 - 0.0136 \times T$$
$$\nu = 10^{n} \tag{98}$$

$$(T)\ ^{\circ}C > 10^{\circ} \leq 40^{\circ}$$
$$n = -5.77592 - 0.010718 \times T$$
$$\nu = 10^{n} \tag{99}$$

An empirically derived conversion factor (CRC Handbook 1981, as cited in Hurst 1992) allows for conversion from pure water kinematic viscosity to the seawater kinematic viscosity:

$$\nu_{sw} = \nu \cdot F \tag{100}$$

$$F = 1.058\left(1 + 0.0000363 \times T^{2}\right) \tag{101}$$

The axial drag coefficient (C_{d1}) can be related to the aspect ratio of the cylindrical object and considered to be independent of axial Reynolds number, (Sumer and Fredsoe 1997). An empirical fit to the axial drag coefficient data for a symmetrical cylinder, (Crowe et al 2001), is developed for (C_{d1}) based on aspect ratio (AR). Aspect Ratio is defined:

$$AR = L/d \tag{102}$$

The empirical axial drag coefficient relationships are expressed:

For AR > 8

$$C_{d1} = 1.0$$

AR > 0.5

$$C_{d1} = 0.75 + \frac{AR}{32.1934} + \frac{0.09612}{(AR)^2} \qquad (103)$$

AR < 0.5

$$C_{d1} = 1.15$$

The empirically fit formulas agree well with experimental drag coefficient data gather and plotted by Rouse (1938). This piecewise, linear fit to data in (Crowe et al 2001) produces a more conservative drag coefficient than the coefficient calculation used by (Arnone and Bowen 1980) and detailed in (Hoerner 1951). To account for imperfections along the flow surface of the cylinder and following conservative engineering practice, the drag coefficient is adjusted 10%, similar to procedures discussed in (Hurst 1992) and (Taber 1999).

$$C_{d1} = 1.1 \cdot C_{d1} \qquad (104)$$

2. Cylinder Cross Flow Drag Force

The cross flow drag force is computed in the drag-lift force coordinate reference frame, as shown in Figure 20. The cross flow relative velocity component ($\vec{V}_2$) is aligned

to simplify drag and lift coefficients using existing empirical data. For any (ω_3'), the cross flow drag force can be expressed:

$$\begin{aligned}\vec{F}_{d2} &= \frac{\int_{-\frac{L}{2}-\chi}^{\frac{L}{2}-\chi} \frac{1}{2} C_{d2}\left(V_0 - \omega_3' y\right)^2 d \cdot \rho_w \cdot dy}{f_{k2}} \cdot \vec{j}_F \\ &= \frac{\frac{1}{2} C_{d2} d \cdot L \cdot \rho_w \left(\left(V_2 + \chi \omega_3'\right)^2 + \frac{1}{12} L^2 \omega_3'^2\right)}{f_{k2}} \cdot \vec{j}_F \\ &= \left(C_{f2} \cdot V_2 + f_{cf2}\right) \cdot \left(e_{12}' \vec{i} + e_{22}' \vec{j} + e_{32}' \vec{k}\right)\end{aligned} \tag{105}$$

$$C_{f2} = \frac{C_{d2} d \cdot L \cdot \rho_w \left(\frac{V_2}{2} + \chi \cdot \omega_3'\right)}{f_{k2}} \tag{106}$$

$$f_{cf2} = \frac{C_{d2} d \cdot L \cdot \rho_w \left(\frac{1}{2}\chi^2 + \frac{1}{24} L^2\right) \cdot \omega_3'^2}{f_{k2}} \tag{107}$$

$$\begin{aligned}\vec{F}_{d2} = &-C_{f2} \cdot \begin{bmatrix} e_{12}'^2 & 0 & 0 \\ 0 & e_{22}'^2 & 0 \\ 0 & 0 & e_{32}'^2 \end{bmatrix} \begin{bmatrix} u_o \\ v_o \\ w_o \end{bmatrix} - C_{f2} \times \begin{bmatrix} 0 & e_{12}' \cdot e_{22}' & e_{12}' \cdot e_{32}' \\ e_{22}' \cdot e_{12}' & 0 & e_{22}' \cdot e_{32}' \\ e_{32}' \cdot e_{12}' & e_{32}' \cdot e_{22}' & 0 \end{bmatrix} \begin{bmatrix} u_o \\ v_o \\ w_o \end{bmatrix} \\ &+ C_{f2} \cdot \begin{bmatrix} e_{12}'^2 & e_{12}' \cdot e_{22}' & e_{12}' \cdot e_{32}' \\ e_{22}' \cdot e_{12}' & e_{22}'^2 & e_{22}' \cdot e_{32}' \\ e_{32}' \cdot e_{12}' & e_{32}' \cdot e_{22}' & e_{32}'^2 \end{bmatrix} \begin{bmatrix} u_w \\ v_w \\ w_w \end{bmatrix} + f_{cf2} \cdot \begin{bmatrix} e_{12}' \\ e_{22}' \\ e_{32}' \end{bmatrix}\end{aligned} \tag{108}$$

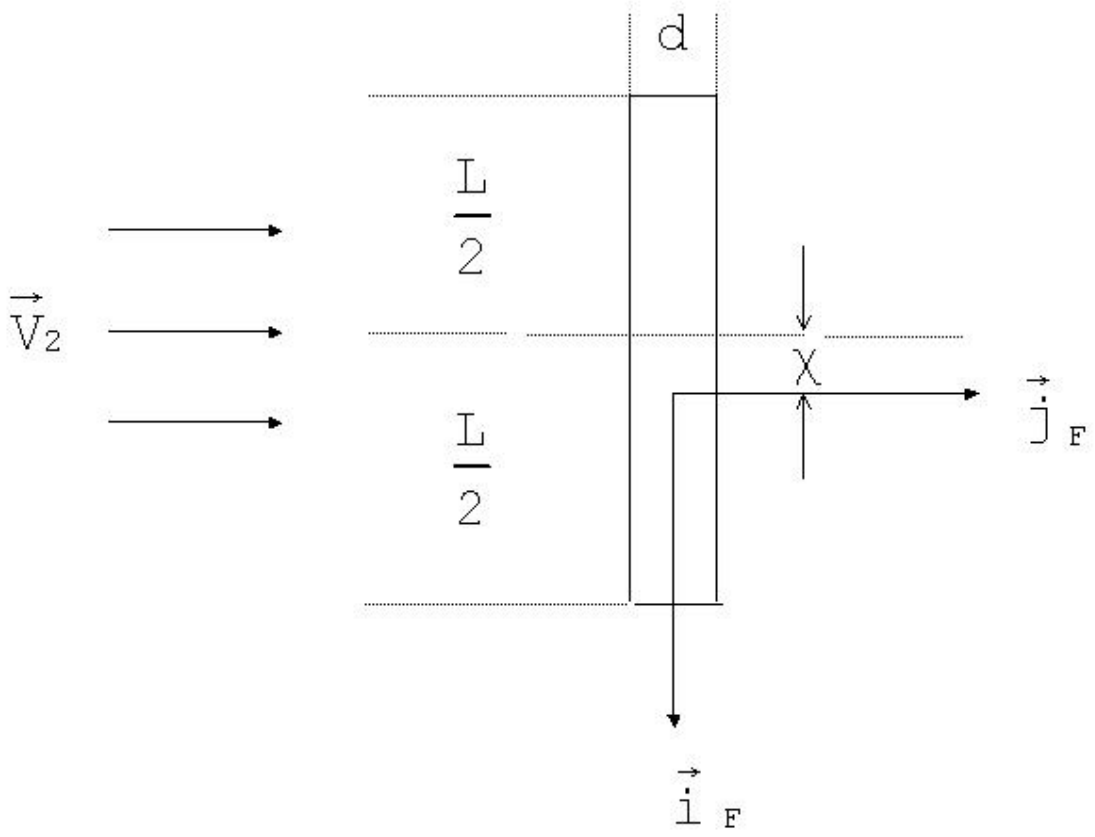

Figure 20. The Drag-lift Force Coordinate Reference Frame Depicting the Cross Flow Velocity Impacting the Mine Shape.

The cross flow drag coefficient is (C_{d2}). An empirically derived relationship is developed from the curve for cross flow around a cylinder of infinite length, Figure 21.

First determine the cross flow Reynolds number, (R_c):

$$R_c = \left| \frac{V_2 d}{\nu} \right| \tag{109}$$

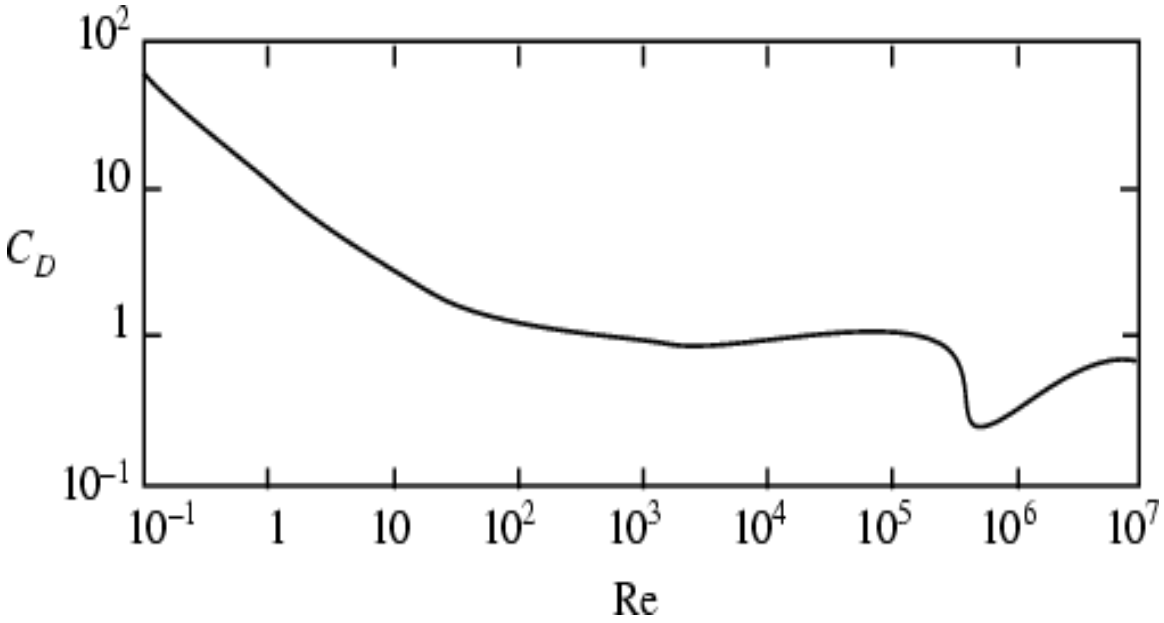

Figure 21. Drag Coefficient Curve for an Infinite Symmetric Circular Cylinder. "From Crowe et al (2001)."

The calculation of the cross flow drag force is directly related to the Reynolds number and AR.

$R_c > 350000$

$$C_{d2} = 1/\left(641550/R_c + 1.5\right) \quad (110)$$

$R_c > 150000$

$$C_{d2} = 1.875 - 0.0000045 \times R_c \quad (111)$$

$R_c > 12000$

The majority of the cross flow drag force coefficients occur calculations used in the model occur in the region of the curve shown in Figure 21 for Reynolds numbers between 1×10^4 and 3×10^5. (Rouse, 1938) shows that for a cylinder of finite length the change in stagnation pressure felt on the

front face of the cylinder is reduced due to leakage around the ends of the cylinder and the cross flow drag coefficient lowers depending on the (AR) of the cylinder. An empirical relationship is derived from (Rouse 1938) for this Reynolds number regime based on (AR) of the given cylinder.

For $AR \geq 10$

$$C_{d2} = 1.20 - 4/AR \tag{112}$$

For $2 \leq AR \leq 10$

$$C_{d2} = 0.835 - 0.35/AR \tag{113}$$

For $AR \leq 2$

$$C_{d2} = 0.7 - 0.08/AR \tag{114}$$

These formulas are empirically derived from a linear piecewise fit to a curve from (Rouse 1938). The drag coefficient values are slightly higher (more conservative) than those derived using the Manning Coefficient used by Arnone and Bowen (1980) for the original model. The more conservative drag coefficient data is used for modeling purposes as the two dimensional model is known to over predict vertical impact velocities, (Satkowiak 1987), (Taber 1999), (Smith 2000), (Gilless 2001) and (Valent et al 2002). The formulas agree well with experimental data plotted in (Hoerner 1951), and (Rouse 1938).

Continuing to lower Reynolds numbers for cross flow conditions the results follow the curve in Figure 21.

$R_c > 2000$

$$C_{d2} = 0.84 + 0.00003 \times R_c \tag{115}$$

$R_c > 180$

$$C_{d2} = 0.8555 + 89/R_c \tag{116}$$

$R_c > 12$

$$C_{d2} = 1.261 + 16/R_c \tag{117}$$

$R_c < 12$

$$C_{d2} = 1.9276 + 8/R_c \tag{118}$$

Again, to account for imperfections in the flow surface around the cylinder the base cross flow drag coefficient is increased by 10%.

$$C_{d2} = 1.1 \times C_{d2} \tag{98}$$

3. Cylinder Lift Force

It is well documented that the lift coefficient for a cylinder can be written:

$$C_L = \frac{\vec{F_l}}{\frac{1}{2}\rho_w \vec{U}^2 A_w} \tag{119}$$

The reference area (A_w) represents the wetted cylinder area in the lift-drag force coordinate frame. The lift force along the ($\vec{k}_F$) director in the drag-lift force coordinate system is expressed:

$$\vec{F}_l = \frac{\frac{1}{2}\Omega \cdot d^2 \cdot \rho_w \int_{-\frac{L}{2}-\chi}^{\frac{L}{2}-\chi} \left(V_2 - \omega'_3 \cdot \eta\right) d\eta}{f_{k2}} \cdot \vec{k}_F = \left(C_{fl} \cdot \vec{V}_2 + f_{cfl}\right) \cdot \left(e'_{13}\vec{i} + e'_{23}\vec{j} + e'_{33}\vec{k}\right) \quad (120)$$

$$C_{fl} = \frac{\frac{1}{2}\Omega \cdot d^2 \cdot \rho_w \cdot L}{f_{k2}} \quad (121)$$

$$f_{cfl} = \frac{\frac{1}{2}\Omega \cdot d^2 \cdot \rho_w \cdot L \cdot \chi}{f_{k2}} \cdot \omega'_3 \quad (122)$$

$$\vec{F}_l = -C_{fl} \cdot \begin{bmatrix} e'_{13} \cdot e'_{12} & 0 & 0 \\ 0 & e'_{23} \cdot e'_{22} & 0 \\ 0 & 0 & e'_{33} \cdot e'_{32} \end{bmatrix} \begin{bmatrix} u_o \\ v_o \\ w_o \end{bmatrix}$$

$$- C_{fl} \cdot \begin{bmatrix} 0 & e'_{13} \cdot e'_{22} & e'_{13} \cdot e'_{32} \\ e'_{23} \cdot e'_{12} & 0 & e'_{23} \cdot e'_{32} \\ e'_{33} \cdot e'_{12} & e'_{33} \cdot e'_{22} & 0 \end{bmatrix} \begin{bmatrix} u_o \\ v_o \\ w_o \end{bmatrix} \quad (123)$$

$$+ C_{fl} \cdot \begin{bmatrix} e'_{13} \cdot e'_{12} & e'_{13} \cdot e'_{22} & e'_{13} \cdot e'_{32} \\ e'_{23} \cdot e'_{12} & e'_{23} \cdot e'_{22} & e'_{23} \cdot e'_{32} \\ e'_{33} \cdot e'_{12} & e'_{33} \cdot e'_{22} & e'_{33} \cdot e'_{32} \end{bmatrix} \begin{bmatrix} u_w \\ v_w \\ w_w \end{bmatrix} + f_{cfl} \cdot \begin{bmatrix} e'_{13} \\ e'_{23} \\ e'_{33} \end{bmatrix}$$

If $\omega_3' = 0$ the flow independence principle discussed earlier is also applicable to the calculation of lift coefficients for a cylindrical mine shape, (Sumer and Fredsoe 1997). Now consider cylinder lift coefficient data, Figure 22. A linear piecewise fit to the plotted experimental data for rotation rates, $\frac{d \cdot \Omega}{|\vec{V}_2|} \leq 8$, around $\vec{i}_F$ produces:

$$C_l \cong \frac{d \cdot \Omega}{|\vec{V}_2|} \tag{124}$$

$$C_{fl} = \frac{1}{2} \Omega \cdot d^2 \cdot L \cdot \rho_w \tag{125}$$

4. Lift Axis Induced Drag Force

If $\omega_2' \neq 0$, as is the case when the center of mass (M) is not coincident with the center of volume (B) in a non-uniform density cylinder the angular velocity will impart an induced drag force on the lift axis, ($\vec{k}_F$):

$$\vec{F}_{d3} = f_{d3} \cdot \vec{k}_F \neq 0 \tag{126}$$

$$\vec{F}_{d3} = \frac{\frac{1}{2} C_{d3} \cdot d \cdot \rho_w \cdot \omega_2' \cdot |\omega_2'|}{f_{k2}} \left(\int_0^{\frac{L}{2} - \chi} y^2 dy - \int_{-\frac{L}{2} - \chi}^{0} y^2 dy \right) \cdot \vec{k}_F \tag{127}$$

$$\vec{F}_{d3} = -\frac{\frac{1}{12} C_{d3} \cdot d \cdot \rho_w \cdot \chi \cdot \left(3L^2 + 4\chi^2\right) \cdot \left|\omega_2'\right| \cdot \omega_2'}{f_{k2}} \cdot \vec{k}_F = C_{f3} \cdot \vec{k}_F$$

$$= C_{f3} \cdot \left(e_{13}' \vec{i} + e_{23}' \vec{j} + e_{33}' \vec{k}\right) \tag{128}$$

Assuming $\frac{d \cdot \Omega}{\left|\vec{V}_2\right|} \leq 8$, in Figure 22, the linear fit can be applied to the curve to provide the empirical relationship where $C_{d3} \cong C_{d2}$. In this case the force coefficient can be simplified and expressed:

$$C_{f3} = \frac{-\frac{1}{12} C_{d2} \cdot d \cdot \rho_w \cdot \chi \cdot \left(3L^2 + 4\chi^2\right) \cdot \left|\omega_2'\right| \cdot \omega_2'}{f_{k2}} \tag{129}$$

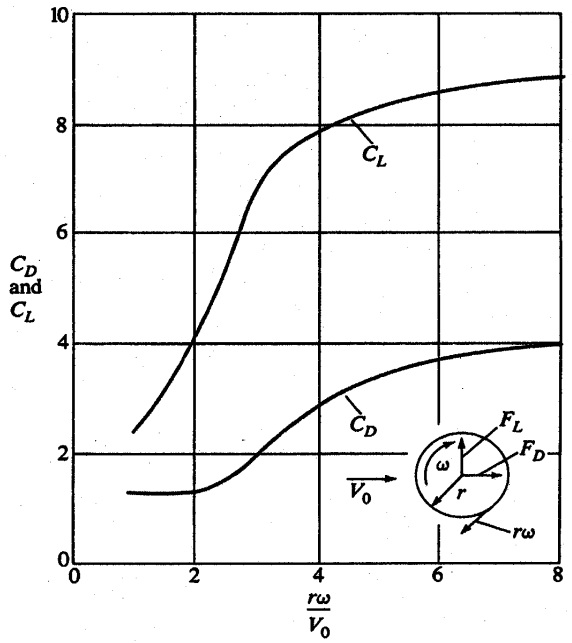

Figure 22. Cross Flow Coefficients for Drag and Lift on a Rotating Cylinder. “From Crowe et al (2001), After Rouse (1938).”

H. DRAG AND LIFT MOMENTS ON MOVING ROTATING CYLINDERS

The composite rotation of a cylindrical mine shape about the three drag-lift force coordinate axes directors $\left(\vec{i}_F, \vec{j}_F, \vec{k}_F\right)$ will produce response moments on a position near the body center of mass due to interaction with the fluid medium creating drag and lift.

Here it is established that at oblique angles of attack the moment arm center occurs neither at the center of mass (M) of the object nor at the center of volume (B) but at some point between the two, (Maxwell 1890, as cited in Lugt 1983). When the mine shape is at oblique angles to the incoming flow an empirical adjustment $\varepsilon = \varepsilon_m(\sin 2\psi_2)$ is applied to the moment arm calculations, as shown in Figure 23.

The value (ε_M) is the maximum percentage of the distance between the between the center of mass (M) and the center of volume (B). This is set as the default in the source code, but an input line allows this value to be changed by the operator running the code to evaluate the effect of changing it. The correction diminishes to zero as the flow orients towards either purely axial or cross flow and reaches a maximum value when $\psi_2 = 45°$.

The technique improves the three-dimensional model performance when compared to actual mine drop results, but this technique may oversimplify the actual moment dynamics affecting the solid body motion.

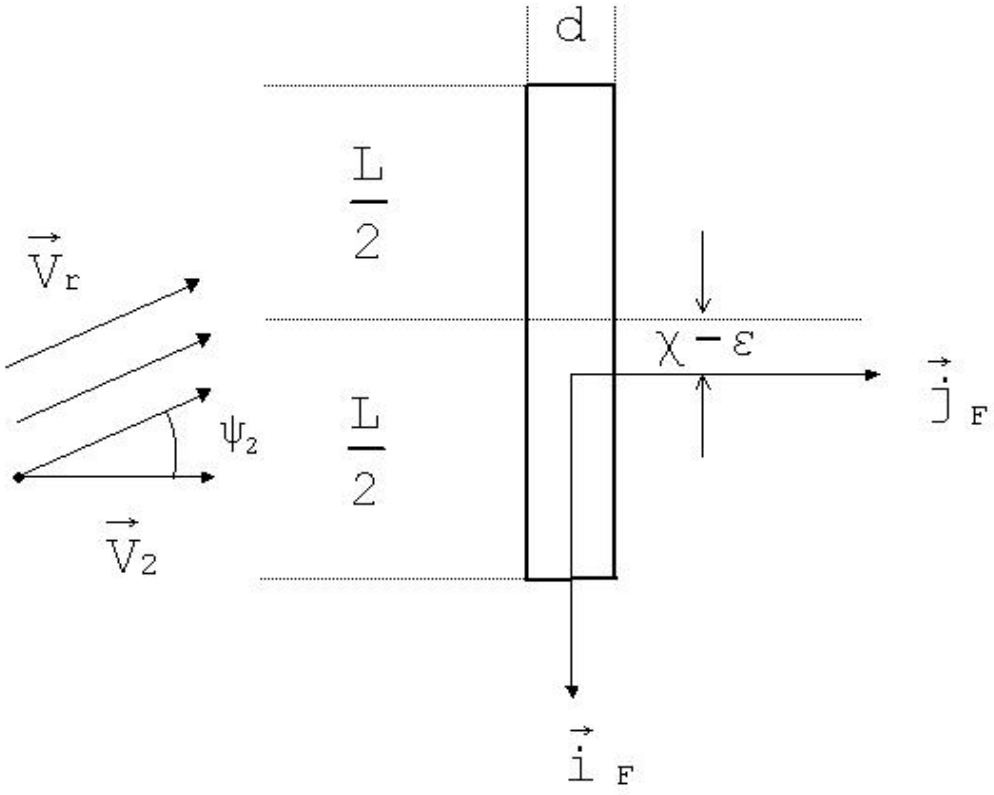

Figure 23. The Mine Body Coordinate Reference Frame in Oblique Flow Conditions Across the Solid Body, Showing the Correction Factor ε Applied to the Center of Mass offset, χ, to Approximate the Drag-Lift Force Moment Center.

1. Cylinder Axial Moment

Consider a steady flow between two cylinders with a common center. The moment of momentum around the ($\vec{i}_F$) axis will be, (White 1974):

$$M = 4\pi\mu \cdot \frac{r_1^2 \cdot r_0^2}{r_1^2 - r_0^2}\left(\omega_1 - \omega_0\right) \qquad (130)$$

The radii (r_1, r_0) are the inside and outside cylinder radius, (ω_1) and (ω_0) are inside and outside angular velocities. When $r_0 \to \infty$ and $\omega_0 = 0$:

$$M = -4\pi\mu \cdot r_1^2 \cdot \omega_1 \tag{131}$$

$$\vec{M}_{s1} = -\pi \cdot \mu \cdot L \cdot d^2 \cdot \Omega \cdot \vec{i}_F = C_{m1} \cdot \Omega \cdot \vec{i}_F \tag{132}$$

$$C_{m1} = -\pi\mu \cdot L \cdot d^2 \tag{133}$$

2. Lift Axis Drag Moment

The lift axis drag moment is calculated much as the cylinder axial moment, but taken about ($\vec{k}_F$) and expressed:

$$\vec{M}_{sd3} = M_{sd3} \cdot \vec{k}_F = M_{sd3} \cdot \left(d_{23}\vec{j}_M + d_{33}\vec{k}_M \right) \tag{134}$$

$$\vec{M}_{sd3} = \frac{\int_{-\frac{L}{2}-\chi}^{\frac{L}{2}-\chi} \frac{1}{2} C_{d2} \cdot d \cdot \rho_w \left(V_2 - \omega_3' y \right)^2 y}{f_{kr}} \cdot dy = C_{m3} \cdot \omega_3' + m_{cm3} \tag{135}$$

$$C_{m3} = \frac{-C_{d2} \cdot d \cdot \rho_w \left(\frac{1}{12} V_2 L^3 + V_2 L \chi^2 + \frac{1}{8} L^3 \omega_3' \chi + \frac{L}{2} \chi^3 \omega_3' \right)}{f_{kr}} \tag{136}$$

$$m_{cm3} = \frac{-\frac{1}{2} C_{d2} \cdot d \cdot \rho_w \cdot V_2^2 \cdot L \cdot (\chi - \varepsilon)}{f_{kr}} \tag{137}$$

Let $\omega'_3 = \vec{\omega} \cdot \vec{k}_F = \omega_2 \cdot d_{32} + \omega_3 \cdot d_{33}$, and perform the rotation from the drag-lift force coordinate $\left(\vec{j}_F, \vec{k}_F\right)$ to body-fixed coordinates $\left(\vec{j}_M, \vec{k}_M\right)$:

$$\vec{M}_{sd3} = C_{m3} \cdot \begin{bmatrix} \left(\omega_2 \cdot d_{23} + \omega_3 \cdot d_{33}\right) \cdot d_{23} \\ \left(\omega_2 \cdot d_{23} + \omega_3 \cdot d_{33}\right) \cdot d_{33} \end{bmatrix} + m_{cm3} \cdot \begin{bmatrix} d_{23} \\ d_{33} \end{bmatrix}$$

$$= C_{m3} \cdot \begin{bmatrix} {d_{23}}^2 & 0 \\ 0 & {d_{33}}^2 \end{bmatrix} \begin{bmatrix} \omega_2 \\ \omega_3 \end{bmatrix} + C_{m3} \cdot \begin{bmatrix} 0 & d_{23} \cdot d_{33} \\ d_{33} \cdot d_{23} & 0 \end{bmatrix} \begin{bmatrix} \omega_2 \\ \omega_3 \end{bmatrix} + m_{cm3} \cdot \begin{bmatrix} d_{23} \\ d_{33} \end{bmatrix} \tag{138}$$

3. Cross Flow Axis Drag Moment

Following a similar process the moment around ($\vec{j}_F$) can be expressed:

$$\vec{M}_{sd2} = M_{sd2} \cdot \vec{j}_F = M_{sd2} \cdot \left(d_{22}\vec{j}_M + d_{32}\vec{k}_M\right) \tag{139}$$

The Reynolds number for cross flow moment calculations is based on the angular velocity around the drag-lift force coordinate director ($\vec{i}_F$). In this case, the rotation is $\Omega_o \cong 0$ and $R_e \leq 2$. This allows the drag moment coefficient to be approximated as $C_{d2} \cong \left(8/R_e\right)$, (Crowe et al 2001). This empirical technique allows the drag moment coefficient to be written in the form:

$$C_{d2} \cong \left(\frac{8\nu}{|y| \cdot |w'_2| \cdot d}\right) \tag{140}$$

$$\mu = \rho_w \nu \tag{141}$$

$$M_{sd2} = \frac{-\omega_2' \left|\omega_2'\right| \int_{-\frac{L}{2}-\chi}^{\frac{L}{2}-\chi} \frac{1}{2} C_{d2} \cdot d \cdot \rho_w \cdot y^2 \cdot |y|}{f_{kr}} \times dy \tag{142}$$

Substituting for (C_{d2}), the torque can be expressed:

$$M_{sd2} = \frac{-4\mu\omega_2' \int_{-L/2-\chi}^{L/2-\chi} y^2}{f_{kr}} dy = C_{m2} \cdot \left(d_{22} \cdot \omega_2 + d_{23} \cdot \omega_3\right) \tag{143}$$

$$C_{m2} = \frac{-\mu\left(L^3/3 + 4L\chi^2\right)}{f_{kr}} \tag{144}$$

Now using the relationship $\omega_2' = \vec{\omega} \cdot \vec{j}_M = \omega_2 \cdot d_{22} + \omega_3 \cdot d_{23}$, the torque can be rotated from the drag-lift force coordinate frame $\left(\vec{j}_F, \vec{k}_F\right)$ to the fixed body coordinate frame $\left(\vec{j}_M, \vec{k}_M\right)$:

$$\vec{M}_{sd2} = C_{m2} \cdot \begin{bmatrix} d_{22}^2 & 0 \\ 0 & d_{32}^2 \end{bmatrix} \begin{bmatrix} \omega_2 \\ \omega_3 \end{bmatrix} + C_{m2} \cdot \begin{bmatrix} 0 & d_{22} \cdot d_{32} \\ d_{32} \cdot d_{22} & 0 \end{bmatrix} \begin{bmatrix} \omega_2 \\ \omega_3 \end{bmatrix} \tag{145}$$

4. Cross Flow Axis Lift Moment

Last consider the moment due to pure lift around ($\vec{j}_F$) due to established rotation about the axis:

$$\vec{M}_{sl} = M_{sl} \cdot \vec{j}_F = M_{sl} \cdot \left(d_{22}\vec{j}_m + d_{32}\vec{k}_m\right) \tag{146}$$

$$M_{sl} = \frac{\int_{-\frac{L}{2}-\chi}^{\frac{L}{2}-\chi} \frac{1}{2} C_l \cdot d \cdot \rho_w \left(V_2 - \omega_3' y\right) y}{f_{kr}} - dy = \frac{-\frac{1}{2}\Omega \cdot d^2 \cdot \rho_w}{f_{kr}} \int_{-\frac{L}{2}-\chi}^{\frac{L}{2}-\chi} \left(V_2 - \omega_3' y\right) y dy \quad (147)$$

$$M_{sl} = \frac{\frac{1}{2}\Omega \cdot d^2 \cdot \rho_w \cdot L}{f_{kr}} \cdot \left(V_2 \chi + \frac{1}{12} L^2 \omega_3' + \chi^2 \omega_3'\right) = C_{ml} \cdot \omega_3' + m_{cml} \quad (148)$$

$$C_{ml} = \frac{\Omega \cdot d^2 \cdot \rho_w \cdot L \cdot \left(\frac{1}{24} L^2 + \frac{\chi^2}{2}\right)}{f_{kr}} \quad (149)$$

$$m_{cml} = \frac{\frac{1}{2}\Omega \cdot d^2 \cdot \rho_w \cdot L \cdot V_2 \cdot \chi}{f_{kr}} \quad (150)$$

Let $\omega_3' = \vec{\omega} \cdot \vec{k}_F = \omega_2 \cdot d_{32} + \omega_3 \cdot d_{33}$ this torque can also be rotated from the drag-lift force coordinates $\left(\vec{j}_F, \vec{k}_F\right)$ to the fixed body coordinates $\left(\vec{j}_M, \vec{k}_M\right)$:

$$\vec{M}_{sl} = C_{ml} \cdot \begin{bmatrix} d_{22} \cdot d_{23} & 0 \\ 0 & d_{32} \cdot d_{33} \end{bmatrix} \begin{bmatrix} \omega_2 \\ \omega_3 \end{bmatrix} + C_{ml} \cdot \begin{bmatrix} 0 & d_{22} \cdot d_{33} \\ d_{32} \cdot d_{23} & 0 \end{bmatrix} \begin{bmatrix} \omega_2 \\ \omega_3 \end{bmatrix} + m_{cml} \cdot \begin{bmatrix} d_{22} \\ d_{32} \end{bmatrix} \quad (151)$$

I. MODEL LINEAR ORDINARY DIFFERENTIAL EQUATION SOLUTIONS

In each time step $(0 \le t \le t_f)$, where (t_f) is synonymous with the mine shape reaching the bottom, the variable $(\vec{q})$ is defines the vector: $\vec{q}$ = [u,v,w,Ω, ω_2, and ω_3].

The system of force-balance equations for the solid body can be represented in matrix notation as a system of differential equations, (Cannon 1967). In this case the system of ordinary differential equations simplifies to a system of first order linear ordinary differential equations of the form:

$$\frac{dq}{dt} = a \cdot q + b \quad (a \neq 0) \tag{152}$$

The analytical solution will take the form, (Cannon 1967) and (Boyce and Diprima 1997):

$$q(t) = q(0) + b \cdot t \quad (a = 0) \tag{153}$$

This represents ordinary integration in a single variable, $q = f(t)$. Otherwise:

$$q(t) = \left(q(0) + \frac{b}{a} \right) e^{a \cdot t} - \frac{b}{a} \quad (a \neq 0) \tag{154}$$

The solution for single variable integration will take on form:

$$\int_0^{t_f} q(t)dt = q(0)\cdot t + \frac{1}{2} b\cdot t^2 \quad (a=0) \tag{155}$$

The system of first order, linear ordinary differential equations have solutions of form, (Boyce and Diprima 1997):

$$\int_0^{t_f} q(t)dt = \frac{1}{a}\left(q(0)+\frac{b}{a}\right)e^{a\cdot t} - \frac{b}{a}t \quad (a\neq 0) \tag{156}$$

The modeling numerical procedure is outlined in Appendix D. The MATLAB application model source code is found in Appendix B.

VI. DATA RETRIEVAL AND ANALYSIS

A. DATA RETRIEVAL

Two separate data sets exist for analysis and validation of the three dimensional model discussed previously. Upon completion of the drop phase in both the MIDEX and Carderock experiments, the video clips from each camera were converted to digital format and archived for subsequent analysis. All the data analyzed was acquired within a controlled environment where drop angles and initial velocities had some controllable tolerances about desired values. All values derived from the digital video clips and archived to data sets are reported in SI units.

1. MIDEX Data

The digital video clip files for each view of MIDEX data (9 model variations and 5 different drop angles from two cameras) were analyzed frame by frame (30 fps) in order to determine the mine's position in the x, -z and -y, -z planes (Gilless 2001). These two dimensional positions were then combined into one data file for each drop containing elapsed time, (x, y, z) positions, (ψ_2, ψ_3) pitch and yaw angles, derived (u, v, w) linear velocities and (ω_2, ω_3) derived angular velocities. Data files were created and archived by drop angle (15, 30, 45, 69, 75) degrees. Inquiries for access to the MIDEX data archive for use in mine burial prediction program research should be directed to NPS, point of contact Dr. Peter C. Chu; (Gilless 2001).

2. Carderock Experiment Data

The digital video clips and digital data analyzer output from the Carderock experiments were analyzed by NRL-SSC personnel (Valent and Holland 2001) and condensed into a primary data record for each drop containing elapsed time, (x, y, z) positions, (ψ_2, ψ_3) pitch and yaw angles, derived (u, v, w) linear velocities and (ω_2, ω_3) derived angular velocities. Other secondary data such as initial point tracked and final point tracked are included in the data set for downstream research use. In addition to the data record a digital video record at 125 fps from three cameras and an analog video record at 30 fps from one camera were generated for each mine shape drop. This allows researchers the chance to observe each drop visually and investigate common characteristics as well as anomalies noticed in drop data. The complete data set from the Carderock experiment contains over 150 drops. This thesis investigated and analyzed only those drops of blunt nosed cylinders, 44 drops. Inquiries for access to the Carderock mine drop experiment data for use in mine burial prediction research should be directed to NRL-SSC, point of contact Dr. Philip Valent, (Valent and Holland 2001) and (Valent et al 2002).

B. SOURCES OF ERROR

1. Data Error

There were several sources of error that hindered the determination of the mine's exact position within the water column. Locations above or below the camera's focal point

were subjected to parallax distortion for both experiments. Placing the cameras as far away from the expected fall path, while still being able to resolve the mine shape motion, minimized this error. An object injected into the water will generate an air cavity. This air cavity can greatly affect the initial motion, particularly at very high speeds (hydro ballistics). Many of the drops could not be tracked until 10 – 20 frames into the drop after the air cavity bubble formation had diminished. The initial position and angle error is estimated to be 1-2% for the MIDEX data (Gilless 2000) and 2-3% for the Carderock Data (Valent and Holland 2000). The error while not itself large can lead to larger error in both the initial linear velocity calculations and the initial angular velocity calculations used to initialize the three dimensional model. Estimates of linear velocity error and angular velocity error are 0.17 m/s and .1 rad/sec respectively.

2. Model Simplification Error

The initial conditions fed to the three dimensional model from the 270 experimental data cases all assume the mine shape is fully wetted and feels no residual effects from the air-water cavity surface interaction when it begins the hydrodynamic phase at model $t_o = 0$. As modeled previously by Arnone and Bowen (1980), Satkowiak (1987), and Hurst (1992), it was assumed that once the mine is fully wetted it moves directly to the hydrodynamic flow regime without any residual effects from the previous regime. This is deemed an acceptable assumption for the Carderock mine drops. These drops all occurred with the

mine fully wetted and any initial movement had been damped out. The MIDEX data begins tracking the mine shapes once the bubble cavity collapses and the mine shape is visible against the grid in the background. This point was set as $t_o = 0$, and the initial positions and subsequent tracking are based on that point.

While this simplification is acceptable in both cases, Hurst (1992) discusses the fact that a singular point transition does not exist in the real motion but would actually occur as a transition zone where the remote effects of the cavity zone would continue to diminish for a short period after the mine shape enters the fully wetted hydrodynamic phase. Currently no method or technique is available to include in the modeling to handle this more complex motion and effects of the air-water cavity phase as it transitions to fully wetted purely hydrodynamic flow.

A second simplification consists of assuming that both the axial and cross components of flow remain laminar during the bodies free fall through the water column. A long body or a tapered body would tend towards turbulent flow as the flow continued further aft on the solid body in the axial direction, (Schlichting 1979). Purday (1949) presents a method to handle this phenomenon if data becomes available to suggest a transition to turbulent flow does occur in the axial direction along a cylinder, or tapered shapes are considered in the future.

Third under oblique flow condition it is assumed the end plates continue to feel laminar flow. It could be argued that at oblique angles of attack the front end plate would feel laminar flow while the rear end plate would

transition to turbulent flow and a change would occur in the torques on the solid body. No data currently exists for oblique flow around cylinders to support this hypothesis. Panton (1996) presents methods to handle this effect if data or a coupling principle becomes available to support the hypothesis. 10 test cases were run using the Faulkner-Skan similarity method (Panton 1996). The method was used to determine the differences in flow across each of the end plates. The effect was determined to be a second order effect for the Reynolds number regime of concern.

Last, vortex shedding in the wake of a cylinder placed into a flow pattern is well documented to occur in the Reynolds number regimes of concern, (von Karmen 1911, in Rouse 1938) and (Sumer and Fredsoe 1997). This is a nonlinear effect that can remotely affect the solid body momentum and moments of momentum, (Sumer and Fredsoe 1997). The three-dimensional model first order solution assumes the vortex shedding is decoupled from the solid body motion and has no effect on the momentum and moments of momentum.

C. DATA ANALYSIS

The data set analysis centered around three central goals: 1) create experiment drop results in a plot format easily compared to the model output plots, 2) provide necessary initial conditions from each of the experiment drops to the three dimensional model and create a plot of the model results, and 3) Create initial conditions for entry into the existing mine burial prediction model, IMPACT28. The key comparison parameters at the end of each drop were the impact fall velocity and the pitch angle of

the shape. These values were archived from all 270 cases for the experimental drops, three-dimensional model and IMPACT28.

1. Mine Modeling Parameters

The required model inputs consist of three linked sets of parameters, Table 7, Table 8, and Table 9.

Mine Characteristics	
χ	center of mass offset
ρ_m	mine mean density
l	mine length
d	mine diameter
m	mine mass
$\vec{J}$	moment of inertia tensor

Table 7. Mine Characteristics Required for the Three Dimensional Model.

Initial Conditions	
x_o, y_o, z_o	initial position vector
u_o, v_o, w_o	initial velocity vector
Ω_o, ω_{1_o}, ω_{2_o}	initial angular velocity vector
ψ_{2_o}, ψ_{3_o}	initial angle vector
Δt	time step increment

Table 8. Initial Conditions Required for the Three Dimensional Model.

Hydrodynamic Characteristics	
$\vec{V}_r=\vec{V}_1+\vec{V}_2$	relative water velocity vector
R_e	reynolds number
C_{d_a}	axial flow drag coefficient
C_{d_f}	cross flow drag coefficient
C_l	lift coefficient
T_w	water temperature
ρ_w	water density
ν	water kinematic viscosity

Table 9. Hydrodynamic Characteristics Required for the Three Dimensional Model.

Although both data sets and the three dimensional model are referenced to a conventional earth fixed coordinate reference frame (right hand rule), all three initialize the mine orientation differently. The model initializes with the head of the mine pointing along the positive x-axis direction, the MIDEX data set has the head of the mine pointed in the negative y-axis direction, and the Carderock data set has the head of the mine pointed in the negative x-axis direction.

Both data sets positions and velocities values had to be transferred to the same orientation as the model to perform comparisons of model output plus evaluate comparisons of impact fall velocities and impact angle. This simple conversion at times became very confusing throughout the analysis process.

A second data conversion issue occurred because approximately fifteen percent of the Carderock experiment drops did not have data at $t_o = 0$. These particular drops were adjusted to create initial conditions for a psuedo $t_o = 0$ by subtracting the initial value of the drop from every position, angle, and time value column to create a new $t_o = 0$ referenced data set for that drop. Resetting drops to the new initial conditions at the new pseudo $t_o = 0$ maintained the maximum number of drops in the data set.

Three blunt nosed mine shape drops in the Carderock data set were not investigated and analyzed in this investigation due to an excessive gap where no data was recorded during the mine shape's fall. The drops not considered during analysis are, 2w-5, 10w-5, and 17w-1.

2. Mine Drop Model Comparison Plots

The mine drop experimental data is plotted alongside the model output for each experimental case. An example plot of a drop case form the Carderock data is shown in Figure 24. The two-dimensional x-z planar sub-plots present the cumulative distance traveled by the mine shape for both the experimental data and the model output. This gives an indication for how well the first order model solution deals with the nonlinear motion the actual mine experiences as it falls through the water column. The second set of sub-plots shows a trace of the mine travel projected onto an x-y plane as the mine falls. And lastly

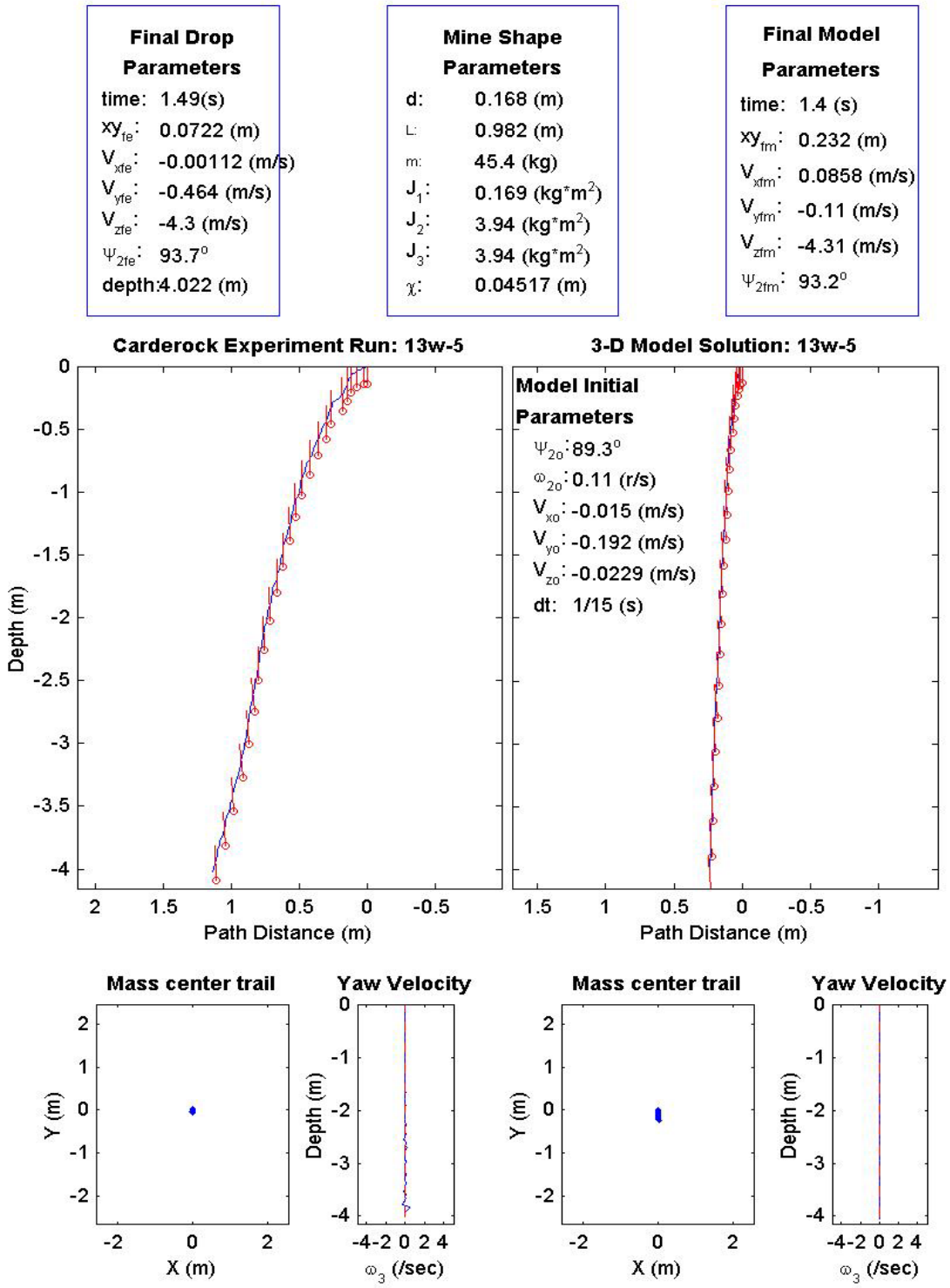

Figure 24. Example of Mine Drop to Model Comparison Plot Showing the x-z Depiction, x-y Depiction, "Mass Center Trail" and the yaw velocity Trace as the Mine Shape Falls Through the Water Column

the third set of sub-plots shows the incremental values of yaw angular velocity (rad/sec) of both the experimental mine shape and the model output. These last two sets of plots also gives a good comparison of the 1st order model solution approximation to the actual nonlinear motion the mine shape experiences as it falls through the water column. The entire group of 270 plots for both data sets is presented in Appendix A.

3. Impact Parameter Comparison Plots

A comparison of the experimental data to the current operational model IMPACT28 required conversion to still another coordinate depiction because the IMPACT28 rotation angle directions are reverse of the angle rotation directions for the three dimensional model. The initial conditions were converted from the three dimensional model initial conditions to IMPACT28 format and saved to a spreadsheet.

IMPACT28 is not an easy application to use. It is written in obsolete code and requires manual entry of all the modeling parameters discussed earlier for each of the 270 cases of Appendix A. The impact fall velocity and impact angle output from IMPACT28 for each of the 270 experimental drops was saved as a text file and then manually entered into a spreadsheet of final conditions for impact fall velocity and impact angle from the experimental data, IMPACT28 model and the three dimensional model.

An example of a typical comparison scatter plot for the 270 cases is presented in Figure 25. Additional comparison plots are presented in the following chapter.

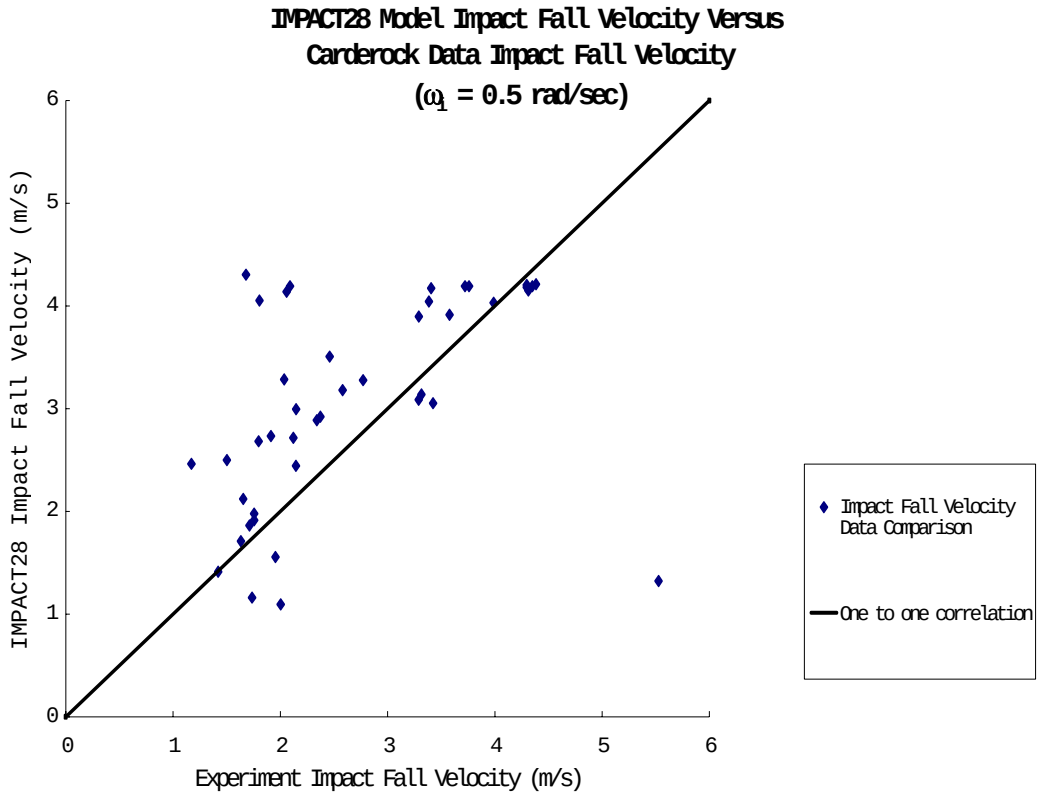

Figure 25. Data Comparison Example for Final Impact Conditions. This Case Compares IMPACT28 Fall Velocity to Carderock Data Fall Velocity for Arbitrarily Introduced IMPACT28 Angular Velocity Value, $\omega_1 = 0.5$ (rad/sec).

THIS PAGE INTENTIONALLY LEFT BLANK

VII. RESULTS

A. TRAJECTORY PATTERNS

Gilless (2001) developed six descriptive trajectory patterns referenced to the body-fixed coordinate reference frame that are commonly seen for solid bodies undergoing free fall through a fluid medium, Table 10. Figure 26 presents the five basic trajectories patterns that can be combined to produce the more complex motion of a combination trajectory. In Figure 26 the final frame shows a flip flat combination as an example of a complex trajectory. The combination trajectory is the most common trajectory pattern occurring in 80% of the 270 mine drop cases investigated. This becomes the first indication the a mine shape's free fall motion is not linear and simple but tends more towards chaotic motion as discussed in Aref and Jones (1993). The chaotic motion tendency has repeatedly been observed and discussed by authors throughout the Impact Mine Burial Prediction model development.

B. CARDEROCK TRAJECTORY PATTERNS

The fifty blunt nosed mine shape experimental drops comprising the Carderock data were evaluated to determine individual trajectory patterns. The trajectories were determined through use of different views of the experimental data from different cameras. Analog and/or digital video clips for each drop were analyzed if available. The forty-two drops that contained sufficient tracking data for determining position were analyzed by looking at the experimental drop data plots. An example of

the data plots is presented in Figure 27. Appendix A contains the complete set of the MIDEX and Carderock experiment drop data plots.

The video and tracking position analysis results were compared and a composite trajectory pattern type was selected for each of the Carderock experimental drops, Table 11. The Carderock drops display trajectory results consistent with those determined for the MIDEX drops, (Gilless 2001). The combination trajectory dominated the Carderock results.

Mine Trajectory Pattern	Description
Straight or Slant	Mine exhibited little angular change about z-axis. For straight mine attitude remained nearly parallel with z-axis (± 15°). For slant, mine attitude was 45° off z-axis (± 15°).
Spiral	Mine experienced rotation about z-axis throughout its water phase trajectory.
Flip	Initial water entry point rotated at least 180° during mine motion.
Flat	Mine's angle with vertical near 90° for most of the trajectory.
Seesaw	Similar to the flat pattern except that mine's angle with vertical would oscillate between greater (less) than 90° and less (greater) than 90° - like a seesaw.
Combination	Complex trajectory where mine exhibited several of the above patterns.

Table 10. Description of Mine Shape Trajectory Patterns. “Adapted from (Gilless 2001).”

Mine Drop Number:	1	2	3	4	5	6
Blunt Nosed Mine Shapes						
Horizontial Drops						
1w-series	Flat-Spiral	Flat-Spiral	Flat	Flat-Spiral	Slant	Slant-Spiral
10w-series	Flat	Flat	Flat	Flat	Slant	Slant-Spiral
11w-series	Flat-Spiral	Flat	Flat	Flat	Slant-Flat	Slant-Spiral
Vertical Drops						
2w-series	Straight-Flat	Straight-Flat	Straight	Straight	Straight	Straight-Slant
12w-series	Straight-Flat-Seesaw	Straight-Flat-Spiral	Straight-Spiral	(flooded mine)	Straight	Straight
13w-series	Straight-Flat	Straight-Flat	Straight	(flooded mine)	Straight	Straight
45 degree down						
17w-series	Flat-Seesaw-Spiral	Flat-Seesaw	Flat-Seesaw	Slant-Flat	Straight-Slant	Slant-Spiral
20w-series	Flat-Seesaw	Flat-Seesaw	Slant-Flat-Seesaw	(flooded mine)	Slant-Spiral	Slant-Spiral
21w-series	Seesaw-Spiral	Flat-Seesaw	Flat-Seesaw	(flooded mine)	Slant-Spiral	Slant

Table 11. Observed Trajectory Patterns for the Blunt Nosed Mine Shapes Dropped at NSWC-CCD, Carderock, MD, 10-14 September 2001.

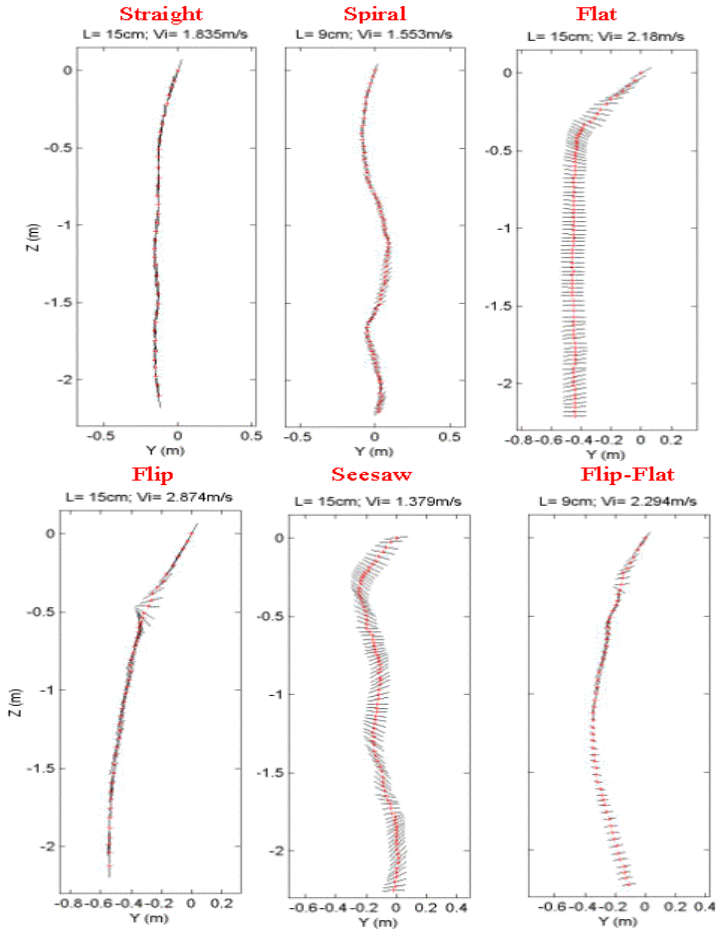

Figure 26. Blunt Nose Mine Shape Trajectory Type Examples. “Adapted from (Gilless 2001).”

C. MODEL SIMPLE MOTION MECHANICS

The three dimensional model output was investigated and compared to experiment results for two simple motion types, axial flow and cross flow. This comparison demonstrates that the three dimensional model can skillfully produce output results consistent with the experimental results for simple motion flow orientations.

1. Simple Axial Flow Motion

A vertical model mine shape drop (2w-4), where pure axial flow dominates the flow, shows the model can replicate with skill characteristics seen in the experimental results Figure 27.

2. Simple Cross Flow Motion

A horizontal model mine shape drop (11w-4), Figure 28 demonstrates the model can skillfully replicate the experimental results for a case where pure cross flow dominates the flow pattern. Both Figure 27 and Figure 28 demonstrate that the three dimensional model can handle simple dynamic motion that equates to calculations of external forces and torques acting on the mine shape solely along primary axes.

3. Oblique Flow Complexity

Oblique angles of attack present more complex impinging flow conditions. The model simplifies the calculation by applying the independence rule (Sumer and

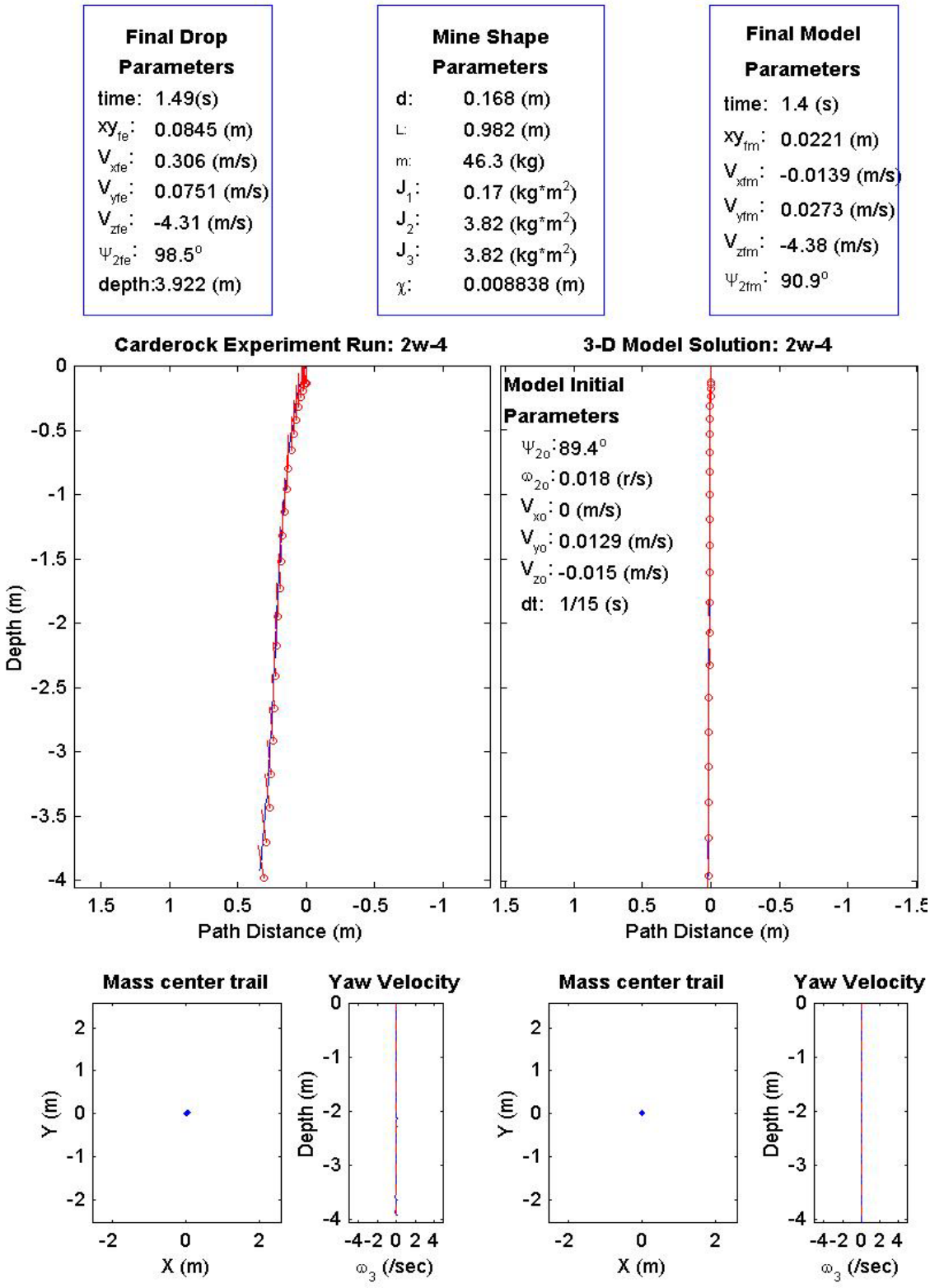

Figure 27. Simple Model Motion Mechanics for Purely Axial Flow.

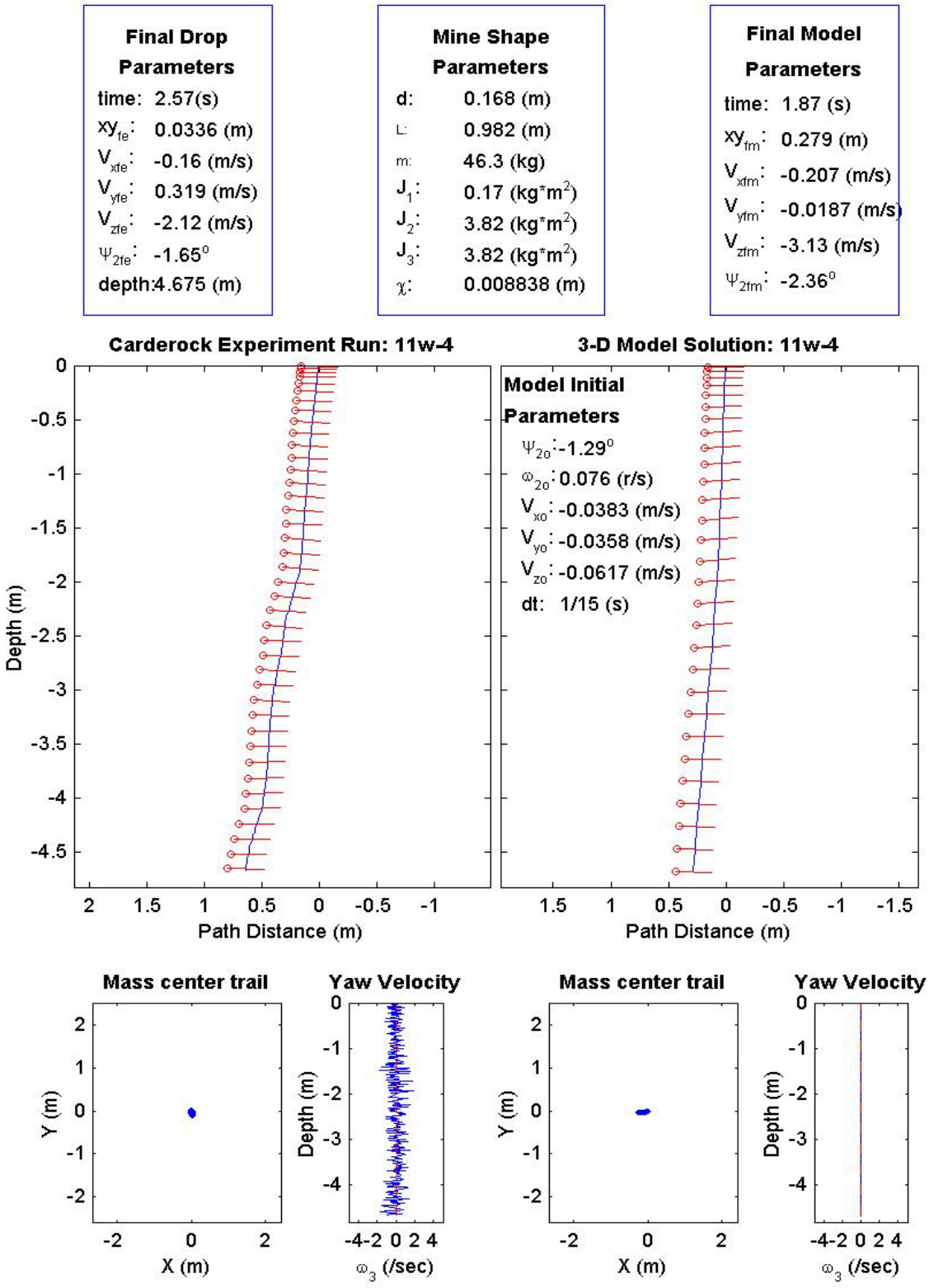

Figure 28. Simple Model Motion Mechanics for Purely Cross Flow Case.

Fredsoe 1997). The velocity components are broken down into relative components acting on the drag-lift force coordinate reference frame. The axial and cross flow velocity components are independently used to derive drag and lift coefficients and calculate the external forces and torques acting on the solid body during free fall. Sumer and Fredsoe (1997) conclude this technique provides an adequate solution for the dynamics problem until more advanced techniques are fully developed to define the axial flow component and cross flow component interactions. Lugt (1983) suggests this simplification be used but with caution in oblique flow situations.

D. MODEL COMPLEX MOTION MECHANICS

The three-dimensional model handles the more complex slant motion trajectory pattern Figure 29, and flipping motion trajectory pattern Figure 30, although not consistently. This type of motion causes larger and higher frequency oscillations in the yaw velocity trace sub-plots for mine drops displaying this motion type. This is an indication of the nonlinear effects on the solid body.

This oscillation appears tied to the non-linear processes acting on a mine shape at high angle of attack in the impinging flow across the mine shape. Lugt (1983) presents empirical evidence and discussion that the drag and lift coefficients for solid bodies at oblique angles to the flow are nonlinear vice the constancy assumption used presently in modeling where components are broken into purely axial and cross flow components.

The experimental data suggests the non-linearity is tied to both subtle variation of initial conditions and the angle of attack, (drop angle) from which the mine shape is released. This variation of angle of attack (drop angle) in hydrodynamic oblique flow conditions is the same as high angle of attack aerodynamics where separation of the boundary layer occurs, (Schlichting 1979).

Sumer and Fredsoe (1997) discuss the interaction of the solid body and the vortex phenomena that occurs in the wake of a solid body. The frequency and amplitude of vortex shedding changes with oblique flow conditions causing large nonlinear oscillations in the wake region behind the solid body. The vortex shedding is coupled to the local mine flow conditions and thus would affect the forces and moments acting on the solid body. The vortex shedding effects causing nonlinear mine shape motion are not investigated here. Evidence of the nonlinear body responses is seen to varying degrees in the data plots in Appendix A and suggests this type of coupling occurs in oblique flow.

E. INITIAL CONDITION DISTRIBUTION EFFECTS

Complete investigation and analysis of all 270 cases demonstrates that small changes to the many input variables could cause substantial changes in the mine shape trajectory, impact fall velocity and impact angle. The effects fuel discussion of nonlinear chaotic motion due to variation and randomization in the final results. This was briefly discussed in the previous section. Figure 31 and Figure 32 show the trajectories of the same mine shape under the same drop conditions for two drops 15-2-15-1, and

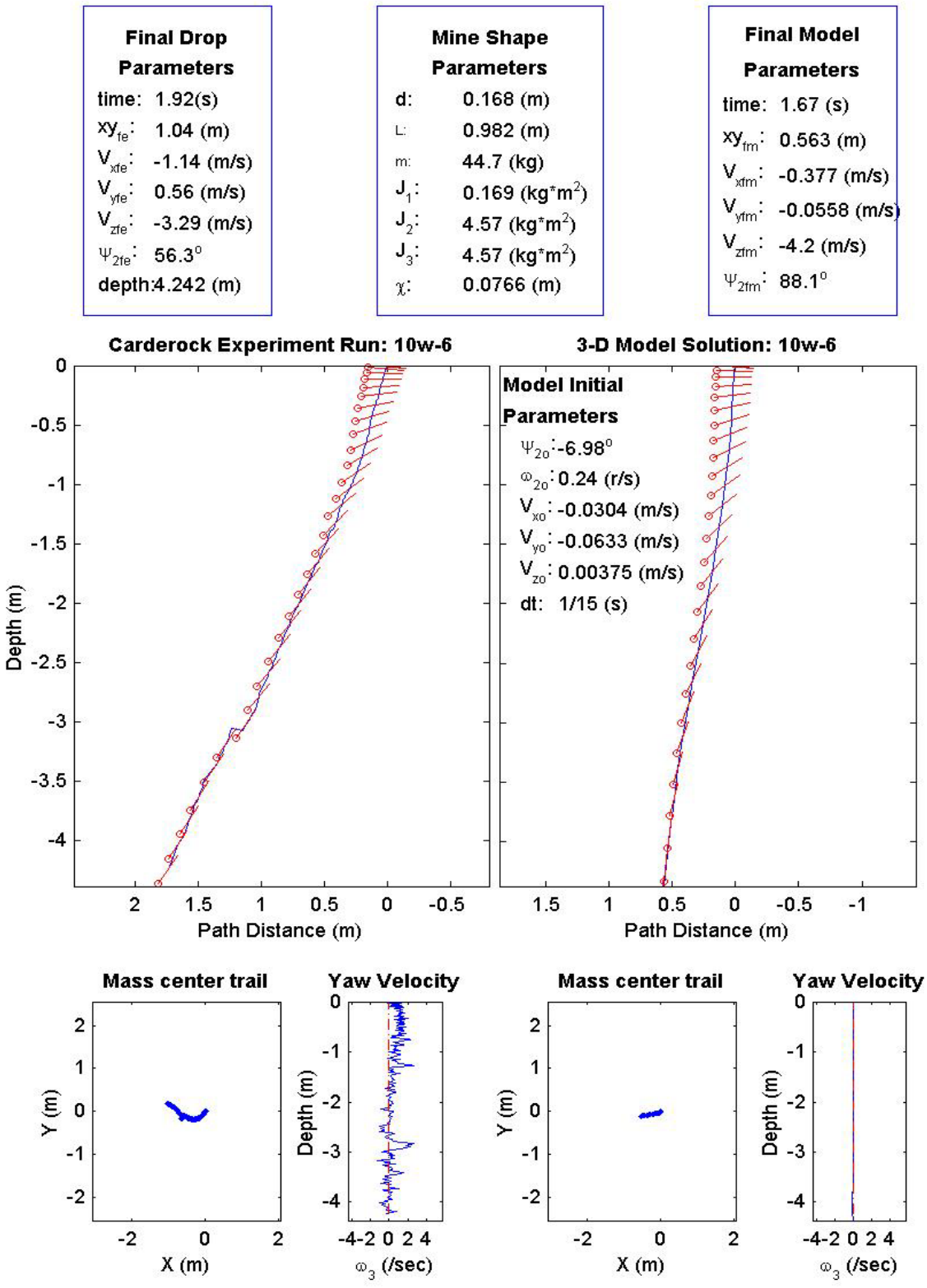

Figure 29. Model Motion Mechanics for More Complex Slant Trajectory Case.

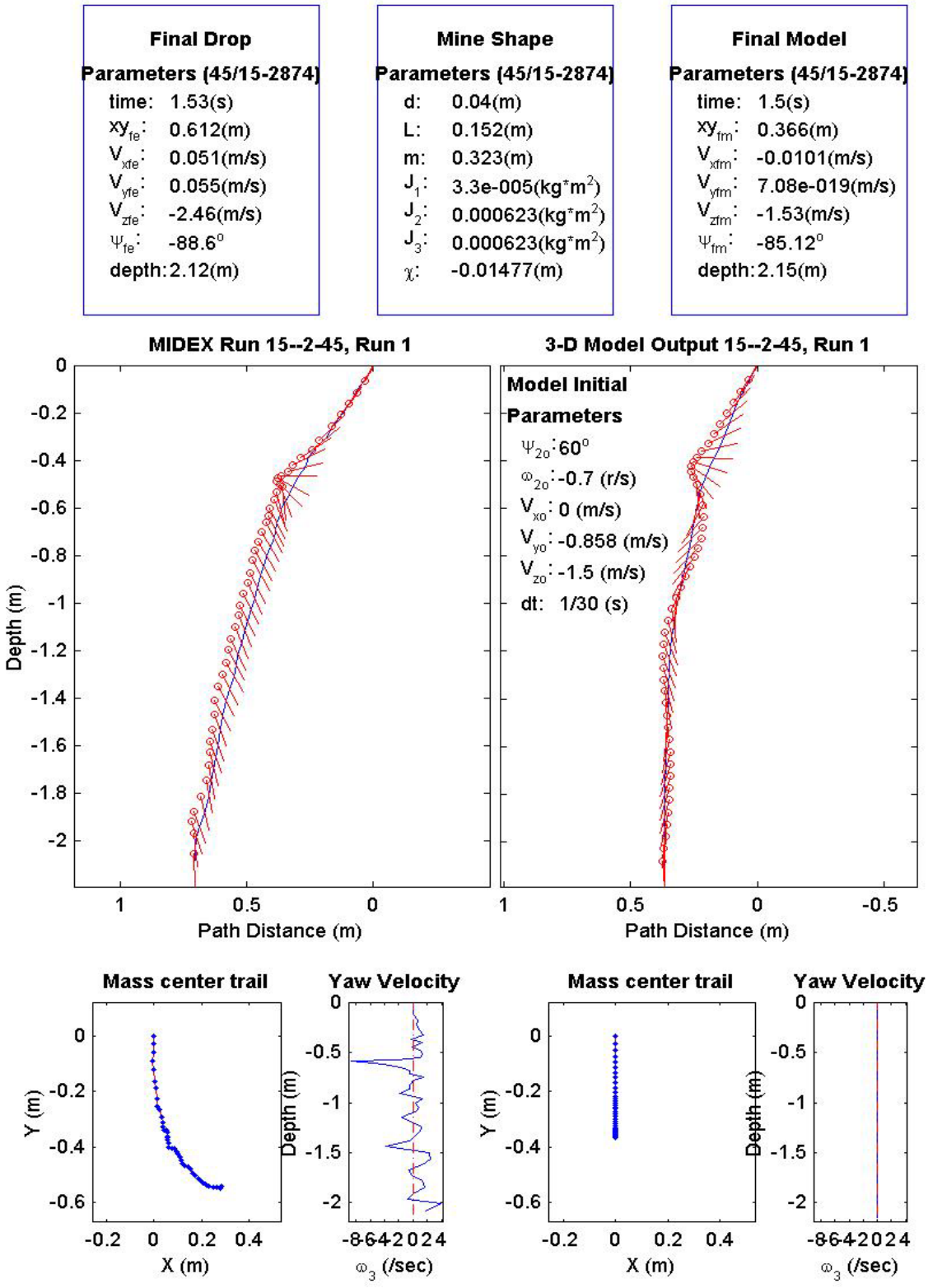

Figure 30. Model Motion Mechanics for Complex Flipping Mine Trajectory Case.

15-2-15-2. Small changes in initial linear and angular velocities occur for these two drops. The experimental results show that the subtle changes in initial conditions cause the mine to follow completely different trajectories.

The three dimensional model does not handle the change in initial conditions well for drop 15-2-15-2. The model drop trajectory takes on different orientations during the free fall and also takes a different path to the bottom. Interestingly in comparison, the final impact (x-y) planar position is comparable with drop 15-2-15-1. The drop does develop substantial impact angle error though it maintains similar impact fall velocity to 15-2-15-1 at the bottom.

F. IMPACT VELOCITY AND IMPACT ANGLE CORRELATION

There exists a wide array of input parameters that could have some random effects on the final trajectory and associated parameters at impact with the bottom. The mine shape free fall could be considered a random process and many truly believe it is due to the coupled local and remote nonlinear effects acting on the mine body.

It was stated previously there are two primary parameters required at the sediment interface to produce accurate burial estimates, impact fall velocity (w component) and impact angle. The experiment results and model output were maintained in a dimensional form to create several correlation scatter plots for all 270 cases in the investigation. The scatter plots allow for easy comparison of both impact fall velocity and impact angle from the experiment and model results. The correlation of experiment impact fall velocity (w component) compared to

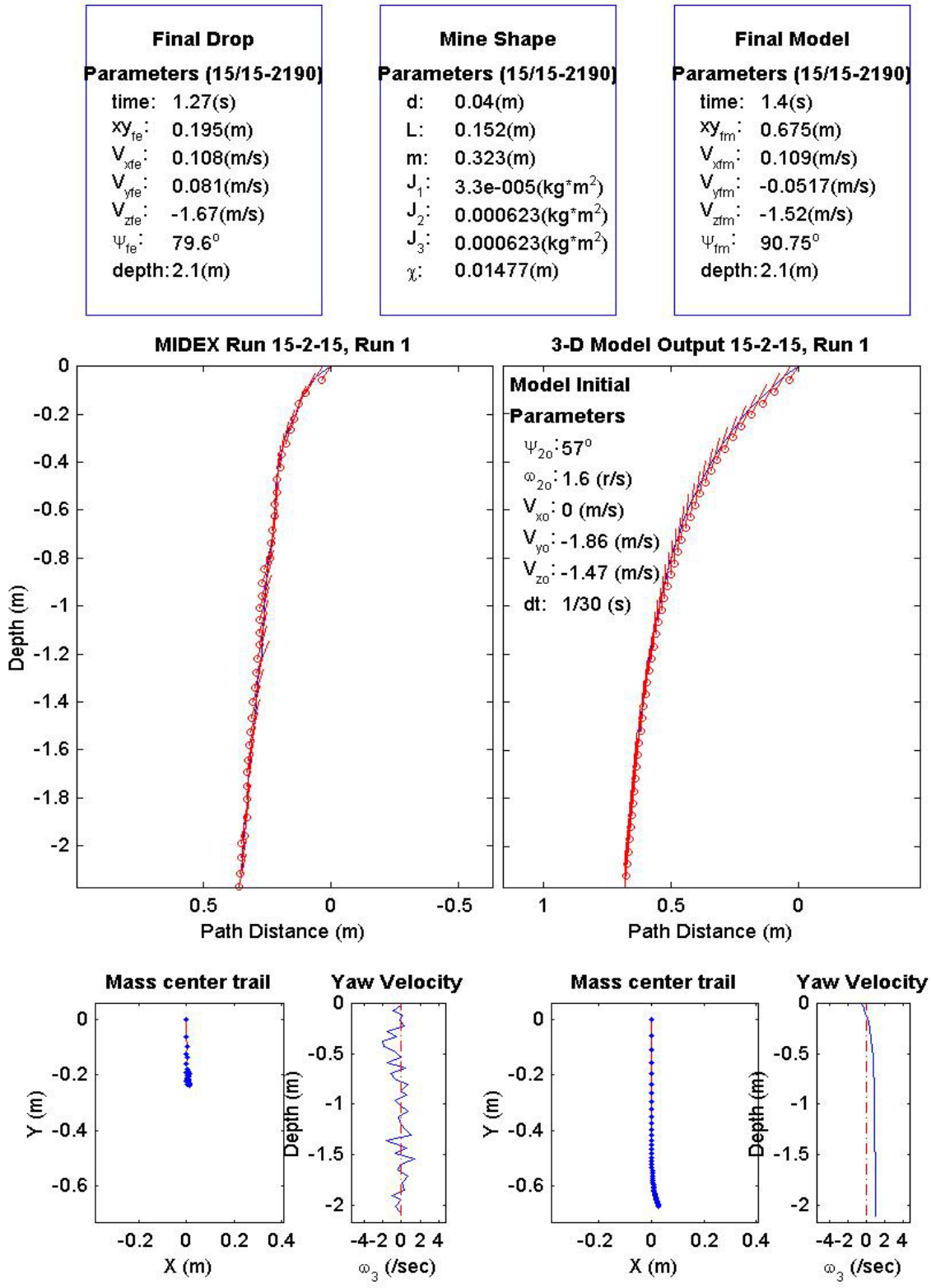

Figure 31. MIDEX Drop Data Plot 15-2-15-1.

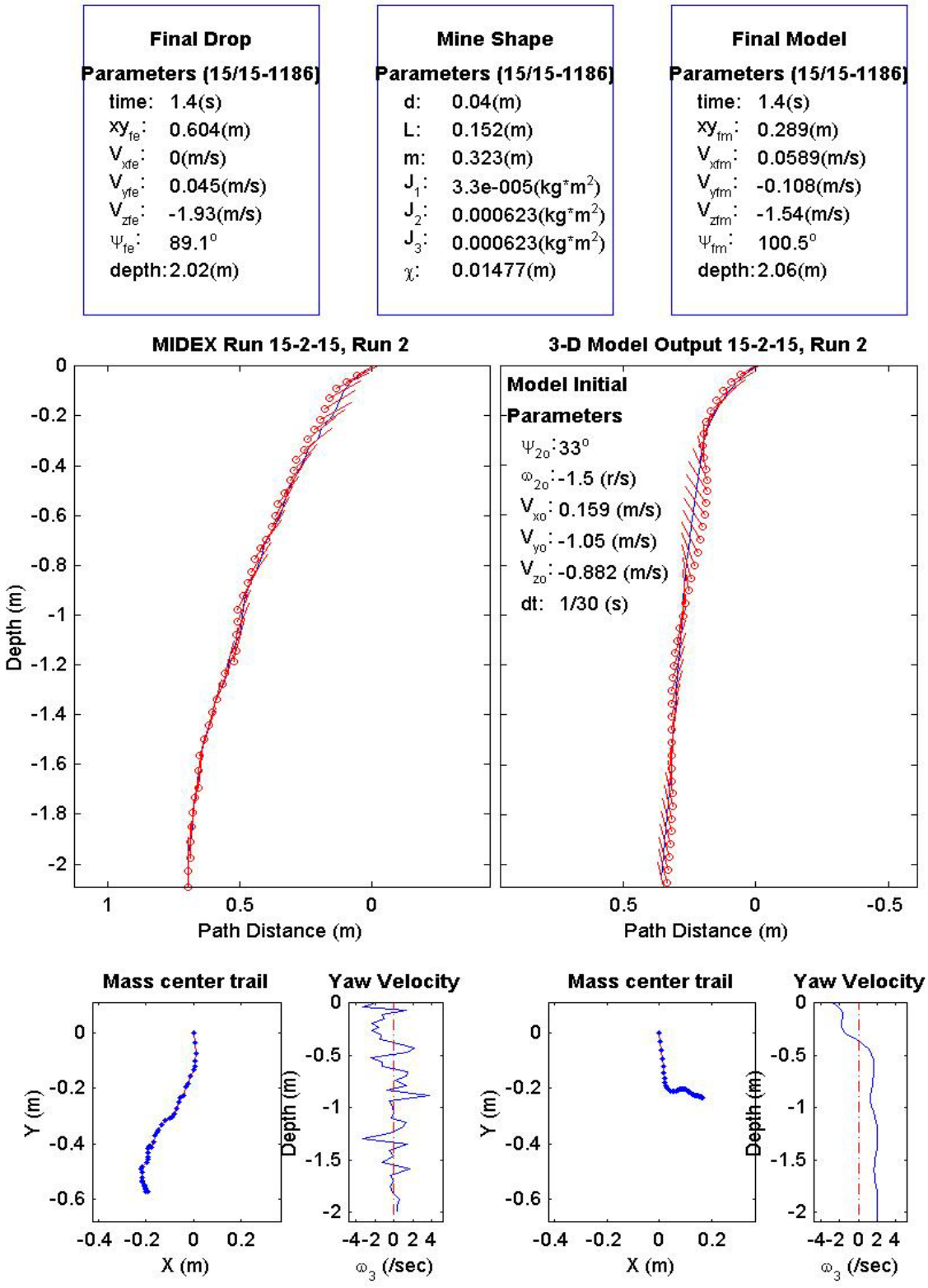

Figure 32. MIDEX Drop Data Plot 15-2-15-2.

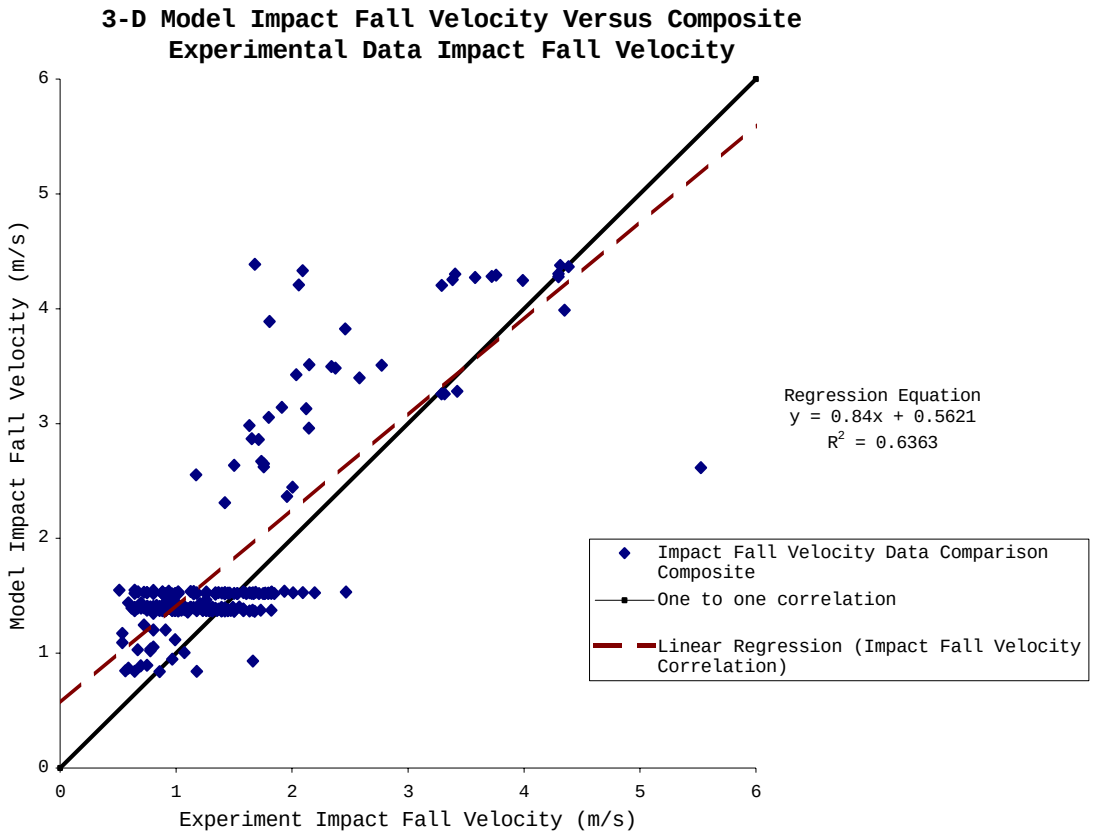

Figure 33. Three Dimensional Model Impact Fall Velocity Versus Composite Experimental Data Impact Fall Velocity, 270 drop cases.

the three-dimensional model impact fall velocity Figure 33, does show the model tends to over predict impact fall velocity magnitude.

If the experiment and three-dimensional model results in Figure 33 are considered random distributions, a linear regression line can be calculated (Montgomery et al 2001), for the experiment and model impact fall velocity scatter plot joint distribution. In a perfect world, a model developer hopes for slopes and correlation coefficients approaching 1.0. The linear regression line and respective equation in this case show high correlation for impact fall

velocity results between the experiment data and the three dimensional model output with a slope of 0.84, goodness of fit r^2 = 0.636 and a correlation coefficient r = 0.8. Thus there is a strong linear association between the impact fall velocity experiment results and the impact fall velocity model output. Other regression techniques could be considered. But since the model is first order a linear technique is appropriate. The comparison and regression results shows that a first order model from a statistical standpoint can skillfully predict a mine shape's impact fall velocity.

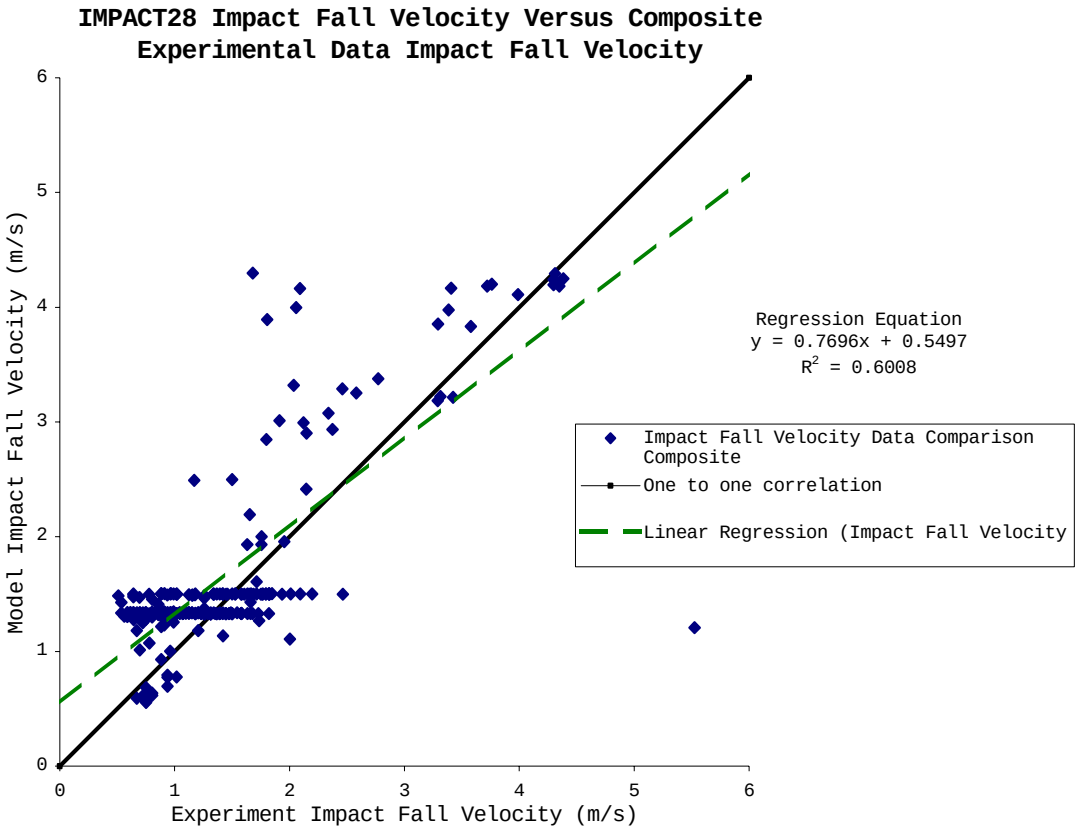

Figure 34. IMPACT28 Model Impact Fall Velocity Versus Composite Experimental Data Impact Fall Velocity, 270 drop cases.

The experimental impact fall velocity results were also compared to IMPACT28 model impact fall velocity results and a scatter plot produced, Figure 34. A linear regression line calculated for the resulting experiment to IMPACT28 model fall velocity distribution shows the three dimensional model produces slightly better statistical results than IMPACT28 for the sample domain considered, 270 drops.

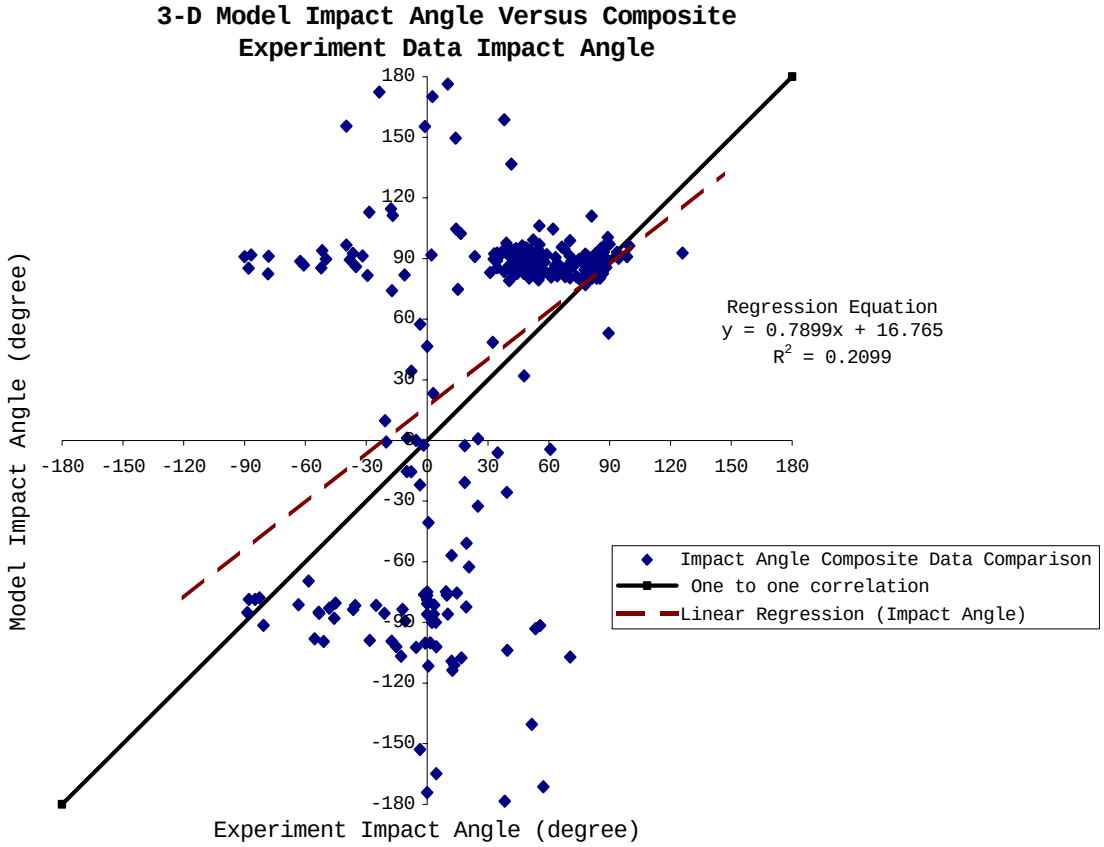

Figure 35. Three Dimensional Model Impact Angle Versus Composite Experimental Data Impact Angle, 270 drop cases.

A similar comparison of experiment results to three-dimensional model output for impact angle (ψ_2) is shown in

Figure 35. The linear regression line and respective equation are calculated from the highly dispersive scatter plot joint distribution. The results statistically do not show a high degree of linear association or correlation for the impact angle distribution.

The experimental impact angle results were also compared to IMPACT28 model output impact angle results and a scatter plot produced, Figure 36. A linear regression line was calculated for the resulting experiment to IMPACT28 model impact angle scatter plot joint distribution. The regression line and respective equation shows the IMPACT28 model produces better statistical results for impact angle than the three dimensional model for the sample domain considered, 270 mine drops.

Limiting the degrees of freedom within IMPACT28 thus limiting interacting motion most likely drives the improvement in impact angle prediction performance. The inclusion of all six degrees of freedom fuels the cross interaction of motion thus feeding the non-linearity and the more random dispersive three dimensional model impact angles at the bottom. The first order model approximations for the remainder of the degrees of freedom used in the three dimensional model currently provide no statistical improvement in prediction performance over IMPACT28. The model cannot deterministically encompass the nonlinear effects that produce the chaotic motion and random impact angle results at the end of a drop’s trajectory.

The Carderock results allow an investigation into what effect variations in initial angular velocity ω_{2_o} have on

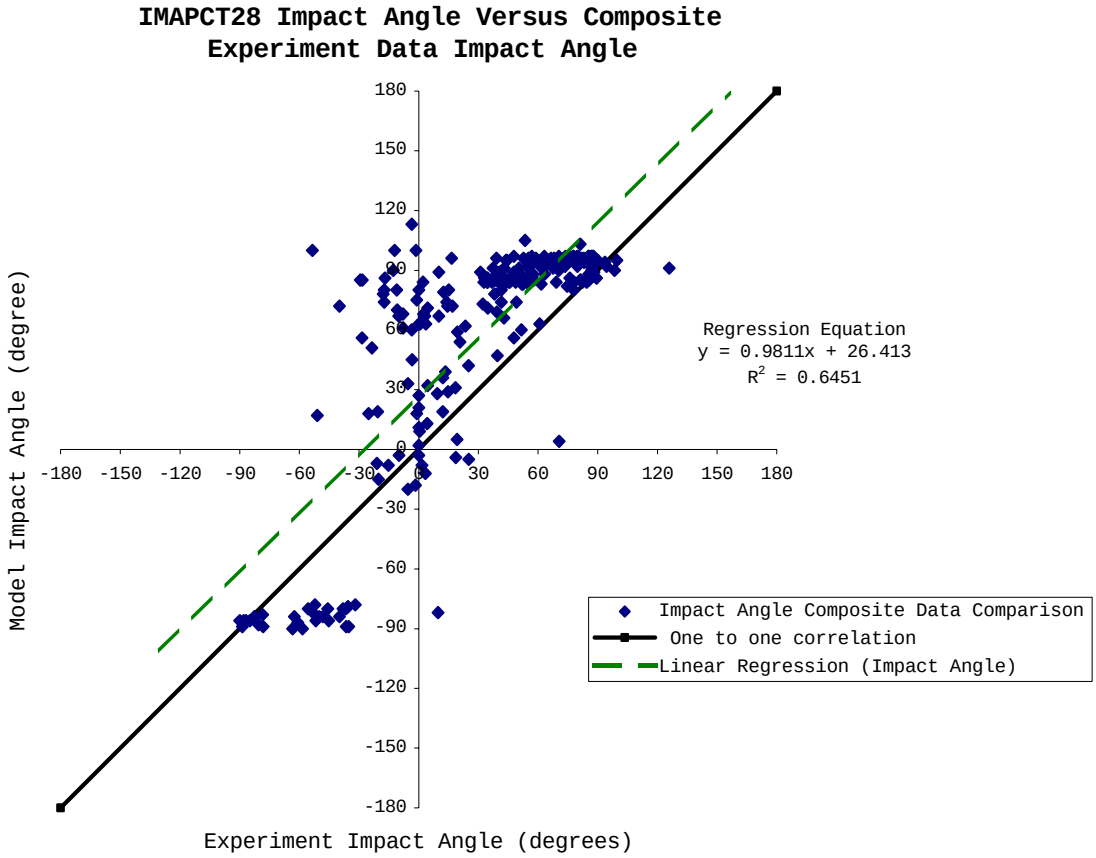

Figure 36. IMPACT28 Model Impact Angle Versus Composite Experimental Data Impact Angle, 270 drop cases.

the final results in IMPACT28. The Carderock data set had angular velocities with a mean value $\omega_{2_o} = 0.1$ rad/sec. This angular velocity ω_{2_o} was increased an order of magnitude to investigate how the initial mine tumbling affects the IMPACT28 impact fall velocity results and impact angle results. The tumbling effect variation about the mine shape's y-axis it was hypothesized would yield large variation in results. This was not the case. The results for impact fall velocity for the Carderock data are shown in Figure 37.

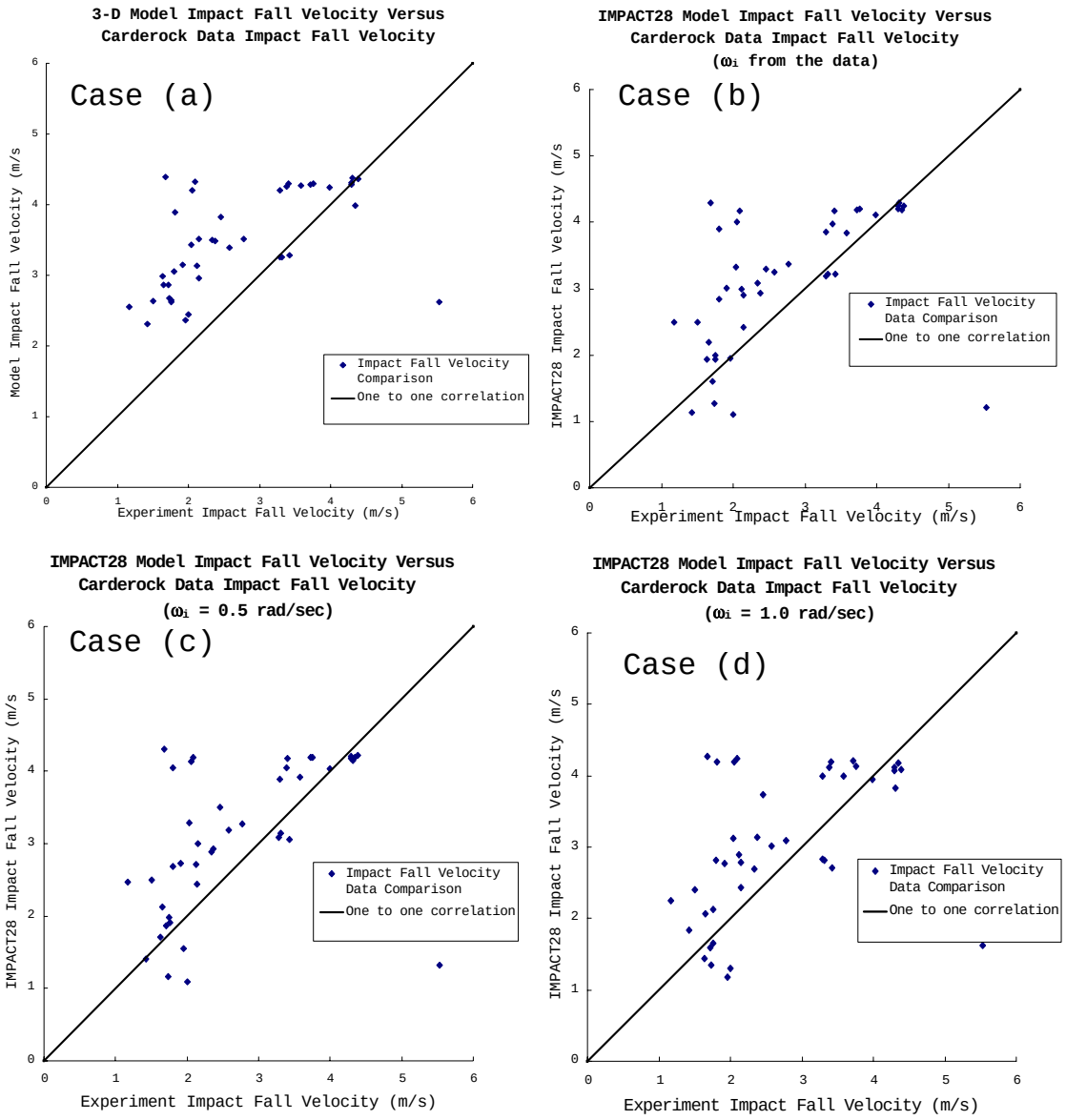

Figure 37. Scatter Plots of Impact Fall Velocity Comparing Carderock Experiment Results with the Three-Dimensional Model and Impact28 Outputs for Three Cases with Variable ω_{2_o} Input to IMPACT28.

Figure 37 contains four separate scatter plot comparison cases for varying angular velocities. Case (a) shows the scatter plot of impact fall velocity comparing Carderock experiment results with the three-dimensional

model output. Case (b) shows the scatter plot of impact fall velocity comparing Carderock experiment results with IMPACT28 model output using the Carderock data supplied initial angular velocity values. Case (c) shows the scatter plot of impact fall velocity comparing Carderock experiment results with IMPACT28 model output using an initial angular velocity value $\omega_{2_o} = 0.5$ rad/sec. Case (d) shows the scatter plot of impact fall velocity comparing Carderock experiment results with IMPACT28 model output using an initial angular velocity value $\omega_{2_o} = 1.0$ rad/sec.

The scatter plot comparison shows that varying the value for the initial rotation rate used to initialize IMPACT28 changes the scatter plot very little. It also shows that the three-dimensional model produces a slightly better estimate of impact fall velocity. Although both models still tend to over predict fall velocity as discussed in Valent et al (2002). A comparison of experiment impact angle results to three dimensional model output and IMPACT28, Figure 38, yields similar results showing that varying the angular velocity used to initialize IMPACT28 has little effect (only 3% change in correlation) on the final impact angle scatter plots.

Past model sensitivity studies have been of limited scope and used sparse data fields to conduct those sensitivity analyzes. Smith (2000) discussed the need to acquire a complete set of data to validate model performance. In this case the model in question was IMPACT25.

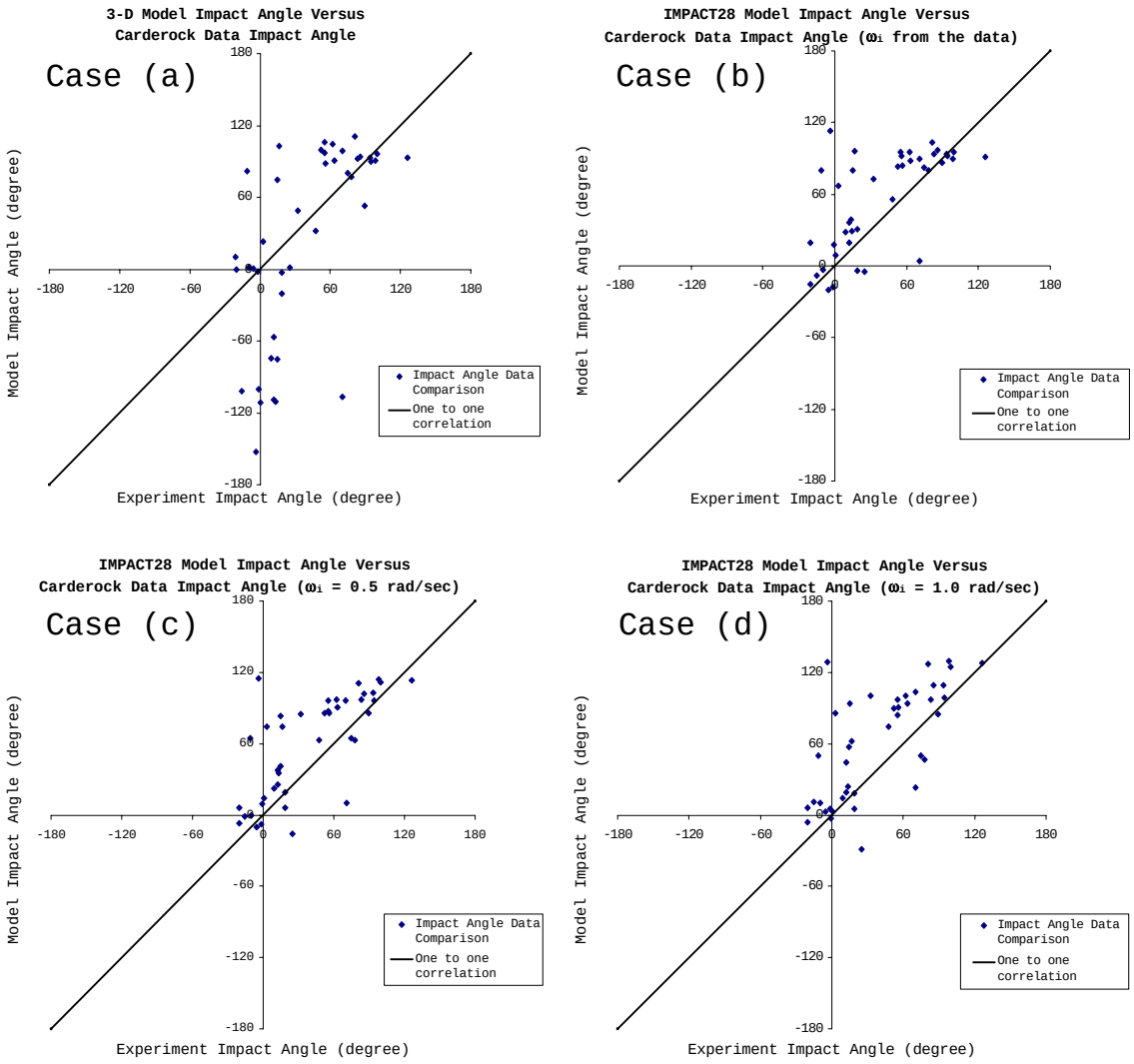

Figure 38. Scatter Plots of Impact Angle Comparing Carderock Experiment Results with the Three-Dimensional Model and Impact28 Outputs for Three Cases with Variable ω_{2_o} Input to IMPACT28.

This large data set allows one to look for the first time at model performance from a statistical standpoint for both the three dimensional model and the IMPACT28 model. To assess the models from a statistical standpoint one must assume acceptable controls were placed on the initialization parameters. Also the assumption must be made

that the data measurements made during the mine shape's free fall fairly resolved and accurate.

The first order three-dimensional model produces a statistically skillful prediction for impact fall velocity, although for a deterministic prediction it tends to follow the IMPACT28 model and over predict impact fall velocity. The error in the prediction though is smaller and an improvement on performance over IMPACT28. Valent et al (2002) discussed the desire for improvement in the prediction of vertical speeds, as the predictions from IMPACT28 were at times 150% greater than the observations. A more accurate prediction of impact fall velocity (vertical speed) leads to a more realistic mine shape kinetic energy dissipation into the bottom sediment

The first order three-dimensional model does not produce a statistically skillful prediction for impact angle, and does not produce deterministic results that are any better than the IMPACT28 model. Satkowiak (1988) discusses the fact that for given sediments the impact angle at the water sediment interface is critical to determination of percent mine burial in the sediment. This area of the three dimensional model requires more attention and focus to provide methods to improve impact angle prediction.

VIII. DISCUSSION

The water phase trajectory a mine shape experiences drives the resultant impact fall velocity and impact angle it will have when it encounters the bottom sediment. Modeling the hydrodynamic free fall is not an exact science and currently possesses no true analytical solution. Only through parameterizations are numerical models developed to predict the highly non-linear behavior of a mine shape. Today's active numerical model for mine burial prediction, IMPACT28, makes extensive use of empirical data, curve fitting and constants to simplify the numerical procedure to obtain solutions. INPACT28 also confines its motion to 3 degrees of freedom; (x, z) linear motion and (ψ_2) angular motion. The three dimensional model incorporates all six degrees of freedom. It produces modeled mine drop trajectories using a first order numerical solution approximation.

A. NONLINEAR MOTION EFFECTS

It was determined during preliminary analysis of the video clips from the Carderock experiment drops that clearly small changes in mine shape orientation, linear velocities and angular velocities lead to chaotic trajectories and dispersive impact points at the bottom of the water column. Follow-up analysis of all the drops plots from both Carderock and MIDEX confirm this initial conclusion. Aref and Jones (1993) support this conclusion with theoretical evidence that even simple solid body motion can develop chaotic tendencies given small

perturbations to an otherwise incompressible, inviscid, irrotational fluid at rest. With nonlinear effects in mind, the model has several areas where it deviates from the experimental results.

1. Yaw Velocity Deviations

The model tends to produce more conservative cumulative horizontal excursions than the actual mine drops experience. The actual mine drops also display a great deal of yaw velocity movement. This component of angular velocity gives a clear indication of the large angular velocity changes occurring on the actual body. The model on the other hand presents constant angular velocities around the yaw axis or angular velocities that change very smoothly. This is a trait consistent with a first order numerical solution used in the three dimensional model, and combined with the empirical data used to calculate the external forces.

2. Horizontal Position Deviations

In 70% of the comparison cases the x-y plane horizontal excursions were within 30% of each other when model results were compared to the actual drops. Comparisons of model to experiment in the simple motion cases produced the best results overall. This is the best comparison metric to demonstrate the model produces skillful results for semi-linear simple motion. The empirical data used for external forcing calculations was collected in conditions of simple flow; either axial or

cross flow conditions. Thus one expects he model to perform skillfully under those flow conditions

3. Vertical Fall Velocity Deviations

The model still over predicts impact fall velocity values but to a lesser degree statistically than IMPACT28. This trait is tied to both the nonlinear motion and model simplification. The model assumes the relative flow across the solid body can be broken down into purely axial and cross flow velocity components. Although useful for conceptual discussions the velocities realistically must interact to some degree at oblique flow angles. The order of magnitude of this effect currently remains unknown.

Also vortex shedding and possible coupling to the solid body motion are not included in the model. It is well documented in literature that this phenomenon does occur, and does affect the solid body motion to some degree.

The fall velocity over prediction also results from the fact that actual drops for complex motion produce higher horizontal velocity components (u,v) than the model produces. The model continues to proceed towards terminal velocity (w velocity component) and produces much smaller horizontal velocity components. The experimental results show lower magnitude and more dispersive magnitude fall velocities for the composite data set, Figure 33.

4. Trajectory Deviations

The last chapter discussed small differences in initial conditions causing the actual mine drops and the

model to behave differently, Figure 31 and Figure 32. An investigation of all the drops show the model and experimental trajectory results do remain similar through the first 25% to 35% of the free fall. After this point is where the divergence in the solutions first appears. Again the simpler the motion, the less likely the model is to diverge rapidly from actual drop results.

5. Model Instability

A possible stability problem exists in the three dimensional model. As the center of mass is moved towards the center of volume the model begins to produce inconsistent results. Also, as the aspect ration (L/d) decreases the model produces inconsistent results. This is a future area for improvement that was not investigated.

6. Impact Angle Deviations

The previous chapter discussed the large dispersion in impact angle produced by the three-dimensional model, Figure 35. One can relate the dispersion of the model to a combination of the effects discussed above. A key to improving the impact angle results resides in the future stability analysis and incorporation of those results into model improvements. When the stability is addressed for the more neutrally stable mine the model will tend to emulate more closely the actual mine drops for all cases producing a better impact angle correlation.

7. IMPACT28 Pitch Axis Angular Velocity Analysis

IMAPCT28 does currently produce better statistical results for impact angle than the three-dimensional model. The analysis of the angular velocity variation around the pitch axis in IMPACT28, Figure 37 and Figure 38, does provides some critical thought on the IMPACT28 impact angle results. As the angular velocity is increased an order of magnitude there is little statistical effect on the impact fall velocities, Figure 37 or the impact angles, Figure 38.

The impact angle correlation changes 3%. Granted the sample size considered only contained 42 points. The analysis of the damping moment effect (Hurst 1992) used in IMPACT28 produces unexpected results. This small variation in correlation as angular velocity is changed suggests that when a large sample is considered, IMPACT28 will statistically produce the same linear regression curve within some tolerance regardless of the angular velocity input.

B. PROBABILITY-TYPE MODEL SOLUTIONS

Arnone and Bowen (1980), Satkowiak (1988) and Hurst (1992) all made observations that mine-like shapes impact the sea bottom in nearly random orientations. Hurst (1992) was the first to suggest that due to the complexity of the problem and lack of accurate initial conditions, when available at all, a statistical distribution of burials may provide the best prediction; a probabilistic model vice a deterministic model. This type of modeling is an effort to statistically encompass and quantify the nonlinear motion effects.

1. Chaotic Mine Burial

Mine Warfare and specifically Mine Countermeasures is one of the most complex realms of Naval Warfare. The complexity of the threat, the myriad influences of the environment and the ingenuity of any adversary (NMWP 2000) make development of any truly deterministic prediction tool unattainable for the hydrodynamic trajectory prediction. Soulsby (1997) compiled a list of uncertainty for many of the environmental parameters encountered in mine burial impact prediction.

This list is not complete by any means. The undefined variables are numerous and the uncertainty and variation in the defined variables can be large. This readily applies to the three dimensional hydrodynamic modeling portion used within any integrated mine burial prediction tool where initial values are supplied to the model and they may posses both variation and uncertainty. A probabilistic modeling approach would handle this variation and uncertainty.

2. Meteorology Numerical Weather Prediction Analogy

Meteorogical forecasts have long been viewed in a deterministic sense. The truth of the situation is the initial state used to initialize numerical weather prediction (NWP) models is always incompletely defined. Growth of small errors in the initial conditions can cause the forecast to diverge with time from actual conditions. And, the closed sets of mathematical equations are approximations that make use of parameterizations to produce operationally significant model results, (Gottshall

1997). A precedent exists and the same solution type is proposed on a much finer spatial and temporal scale for mine trajectory prediction.

Meteorologists have found the use of ensemble prediction models increasingly attractive over the past decade. These models are based on probability and applied applications. Numerical Weather Prediction Models of this type demonstrate skillful performance past the 4-5 day point over a single model deterministic forecast by computing the mean of a parameter and a standard deviation on the parameter. The improved skill is achieved by using the statistics of a set of models or one model perturbed multiple times around a set of initial conditions.

Interestingly enough, the National Weather Service uses Model output Statistics (MOS) without human intervention to produce city temperature forecasts. These probabilistic outputs are preferred due to the models consistent skill at producing weather elements that consistently validate. Here again, parameter outputs are based on statistics and probability to improve skill. It is on this basis that a probabilistic modeling approach seems appropriate for handling the nonlinear effects on the solid body motion.

3. Short Range Mine Burial Model Development

Dolan et al (1999) during a visit to NATO countries to discuss general mine hunting prediction tools reached the conclusion that existing error terms for some parameters in current models exceed tolerances required by the mine warfare community. They speculated that a deterministic

integrated mine burial model with errors less +/- 10% would not be developed within the next decade. Today this easily appears to be a conservative estimate. They concluded development of a model based on probabilities would be most useful in the short term.

Shortly after that assessment, the Mine Burial Prediction Group evolved. No association could be found between that assessment and the initial meetings of the group but they are closely tied in time. The group's primary short-range goal is the development of a framework for obtaining probability distribution functions (pdf)s for all required inputs to an integrated and improved IBPM, (Bennett 2000). A mid to long-range goal is the development of a statistically dynamical mine burial prediction system.

4. Current Probabilistic Model Solutions

Goff (2002), a member of the MBPG, has suggested development of a stochastic framework to modeling mine burial using Monte Carlo methods. A complete probabilistic solution requires (pdf)s for both uncertainty and variability of input parameters. Some parameters would have both uncertainty and variability (pdf)s. Others would only have one (pdf). The input (pdf)s are then used within some integrated mine burial prediction model. The input (pdf)s would be used to initialize a model, like the three dimensional hydrodynamic model and provide output (pdf)s to follow-on sediment models. This continues until an output is obtained at some forecast time for the percent burial based on all factors affecting burial to that point.

A Mine Burial Expert System Model (MBESM) Figure 39, is currently being developed at John Hopkins University for inclusion in tactical decision aids such as the Mine Warfare Environmental Decision Aids Library (MEDAL), by Rennie et al (2002). It is based on Bayesian probabilistic networks and nodes that analyze the causal relationships between key parameters and how they affect each other. The causal effects are quantified by conditional probability distributions (cdp)s.

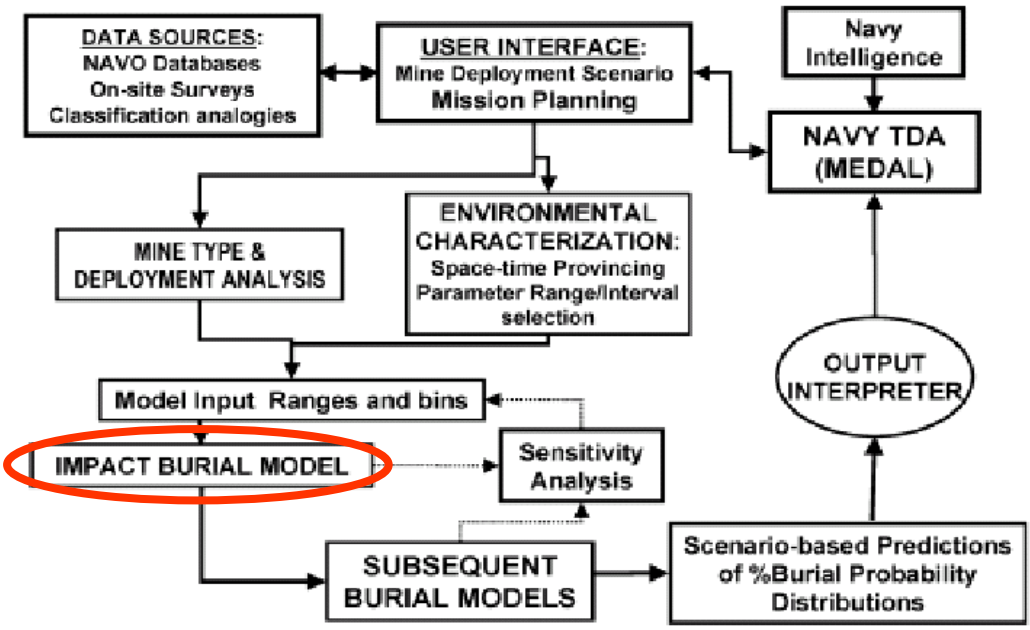

Figure 39. Mine Burial Expert System Model Concept Overview. “Adapted from (Rennie et al 2002).”

In the expert system the core information is conditional probability tables (cpt)s based on histograms developed through Monte Carlo exercises of the physics based models associated with mine impact and burial. An improved three-dimensional hydrodynamic model would perform the calculation of trajectories and develop fall velocity

and impact angle histograms to feed to sediment models. The hydrodynamic model (three dimensional model) fits into (MBESM) in the Impact Burial Prediction section as outline in red in Figure 39.

C. EFFECTIVE MINE IMPACT BURIAL PREDICTION METRIC

The output mine burial metrics to the navy mine countermeasure planner would consist of (pdf)s for percent mine burial with composite error estimate and degree of confidence. This parameter would then be tied to the acoustic detection prediction for the mine shape within a given battlespace environment. Strategic and operational planning doctrine would be developed by COMMINWARCOM based on this set of output metrics covering a specific battlespace environment. The relevant tactical question that needs to be answered by this knowledge; do we hunt or do we sweep this particular battlespace?

The results of the current investigation and three-dimensional model development agree that an integrated probability model presents the best solution available currently to deal with this highly nonlinear hydrodynamic flow problem. Thus it is envisioned that an improved three-dimensional model will be integrated into the ONR/NRL framework for a stochastic approach to mine burial prediction, (Richardson et al 2001b).

IX. CONCLUSIONS

The mine warfare community needs improved mine burial prediction capability. The community agrees the current prediction models in use today provide unreliable information. Commander Jim Berdeguez a former N75 expeditionary warfare METOC liaison summed up the mine warfare communities plea in one word, “Help.”

Scientists and researchers agree that an arbitrary mine dropped through a given water column will exhibit varying degrees of nonlinearity as the shape proceeds towards the bottom. The scenario presents a tough modeling challenge. Scientists and researchers also agree that the two critical parameters from the hydrodynamic portion of the mine drop trajectory are impact fall velocity and the impact angle. Those two parameters determine the amount of vertical kinetic energy that must be dissipated in the sediment and the orientation under which that dissipation begins to occur in the sediment.

Existing models for mine burial prediction are rudimentary at best. Even the impact burial prediction program requires improvements as demonstrated by Valent et al (2002). They demonstrated that IMPACT28 over predicted fall velocity by 150%. The current analysis shows that varying the rotation rate in IMPACT28 has relatively little statistical effect on either impact fall velocity or impact angle for the group of mine shape drops.

A. SUMMARY OF FINDINGS

A first order three-dimensional model was developed that includes the full physics package to predict the orientation of a solid body at an increment in time. The solid body in this case would be a simple right axially symmetric cylinder with blunt ends. A wealth of knowledge exists in the literature for cylinders thus simplifying the investigation and model development. The model obeys the two Newtonian principles of conservation of momentum and conservation of moments of momentum thus encompassing all 6 degrees of freedom that can possibly occur for a solid body moving through a fluid medium.

The model was developed using MATLAB, a modern scientific computation and visualization tool. It is well suited to work on matrices and systems of equations then produce graphic output. In this case, the system of nine equations governs the linear velocity, angular velocity and Euler angles.

Two robust data sets were used to validate the mechanics of the model. The data sets come from two experiments, MIDEX, and the Carderock Mine Drop Experiment. The Carderock data set had not previously been extensively investigated. MIDEX had. Gilless (2001) had developed a table of common trajectory types for right axially symmetric cylinders using the MIDEX results. The Carderock data set contained a subset of right axially symmetric cylinder drops initiated within the water column. The drops were similar in structure and release conditions to the shapes used in MIDEX, although the scales were different. These drops possess characteristics from the trajectory

table previously developed for the MIDEX data with the combination trajectory being dominant occurring in 80% of the cases. The two data sets were combined to create a single dataset to validate the three-dimensional model mechanics and overall performance.

The model correctly handles what can be characterized as simple motion; purely axial flow conditions and cross flow conditions. The model can produce skillful results for more complex trajectories such as slant motion or flips, but not consistently.

The three dimensional model is statistically more skillful than IMPACT28 at prediction of vertical fall velocity. The three-dimensional model shows poor skill at predicting the impact angle for a mine as it impacts the bottom. The impact angle prediction showed little correlation to the experiment results. The resulting scatter plot was very dispersed. The same mine released with nearly identical initial release parameters develop impact angles sometimes 90° apart.

B. FUTURE RESEARCH

A trend observed in the data plots centered around two issues concerning mine stability. Mines in which the center of mass is coincident with the center of volume are neutrally stable and tend to produce inconsistent predictions especially for impact angle. Also, mines that had lower aspect ratio (L/D) tended to produce inconsistent prediction for impact angle. These trends appear related to solid body stability. Future work in this area is necessary

and centers on analyzing the stability of the mine shape during its free fall trajectory.

A database now exists for 270 blunt nosed right cylinders tracked during free fall with the final conditions just before sediment impact calculated and archived. The Carderock data set contains a subset of mine shapes with hemispheric noses. Future work would include the capability to handle hemispheric noses in the model. An analysis of the Carderock hemispheric nose mine drop data could be completed.

A full-scale mine data set exists that contains a subset of mines released below the surface. The release from below the surface criteria makes analysis and comparison to model results easier. Data set exists from full scale mine drops in September 2000, November 2000, January 2002, and May 2002. The set of full-scale drops include both blunt nose mine drops and hemispheric nose mine drops. Future work would also include this data set into the master data set and perform a validation of model performance against those mine shape drops.

The data sets considered in this investigation for model development were obtained in a controlled environment without external influences such as wave and current forcing. Routines exist within the model for using some type of current data (like Advanced Doppler Current Profiler data) within the model to investigate differences in model output by neglecting the current forcing versus inclusion of the current forcing. When this type of data is collected in conjunction with future mine drop experiments environmental current effects could be investigated.

Throughout the course of model development and data analysis indications of nonlinear motion are evident in the mine drop data plots. When the nonlinear development occurs in a drop the model does not perform as well as when the development remains insignificant over duration of the free fall. The dispersive nature of the impact angle results caused by subtle deviations in initial release parameters indicates the motion is chaotic. Thus a statistical modeling approach (similar to ensemble prediction for the atmosphere) would provide the most effective output metric to input into a navy tactical decision aid.

The three dimensional model takes a step in the correct direction. It allows prediction based on an entire set of dynamic equations. Although a first order solution it provides skillful fall velocity predictions and with further work will provide skillful impact angle predictions. These are the two critical parameters necessary to correctly predict the percentage mine burial for a given battlespace. An accurate percent burial and confidence represents the effective metrics answering the cry for “help” from the mine warfare community.

THIS PAGE INTENTIONALLY LEFT BLANK

APPENDIX A. MODEL AND EXPERIMENT DATA PLOTS

1. CARDEROCK DATA PLOTS

Index of blunt nosed mine shape drops conducted at NSWC, Carderock, MD, 10-14 Sep 2001; adapted from (Valent and Holland 2001). Subsequent pages contain the data plots for both the experimental data and the model output initialized from the Carderock mine drop experimental data, 42 plots, read top to bottom, left to right.

Vertical	Horizontal	45° Down Angle
2w-2	1w-1	17w-3
2w-3	1w-2	17w-4
2w-4	1w-3	17w-5
2w-6	1w-4	17w-6
12w-1	1w-5	20w-1
12w-2	1w-6	20w-2
12w-3	10w-6	20w-3
12w-5	11w-1	20w-5
12w-6	11w-2	20w-6
13w-1	11w-3	21w-1
13w-2	11w-4	21w-2
13w-3	11w-5	21w-3
13w-5	11w-6	21w-5
13w-6	17w-2	21w-6

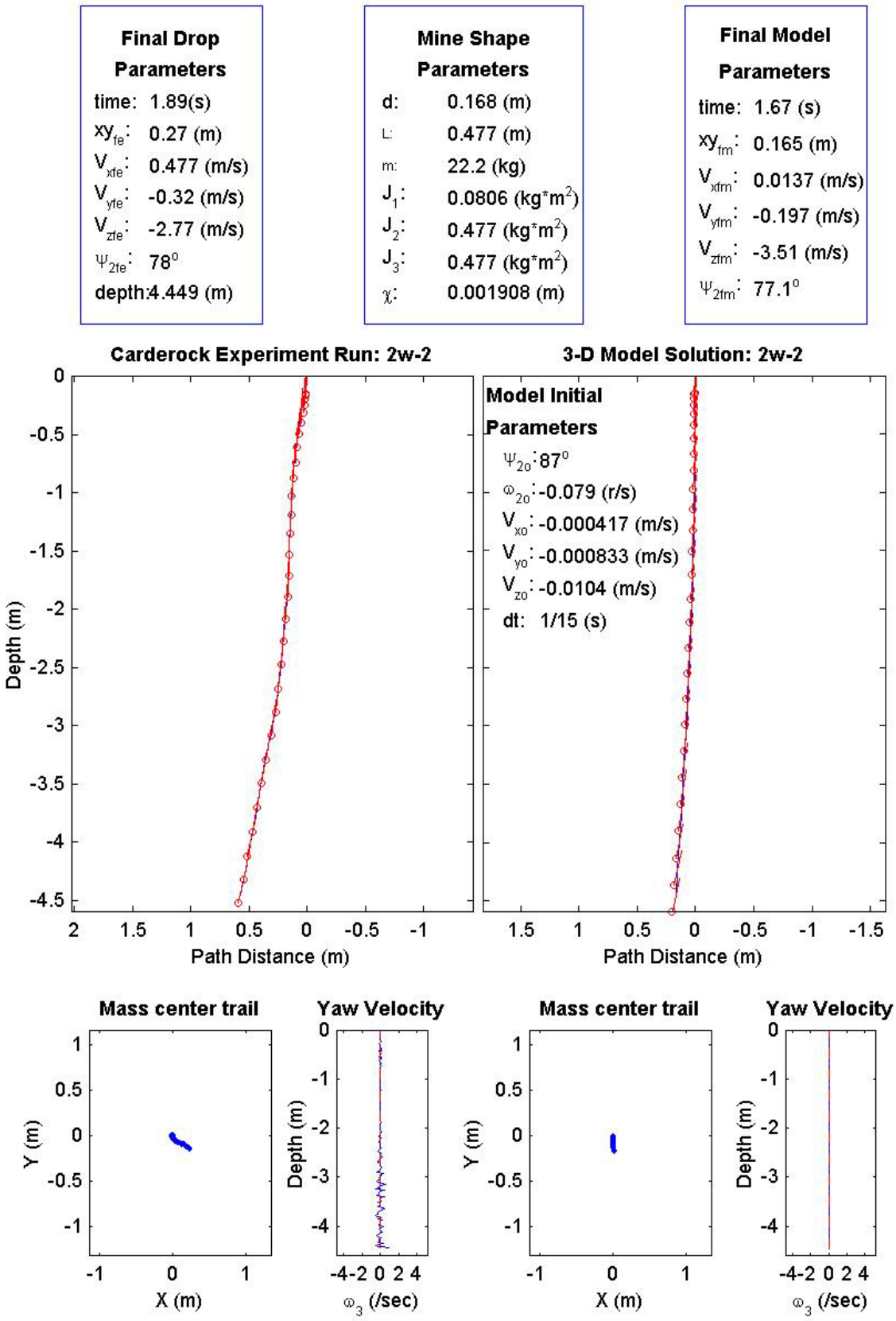
Final Drop Parameters
time: 1.89(s)
xy_fe: 0.27 (m)
V_xfe: 0.477 (m/s)
V_yfe: -0.32 (m/s)
V_zfe: -2.77 (m/s)
Ψ_2fe: 78°
depth:4.449 (m)
Mine Shape Parameters
d: 0.168 (m)
L: 0.477 (m)
m: 22.2 (kg)
J_1: 0.0806 (kg*m^2)
J_2: 0.477 (kg*m^2)
J_3: 0.477 (kg*m^2)
χ: 0.001908 (m)
Final Model Parameters
time: 1.67 (s)
xy_fm: 0.165 (m)
V_xfm: 0.0137 (m/s)
V_yfm: -0.197 (m/s)
V_zfm: -3.51 (m/s)
Ψ_2fm: 77.1°
Carderock Experiment Run: 2w-2
3-D Model Solution: 2w-2
Model Initial Parameters
Ψ_2o: 87°
ω_2o: -0.079 (r/s)
V_xo: -0.000417 (m/s)
V_yo: -0.000833 (m/s)
V_zo: -0.0104 (m/s)
dt: 1/15 (s)
Depth (m)
Path Distance (m)
Path Distance (m)
Mass center trail
Yaw Velocity
Mass center trail
Yaw Velocity
Y (m)
X (m)
Depth (m)
ω_3 (/sec)
Y (m)
X (m)
Depth (m)
ω_3 (/sec)

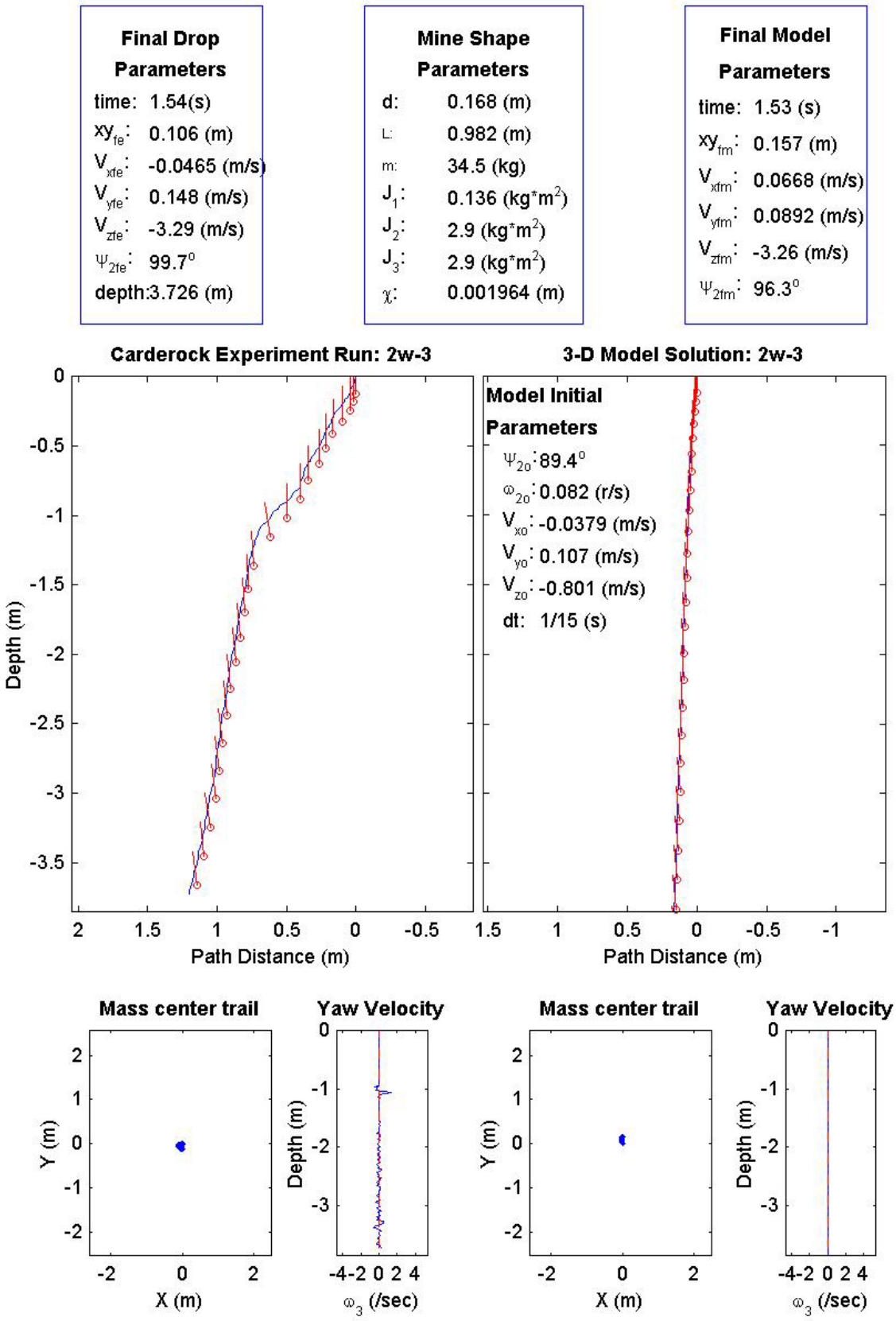
Final Drop Parameters
time: 1.54(s)
xy_fe: 0.106 (m)
V_xfe: -0.0465 (m/s)
V_yfe: 0.148 (m/s)
V_zfe: -3.29 (m/s)
Ψ_2fe: 99.7°
depth: 3.726 (m)
Mine Shape Parameters
d: 0.168 (m)
L: 0.982 (m)
m: 34.5 (kg)
J_1: 0.136 (kg*m^2)
J_2: 2.9 (kg*m^2)
J_3: 2.9 (kg*m^2)
χ: 0.001964 (m)
Final Model Parameters
time: 1.53 (s)
xy_fm: 0.157 (m)
V_xfm: 0.0668 (m/s)
V_yfm: 0.0892 (m/s)
V_zfm: -3.26 (m/s)
Ψ_2fm: 96.3°
Carderock Experiment Run: 2w-3
3-D Model Solution: 2w-3
Model Initial Parameters
Ψ_2o: 89.4°
ω_2o: 0.082 (r/s)
V_xo: -0.0379 (m/s)
V_yo: 0.107 (m/s)
V_zo: -0.801 (m/s)
dt: 1/15 (s)
Depth (m)
Path Distance (m)
Path Distance (m)
Mass center trail
Yaw Velocity
Mass center trail
Yaw Velocity
Y (m)
X (m)
Depth (m)
ω_3 (/sec)
Y (m)
X (m)
Depth (m)
ω_3 (/sec)

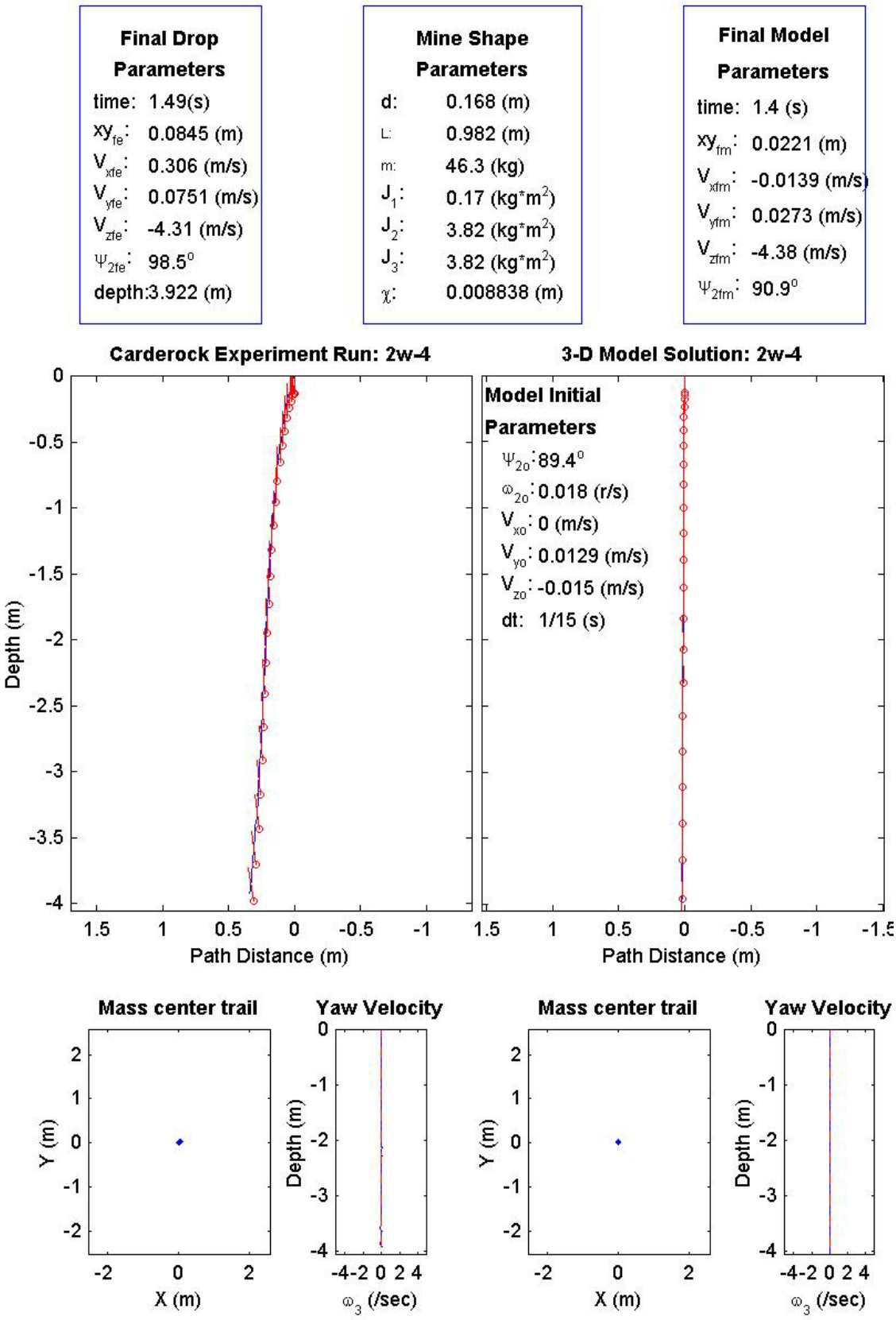
Final Drop Parameters
time: 1.49(s)
xy_fe: 0.0845 (m)
V_xfe: 0.306 (m/s)
V_yfe: 0.0751 (m/s)
V_zfe: -4.31 (m/s)
ψ_2fe: 98.5°
depth: 3.922 (m)
Mine Shape Parameters
d: 0.168 (m)
L: 0.982 (m)
m: 46.3 (kg)
J_1: 0.17 (kg*m^2)
J_2: 3.82 (kg*m^2)
J_3: 3.82 (kg*m^2)
χ: 0.008838 (m)
Final Model Parameters
time: 1.4 (s)
xy_fm: 0.0221 (m)
V_xfm: -0.0139 (m/s)
V_yfm: 0.0273 (m/s)
V_zfm: -4.38 (m/s)
ψ_2fm: 90.9°
Carderock Experiment Run: 2w-4
3-D Model Solution: 2w-4
Model Initial Parameters
ψ_2o: 89.4°
ω_2o: 0.018 (r/s)
V_xo: 0 (m/s)
V_yo: 0.0129 (m/s)
V_zo: -0.015 (m/s)
dt: 1/15 (s)
Depth (m)
Path Distance (m)
Path Distance (m)
Mass center trail
Yaw Velocity
Mass center trail
Yaw Velocity
Y (m)
X (m)
Depth (m)
ω_3 (/sec)
Y (m)
X (m)
Depth (m)
ω_3 (/sec)

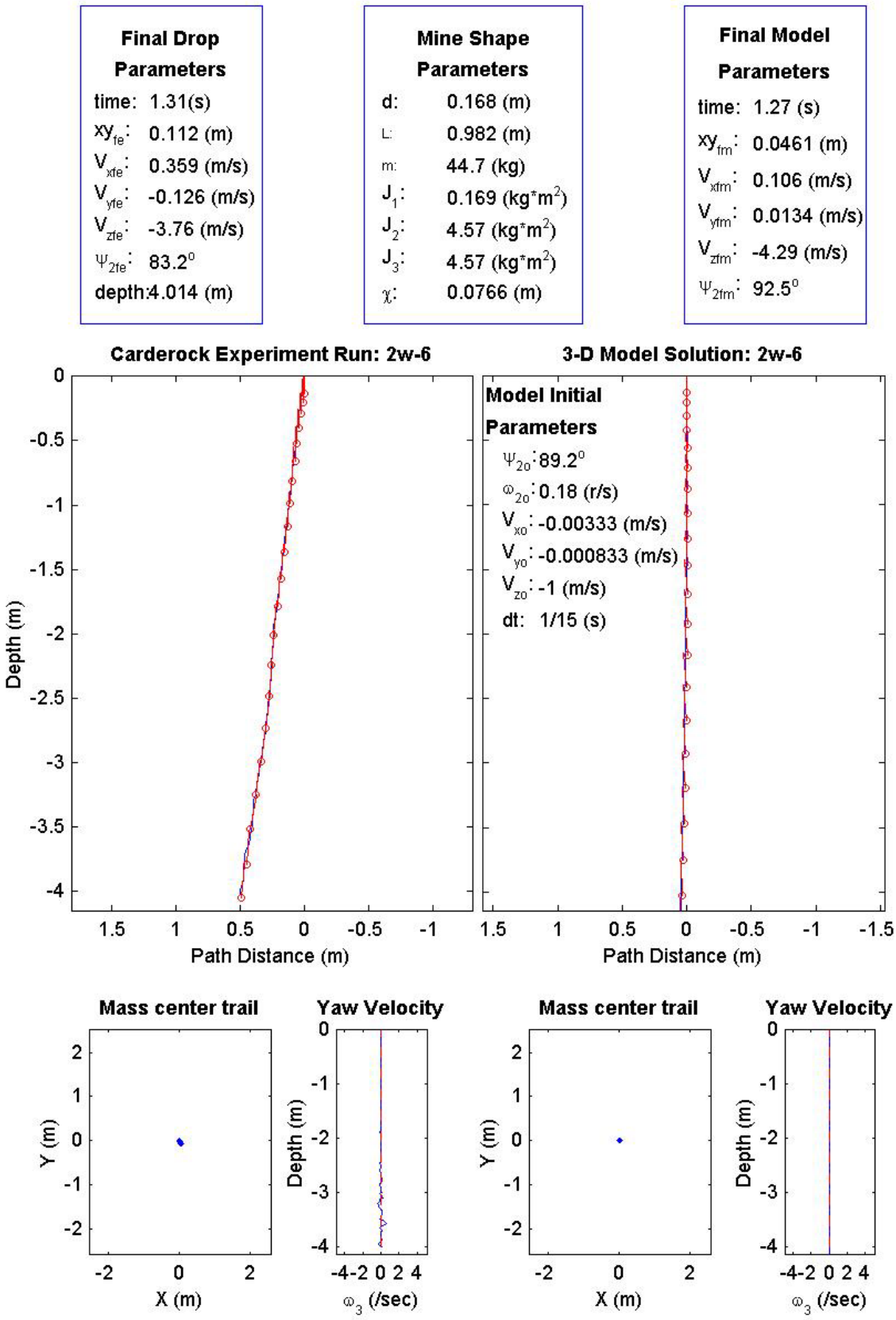
Final Drop Parameters
time: 1.31(s)
xy_fe: 0.112 (m)
V_xfe: 0.359 (m/s)
V_yfe: -0.126 (m/s)
V_zfe: -3.76 (m/s)
ψ_2fe: 83.2°
depth:4.014 (m)
Mine Shape Parameters
d: 0.168 (m)
L: 0.982 (m)
m: 44.7 (kg)
J_1: 0.169 (kg*m^2)
J_2: 4.57 (kg*m^2)
J_3: 4.57 (kg*m^2)
χ: 0.0766 (m)
Final Model Parameters
time: 1.27 (s)
xy_fm: 0.0461 (m)
V_xfm: 0.106 (m/s)
V_yfm: 0.0134 (m/s)
V_zfm: -4.29 (m/s)
ψ_2fm: 92.5°
Carderock Experiment Run: 2w-6
3-D Model Solution: 2w-6
Model Initial Parameters
ψ_2o: 89.2°
ω_2o: 0.18 (r/s)
V_xo: -0.00333 (m/s)
V_yo: -0.000833 (m/s)
V_zo: -1 (m/s)
dt: 1/15 (s)
Depth (m)
Path Distance (m)
Mass center trail
Yaw Velocity
Y (m)
X (m)
ω_3 (/sec)

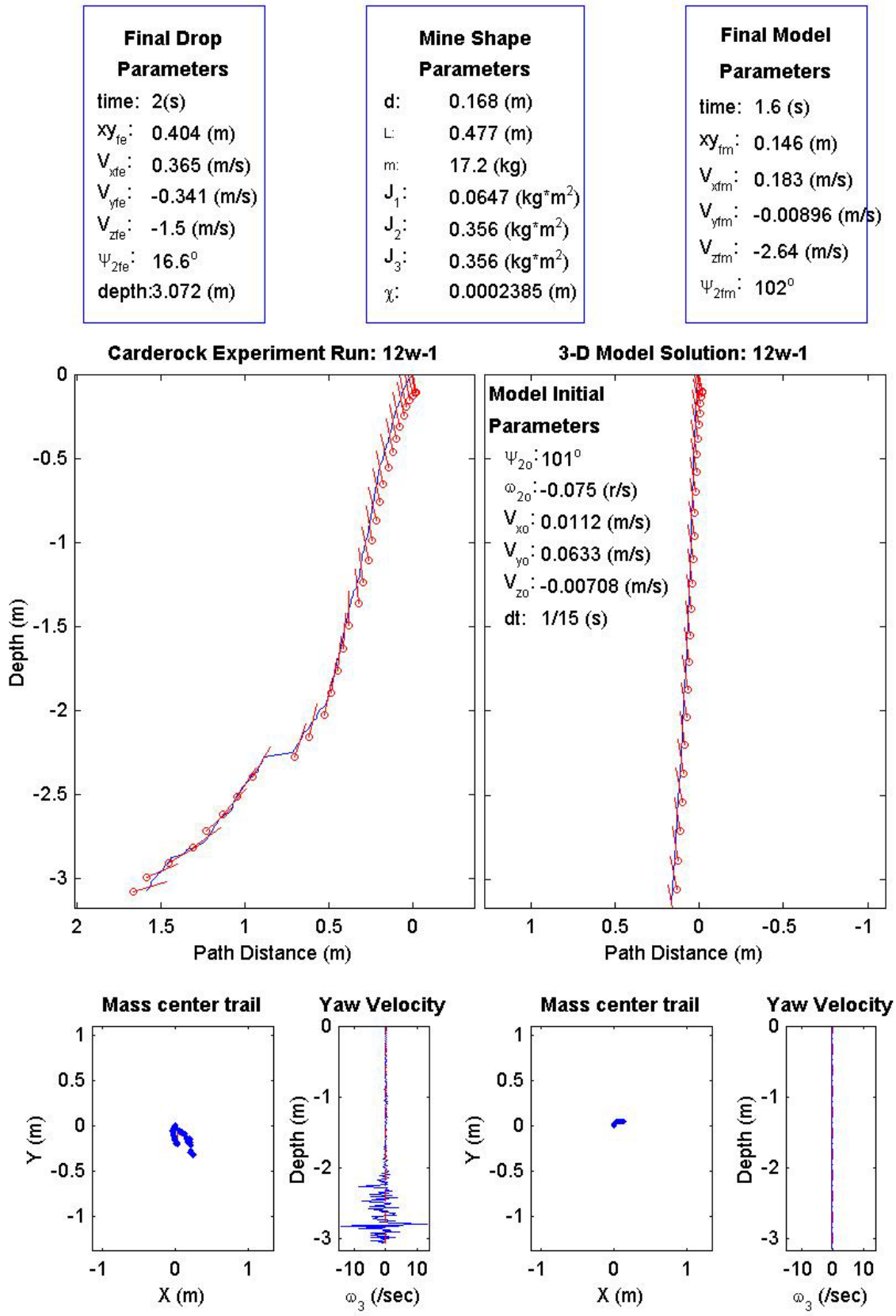
Final Drop Parameters
time: 2(s)
xy_fe: 0.404 (m)
V_xfe: 0.365 (m/s)
V_yfe: -0.341 (m/s)
V_zfe: -1.5 (m/s)
Ψ_2fe: 16.6°
depth:3.072 (m)
Mine Shape Parameters
d: 0.168 (m)
L: 0.477 (m)
m: 17.2 (kg)
J_1: 0.0647 (kg*m^2)
J_2: 0.356 (kg*m^2)
J_3: 0.356 (kg*m^2)
χ: 0.0002385 (m)
Final Model Parameters
time: 1.6 (s)
xy_fm: 0.146 (m)
V_xfm: 0.183 (m/s)
V_yfm: -0.00896 (m/s)
V_zfm: -2.64 (m/s)
Ψ_2fm: 102°
Carderock Experiment Run: 12w-1
3-D Model Solution: 12w-1
Model Initial Parameters
Ψ_2o: 101°
ω_2o: -0.075 (r/s)
V_xo: 0.0112 (m/s)
V_yo: 0.0633 (m/s)
V_zo: -0.00708 (m/s)
dt: 1/15 (s)
Depth (m)
Path Distance (m)
Path Distance (m)
Mass center trail
Yaw Velocity
Mass center trail
Yaw Velocity
Y (m)
X (m)
Depth (m)
ω_3 (/sec)
Y (m)
X (m)
Depth (m)
ω_3 (/sec)

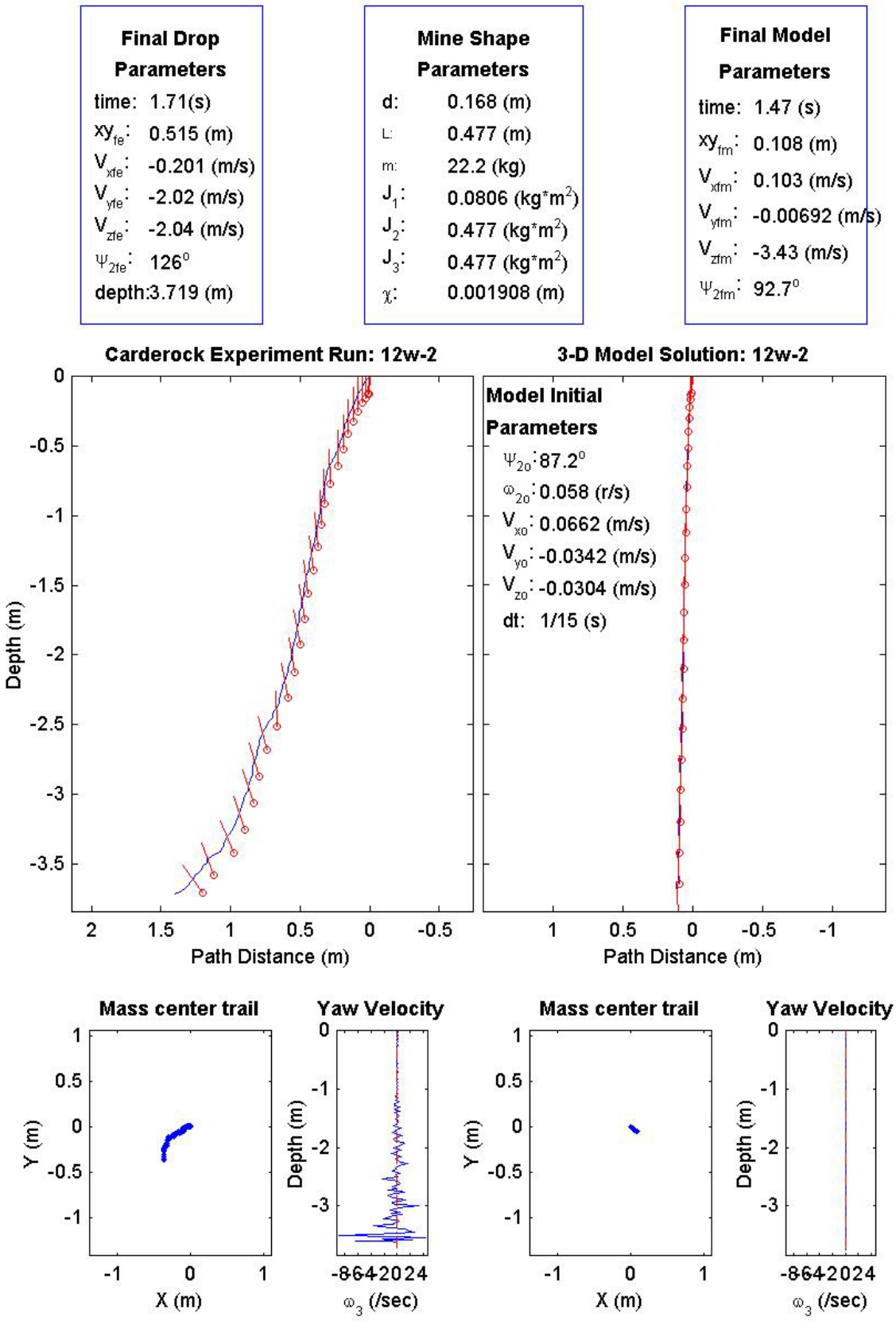
Final Drop Parameters
time: 1.71(s)
xy_fe: 0.515 (m)
V_xfe: -0.201 (m/s)
V_yfe: -2.02 (m/s)
V_zfe: -2.04 (m/s)
ψ_2fe: 126°
depth:3.719 (m)
Mine Shape Parameters
d: 0.168 (m)
L: 0.477 (m)
m: 22.2 (kg)
J_1: 0.0806 (kg*m^2)
J_2: 0.477 (kg*m^2)
J_3: 0.477 (kg*m^2)
χ: 0.001908 (m)
Final Model Parameters
time: 1.47 (s)
xy_fm: 0.108 (m)
V_xfm: 0.103 (m/s)
V_yfm: -0.00692 (m/s)
V_zfm: -3.43 (m/s)
ψ_2fm: 92.7°
Carderock Experiment Run: 12w-2
3-D Model Solution: 12w-2
Model Initial Parameters
ψ_2o: 87.2°
ω_2o: 0.058 (r/s)
V_xo: 0.0662 (m/s)
V_yo: -0.0342 (m/s)
V_zo: -0.0304 (m/s)
dt: 1/15 (s)
Depth (m)
Path Distance (m)
Path Distance (m)
Mass center trail
Yaw Velocity
Mass center trail
Yaw Velocity
Y (m)
X (m)
Depth (m)
ω_3 (/sec)
Y (m)
X (m)
Depth (m)
ω_3 (/sec)

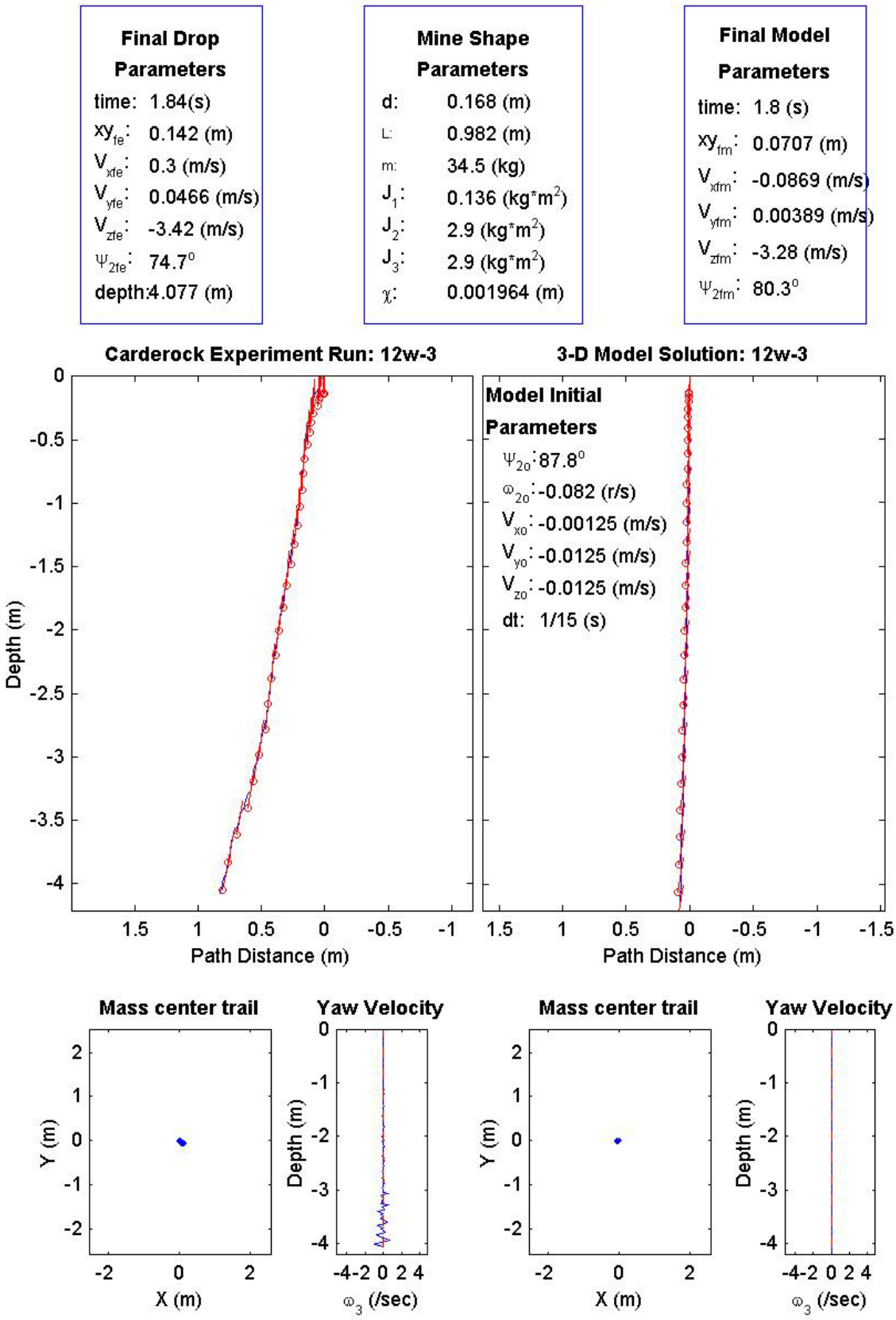
Final Drop Parameters
time: 1.84(s)
xy_fe: 0.142 (m)
V_xfe: 0.3 (m/s)
V_yfe: 0.0466 (m/s)
V_zfe: -3.42 (m/s)
Ψ_2fe: 74.7°
depth: 4.077 (m)
Mine Shape Parameters
d: 0.168 (m)
L: 0.982 (m)
m: 34.5 (kg)
J_1: 0.136 (kg*m^2)
J_2: 2.9 (kg*m^2)
J_3: 2.9 (kg*m^2)
χ: 0.001964 (m)
Final Model Parameters
time: 1.8 (s)
xy_fm: 0.0707 (m)
V_xfm: -0.0869 (m/s)
V_yfm: 0.00389 (m/s)
V_zfm: -3.28 (m/s)
Ψ_2fm: 80.3°
Carderock Experiment Run: 12w-3
3-D Model Solution: 12w-3
Model Initial Parameters
Ψ_2o: 87.8°
ω_2o: -0.082 (r/s)
V_xo: -0.00125 (m/s)
V_yo: -0.0125 (m/s)
V_zo: -0.0125 (m/s)
dt: 1/15 (s)
Depth (m)
Path Distance (m)
Path Distance (m)
Mass center trail
Yaw Velocity
Mass center trail
Yaw Velocity
Y (m)
X (m)
Depth (m)
ω_3 (/sec)
Y (m)
X (m)
Depth (m)
ω_3 (/sec)

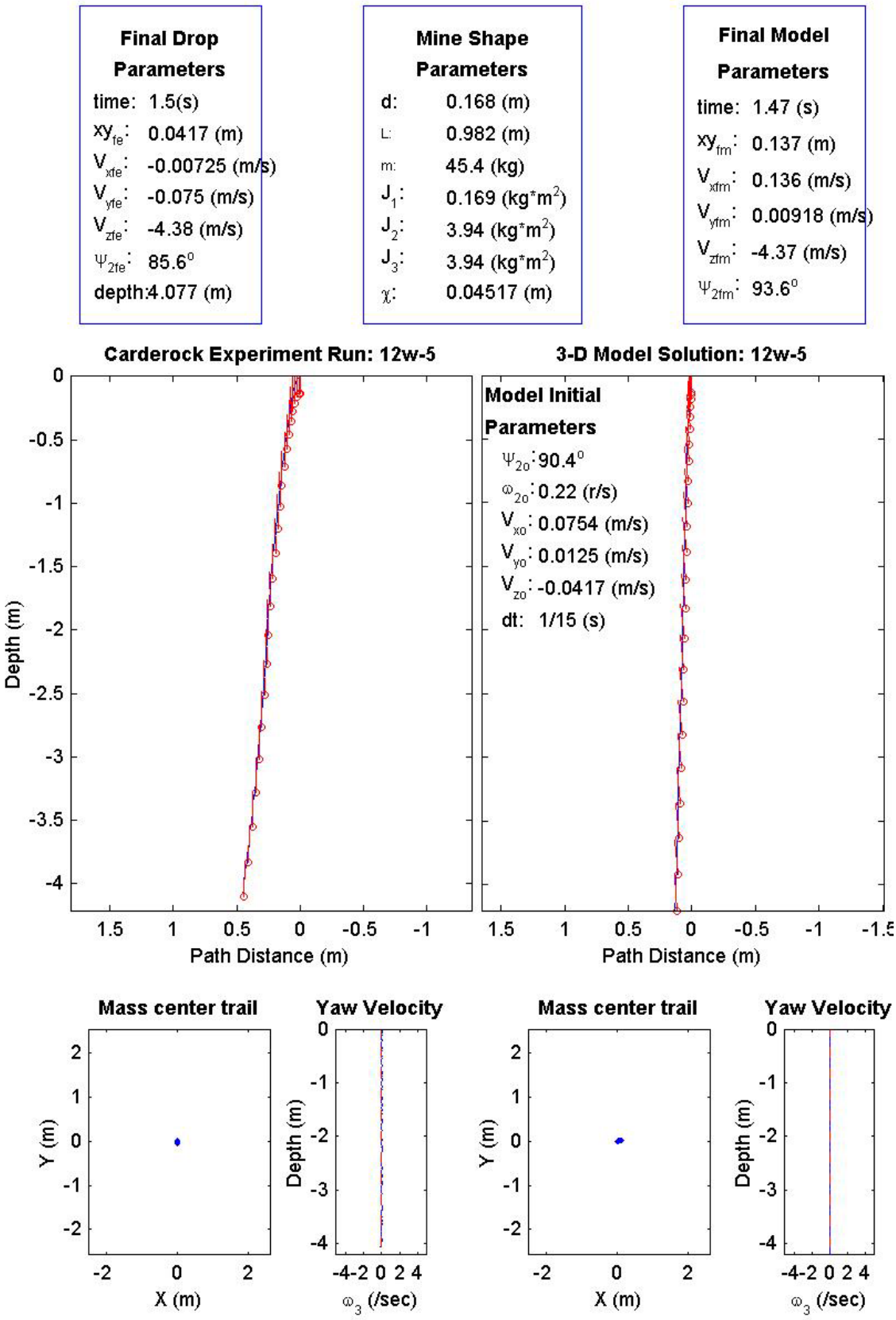
Final Drop Parameters
time: 1.5(s)
xy_fe: 0.0417 (m)
V_xfe: -0.00725 (m/s)
V_yfe: -0.075 (m/s)
V_zfe: -4.38 (m/s)
ψ_2fe: 85.6°
depth: 4.077 (m)
Mine Shape Parameters
d: 0.168 (m)
L: 0.982 (m)
m: 45.4 (kg)
J_1: 0.169 (kg*m^2)
J_2: 3.94 (kg*m^2)
J_3: 3.94 (kg*m^2)
χ: 0.04517 (m)
Final Model Parameters
time: 1.47 (s)
xy_fm: 0.137 (m)
V_xfm: 0.136 (m/s)
V_yfm: 0.00918 (m/s)
V_zfm: -4.37 (m/s)
ψ_2fm: 93.6°
Carderock Experiment Run: 12w-5
3-D Model Solution: 12w-5
Model Initial Parameters
ψ_2o: 90.4°
ω_2o: 0.22 (r/s)
V_xo: 0.0754 (m/s)
V_yo: 0.0125 (m/s)
V_zo: -0.0417 (m/s)
dt: 1/15 (s)
Depth (m)
Path Distance (m)
Mass center trail
Yaw Velocity
Y (m)
X (m)
ω_3 (/sec)

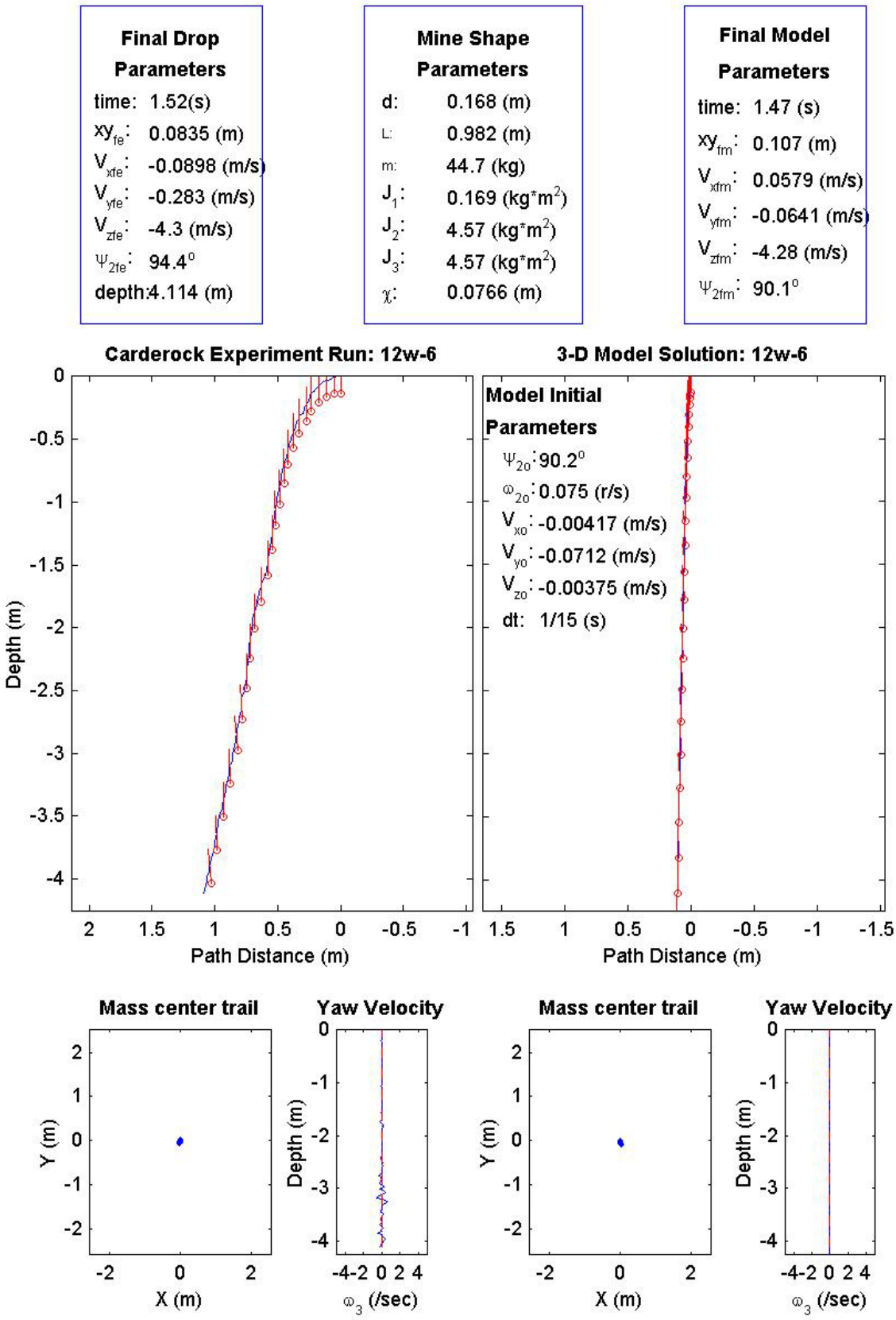
Final Drop Parameters
time: 1.52(s)
xy_fe: 0.0835 (m)
V_xfe: -0.0898 (m/s)
V_yfe: -0.283 (m/s)
V_zfe: -4.3 (m/s)
ψ_2fe: 94.4°
depth: 4.114 (m)
Mine Shape Parameters
d: 0.168 (m)
L: 0.982 (m)
m: 44.7 (kg)
J_1: 0.169 (kg*m^2)
J_2: 4.57 (kg*m^2)
J_3: 4.57 (kg*m^2)
χ: 0.0766 (m)
Final Model Parameters
time: 1.47 (s)
xy_fm: 0.107 (m)
V_xfm: 0.0579 (m/s)
V_yfm: -0.0641 (m/s)
V_zfm: -4.28 (m/s)
ψ_2fm: 90.1°
Carderock Experiment Run: 12w-6
3-D Model Solution: 12w-6
Model Initial Parameters
ψ_2o: 90.2°
ω_2o: 0.075 (r/s)
V_xo: -0.00417 (m/s)
V_yo: -0.0712 (m/s)
V_zo: -0.00375 (m/s)
dt: 1/15 (s)
Depth (m)
Path Distance (m)
Path Distance (m)
Mass center trail
Yaw Velocity
Mass center trail
Yaw Velocity
Y (m)
X (m)
Depth (m)
ω_3 (/sec)
Y (m)
X (m)
Depth (m)
ω_3 (/sec)

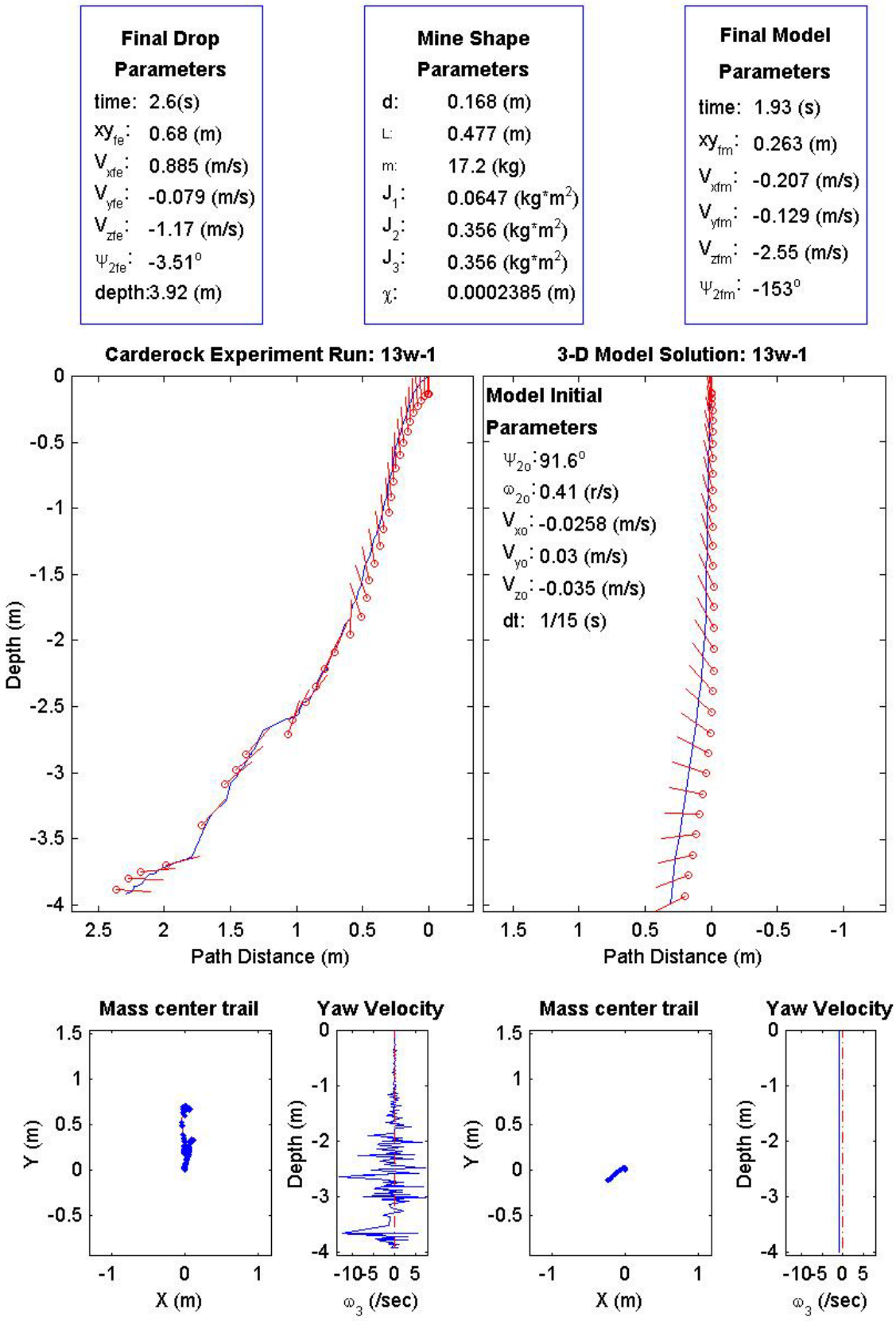
Final Drop Parameters
time: 2.6(s)
xy_fe: 0.68 (m)
V_xfe: 0.885 (m/s)
V_yfe: -0.079 (m/s)
V_zfe: -1.17 (m/s)
Ψ_2fe: -3.51°
depth:3.92 (m)
Mine Shape Parameters
d: 0.168 (m)
L: 0.477 (m)
m: 17.2 (kg)
J_1: 0.0647 (kg*m^2)
J_2: 0.356 (kg*m^2)
J_3: 0.356 (kg*m^2)
χ: 0.0002385 (m)
Final Model Parameters
time: 1.93 (s)
xy_fm: 0.263 (m)
V_xfm: -0.207 (m/s)
V_yfm: -0.129 (m/s)
V_zfm: -2.55 (m/s)
Ψ_2fm: -153°
Carderock Experiment Run: 13w-1
3-D Model Solution: 13w-1
Model Initial Parameters
Ψ_2o: 91.6°
ω_2o: 0.41 (r/s)
V_xo: -0.0258 (m/s)
V_yo: 0.03 (m/s)
V_zo: -0.035 (m/s)
dt: 1/15 (s)
Depth (m)
Path Distance (m)
Path Distance (m)
Mass center trail
Yaw Velocity
Mass center trail
Yaw Velocity
Y (m)
X (m)
Depth (m)
ω_3 (/sec)
Y (m)
X (m)
Depth (m)
ω_3 (/sec)

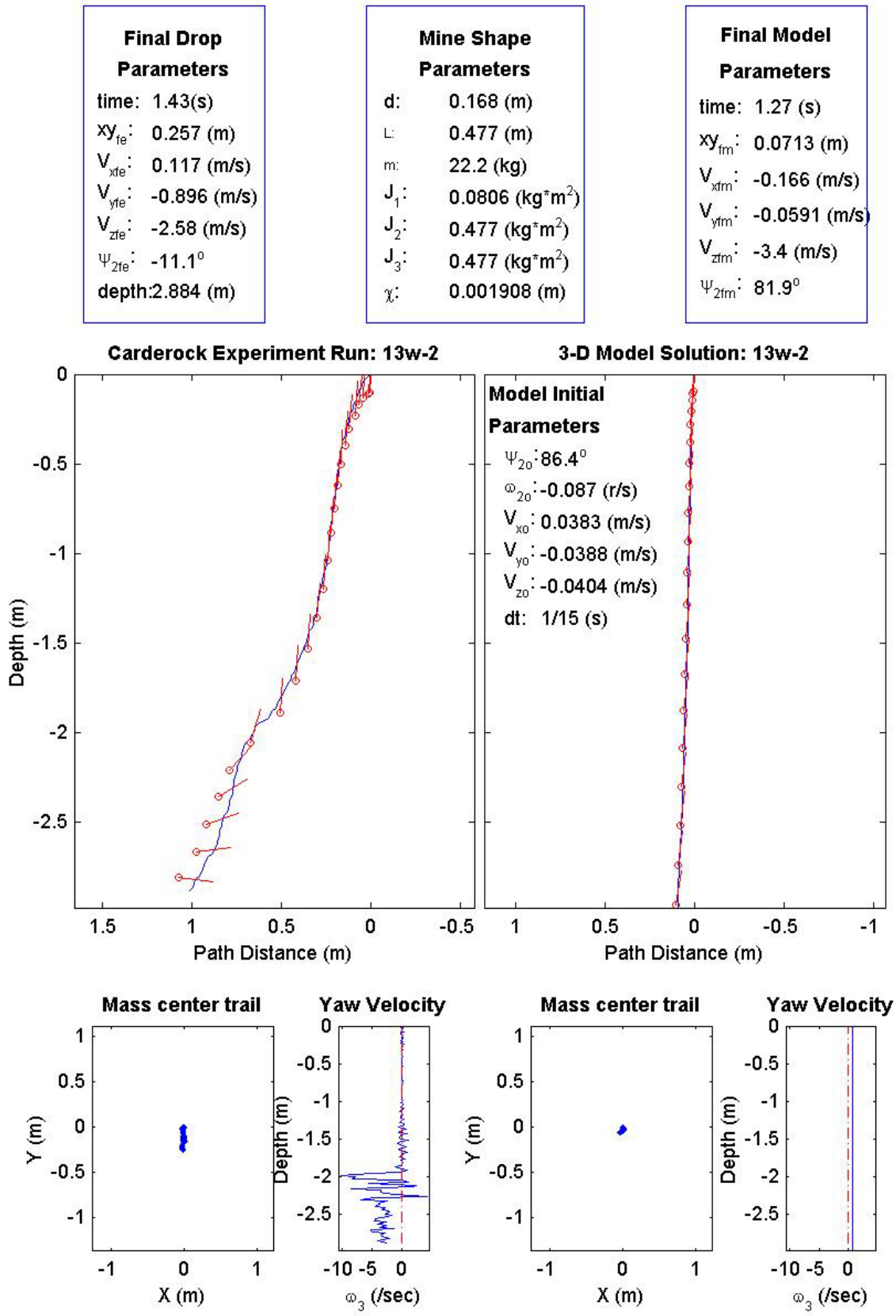
Final Drop Parameters
time: 1.43(s)
xy_fe: 0.257 (m)
V_xfe: 0.117 (m/s)
V_yfe: -0.896 (m/s)
V_zfe: -2.58 (m/s)
Ψ_2fe: -11.1°
depth:2.884 (m)
Mine Shape Parameters
d: 0.168 (m)
L: 0.477 (m)
m: 22.2 (kg)
J_1: 0.0806 (kg*m^2)
J_2: 0.477 (kg*m^2)
J_3: 0.477 (kg*m^2)
χ: 0.001908 (m)
Final Model Parameters
time: 1.27 (s)
xy_fm: 0.0713 (m)
V_xfm: -0.166 (m/s)
V_yfm: -0.0591 (m/s)
V_zfm: -3.4 (m/s)
Ψ_2fm: 81.9°
Carderock Experiment Run: 13w-2
3-D Model Solution: 13w-2
Model Initial Parameters
Ψ_2o: 86.4°
ω_2o: -0.087 (r/s)
V_xo: 0.0383 (m/s)
V_yo: -0.0388 (m/s)
V_zo: -0.0404 (m/s)
dt: 1/15 (s)
Depth (m)
Path Distance (m)
Path Distance (m)
Mass center trail
Yaw Velocity
Mass center trail
Yaw Velocity
Y (m)
X (m)
Depth (m)
ω_3 (/sec)
Y (m)
X (m)
Depth (m)
ω_3 (/sec)

Final Drop Parameters

time: 1.88(s)
xy_{fe}: 0.14 (m)
V_{xfe}: -0.112 (m/s)
V_{yfe}: 0.635 (m/s)
V_{zfe}: -3.32 (m/s)
Ψ_{2fe}: 81.2°
depth: 4.307 (m)

Mine Shape Parameters

d: 0.168 (m)
L: 0.982 (m)
m: 34.5 (kg)
J_1: 0.136 (kg*m^2)
J_2: 2.9 (kg*m^2)
J_3: 2.9 (kg*m^2)
χ: 0.001964 (m)

Final Model Parameters

time: 1.87 (s)
xy_{fm}: 0.187 (m)
V_{xfm}: 0.0815 (m/s)
V_{yfm}: 0.175 (m/s)
V_{zfm}: -3.26 (m/s)
Ψ_{2fm}: 111°

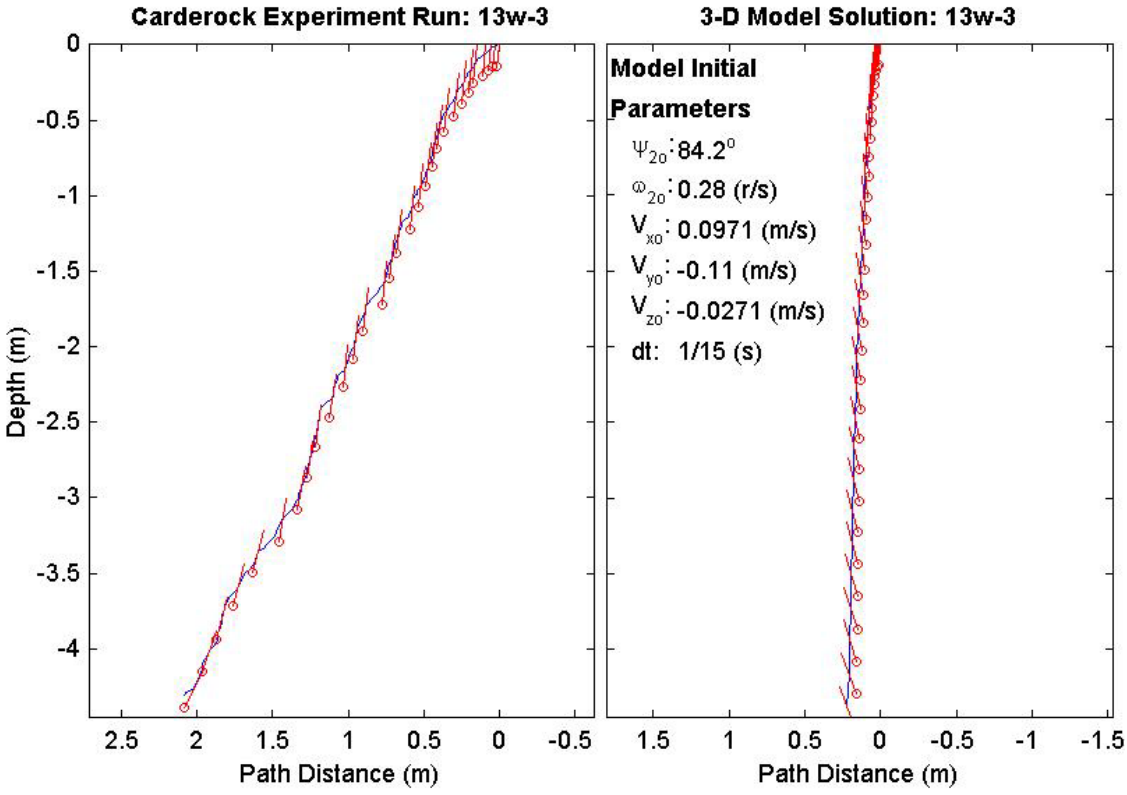

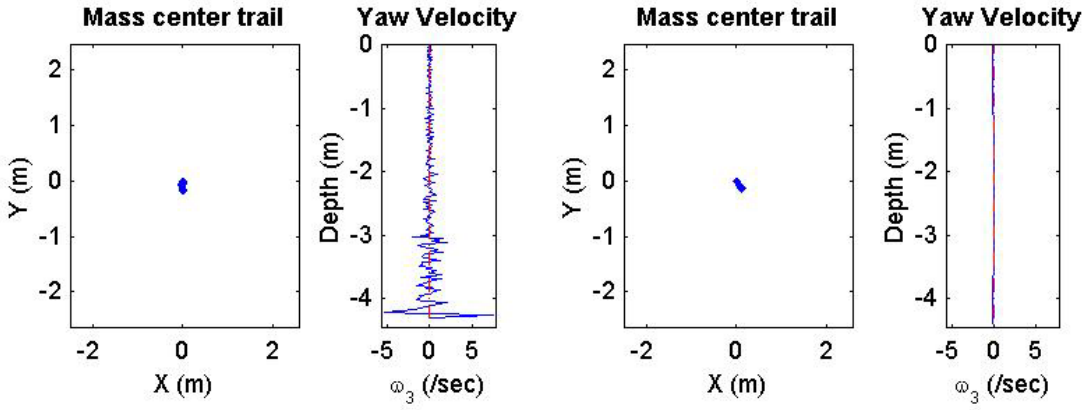

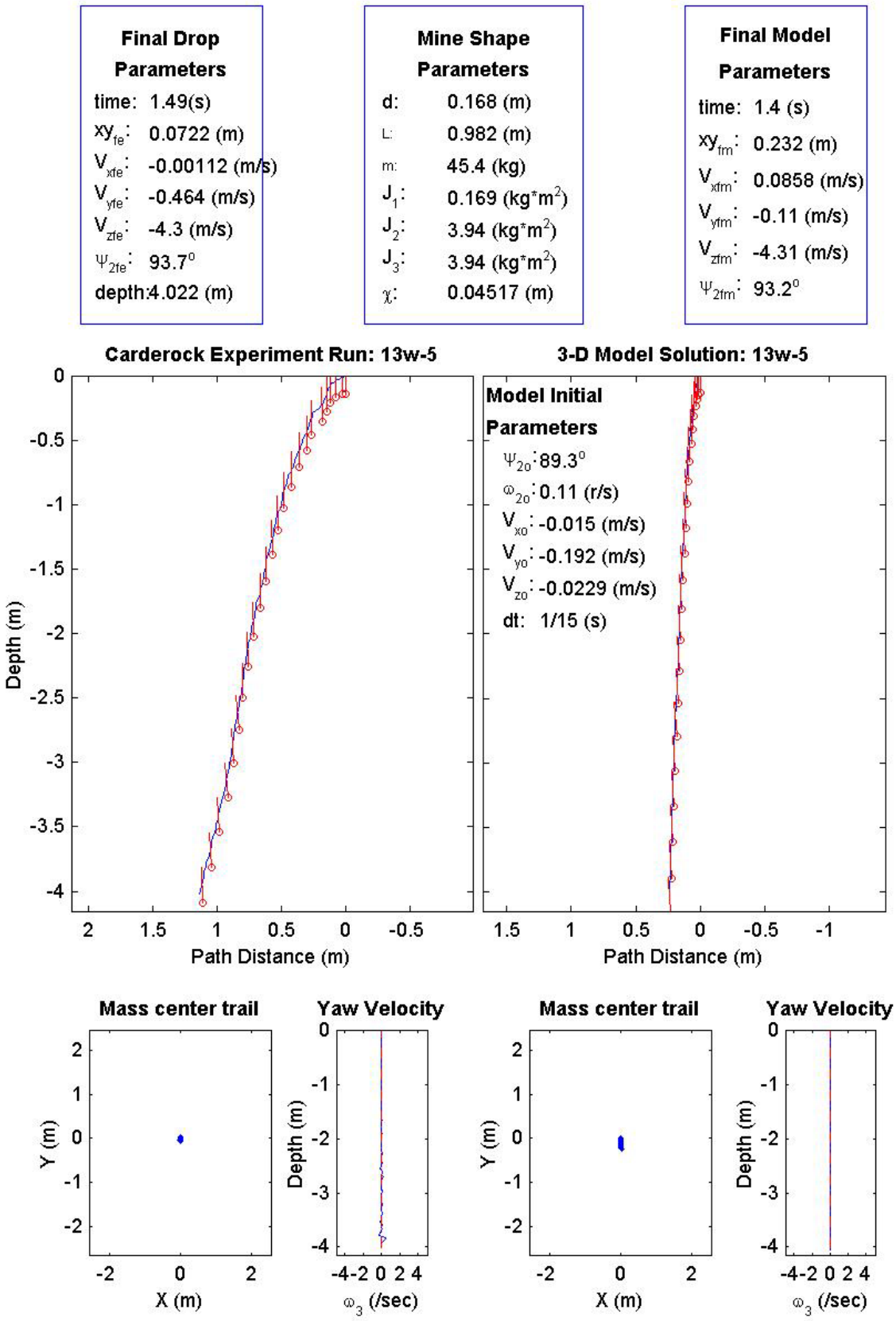
Final Drop Parameters
time: 1.49(s)
xy_fe: 0.0722 (m)
V_xfe: -0.00112 (m/s)
V_yfe: -0.464 (m/s)
V_zfe: -4.3 (m/s)
ψ_2fe: 93.7°
depth: 4.022 (m)
Mine Shape Parameters
d: 0.168 (m)
L: 0.982 (m)
m: 45.4 (kg)
J_1: 0.169 (kg*m^2)
J_2: 3.94 (kg*m^2)
J_3: 3.94 (kg*m^2)
χ: 0.04517 (m)
Final Model Parameters
time: 1.4 (s)
xy_fm: 0.232 (m)
V_xfm: 0.0858 (m/s)
V_yfm: -0.11 (m/s)
V_zfm: -4.31 (m/s)
ψ_2fm: 93.2°
Carderock Experiment Run: 13w-5
3-D Model Solution: 13w-5
Model Initial Parameters
ψ_2o: 89.3°
ω_2o: 0.11 (r/s)
V_xo: -0.015 (m/s)
V_yo: -0.192 (m/s)
V_zo: -0.0229 (m/s)
dt: 1/15 (s)
Depth (m)
Path Distance (m)
Path Distance (m)
Mass center trail
Yaw Velocity
Mass center trail
Yaw Velocity
Y (m)
X (m)
Depth (m)
ω_3 (/sec)
Y (m)
X (m)
Depth (m)
ω_3 (/sec)

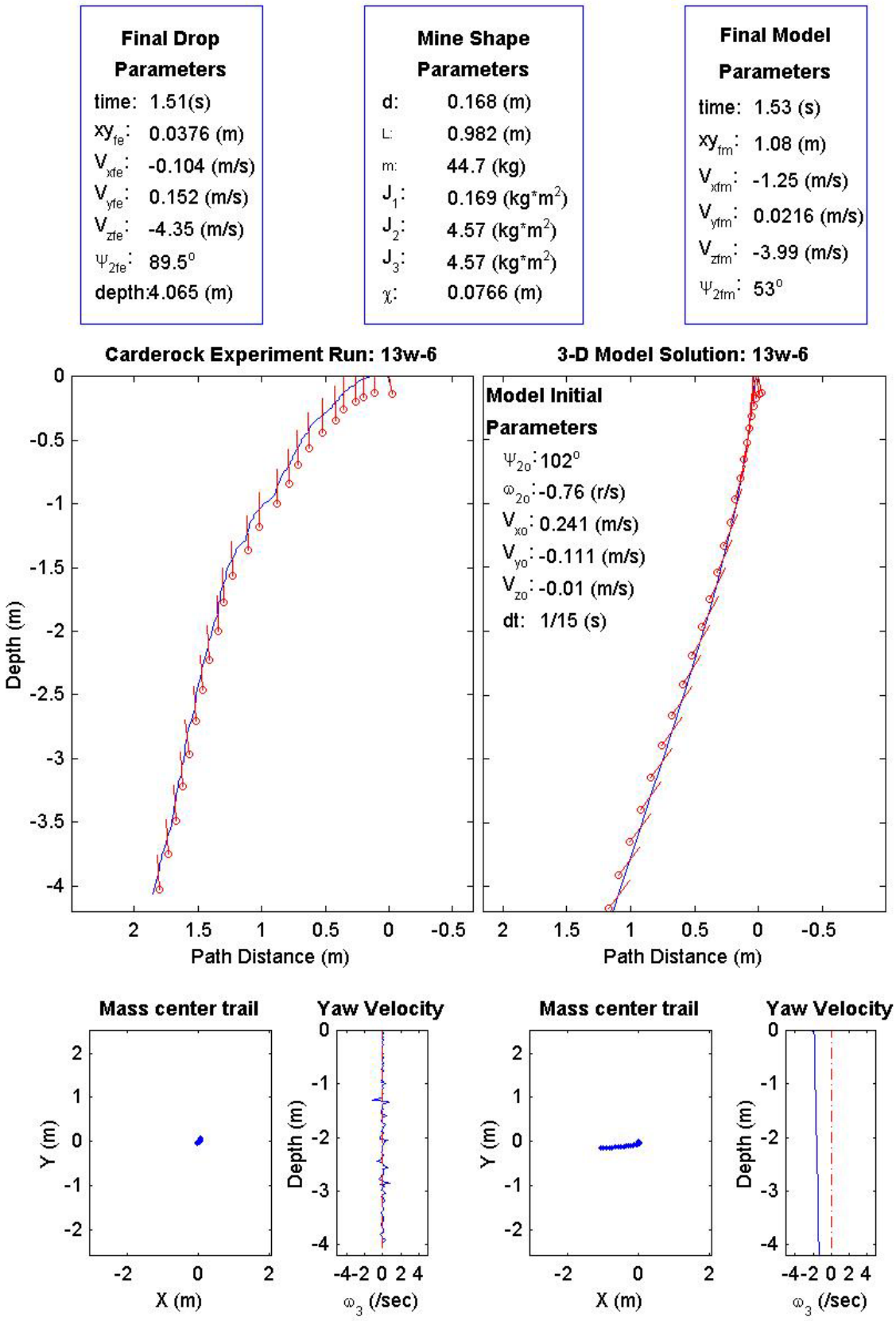
Final Drop Parameters
time: 1.51(s)
xy_fe: 0.0376 (m)
V_xfe: -0.104 (m/s)
V_yfe: 0.152 (m/s)
V_zfe: -4.35 (m/s)
ψ_2fe: 89.5°
depth: 4.065 (m)
Mine Shape Parameters
d: 0.168 (m)
L: 0.982 (m)
m: 44.7 (kg)
J_1: 0.169 (kg*m^2)
J_2: 4.57 (kg*m^2)
J_3: 4.57 (kg*m^2)
χ: 0.0766 (m)
Final Model Parameters
time: 1.53 (s)
xy_fm: 1.08 (m)
V_xfm: -1.25 (m/s)
V_yfm: 0.0216 (m/s)
V_zfm: -3.99 (m/s)
ψ_2fm: 53°
Carderock Experiment Run: 13w-6
3-D Model Solution: 13w-6
Model Initial Parameters
ψ_2o: 102°
ω_2o: -0.76 (r/s)
V_xo: 0.241 (m/s)
V_yo: -0.111 (m/s)
V_zo: -0.01 (m/s)
dt: 1/15 (s)
Depth (m)
Path Distance (m)
Mass center trail
Yaw Velocity
Y (m)
X (m)
ω_3 (/sec)

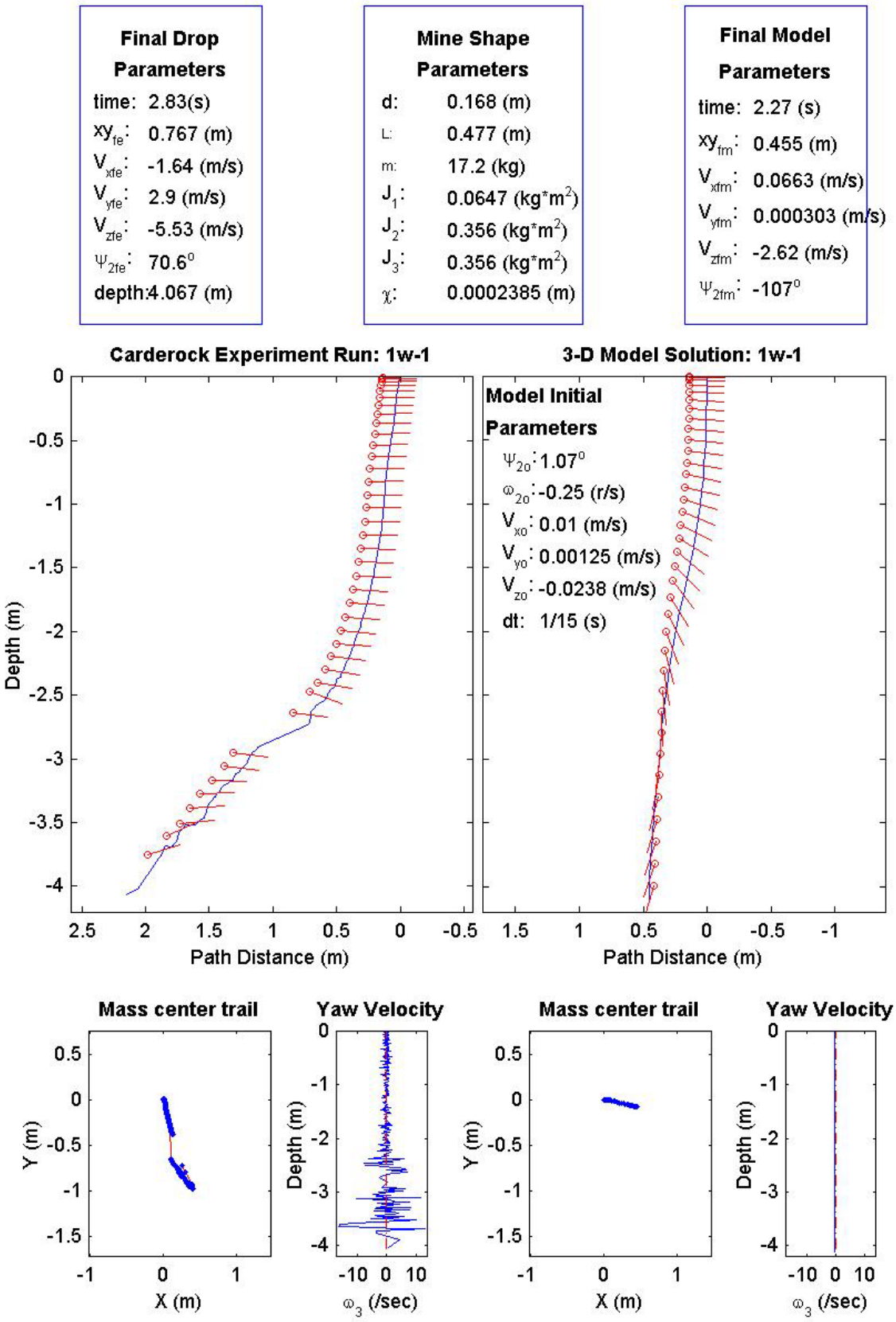
Final Drop Parameters
time: 2.83(s)
xy_fe: 0.767 (m)
V_xfe: -1.64 (m/s)
V_yfe: 2.9 (m/s)
V_zfe: -5.53 (m/s)
ψ_2fe: 70.6°
depth: 4.067 (m)
Mine Shape Parameters
d: 0.168 (m)
L: 0.477 (m)
m: 17.2 (kg)
J_1: 0.0647 (kg*m^2)
J_2: 0.356 (kg*m^2)
J_3: 0.356 (kg*m^2)
χ: 0.0002385 (m)
Final Model Parameters
time: 2.27 (s)
xy_fm: 0.455 (m)
V_xfm: 0.0663 (m/s)
V_yfm: 0.000303 (m/s)
V_zfm: -2.62 (m/s)
ψ_2fm: -107°
Carderock Experiment Run: 1w-1
3-D Model Solution: 1w-1
Model Initial Parameters
ψ_2o: 1.07°
ω_2o: -0.25 (r/s)
V_xo: 0.01 (m/s)
V_yo: 0.00125 (m/s)
V_zo: -0.0238 (m/s)
dt: 1/15 (s)
Depth (m)
Path Distance (m)
Path Distance (m)
Mass center trail
Yaw Velocity
Mass center trail
Yaw Velocity
Y (m)
X (m)
Depth (m)
ω_3 (/sec)
Y (m)
X (m)
Depth (m)
ω_3 (/sec)

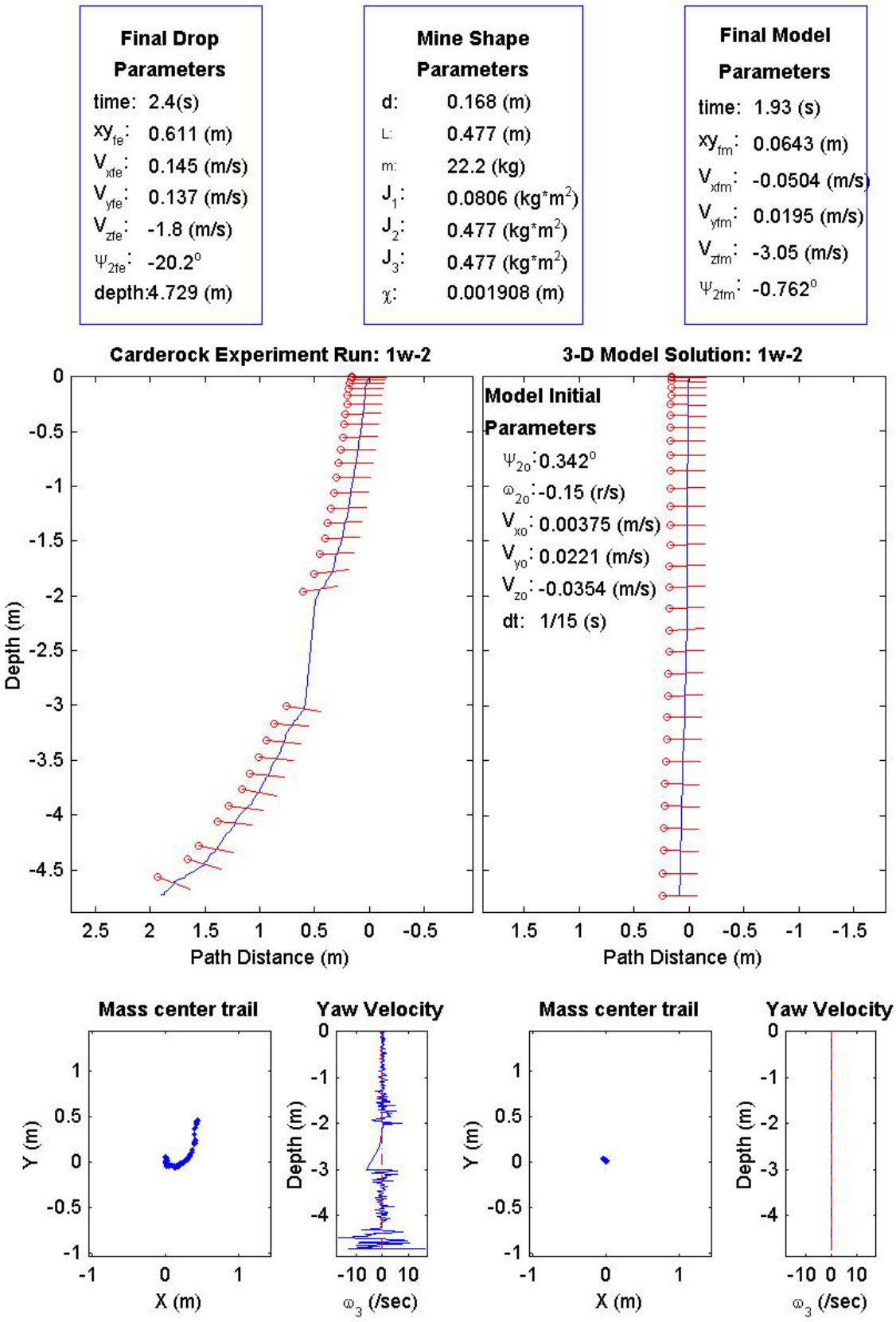
Final Drop Parameters
time: 2.4(s)
xy_fe: 0.611 (m)
V_xfe: 0.145 (m/s)
V_yfe: 0.137 (m/s)
V_zfe: -1.8 (m/s)
Ψ_2fe: -20.2°
depth:4.729 (m)
Mine Shape Parameters
d: 0.168 (m)
L: 0.477 (m)
m: 22.2 (kg)
J_1: 0.0806 (kg*m^2)
J_2: 0.477 (kg*m^2)
J_3: 0.477 (kg*m^2)
χ: 0.001908 (m)
Final Model Parameters
time: 1.93 (s)
xy_fm: 0.0643 (m)
V_xfm: -0.0504 (m/s)
V_yfm: 0.0195 (m/s)
V_zfm: -3.05 (m/s)
Ψ_2fm: -0.762°
Carderock Experiment Run: 1w-2
3-D Model Solution: 1w-2
Model Initial Parameters
Ψ_2o: 0.342°
ω_2o: -0.15 (r/s)
V_xo: 0.00375 (m/s)
V_yo: 0.0221 (m/s)
V_zo: -0.0354 (m/s)
dt: 1/15 (s)
Depth (m)
Path Distance (m)
Path Distance (m)
Mass center trail
Yaw Velocity
Mass center trail
Yaw Velocity
Y (m)
X (m)
Depth (m)
ω_3 (/sec)
Y (m)
X (m)
Depth (m)
ω_3 (/sec)

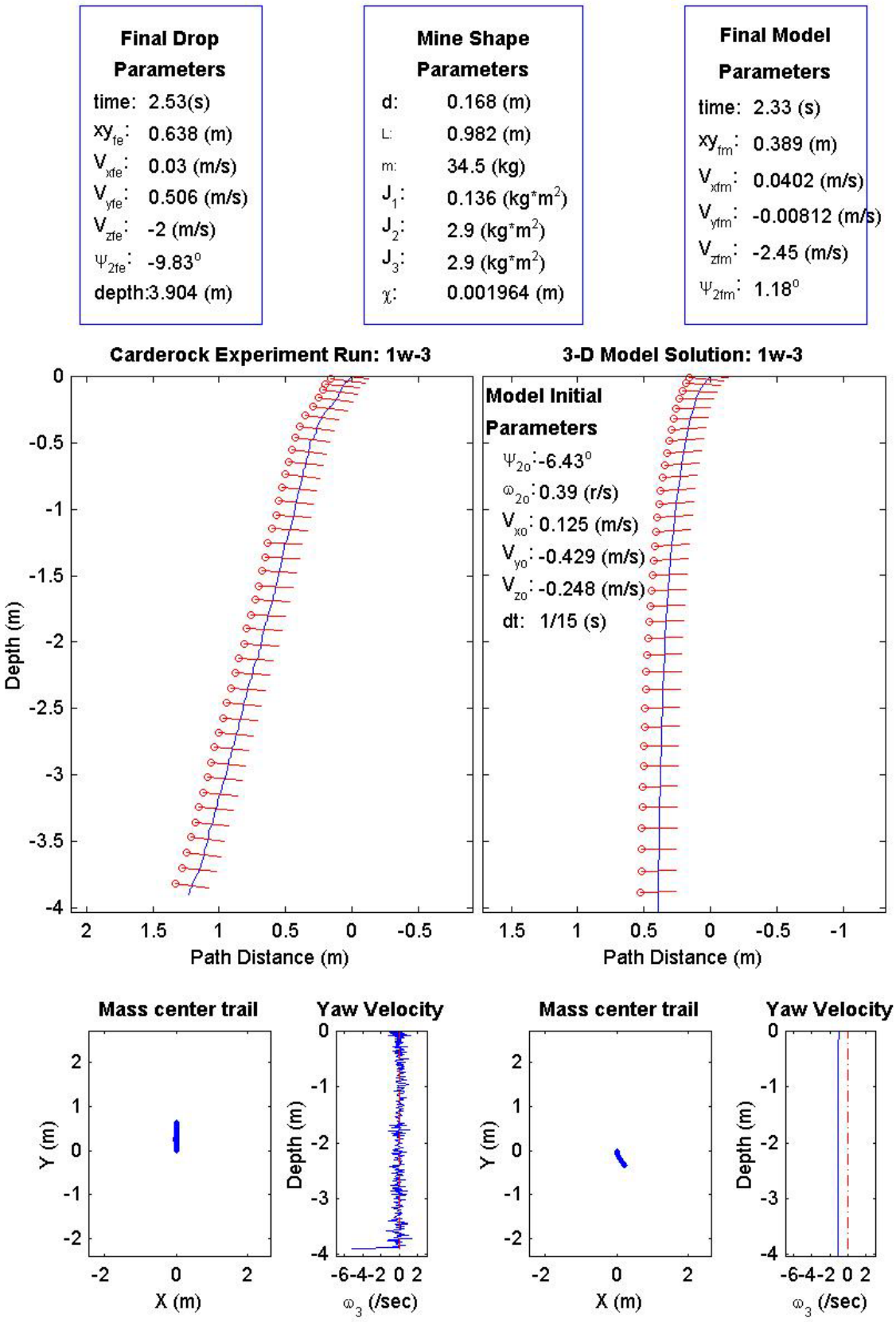
Final Drop Parameters
time: 2.53(s)
xy_fe: 0.638 (m)
V_xfe: 0.03 (m/s)
V_yfe: 0.506 (m/s)
V_zfe: -2 (m/s)
ψ_2fe: -9.83°
depth:3.904 (m)
Mine Shape Parameters
d: 0.168 (m)
L: 0.982 (m)
m: 34.5 (kg)
J_1: 0.136 (kg*m^2)
J_2: 2.9 (kg*m^2)
J_3: 2.9 (kg*m^2)
χ: 0.001964 (m)
Final Model Parameters
time: 2.33 (s)
xy_fm: 0.389 (m)
V_xfm: 0.0402 (m/s)
V_yfm: -0.00812 (m/s)
V_zfm: -2.45 (m/s)
ψ_2fm: 1.18°
Carderock Experiment Run: 1w-3
3-D Model Solution: 1w-3
Model Initial Parameters
ψ_2o: -6.43°
ω_2o: 0.39 (r/s)
V_xo: 0.125 (m/s)
V_yo: -0.429 (m/s)
V_zo: -0.248 (m/s)
dt: 1/15 (s)
Depth (m)
Path Distance (m)
Path Distance (m)
Mass center trail
Yaw Velocity
Mass center trail
Yaw Velocity
Y (m)
X (m)
Depth (m)
ω_3 (/sec)
Y (m)
X (m)
Depth (m)
ω_3 (/sec)

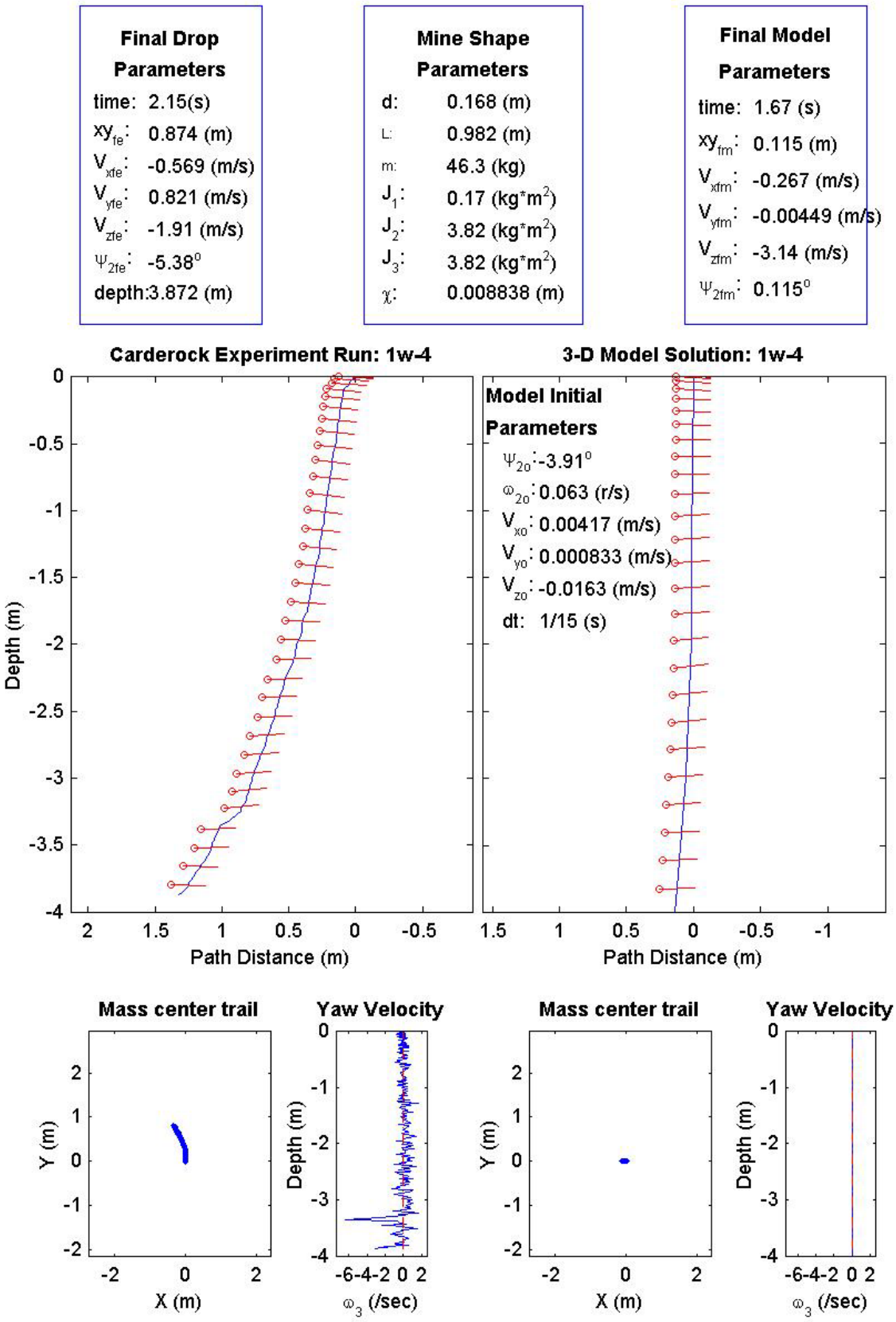
Final Drop Parameters
time: 2.15(s)
xy_fe: 0.874 (m)
V_xfe: -0.569 (m/s)
V_yfe: 0.821 (m/s)
V_zfe: -1.91 (m/s)
ψ_2fe: -5.38°
depth: 3.872 (m)
Mine Shape Parameters
d: 0.168 (m)
L: 0.982 (m)
m: 46.3 (kg)
J_1: 0.17 (kg*m^2)
J_2: 3.82 (kg*m^2)
J_3: 3.82 (kg*m^2)
χ: 0.008838 (m)
Final Model Parameters
time: 1.67 (s)
xy_fm: 0.115 (m)
V_xfm: -0.267 (m/s)
V_yfm: -0.00449 (m/s)
V_zfm: -3.14 (m/s)
ψ_2fm: 0.115°
Carderock Experiment Run: 1w-4
3-D Model Solution: 1w-4
Model Initial Parameters
ψ_2o: -3.91°
ω_2o: 0.063 (r/s)
V_xo: 0.00417 (m/s)
V_yo: 0.000833 (m/s)
V_zo: -0.0163 (m/s)
dt: 1/15 (s)
Depth (m)
Path Distance (m)
Path Distance (m)
Mass center trail
Yaw Velocity
Mass center trail
Yaw Velocity
Y (m)
X (m)
Depth (m)
ω_3 (/sec)
Y (m)
X (m)
Depth (m)
ω_3 (/sec)

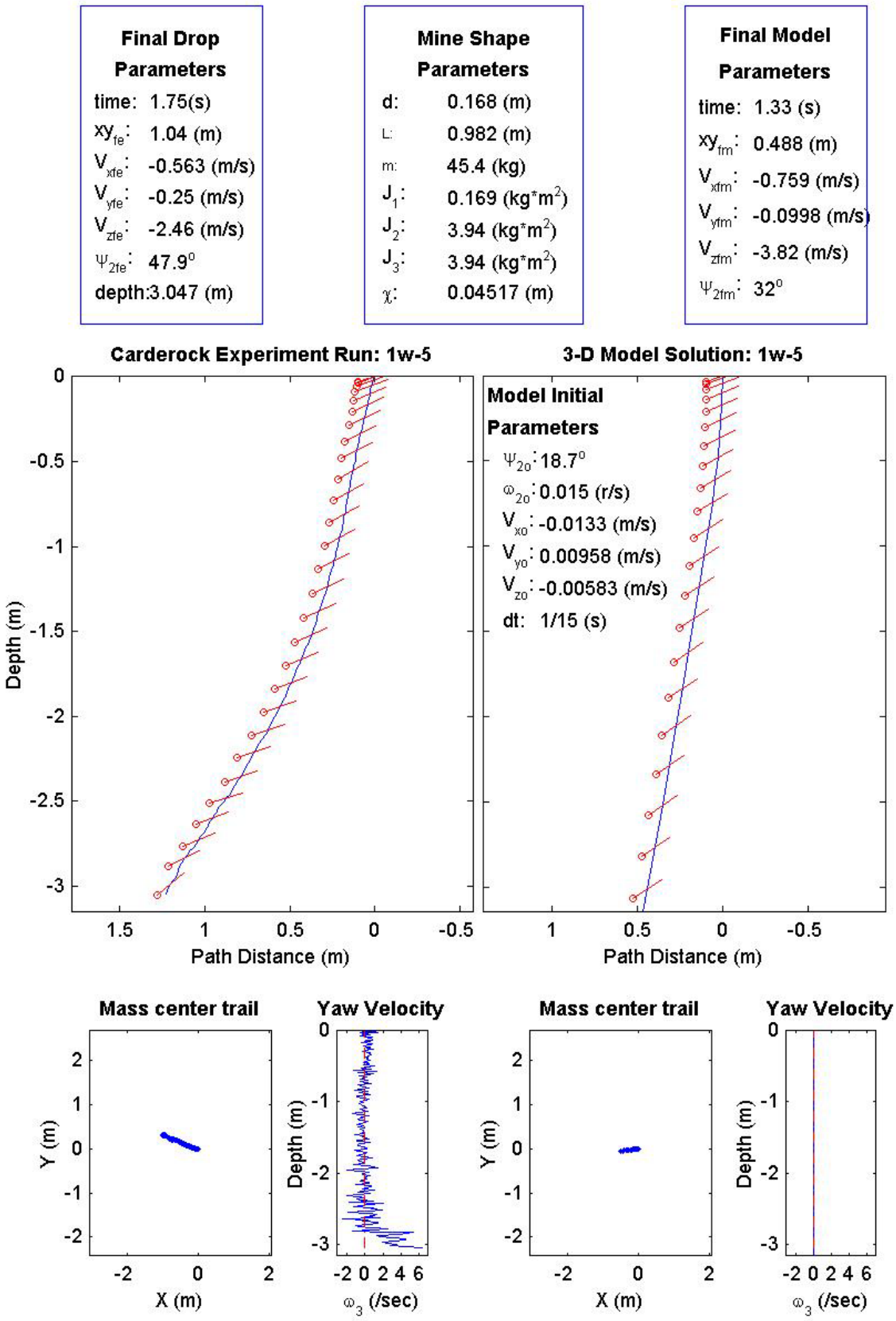
Final Drop Parameters
time: 1.75(s)
xy_fe: 1.04 (m)
V_xfe: -0.563 (m/s)
V_yfe: -0.25 (m/s)
V_zfe: -2.46 (m/s)
Ψ_2fe: 47.9°
depth:3.047 (m)
Mine Shape Parameters
d: 0.168 (m)
L: 0.982 (m)
m: 45.4 (kg)
J_1: 0.169 (kg*m^2)
J_2: 3.94 (kg*m^2)
J_3: 3.94 (kg*m^2)
χ: 0.04517 (m)
Final Model Parameters
time: 1.33 (s)
xy_fm: 0.488 (m)
V_xfm: -0.759 (m/s)
V_yfm: -0.0998 (m/s)
V_zfm: -3.82 (m/s)
Ψ_2fm: 32°
Carderock Experiment Run: 1w-5
3-D Model Solution: 1w-5
Model Initial Parameters
Ψ_2o: 18.7°
ω_2o: 0.015 (r/s)
V_xo: -0.0133 (m/s)
V_yo: 0.00958 (m/s)
V_zo: -0.00583 (m/s)
dt: 1/15 (s)
Depth (m)
Path Distance (m)
Path Distance (m)
Mass center trail
Yaw Velocity
Mass center trail
Yaw Velocity
Y (m)
X (m)
Depth (m)
ω_3 (/sec)
Y (m)
X (m)
Depth (m)
ω_3 (/sec)

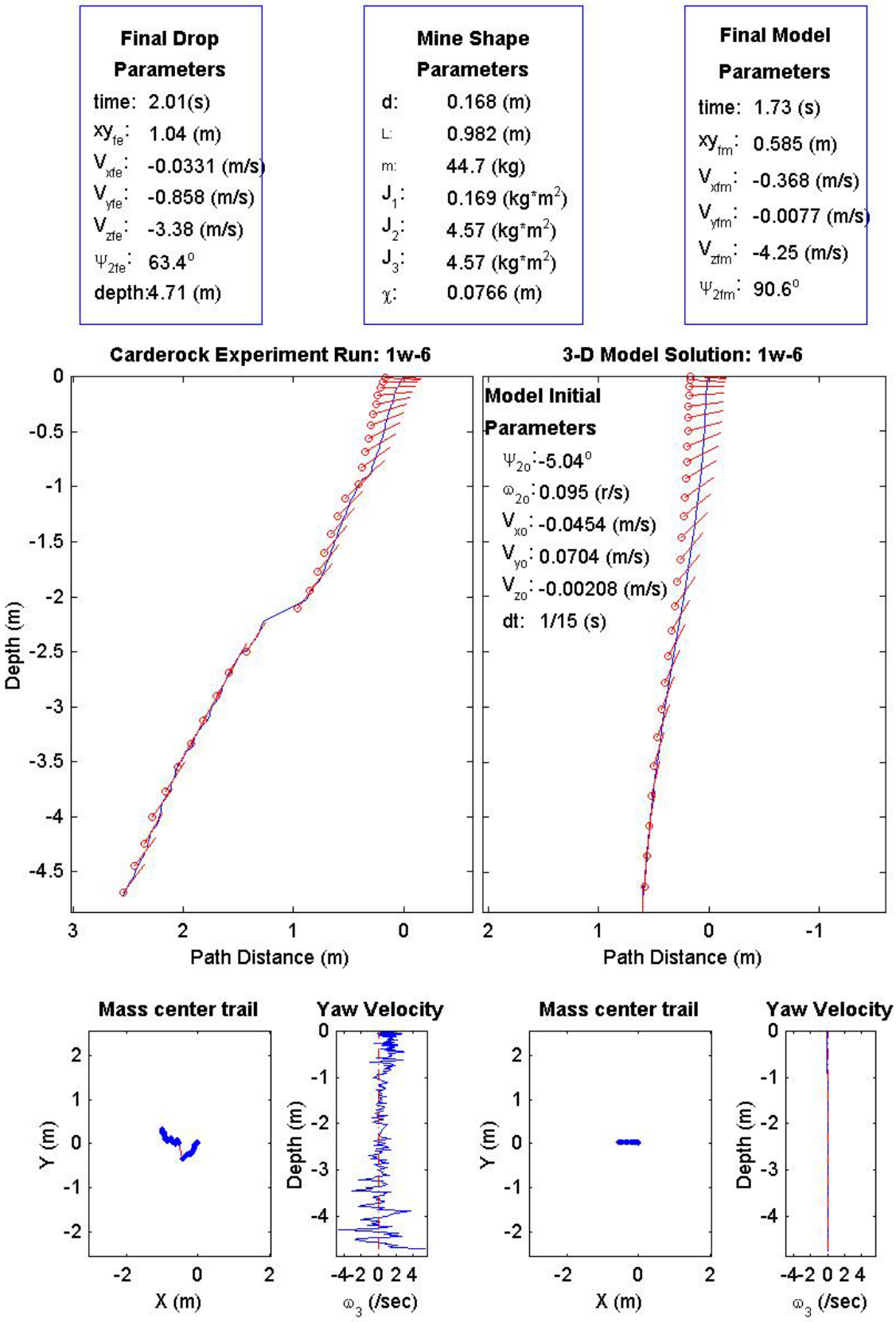
Final Drop Parameters
time: 2.01(s)
xy_fe: 1.04 (m)
V_xfe: -0.0331 (m/s)
V_yfe: -0.858 (m/s)
V_zfe: -3.38 (m/s)
Ψ_2fe: 63.4°
depth:4.71 (m)
Mine Shape Parameters
d: 0.168 (m)
L: 0.982 (m)
m: 44.7 (kg)
J_1: 0.169 (kg*m^2)
J_2: 4.57 (kg*m^2)
J_3: 4.57 (kg*m^2)
χ: 0.0766 (m)
Final Model Parameters
time: 1.73 (s)
xy_fm: 0.585 (m)
V_xfm: -0.368 (m/s)
V_yfm: -0.0077 (m/s)
V_zfm: -4.25 (m/s)
Ψ_2fm: 90.6°
Carderock Experiment Run: 1w-6
3-D Model Solution: 1w-6
Model Initial Parameters
Ψ_2o: -5.04°
ω_2o: 0.095 (r/s)
V_xo: -0.0454 (m/s)
V_yo: 0.0704 (m/s)
V_zo: -0.00208 (m/s)
dt: 1/15 (s)
Depth (m)
Path Distance (m)
Path Distance (m)
Mass center trail
Yaw Velocity
Mass center trail
Yaw Velocity
Y (m)
X (m)
Depth (m)
ω_3 (/sec)
Y (m)
X (m)
Depth (m)
ω_3 (/sec)

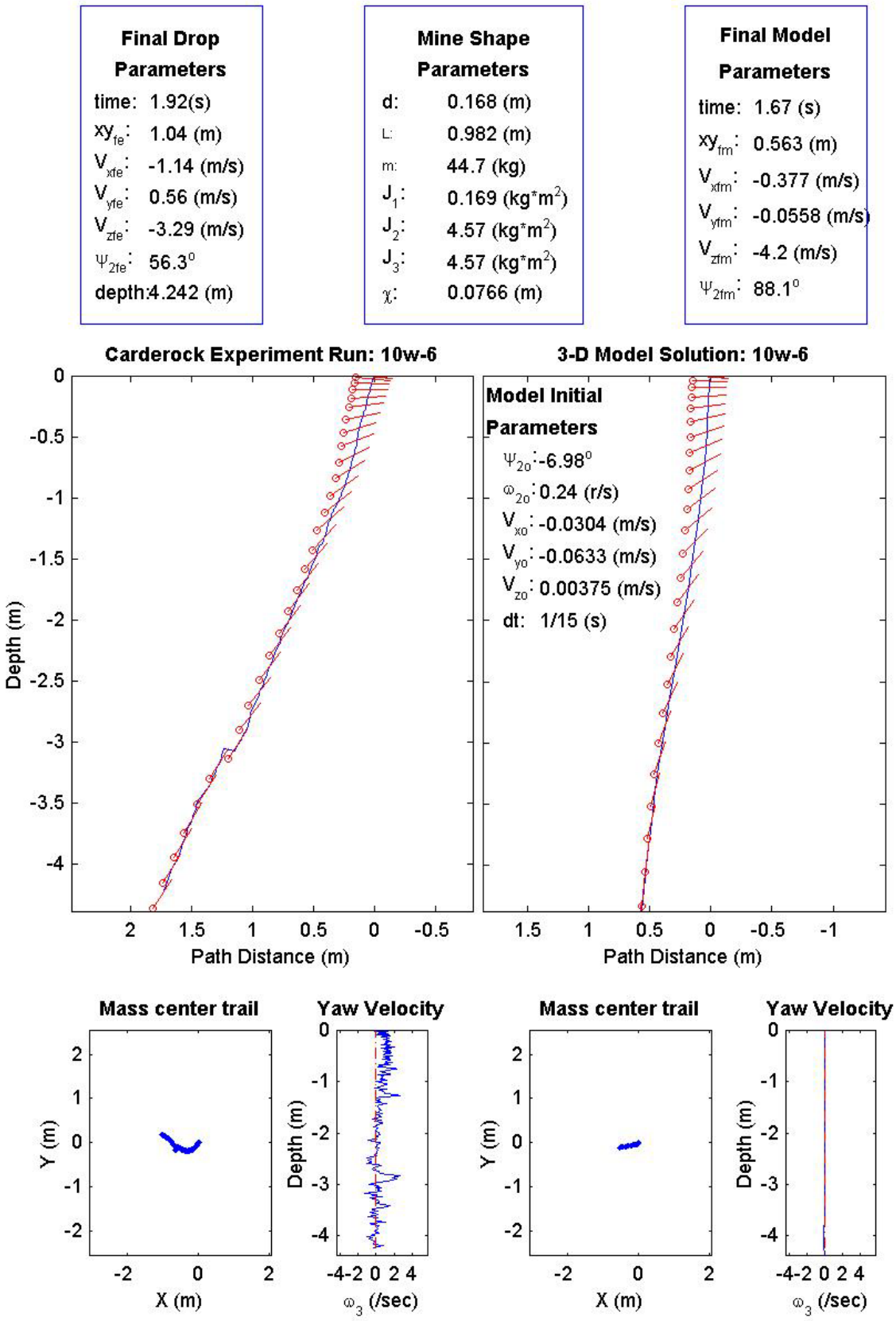
Final Drop Parameters
time: 1.92(s)
xy_fe: 1.04 (m)
V_xfe: -1.14 (m/s)
V_yfe: 0.56 (m/s)
V_zfe: -3.29 (m/s)
ψ_2fe: 56.3°
depth: 4.242 (m)
Mine Shape Parameters
d: 0.168 (m)
L: 0.982 (m)
m: 44.7 (kg)
J_1: 0.169 (kg*m^2)
J_2: 4.57 (kg*m^2)
J_3: 4.57 (kg*m^2)
χ: 0.0766 (m)
Final Model Parameters
time: 1.67 (s)
xy_fm: 0.563 (m)
V_xfm: -0.377 (m/s)
V_yfm: -0.0558 (m/s)
V_zfm: -4.2 (m/s)
ψ_2fm: 88.1°
Carderock Experiment Run: 10w-6
3-D Model Solution: 10w-6
Model Initial Parameters
ψ_2o: -6.98°
ω_2o: 0.24 (r/s)
V_xo: -0.0304 (m/s)
V_yo: -0.0633 (m/s)
V_zo: 0.00375 (m/s)
dt: 1/15 (s)
Depth (m)
Path Distance (m)
Path Distance (m)
Mass center trail
Yaw Velocity
Mass center trail
Yaw Velocity
Y (m)
X (m)
Depth (m)
ω_3 (/sec)
Y (m)
X (m)
Depth (m)
ω_3 (/sec)

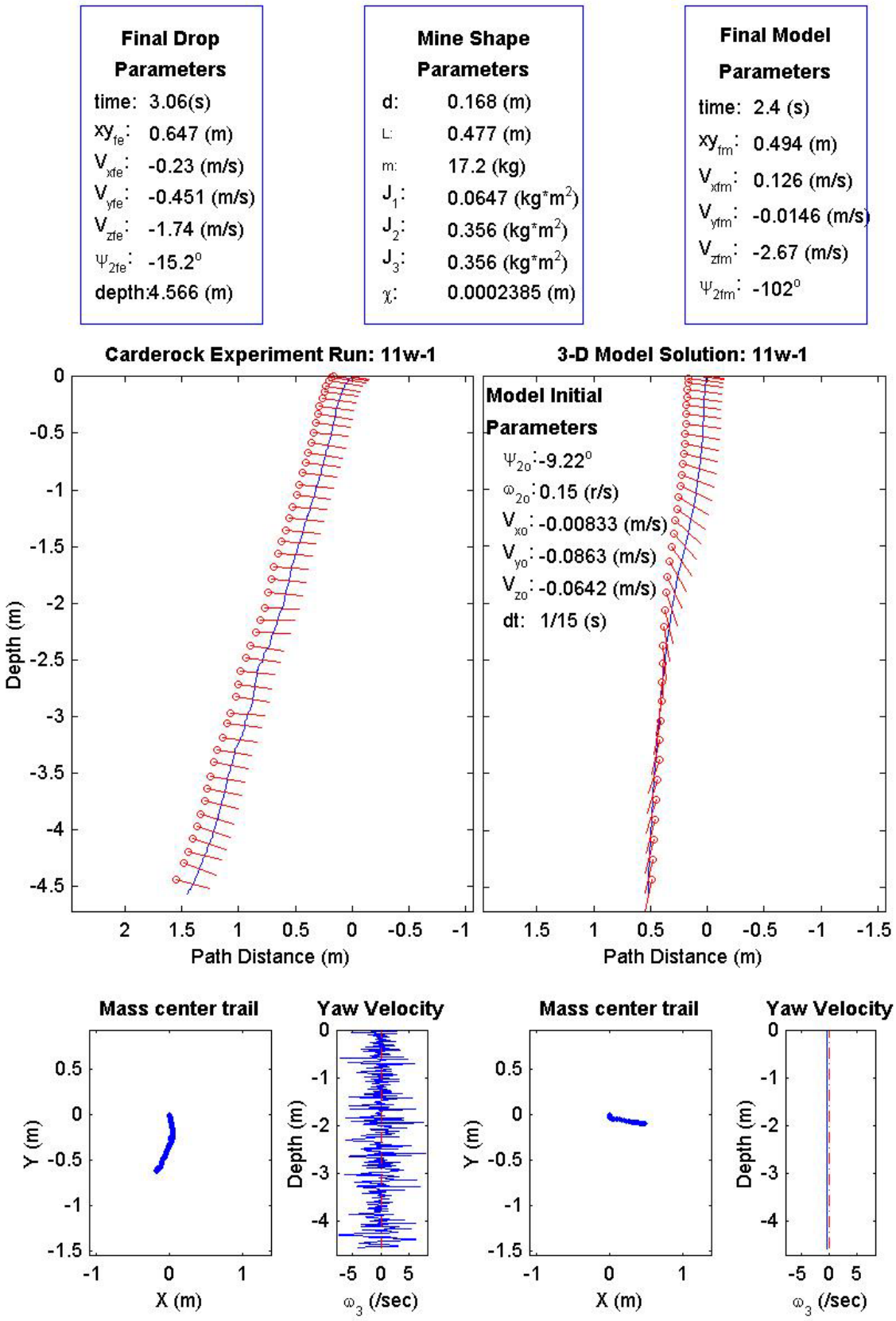
Final Drop Parameters
time: 3.06(s)
xy_fe: 0.647 (m)
V_xfe: -0.23 (m/s)
V_yfe: -0.451 (m/s)
V_zfe: -1.74 (m/s)
ψ_2fe: -15.2°
depth: 4.566 (m)
Mine Shape Parameters
d: 0.168 (m)
L: 0.477 (m)
m: 17.2 (kg)
J_1: 0.0647 (kg*m^2)
J_2: 0.356 (kg*m^2)
J_3: 0.356 (kg*m^2)
χ: 0.0002385 (m)
Final Model Parameters
time: 2.4 (s)
xy_fm: 0.494 (m)
V_xfm: 0.126 (m/s)
V_yfm: -0.0146 (m/s)
V_zfm: -2.67 (m/s)
ψ_2fm: -102°
Carderock Experiment Run: 11w-1
3-D Model Solution: 11w-1
Model Initial Parameters
ψ_2o: -9.22°
ω_2o: 0.15 (r/s)
V_xo: -0.00833 (m/s)
V_yo: -0.0863 (m/s)
V_zo: -0.0642 (m/s)
dt: 1/15 (s)
Depth (m)
Path Distance (m)
Path Distance (m)
Mass center trail
Yaw Velocity
Mass center trail
Yaw Velocity
Y (m)
X (m)
Depth (m)
ω_3 (/sec)
Y (m)
X (m)
Depth (m)
ω_3 (/sec)

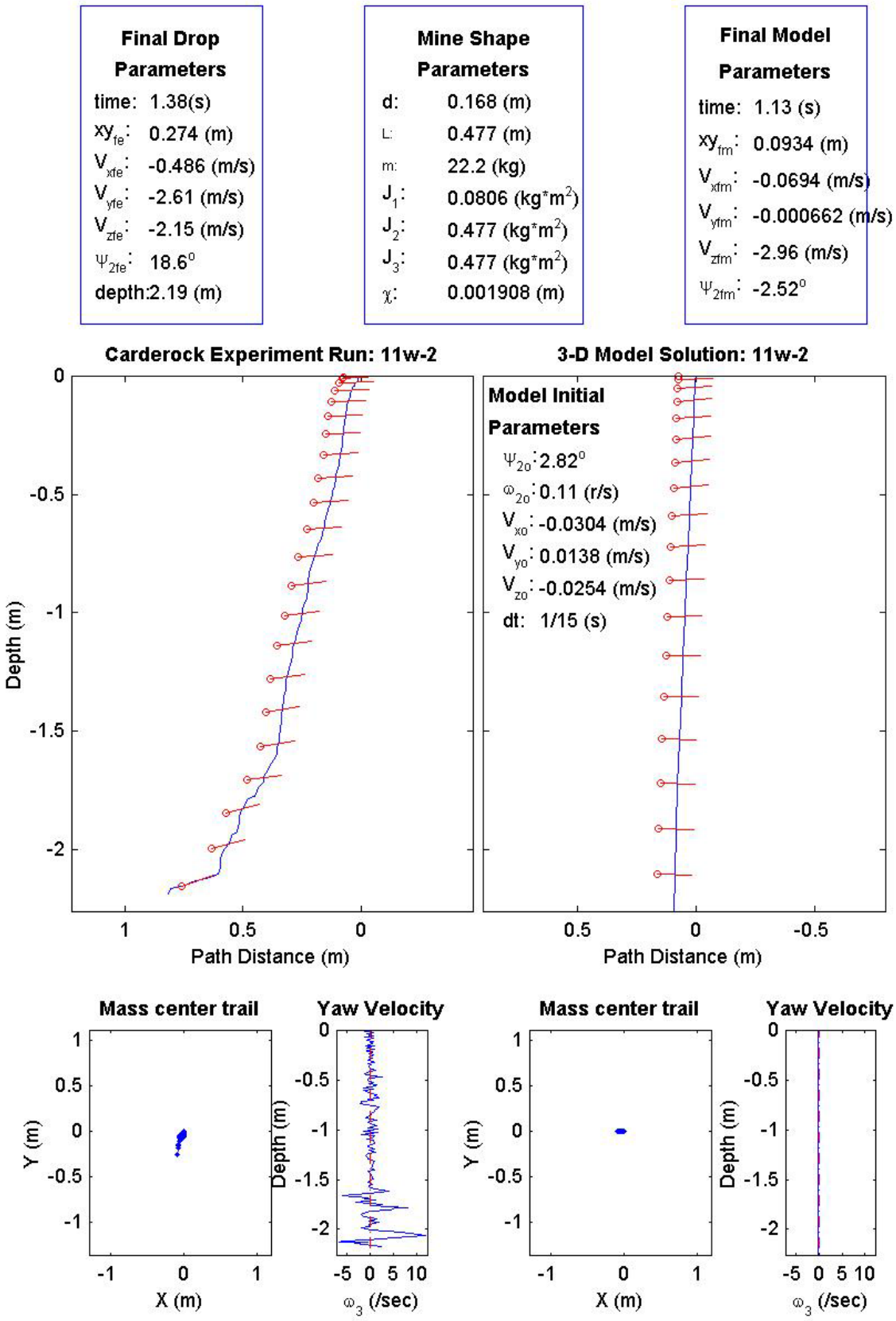
Final Drop Parameters
time: 1.38(s)
xy_fe: 0.274 (m)
V_xfe: -0.486 (m/s)
V_yfe: -2.61 (m/s)
V_zfe: -2.15 (m/s)
Ψ_2fe: 18.6°
depth:2.19 (m)
Mine Shape Parameters
d: 0.168 (m)
L: 0.477 (m)
m: 22.2 (kg)
J_1: 0.0806 (kg*m^2)
J_2: 0.477 (kg*m^2)
J_3: 0.477 (kg*m^2)
χ: 0.001908 (m)
Final Model Parameters
time: 1.13 (s)
xy_fm: 0.0934 (m)
V_xfm: -0.0694 (m/s)
V_yfm: -0.000662 (m/s)
V_zfm: -2.96 (m/s)
Ψ_2fm: -2.52°
Carderock Experiment Run: 11w-2
3-D Model Solution: 11w-2
Model Initial Parameters
Ψ_2o: 2.82°
ω_2o: 0.11 (r/s)
V_xo: -0.0304 (m/s)
V_yo: 0.0138 (m/s)
V_zo: -0.0254 (m/s)
dt: 1/15 (s)
Depth (m)
Path Distance (m)
Path Distance (m)
Mass center trail
Yaw Velocity
Mass center trail
Yaw Velocity
Y (m)
X (m)
Depth (m)
ω_3 (/sec)
Y (m)
X (m)
Depth (m)
ω_3 (/sec)

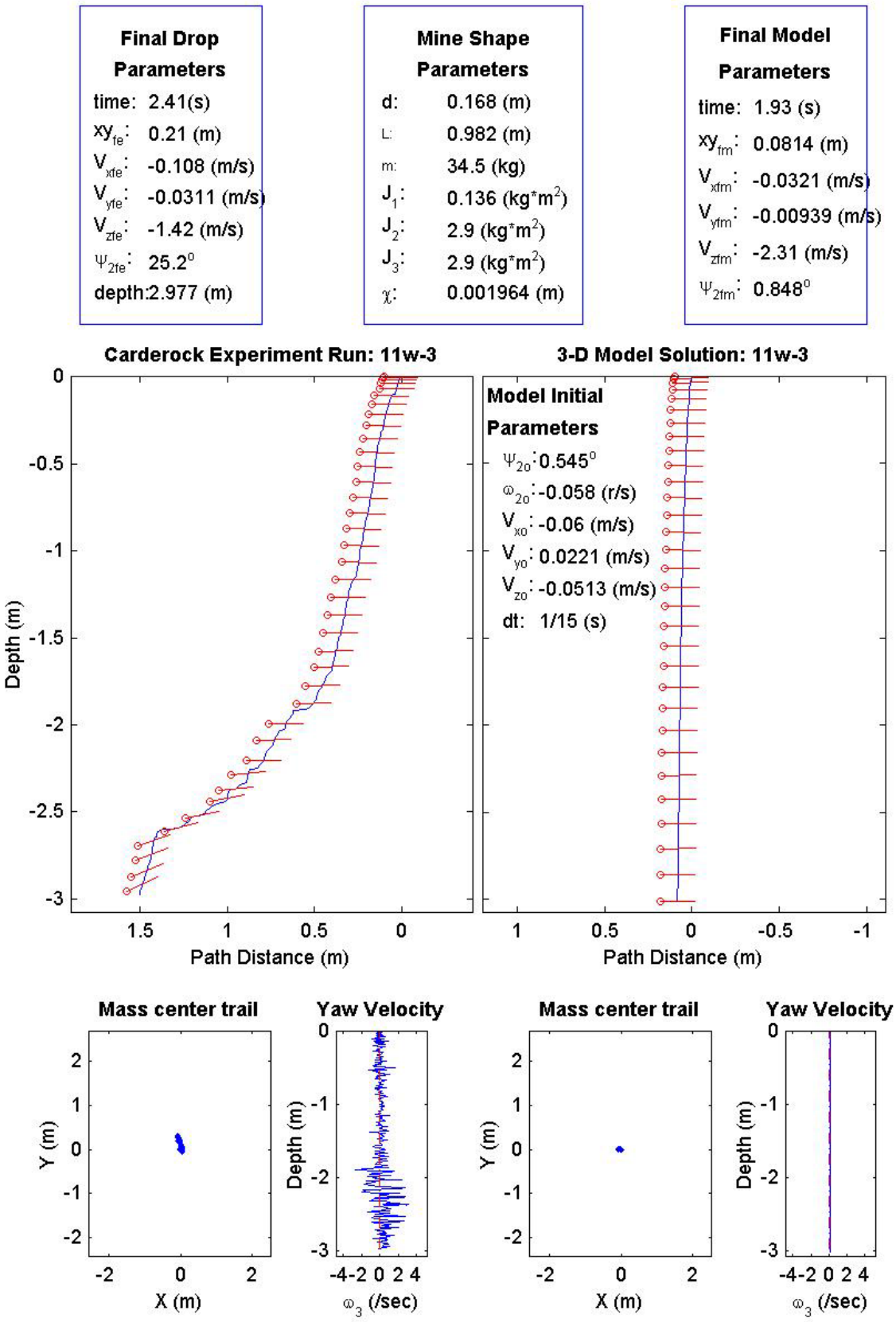
Final Drop Parameters
time: 2.41(s)
xy_fe: 0.21 (m)
V_xfe: -0.108 (m/s)
V_yfe: -0.0311 (m/s)
V_zfe: -1.42 (m/s)
Ψ_2fe: 25.2°
depth:2.977 (m)
Mine Shape Parameters
d: 0.168 (m)
L: 0.982 (m)
m: 34.5 (kg)
J_1: 0.136 (kg*m^2)
J_2: 2.9 (kg*m^2)
J_3: 2.9 (kg*m^2)
χ: 0.001964 (m)
Final Model Parameters
time: 1.93 (s)
xy_fm: 0.0814 (m)
V_xfm: -0.0321 (m/s)
V_yfm: -0.00939 (m/s)
V_zfm: -2.31 (m/s)
Ψ_2fm: 0.848°
Carderock Experiment Run: 11w-3
3-D Model Solution: 11w-3
Model Initial Parameters
Ψ_2o: 0.545°
ω_2o: -0.058 (r/s)
V_xo: -0.06 (m/s)
V_yo: 0.0221 (m/s)
V_zo: -0.0513 (m/s)
dt: 1/15 (s)
Depth (m)
Path Distance (m)
Path Distance (m)
Mass center trail
Yaw Velocity
Y (m)
X (m)
Depth (m)
ω_3 (/sec)
Mass center trail
Yaw Velocity
Y (m)
X (m)
Depth (m)
ω_3 (/sec)

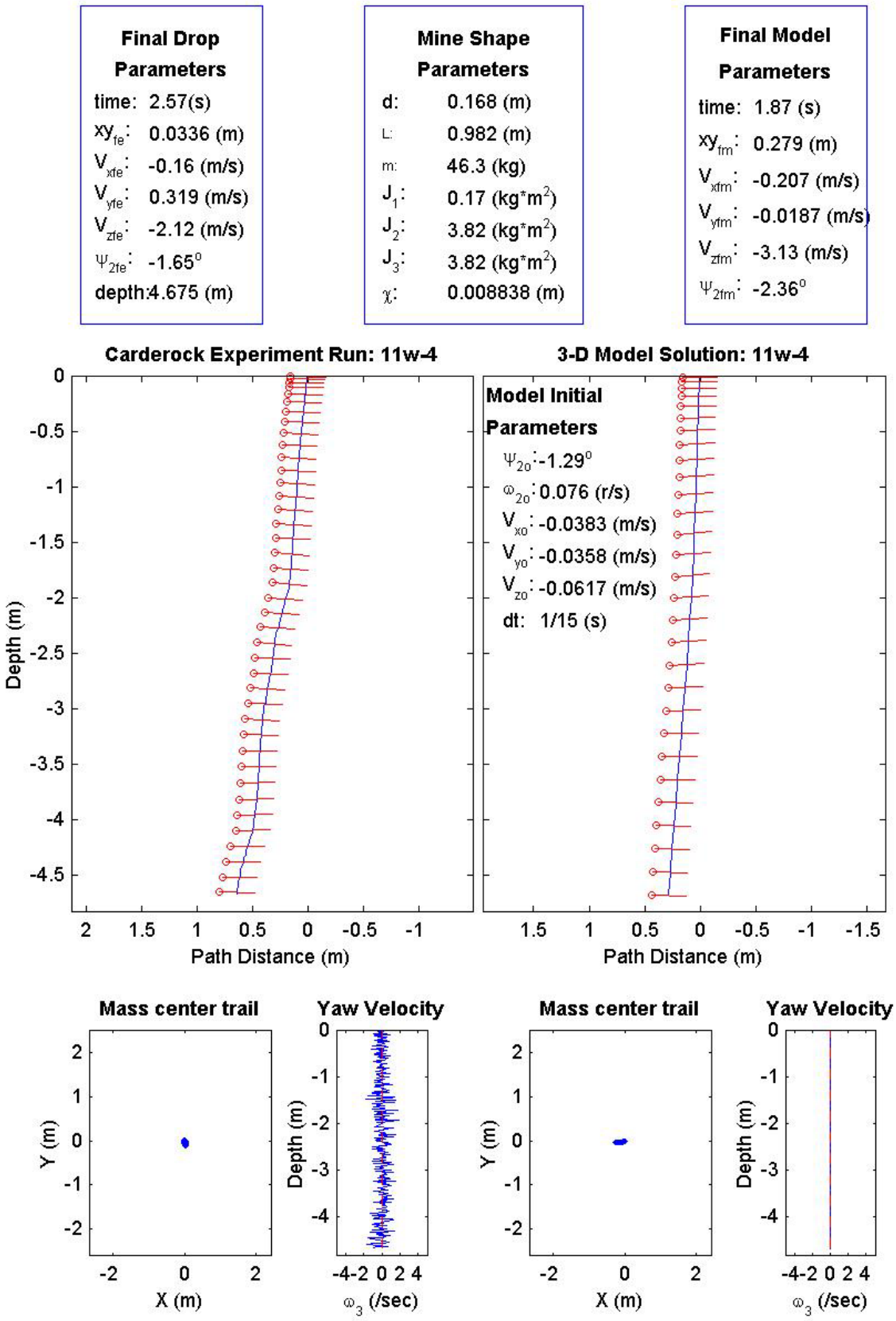
Final Drop Parameters
time: 2.57(s)
xy_fe: 0.0336 (m)
V_xfe: -0.16 (m/s)
V_yfe: 0.319 (m/s)
V_zfe: -2.12 (m/s)
Ψ_2fe: -1.65°
depth: 4.675 (m)
Mine Shape Parameters
d: 0.168 (m)
L: 0.982 (m)
m: 46.3 (kg)
J_1: 0.17 (kg*m^2)
J_2: 3.82 (kg*m^2)
J_3: 3.82 (kg*m^2)
χ: 0.008838 (m)
Final Model Parameters
time: 1.87 (s)
xy_fm: 0.279 (m)
V_xfm: -0.207 (m/s)
V_yfm: -0.0187 (m/s)
V_zfm: -3.13 (m/s)
Ψ_2fm: -2.36°
Carderock Experiment Run: 11w-4
3-D Model Solution: 11w-4
Model Initial Parameters
Ψ_2o: -1.29°
ω_2o: 0.076 (r/s)
V_xo: -0.0383 (m/s)
V_yo: -0.0358 (m/s)
V_zo: -0.0617 (m/s)
dt: 1/15 (s)
Depth (m)
Path Distance (m)
Path Distance (m)
Mass center trail
Yaw Velocity
Mass center trail
Yaw Velocity
Y (m)
X (m)
Depth (m)
ω_3 (/sec)
Y (m)
X (m)
Depth (m)
ω_3 (/sec)

Final Drop Parameters

time: 2.51(s)
xy_{fe}: 2.19 (m)
V_{xfe}: -1.15 (m/s)
V_{yfe}: -0.087 (m/s)
V_{zfe}: -1.81 (m/s)
Ψ_{2fe}: 3.04°
depth: 4.471 (m)

Mine Shape Parameters

d: 0.168 (m)
L: 0.982 (m)
m: 45.4 (kg)
J_1: 0.169 (kg*m^2)
J_2: 3.94 (kg*m^2)
J_3: 3.94 (kg*m^2)
χ: 0.04517 (m)

Final Model Parameters

time: 1.67 (s)
xy_{fm}: 0.838 (m)
V_{xfm}: -0.993 (m/s)
V_{yfm}: 0.328 (m/s)
V_{zfm}: -3.89 (m/s)
Ψ_{2fm}: 23.2°

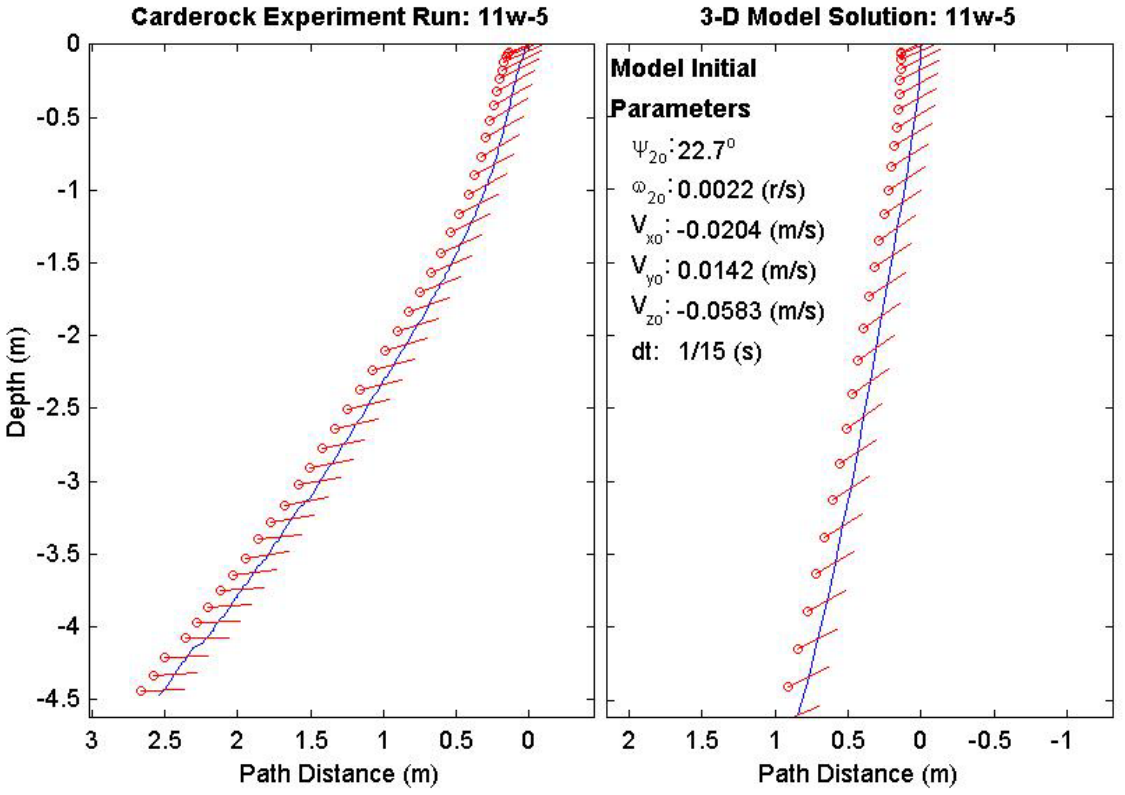

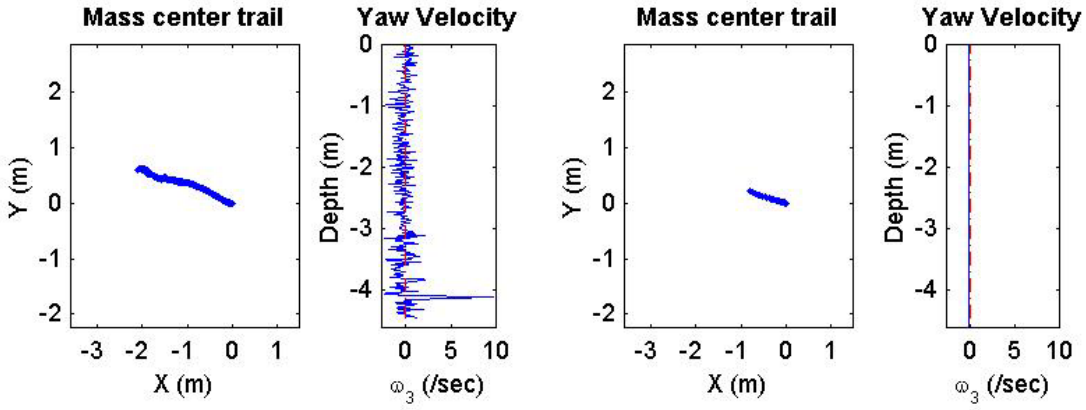

Final Drop Parameters

time: 1.95(s)
xy_{fe}: 1.15 (m)
V_{xfe}: -0.862 (m/s)
V_{yfe}: -0.883 (m/s)
V_{zfe}: -3.58 (m/s)
Ψ_{2fe}: 52.4°
depth: 4.403 (m)

Mine Shape Parameters

d: 0.168 (m)
L: 0.982 (m)
m: 44.7 (kg)
J_1: 0.169 ($kg*m^2$)
J_2: 4.57 ($kg*m^2$)
J_3: 4.57 ($kg*m^2$)
χ: 0.0766 (m)

Final Model Parameters

time: 1.67 (s)
xy_{fm}: 0.3 (m)
V_{xfm}: -0.232 (m/s)
V_{yfm}: -0.0156 (m/s)
V_{zfm}: -4.27 (m/s)
Ψ_{2fm}: 99.2°

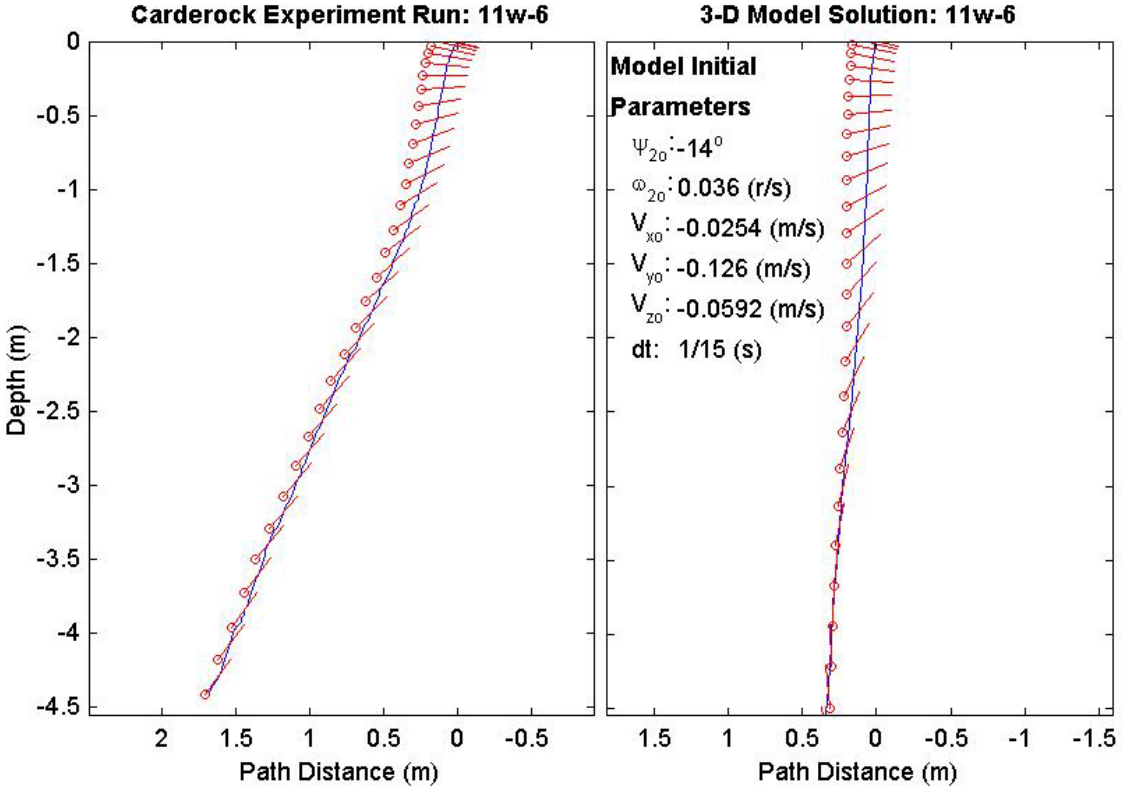

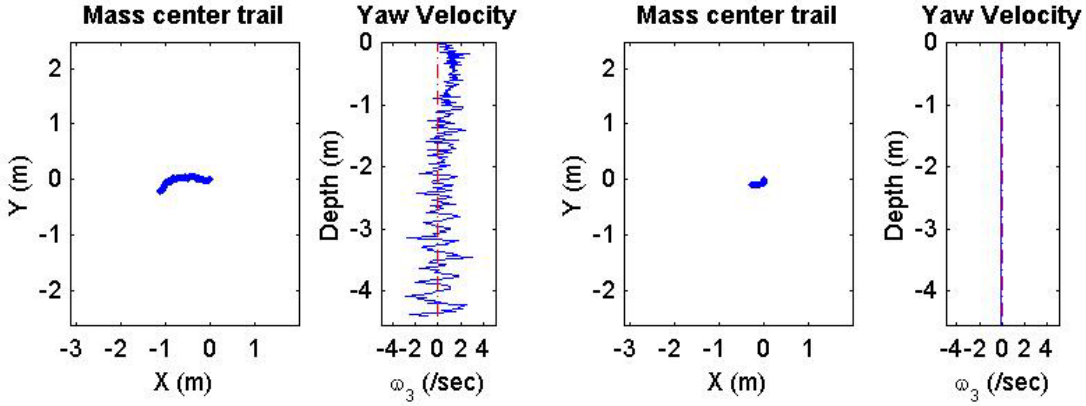

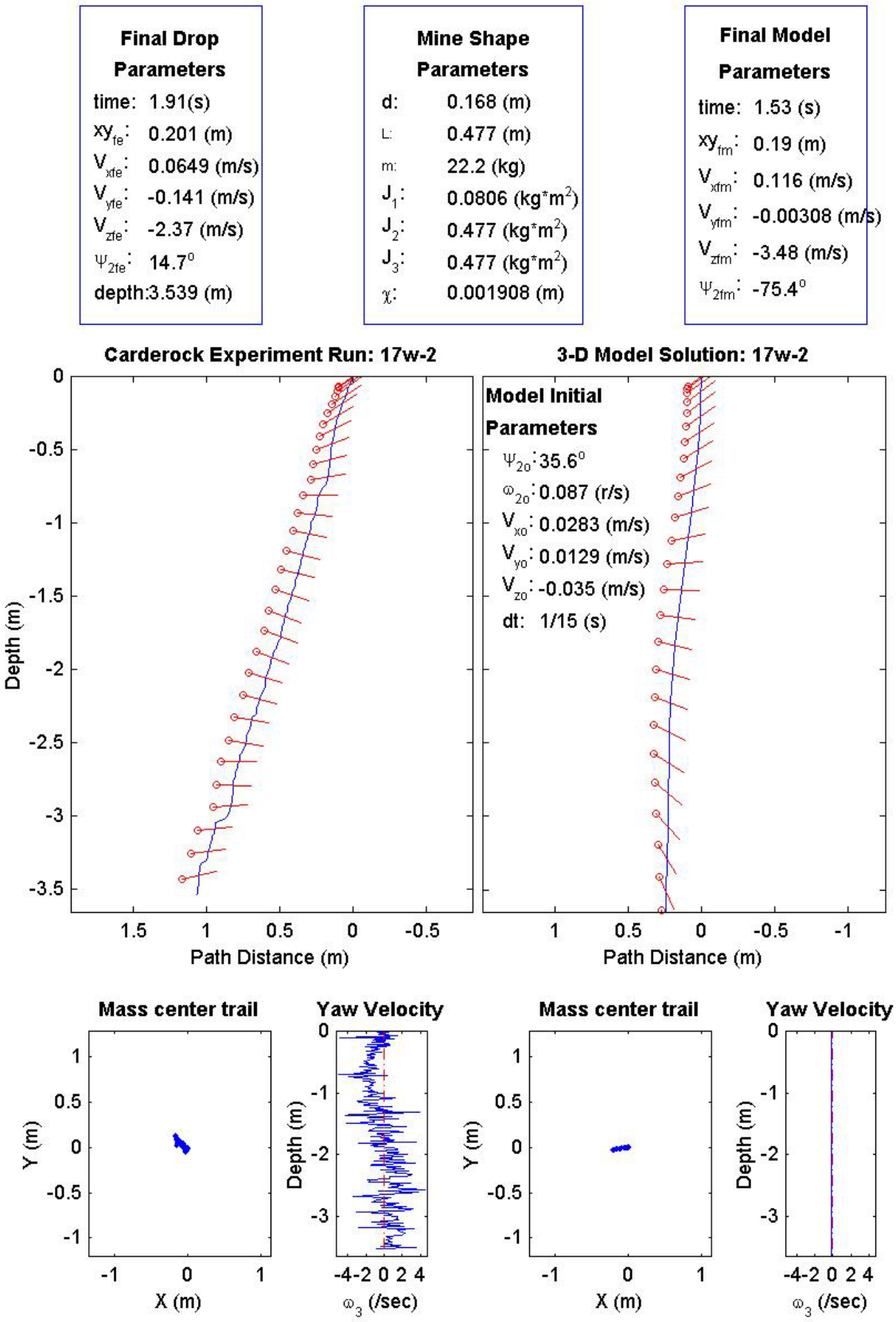
Final Drop Parameters
time: 1.91(s)
xy_fe: 0.201 (m)
V_xfe: 0.0649 (m/s)
V_yfe: -0.141 (m/s)
V_zfe: -2.37 (m/s)
Ψ_2fe: 14.7°
depth:3.539 (m)
Mine Shape Parameters
d: 0.168 (m)
L: 0.477 (m)
m: 22.2 (kg)
J_1: 0.0806 (kg*m^2)
J_2: 0.477 (kg*m^2)
J_3: 0.477 (kg*m^2)
χ: 0.001908 (m)
Final Model Parameters
time: 1.53 (s)
xy_fm: 0.19 (m)
V_xfm: 0.116 (m/s)
V_yfm: -0.00308 (m/s)
V_zfm: -3.48 (m/s)
Ψ_2fm: -75.4°
Carderock Experiment Run: 17w-2
3-D Model Solution: 17w-2
Model Initial Parameters
Ψ_2o: 35.6°
ω_2o: 0.087 (r/s)
V_xo: 0.0283 (m/s)
V_yo: 0.0129 (m/s)
V_zo: -0.035 (m/s)
dt: 1/15 (s)
Depth (m)
Path Distance (m)
Path Distance (m)
Mass center trail
Yaw Velocity
Mass center trail
Yaw Velocity
Y (m)
X (m)
Depth (m)
ω_3 (/sec)
Y (m)
X (m)
Depth (m)
ω_3 (/sec)

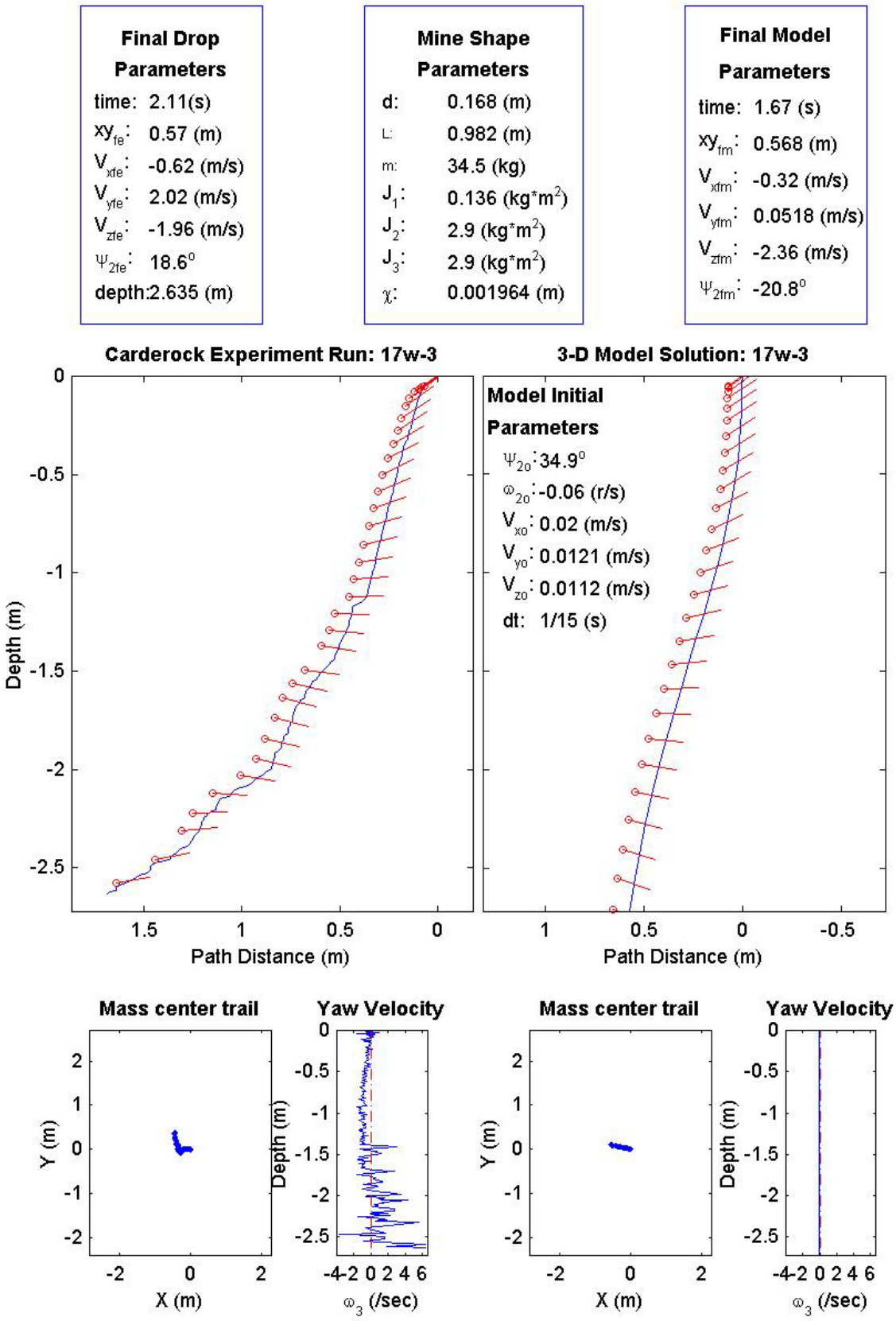
Final Drop Parameters
time: 2.11(s)
xy_fe: 0.57 (m)
V_xfe: -0.62 (m/s)
V_yfe: 2.02 (m/s)
V_zfe: -1.96 (m/s)
Ψ_2fe: 18.6°
depth: 2.635 (m)
Mine Shape Parameters
d: 0.168 (m)
L: 0.982 (m)
m: 34.5 (kg)
J_1: 0.136 (kg*m^2)
J_2: 2.9 (kg*m^2)
J_3: 2.9 (kg*m^2)
χ: 0.001964 (m)
Final Model Parameters
time: 1.67 (s)
xy_fm: 0.568 (m)
V_xfm: -0.32 (m/s)
V_yfm: 0.0518 (m/s)
V_zfm: -2.36 (m/s)
Ψ_2fm: -20.8°
Carderock Experiment Run: 17w-3
3-D Model Solution: 17w-3
Model Initial Parameters
Ψ_2o: 34.9°
ω_2o: -0.06 (r/s)
V_xo: 0.02 (m/s)
V_yo: 0.0121 (m/s)
V_zo: 0.0112 (m/s)
dt: 1/15 (s)
Depth (m)
Path Distance (m)
Path Distance (m)
Mass center trail
Yaw Velocity
Mass center trail
Yaw Velocity
Y (m)
X (m)
Depth (m)
ω_3 (/sec)
Y (m)
X (m)
Depth (m)
ω_3 (/sec)

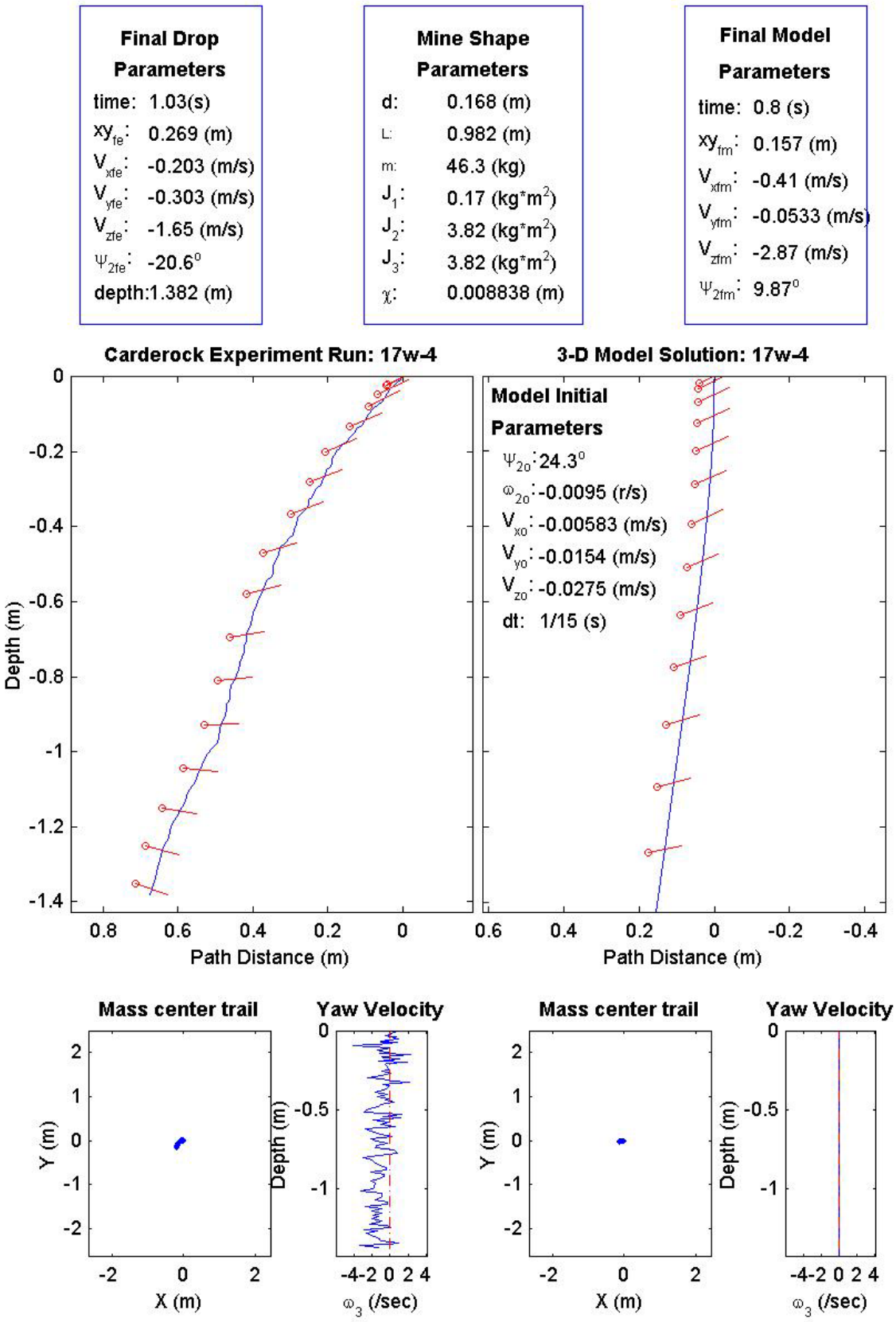
Final Drop Parameters
time: 1.03(s)
xy_fe: 0.269 (m)
V_xfe: -0.203 (m/s)
V_yfe: -0.303 (m/s)
V_zfe: -1.65 (m/s)
Ψ_2fe: -20.6°
depth:1.382 (m)
Mine Shape Parameters
d: 0.168 (m)
L: 0.982 (m)
m: 46.3 (kg)
J_1: 0.17 (kg*m^2)
J_2: 3.82 (kg*m^2)
J_3: 3.82 (kg*m^2)
χ: 0.008838 (m)
Final Model Parameters
time: 0.8 (s)
xy_fm: 0.157 (m)
V_xfm: -0.41 (m/s)
V_yfm: -0.0533 (m/s)
V_zfm: -2.87 (m/s)
Ψ_2fm: 9.87°
Carderock Experiment Run: 17w-4
3-D Model Solution: 17w-4
Model Initial Parameters
Ψ_2o: 24.3°
ω_2o: -0.0095 (r/s)
V_xo: -0.00583 (m/s)
V_yo: -0.0154 (m/s)
V_zo: -0.0275 (m/s)
dt: 1/15 (s)
Depth (m)
Path Distance (m)
Path Distance (m)
Mass center trail
Yaw Velocity
Mass center trail
Yaw Velocity
Y (m)
X (m)
Depth (m)
ω_3 (/sec)
Y (m)
X (m)
Depth (m)
ω_3 (/sec)

Final Drop Parameters

time: 1.91(s)
xy_{fe}: 1.62 (m)
V_{xfe}: -1.43 (m/s)
V_{yfe}: 0.136 (m/s)
V_{zfe}: -2.06 (m/s)
Ψ_{2fe}: 32.3°
depth: 3.951 (m)

Mine Shape Parameters

d: 0.168 (m)
L: 0.982 (m)
m: 45.4 (kg)
J_1: 0.169 ($kg*m^2$)
J_2: 3.94 ($kg*m^2$)
J_3: 3.94 ($kg*m^2$)
χ: 0.04517 (m)

Final Model Parameters

time: 1.47 (s)
xy_{fm}: 0.655 (m)
V_{xfm}: -0.68 (m/s)
V_{yfm}: 0.0173 (m/s)
V_{zfm}: -4.21 (m/s)
Ψ_{2fm}: 48.6°

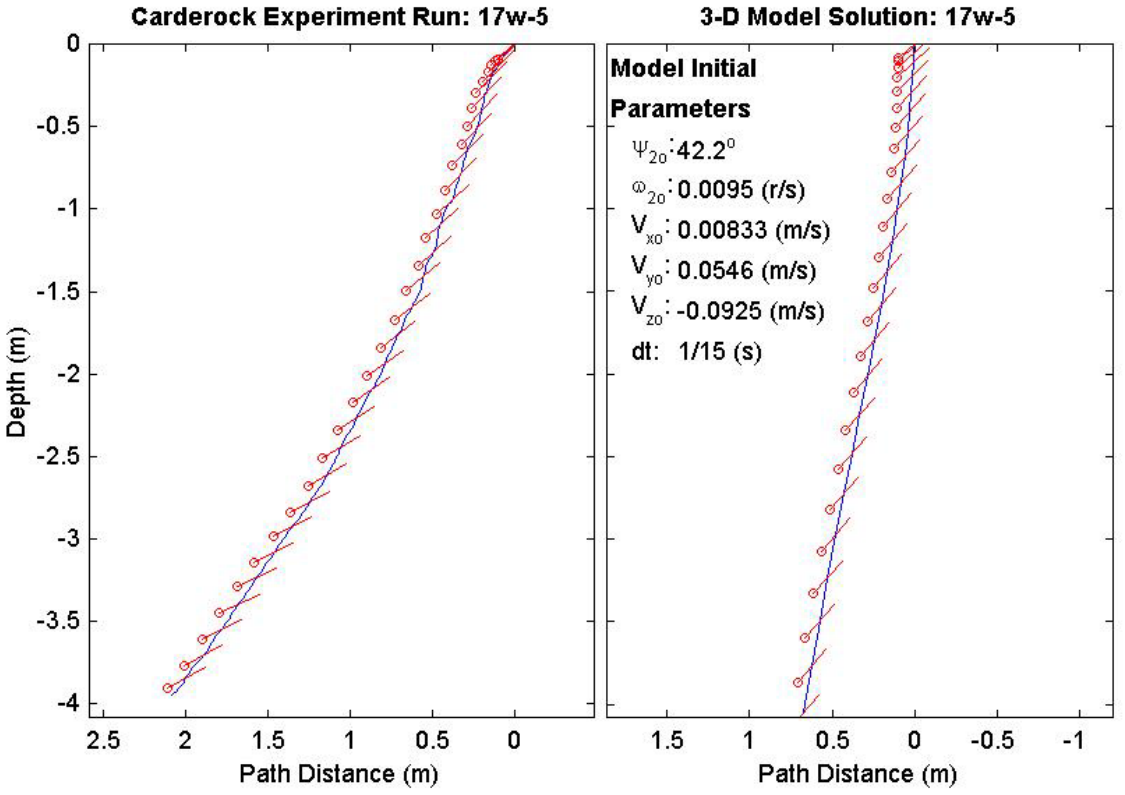

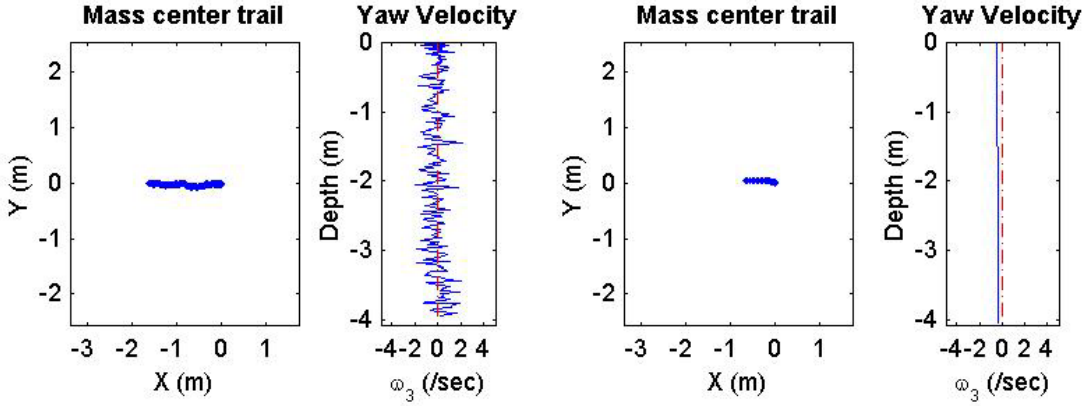

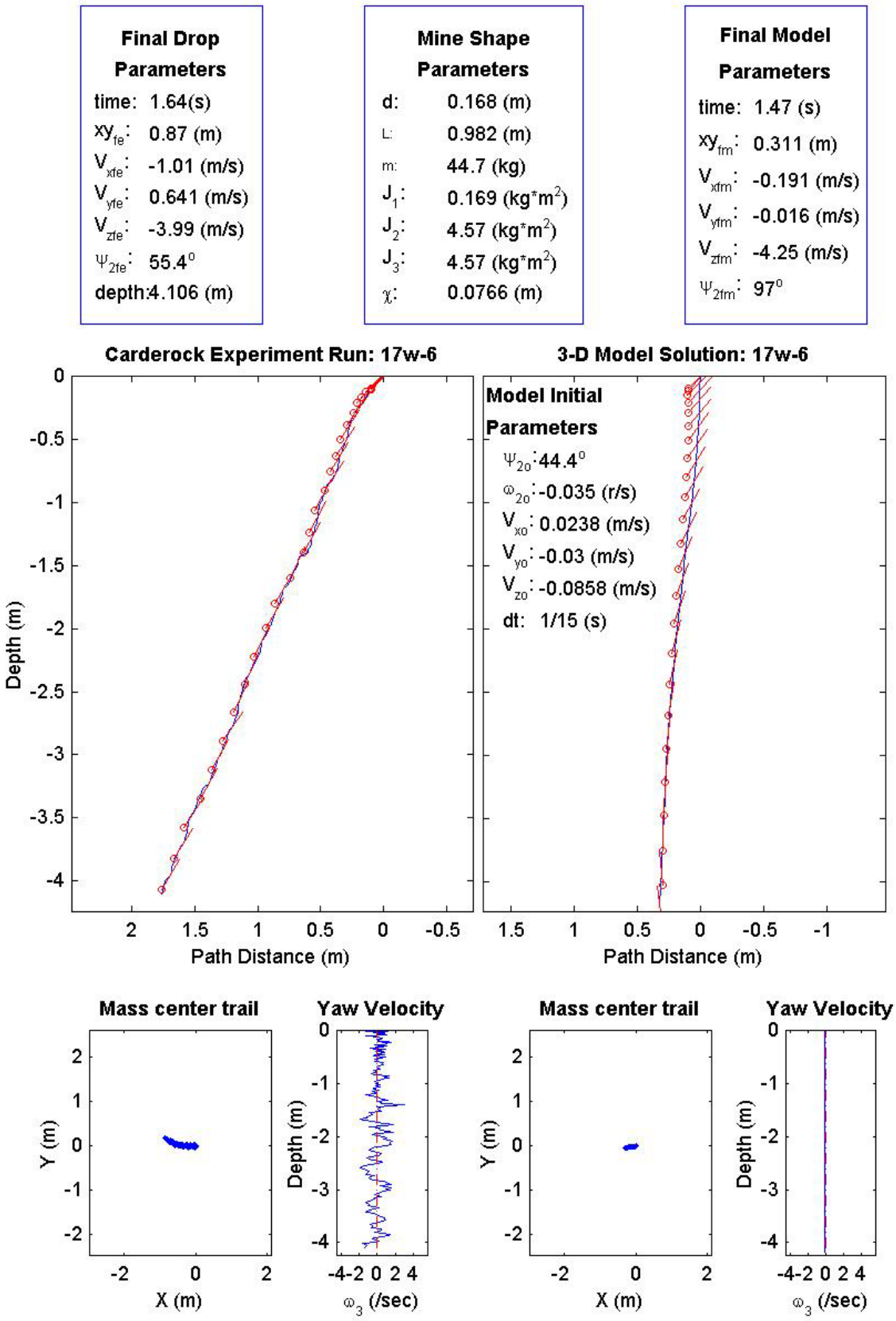
Final Drop Parameters
time: 1.64(s)
xy_fe: 0.87 (m)
V_xfe: -1.01 (m/s)
V_yfe: 0.641 (m/s)
V_zfe: -3.99 (m/s)
ψ_2fe: 55.4°
depth:4.106 (m)
Mine Shape Parameters
d: 0.168 (m)
L: 0.982 (m)
m: 44.7 (kg)
J_1: 0.169 (kg*m^2)
J_2: 4.57 (kg*m^2)
J_3: 4.57 (kg*m^2)
χ: 0.0766 (m)
Final Model Parameters
time: 1.47 (s)
xy_fm: 0.311 (m)
V_xfm: -0.191 (m/s)
V_yfm: -0.016 (m/s)
V_zfm: -4.25 (m/s)
ψ_2fm: 97°
Carderock Experiment Run: 17w-6
3-D Model Solution: 17w-6
Model Initial Parameters
ψ_2o: 44.4°
ω_2o: -0.035 (r/s)
V_xo: 0.0238 (m/s)
V_yo: -0.03 (m/s)
V_zo: -0.0858 (m/s)
dt: 1/15 (s)
Depth (m)
Path Distance (m)
Path Distance (m)
Mass center trail
Yaw Velocity
Mass center trail
Yaw Velocity
Y (m)
X (m)
Depth (m)
ω_3 (/sec)
Y (m)
X (m)
Depth (m)
ω_3 (/sec)

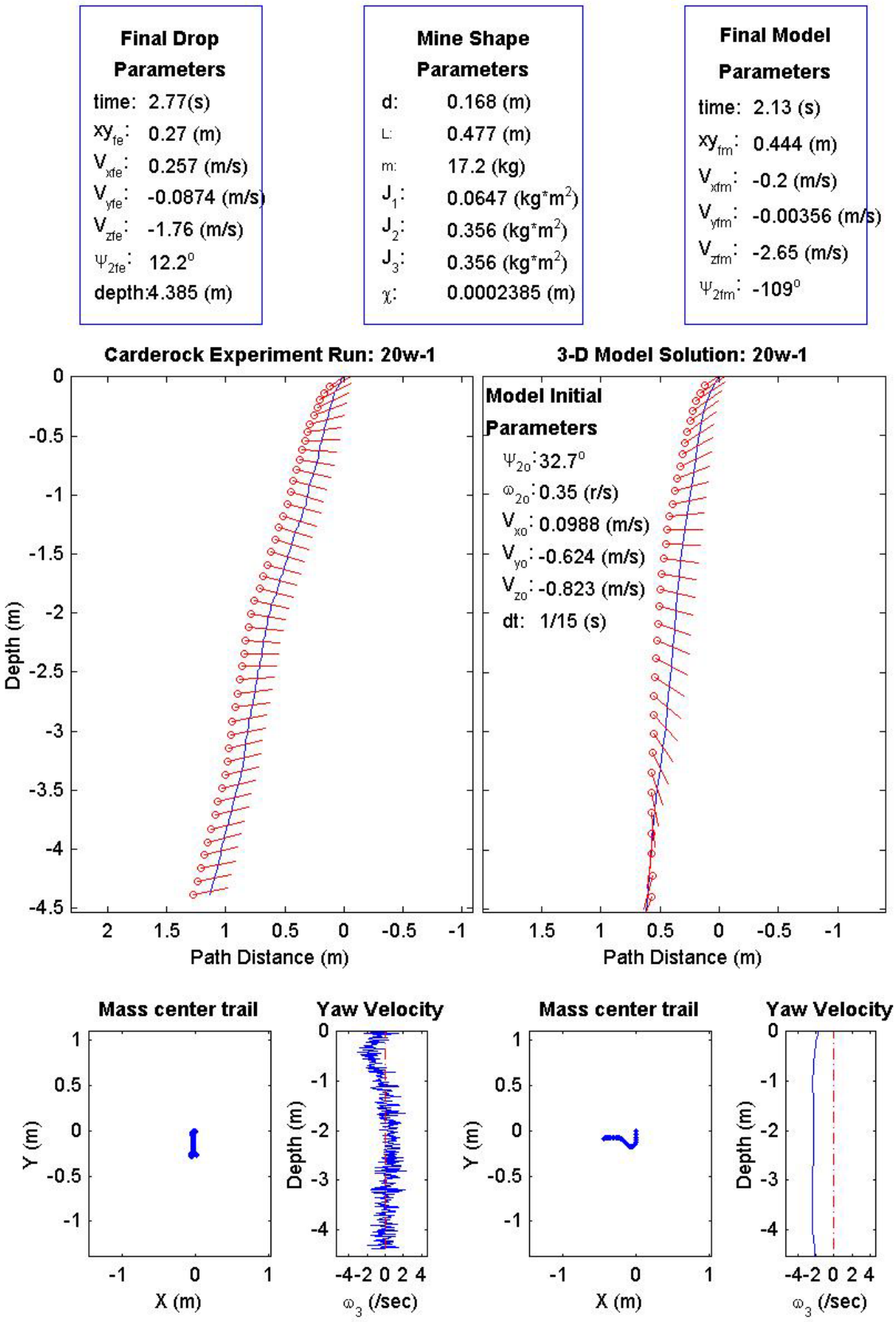
Final Drop Parameters
time: 2.77(s)
xy_fe: 0.27 (m)
V_xfe: 0.257 (m/s)
V_yfe: -0.0874 (m/s)
V_zfe: -1.76 (m/s)
ψ_2fe: 12.2°
depth: 4.385 (m)
Mine Shape Parameters
d: 0.168 (m)
L: 0.477 (m)
m: 17.2 (kg)
J_1: 0.0647 (kg*m^2)
J_2: 0.356 (kg*m^2)
J_3: 0.356 (kg*m^2)
χ: 0.0002385 (m)
Final Model Parameters
time: 2.13 (s)
xy_fm: 0.444 (m)
V_xfm: -0.2 (m/s)
V_yfm: -0.00356 (m/s)
V_zfm: -2.65 (m/s)
ψ_2fm: -109°
Carderock Experiment Run: 20w-1
3-D Model Solution: 20w-1
Model Initial Parameters
ψ_2o: 32.7°
ω_2o: 0.35 (r/s)
V_xo: 0.0988 (m/s)
V_yo: -0.624 (m/s)
V_zo: -0.823 (m/s)
dt: 1/15 (s)
Depth (m)
Path Distance (m)
Mass center trail
Yaw Velocity
Y (m)
X (m)
ω_3 (/sec)

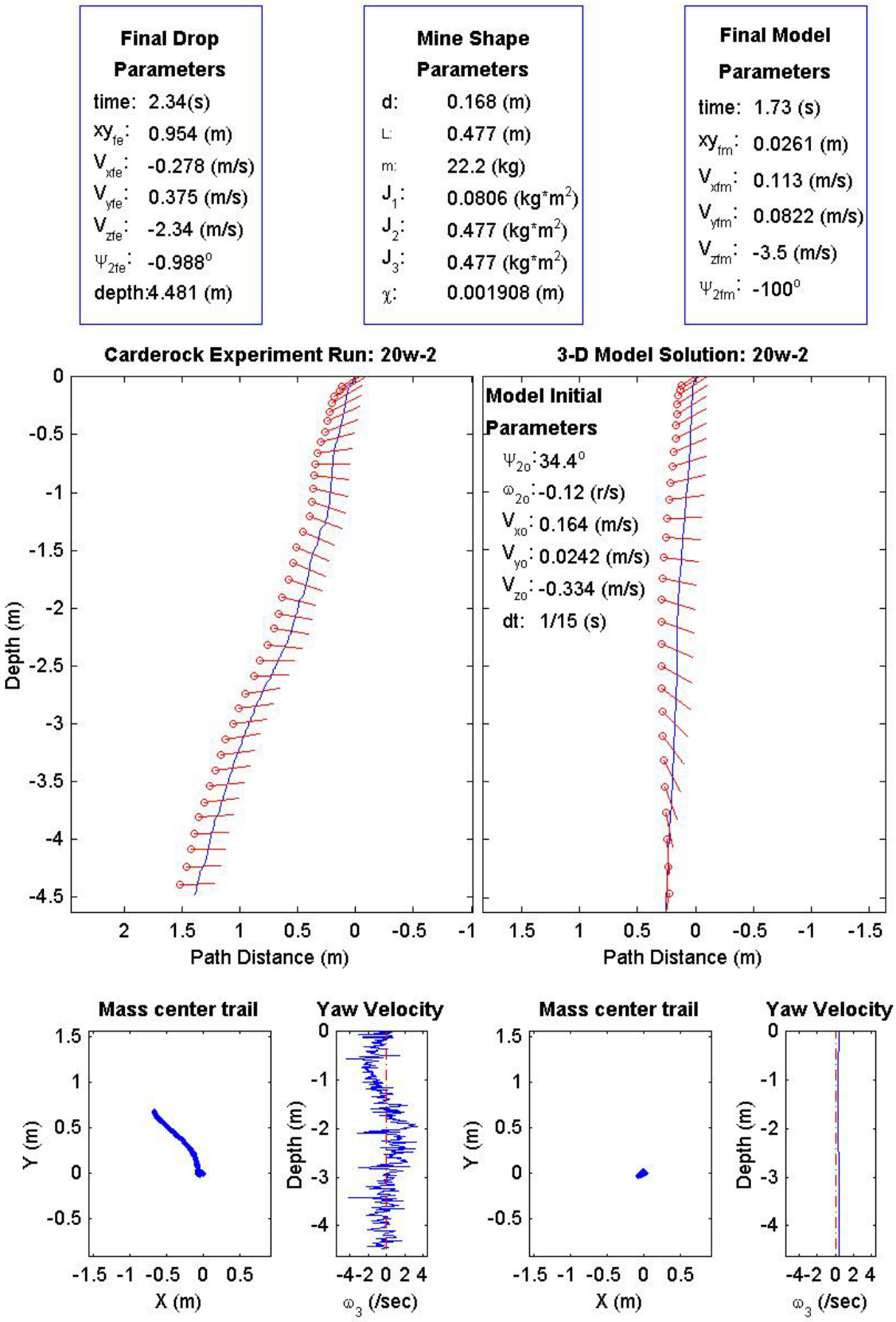
Final Drop Parameters
time: 2.34(s)
xy_fe: 0.954 (m)
V_xfe: -0.278 (m/s)
V_yfe: 0.375 (m/s)
V_zfe: -2.34 (m/s)
ψ_2fe: -0.988°
depth: 4.481 (m)
Mine Shape Parameters
d: 0.168 (m)
L: 0.477 (m)
m: 22.2 (kg)
J_1: 0.0806 (kg*m^2)
J_2: 0.477 (kg*m^2)
J_3: 0.477 (kg*m^2)
χ: 0.001908 (m)
Final Model Parameters
time: 1.73 (s)
xy_fm: 0.0261 (m)
V_xfm: 0.113 (m/s)
V_yfm: 0.0822 (m/s)
V_zfm: -3.5 (m/s)
ψ_2fm: -100°
Carderock Experiment Run: 20w-2
3-D Model Solution: 20w-2
Model Initial Parameters
ψ_2o: 34.4°
ω_2o: -0.12 (r/s)
V_xo: 0.164 (m/s)
V_yo: 0.0242 (m/s)
V_zo: -0.334 (m/s)
dt: 1/15 (s)
Depth (m)
Path Distance (m)
Path Distance (m)
Mass center trail
Yaw Velocity
Mass center trail
Yaw Velocity
Y (m)
X (m)
Depth (m)
ω_3 (/sec)
Y (m)
X (m)
Depth (m)
ω_3 (/sec)

Final Drop Parameters

time: 2.81(s)
xy_{fe}: 0.399 (m)
V_{xfe}: 0.0985 (m/s)
V_{yfe}: -0.017 (m/s)
V_{zfe}: -1.71 (m/s)
Ψ_{2fe}: 12.1°
depth: 4.285 (m)

Mine Shape Parameters

d: 0.168 (m)
L: 0.982 (m)
m: 34.5 (kg)
J_1: 0.136 (kg*m^2)
J_2: 2.9 (kg*m^2)
J_3: 2.9 (kg*m^2)
χ: 0.001964 (m)

Final Model Parameters

time: 2.13 (s)
xy_{fm}: 0.344 (m)
V_{xfm}: 0.438 (m/s)
V_{yfm}: 0.25 (m/s)
V_{zfm}: -2.86 (m/s)
Ψ_{2fm}: -56.9°

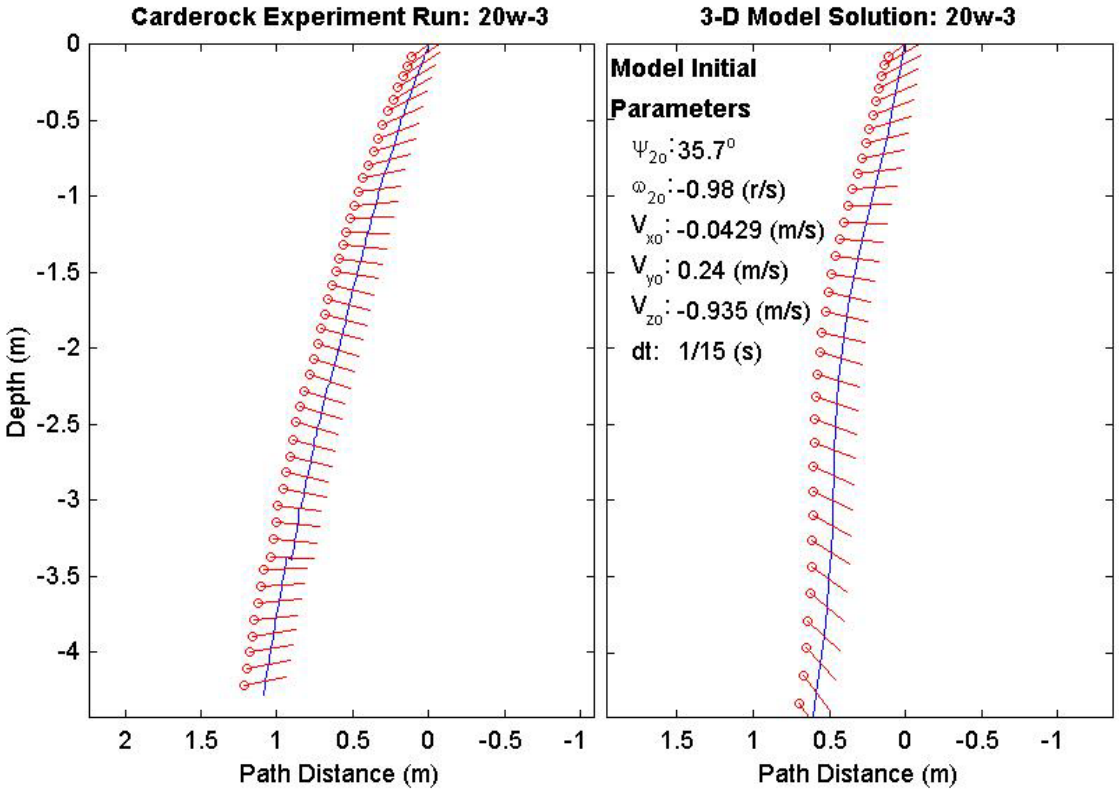

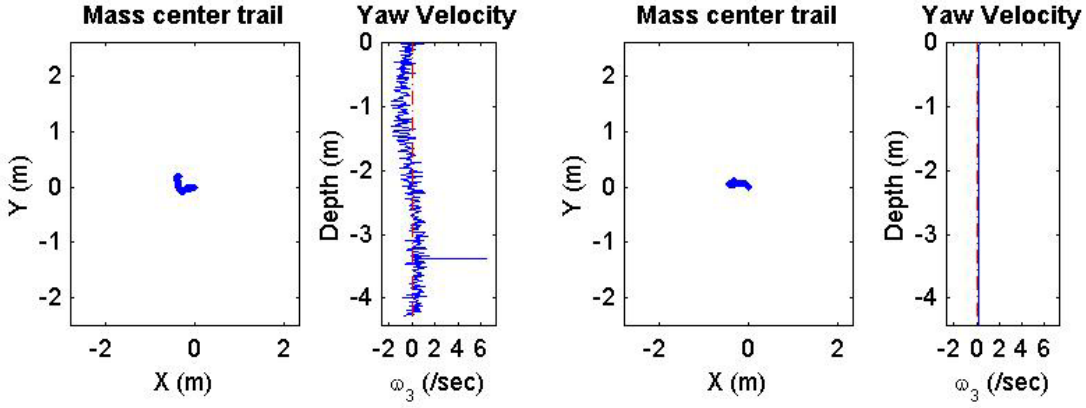

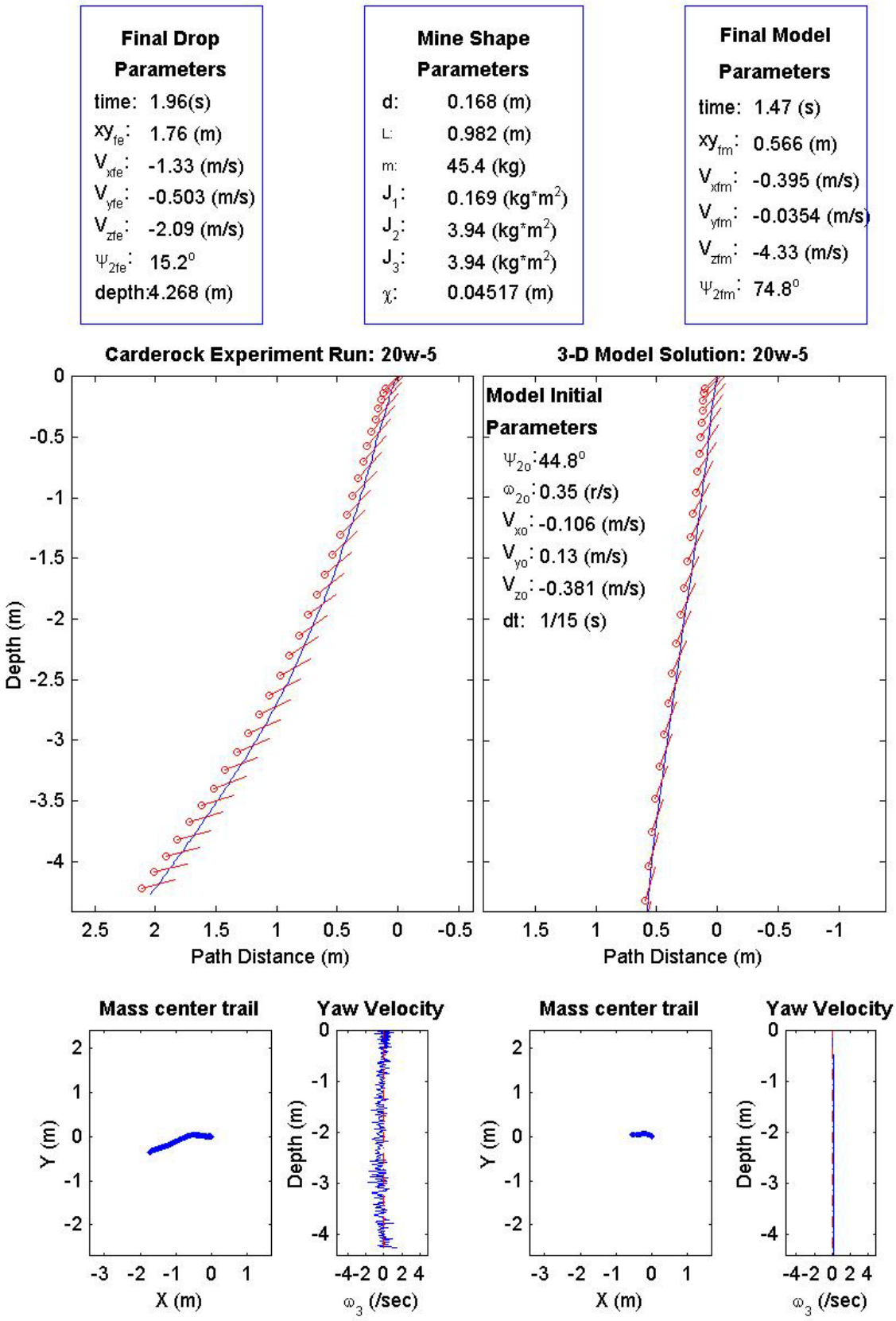
Final Drop Parameters
time: 1.96(s)
xy_fe: 1.76 (m)
V_xfe: -1.33 (m/s)
V_yfe: -0.503 (m/s)
V_zfe: -2.09 (m/s)
ψ_2fe: 15.2°
depth:4.268 (m)
Mine Shape Parameters
d: 0.168 (m)
L: 0.982 (m)
m: 45.4 (kg)
J_1: 0.169 (kg*m^2)
J_2: 3.94 (kg*m^2)
J_3: 3.94 (kg*m^2)
χ: 0.04517 (m)
Final Model Parameters
time: 1.47 (s)
xy_fm: 0.566 (m)
V_xfm: -0.395 (m/s)
V_yfm: -0.0354 (m/s)
V_zfm: -4.33 (m/s)
ψ_2fm: 74.8°
Carderock Experiment Run: 20w-5
3-D Model Solution: 20w-5
Model Initial Parameters
ψ_2o: 44.8°
ω_2o: 0.35 (r/s)
V_xo: -0.106 (m/s)
V_yo: 0.13 (m/s)
V_zo: -0.381 (m/s)
dt: 1/15 (s)
Depth (m)
Path Distance (m)
Path Distance (m)
Mass center trail
Yaw Velocity
Mass center trail
Yaw Velocity
Y (m)
X (m)
Depth (m)
ω_3 (/sec)
Y (m)
X (m)
Depth (m)
ω_3 (/sec)

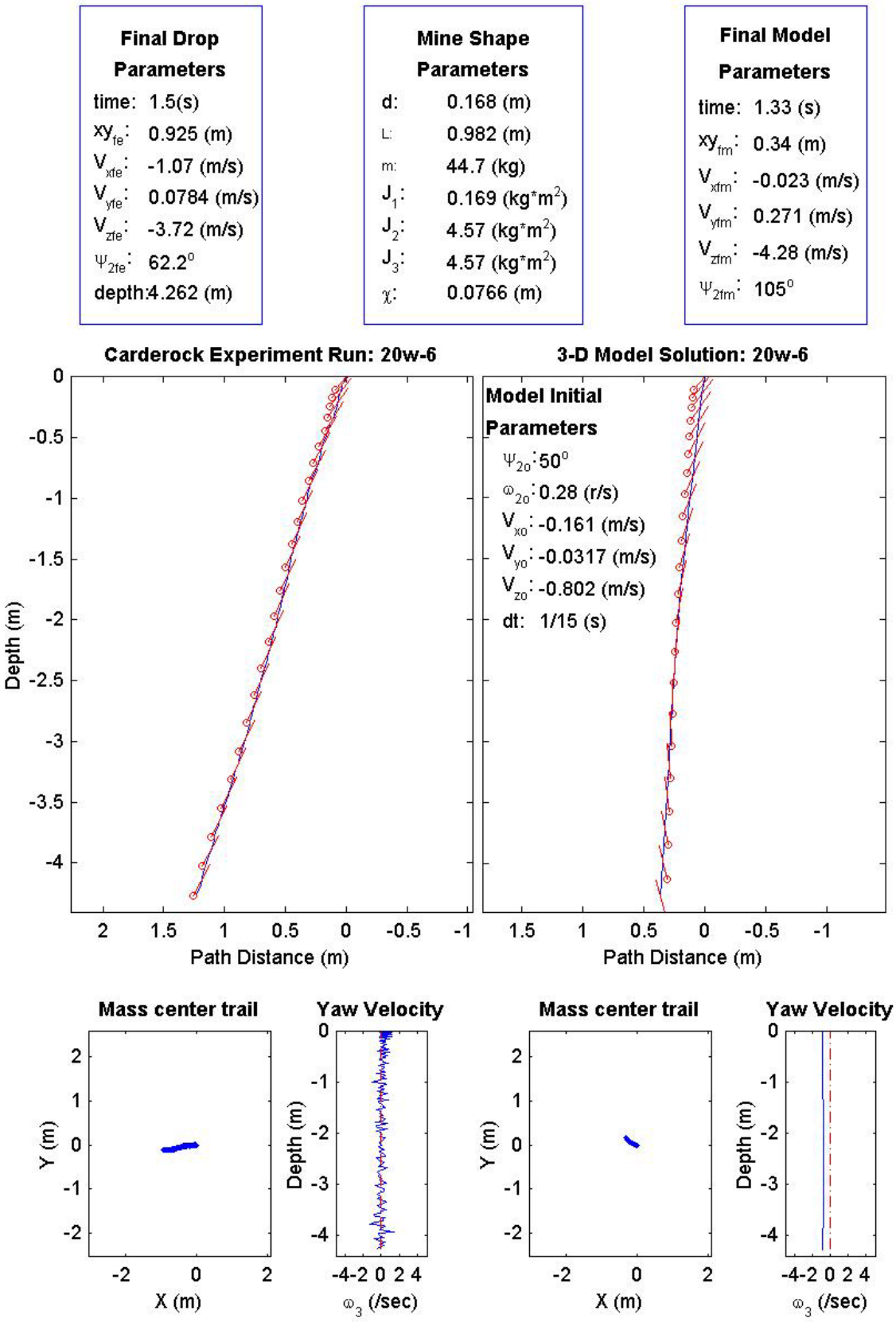
Final Drop Parameters
time: 1.5(s)
xy_fe: 0.925 (m)
V_xfe: -1.07 (m/s)
V_yfe: 0.0784 (m/s)
V_zfe: -3.72 (m/s)
ψ_2fe: 62.2°
depth:4.262 (m)
Mine Shape Parameters
d: 0.168 (m)
L: 0.982 (m)
m: 44.7 (kg)
J_1: 0.169 (kg*m^2)
J_2: 4.57 (kg*m^2)
J_3: 4.57 (kg*m^2)
χ: 0.0766 (m)
Final Model Parameters
time: 1.33 (s)
xy_fm: 0.34 (m)
V_xfm: -0.023 (m/s)
V_yfm: 0.271 (m/s)
V_zfm: -4.28 (m/s)
ψ_2fm: 105°
Carderock Experiment Run: 20w-6
3-D Model Solution: 20w-6
Model Initial Parameters
ψ_2o: 50°
ω_2o: 0.28 (r/s)
V_xo: -0.161 (m/s)
V_yo: -0.0317 (m/s)
V_zo: -0.802 (m/s)
dt: 1/15 (s)
Depth (m)
Path Distance (m)
Path Distance (m)
Mass center trail
Yaw Velocity
Mass center trail
Yaw Velocity
Y (m)
X (m)
Depth (m)
ω_3 (/sec)
Y (m)
X (m)
Depth (m)
ω_3 (/sec)

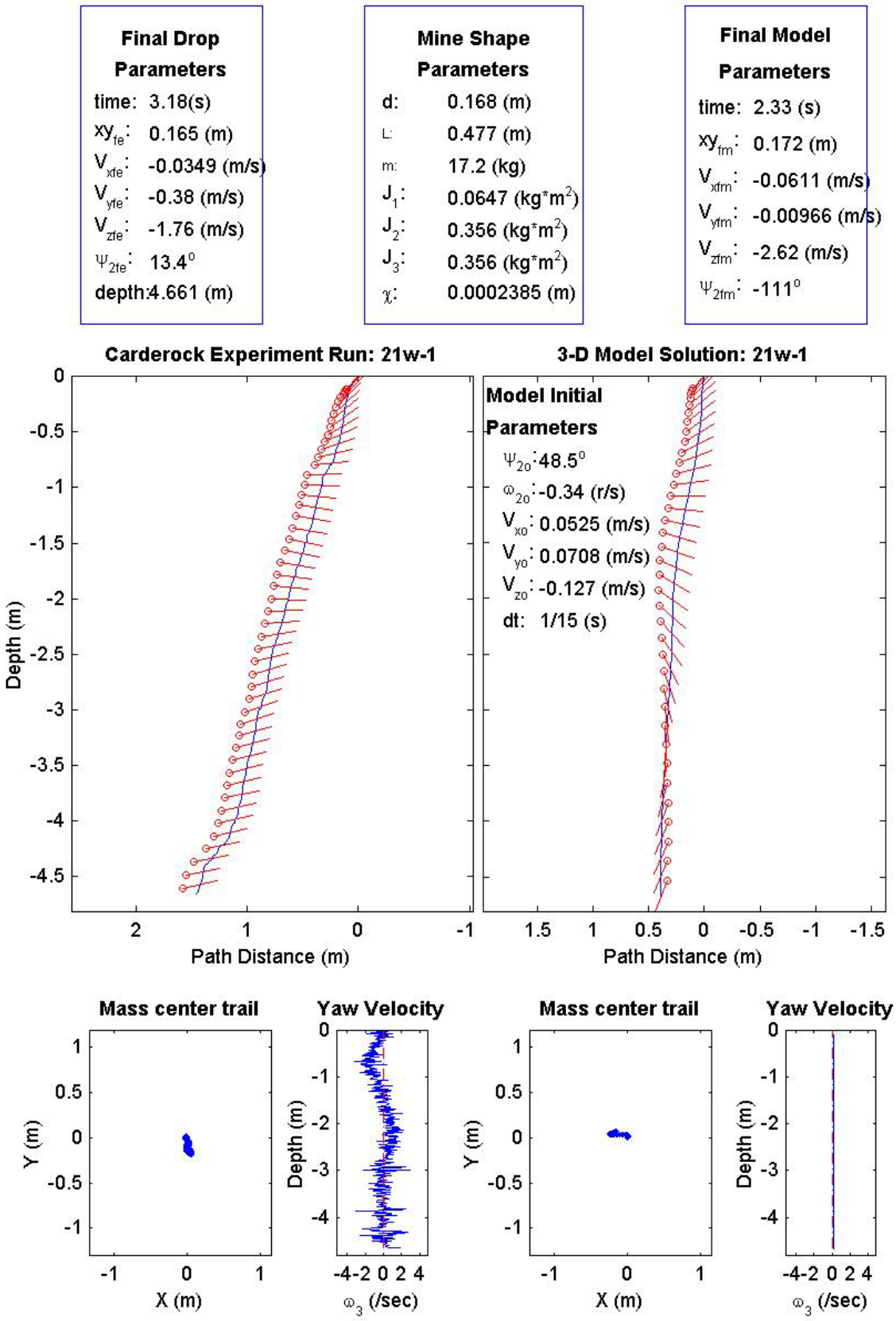
Final Drop Parameters
time: 3.18(s)
xy_fe: 0.165 (m)
V_xfe: -0.0349 (m/s)
V_yfe: -0.38 (m/s)
V_zfe: -1.76 (m/s)
ψ_2fe: 13.4°
depth:4.661 (m)
Mine Shape Parameters
d: 0.168 (m)
L: 0.477 (m)
m: 17.2 (kg)
J_1: 0.0647 (kg*m^2)
J_2: 0.356 (kg*m^2)
J_3: 0.356 (kg*m^2)
χ: 0.0002385 (m)
Final Model Parameters
time: 2.33 (s)
xy_fm: 0.172 (m)
V_xfm: -0.0611 (m/s)
V_yfm: -0.00966 (m/s)
V_zfm: -2.62 (m/s)
ψ_2fm: -111°
Carderock Experiment Run: 21w-1
3-D Model Solution: 21w-1
Model Initial Parameters
ψ_2o: 48.5°
ω_2o: -0.34 (r/s)
V_xo: 0.0525 (m/s)
V_yo: 0.0708 (m/s)
V_zo: -0.127 (m/s)
dt: 1/15 (s)
Depth (m)
Path Distance (m)
Path Distance (m)
Mass center trail
Yaw Velocity
Mass center trail
Yaw Velocity
Y (m)
X (m)
Depth (m)
ω_3 (/sec)
Y (m)
X (m)
Depth (m)
ω_3 (/sec)

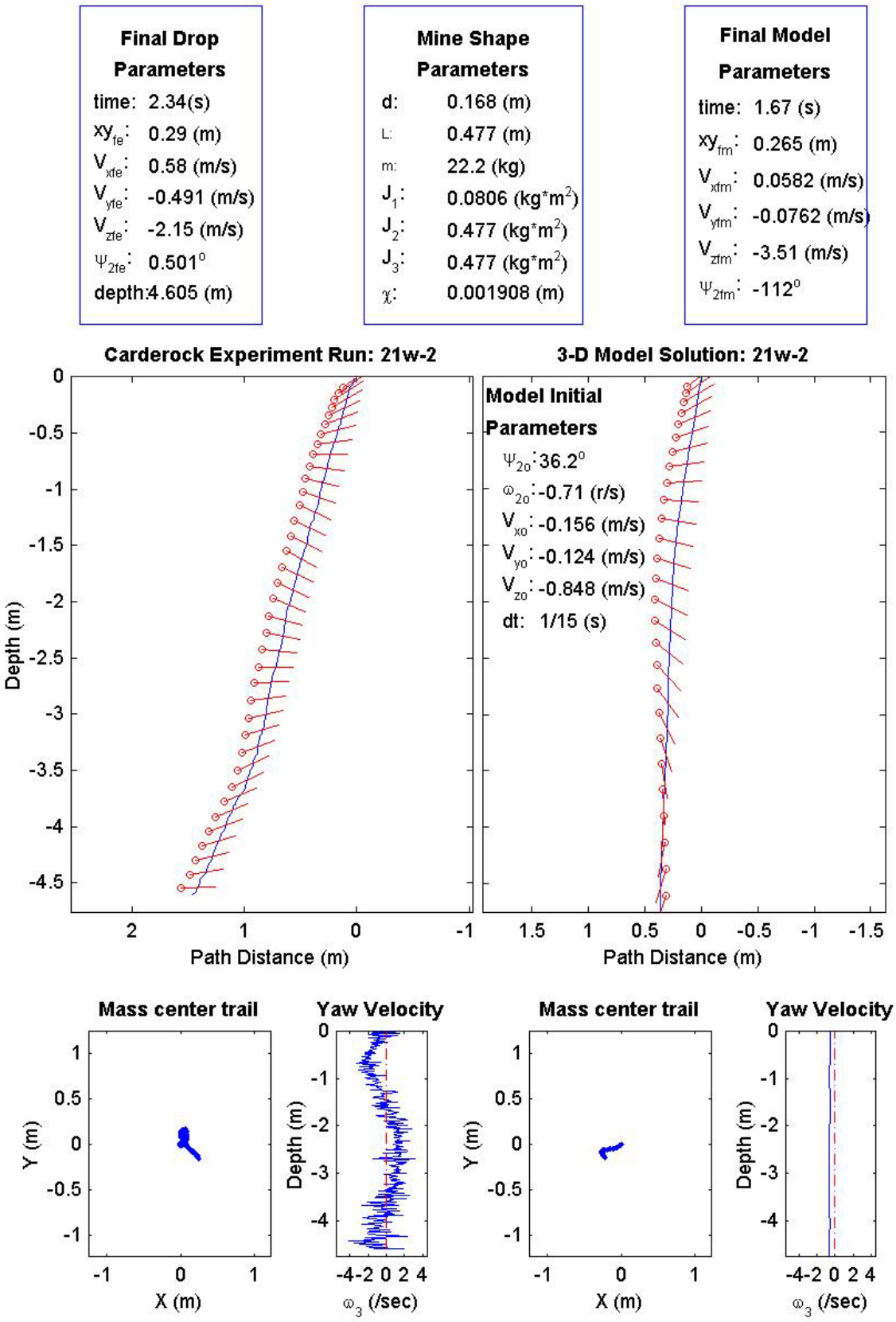
Final Drop Parameters
time: 2.34(s)
xy_fe: 0.29 (m)
V_xfe: 0.58 (m/s)
V_yfe: -0.491 (m/s)
V_zfe: -2.15 (m/s)
Ψ_2fe: 0.501°
depth: 4.605 (m)
Mine Shape Parameters
d: 0.168 (m)
L: 0.477 (m)
m: 22.2 (kg)
J_1: 0.0806 (kg*m^2)
J_2: 0.477 (kg*m^2)
J_3: 0.477 (kg*m^2)
χ: 0.001908 (m)
Final Model Parameters
time: 1.67 (s)
xy_fm: 0.265 (m)
V_xfm: 0.0582 (m/s)
V_yfm: -0.0762 (m/s)
V_zfm: -3.51 (m/s)
Ψ_2fm: -112°
Carderock Experiment Run: 21w-2
3-D Model Solution: 21w-2
Model Initial Parameters
Ψ_2o: 36.2°
ω_2o: -0.71 (r/s)
V_xo: -0.156 (m/s)
V_yo: -0.124 (m/s)
V_zo: -0.848 (m/s)
dt: 1/15 (s)
Depth (m)
Path Distance (m)
Path Distance (m)
Mass center trail
Yaw Velocity
Mass center trail
Yaw Velocity
Y (m)
X (m)
Depth (m)
ω_3 (/sec)
Y (m)
X (m)
Depth (m)
ω_3 (/sec)

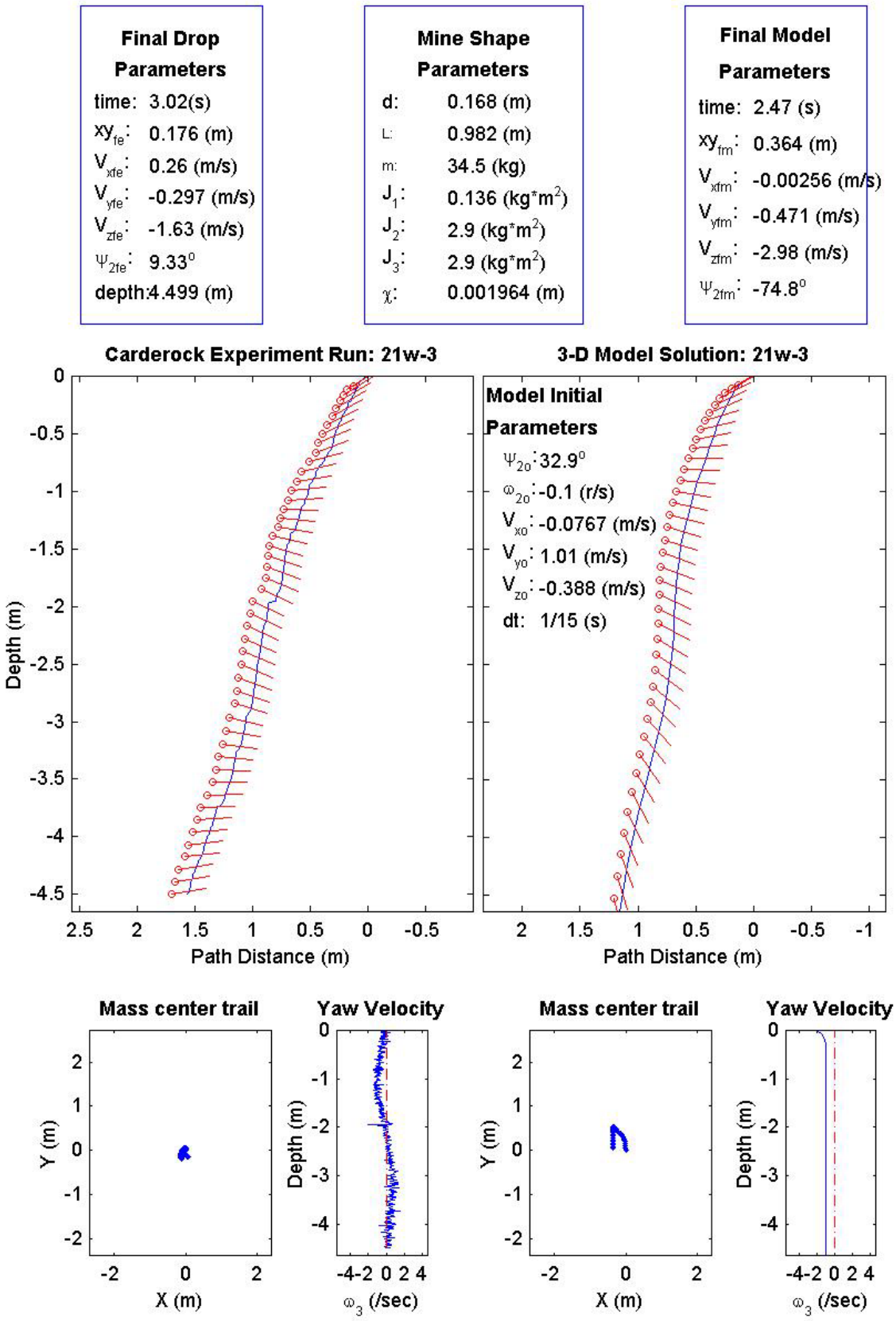
Final Drop Parameters
time: 3.02(s)
xy_fe: 0.176 (m)
V_xfe: 0.26 (m/s)
V_yfe: -0.297 (m/s)
V_zfe: -1.63 (m/s)
Ψ_2fe: 9.33°
depth: 4.499 (m)
Mine Shape Parameters
d: 0.168 (m)
L: 0.982 (m)
m: 34.5 (kg)
J_1: 0.136 (kg*m^2)
J_2: 2.9 (kg*m^2)
J_3: 2.9 (kg*m^2)
χ: 0.001964 (m)
Final Model Parameters
time: 2.47 (s)
xy_fm: 0.364 (m)
V_xfm: -0.00256 (m/s)
V_yfm: -0.471 (m/s)
V_zfm: -2.98 (m/s)
Ψ_2fm: -74.8°
Carderock Experiment Run: 21w-3
3-D Model Solution: 21w-3
Model Initial Parameters
Ψ_2o: 32.9°
ω_2o: -0.1 (r/s)
V_xo: -0.0767 (m/s)
V_yo: 1.01 (m/s)
V_zo: -0.388 (m/s)
dt: 1/15 (s)
Depth (m)
Path Distance (m)
Path Distance (m)
Mass center trail
Yaw Velocity
Mass center trail
Yaw Velocity
Y (m)
X (m)
Depth (m)
ω_3 (/sec)
Y (m)
X (m)
Depth (m)
ω_3 (/sec)

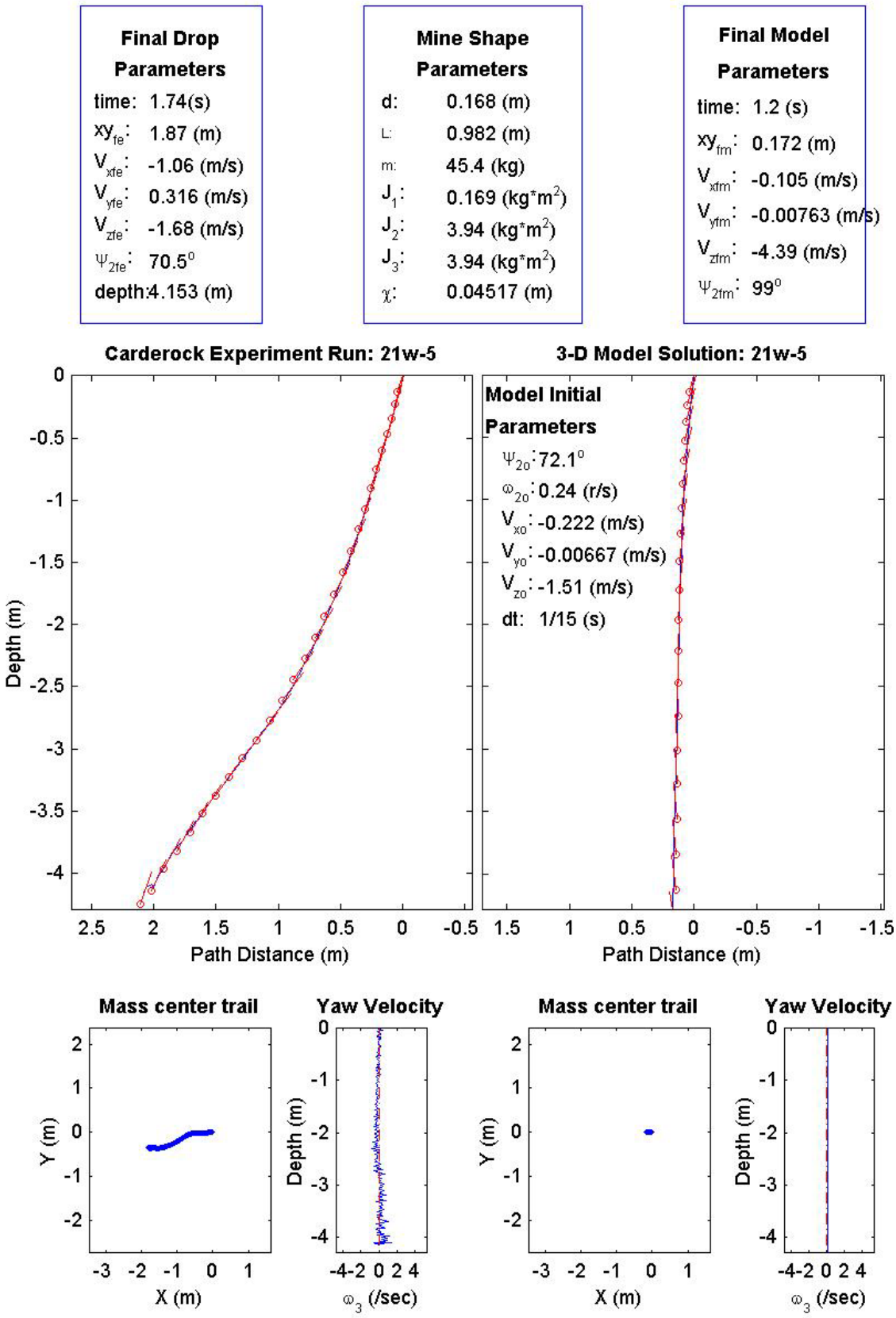
Final Drop Parameters
time: 1.74(s)
xy_fe: 1.87 (m)
V_xfe: -1.06 (m/s)
V_yfe: 0.316 (m/s)
V_zfe: -1.68 (m/s)
ψ_2fe: 70.5°
depth: 4.153 (m)
Mine Shape Parameters
d: 0.168 (m)
L: 0.982 (m)
m: 45.4 (kg)
J_1: 0.169 (kg*m^2)
J_2: 3.94 (kg*m^2)
J_3: 3.94 (kg*m^2)
χ: 0.04517 (m)
Final Model Parameters
time: 1.2 (s)
xy_fm: 0.172 (m)
V_xfm: -0.105 (m/s)
V_yfm: -0.00763 (m/s)
V_zfm: -4.39 (m/s)
ψ_2fm: 99°
Carderock Experiment Run: 21w-5
3-D Model Solution: 21w-5
Model Initial Parameters
ψ_2o: 72.1°
ω_2o: 0.24 (r/s)
V_xo: -0.222 (m/s)
V_yo: -0.00667 (m/s)
V_zo: -1.51 (m/s)
dt: 1/15 (s)
Depth (m)
Path Distance (m)
Path Distance (m)
Mass center trail
Yaw Velocity
Mass center trail
Yaw Velocity
Y (m)
X (m)
Depth (m)
ω_3 (/sec)
Y (m)
X (m)
Depth (m)
ω_3 (/sec)

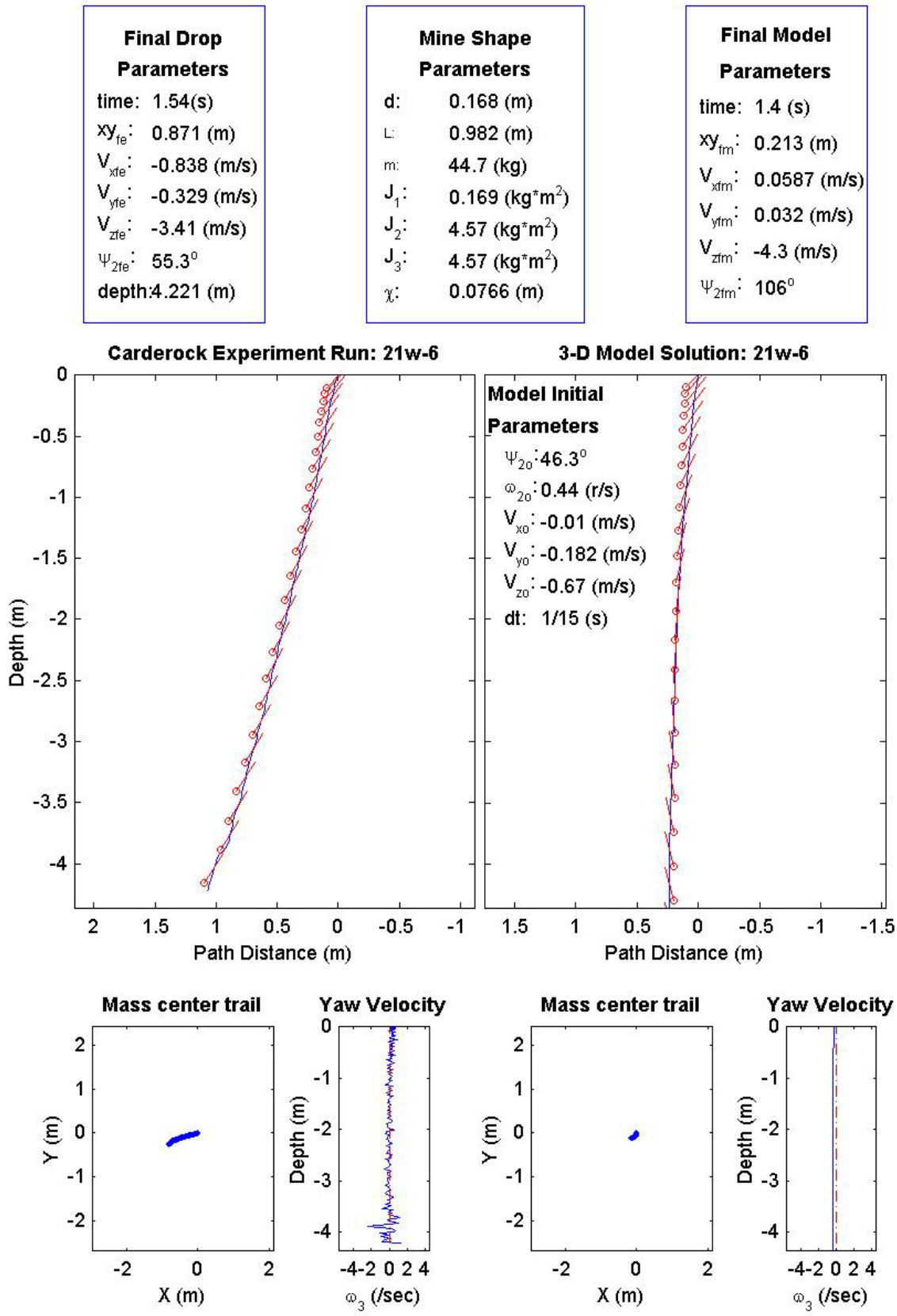
Final Drop Parameters
time: 1.54(s)
xy_fe: 0.871 (m)
V_xfe: -0.838 (m/s)
V_yfe: -0.329 (m/s)
V_zfe: -3.41 (m/s)
Ψ_2fe: 55.3°
depth:4.221 (m)
Mine Shape Parameters
d: 0.168 (m)
L: 0.982 (m)
m: 44.7 (kg)
J_1: 0.169 (kg*m^2)
J_2: 4.57 (kg*m^2)
J_3: 4.57 (kg*m^2)
χ: 0.0766 (m)
Final Model Parameters
time: 1.4 (s)
xy_fm: 0.213 (m)
V_xfm: 0.0587 (m/s)
V_yfm: 0.032 (m/s)
V_zfm: -4.3 (m/s)
Ψ_2fm: 106°
Carderock Experiment Run: 21w-6
3-D Model Solution: 21w-6
Model Initial Parameters
Ψ_2o: 46.3°
ω_2o: 0.44 (r/s)
V_xo: -0.01 (m/s)
V_yo: -0.182 (m/s)
V_zo: -0.67 (m/s)
dt: 1/15 (s)
Depth (m)
Path Distance (m)
Path Distance (m)
Mass center trail
Yaw Velocity
Mass center trail
Yaw Velocity
Y (m)
X (m)
Depth (m)
ω_3 (/sec)
Y (m)
X (m)
Depth (m)
ω_3 (/sec)

2. MIDEX DATA PLOTS

Index of blunt nosed mine shape drops conducted at NPS, Monterey, CA, 1-2 July 2001; adapted from (Gilless 2001). Subsequent pages contain the data plots for both the experimental data and the model output initialized from the MIDEX mine drop experimental data, 230 plots, read top to bottom, left to right, page one then page two.

15-2-15-1	12-2-45-2	9-2-75-3
15-2-15-2	12-2-45-3	9-2-75-4
15-2-15-3	12-2-45-4	15-1-15-1
15-2-15-4	12-2-45-5	15-1-15-2
15-2-15-5	9-2-45-1	15-1-15-3
12-2-15-1	9-2-45-2	12-1-15-1
12-2-15-2	9-2-45-3	12-1-15-2
12-2-15-3	9-2-45-4	12-1-15-3
12-2-15-4	9-2-45-5	9-1-15-1
9-2-15-1	15-2-60-1	9-1-15-2
9-2-15-2	15-2-60-2	9-1-15-3
9-2-15-3	15-2-60-3	15-1-30-1
9-2-15-4	15-2-60-4	15-1-30-2
15-2-30-1	15-2-60-5	15-1-30-3
15-2-30-2	12-2-60-1	15-1-30-4
15-2-30-3	12-2-60-2	15-1-30-5
15-2-30-4	12-2-60-3	12-1-30-1
15-2-30-5	12-2-60-4	12-1-30-2
12-2-30-1	12-2-60-5	12-1-30-3
12-2-30-2	9-2-60-1	12-1-30-4
12-2-30-3	9-2-60-2	12-1-30-5
12-2-30-4	9-2-60-3	9-1-30-1
12-2-30-5	9-2-60-4	9-1-30-2
9-2-30-1	9-2-60-5	9-1-30-3
9-2-30-2	15-2-75-1	9-1-30-4
9-2-30-3	15-2-75-2	9-1-30-5
9-2-30-4	15-2-75-3	15-1-45-1
9-2-30-5	15-2-75-4	15-1-45-2
15-2-45-1	12-2-75-1	15-1-45-3
15-2-45-2	12-2-75-2	15-1-45-4
15-2-45-3	12-2-75-3	15-1-45-5
15-2-45-4	12-2-75-4	12-1-45-1
15-2-45-5	9-2-75-1	12-1-45-2
12-2-45-1	9-2-75-2	12-1-45-3

12-1-45-4	9-0-15-4	9-0-60-1
12-1-45-5	15-0-30-1	9-0-60-2
9-1-45-1	15-0-30-2	9-0-60-3
9-1-45-2	15-0-30-3	9-0-60-4
9-1-45-3	15-0-30-4	9-0-60-5
9-1-45-4	15-0-30-5	9-0-60-6
9-1-45-5	12-0-30-1	15-0-75-1
15-1-60-1	12-0-30-2	15-0-75-2
15-1-60-2	12-0-30-3	12-0-75-1
15-1-60-3	12-0-30-4	12-0-75-2
15-1-60-4	12-0-30-5	9-0-75-1
15-1-60-5	9-0-30-1	9-0-75-2
12-1-60-1	9-0-30-2	15--1-30-1
12-1-60-2	9-0-30-3	15--1-30-2
12-1-60-3	9-0-30-4	12--1-30-1
12-1-60-4	9-0-30-5	12--1-30-2
12-1-60-5	15-0-45-1	9--1-30-1
9-1-60-1	15-0-45-2	9--1-30-2
9-1-60-2	15-0-45-3	15--1-45-1
9-1-60-3	15-0-45-4	15--1-45-2
9-1-60-4	12-0-45-1	12--1-45-1
9-1-60-5	12-0-45-2	12--1-45-2
15-1-75-1	12-0-45-3	9--1-45-1
15-1-75-2	12-0-45-4	9--1-45-2
15-1-75-3	12-0-45-5	15--1-60-1
12-1-75-1	9-0-45-1	15--1-60-2
12-1-75-2	9-0-45-2	12--1-60-1
12-1-75-3	9-0-45-3	12--1-60-2
9-1-75-1	9-0-45-4	9--1-60-1
9-1-75-2	9-0-45-5	9--1-60-2
9-1-75-3	15-0-60-1	15--2-30-1
15-0-15-1	15-0-60-2	15--2-30-2
15-0-15-2	15-0-60-3	12--2-30-1
15-0-15-3	15-0-60-4	12--2-30-2
15-0-15-4	15-0-60-5	9--2-30-1
12-0-15-1	15-0-60-6	9--2-30-2
12-0-15-2	12-0-60-1	15--2-45-1
12-0-15-3	12-0-60-2	15--2-45-2
12-0-15-4	12-0-60-3	12--2-45-1
9-0-15-1	12-0-60-4	12--2-45-2
9-0-15-2	12-0-60-5	9--2-45-1
9-0-15-3	12-0-60-6	9--2-45-2

Final Drop

Parameters (15/15-2190)

time: 1.27(s)
xy_{fe}: 0.195(m)
V_{xfe}: 0.108(m/s)
V_{yfe}: 0.081(m/s)
V_{zfe}: -1.67(m/s)
Ψ_{fe}: 79.6°
depth: 2.1(m)

Mine Shape

Parameters (15/15-2190)

d: 0.04(m)
L: 0.152(m)
m: 0.323(m)
J_1: 3.3e-005(kg*m^2)
J_2: 0.000623(kg*m^2)
J_3: 0.000623(kg*m^2)
χ: 0.01477(m)

Final Model

Parameters (15/15-2190)

time: 1.4(s)
xy_{fm}: 0.675(m)
V_{xfm}: 0.109(m/s)
V_{yfm}: -0.0517(m/s)
V_{zfm}: -1.52(m/s)
Ψ_{fm}: 90.75°
depth: 2.1(m)

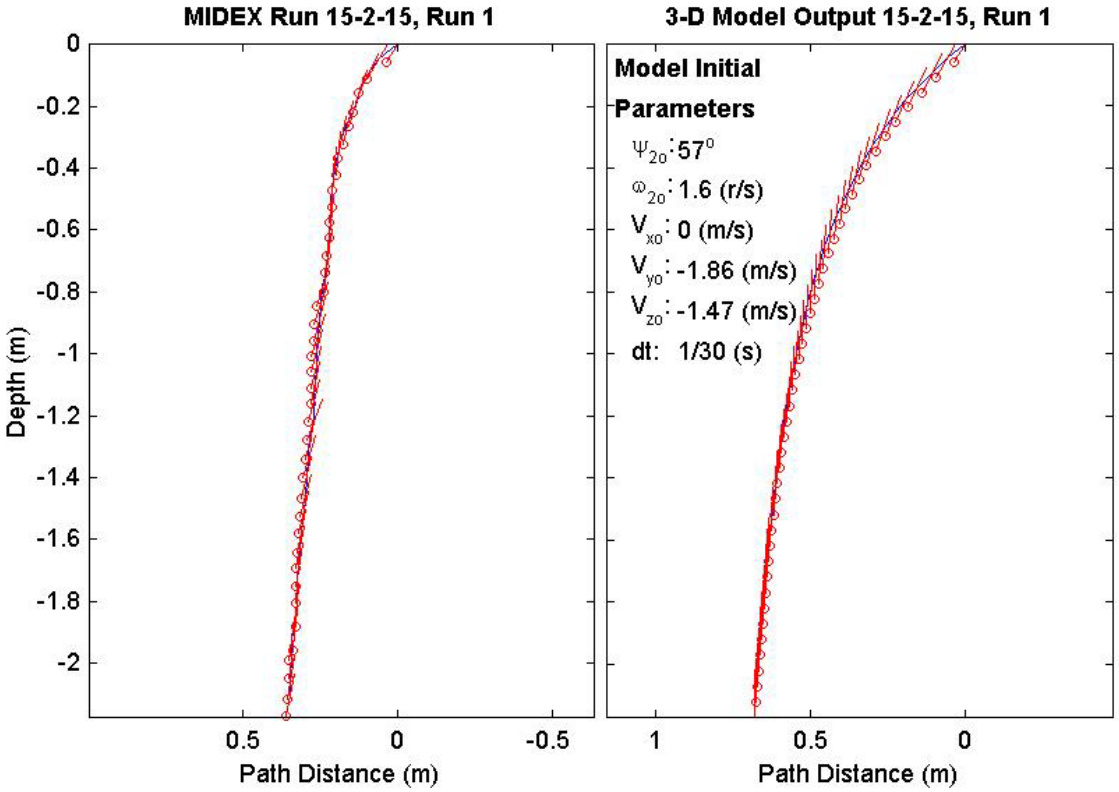

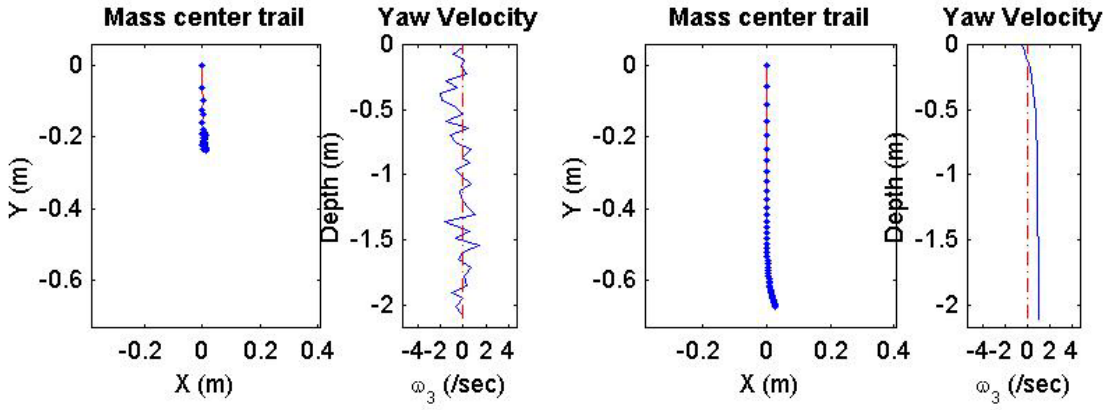

Final Drop Parameters (15/15-1186)

time: 1.4(s)
xy_{fe}: 0.604(m)
V_{xfe}: 0(m/s)
V_{yfe}: 0.045(m/s)
V_{zfe}: -1.93(m/s)
Ψ_{fe}: 89.1°
depth: 2.02(m)

Mine Shape Parameters (15/15-1186)

d: 0.04(m)
L: 0.152(m)
m: 0.323(m)
J_1: 3.3e-005(kg*m^2)
J_2: 0.000623(kg*m^2)
J_3: 0.000623(kg*m^2)
χ: 0.01477(m)

Final Model Parameters (15/15-1186)

time: 1.4(s)
xy_{fm}: 0.289(m)
V_{xfm}: 0.0589(m/s)
V_{yfm}: -0.108(m/s)
V_{zfm}: -1.54(m/s)
Ψ_{fm}: 100.5°
depth: 2.06(m)

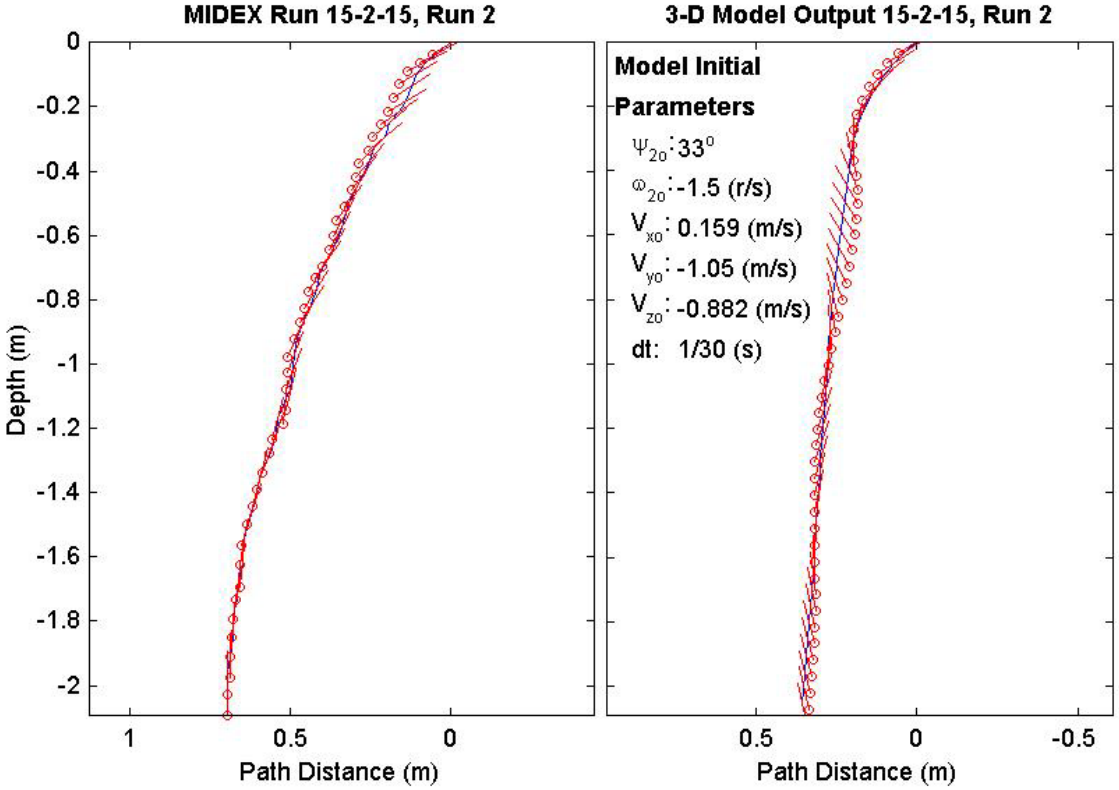

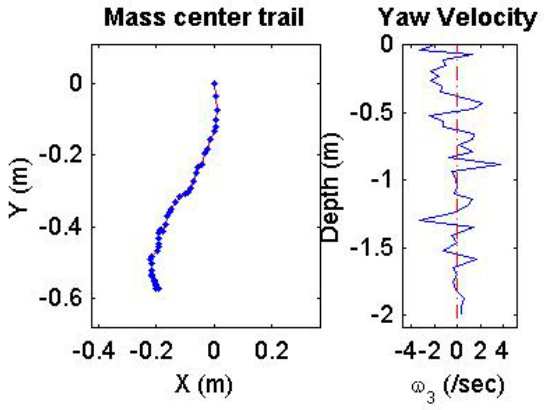

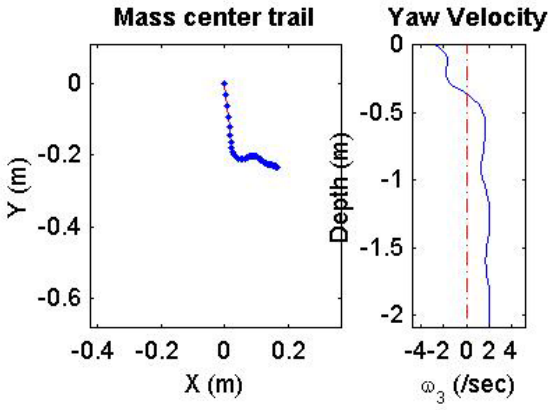

Final Drop Parameters (15/15-1897)

time: 1.23(s)
xy_{fe}: 0.39(m)
V_{xfe}: 0.051(m/s)
V_{yfe}: -0.045(m/s)
V_{zfe}: -2.09(m/s)
Ψ_{fe}: 90°
depth: 2.12(m)

Mine Shape Parameters (15/15-1897)

d: 0.04(m)
L: 0.152(m)
m: 0.323(m)
J_1: 3.3e-005(kg*m^2)
J_2: 0.000623(kg*m^2)
J_3: 0.000623(kg*m^2)
χ: 0.01477(m)

Final Model Parameters (15/15-1897)

time: 1.3(s)
xy_{fm}: 0.35(m)
V_{xfm}: 0.033(m/s)
V_{yfm}: -0.071(m/s)
V_{zfm}: -1.53(m/s)
Ψ_{fm}: 97.05°
depth: 2.13(m)

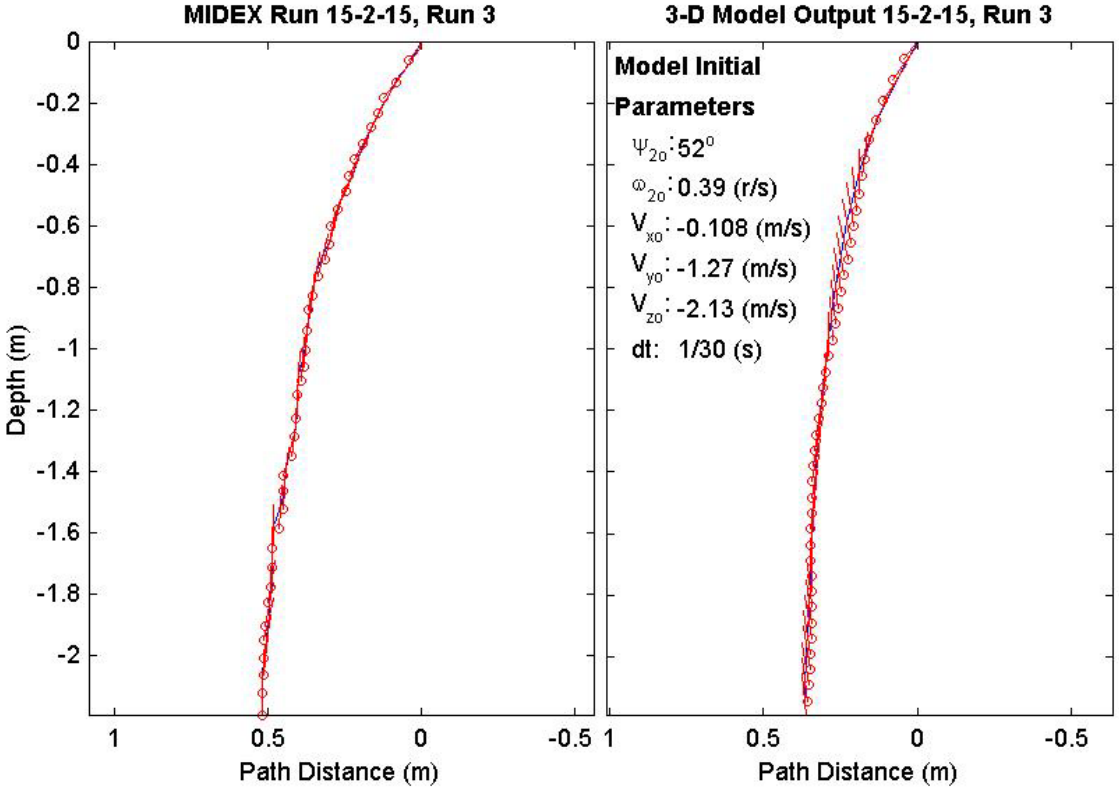

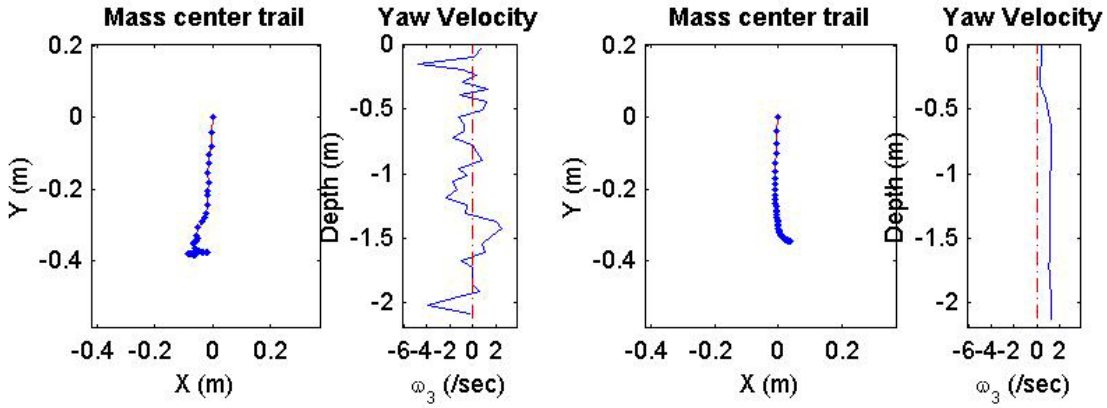

Final Drop Parameters (15/15-2637)

time: 1.27(s)
xy_{fe}: 0.22(m)
V_{xfe}: 0.055(m/s)
V_{yfe}: 0.045(m/s)
V_{zfe}: -1.65(m/s)
Ψ_{fe}: 87.9°
depth: 2.09(m)

Mine Shape Parameters (15/15-2637)

d: 0.04(m)
L: 0.152(m)
m: 0.323(m)
J_1: 3.3e-005(kg*m^2)
J_2: 0.000623(kg*m^2)
J_3: 0.000623(kg*m^2)
χ: 0.01477(m)

Final Model Parameters (15/15-2637)

time: 1.33(s)
xy_{fm}: 0.475(m)
V_{xfm}: 0.0348(m/s)
V_{yfm}: -0.114(m/s)
V_{zfm}: -1.52(m/s)
Ψ_{fm}: 87.67°
depth: 2.12(m)

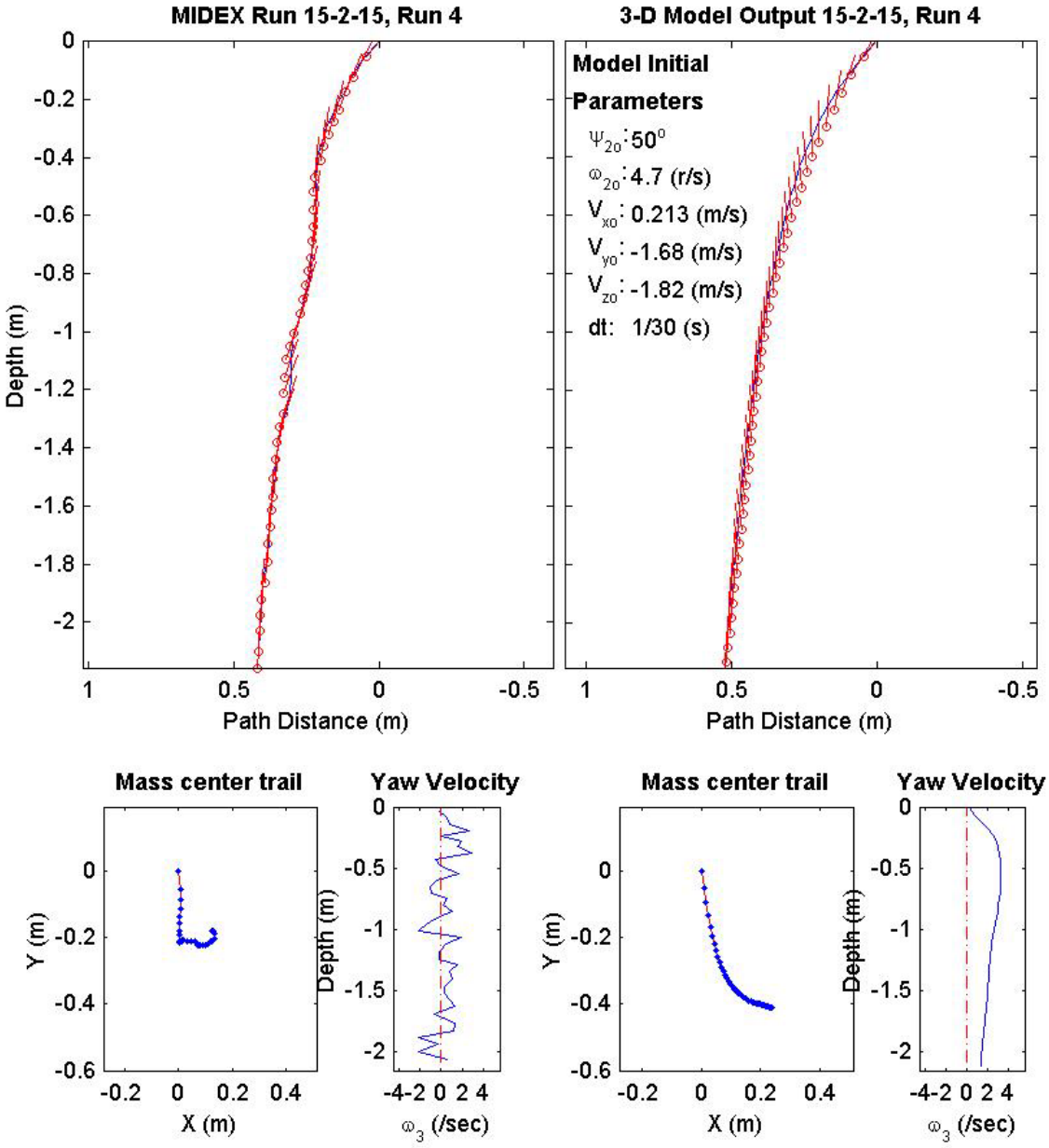

Final Drop Parameters (15/15-2302)

time: 1.27(s)
xy_{fe}: 0.223(m)
V_{xfe}: -0.055(m/s)
V_{yfe}: 0.055(m/s)
V_{zfe}: -1.61(m/s)
Ψ_{fe}: 86.9°
depth: 2.1(m)

Mine Shape Parameters (15/15-2302)

d: 0.04(m)
L: 0.152(m)
m: 0.323(m)
J_1: 3.3e-005(kg*m^2)
J_2: 0.000623(kg*m^2)
J_3: 0.000623(kg*m^2)
χ: 0.01477(m)

Final Model Parameters (15/15-2302)

time: 1.4(s)
xy_{fm}: 0.678(m)
V_{xfm}: 0.0798(m/s)
V_{yfm}: -0.101(m/s)
V_{zfm}: -1.52(m/s)
Ψ_{fm}: 91.14°
depth: 2.13(m)

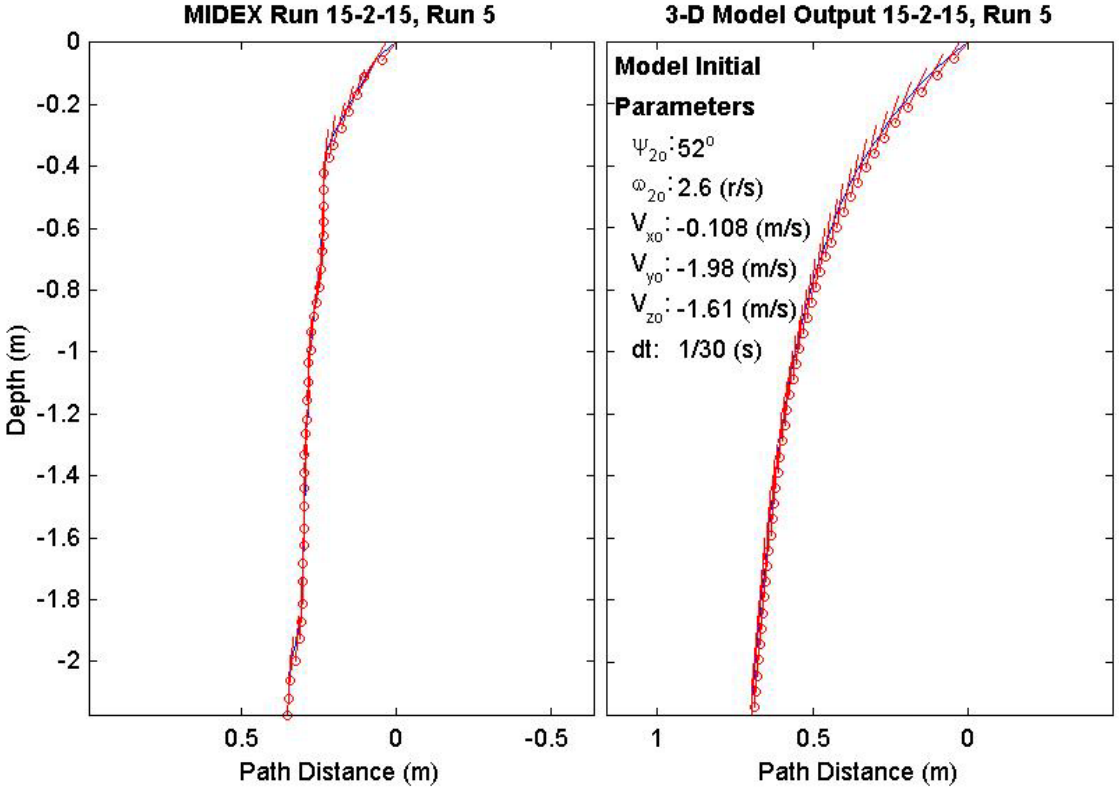

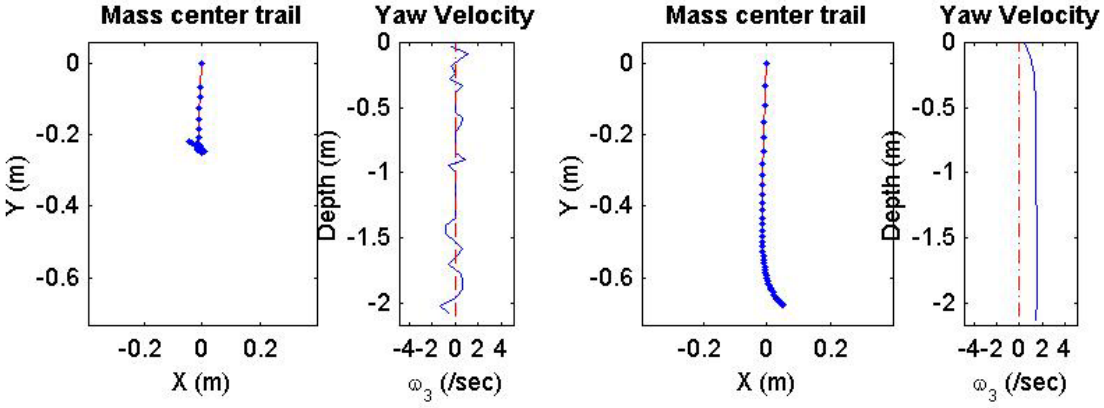

Final Drop Parameters (15/12-1406)

time: 1.37(s)
xy_{fe}: 0.224(m)
V_{xfe}: 0.054(m/s)
V_{yfe}: 0.633(m/s)
V_{zfe}: -1.45(m/s)
Ψ_{fe}: 73.7°
depth: 2.08(m)

Mine Shape Parameters (15/12-1406)

d: 0.04(m)
L: 0.121(m)
m: 0.254(m)
J_1: 2.71e-005(kg*m^2)
J_2: 0.000331(kg*m^2)
J_3: 0.000331(kg*m^2)
χ: 0.00997(m)

Final Model Parameters (15/12-1406)

time: 1.5(s)
xy_{fm}: 0.319(m)
V_{xfm}: 0.0572(m/s)
V_{yfm}: -0.0522(m/s)
V_{zfm}: -1.37(m/s)
Ψ_{fm}: 87.96°
depth: 2.09(m)

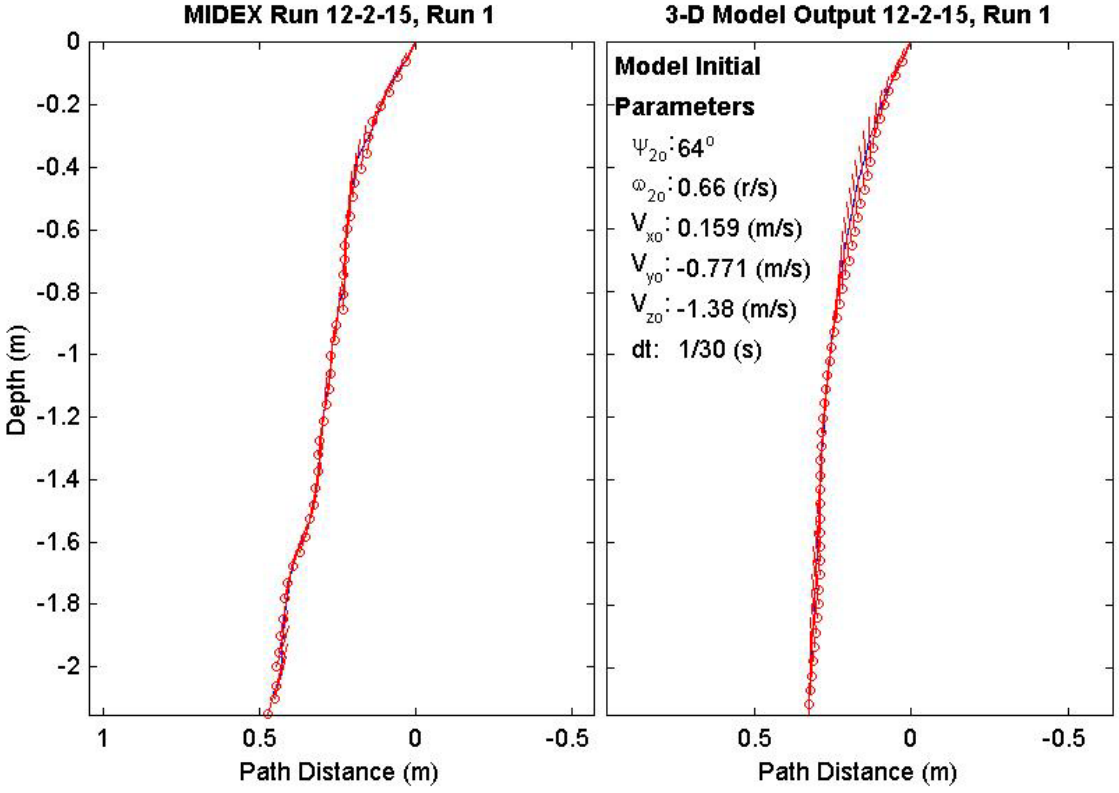

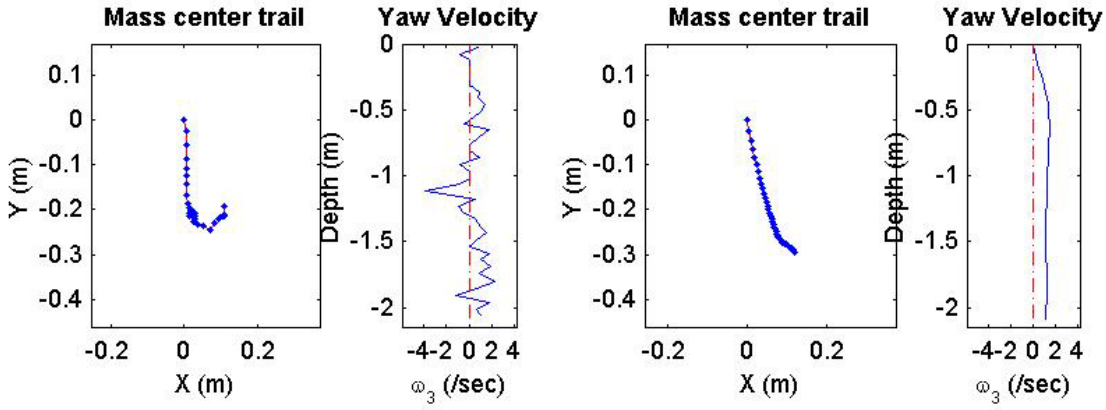

Final Drop
Parameters (15/12-1918)

time: 1.57(s)
xy_{fe}: 0.0136(m)
V_{xfe}: -0.054(m/s)
V_{yfe}: 0.228(m/s)
V_{zfe}: -1.73(m/s)
Ψ_{fe}: 79.7°
depth: 2.15(m)

Mine Shape
Parameters (15/12-1918)

d: 0.04(m)
L: 0.121(m)
m: 0.254(m)
J_1: 2.71e-005(kg*m^2)
J_2: 0.000331(kg*m^2)
J_3: 0.000331(kg*m^2)
χ: 0.00997(m)

Final Model
Parameters (15/12-1918)

time: 1.6(s)
xy_{fm}: 0.263(m)
V_{xfm}: -0.0184(m/s)
V_{yfm}: -0.0102(m/s)
V_{zfm}: -1.37(m/s)
Ψ_{fm}: 86.3°
depth: 2.2(m)

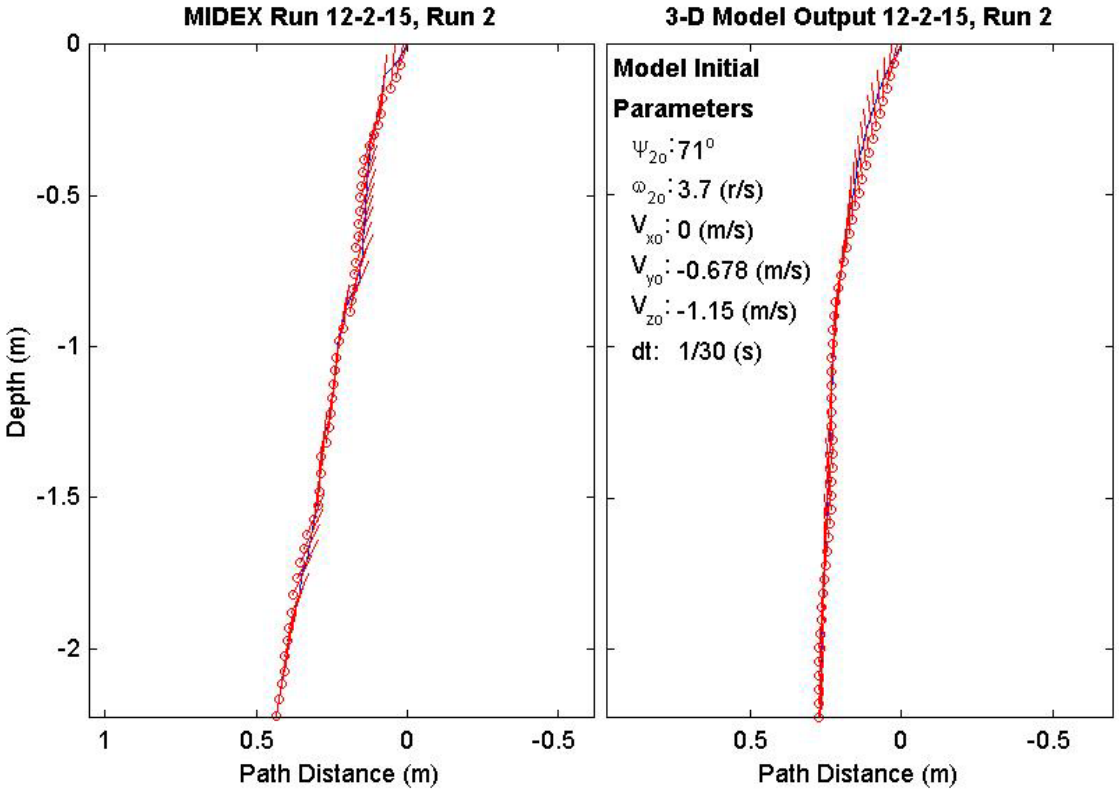

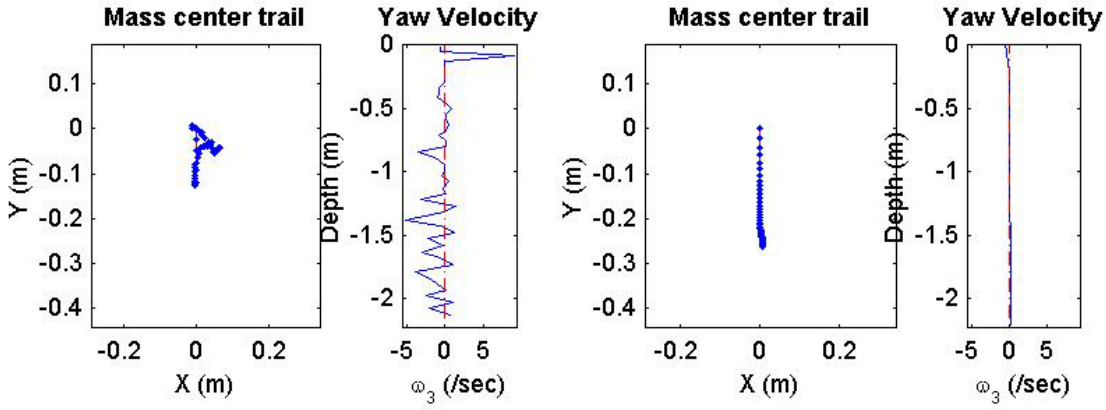

Final Drop

Parameters (15/12-2761)

time: 1.6(s)
xy_{fe}: 0.403(m)
V_{xfe}: 0.105(m/s)
V_{yfe}: 0.228(m/s)
V_{zfe}: -1.68(m/s)
Ψ_{fe}: 79.2°
depth: 2.15(m)

Mine Shape

Parameters (15/12-2761)

d: 0.04(m)
L: 0.121(m)
m: 0.254(m)
J_1: 2.71e-005(kg*m^2)
J_2: 0.000331(kg*m^2)
J_3: 0.000331(kg*m^2)
χ: 0.00997(m)

Final Model

Parameters (15/12-2761)

time: 1.57(s)
xy_{fm}: 0.541(m)
V_{xfm}: 0.0672(m/s)
V_{yfm}: -0.0482(m/s)
V_{zfm}: -1.37(m/s)
Ψ_{fm}: 90.91°
depth: 2.18(m)

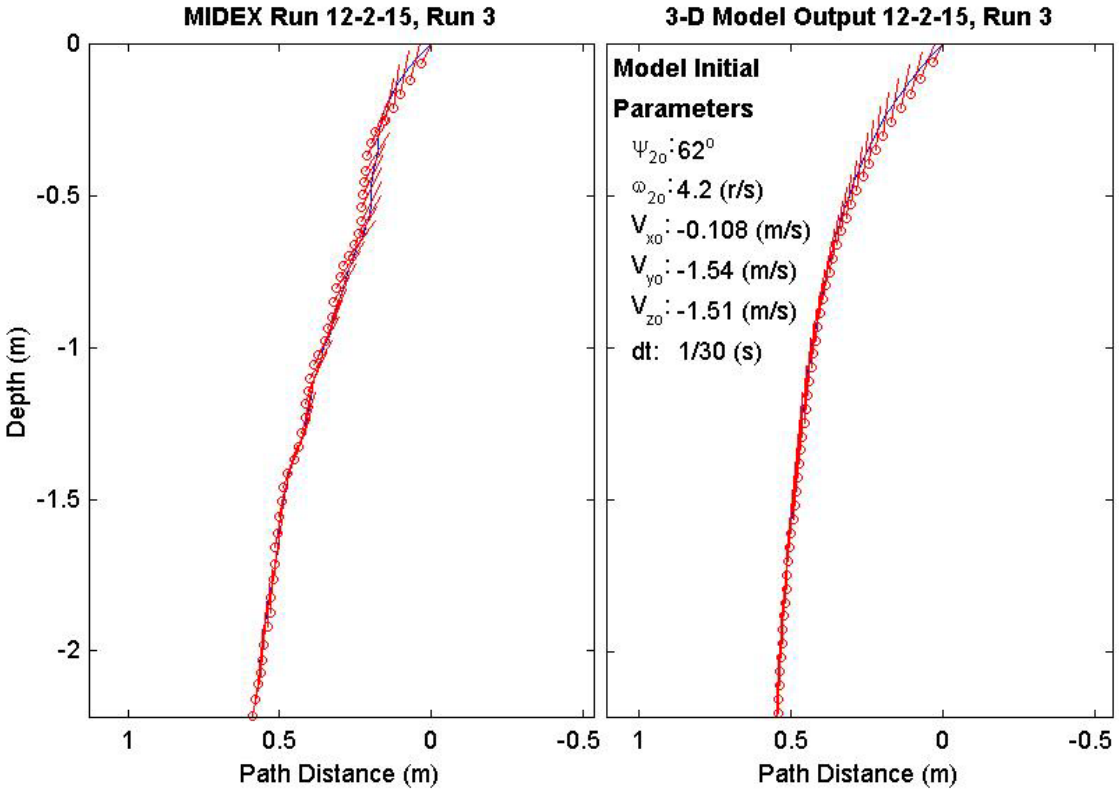

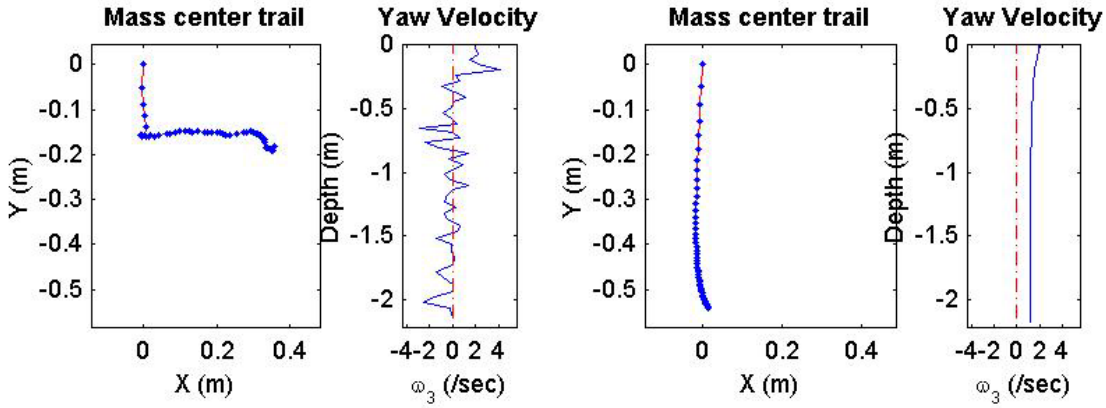

Final Drop Parameters (15/12-1448)

time: 1.43(s)
xy_{fe}: 0.139(m)
V_{xfe}: 0(m/s)
V_{yfe}: 0.321(m/s)
V_{zfe}: -1.39(m/s)
Ψ_{fe}: 77.7°
depth: 2.01(m)

Mine Shape Parameters (15/12-1448)

d: 0.04(m)
L: 0.121(m)
m: 0.254(m)
J_1: 2.71e-005(kg*m^2)
J_2: 0.000331(kg*m^2)
J_3: 0.000331(kg*m^2)
χ: 0.00997(m)

Final Model Parameters (15/12-1448)

time: 1.47(s)
xy_{fm}: 0.296(m)
V_{xfm}: 0.0479(m/s)
V_{yfm}: -0.0715(m/s)
V_{zfm}: -1.37(m/s)
Ψ_{fm}: 91.41°
depth: 2.05(m)

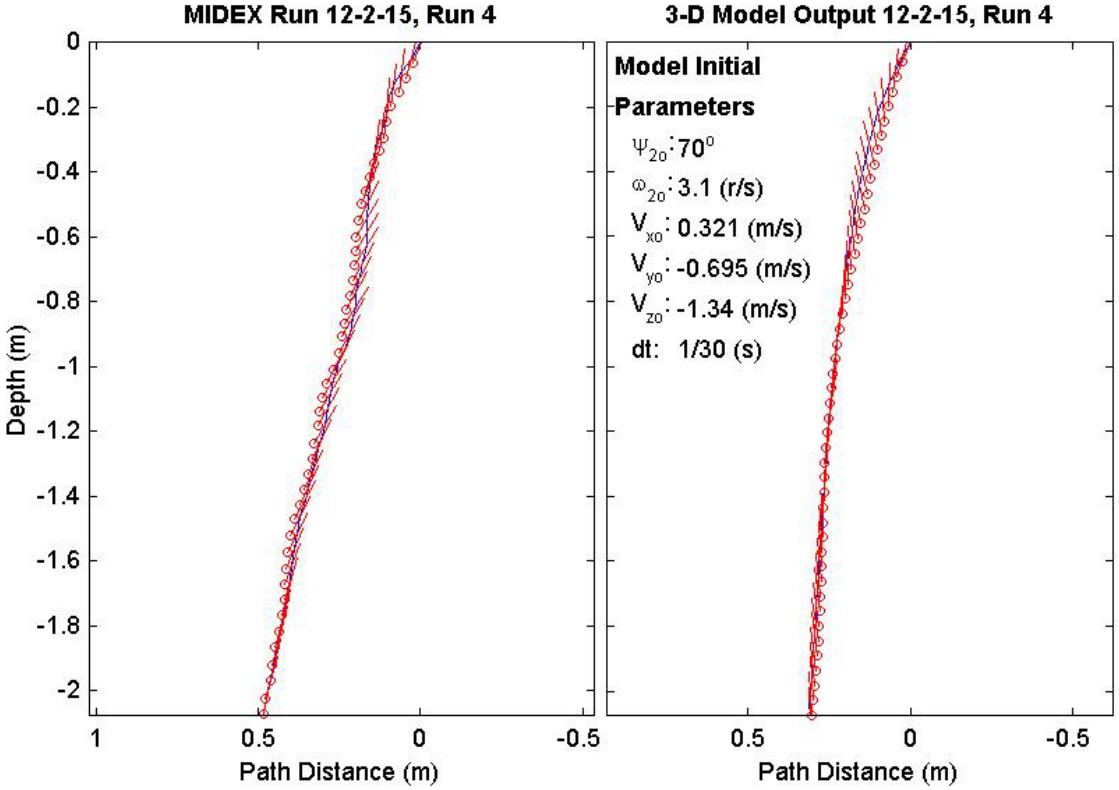

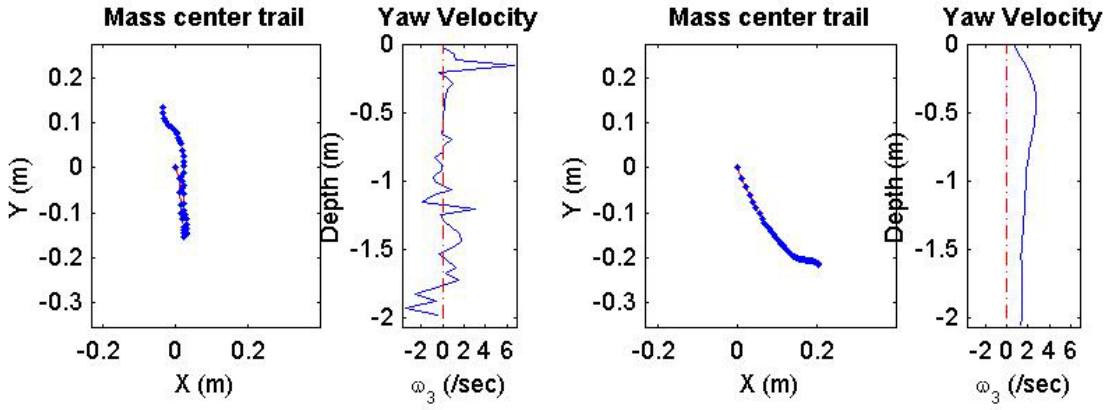

Final Drop
Parameters (15/9-1512)

time: 1.67(s)
xy_{fe}: 0.0783(m)
V_{xfe}: 0(m/s)
V_{yfe}: -0.315(m/s)
V_{zfe}: -1.54(m/s)
Ψ_{fe}: 73.6°
depth: 2.23(m)

Mine Shape
Parameters (15/9-1512)

d: 0.04(m)
L: 0.0912(m)
m: 0.215(m)
J_1: 2.35e-005(kg*m^2)
J_2: 0.000156(kg*m^2)
J_3: 0.000156(kg*m^2)
χ: 0.005796(m)

Final Model
Parameters (15/9-1512)

time: 1.57(s)
xy_{fm}: 0.255(m)
V_{xfm}: -0.0101(m/s)
V_{yfm}: 0.000595(m/s)
V_{zfm}: -1.4(m/s)
Ψ_{fm}: 81.13°
depth: 2.23(m)

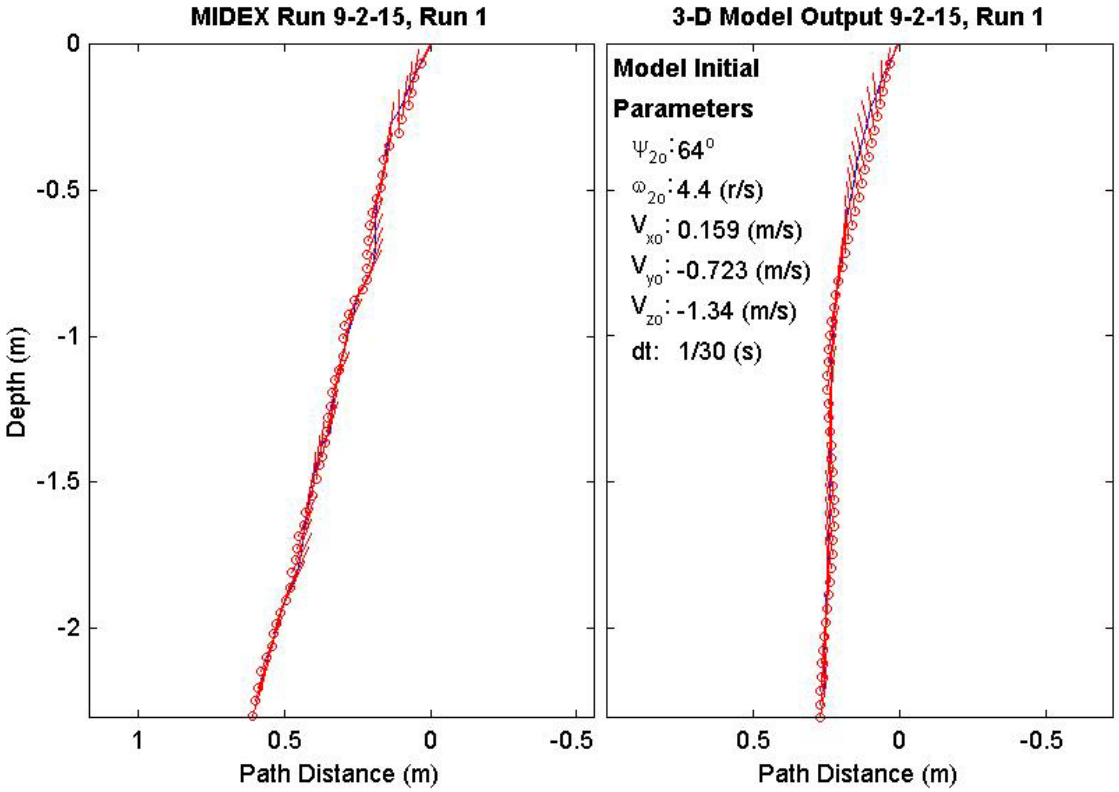

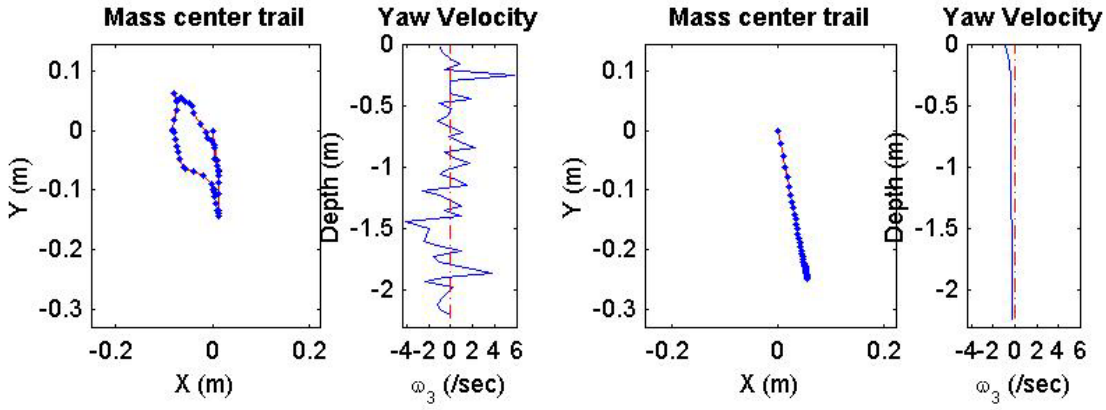

Final Drop
Parameters (15/9-2397)

time: 1.77(s)
xy_{fe}: 0.338(m)
V_{xfe}: 0.213(m/s)
V_{yfe}: 0.117(m/s)
V_{zfe}: -1.49(m/s)
Ψ_{fe}: 70.5°
depth: 2.11(m)

Mine Shape
Parameters (15/9-2397)

d: 0.04(m)
L: 0.0912(m)
m: 0.215(m)
J_1: 2.35e-005(kg*m^2)
J_2: 0.000156(kg*m^2)
J_3: 0.000156(kg*m^2)
χ: 0.005796(m)

Final Model
Parameters (15/9-2397)

time: 1.47(s)
xy_{fm}: 0.28(m)
V_{xfm}: 0.0169(m/s)
V_{yfm}: -0.0149(m/s)
V_{zfm}: -1.4(m/s)
Ψ_{fm}: 80.5°
depth: 2.14(m)

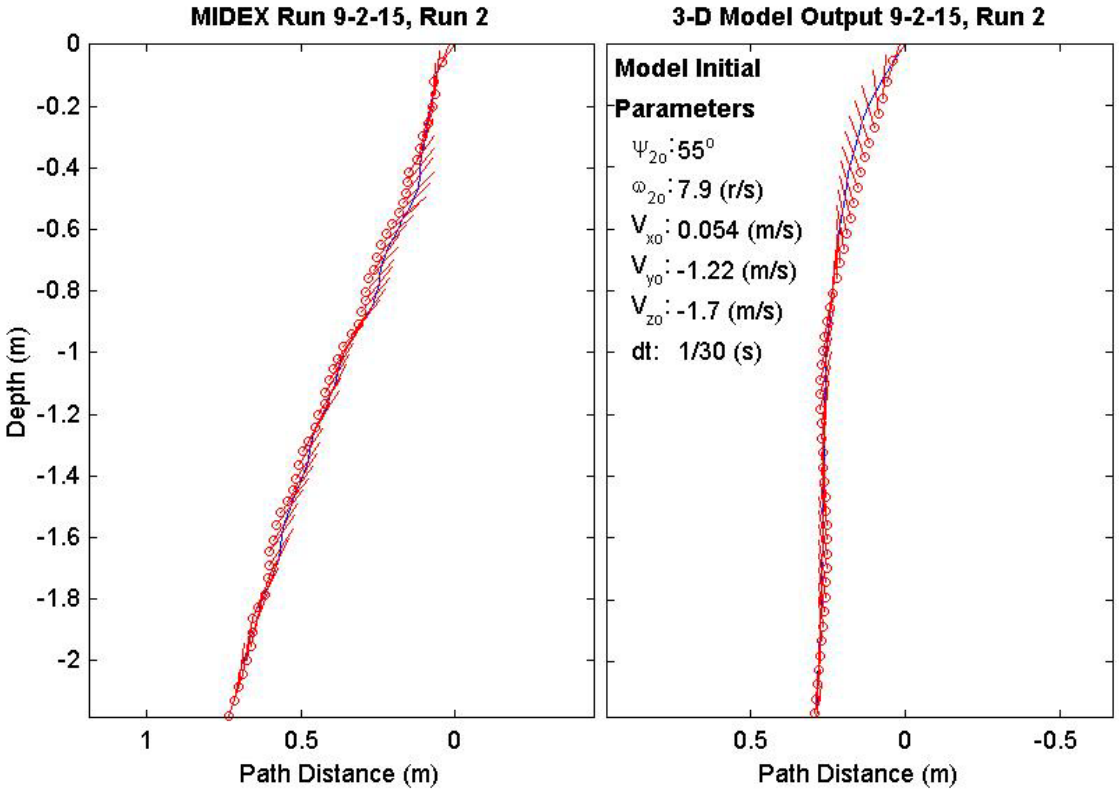

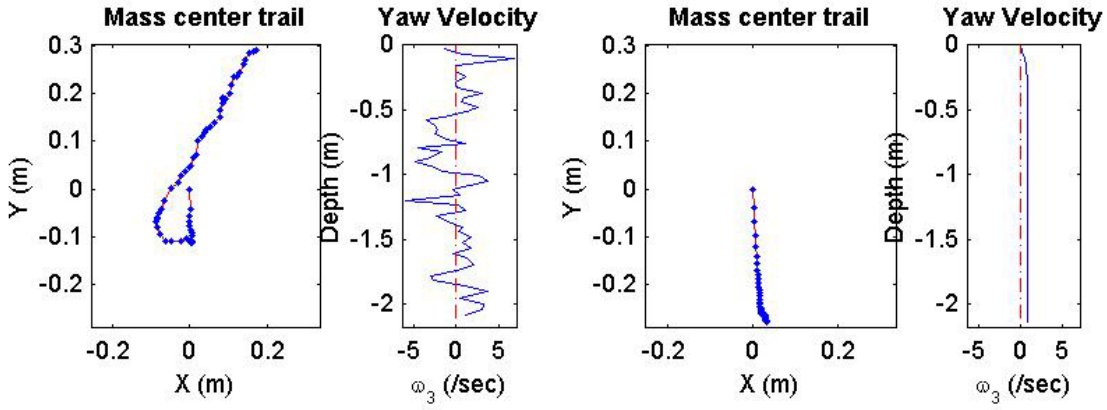

Final Drop

Parameters (15/9-2685)

time: 1.9(s)
xy_{fe}: 0.428(m)
V_{xfe}: 0.429(m/s)
V_{yfe}: 0.498(m/s)
V_{zfe}: -1.24(m/s)
Ψ_{fe}: 55°
depth: 2.19(m)

Mine Shape

Parameters (15/9-2685)

d: 0.04(m)
L: 0.0912(m)
m: 0.215(m)
J_1: 2.35e-005(kg*m^2)
J_2: 0.000156(kg*m^2)
J_3: 0.000156(kg*m^2)
χ: 0.005796(m)

Final Model

Parameters (15/9-2685)

time: 1.53(s)
xy_{fm}: 0.262(m)
V_{xfm}: 0.012(m/s)
V_{yfm}: -0.0193(m/s)
V_{zfm}: -1.4(m/s)
Ψ_{fm}: 81.16°
depth: 2.2(m)

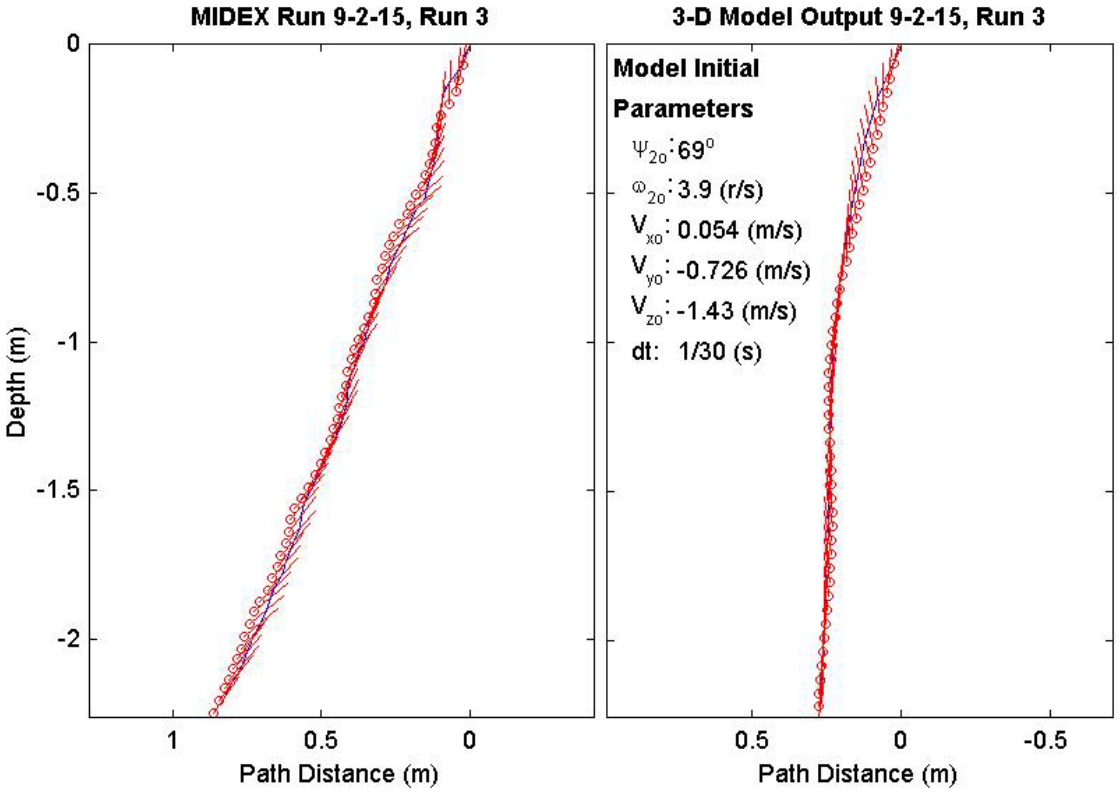

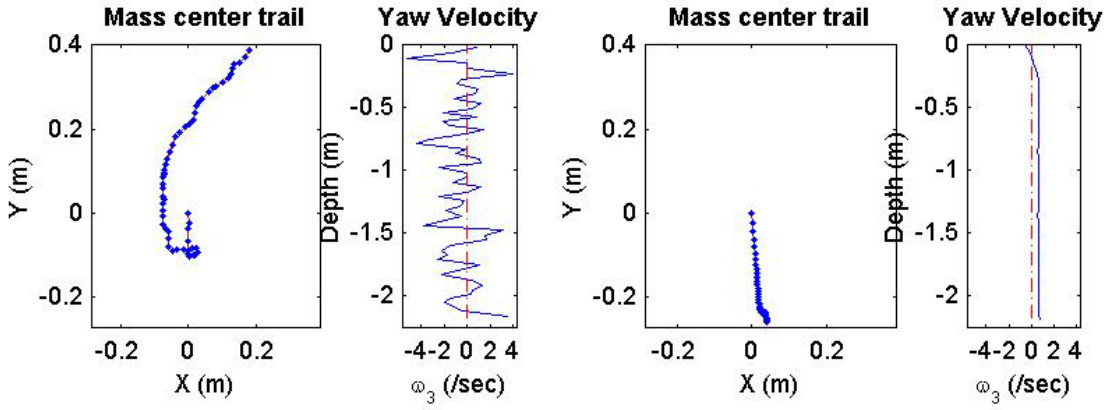

Final Drop
Parameters (15/9-1720)

time: 1.63(s)
xy_{fe}: 0.095(m)
V_{xfe}: 0(m/s)
V_{yfe}: -0.27(m/s)
V_{zfe}: -1.04(m/s)
Ψ_{fe}: 65.5°
depth: 2.08(m)

Mine Shape
Parameters (15/9-1720)

d: 0.04(m)
L: 0.0912(m)
m: 0.215(m)
J_1: 2.35e-005(kg*m^2)
J_2: 0.000156(kg*m^2)
J_3: 0.000156(kg*m^2)
χ: 0.005796(m)

Final Model
Parameters (15/9-1720)

time: 1.5(s)
xy_{fm}: 0.451(m)
V_{xfm}: 0.0634(m/s)
V_{yfm}: -0.0194(m/s)
V_{zfm}: -1.39(m/s)
Ψ_{fm}: 86.46°
depth: 2.11(m)

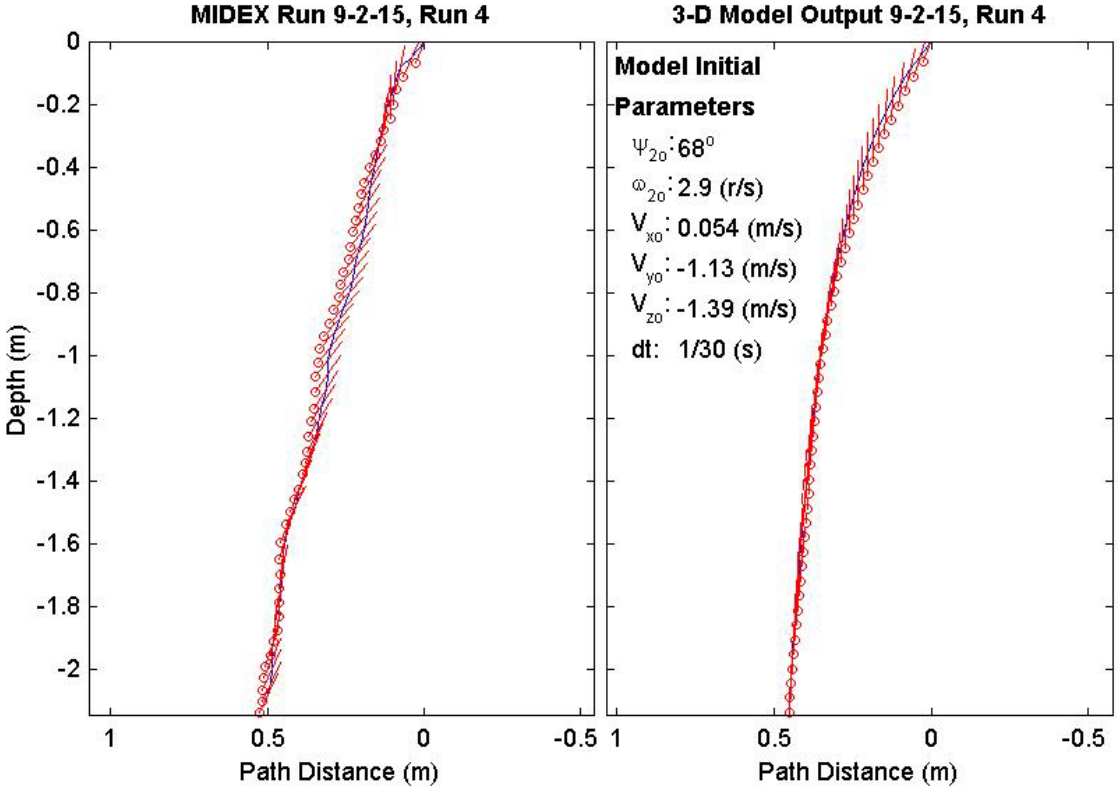

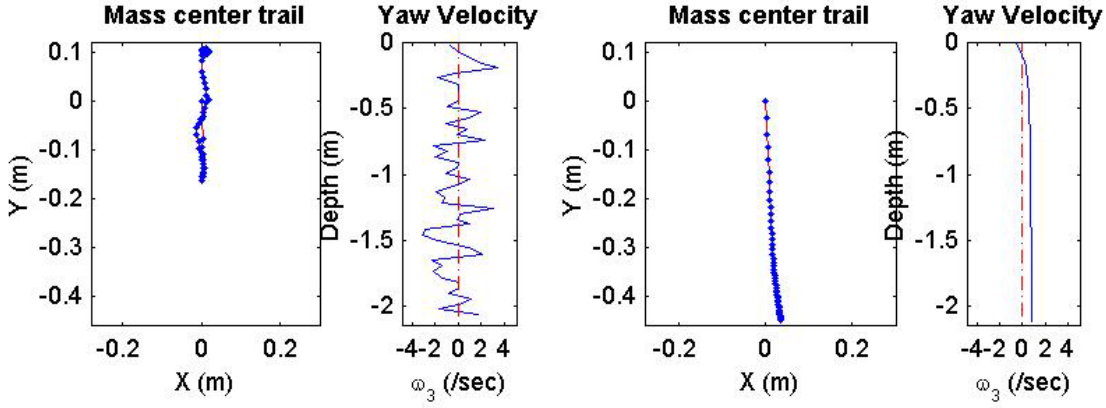

Final Drop Parameters (30/15-2082)

time: 1.2(s)
xy_{fe}: 0.258(m)
V_{xfe}: 0.045(m/s)
V_{yfe}: 0.045(m/s)
V_{zfe}: -1.75(m/s)
Ψ_{fe}: 82.9°
depth: 2.09(m)

Mine Shape Parameters (30/15-2082)

d: 0.04(m)
L: 0.152(m)
m: 0.323(m)
J_1: 3.3e-005(kg*m^2)
J_2: 0.000623(kg*m^2)
J_3: 0.000623(kg*m^2)
χ: 0.01477(m)

Final Model Parameters (30/15-2082)

time: 1.33(s)
xy_{fm}: 0.557(m)
V_{xfm}: 0.103(m/s)
V_{yfm}: -0.0623(m/s)
V_{zfm}: -1.52(m/s)
Ψ_{fm}: 90.43°
depth: 2.1(m)

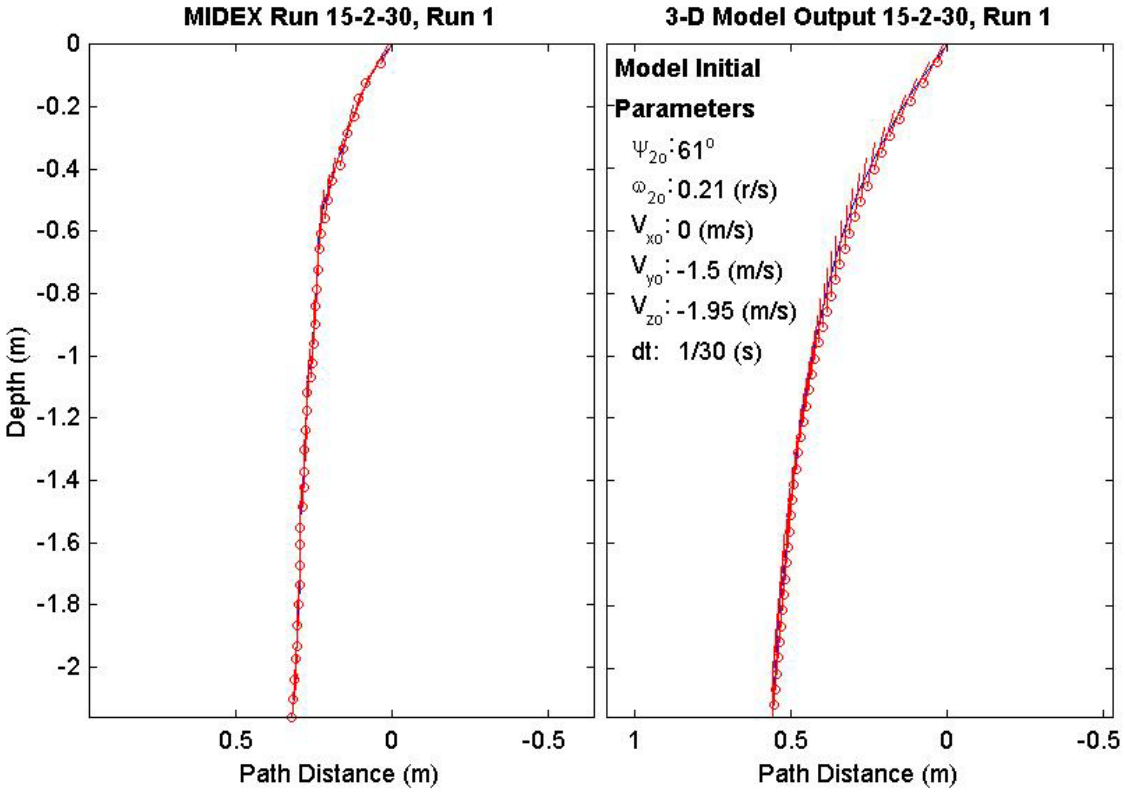

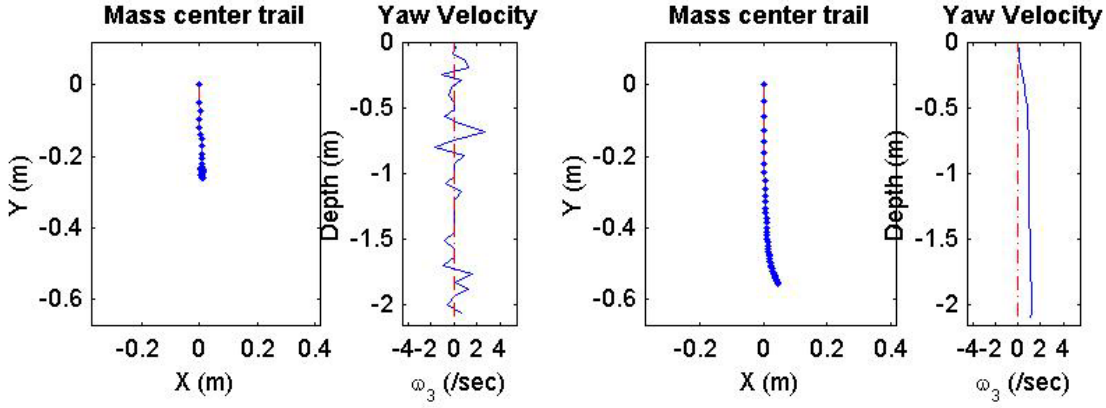

Final Drop Parameters (30/15-2309)

time: 1.27(s)
xy_{fe}: 0.203(m)
V_{xfe}: -0.055(m/s)
V_{yfe}: 0.408(m/s)
V_{zfe}: -1.76(m/s)
Ψ_{fe}: 86.4°
depth: 2.12(m)

Mine Shape Parameters (30/15-2309)

d: 0.04(m)
L: 0.152(m)
m: 0.323(m)
J_1: 3.3e-005(kg*m^2)
J_2: 0.000623(kg*m^2)
J_3: 0.000623(kg*m^2)
χ: 0.01477(m)

Final Model Parameters (30/15-2309)

time: 1.43(s)
xy_{fm}: 0.443(m)
V_{xfm}: 0.0771(m/s)
V_{yfm}: 0.0617(m/s)
V_{zfm}: -1.52(m/s)
Ψ_{fm}: 87.95°
depth: 2.15(m)

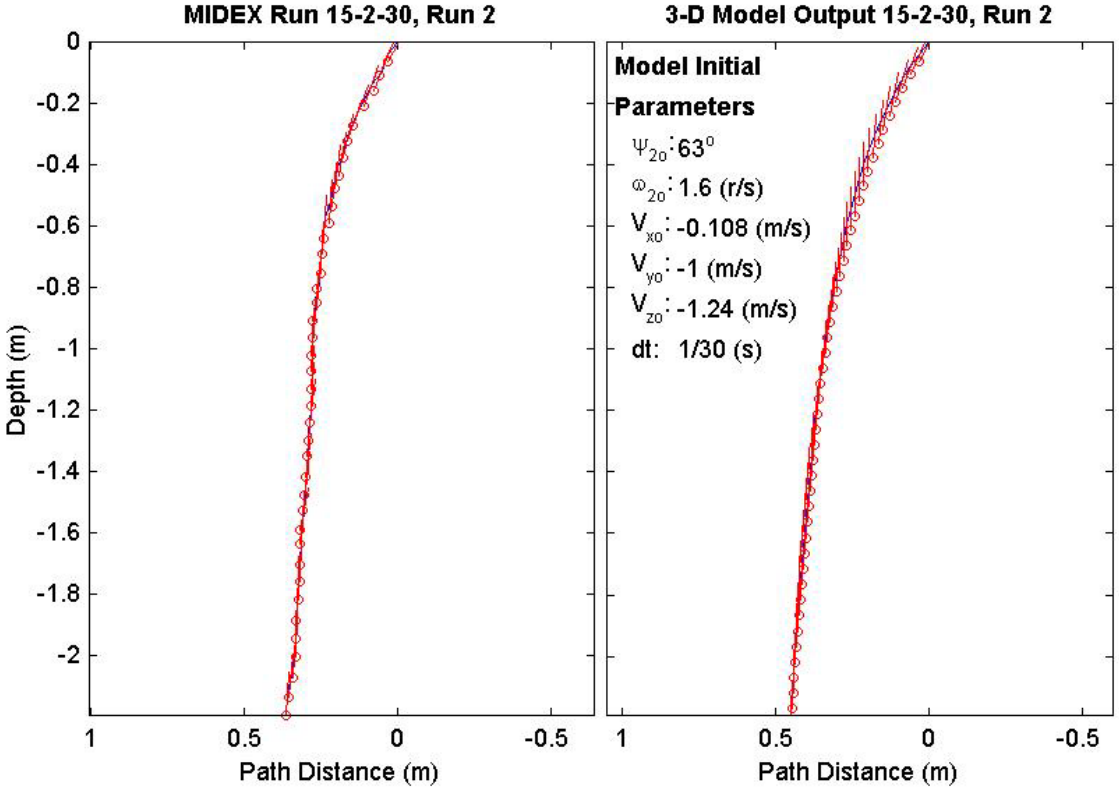

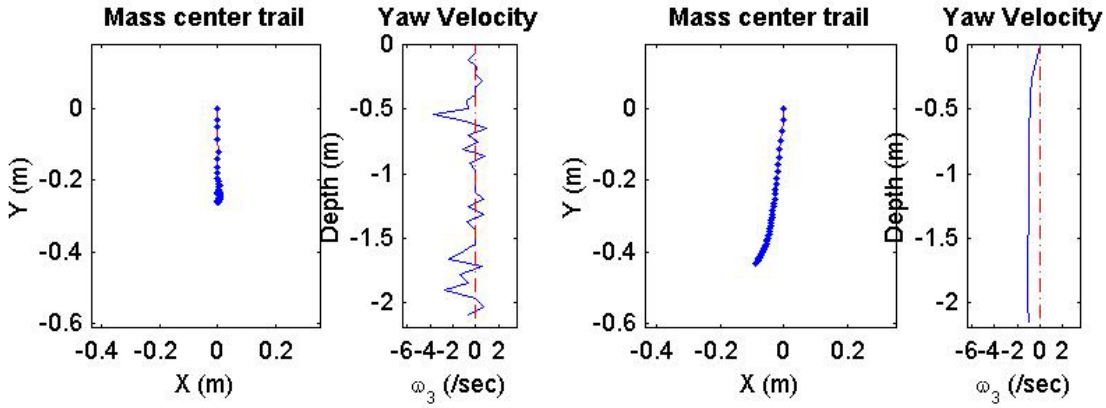

Final Drop Parameters (30/15-1525)

time: 1.3(s)
xy_{fe}: 0.468(m)
V_{xfe}: 0(m/s)
V_{yfe}: -0.375(m/s)
V_{zfe}: -1.53(m/s)
Ψ_{fe}: 87.4°
depth: 2.15(m)

Mine Shape Parameters (30/15-1525)

d: 0.04(m)
L: 0.152(m)
m: 0.323(m)
J_1: 3.3e-005(kg*m^2)
J_2: 0.000623(kg*m^2)
J_3: 0.000623(kg*m^2)
χ: 0.01477(m)

Final Model Parameters (30/15-1525)

time: 1.47(s)
xy_{fm}: 0.613(m)
V_{xfm}: 0.098(m/s)
V_{yfm}: 0.00606(m/s)
V_{zfm}: -1.52(m/s)
Ψ_{fm}: 87.44°
depth: 2.2(m)

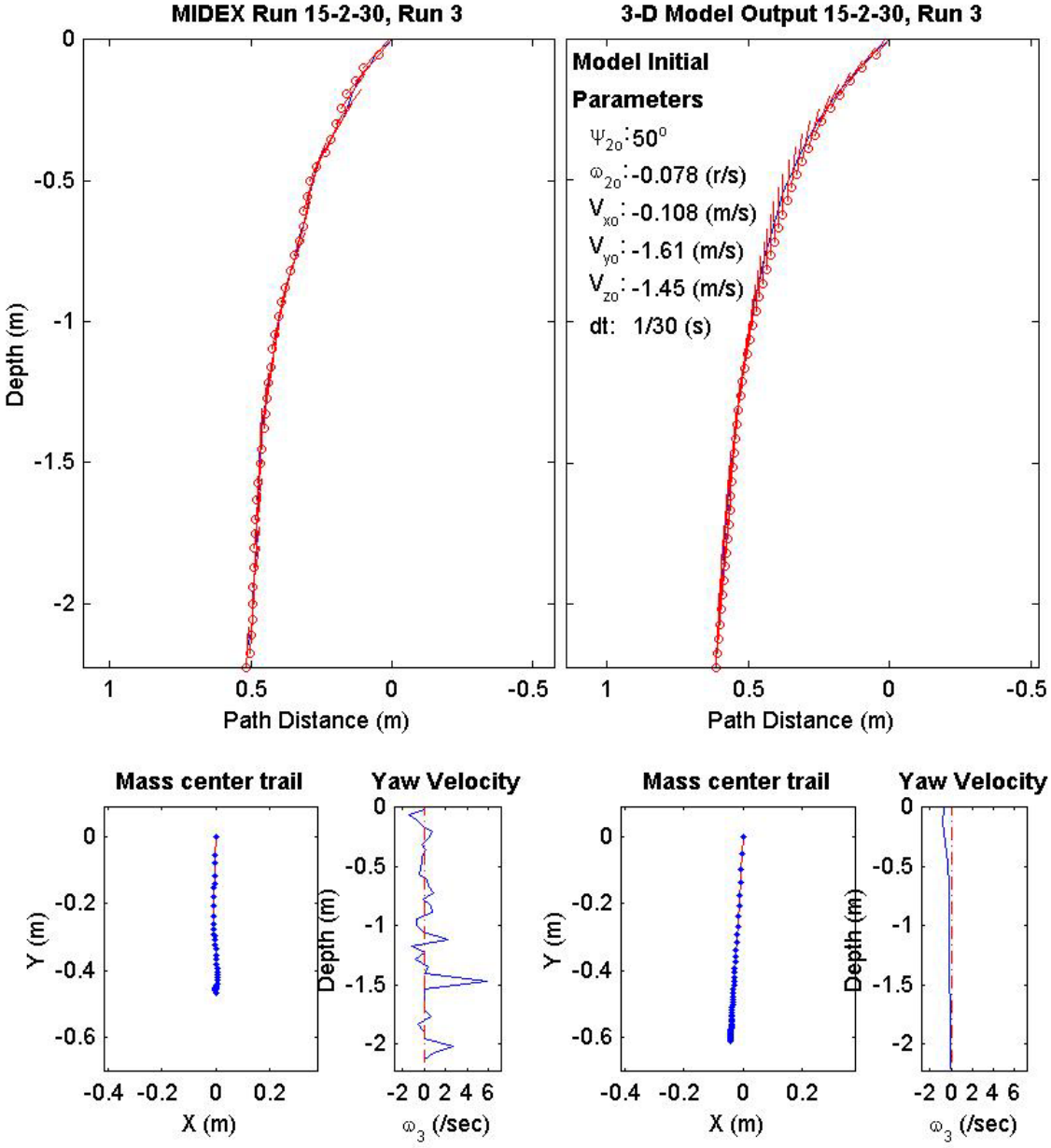

Final Drop Parameters (30/15-1244)

time: 1.37(s)
xy_{fe}: 0.616(m)
V_{xfe}: 0(m/s)
V_{yfe}: 0.159(m/s)
V_{zfe}: -1.69(m/s)
Ψ_{fe}: 88°
depth: 2.13(m)

Mine Shape Parameters (30/15-1244)

d: 0.04(m)
L: 0.152(m)
m: 0.323(m)
J_1: 3.3e-005(kg*m^2)
J_2: 0.000623(kg*m^2)
J_3: 0.000623(kg*m^2)
χ: 0.01477(m)

Final Model Parameters (30/15-1244)

time: 1.5(s)
xy_{fm}: 0.372(m)
V_{xfm}: 0.0382(m/s)
V_{yfm}: -0.0082(m/s)
V_{zfm}: -1.53(m/s)
Ψ_{fm}: 89.21°
depth: 2.15(m)

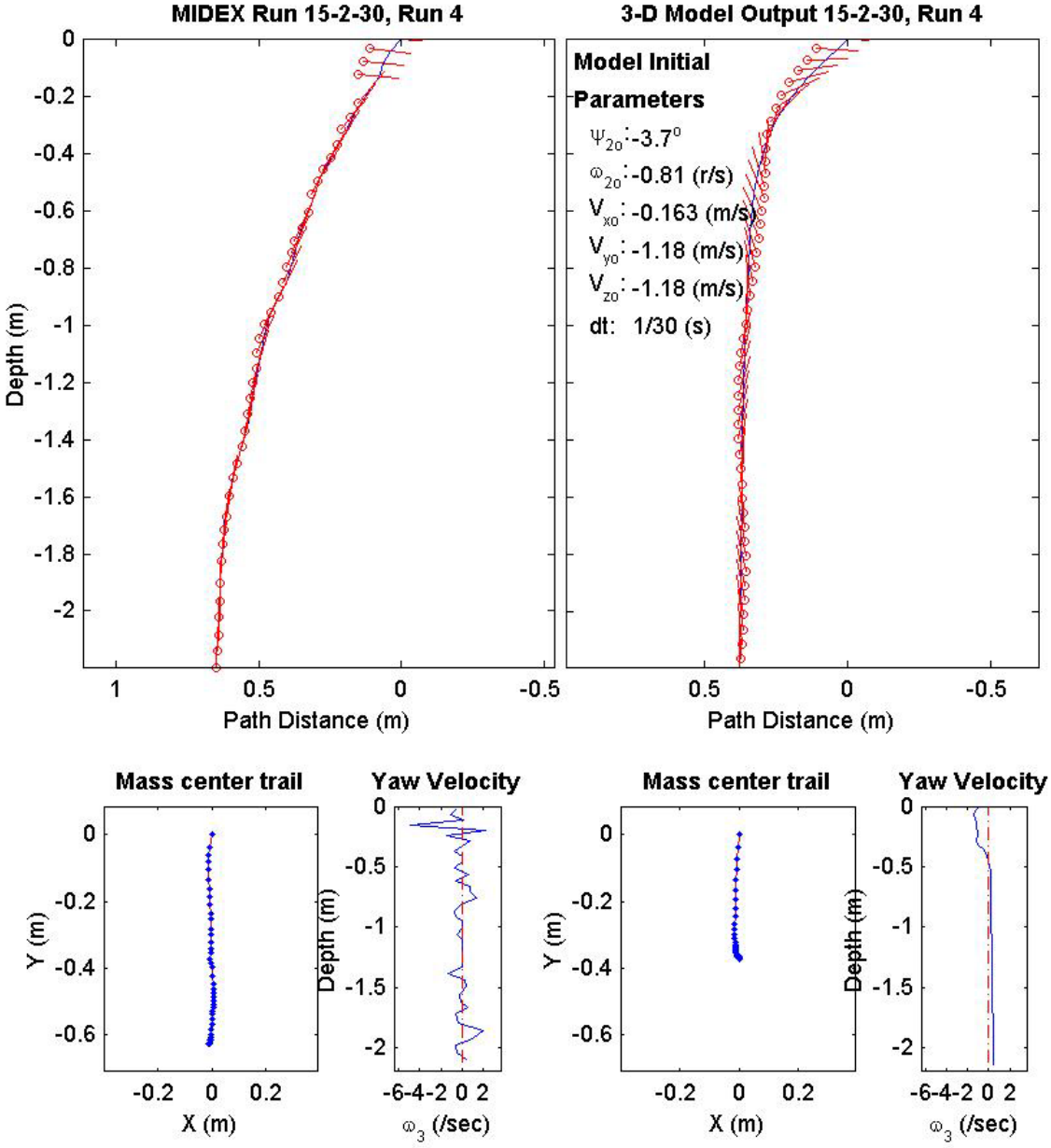

Final Drop Parameters (30/15-1153)

time: 1.43(s)
xy_{fe}: 0.609(m)
V_{xfe}: 0.055(m/s)
V_{yfe}: 0.055(m/s)
V_{zfe}: -1.66(m/s)
Ψ_{fe}: 83°
depth: 2.2(m)

Mine Shape Parameters (30/15-1153)

d: 0.04(m)
L: 0.152(m)
m: 0.323(m)
J_1: 3.3e-005(kg*m^2)
J_2: 0.000623(kg*m^2)
J_3: 0.000623(kg*m^2)
χ: 0.01477(m)

Final Model Parameters (30/15-1153)

time: 1.43(s)
xy_{fm}: 0.252(m)
V_{xfm}: 0.0358(m/s)
V_{yfm}: 0.00238(m/s)
V_{zfm}: -1.53(m/s)
Ψ_{fm}: 86.39°
depth: 2.24(m)

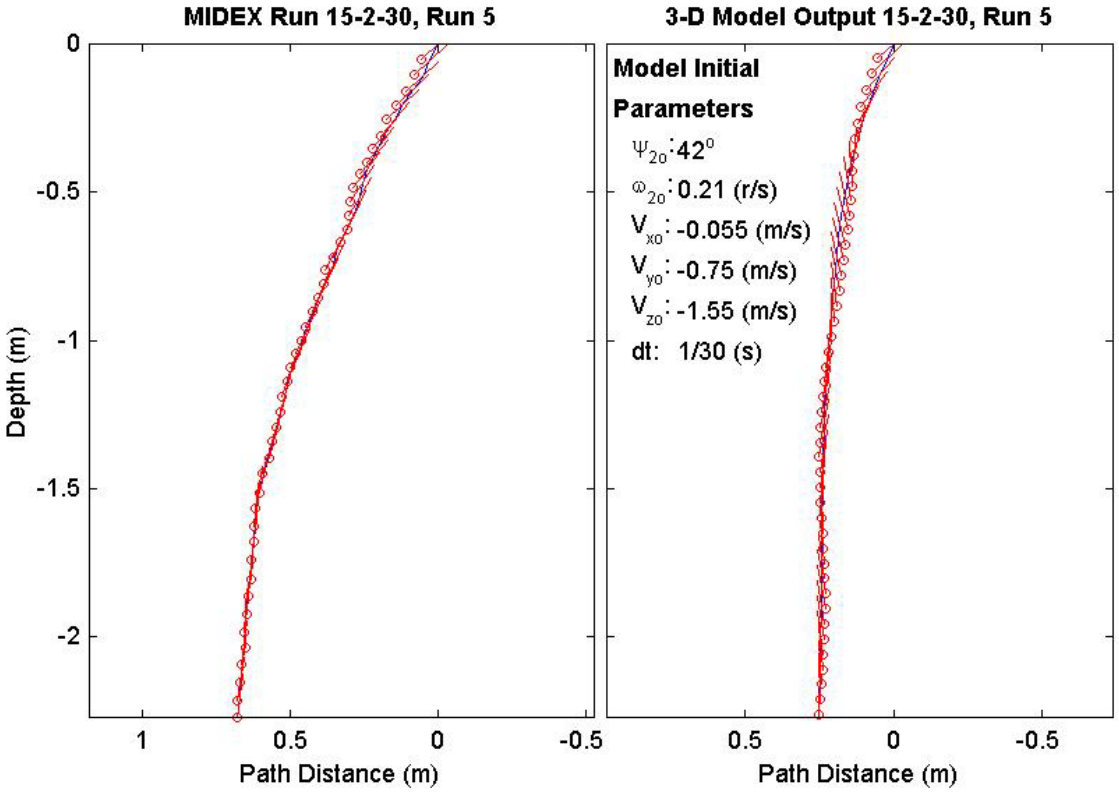

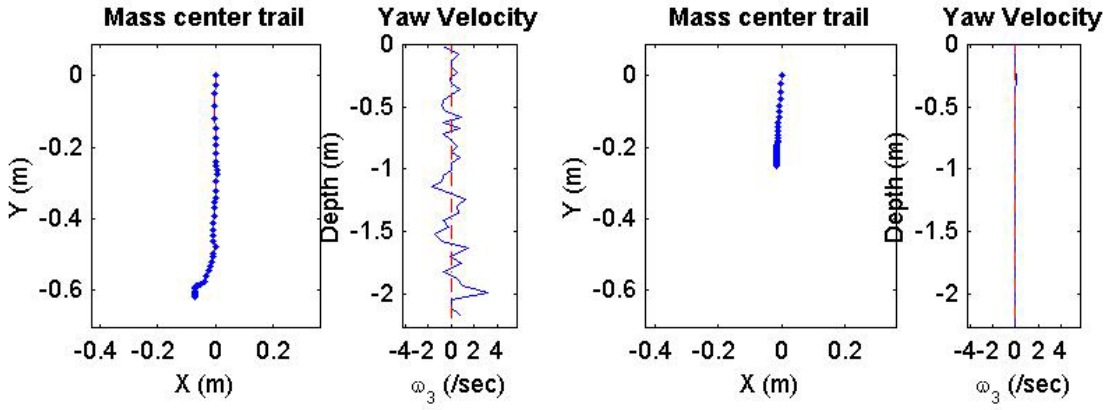

Final Drop

Parameters (30/12-2724)

time: 1.6(s)
xy_{fe}: 0.321(m)
V_{xfe}: -0.108(m/s)
V_{yfe}: -0.228(m/s)
V_{zfe}: -1.35(m/s)
Ψ_{fe}: 83.1°
depth: 2.18(m)

Mine Shape

Parameters (30/12-2724)

d: 0.04(m)
L: 0.121(m)
m: 0.254(m)
J_1: 2.71e-005(kg*m^2)
J_2: 0.000331(kg*m^2)
J_3: 0.000331(kg*m^2)
χ: 0.00997(m)

Final Model

Parameters (30/12-2724)

time: 1.53(s)
xy_{fm}: 0.303(m)
V_{xfm}: 0.0255(m/s)
V_{yfm}: -0.0758(m/s)
V_{zfm}: -1.37(m/s)
Ψ_{fm}: 82.84°
depth: 2.22(m)

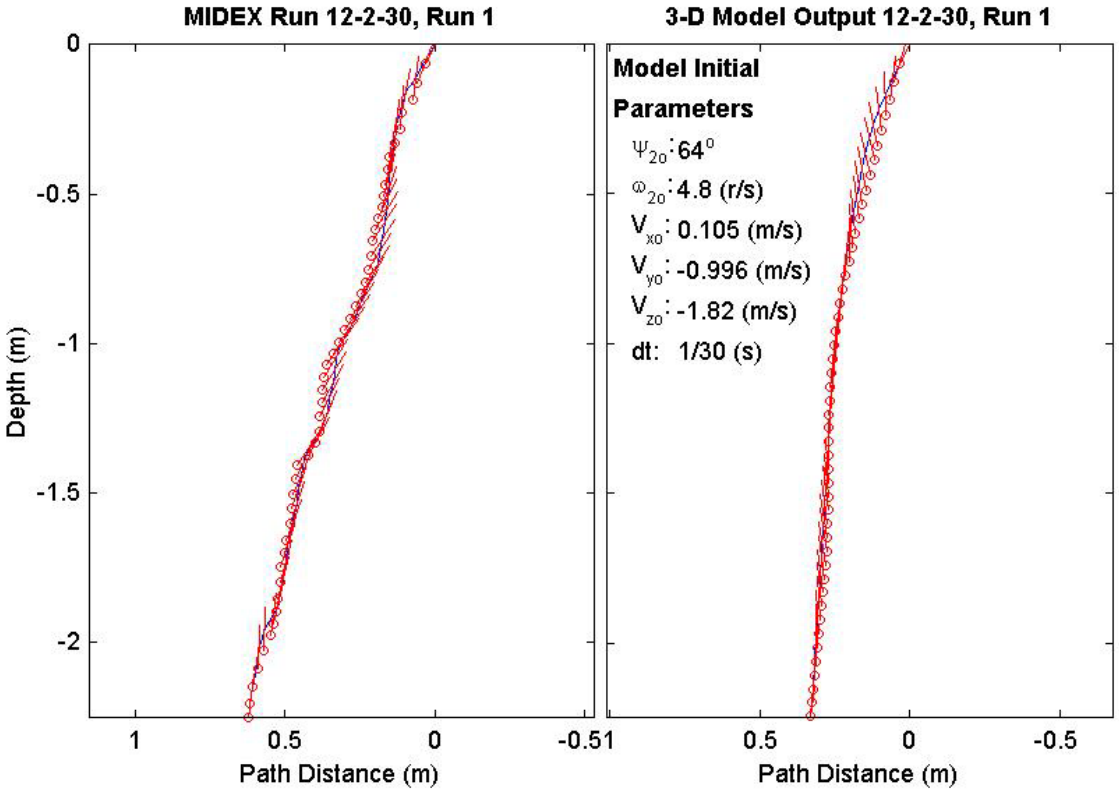

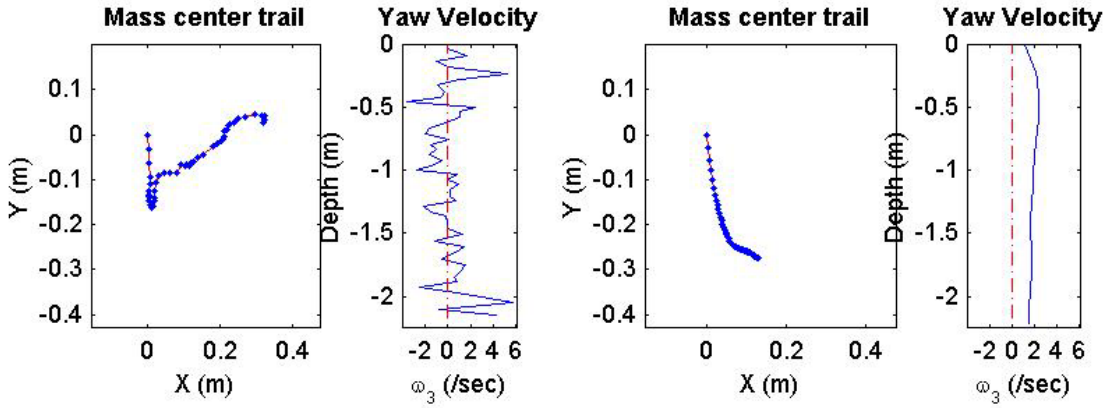

Final Drop Parameters (30/12-1791)

time: 1.43(s)
xy_{fe}: 0.347(m)
V_{xfe}: 0.162(m/s)
V_{yfe}: -0.09(m/s)
V_{zfe}: -1.82(m/s)
Ψ_{fe}: 85.2°
depth: 2.13(m)

Mine Shape Parameters (30/12-1791)

d: 0.04(m)
L: 0.121(m)
m: 0.254(m)
J_1: 2.71e-005(kg*m^2)
J_2: 0.000331(kg*m^2)
J_3: 0.000331(kg*m^2)
χ: 0.00997(m)

Final Model Parameters (30/12-1791)

time: 1.53(s)
xy_{fm}: 0.196(m)
V_{xfm}: 0.000603(m/s)
V_{yfm}: -0.042(m/s)
V_{zfm}: -1.37(m/s)
Ψ_{fm}: 80.34°
depth: 2.17(m)

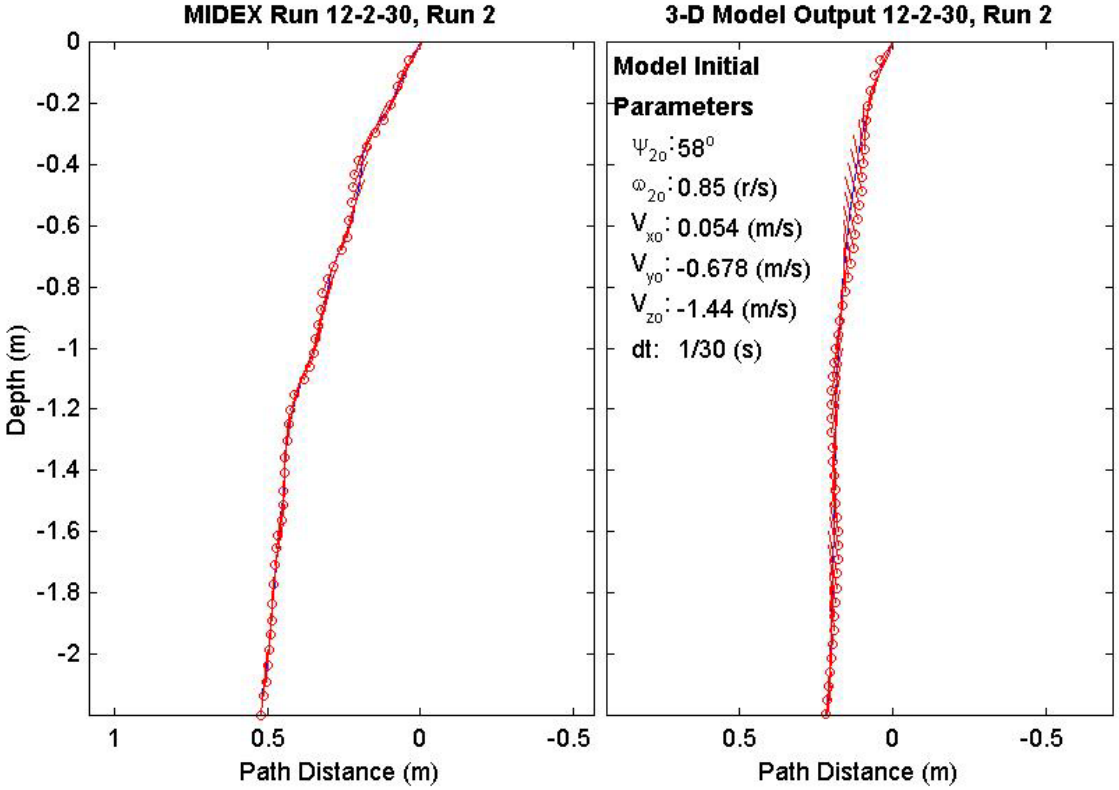

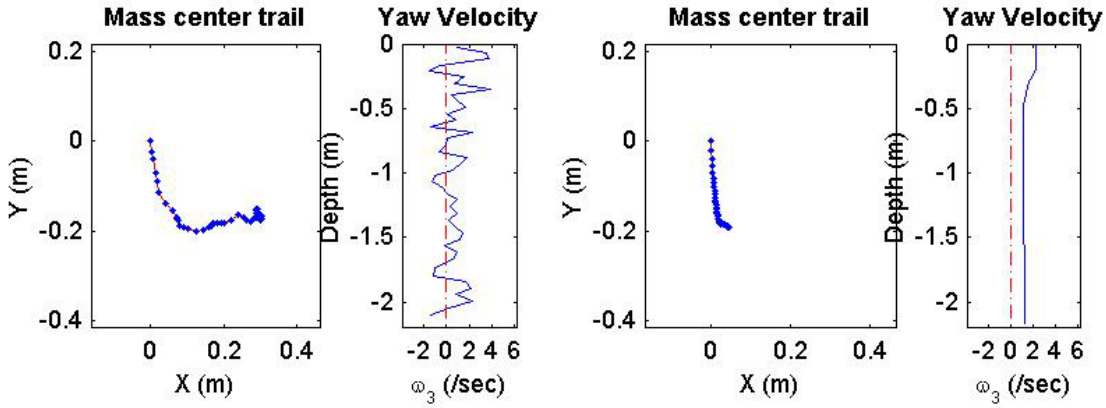

Final Drop
Parameters (30/12-1953)

time: 1.37(s)
xy_{fe}: 0.227(m)
V_{xfe}: -0.213(m/s)
V_{yfe}: -0.375(m/s)
V_{zfe}: -1.31(m/s)
Ψ_{fe}: 56.9°
depth: 2.06(m)

Mine Shape
Parameters (30/12-1953)

d: 0.04(m)
L: 0.121(m)
m: 0.254(m)
J_1: 2.71e-005(kg*m^2)
J_2: 0.000331(kg*m^2)
J_3: 0.000331(kg*m^2)
χ: 0.00997(m)

Final Model
Parameters (30/12-1953)

time: 1.47(s)
xy_{fm}: 0.233(m)
V_{xfm}: 0.0474(m/s)
V_{yfm}: -0.0159(m/s)
V_{zfm}: -1.38(m/s)
Ψ_{fm}: 90.04°
depth: 2.09(m)

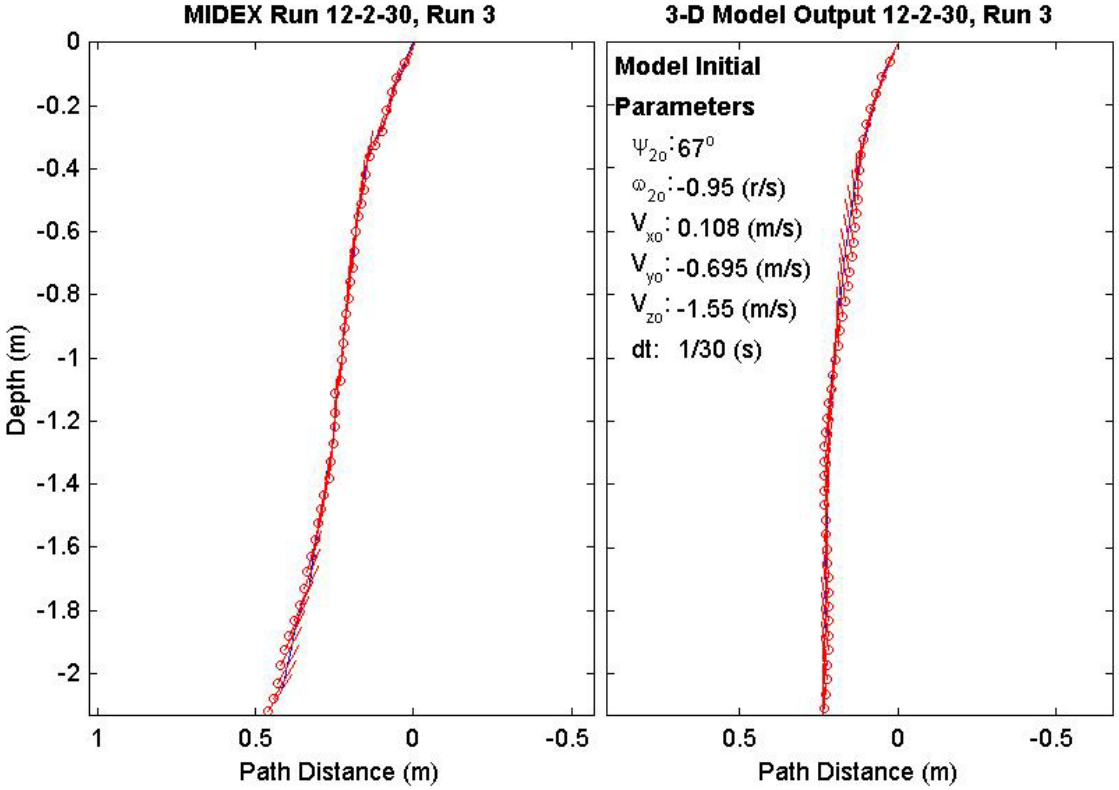

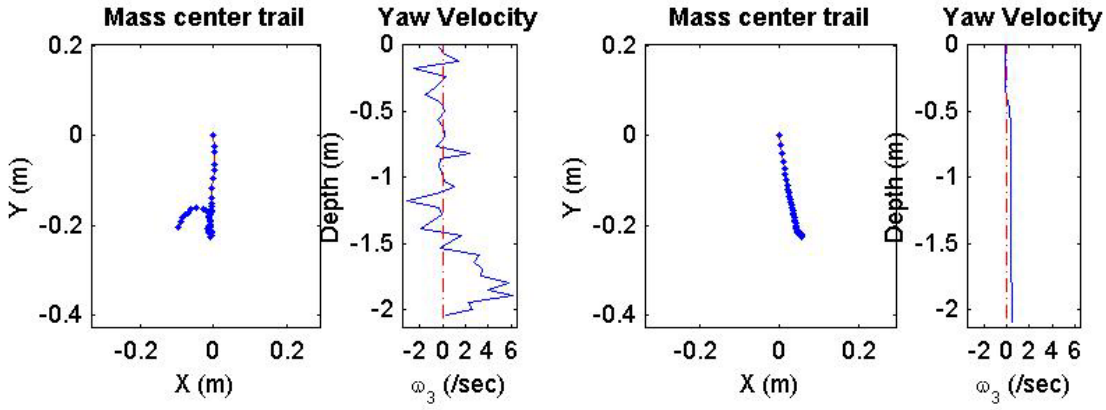

Final Drop
Parameters (30/12-1527)

time: 1.5(s)
xy_{fe}: 0.0228(m)
V_{xfe}: 0.108(m/s)
V_{yfe}: 0.483(m/s)
V_{zfe}: -1.02(m/s)
Ψ_{fe}: 54.7°
depth: 2.19(m)

Mine Shape
Parameters (30/12-1527)

d: 0.04(m)
L: 0.121(m)
m: 0.254(m)
J_1: 2.71e-005(kg*m^2)
J_2: 0.000331(kg*m^2)
J_3: 0.000331(kg*m^2)
χ: 0.00997(m)

Final Model
Parameters (30/12-1527)

time: 1.6(s)
xy_{fm}: 0.269(m)
V_{xfm}: 0.0197(m/s)
V_{yfm}: -0.0624(m/s)
V_{zfm}: -1.37(m/s)
Ψ_{fm}: 81.55°
depth: 2.19(m)

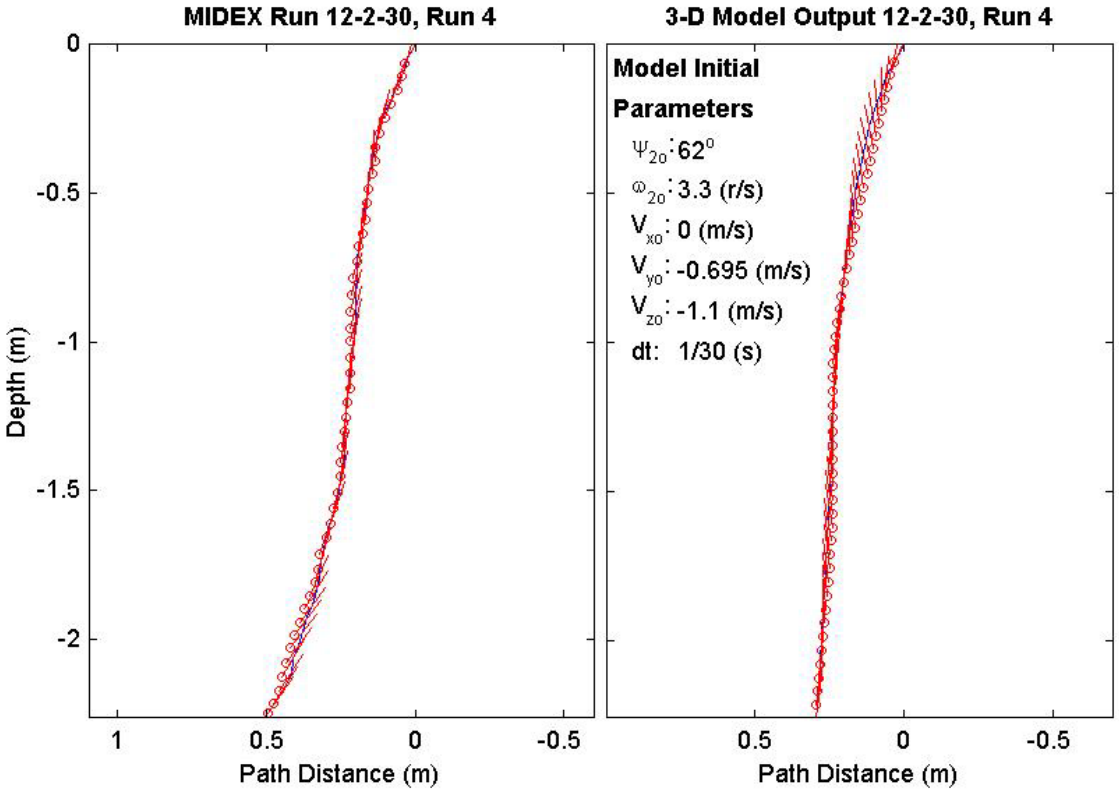

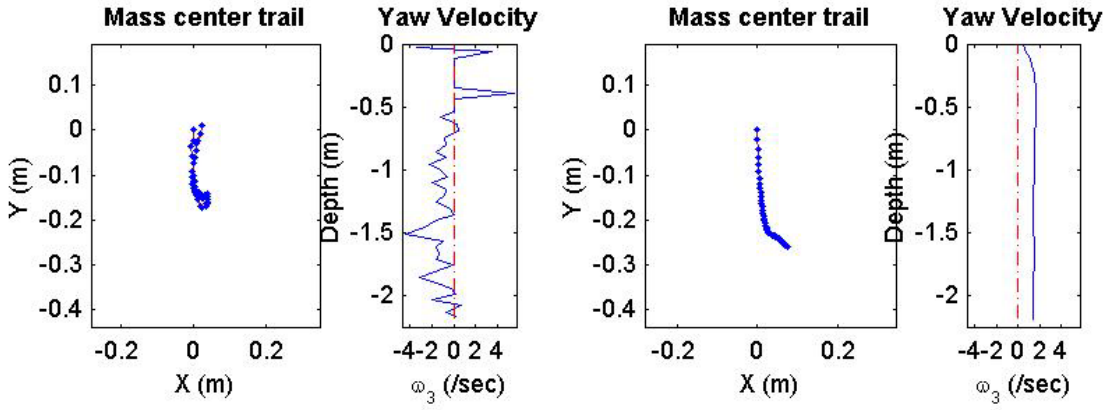

Final Drop Parameters (30/12-1259)

time: 1.63(s)
xy_{fe}: 0.696(m)
V_{xfe}: 0.108(m/s)
V_{yfe}: -0.213(m/s)
V_{zfe}: -1.31(m/s)
Ψ_{fe}: 76°
depth: 2.13(m)

Mine Shape Parameters (30/12-1259)

d: 0.04(m)
L: 0.121(m)
m: 0.254(m)
J_1: 2.71e-005(kg*m^2)
J_2: 0.000331(kg*m^2)
J_3: 0.000331(kg*m^2)
χ: 0.00997(m)

Final Model Parameters (30/12-1259)

time: 1.57(s)
xy_{fm}: 0.135(m)
V_{xfm}: 0.00568(m/s)
V_{yfm}: -0.0165(m/s)
V_{zfm}: -1.38(m/s)
Ψ_{fm}: 79.87°
depth: 2.17(m)

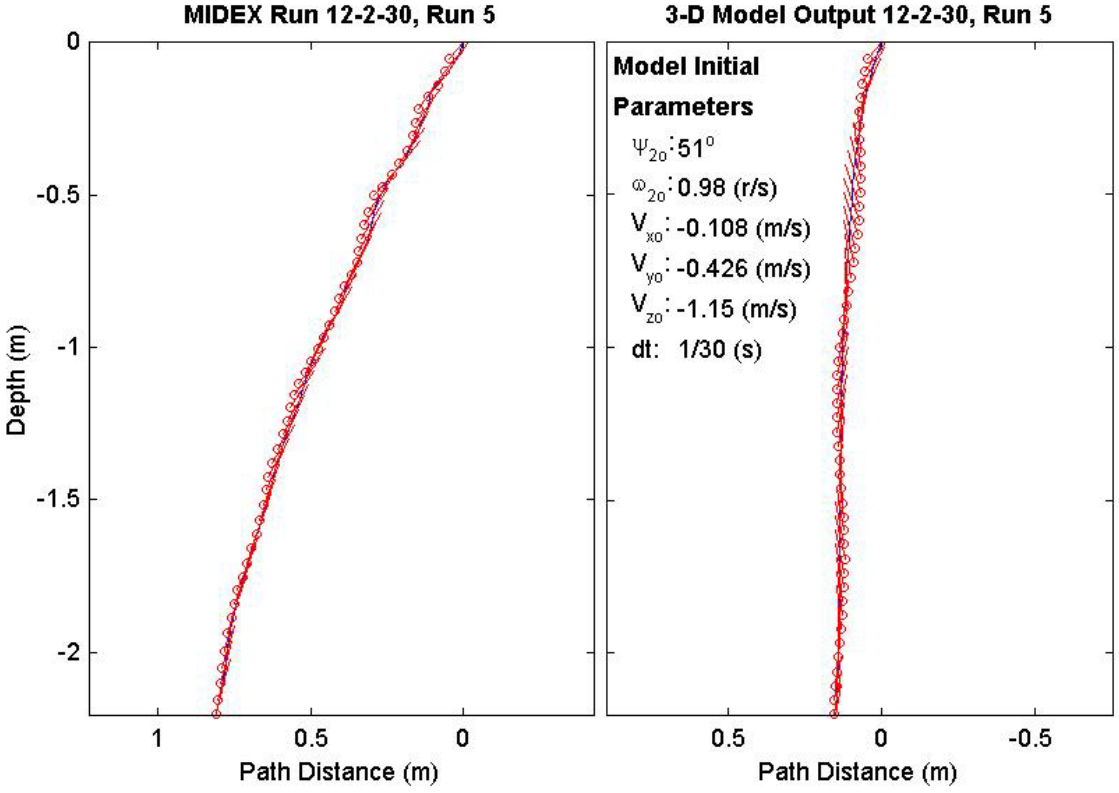

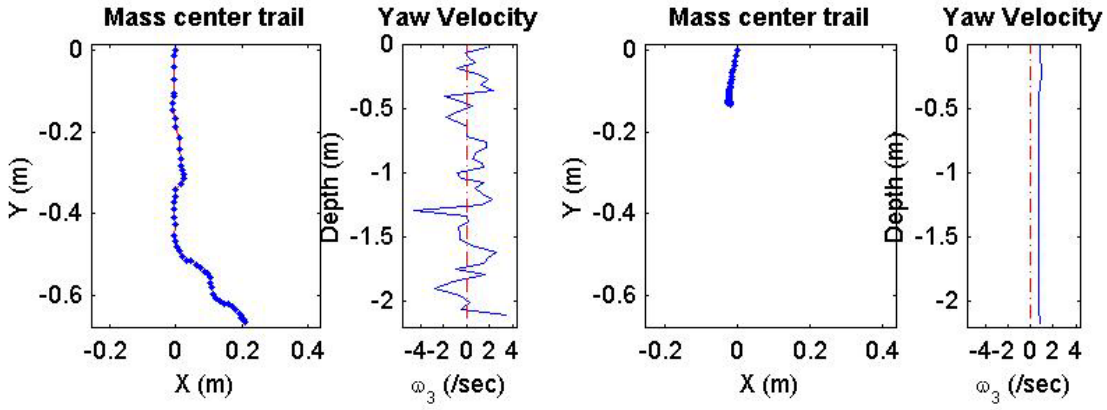

Final Drop

Parameters (30/9-2746)

time: 1.53(s)
xy_{fe}: 0.23(m)
V_{xfe}: -0.159(m/s)
V_{yfe}: 0.273(m/s)
V_{zfe}: -1.39(m/s)
Ψ_{fe}: 81.4°
depth: 2.1(m)

Mine Shape

Parameters (30/9-2746)

d: 0.04(m)
L: 0.0912(m)
m: 0.215(m)
J_1: 2.35e-005(kg*m^2)
J_2: 0.000156(kg*m^2)
J_3: 0.000156(kg*m^2)
χ: 0.005796(m)

Final Model

Parameters (30/9-2746)

time: 1.47(s)
xy_{fm}: 0.19(m)
V_{xfm}: 0.0128(m/s)
V_{yfm}: 0.00176(m/s)
V_{zfm}: -1.4(m/s)
Ψ_{fm}: 80.4°
depth: 2.13(m)

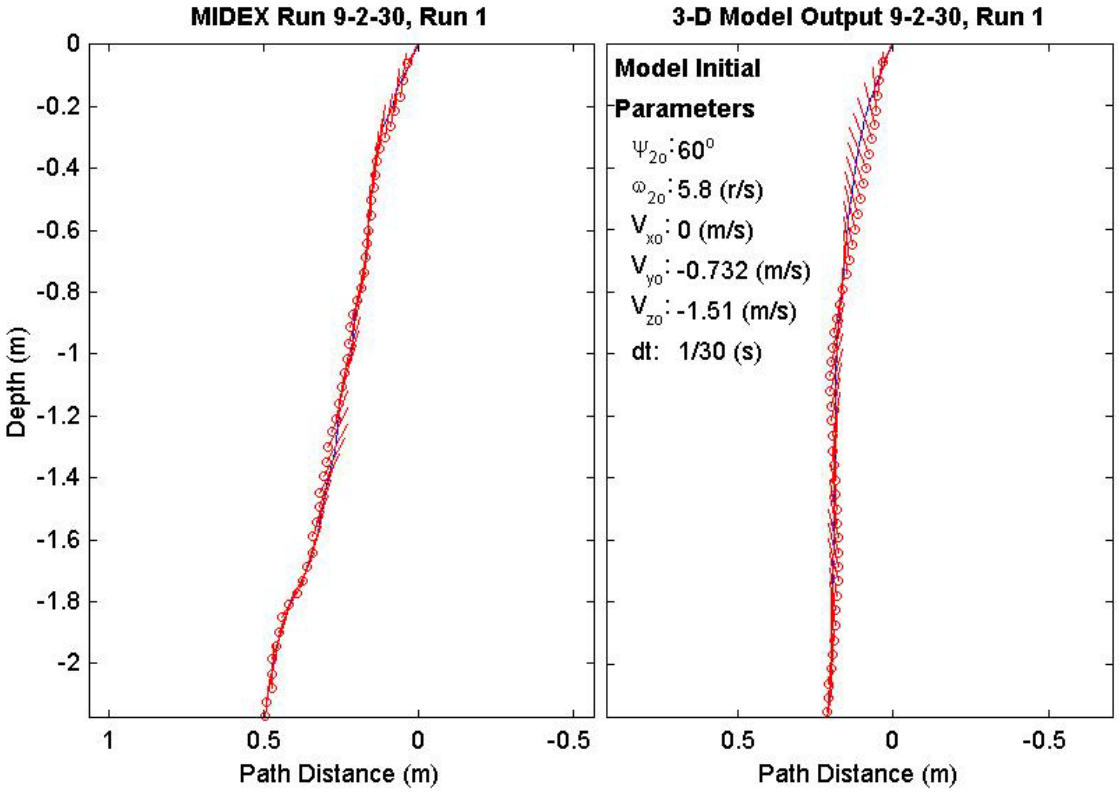

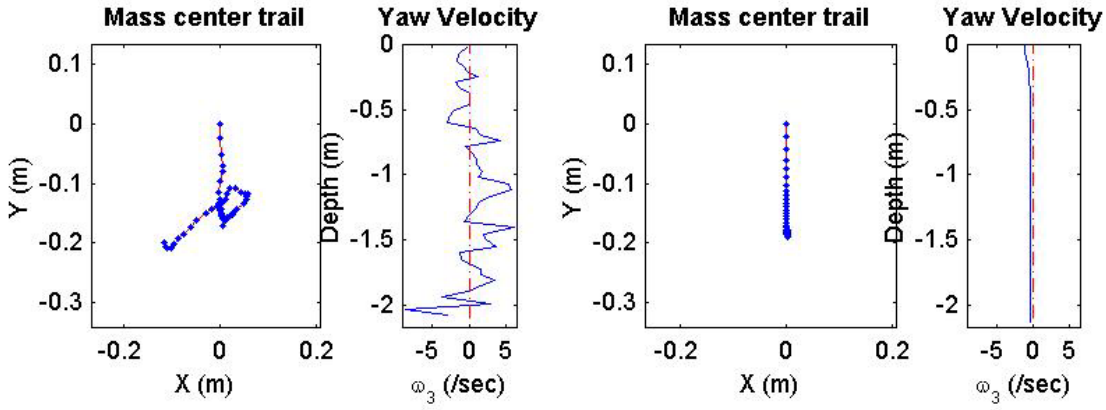

Final Drop
Parameters (30/9-2199)

time: 1.77(s)
xy_{fe}: 0.21(m)
V_{xfe}: -0.483(m/s)
V_{yfe}: -0.093(m/s)
V_{zfe}: -1.25(m/s)
Ψ_{fe}: 43°
depth: 2.23(m)

Mine Shape
Parameters (30/9-2199)

d: 0.04(m)
L: 0.0912(m)
m: 0.215(m)
J_1: 2.35e-005($kg*m^2$)
J_2: 0.000156($kg*m^2$)
J_3: 0.000156($kg*m^2$)
χ: 0.005796(m)

Final Model
Parameters (30/9-2199)

time: 1.57(s)
xy_{fm}: 0.297(m)
V_{xfm}: -0.0101(m/s)
V_{yfm}: 0.00953(m/s)
V_{zfm}: -1.4(m/s)
Ψ_{fm}: 82.26°
depth: 2.25(m)

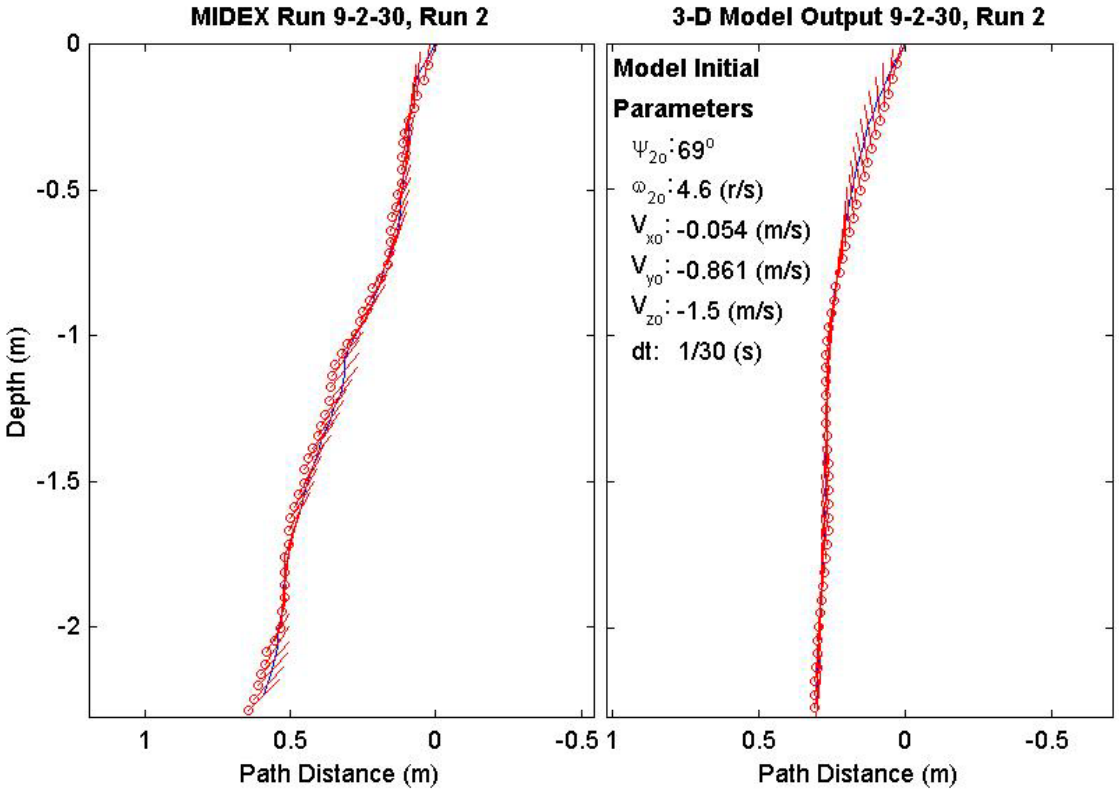

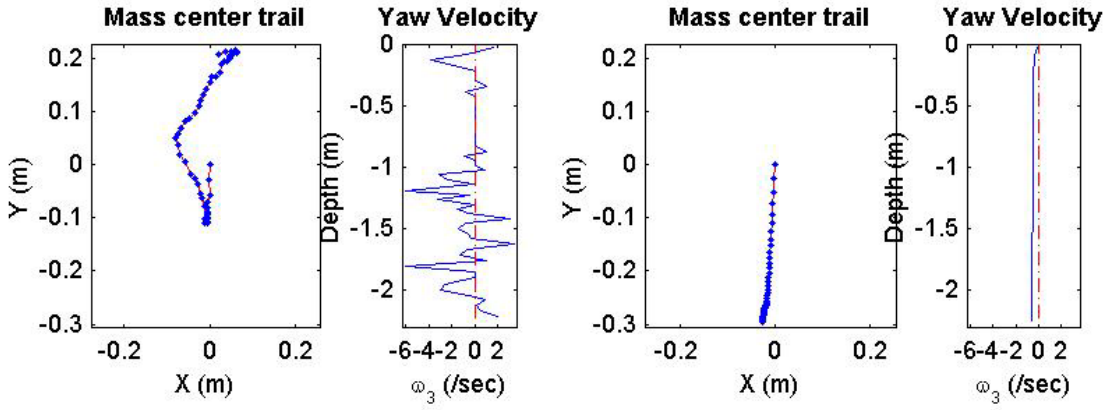

Final Drop
Parameters (30/9-1562)

time: 1.7(s)
xy_{fe}: 0.0694(m)
V_{xfe}: -0.213(m/s)
V_{yfe}: 0.483(m/s)
V_{zfe}: -1.15(m/s)
Ψ_{fe}: 72°
depth: 2.18(m)

Mine Shape
Parameters (30/9-1562)

d: 0.04(m)
L: 0.0912(m)
m: 0.215(m)
J_1: 2.35e-005(kg*m^2)
J_2: 0.000156(kg*m^2)
J_3: 0.000156(kg*m^2)
χ: 0.005796(m)

Final Model
Parameters (30/9-1562)

time: 1.5(s)
xy_{fm}: 0.19(m)
V_{xfm}: 0.0666(m/s)
V_{yfm}: -0.0202(m/s)
V_{zfm}: -1.4(m/s)
Ψ_{fm}: 86.14°
depth: 2.18(m)

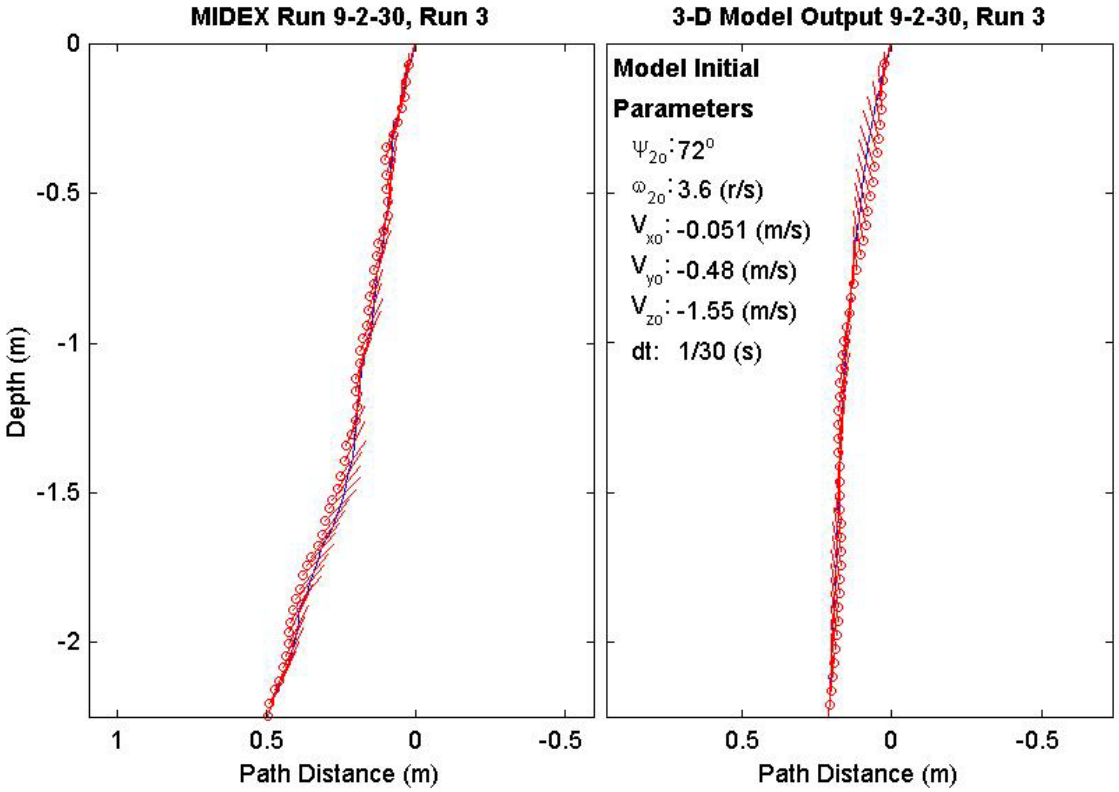

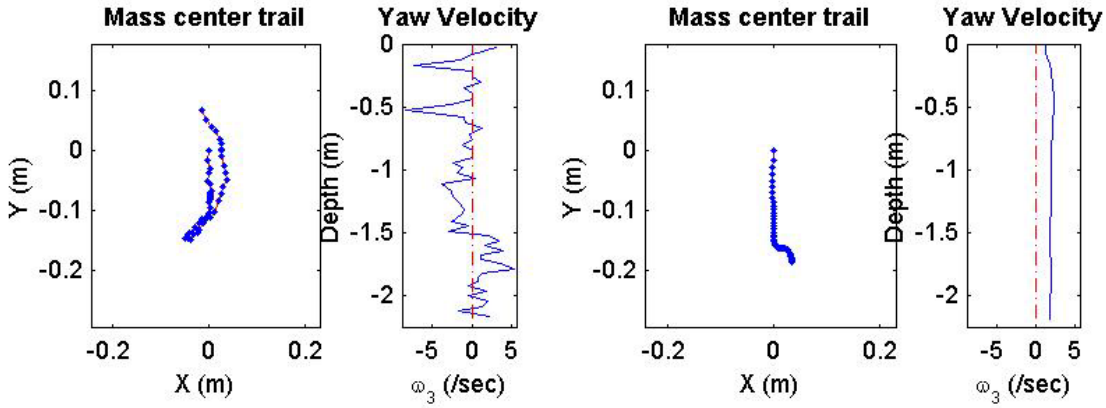

Final Drop
Parameters (30/9-1260)

time: 1.73(s)
xy_{fe}: 0.0781(m)
V_{xfe}: 0.375(m/s)
V_{yfe}: 0.267(m/s)
V_{zfe}: -1.07(m/s)
Ψ_{fe}: 52.7°
depth: 2.22(m)

Mine Shape
Parameters (30/9-1260)

d: 0.04(m)
L: 0.0912(m)
m: 0.215(m)
J_1: 2.35e-005(kg*m^2)
J_2: 0.000156(kg*m^2)
J_3: 0.000156(kg*m^2)
χ: 0.005796(m)

Final Model
Parameters (30/9-1260)

time: 1.53(s)
xy_{fm}: 0.136(m)
V_{xfm}: 0.0509(m/s)
V_{yfm}: 2.8e-005(m/s)
V_{zfm}: -1.4(m/s)
Ψ_{fm}: 85.31°
depth: 2.23(m)

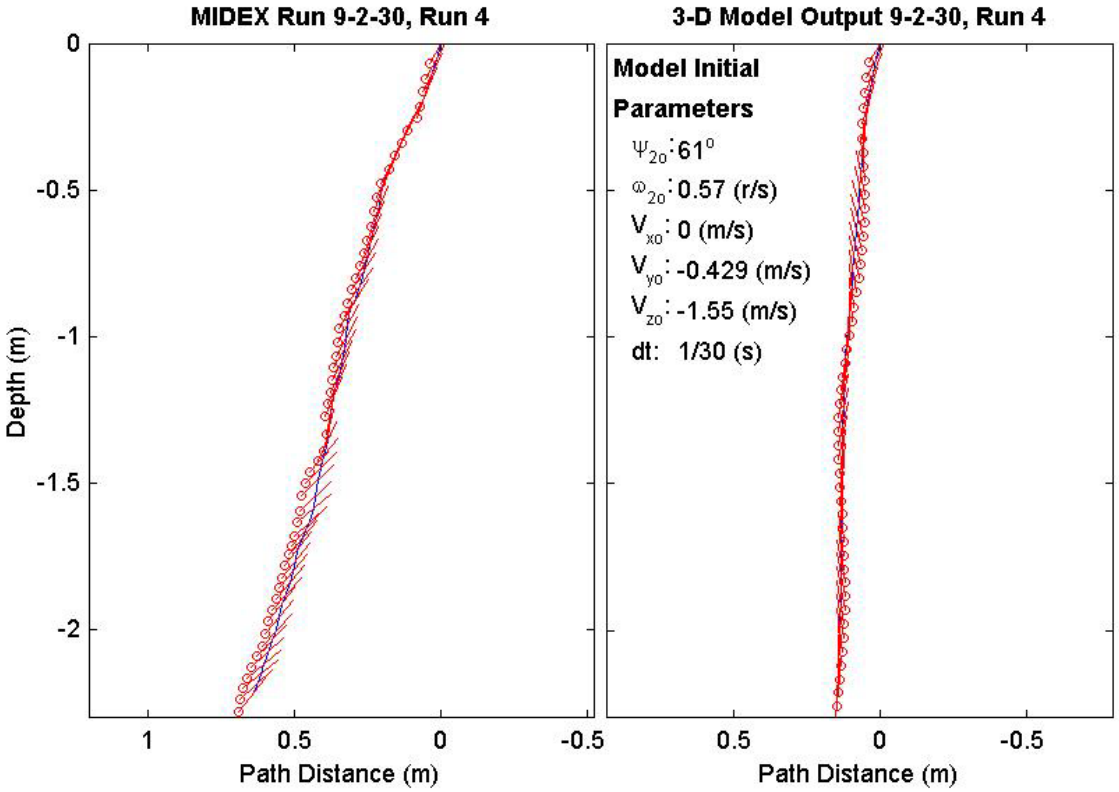

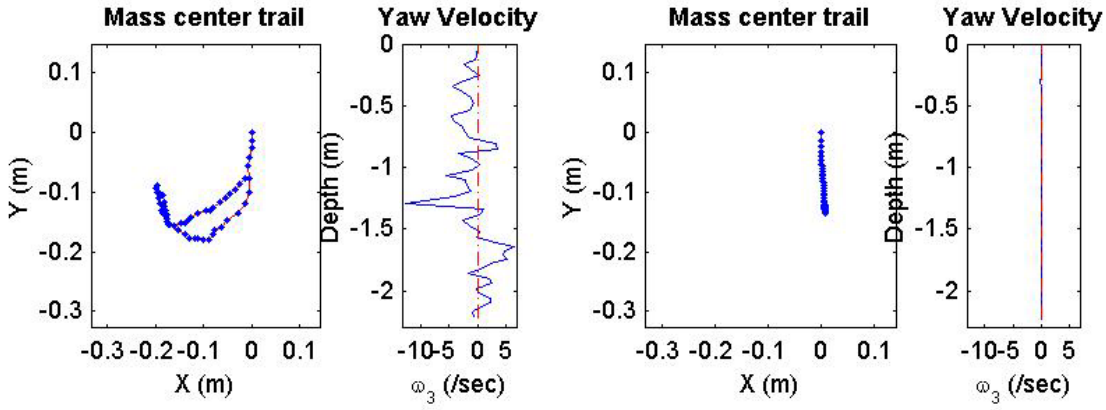

Final Drop

Parameters (30/9-1122)

time: 1.67(s)
xy_{fe}: 0.162(m)
V_{xfe}: -0.108(m/s)
V_{yfe}: -0.213(m/s)
V_{zfe}: -1.07(m/s)
Ψ_{fe}: 55.1°
depth: 2.21(m)

Mine Shape

Parameters (30/9-1122)

d: 0.04(m)
L: 0.0912(m)
m: 0.215(m)
J_1: 2.35e-005(kg*m^2)
J_2: 0.000156(kg*m^2)
J_3: 0.000156(kg*m^2)
χ: 0.005796(m)

Final Model

Parameters (30/9-1122)

time: 1.57(s)
xy_{fm}: 0.248(m)
V_{xfm}: 0.0596(m/s)
V_{yfm}: -0.0064(m/s)
V_{zfm}: -1.4(m/s)
Ψ_{fm}: 86.22°
depth: 2.22(m)

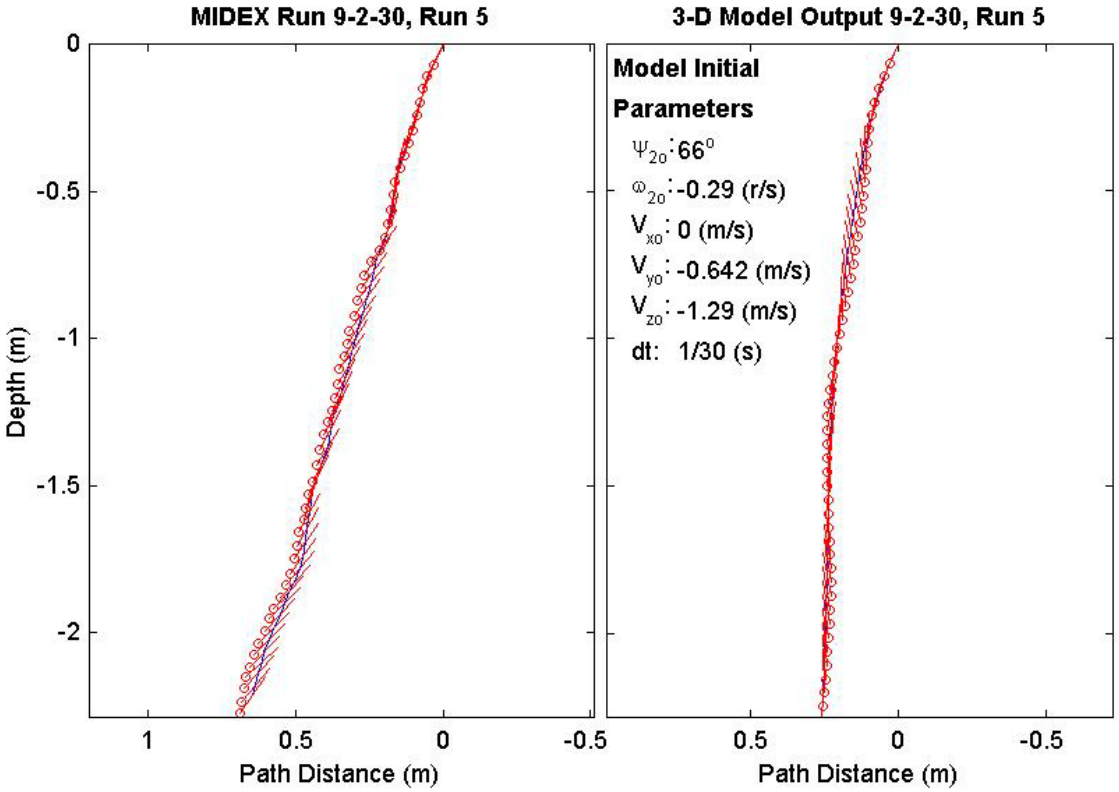

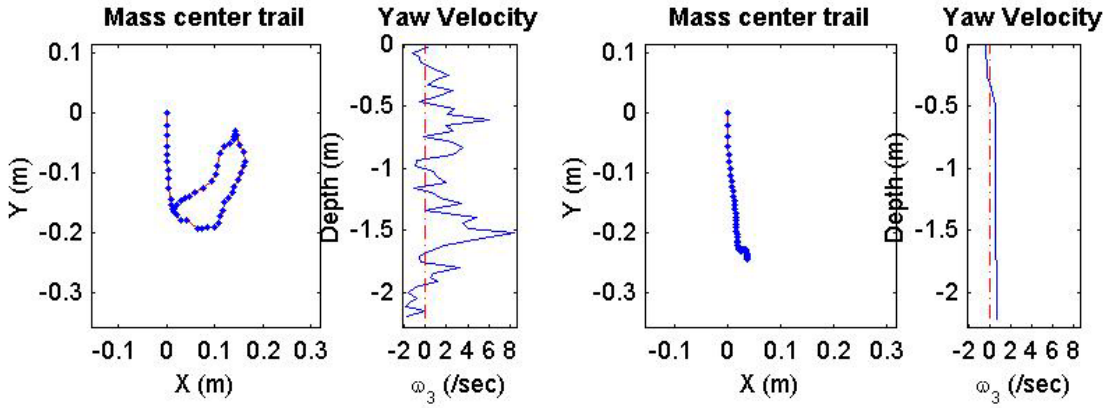

Final Drop

Parameters (45/15-2891)

time: 1.33(s)
xy_{fe}: 0.0513(m)
V_{xfe}: 0(m/s)
V_{yfe}: 0.108(m/s)
V_{zfe}: -1.37(m/s)
Ψ_{fe}: 82.3°
depth: 2.14(m)

Mine Shape

Parameters (45/15-2891)

d: 0.04(m)
L: 0.152(m)
m: 0.323(m)
J_1: 3.3e-005(kg*m^2)
J_2: 0.000623(kg*m^2)
J_3: 0.000623(kg*m^2)
χ: 0.01477(m)

Final Model

Parameters (45/15-2891)

time: 1.37(s)
xy_{fm}: 0.262(m)
V_{xfm}: 0.0462(m/s)
V_{yfm}: 0.0415(m/s)
V_{zfm}: -1.53(m/s)
Ψ_{fm}: 91.03°
depth: 2.17(m)

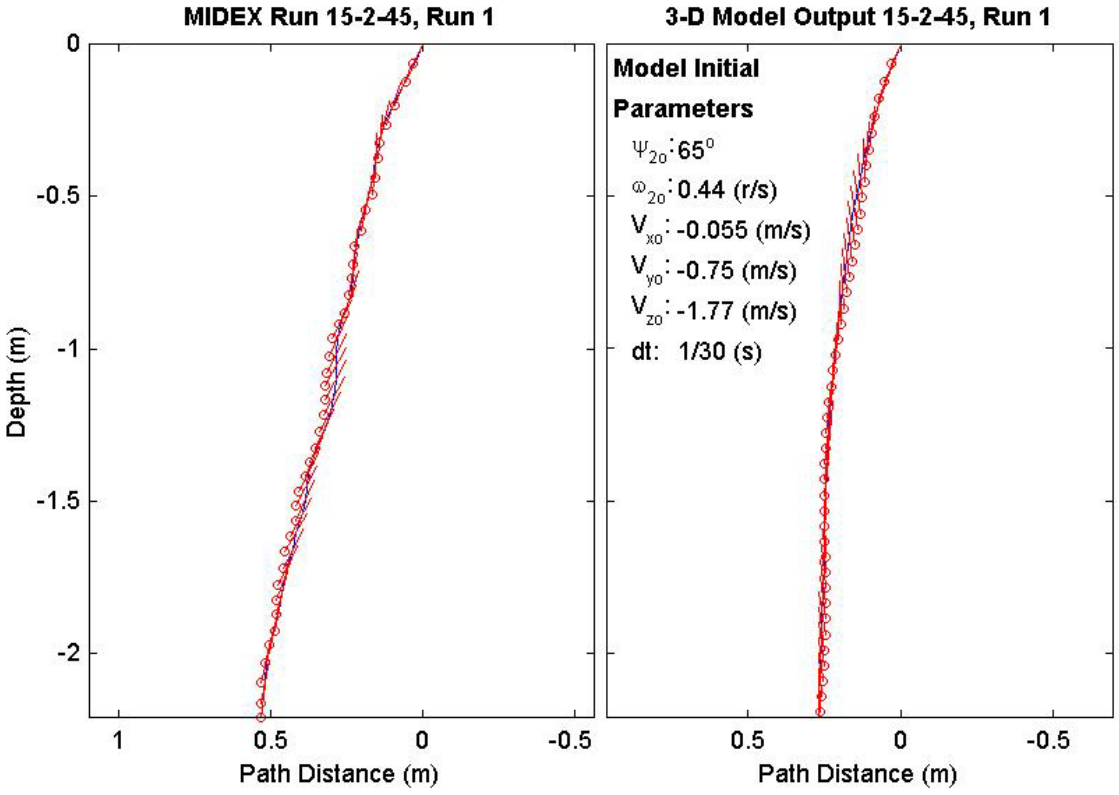

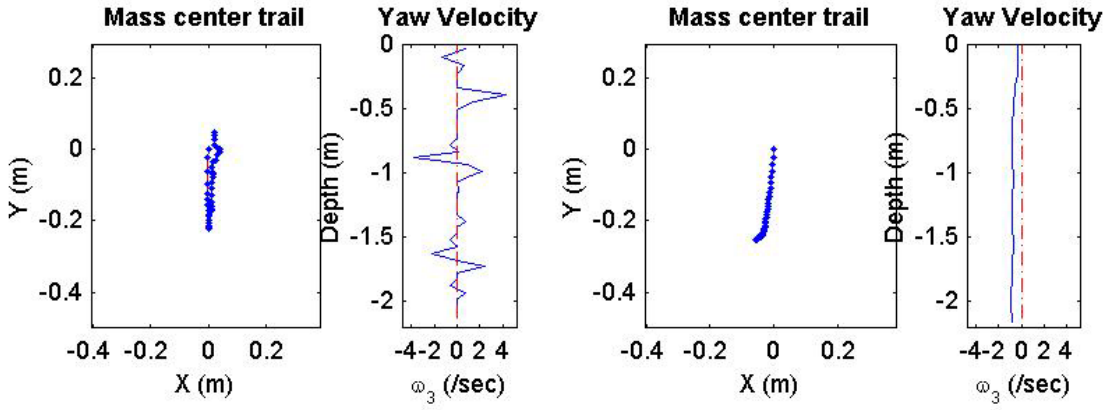

Final Drop
Parameters (45/15-2684)

time: 1.37(s)
xy_{fe}: 0.0644(m)
V_{xfe}: 0.429(m/s)
V_{yfe}: 0.267(m/s)
V_{zfe}: -1.39(m/s)
Ψ_{fe}: 77.7°
depth: 2.19(m)

Mine Shape
Parameters (45/15-2684)

d: 0.04(m)
L: 0.152(m)
m: 0.323(m)
J_1: 3.3e-005(kg*m^2)
J_2: 0.000623(kg*m^2)
J_3: 0.000623(kg*m^2)
χ: 0.01477(m)

Final Model
Parameters (45/15-2684)

time: 1.33(s)
xy_{fm}: 0.33(m)
V_{xfm}: 0.0666(m/s)
V_{yfm}: -0.014(m/s)
V_{zfm}: -1.52(m/s)
Ψ_{fm}: 87.56°
depth: 2.2(m)

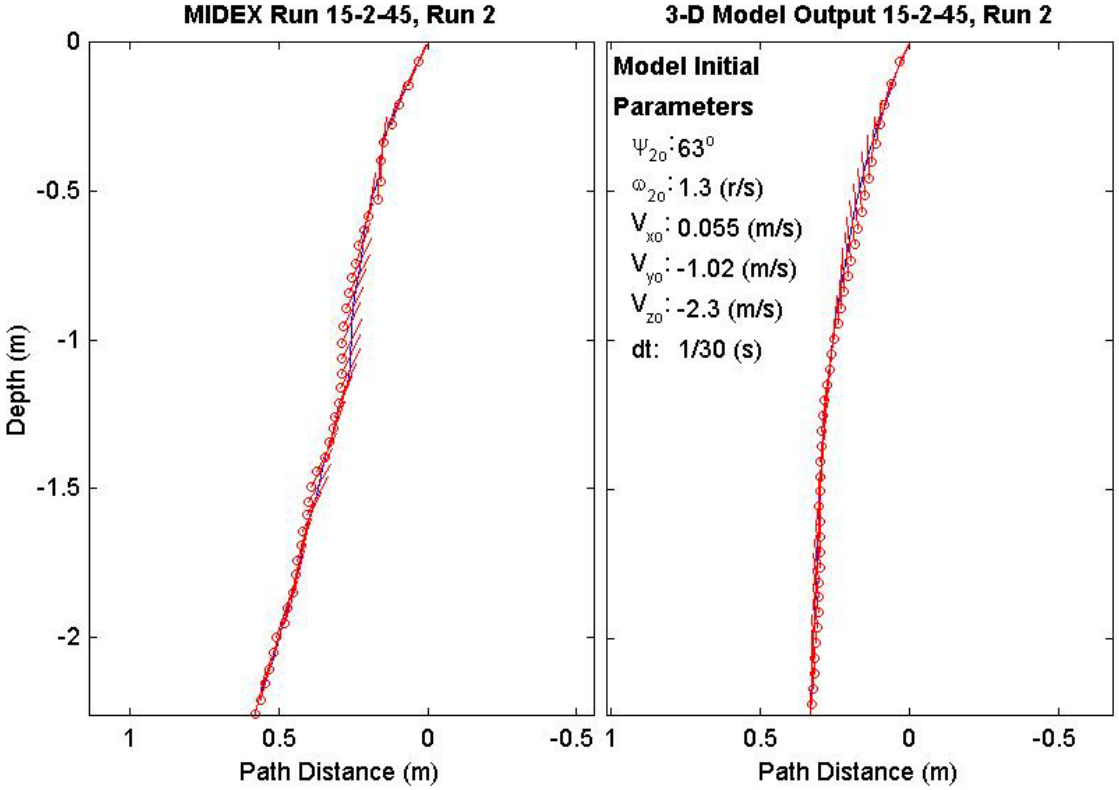

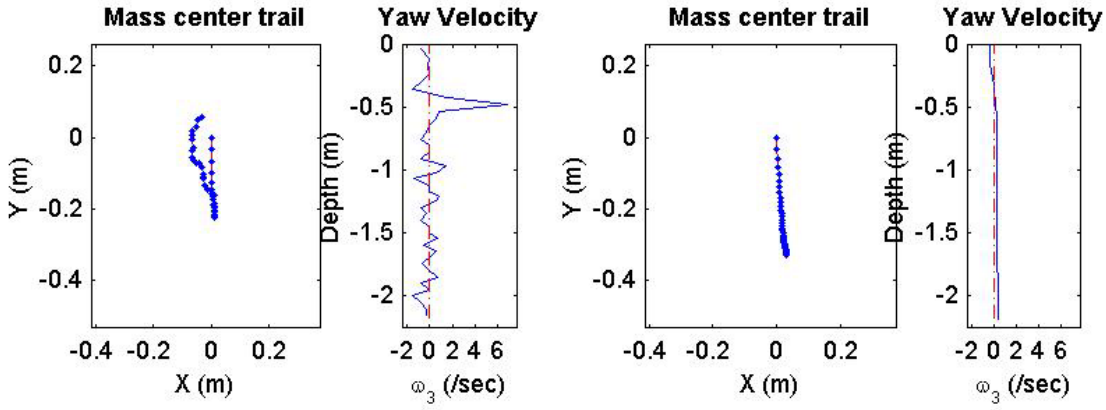

Final Drop

Parameters (45/15-2230)

time: 1.23(s)
xy_{fe}: 0.205(m)
V_{xfe}: 0(m/s)
V_{yfe}: 0.055(m/s)
V_{zfe}: -1.79(m/s)
Ψ_{fe}: 77.8°
depth: 2.15(m)

Mine Shape

Parameters (45/15-2230)

d: 0.04(m)
L: 0.152(m)
m: 0.323(m)
J_1: 3.3e-005(kg*m^2)
J_2: 0.000623(kg*m^2)
J_3: 0.000623(kg*m^2)
χ: 0.01477(m)

Final Model

Parameters (45/15-2230)

time: 1.37(s)
xy_{fm}: 0.35(m)
V_{xfm}: 0.0749(m/s)
V_{yfm}: -0.0286(m/s)
V_{zfm}: -1.52(m/s)
Ψ_{fm}: 86.99°
depth: 2.17(m)

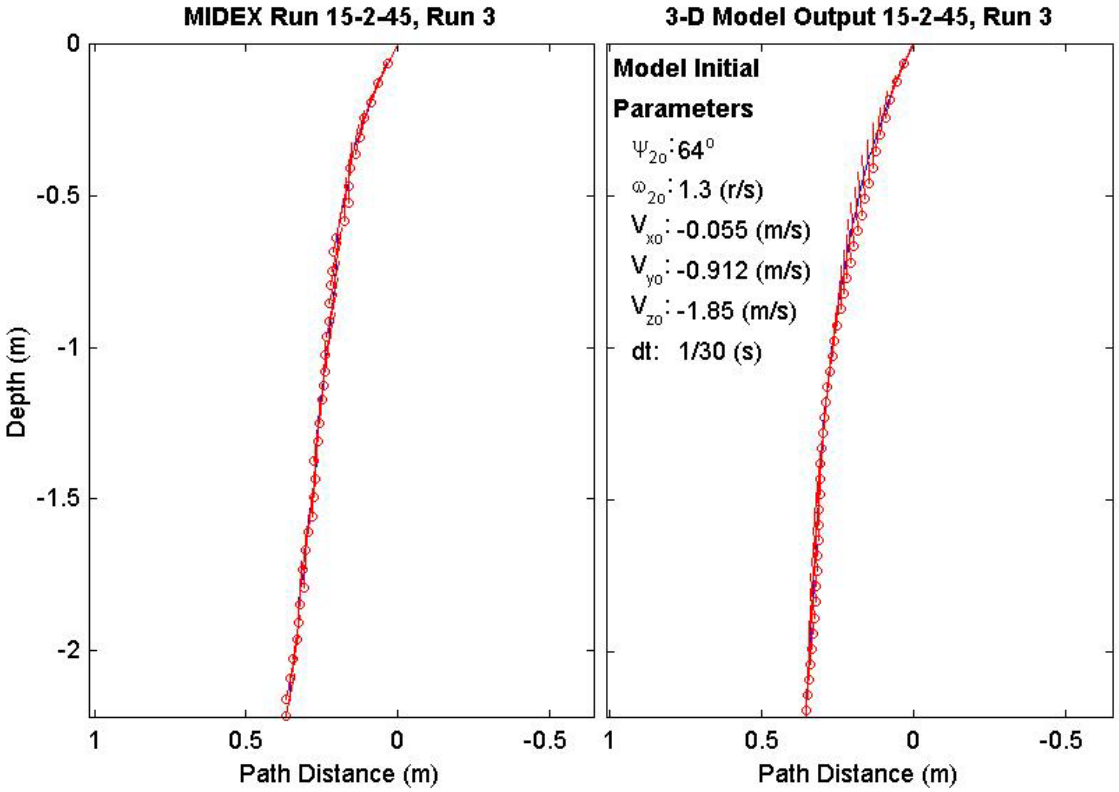

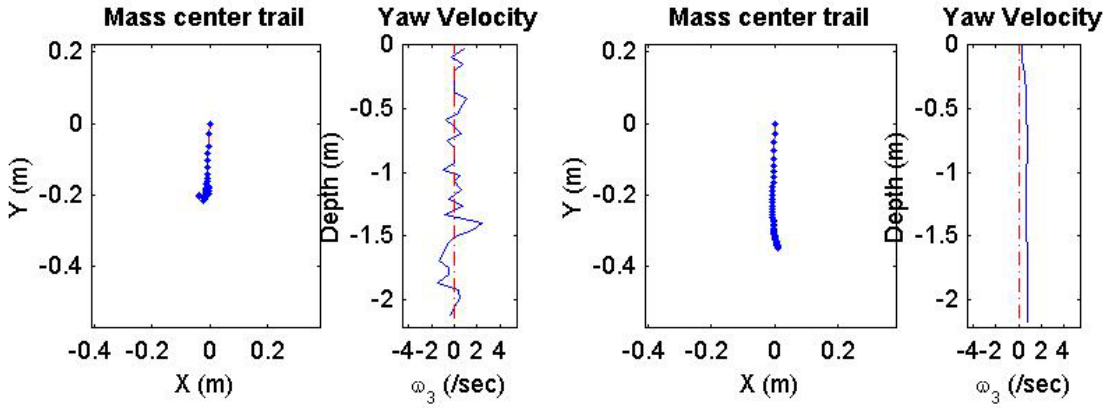

Final Drop

Parameters (45/15-1832)

time: 1.27(s)
xy_{fe}: 0.162(m)
V_{xfe}: -0.055(m/s)
V_{yfe}: 0.163(m/s)
V_{zfe}: -1.63(m/s)
Ψ_{fe}: 77.9°
depth: 2.18(m)

Mine Shape

Parameters (45/15-1832)

d: 0.04(m)
L: 0.152(m)
m: 0.323(m)
J_1: 3.3e-005(kg*m^2)
J_2: 0.000623(kg*m^2)
J_3: 0.000623(kg*m^2)
χ: 0.01477(m)

Final Model

Parameters (45/15-1832)

time: 1.43(s)
xy_{fm}: 0.304(m)
V_{xfm}: 0.0264(m/s)
V_{yfm}: 0.0953(m/s)
V_{zfm}: -1.53(m/s)
Ψ_{fm}: 91.75°
depth: 2.23(m)

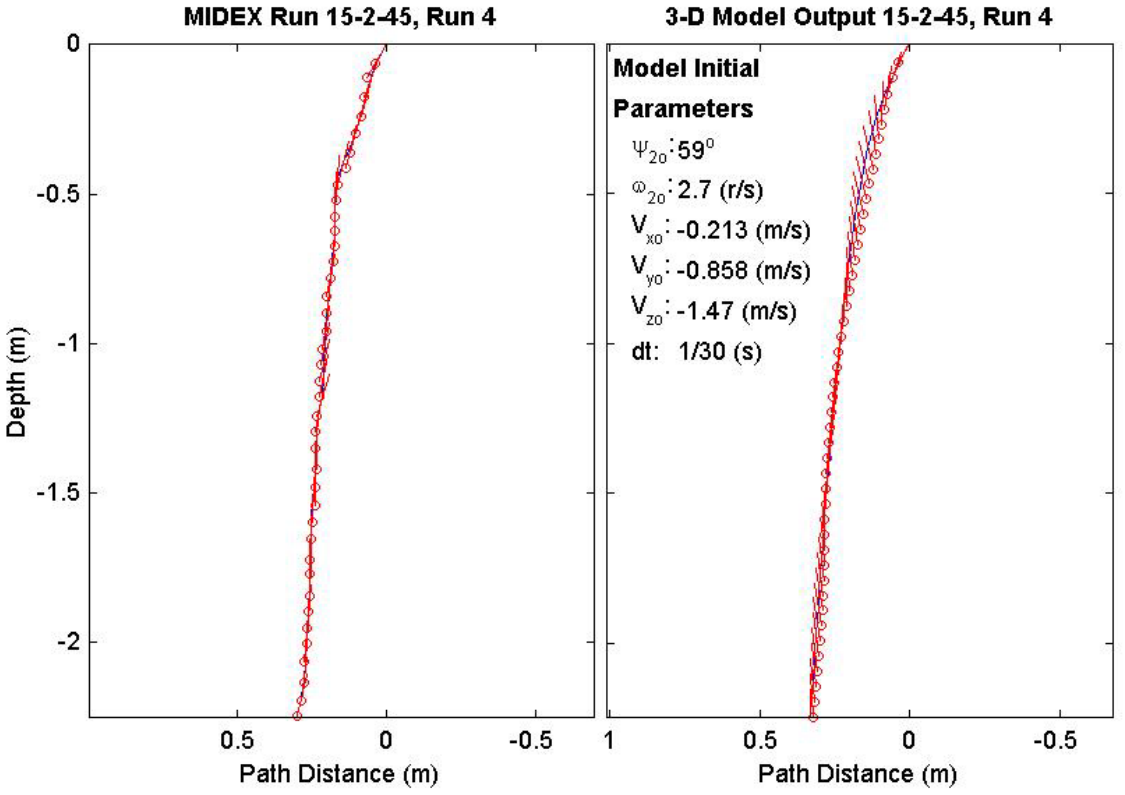

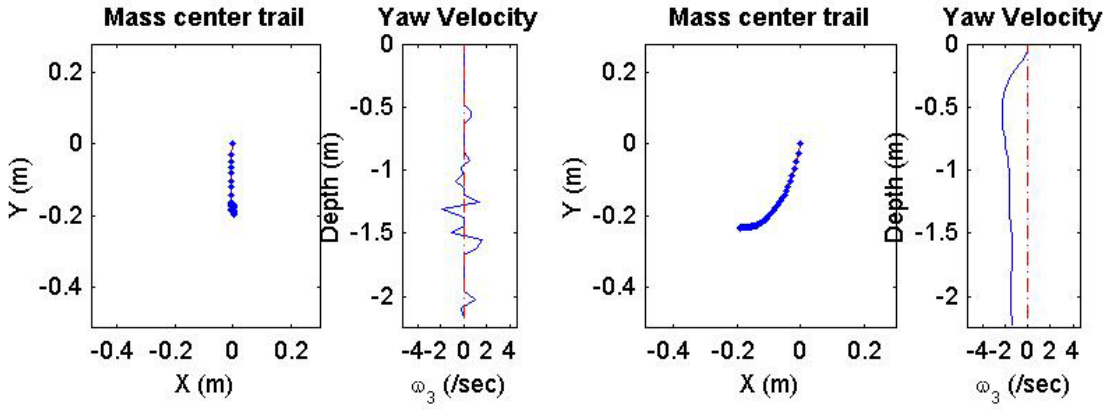

Final Drop
Parameters (45/15-1328)

time: 1.27(s)
xy_{fe}: 0.314(m)
V_{xfe}: -0.106(m/s)
V_{yfe}: -0.108(m/s)
V_{zfe}: -1.82(m/s)
Ψ_{fe}: 85.6°
depth: 2.15(m)

Mine Shape
Parameters (45/15-1328)

d: 0.04(m)
L: 0.152(m)
m: 0.323(m)
J_1: 3.3e-005(kg*m^2)
J_2: 0.000623(kg*m^2)
J_3: 0.000623(kg*m^2)
χ: 0.01477(m)

Final Model
Parameters (45/15-1328)

time: 1.4(s)
xy_{fm}: 0.249(m)
V_{xfm}: 0.0107(m/s)
V_{yfm}: 0.1(m/s)
V_{zfm}: -1.53(m/s)
Ψ_{fm}: 95.04°
depth: 2.16(m)

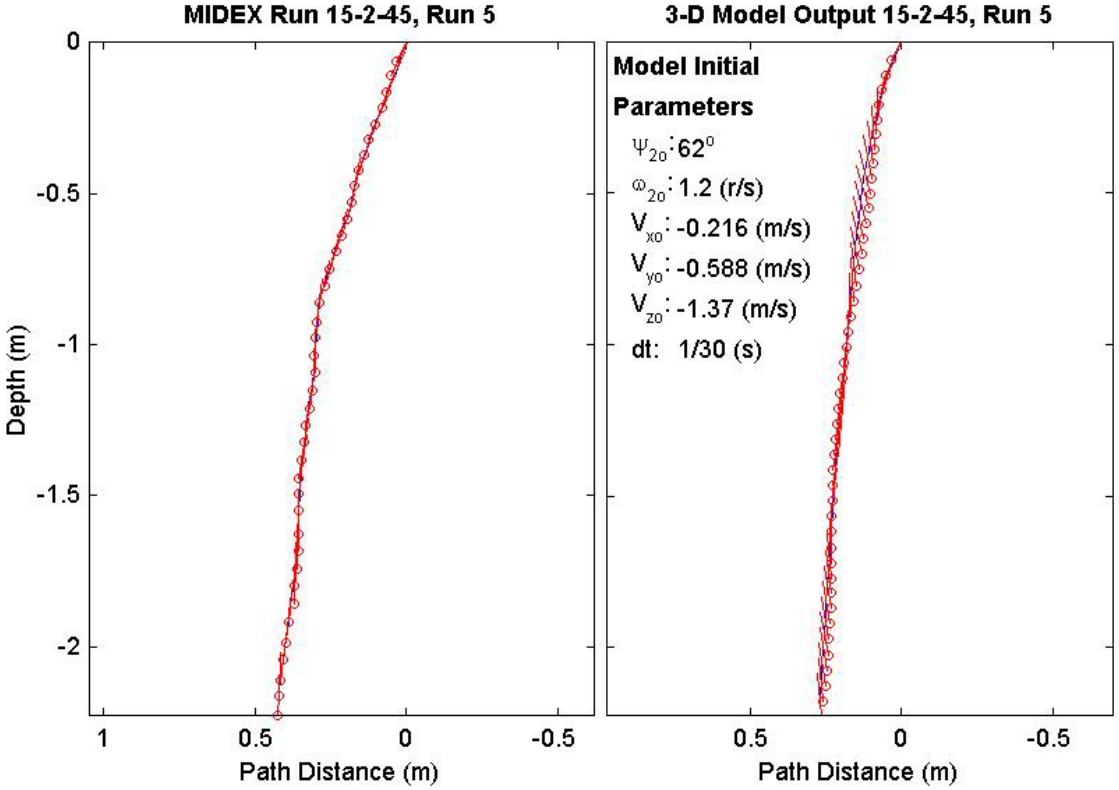

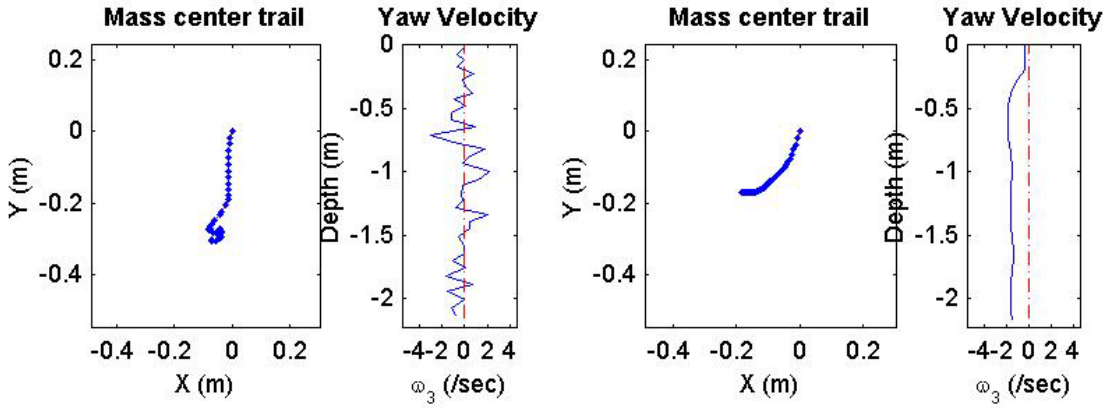

Final Drop

Parameters (45/12-3123)

time: 1.57(s)
xy_{fe}: 0.18(m)
V_{xfe}: -0.054(m/s)
V_{yfe}: 0.108(m/s)
V_{zfe}: -1.39(m/s)
Ψ_{fe}: 86.7°
depth: 2.1(m)

Mine Shape

Parameters (45/12-3123)

d: 0.04(m)
L: 0.121(m)
m: 0.254(m)
J_1: 2.71e-005(kg*m^2)
J_2: 0.000331(kg*m^2)
J_3: 0.000331(kg*m^2)
χ: 0.00997(m)

Final Model

Parameters (45/12-3123)

time: 1.43(s)
xy_{fm}: 0.282(m)
V_{xfm}: 0.0369(m/s)
V_{yfm}: -0.0115(m/s)
V_{zfm}: -1.37(m/s)
Ψ_{fm}: 82.52°
depth: 2.11(m)

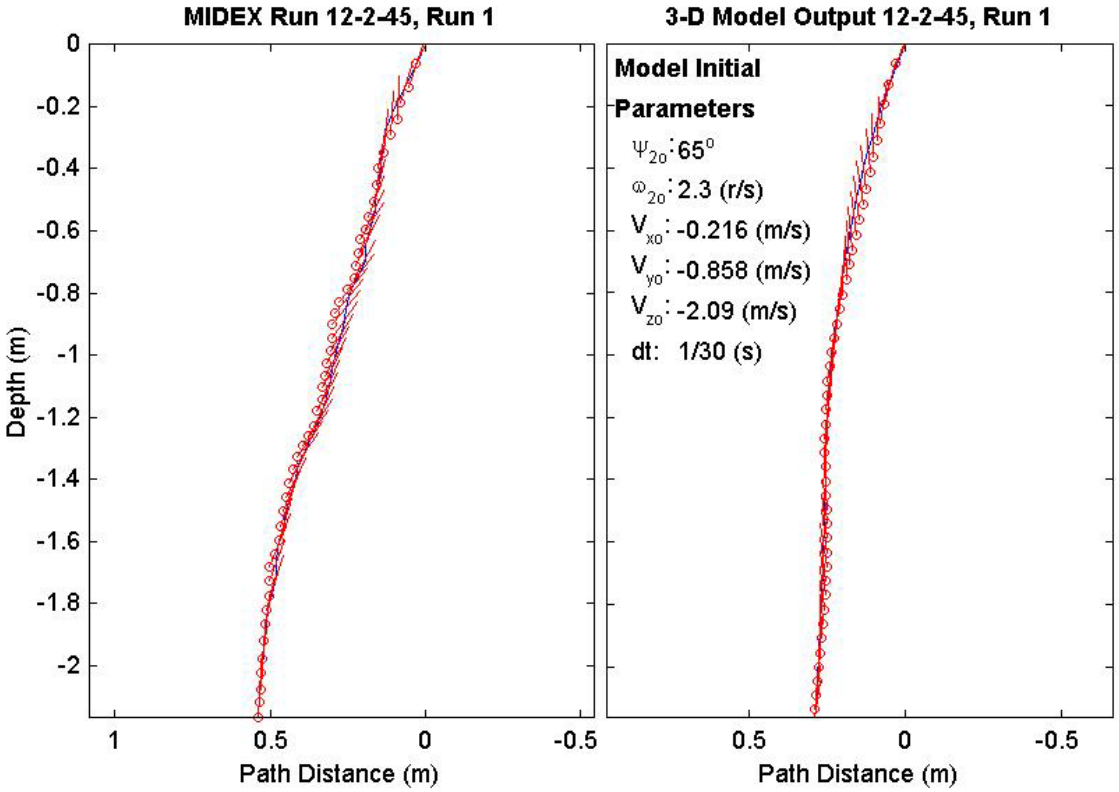

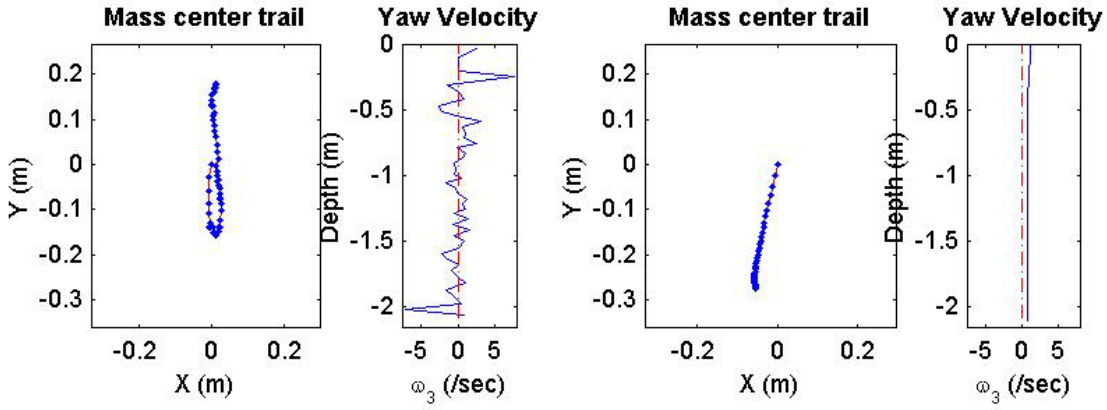

Final Drop

Parameters (45/12-2649)

time: 1.4(s)
xy_{fe}: 0.199(m)
V_{xfe}: -0.108(m/s)
V_{yfe}: 0(m/s)
V_{zfe}: -1.47(m/s)
Ψ_{fe}: 83.6°
depth: 2.15(m)

Mine Shape

Parameters (45/12-2649)

d: 0.04(m)
L: 0.121(m)
m: 0.254(m)
J_1: 2.71e-005(kg*m^2)
J_2: 0.000331(kg*m^2)
J_3: 0.000331(kg*m^2)
χ: 0.00997(m)

Final Model

Parameters (45/12-2649)

time: 1.5(s)
xy_{fm}: 0.169(m)
V_{xfm}: 0.0192(m/s)
V_{yfm}: -0.0422(m/s)
V_{zfm}: -1.37(m/s)
Ψ_{fm}: 80.15°
depth: 2.16(m)

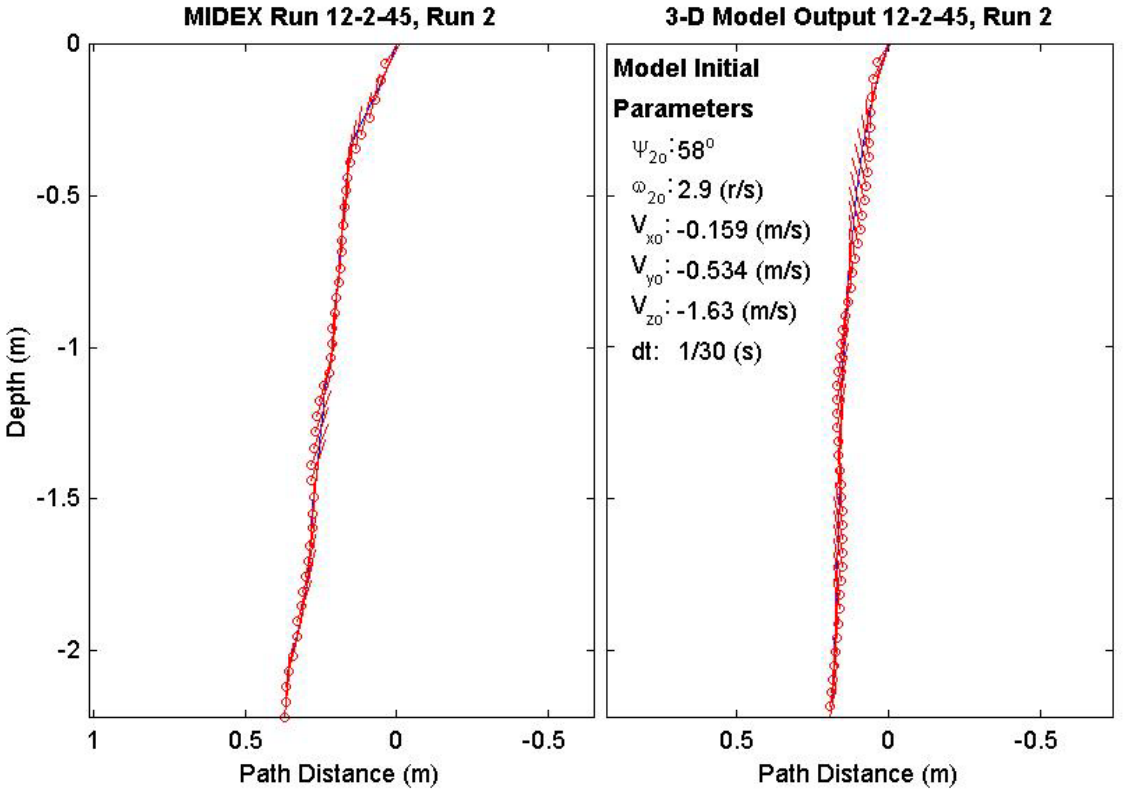

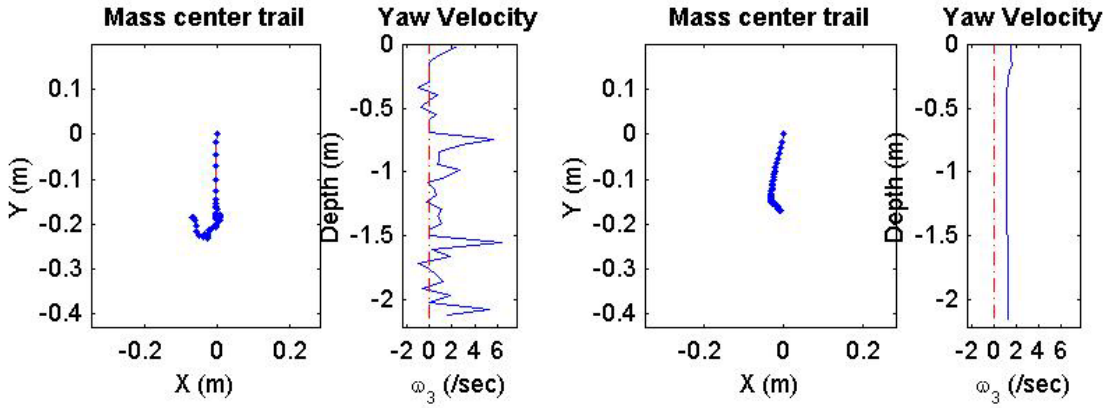

Final Drop

Parameters (45/12-2300)

time: 1.37(s)
xy_{fe}: 0.117(m)
V_{xfe}: 0.054(m/s)
V_{yfe}: -0.27(m/s)
V_{zfe}: -1.66(m/s)
Ψ_{fe}: 80.1°
depth: 2.08(m)

Mine Shape

Parameters (45/12-2300)

d: 0.04(m)
L: 0.121(m)
m: 0.254(m)
J_1: 2.71e-005(kg*m^2)
J_2: 0.000331(kg*m^2)
J_3: 0.000331(kg*m^2)
χ: 0.00997(m)

Final Model

Parameters (45/12-2300)

time: 1.47(s)
xy_{fm}: 0.256(m)
V_{xfm}: 0.0178(m/s)
V_{yfm}: -0.0482(m/s)
V_{zfm}: -1.37(m/s)
Ψ_{fm}: 80.28°
depth: 2.12(m)

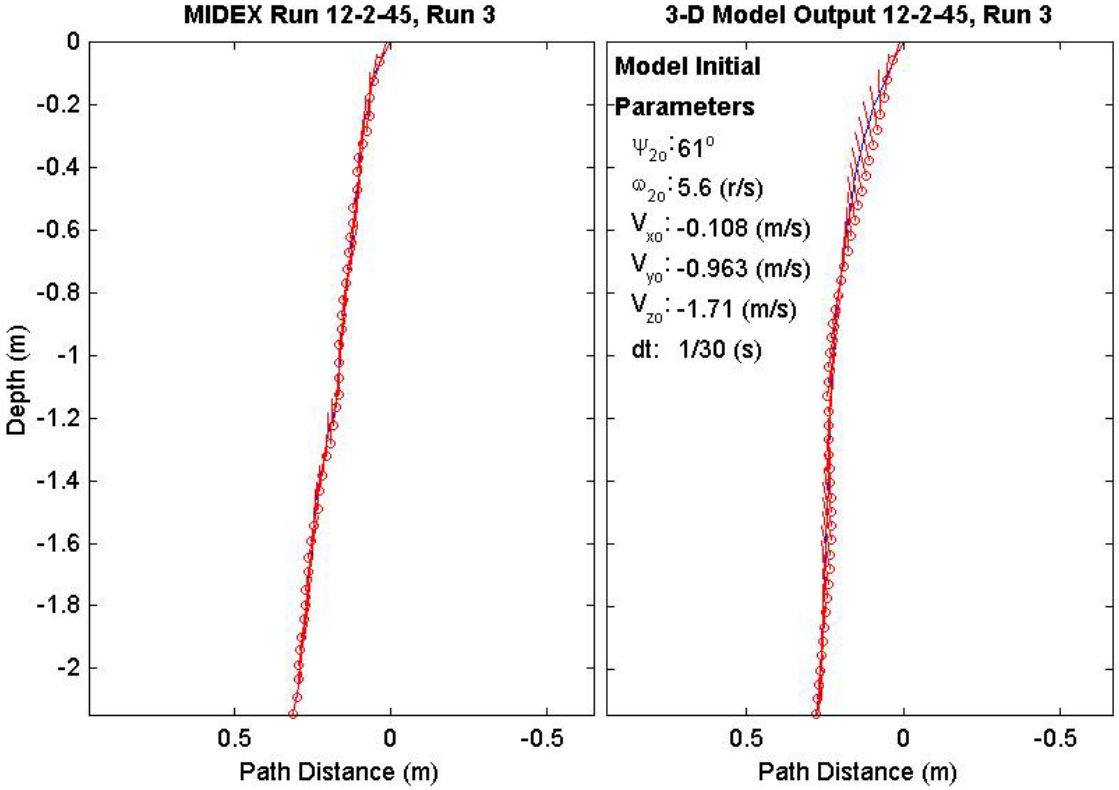

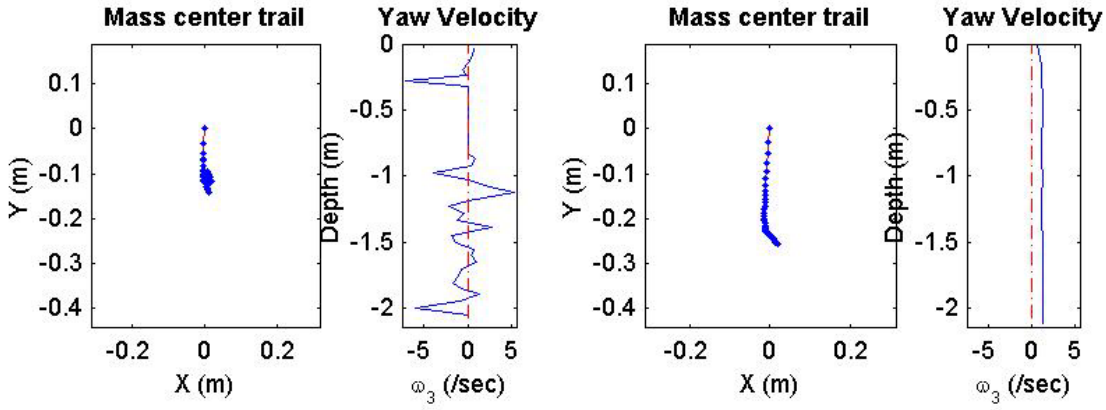

Final Drop

Parameters (45/12-1836)

time: 1.37(s)
xy_{fe}: 0.13(m)
V_{xfe}: 0.375(m/s)
V_{yfe}: 0.321(m/s)
V_{zfe}: -1.29(m/s)
Ψ_{fe}: 80.2^{o}
depth: 2.08(m)

Mine Shape

Parameters (45/12-1836)

d: 0.04(m)
L: 0.121(m)
m: 0.254(m)
J_1: 2.71e-005($kg*m^2$)
J_2: 0.000331($kg*m^2$)
J_3: 0.000331($kg*m^2$)
χ: 0.00997(m)

Final Model

Parameters (45/12-1836)

time: 1.47(s)
xy_{fm}: 0.283(m)
V_{xfm}: 0.0397(m/s)
V_{yfm}: -0.0064(m/s)
V_{zfm}: -1.37(m/s)
Ψ_{fm}: 83.19^{o}
depth: 2.1(m)

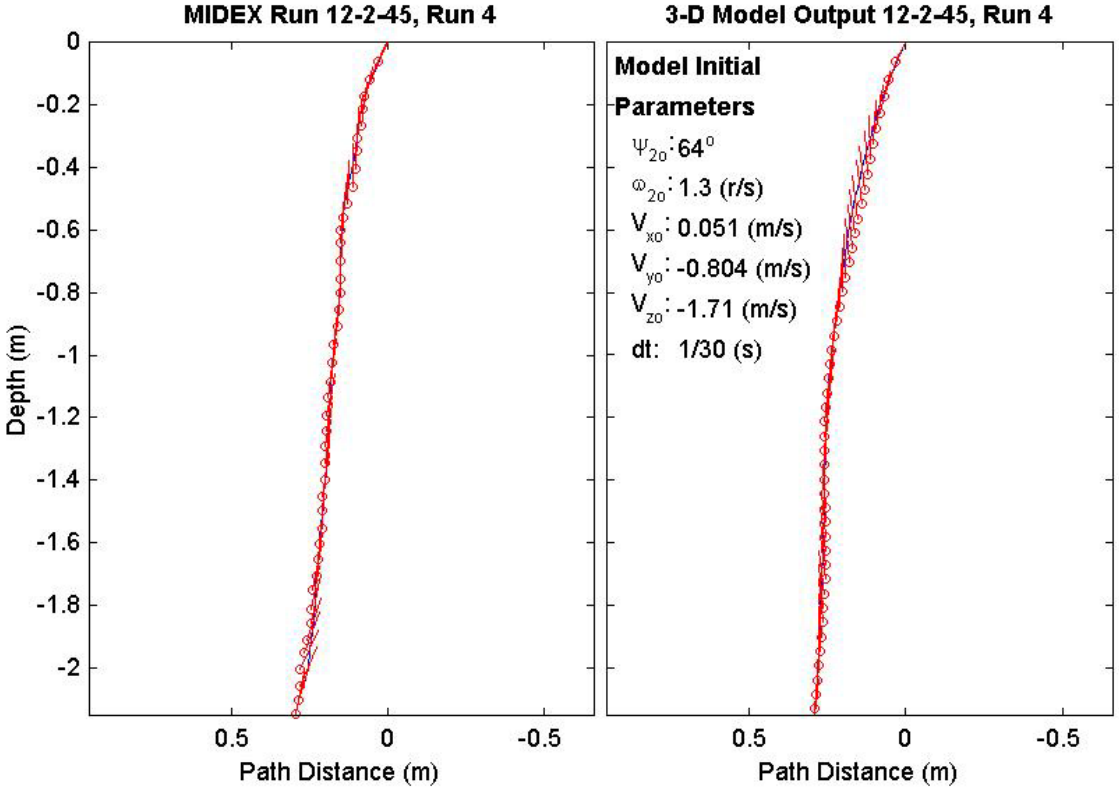

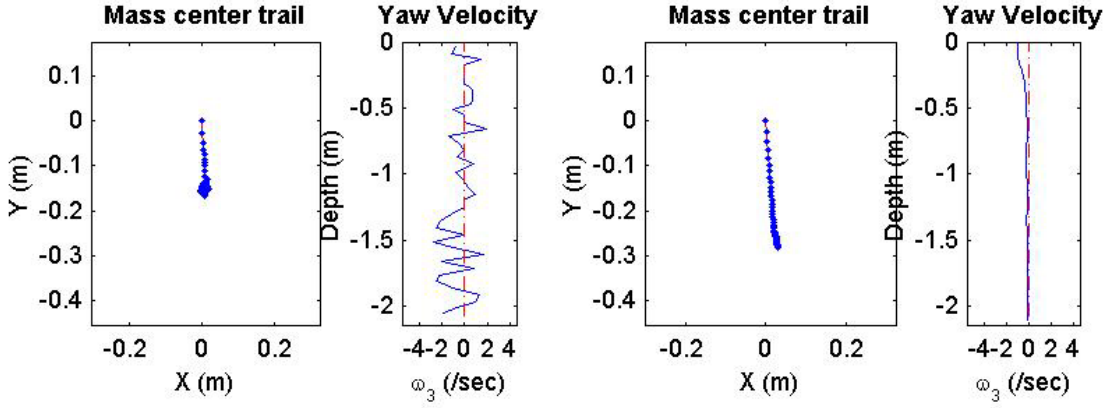

Final Drop

Parameters (45/12-1565)

time: 1.47(s)
xy_{fe}: 0.018(m)
V_{xfe}: 0(m/s)
V_{yfe}: 0.267(m/s)
V_{zfe}: -1.42(m/s)
Ψ_{fe}: 70.5°
depth: 2.14(m)

Mine Shape

Parameters (45/12-1565)

d: 0.04(m)
L: 0.121(m)
m: 0.254(m)
J_1: 2.71e-005(kg*m^2)
J_2: 0.000331(kg*m^2)
J_3: 0.000331(kg*m^2)
χ: 0.00997(m)

Final Model

Parameters (45/12-1565)

time: 1.53(s)
xy_{fm}: 0.331(m)
V_{xfm}: 0.0822(m/s)
V_{yfm}: -0.0254(m/s)
V_{zfm}: -1.37(m/s)
Ψ_{fm}: 87.59°
depth: 2.15(m)

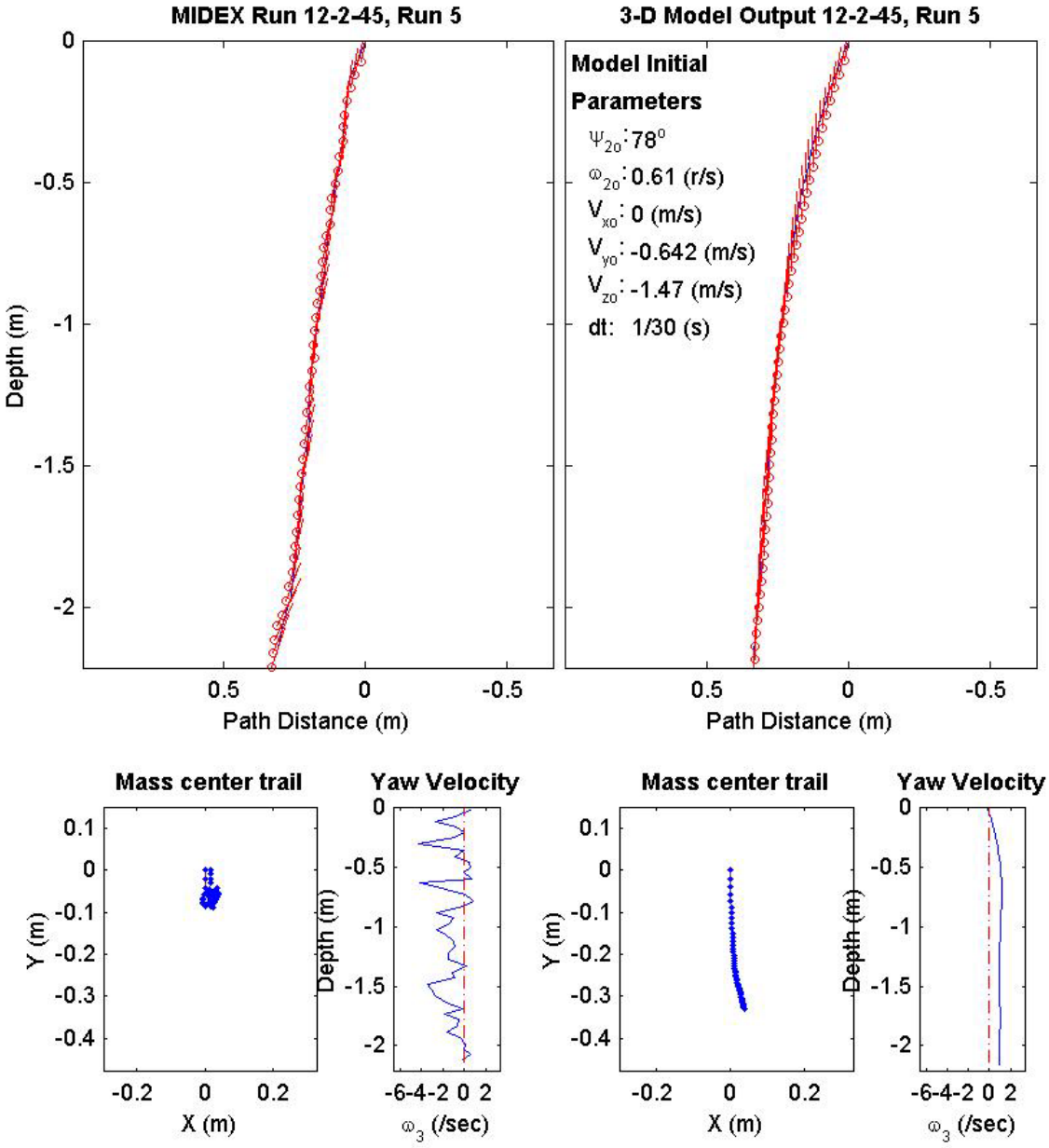

Final Drop
Parameters (45/9-2953)

time: 1.73(s)
xy_{fe}: 0.484(m)
V_{xfe}: 0.267(m/s)
V_{yfe}: 0.162(m/s)
V_{zfe}: -1.31(m/s)
Ψ_{fe}: 54.9°
depth: 2.14(m)

Mine Shape
Parameters (45/9-2953)

d: 0.04(m)
L: 0.0912(m)
m: 0.215(m)
J_1: 2.35e-005(kg*m^2)
J_2: 0.000156(kg*m^2)
J_3: 0.000156(kg*m^2)
χ: 0.005796(m)

Final Model
Parameters (45/9-2953)

time: 1.53(s)
xy_{fm}: 0.244(m)
V_{xfm}: 0.00365(m/s)
V_{yfm}: 3.26e-018(m/s)
V_{zfm}: -1.4(m/s)
Ψ_{fm}: 80.6°
depth: 2.18(m)

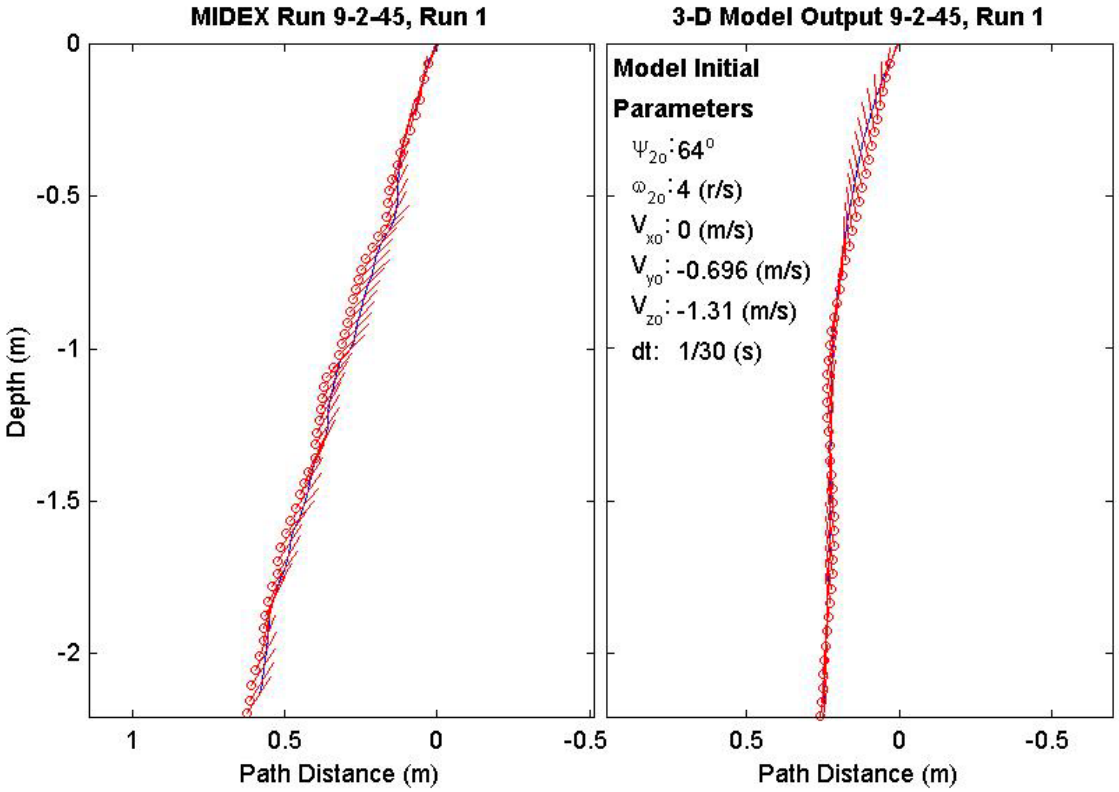

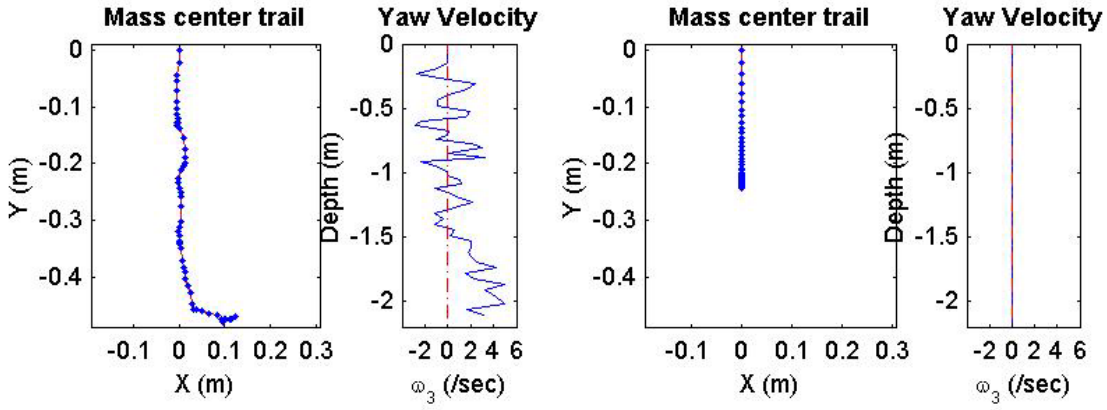

Final Drop

Parameters (45/9-2508)

time: 1.77(s)
xy_{fe}: 0.53(m)
V_{xfe}: 0.108(m/s)
V_{yfe}: -0.108(m/s)
V_{zfe}: -1.13(m/s)
Ψ_{fe}: 50.4°
depth: 2.15(m)

Mine Shape

Parameters (45/9-2508)

d: 0.04(m)
L: 0.0912(m)
m: 0.215(m)
J_1: 2.35e-005(kg*m^2)
J_2: 0.000156(kg*m^2)
J_3: 0.000156(kg*m^2)
χ: 0.005796(m)

Final Model

Parameters (45/9-2508)

time: 1.47(s)
xy_{fm}: 0.207(m)
V_{xfm}: 0.0121(m/s)
V_{yfm}: 4.39e-019(m/s)
V_{zfm}: -1.4(m/s)
Ψ_{fm}: 80.35°
depth: 2.15(m)

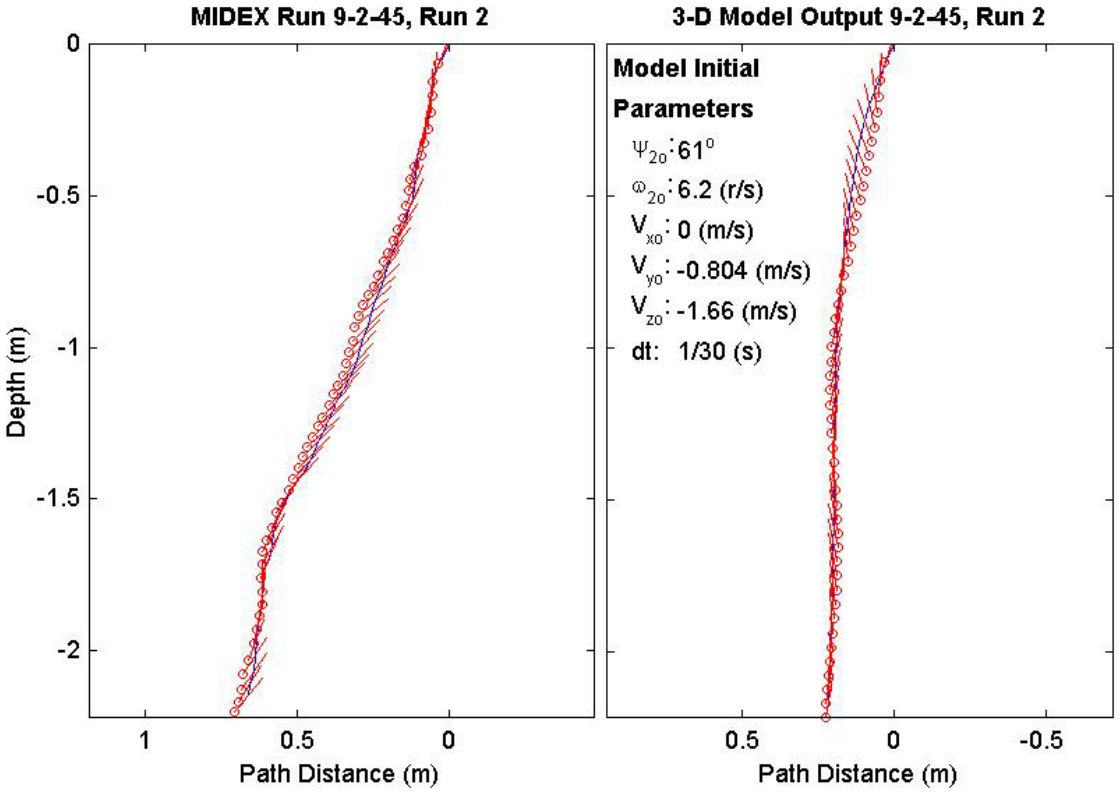

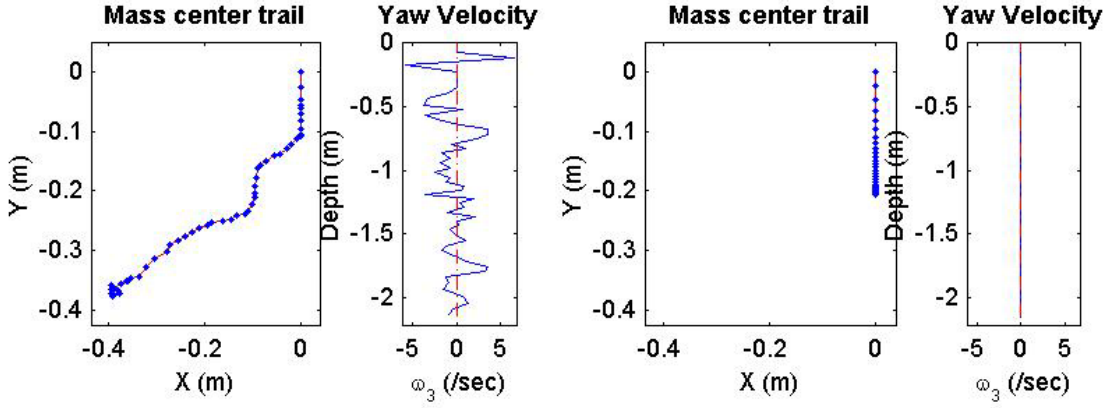

Final Drop

Parameters (45/9-2242)

time: 1.7(s)
xy_{fe}: 0.362(m)
V_{xfe}: 0.051(m/s)
V_{yfe}: 0.108(m/s)
V_{zfe}: -1.23(m/s)
Ψ_{fe}: 63.1°
depth: 2.11(m)

Mine Shape

Parameters (45/9-2242)

d: 0.04(m)
L: 0.0912(m)
m: 0.215(m)
J_1: 2.35e-005(kg*m^2)
J_2: 0.000156(kg*m^2)
J_3: 0.000156(kg*m^2)
χ: 0.005796(m)

Final Model

Parameters (45/9-2242)

time: 1.47(s)
xy_{fm}: 0.189(m)
V_{xfm}: 0.0606(m/s)
V_{yfm}: -0.0131(m/s)
V_{zfm}: -1.39(m/s)
Ψ_{fm}: 86.57°
depth: 2.12(m)

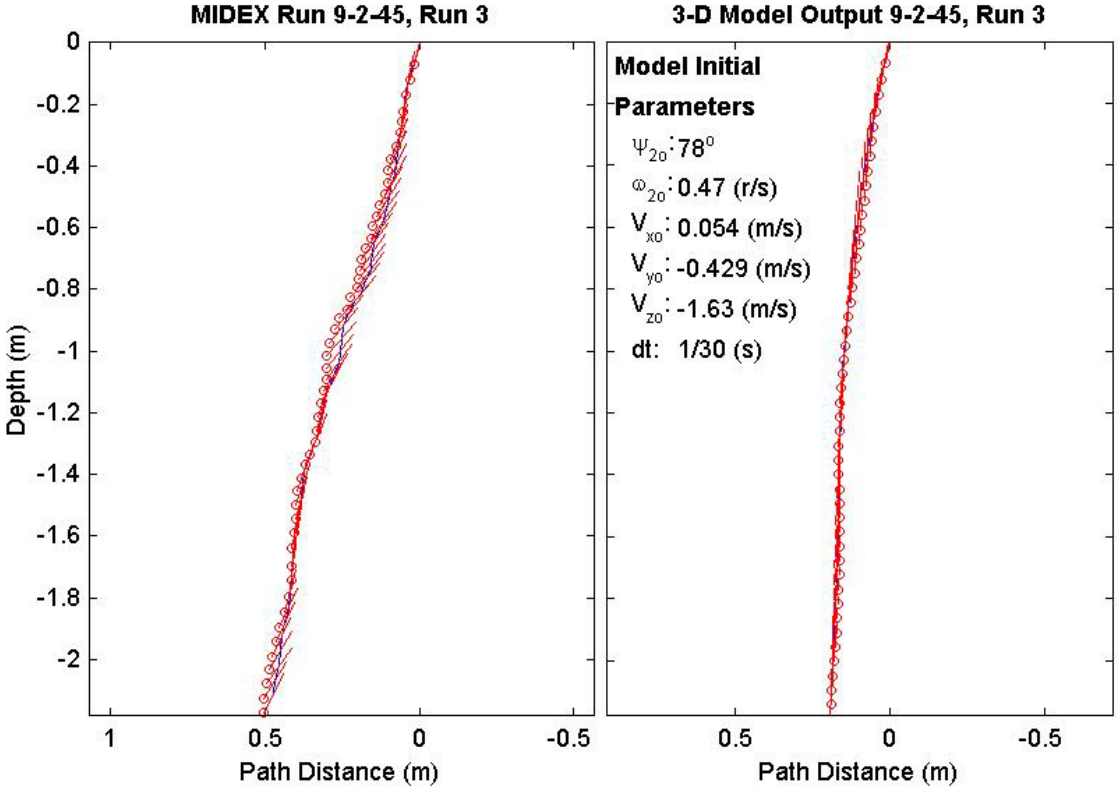

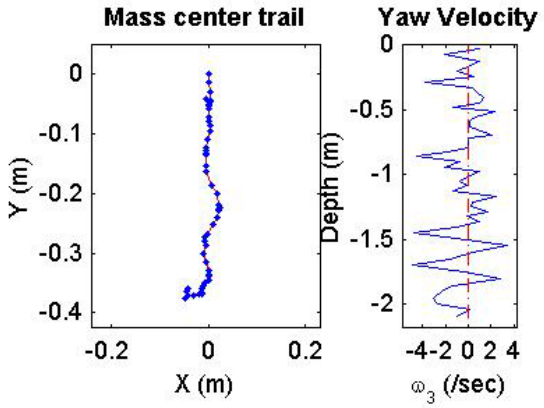

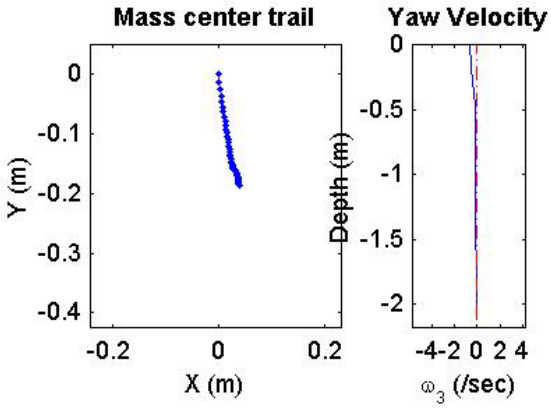

Final Drop

Parameters (45/9-1626)

time: 1.73(s)
xy_{fe}: 0.245(m)
V_{xfe}: -0.108(m/s)
V_{yfe}: 0.054(m/s)
V_{zfe}: -0.883(m/s)
Ψ_{fe}: 61.1°
depth: 2.17(m)

Mine Shape

Parameters (45/9-1626)

d: 0.04(m)
L: 0.0912(m)
m: 0.215(m)
J_1: 2.35e-005(kg*m^2)
J_2: 0.000156(kg*m^2)
J_3: 0.000156(kg*m^2)
χ: 0.005796(m)

Final Model

Parameters (45/9-1626)

time: 1.53(s)
xy_{fm}: 0.114(m)
V_{xfm}: 0.00218(m/s)
V_{yfm}: -0.0108(m/s)
V_{zfm}: -1.4(m/s)
Ψ_{fm}: 80.88°
depth: 2.19(m)

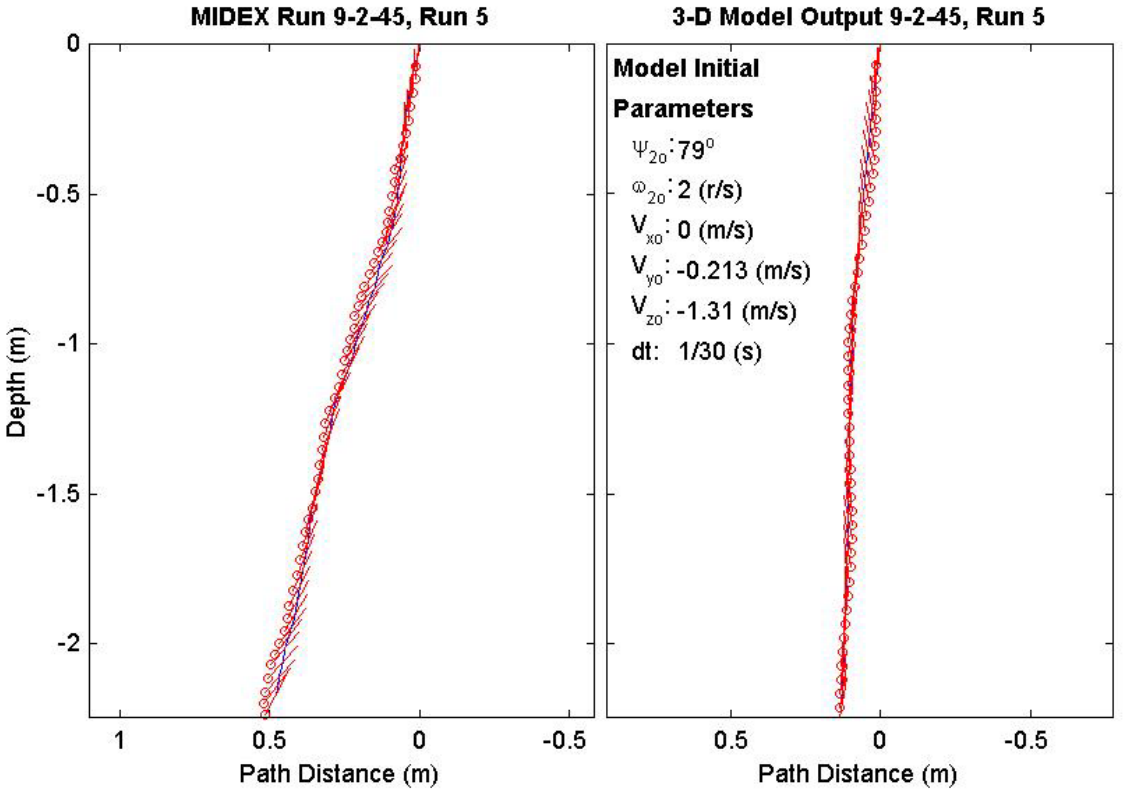

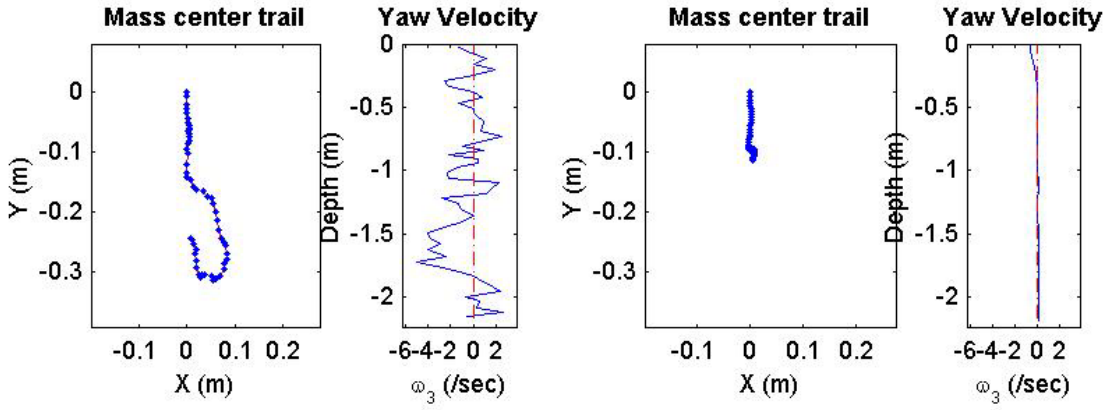

Final Drop Parameters (60/15-3400)

time: 1.17(s)
xy_{fe}: 0.0855(m)
V_{xfe}: 0.213(m/s)
V_{yfe}: -0.108(m/s)
V_{zfe}: -1.34(m/s)
Ψ_{fe}: 87.3°
depth: 2.07(m)

Mine Shape Parameters (60/15-3400)

d: 0.04(m)
L: 0.152(m)
m: 0.323(m)
J_1: 3.3e-005(kg*m^2)
J_2: 0.000623(kg*m^2)
J_3: 0.000623(kg*m^2)
χ: 0.01477(m)

Final Model Parameters (60/15-3400)

time: 1.23(s)
xy_{fm}: 0.327(m)
V_{xfm}: 0.098(m/s)
V_{yfm}: -0.0307(m/s)
V_{zfm}: -1.52(m/s)
Ψ_{fm}: 89.93°
depth: 2.07(m)

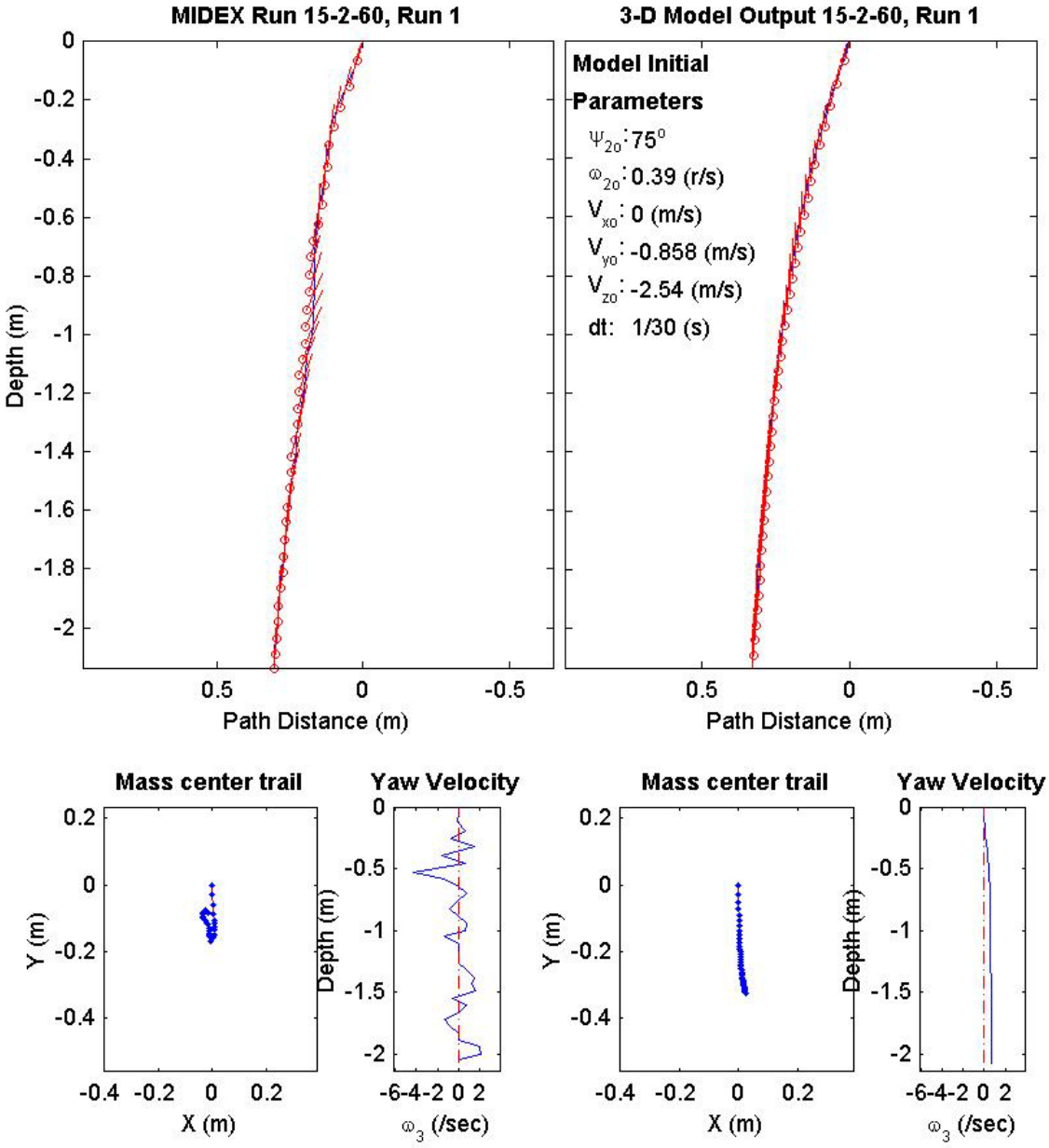

Final Drop

Parameters (45/15-2684)

time: 1.37(s)
xy_{fe}: 0.0644(m)
V_{xfe}: 0.429(m/s)
V_{yfe}: 0.267(m/s)
V_{zfe}: -1.39(m/s)
Ψ_{fe}: 77.7°
depth: 2.19(m)

Mine Shape

Parameters (45/15-2684)

d: 0.04(m)
L: 0.152(m)
m: 0.323(m)
J_1: 3.3e-005(kg*m^2)
J_2: 0.000623(kg*m^2)
J_3: 0.000623(kg*m^2)
χ: 0.01477(m)

Final Model

Parameters (45/15-2684)

time: 1.33(s)
xy_{fm}: 0.33(m)
V_{xfm}: 0.0666(m/s)
V_{yfm}: -0.014(m/s)
V_{zfm}: -1.52(m/s)
Ψ_{fm}: 87.56°
depth: 2.2(m)

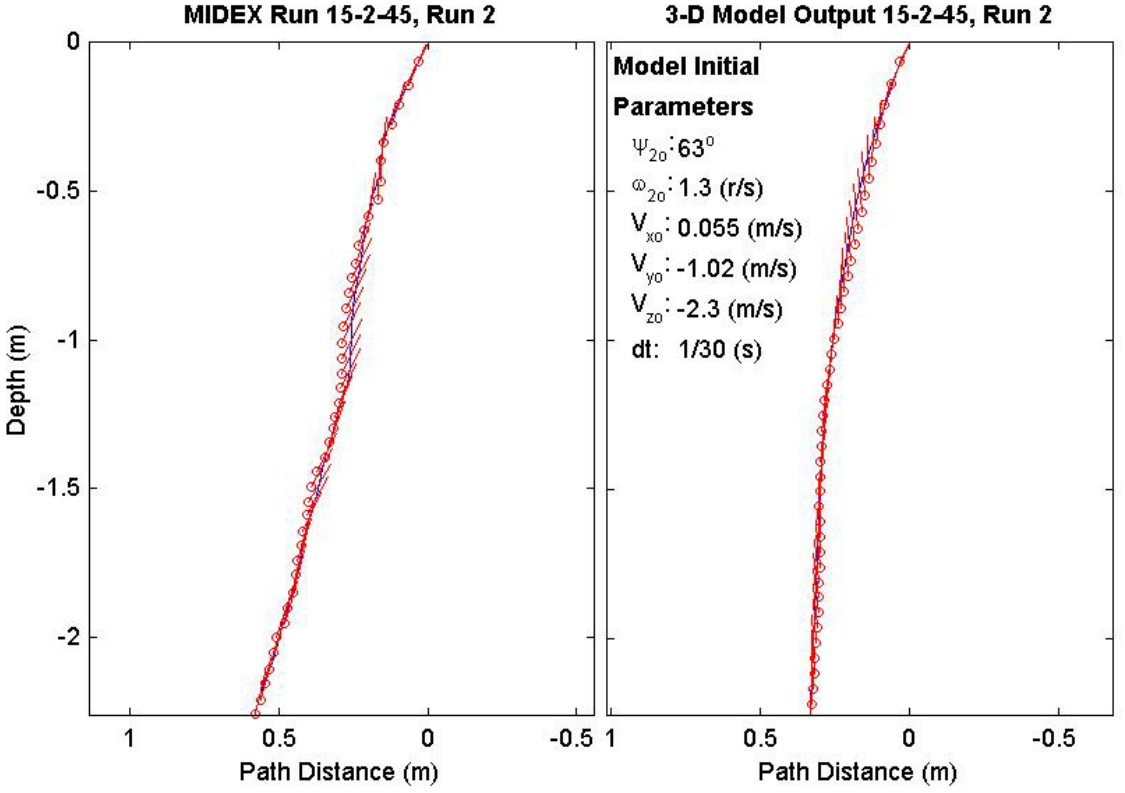

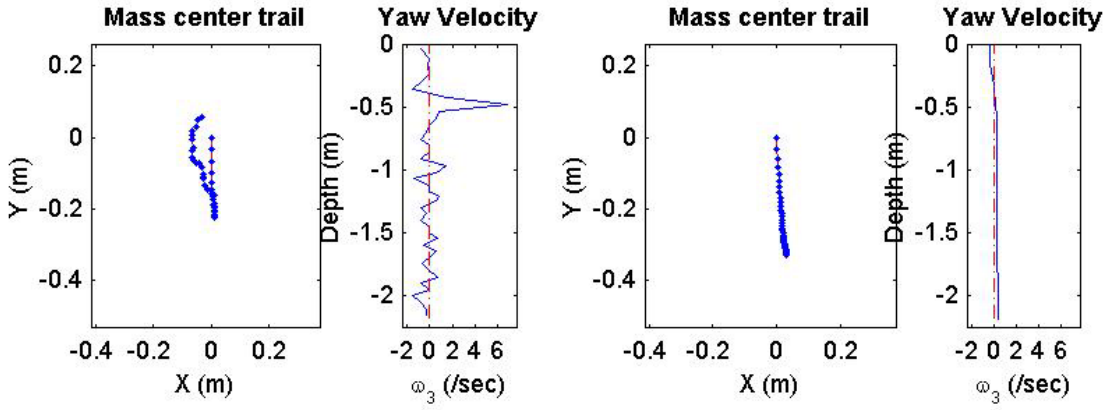

Final Drop

Parameters (60/15-2709)

time: 1.23(s)
xy_{fe}: 0.0773(m)
V_{xfe}: -0.267(m/s)
V_{yfe}: 0.106(m/s)
V_{zfe}: -1.77(m/s)
Ψ_{fe}: 85.4°
depth: 2.14(m)

Mine Shape

Parameters (60/15-2709)

d: 0.04(m)
L: 0.152(m)
m: 0.323(m)
J_1: 3.3e-005(kg*m^2)
J_2: 0.000623(kg*m^2)
J_3: 0.000623(kg*m^2)
χ: 0.01477(m)

Final Model

Parameters (60/15-2709)

time: 1.3(s)
xy_{fm}: 0.225(m)
V_{xfm}: 0.0363(m/s)
V_{yfm}: -0.0505(m/s)
V_{zfm}: -1.52(m/s)
Ψ_{fm}: 84.57°
depth: 2.15(m)

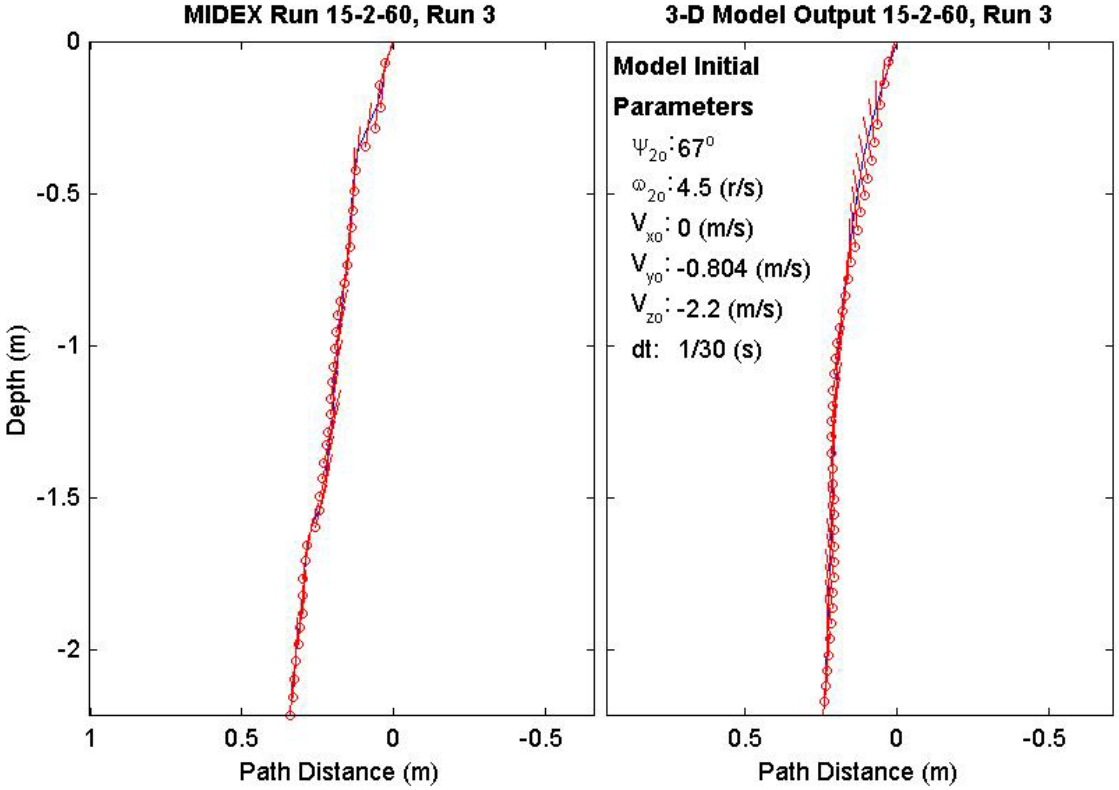

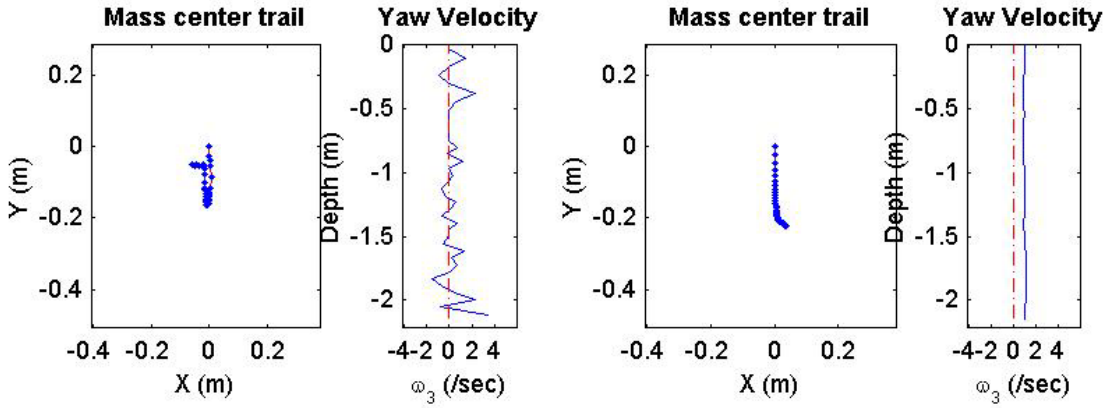

Final Drop Parameters (60/15-1835)

time: 1.2(s)
xy_{fe}: 0.129(m)
V_{xfe}: 0(m/s)
V_{yfe}: 0.321(m/s)
V_{zfe}: -2.01(m/s)
Ψ_{fe}: 84.9°
depth: 2.1(m)

Mine Shape Parameters (60/15-1835)

d: 0.04(m)
L: 0.152(m)
m: 0.323(m)
J_1: 3.3e-005(kg*m^2)
J_2: 0.000623(kg*m^2)
J_3: 0.000623(kg*m^2)
χ: 0.01477(m)

Final Model Parameters (60/15-1835)

time: 1.3(s)
xy_{fm}: 0.227(m)
V_{xfm}: 0.0567(m/s)
V_{yfm}: 1.07e-018(m/s)
V_{zfm}: -1.52(m/s)
Ψ_{fm}: 87.76°
depth: 2.11(m)

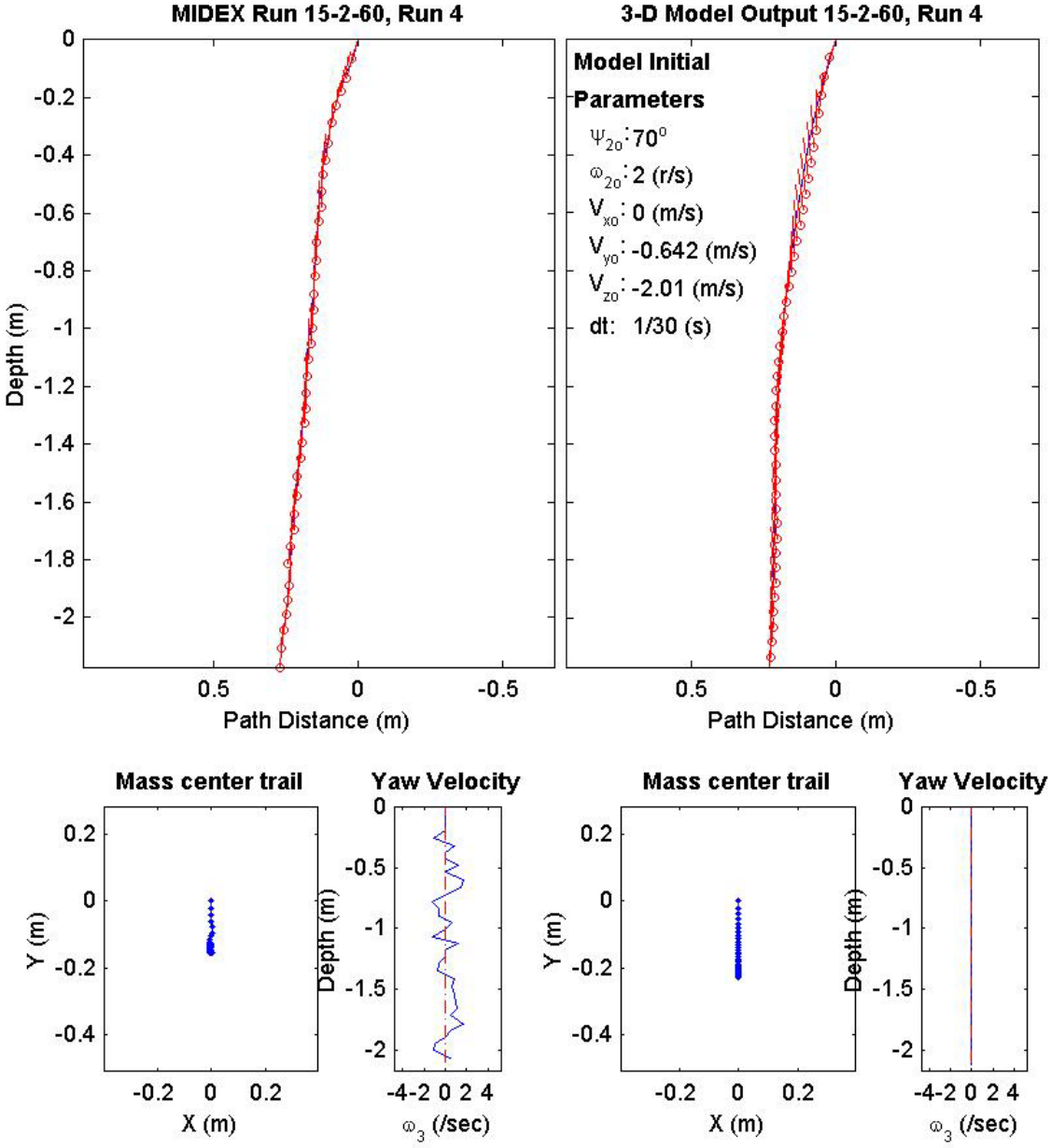

Final Drop

Parameters (60/15-1567)

time: 1.23(s)
xy_{fe}: 0.139(m)
V_{xfe}: 0(m/s)
V_{yfe}: 0(m/s)
V_{zfe}: -1.79(m/s)
Ψ_{fe}: 81.8°
depth: 2.18(m)

Mine Shape

Parameters (60/15-1567)

d: 0.04(m)
L: 0.152(m)
m: 0.323(m)
J_1: 3.3e-005(kg*m^2)
J_2: 0.000623(kg*m^2)
J_3: 0.000623(kg*m^2)
χ: 0.01477(m)

Final Model

Parameters (60/15-1567)

time: 1.37(s)
xy_{fm}: 0.242(m)
V_{xfm}: 0.0403(m/s)
V_{yfm}: 0.00975(m/s)
V_{zfm}: -1.52(m/s)
Ψ_{fm}: 84.14°
depth: 2.21(m)

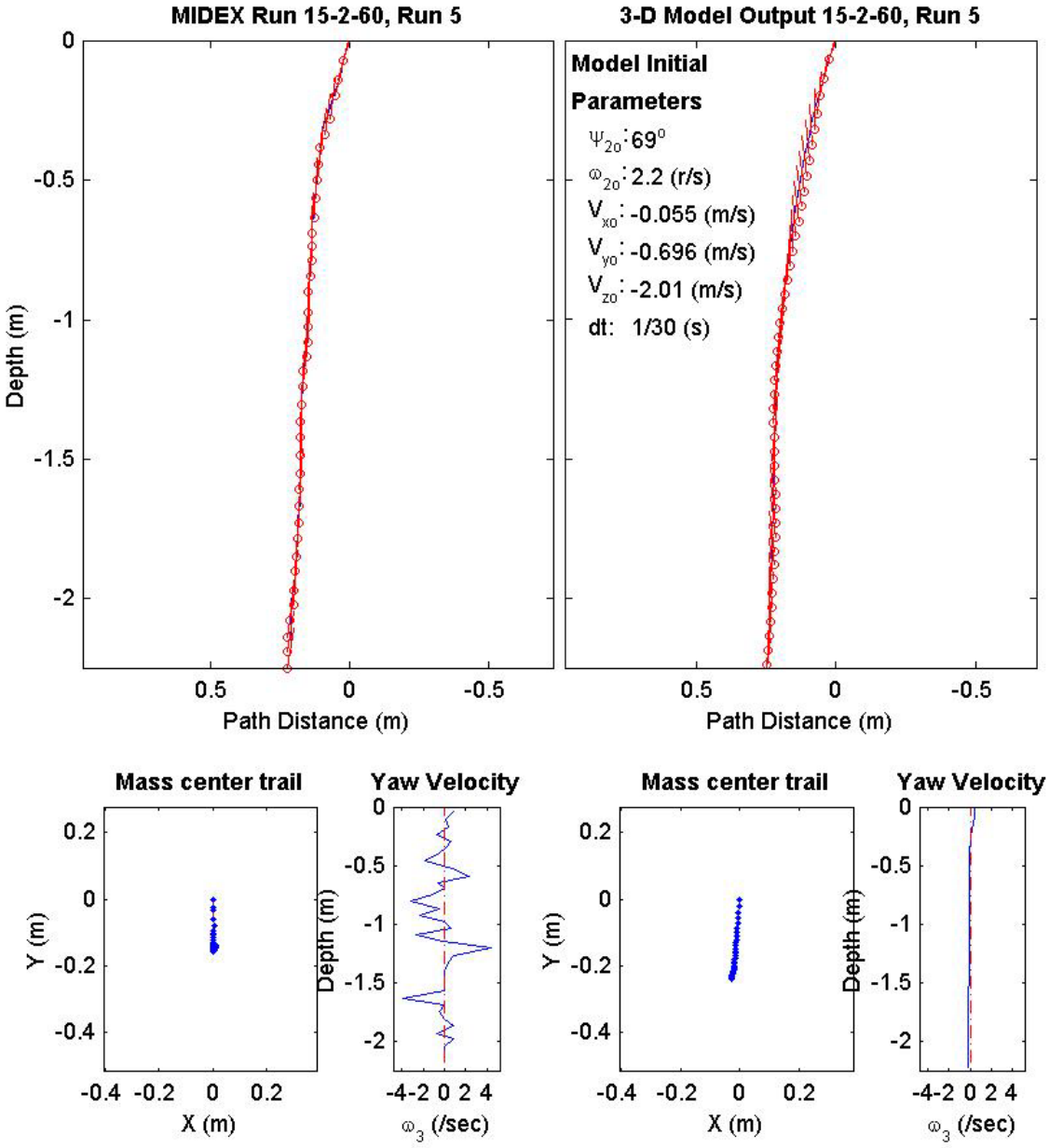

Final Drop

Parameters (60/12-3544)

time: 1.3(s)
xy_{fe}: 0.142(m)
V_{xfe}: 0.321(m/s)
V_{yfe}: 0.162(m/s)
V_{zfe}: -1.18(m/s)
Ψ_{fe}: 79.5°
depth: 2.13(m)

Mine Shape

Parameters (60/12-3544)

d: 0.04(m)
L: 0.121(m)
m: 0.254(m)
J_1: 2.71e-005(kg*m^2)
J_2: 0.000331(kg*m^2)
J_3: 0.000331(kg*m^2)
χ: 0.00997(m)

Final Model

Parameters (60/12-3544)

time: 1.43(s)
xy_{fm}: 0.154(m)
V_{xfm}: 0.05(m/s)
V_{yfm}: -0.0101(m/s)
V_{zfm}: -1.37(m/s)
Ψ_{fm}: 86.26°
depth: 2.17(m)

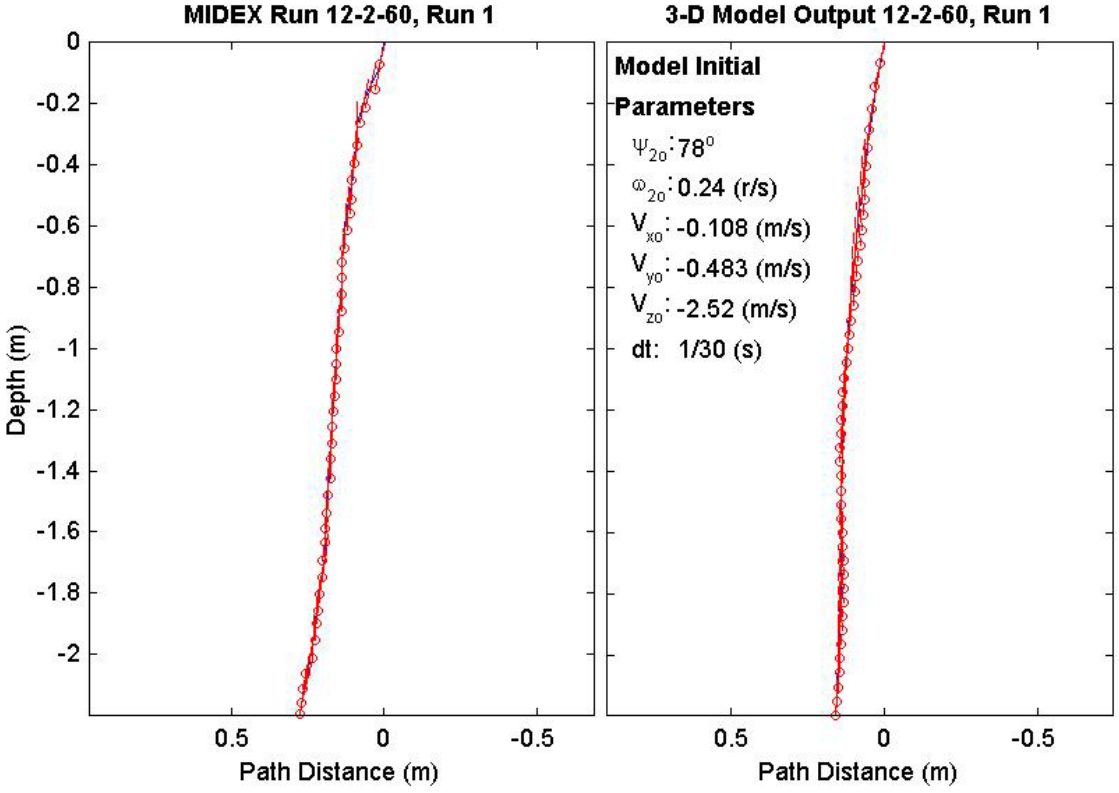

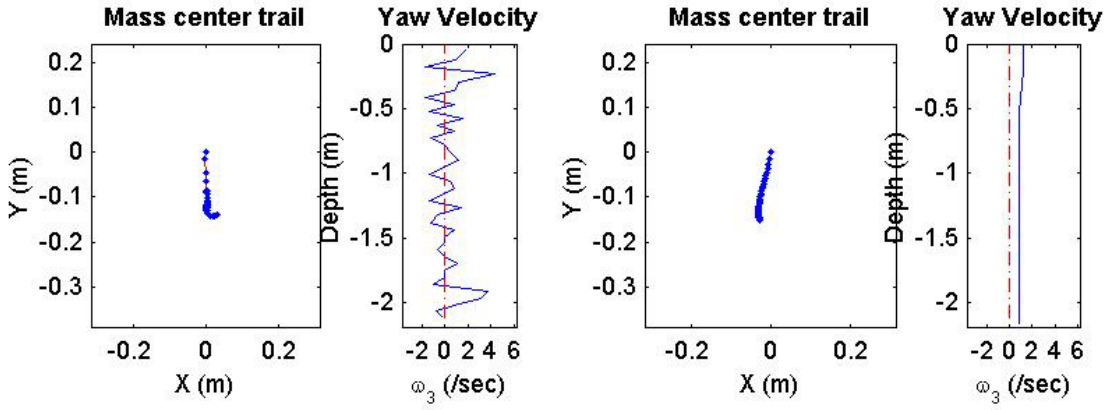

Final Drop

Parameters (60/12-2963)

time: 1.37(s)
xy_{fe}: 0.0211(m)
V_{xfe}: -0.054(m/s)
V_{yfe}: 0.108(m/s)
V_{zfe}: -1.23(m/s)
Ψ_{fe}: 68.1°
depth: 2.12(m)

Mine Shape

Parameters (60/12-2963)

d: 0.04(m)
L: 0.121(m)
m: 0.254(m)
J_1: 2.71e-005(kg*m^2)
J_2: 0.000331(kg*m^2)
J_3: 0.000331(kg*m^2)
χ: 0.00997(m)

Final Model

Parameters (60/12-2963)

time: 1.47(s)
xy_{fm}: 0.145(m)
V_{xfm}: 0.00296(m/s)
V_{yfm}: -0.00382(m/s)
V_{zfm}: -1.38(m/s)
Ψ_{fm}: 81.04°
depth: 2.13(m)

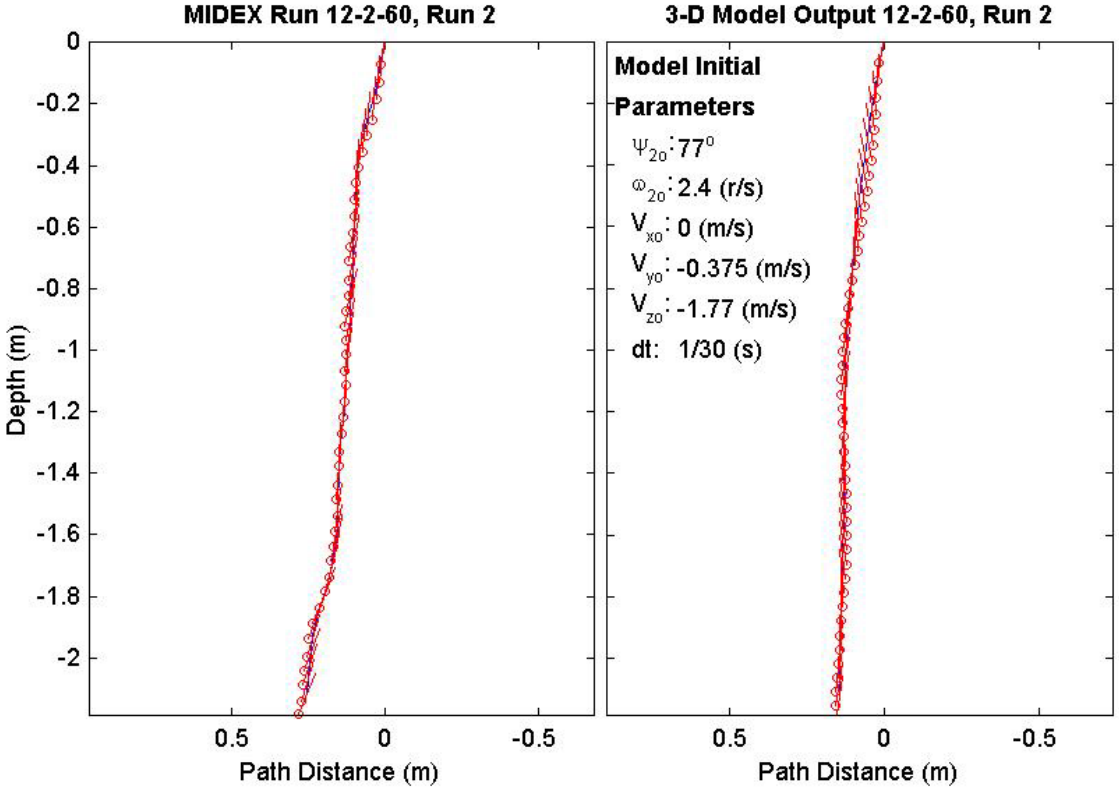

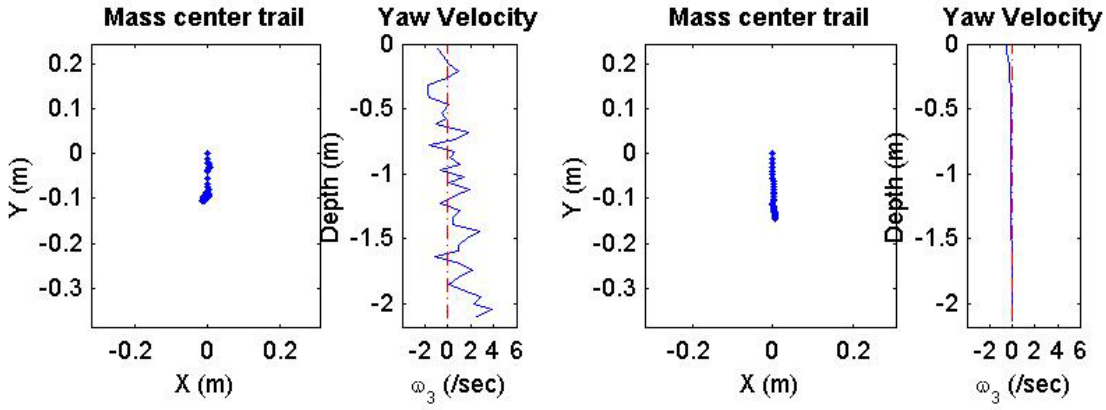

Final Drop

Parameters (60/12-2546)

time: 1.37(s)
xy_{fe}: 0.154(m)
V_{xfe}: 0(m/s)
V_{yfe}: -0.054(m/s)
V_{zfe}: -1.47(m/s)
Ψ_{fe}: 69°
depth: 2.17(m)

Mine Shape

Parameters (60/12-2546)

d: 0.04(m)
L: 0.121(m)
m: 0.254(m)
J_1: 2.71e-005(kg*m^2)
J_2: 0.000331(kg*m^2)
J_3: 0.000331(kg*m^2)
χ: 0.00997(m)

Final Model

Parameters (60/12-2546)

time: 1.5(s)
xy_{fm}: 0.33(m)
V_{xfm}: -0.00109(m/s)
V_{yfm}: 6.91e-018(m/s)
V_{zfm}: -1.37(m/s)
Ψ_{fm}: 84.4°
depth: 2.21(m)

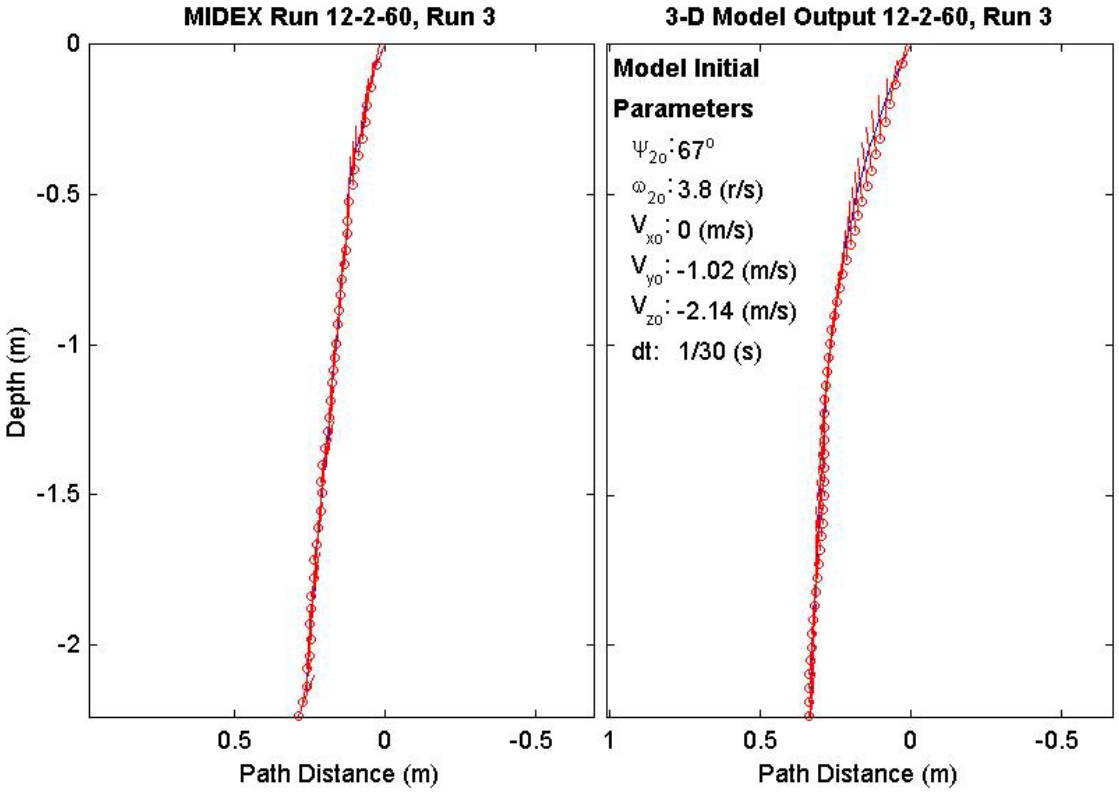

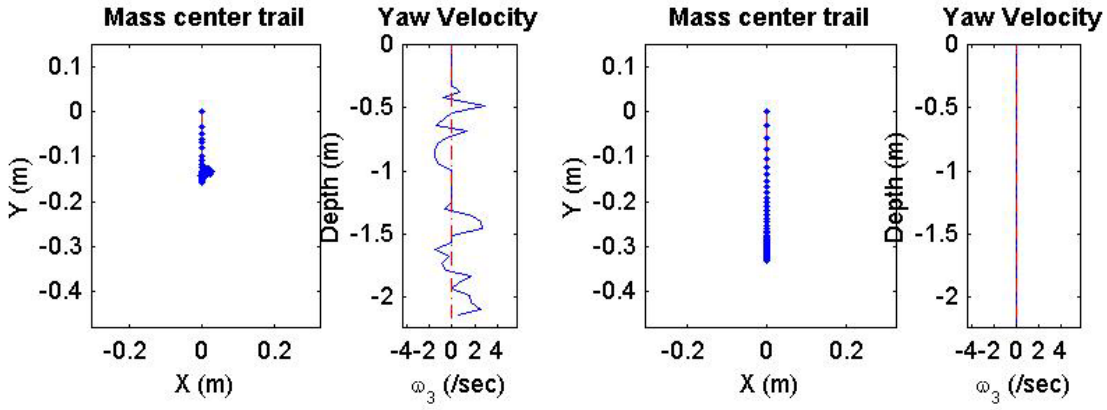

Final Drop

Parameters (60/12-1722)

time: 1.43(s)
xy_{fe}: 0.0857(m)
V_{xfe}: -0.105(m/s)
V_{yfe}: -0.054(m/s)
V_{zfe}: -1.5(m/s)
Ψ_{fe}: 70.3°
depth: 2.19(m)

Mine Shape

Parameters (60/12-1722)

d: 0.04(m)
L: 0.121(m)
m: 0.254(m)
J_1: 2.71e-005(kg*m^2)
J_2: 0.000331(kg*m^2)
J_3: 0.000331(kg*m^2)
χ: 0.00997(m)

Final Model

Parameters (60/12-1722)

time: 1.57(s)
xy_{fm}: 0.479(m)
V_{xfm}: 0.0814(m/s)
V_{yfm}: -0.0349(m/s)
V_{zfm}: -1.37(m/s)
Ψ_{fm}: 91.26°
depth: 2.23(m)

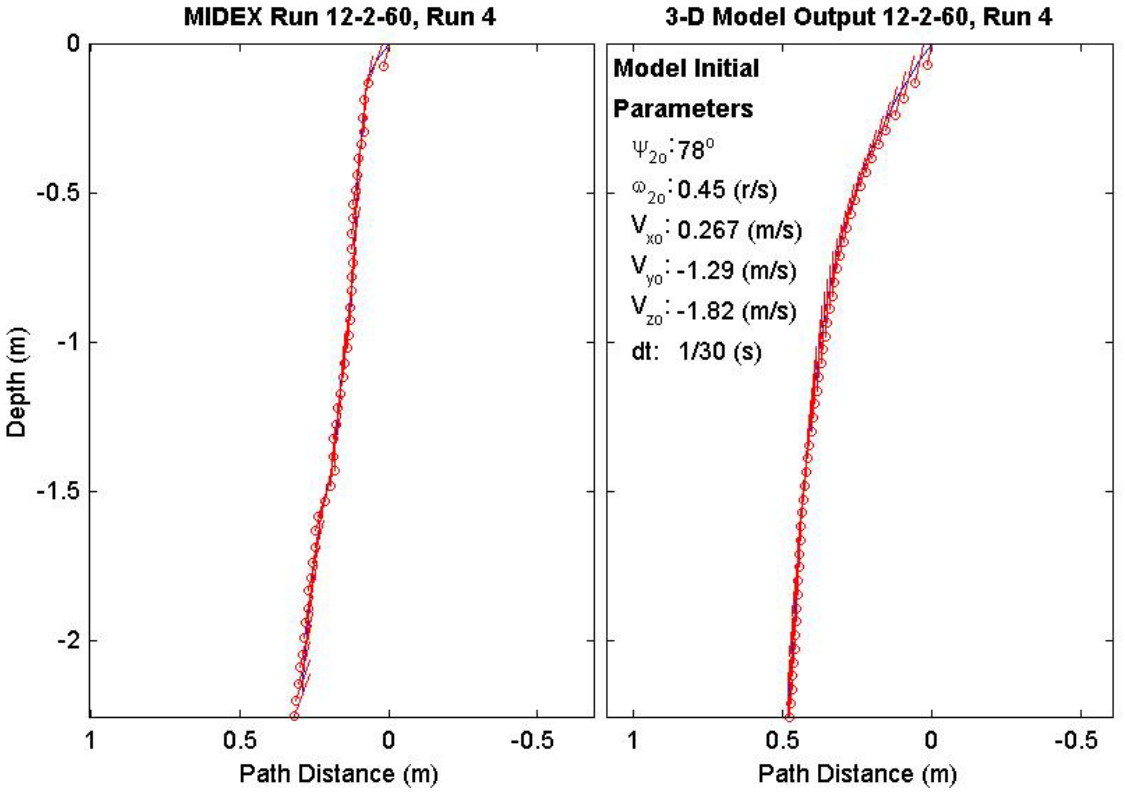

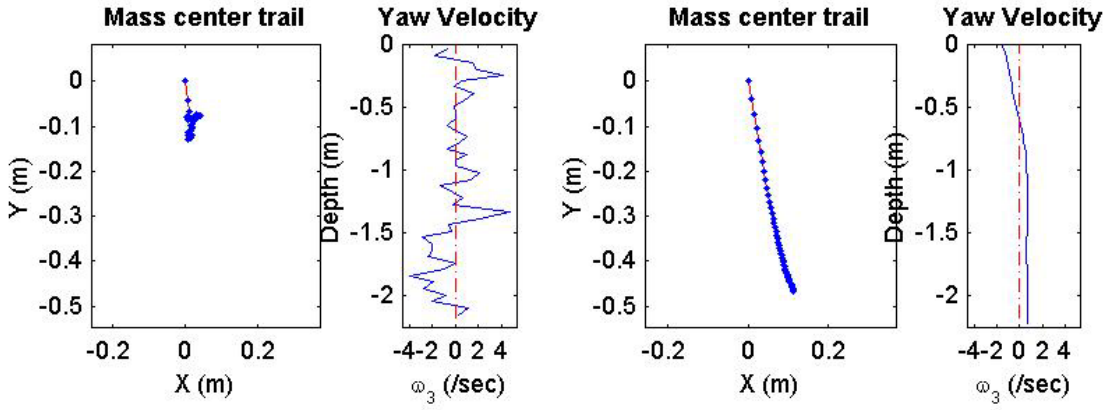

Final Drop

Parameters (60/12-1708)

time: 1.43(s)
xy_{fe}: 0.061(m)
V_{xfe}: 0.054(m/s)
V_{yfe}: 0.054(m/s)
V_{zfe}: -1.39(m/s)
Ψ_{fe}: 77.7°
depth: 2.17(m)

Mine Shape

Parameters (60/12-1708)

d: 0.04(m)
L: 0.121(m)
m: 0.254(m)
J_1: 2.71e-005(kg*m^2)
J_2: 0.000331(kg*m^2)
J_3: 0.000331(kg*m^2)
χ: 0.00997(m)

Final Model

Parameters (60/12-1708)

time: 1.5(s)
xy_{fm}: 0.245(m)
V_{xfm}: 0.0533(m/s)
V_{yfm}: -0.0575(m/s)
V_{zfm}: -1.37(m/s)
Ψ_{fm}: 84.38°
depth: 2.19(m)

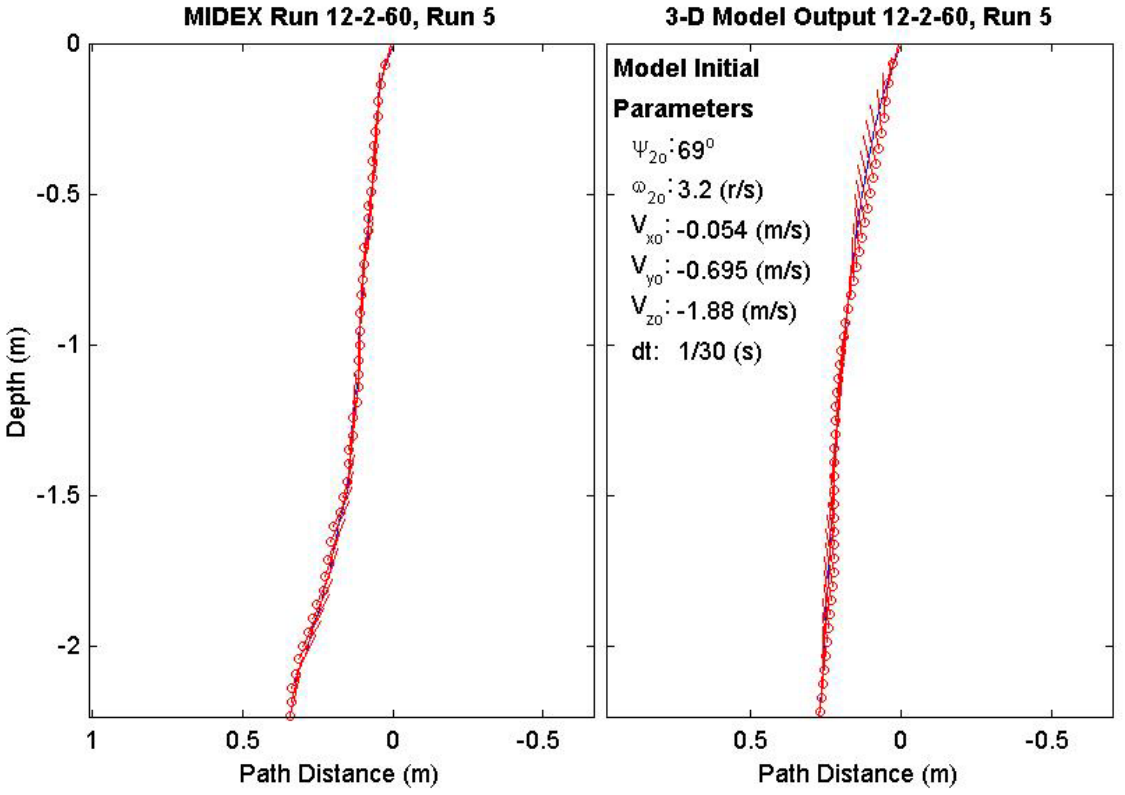

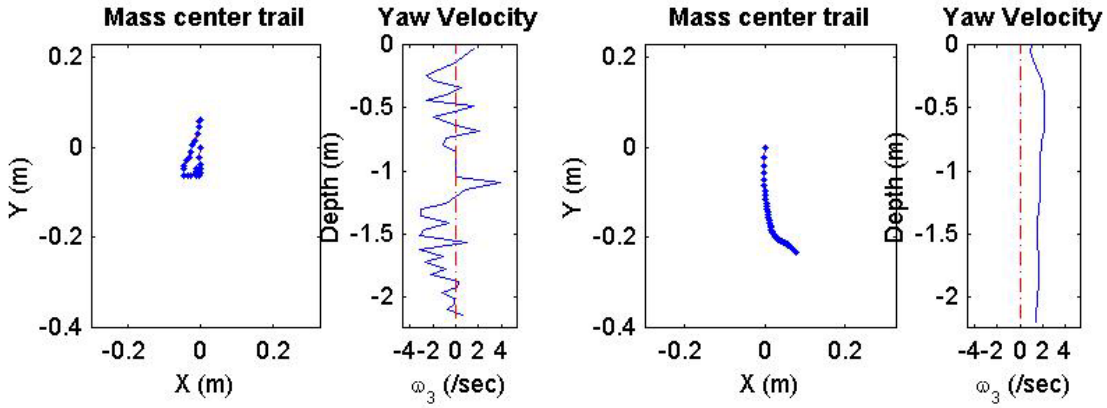

Final Drop

Parameters (60/9-3607)

time: 1.5(s)
xy_{fe}: 0.129(m)
V_{xfe}: 0(m/s)
V_{yfe}: -0.27(m/s)
V_{zfe}: -1.15(m/s)
Ψ_{fe}: 56.3°
depth: 2.18(m)

Mine Shape

Parameters (60/9-3607)

d: 0.04(m)
L: 0.0912(m)
m: 0.215(m)
J_1: 2.35e-005(kg*m^2)
J_2: 0.000156(kg*m^2)
J_3: 0.000156(kg*m^2)
χ: 0.005796(m)

Final Model

Parameters (60/9-3607)

time: 1.5(s)
xy_{fm}: 0.279(m)
V_{xfm}: 0.0586(m/s)
V_{yfm}: 0.0285(m/s)
V_{zfm}: -1.39(m/s)
Ψ_{fm}: 84.83°
depth: 2.22(m)

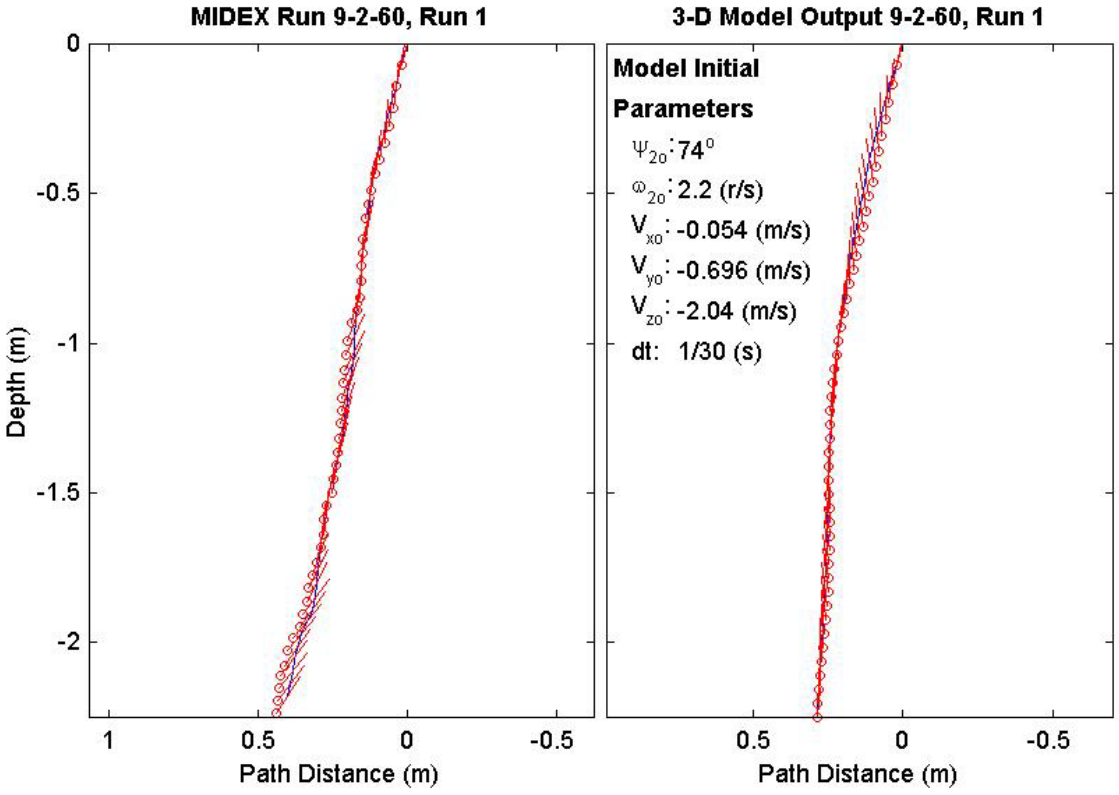

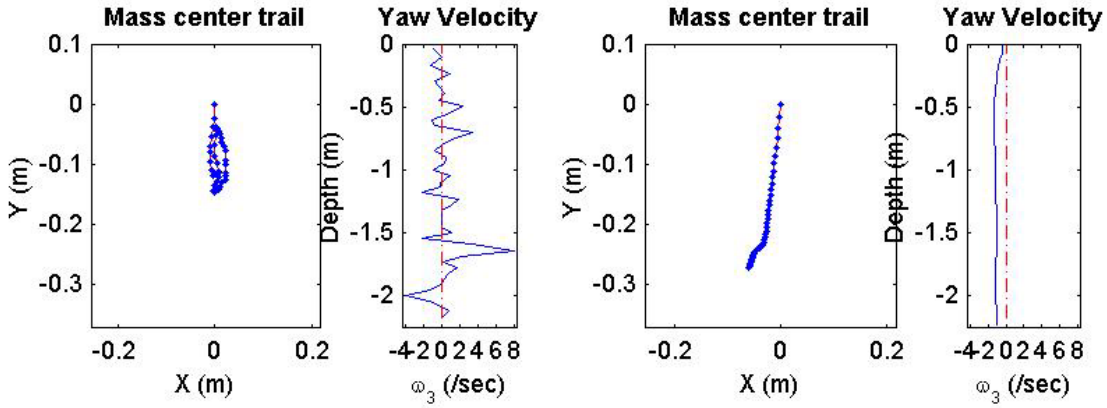

Final Drop
Parameters (60/9-3221)

time: 1.57(s)
xy_{fe}: 0.211(m)
V_{xfe}: -0.267(m/s)
V_{yfe}: -0.108(m/s)
V_{zfe}: -1.21(m/s)
Ψ_{fe}: 64.1°
depth: 2.17(m)

Mine Shape
Parameters (60/9-3221)

d: 0.04(m)
L: 0.0912(m)
m: 0.215(m)
J_1: 2.35e-005(kg*m^2)
J_2: 0.000156(kg*m^2)
J_3: 0.000156(kg*m^2)
χ: 0.005796(m)

Final Model
Parameters (60/9-3221)

time: 1.47(s)
xy_{fm}: 0.28(m)
V_{xfm}: 0.0192(m/s)
V_{yfm}: 3.33e-018(m/s)
V_{zfm}: -1.4(m/s)
Ψ_{fm}: 81.44°
depth: 2.21(m)

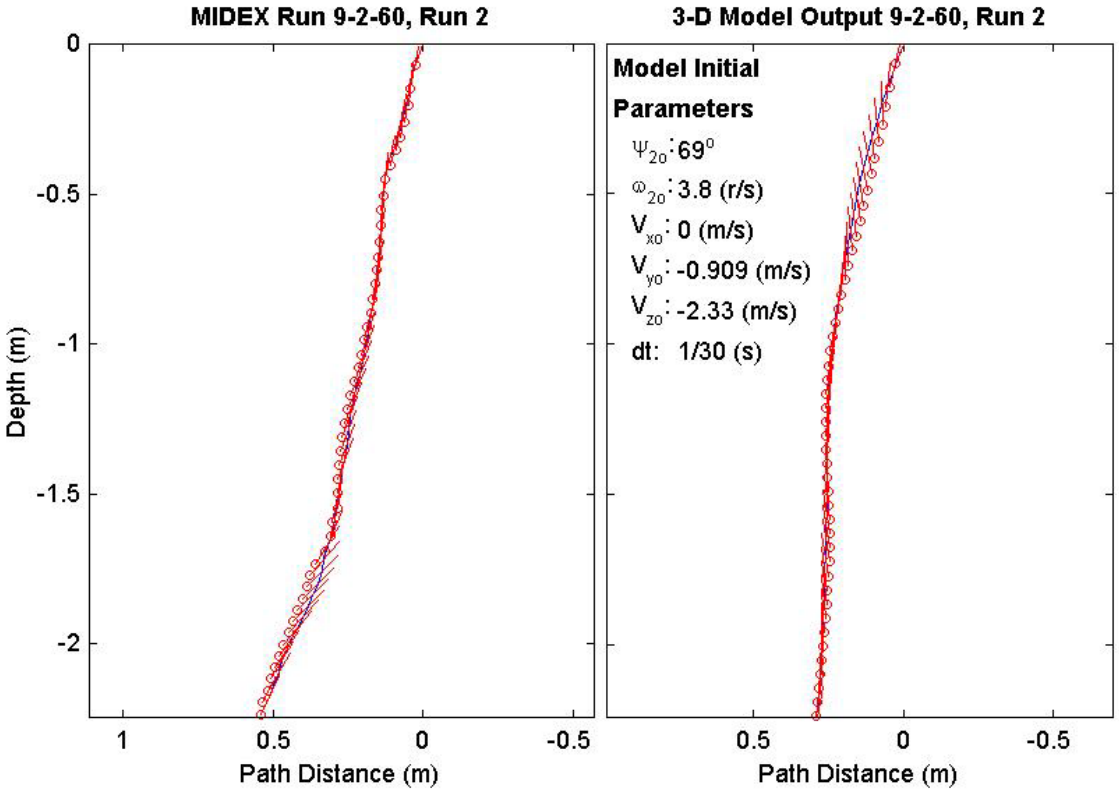

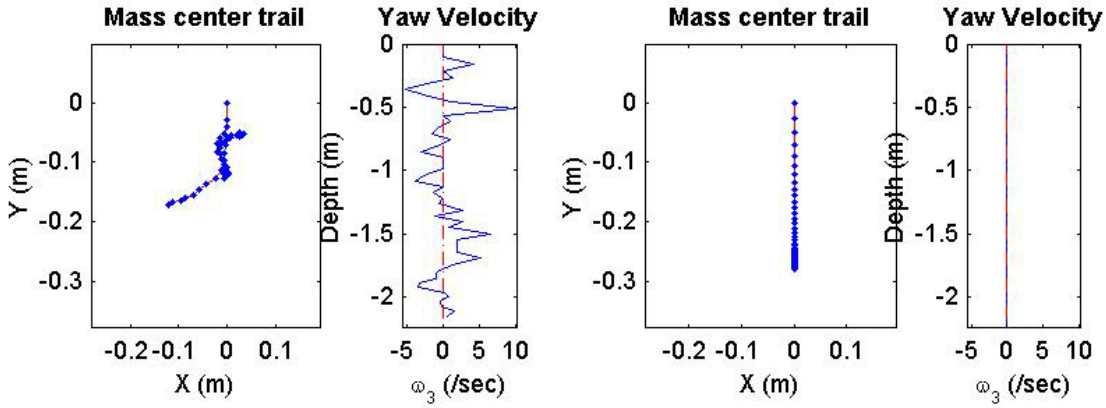

Final Drop

Parameters (60/9-2512)

time: 1.6(s)
xy_{fe}: 0.089(m)
V_{xfe}: 0.375(m/s)
V_{yfe}: -0.054(m/s)
V_{zfe}: -1.29(m/s)
Ψ_{fe}: 67°
depth: 2.19(m)

Mine Shape

Parameters (60/9-2512)

d: 0.04(m)
L: 0.0912(m)
m: 0.215(m)
J_1: 2.35e-005(kg*m^2)
J_2: 0.000156(kg*m^2)
J_3: 0.000156(kg*m^2)
χ: 0.005796(m)

Final Model

Parameters (60/9-2512)

time: 1.5(s)
xy_{fm}: 0.346(m)
V_{xfm}: 0.059(m/s)
V_{yfm}: 0.0257(m/s)
V_{zfm}: -1.39(m/s)
Ψ_{fm}: 84.74°
depth: 2.22(m)

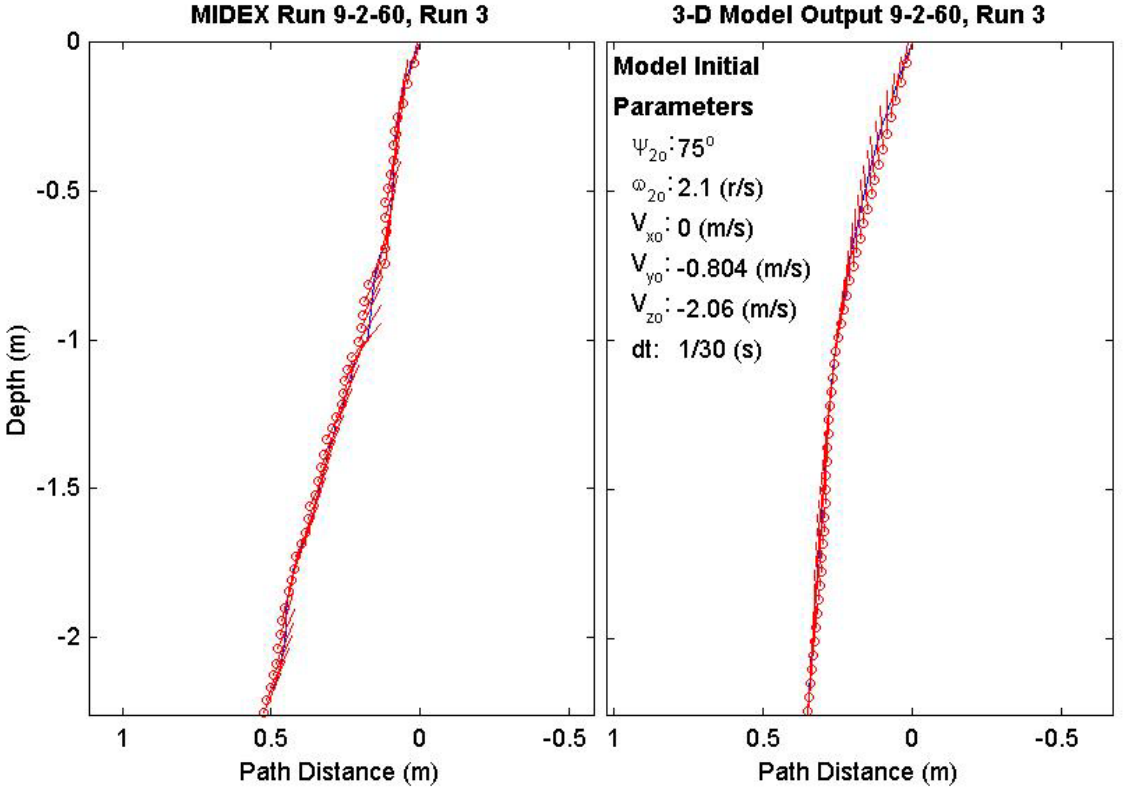

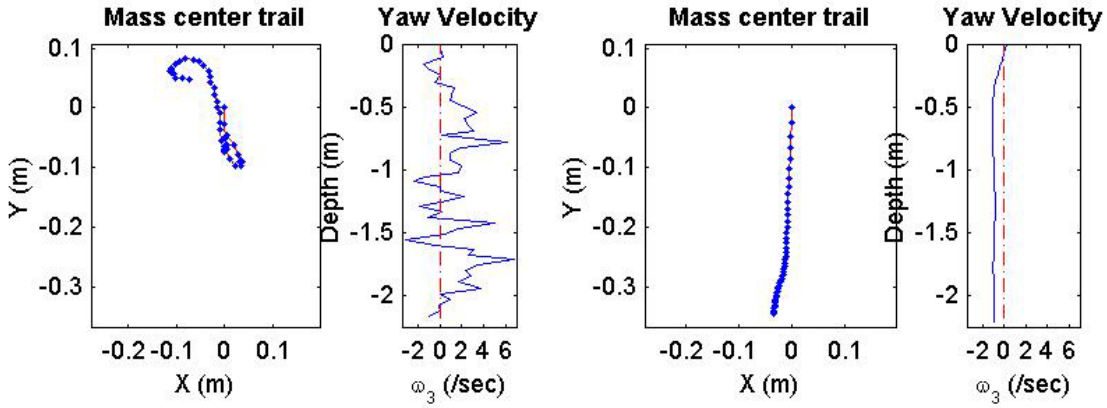

Final Drop
Parameters (60/9-1838)

time: 1.8(s)
xy_{fe}: 0.228(m)
V_{xfe}: 0(m/s)
V_{yfe}: 0.321(m/s)
V_{zfe}: -1.07(m/s)
Ψ_{fe}: 44.4°
depth: 2.21(m)

Mine Shape
Parameters (60/9-1838)

d: 0.04(m)
L: 0.0912(m)
m: 0.215(m)
J_1: 2.35e-005(kg*m^2)
J_2: 0.000156(kg*m^2)
J_3: 0.000156(kg*m^2)
χ: 0.005796(m)

Final Model
Parameters (60/9-1838)

time: 1.57(s)
xy_{fm}: 0.174(m)
V_{xfm}: 0.0192(m/s)
V_{yfm}: -0.00231(m/s)
V_{zfm}: -1.4(m/s)
Ψ_{fm}: 82.62°
depth: 2.25(m)

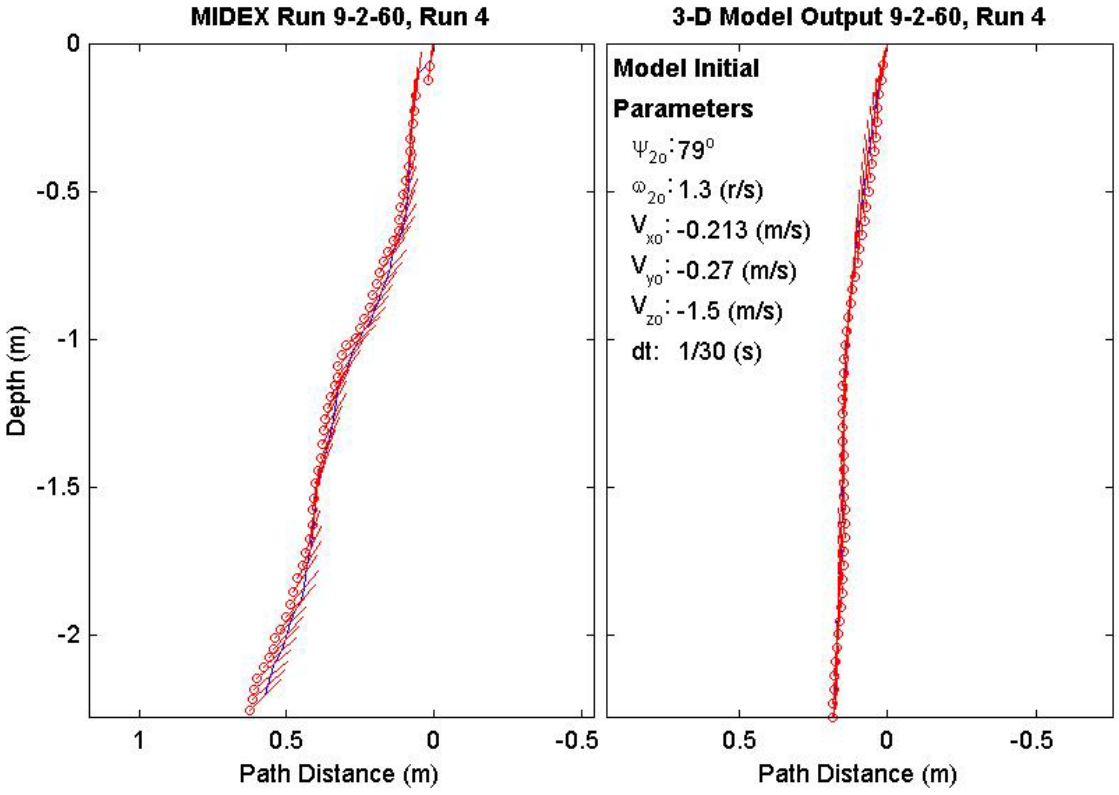

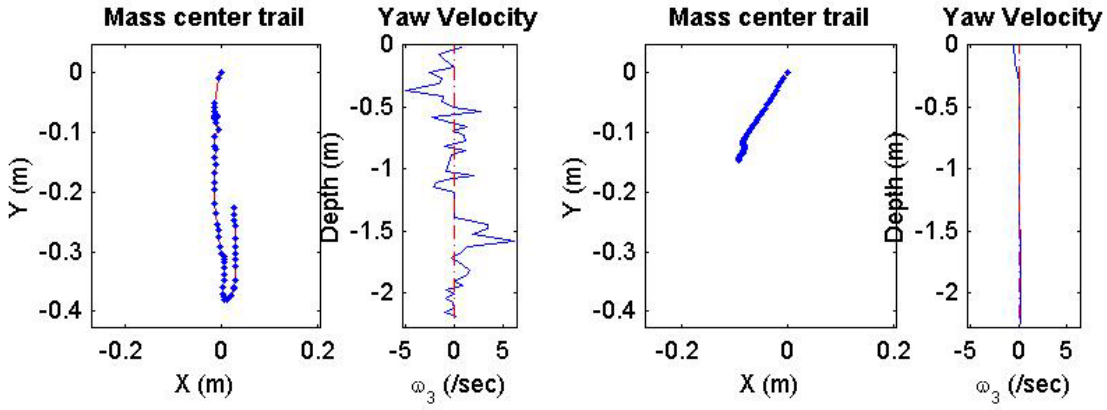

Final Drop
Parameters (60/9-1942)

time: 1.63(s)
xy_{fe}: 0.186(m)
V_{xfe}: 0.267(m/s)
V_{yfe}: 0.054(m/s)
V_{zfe}: -1.34(m/s)
Ψ_{fe}: 70.3°
depth: 2.2(m)

Mine Shape
Parameters (60/9-1942)

d: 0.04(m)
L: 0.0912(m)
m: 0.215(m)
J_1: 2.35e-005(kg*m^2)
J_2: 0.000156(kg*m^2)
J_3: 0.000156(kg*m^2)
χ: 0.005796(m)

Final Model
Parameters (60/9-1942)

time: 1.57(s)
xy_{fm}: 0.337(m)
V_{xfm}: 0.0339(m/s)
V_{yfm}: -0.0246(m/s)
V_{zfm}: -1.39(m/s)
Ψ_{fm}: 86.56°
depth: 2.23(m)

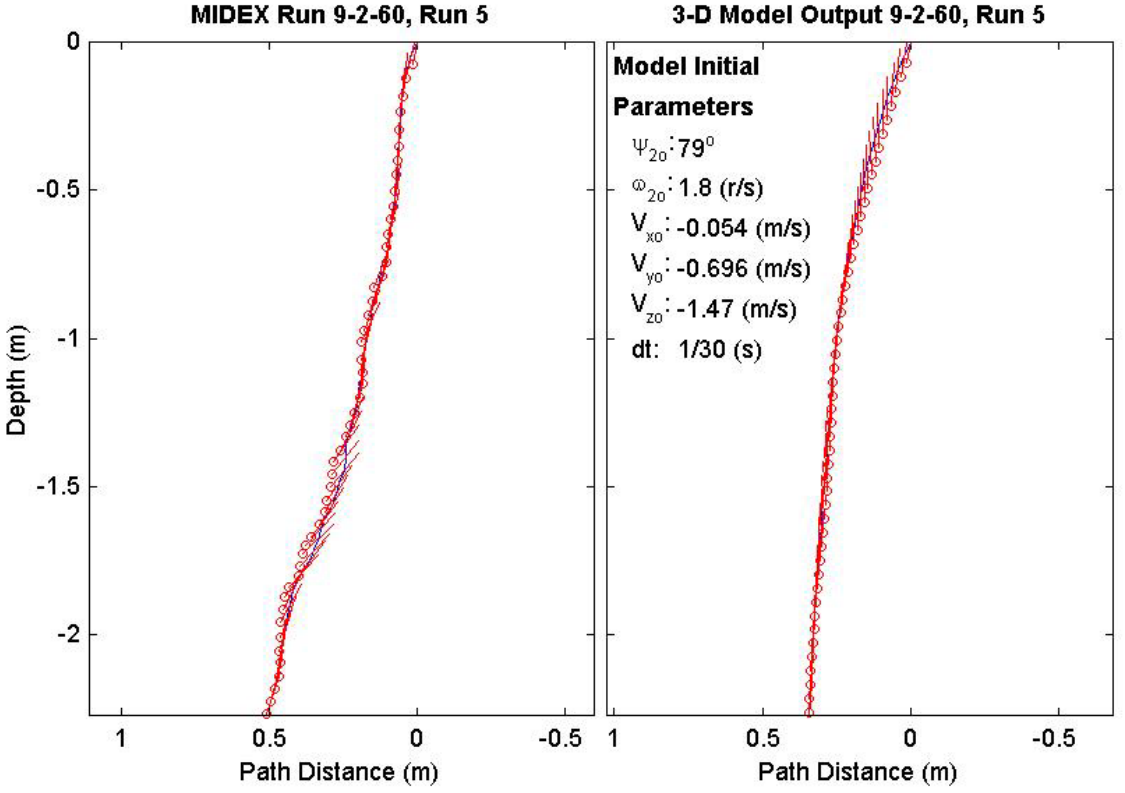

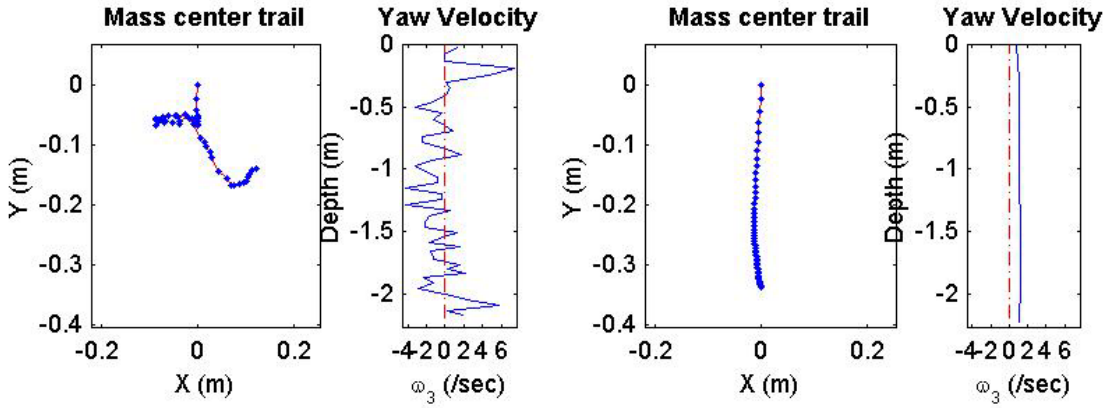

Final Drop Parameters (75/15-3647)

time: 1.1(s)
xy_{fe}: 0.104(m)
V_{xfe}: 0(m/s)
V_{yfe}: 0.051(m/s)
V_{zfe}: -1.42(m/s)
Ψ_{fe}: 88.7°
depth: 2.13(m)

Mine Shape Parameters (75/15-3647)

d: 0.04(m)
L: 0.152(m)
m: 0.323(m)
J_1: 3.3e-005(kg*m^2)
J_2: 0.000623(kg*m^2)
J_3: 0.000623(kg*m^2)
χ: 0.01477(m)

Final Model Parameters (75/15-3647)

time: 1.23(s)
xy_{fm}: 0.419(m)
V_{xfm}: 0.0952(m/s)
V_{yfm}: -0.00803(m/s)
V_{zfm}: -1.52(m/s)
Ψ_{fm}: 89.51°
depth: 2.16(m)

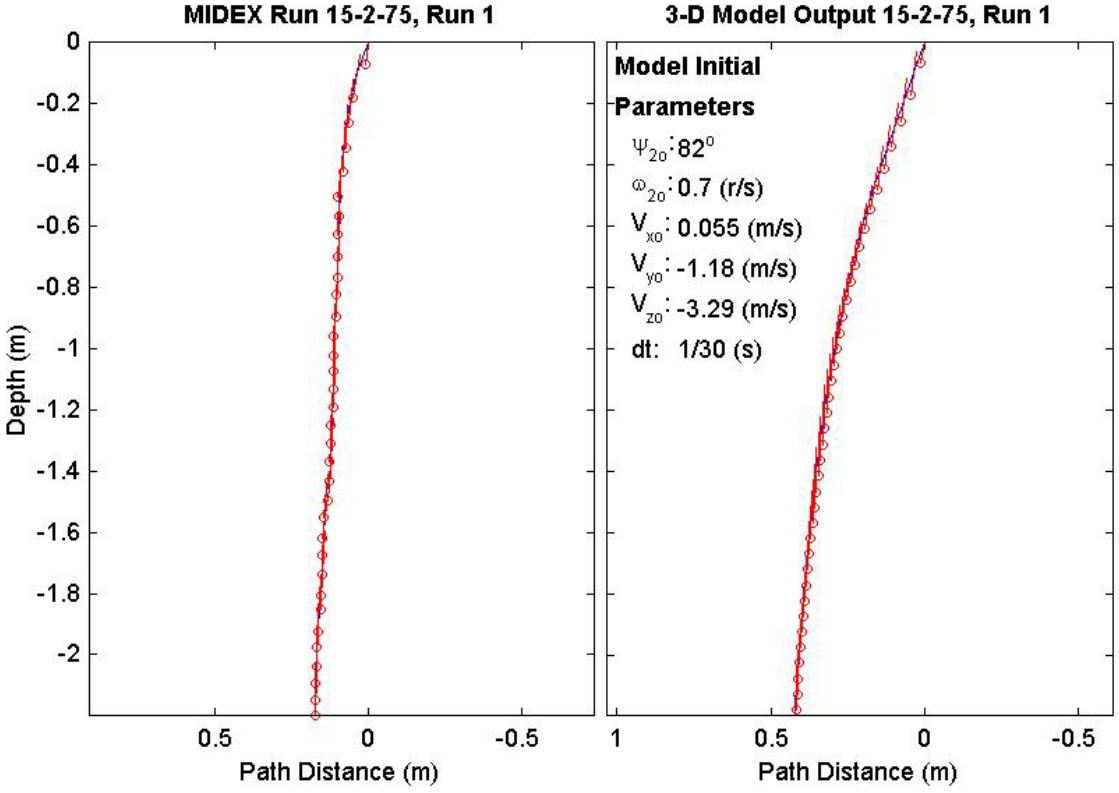

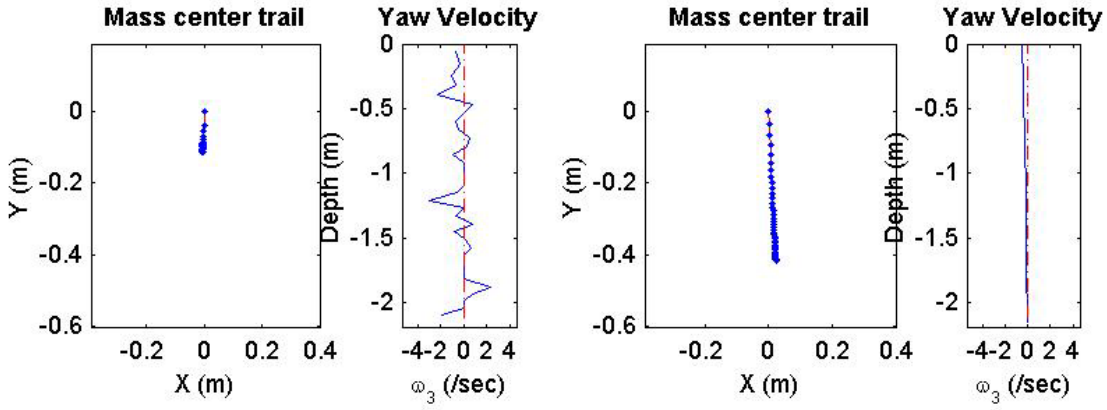

Final Drop

Parameters (75/15-3315)

time: 1.1(s)
xy_{fe}: 0.109(m)
V_{xfe}: -0.051(m/s)
V_{yfe}: 0.216(m/s)
V_{zfe}: -1.82(m/s)
Ψ_{fe}: 87°
depth: 2.14(m)

Mine Shape

Parameters (75/15-3315)

d: 0.04(m)
L: 0.152(m)
m: 0.323(m)
J_1: 3.3e-005(kg*m^2)
J_2: 0.000623(kg*m^2)
J_3: 0.000623(kg*m^2)
χ: 0.01477(m)

Final Model

Parameters (75/15-3315)

time: 1.27(s)
xy_{fm}: 0.203(m)
V_{xfm}: 0.0617(m/s)
V_{yfm}: 0.0657(m/s)
V_{zfm}: -1.52(m/s)
Ψ_{fm}: 90.45°
depth: 2.19(m)

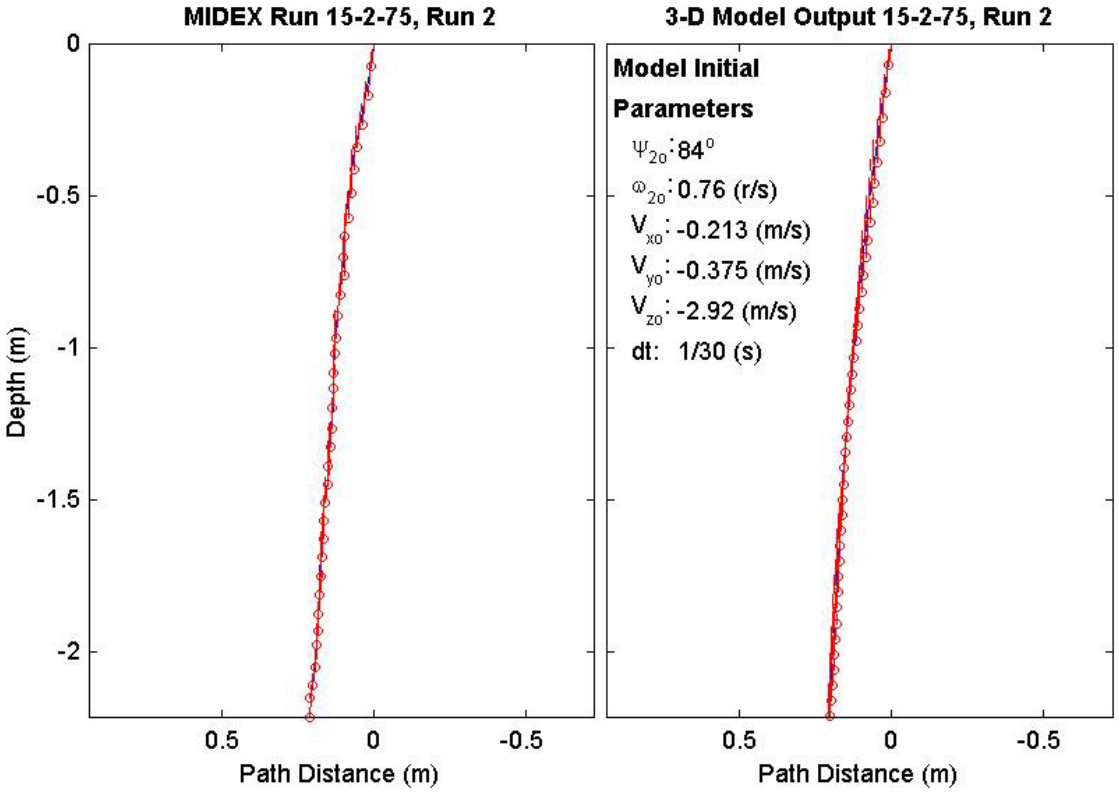

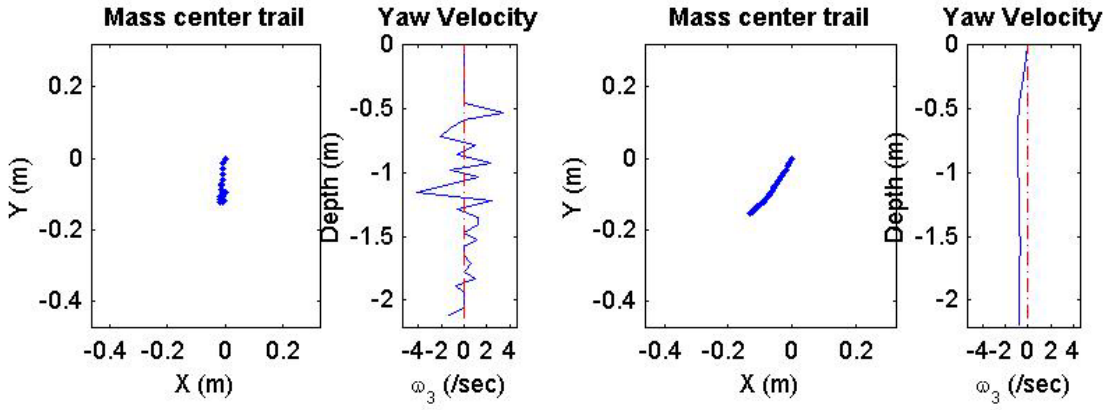

Final Drop

Parameters (75/15-2413)

time: 1.2(s)
xy_{fe}: 0.0301(m)
V_{xfe}: -0.055(m/s)
V_{yfe}: 0.055(m/s)
V_{zfe}: -1.42(m/s)
Ψ_{fe}: 86.9°
depth: 2.17(m)

Mine Shape

Parameters (75/15-2413)

d: 0.04(m)
L: 0.152(m)
m: 0.323(m)
J_1: 3.3e-005(kg*m^2)
J_2: 0.000623(kg*m^2)
J_3: 0.000623(kg*m^2)
χ: 0.01477(m)

Final Model

Parameters (75/15-2413)

time: 1.33(s)
xy_{fm}: 0.123(m)
V_{xfm}: -0.00319(m/s)
V_{yfm}: -0.0408(m/s)
V_{zfm}: -1.52(m/s)
Ψ_{fm}: 95.9°
depth: 2.23(m)

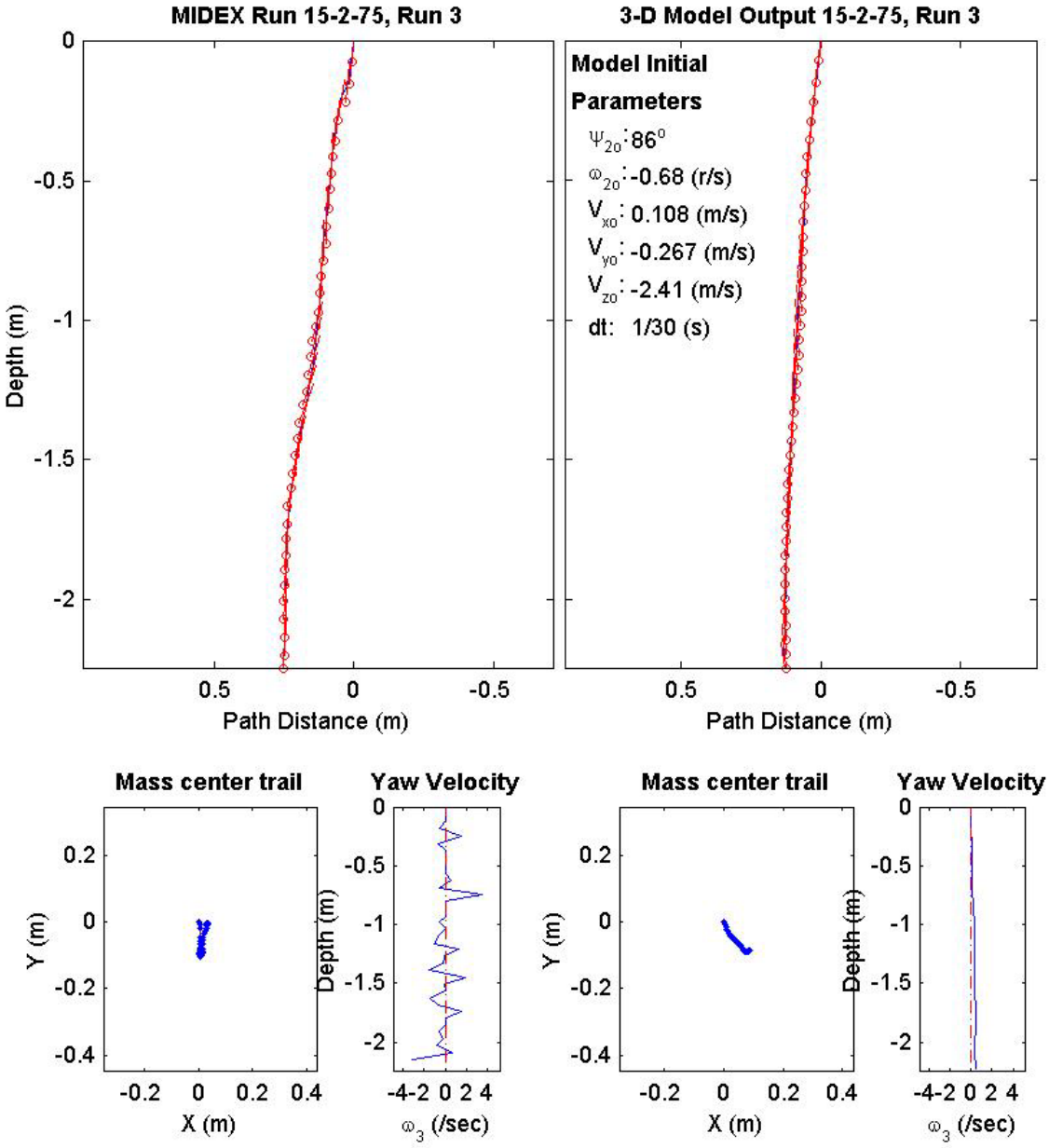

Final Drop Parameters (75/15-2671)

time: 1.1(s)
xy_{fe}: 0.0861(m)
V_{xfe}: -0.108(m/s)
V_{yfe}: 0.051(m/s)
V_{zfe}: -2.2(m/s)
Ψ_{fe}: 87.1°
depth: 2.05(m)

Mine Shape Parameters (75/15-2671)

d: 0.04(m)
L: 0.152(m)
m: 0.323(m)
J_1: 3.3e-005(kg*m^2)
J_2: 0.000623(kg*m^2)
J_3: 0.000623(kg*m^2)
χ: 0.01477(m)

Final Model Parameters (75/15-2671)

time: 1.23(s)
xy_{fm}: 0.142(m)
V_{xfm}: 0.0451(m/s)
V_{yfm}: 0.0453(m/s)
V_{zfm}: -1.53(m/s)
Ψ_{fm}: 93.28°
depth: 2.08(m)

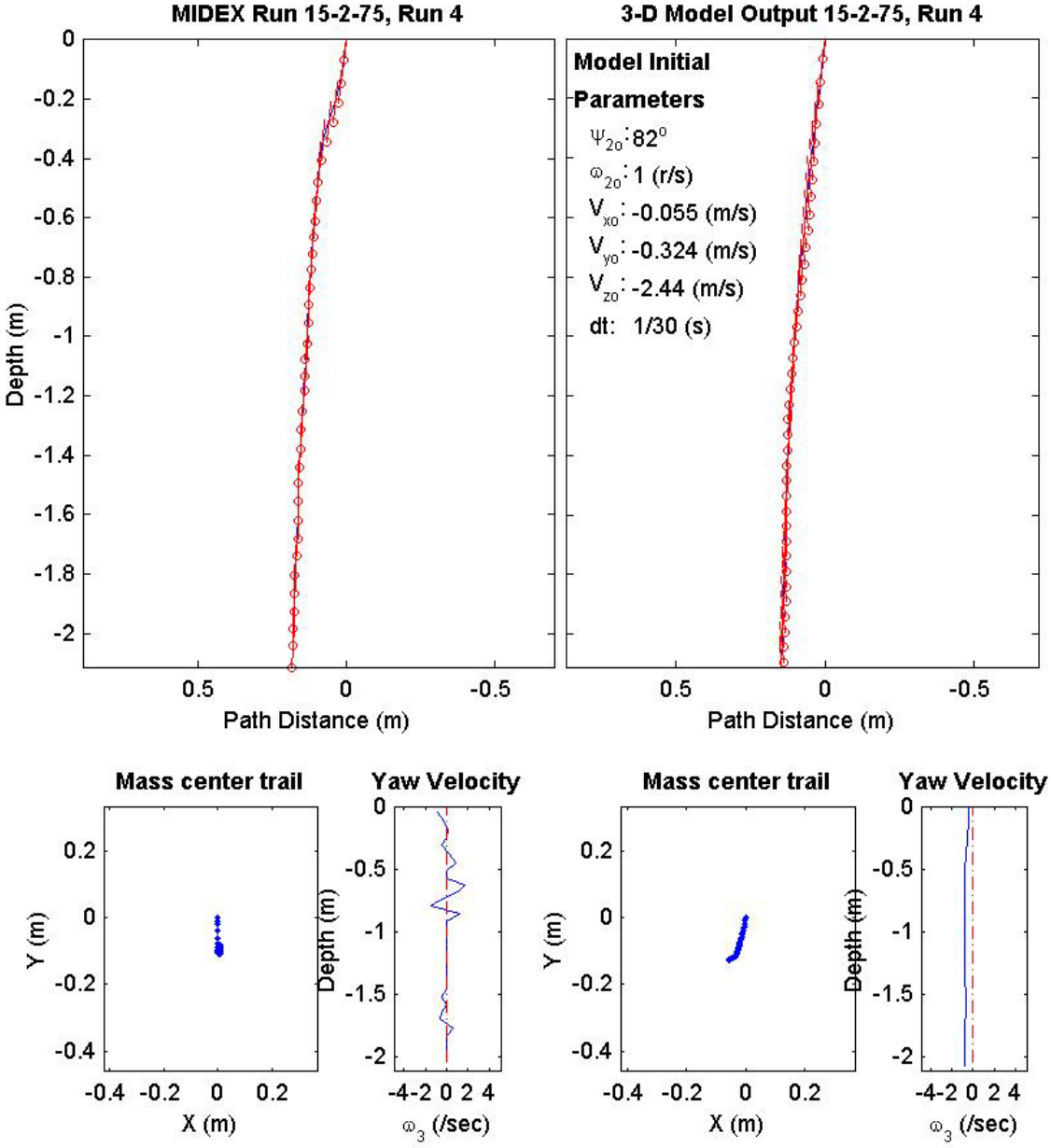

Final Drop Parameters (75/12-3761)

time: 1.33(s)
xy_{fe}: 0.117(m)
V_{xfe}: 0.213(m/s)
V_{yfe}: -0.108(m/s)
V_{zfe}: -1.31(m/s)
Ψ_{fe}: 71.2°
depth: 2.13(m)

Mine Shape Parameters (75/12-3761)

d: 0.04(m)
L: 0.121(m)
m: 0.254(m)
J_1: 2.71e-005(kg*m^2)
J_2: 0.000331(kg*m^2)
J_3: 0.000331(kg*m^2)
χ: 0.00997(m)

Final Model Parameters (75/12-3761)

time: 1.43(s)
xy_{fm}: 0.229(m)
V_{xfm}: 0.0715(m/s)
V_{yfm}: 0.00608(m/s)
V_{zfm}: -1.37(m/s)
Ψ_{fm}: 88.64°
depth: 2.16(m)

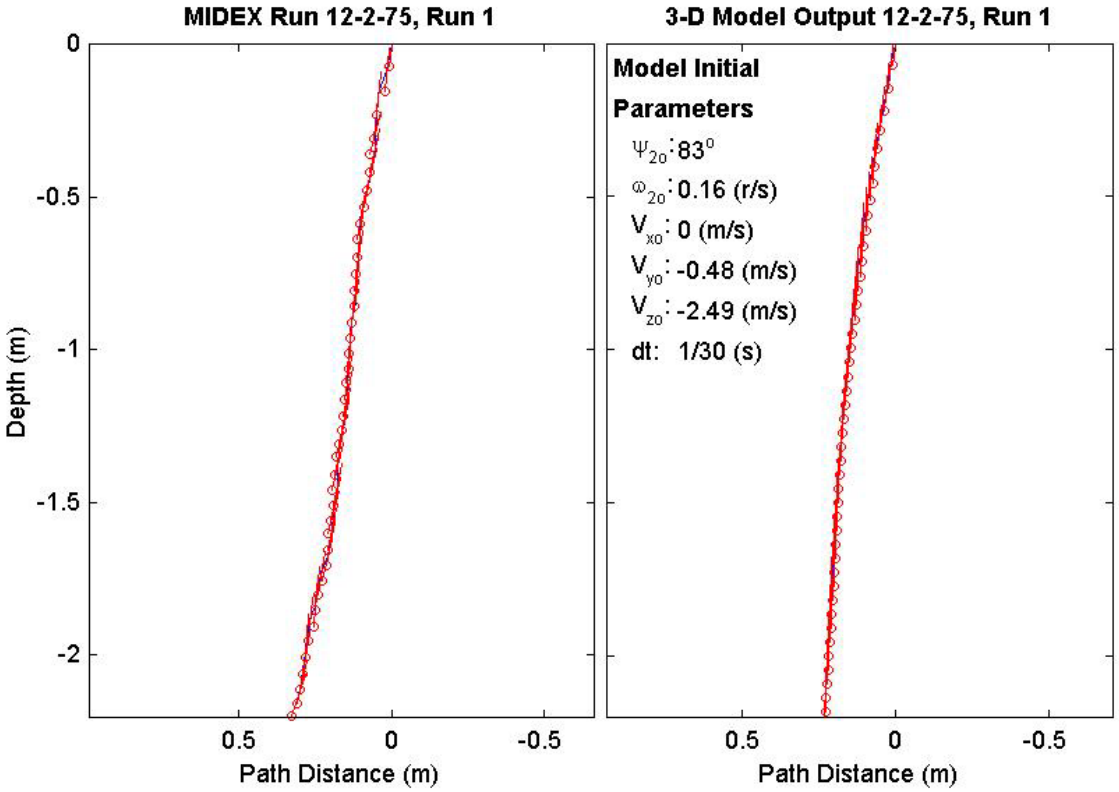

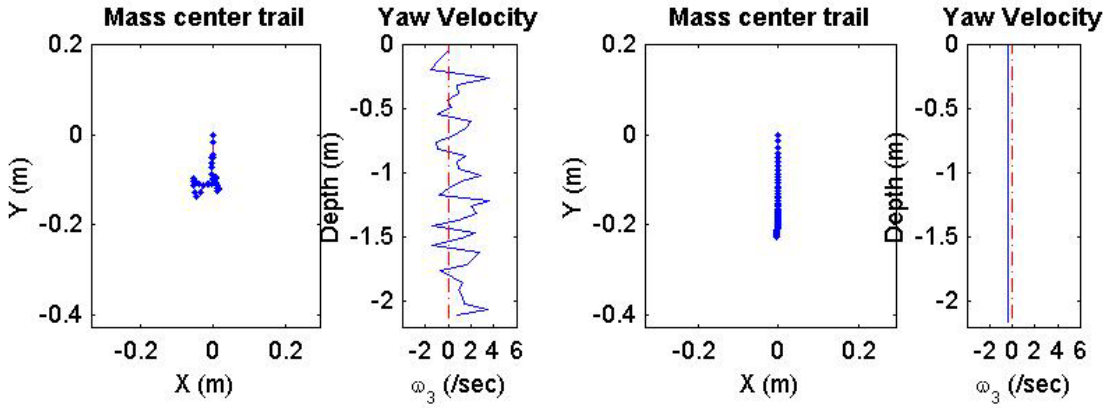

Final Drop Parameters (75/12-3209)

time: 1.3(s)
xy_{fe}: 0.111(m)
V_{xfe}: -0.054(m/s)
V_{yfe}: 0(m/s)
V_{zfe}: -1.45(m/s)
Ψ_{fe}: 84.5°
depth: 2.12(m)

Mine Shape Parameters (75/12-3209)

d: 0.04(m)
L: 0.121(m)
m: 0.254(m)
J_1: 2.71e-005(kg*m^2)
J_2: 0.000331(kg*m^2)
J_3: 0.000331(kg*m^2)
χ: 0.00997(m)

Final Model Parameters (75/12-3209)

time: 1.43(s)
xy_{fm}: 0.151(m)
V_{xfm}: 0.0604(m/s)
V_{yfm}: -0.012(m/s)
V_{zfm}: -1.37(m/s)
Ψ_{fm}: 85.87°
depth: 2.13(m)

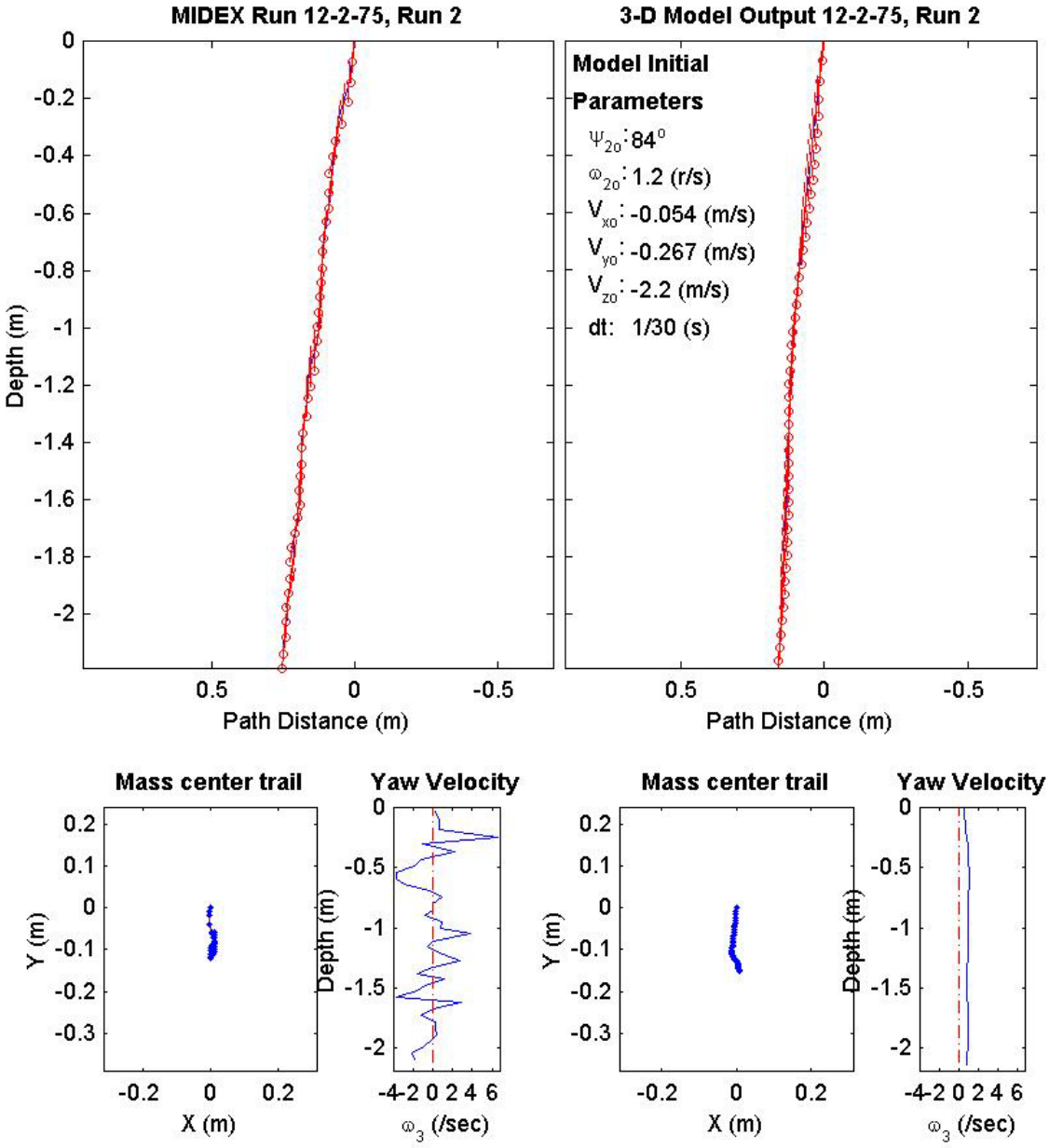

Final Drop

Parameters (75/12-2318)

time: 1.37(s)
xy_{fe}: 0.045(m)
V_{xfe}: -0.108(m/s)
V_{yfe}: -0.054(m/s)
V_{zfe}: -1.5(m/s)
Ψ_{fe}: 75°
depth: 2.16(m)

Mine Shape

Parameters (75/12-2318)

d: 0.04(m)
L: 0.121(m)
m: 0.254(m)
J_1: 2.71e-005(kg*m^2)
J_2: 0.000331(kg*m^2)
J_3: 0.000331(kg*m^2)
χ: 0.00997(m)

Final Model

Parameters (75/12-2318)

time: 1.47(s)
xy_{fm}: 0.219(m)
V_{xfm}: 0.0503(m/s)
V_{yfm}: 3.95e-018(m/s)
V_{zfm}: -1.37(m/s)
Ψ_{fm}: 89.6°
depth: 2.2(m)

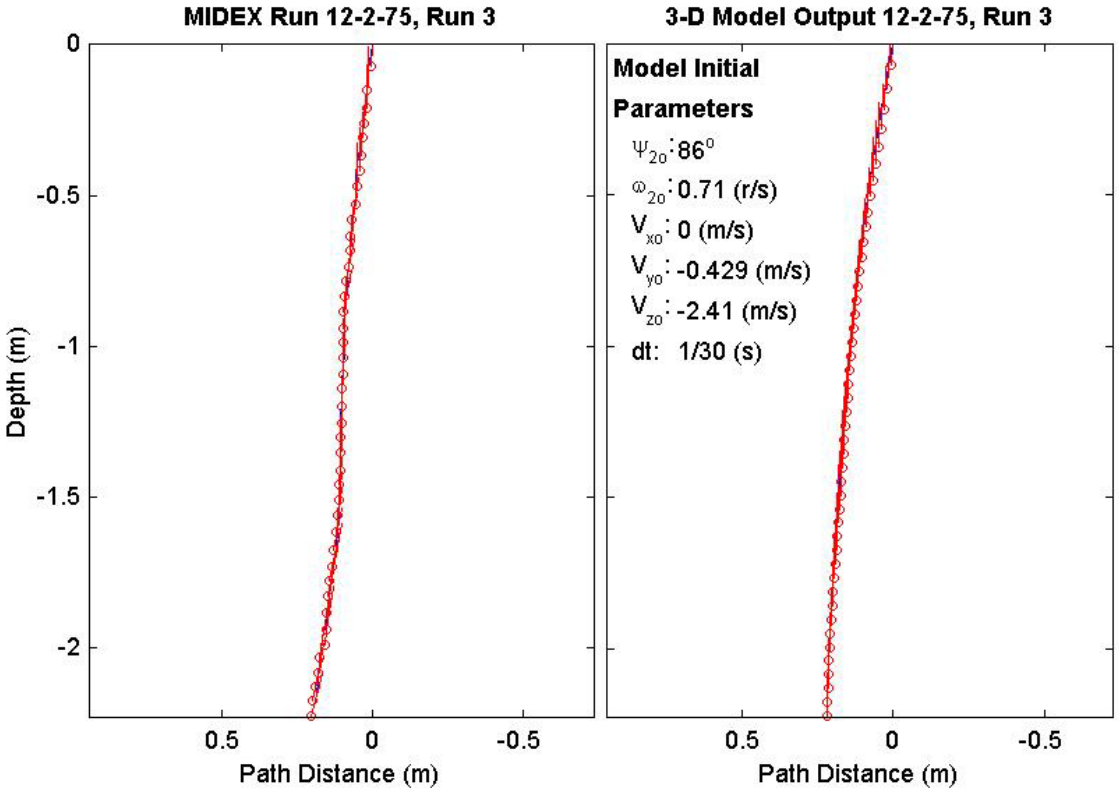

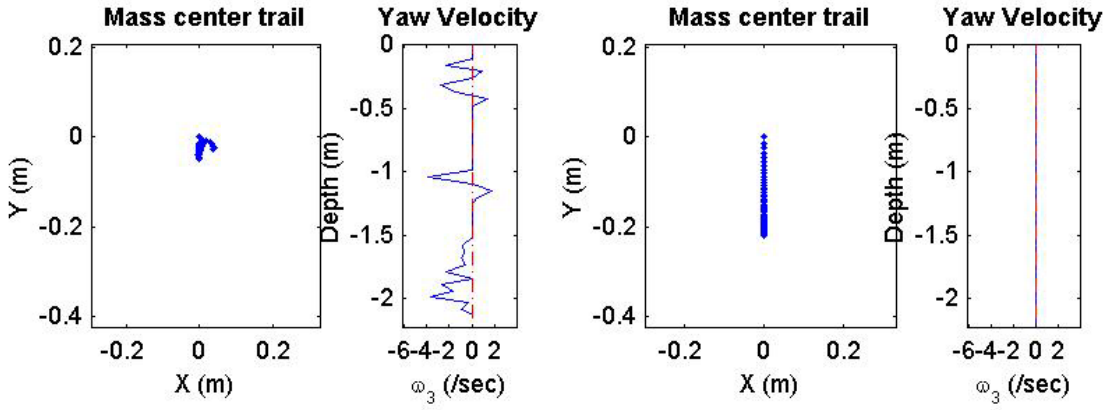

Final Drop

Parameters (75/12-2417)

time: 1.43(s)
xy_{fe}: 0.052(m)
V_{xfe}: 0.429(m/s)
V_{yfe}: -0.162(m/s)
V_{zfe}: -1.26(m/s)
Ψ_{fe}: 67.6°
depth: 2.17(m)

Mine Shape

Parameters (75/12-2417)

d: 0.04(m)
L: 0.121(m)
m: 0.254(m)
J_1: 2.71e-005(kg*m^2)
J_2: 0.000331(kg*m^2)
J_3: 0.000331(kg*m^2)
χ: 0.00997(m)

Final Model

Parameters (75/12-2417)

time: 1.47(s)
xy_{fm}: 0.0852(m)
V_{xfm}: 0.0339(m/s)
V_{yfm}: -0.0183(m/s)
V_{zfm}: -1.37(m/s)
Ψ_{fm}: 94.88°
depth: 2.17(m)

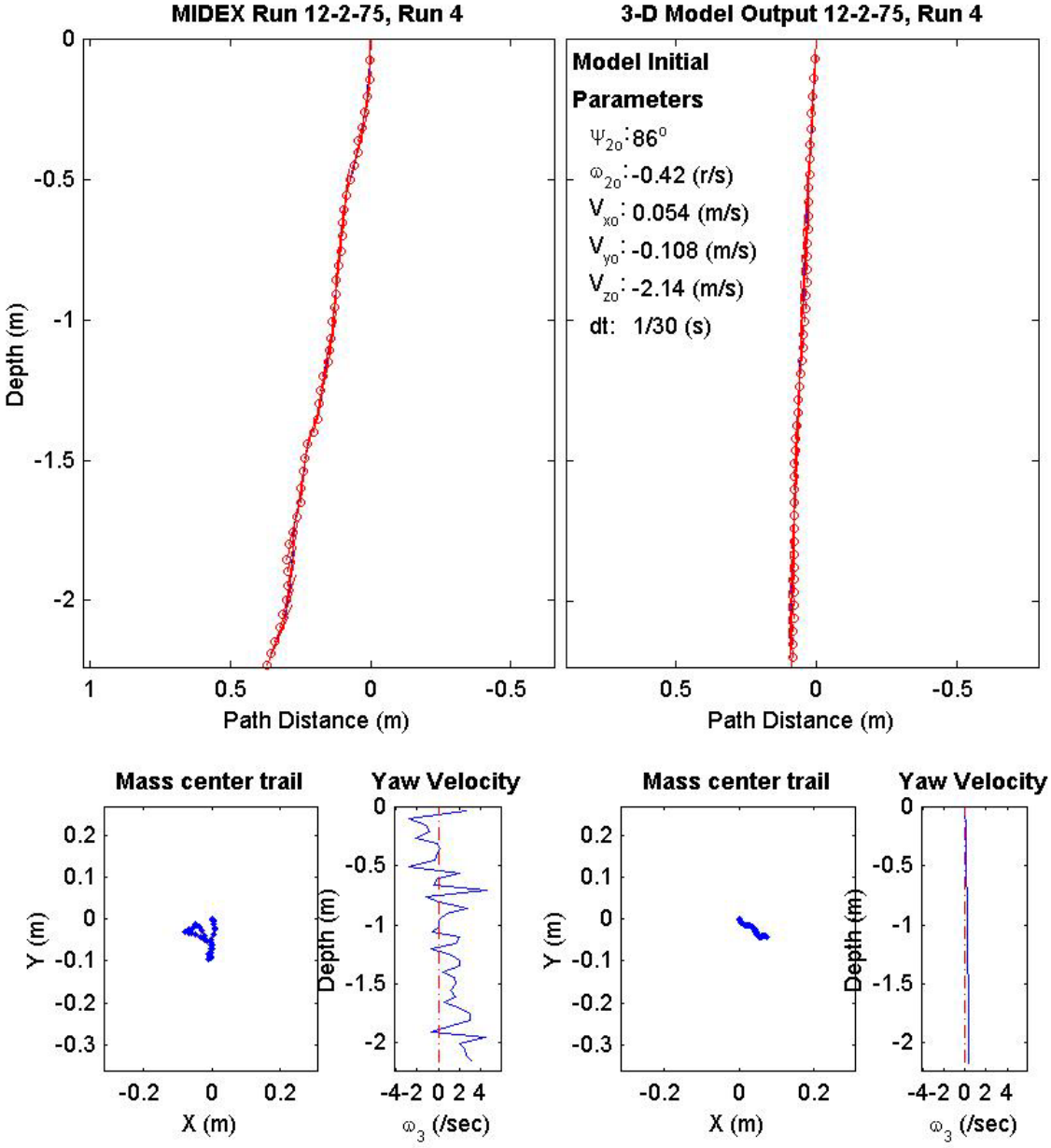

Final Drop
Parameters (75/9-3756)

time: 1.47(s)
xy_{fe}: 0.0362(m)
V_{xfe}: 0(m/s)
V_{yfe}: -0.162(m/s)
V_{zfe}: -1.13(m/s)
Ψ_{fe}: 66.5°
depth: 2.2(m)

Mine Shape
Parameters (75/9-3756)

d: 0.04(m)
L: 0.0912(m)
m: 0.215(m)
J_1: 2.35e-005(kg*m^2)
J_2: 0.000156(kg*m^2)
J_3: 0.000156(kg*m^2)
χ: 0.005796(m)

Final Model
Parameters (75/9-3756)

time: 1.47(s)
xy_{fm}: 0.253(m)
V_{xfm}: 0.0233(m/s)
V_{yfm}: 0.0379(m/s)
V_{zfm}: -1.39(m/s)
Ψ_{fm}: 95.57°
depth: 2.21(m)

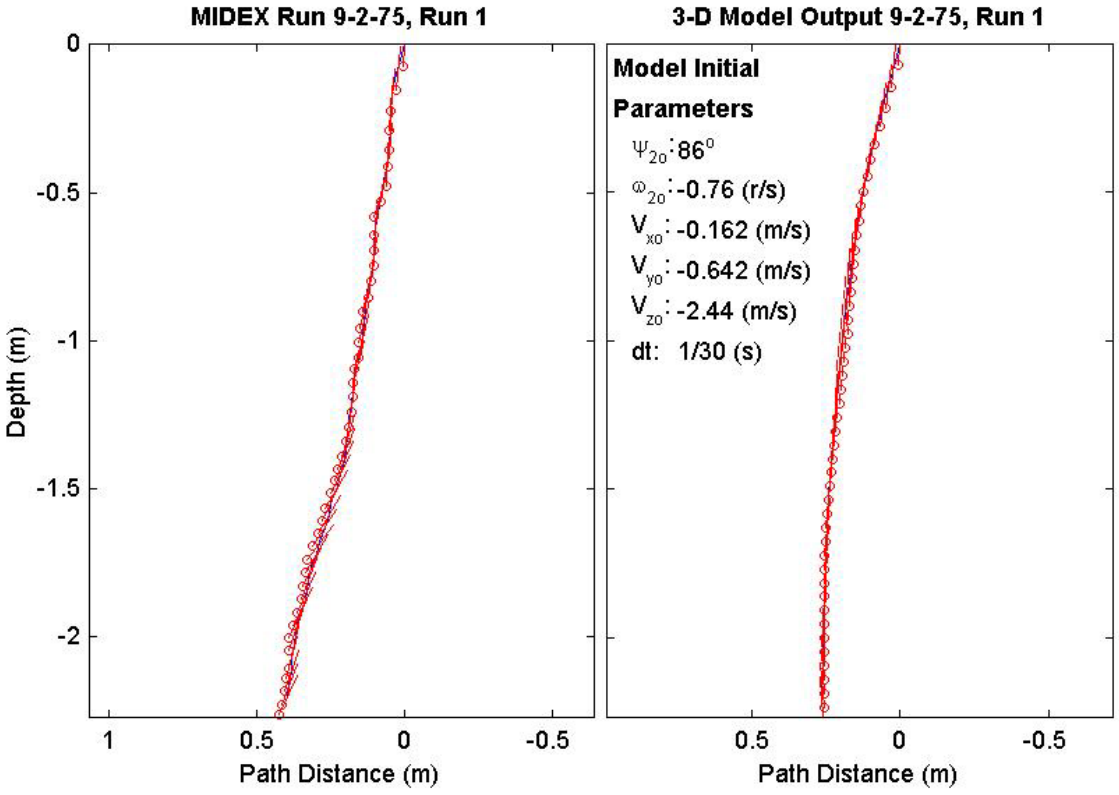

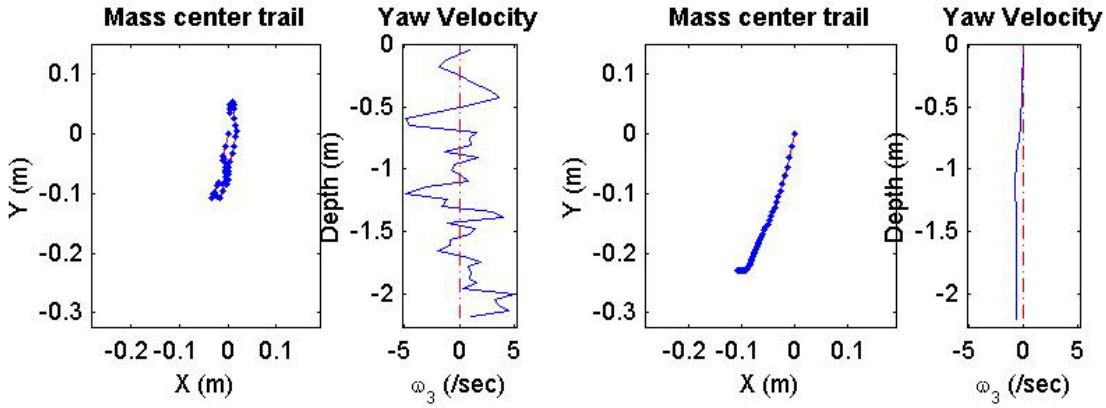

Final Drop

Parameters (75/9-3244)

time: 1.57(s)
xy_{fe}: 0.215(m)
V_{xfe}: -0.216(m/s)
V_{yfe}: -0.429(m/s)
V_{zfe}: -1.07(m/s)
Ψ_{fe}: 53.7°
depth: 2.16(m)

Mine Shape

Parameters (75/9-3244)

d: 0.04(m)
L: 0.0912(m)
m: 0.215(m)
J_1: 2.35e-005(kg*m^2)
J_2: 0.000156(kg*m^2)
J_3: 0.000156(kg*m^2)
χ: 0.005796(m)

Final Model

Parameters (75/9-3244)

time: 1.43(s)
xy_{fm}: 0.155(m)
V_{xfm}: 0.0653(m/s)
V_{yfm}: -0.00483(m/s)
V_{zfm}: -1.4(m/s)
Ψ_{fm}: 92.49°
depth: 2.18(m)

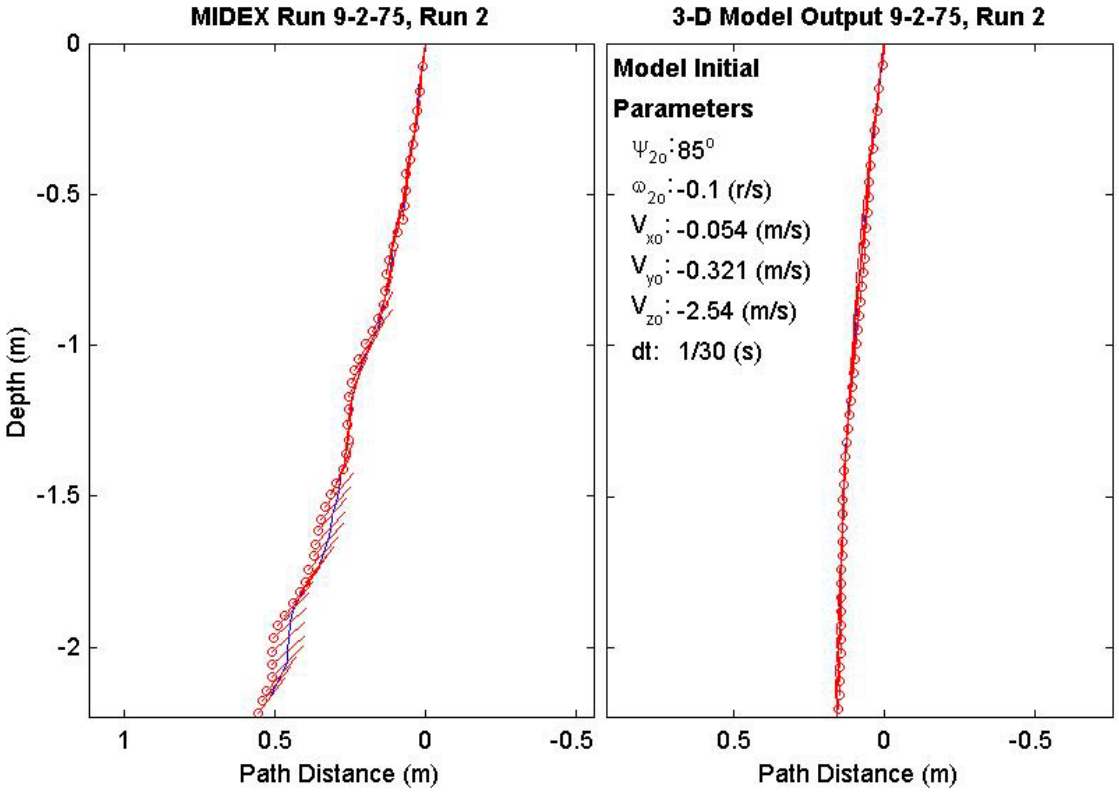

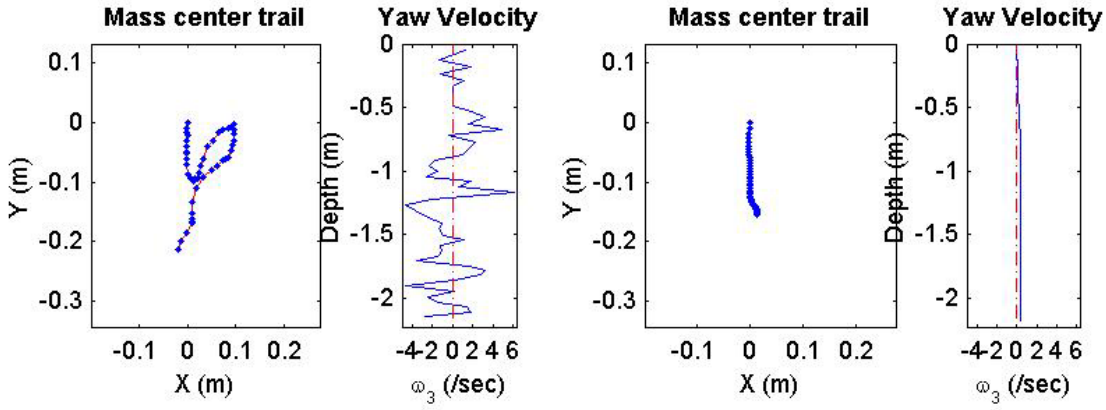

Final Drop
Parameters (75/9-2250)

time:	1.87(s)
xy_{fe}:	0.739(m)
V_{xfe}:	-0.105(m/s)
V_{yfe}:	-0.321(m/s)
V_{zfe}:	-1.07(m/s)
Ψ_{fe}:	39°
depth:	2.16(m)

Mine Shape
Parameters (75/9-2250)

d:	0.04(m)
L:	0.0912(m)
m:	0.215(m)
J_1:	2.35e-005(kg*m^2)
J_2:	0.000156(kg*m^2)
J_3:	0.000156(kg*m^2)
χ:	0.005796(m)

Final Model
Parameters (75/9-2250)

time:	1.5(s)
xy_{fm}:	0.236(m)
V_{xfm}:	0.0467(m/s)
V_{yfm}:	-0.0171(m/s)
V_{zfm}:	-1.41(m/s)
Ψ_{fm}:	97.65°
depth:	2.16(m)

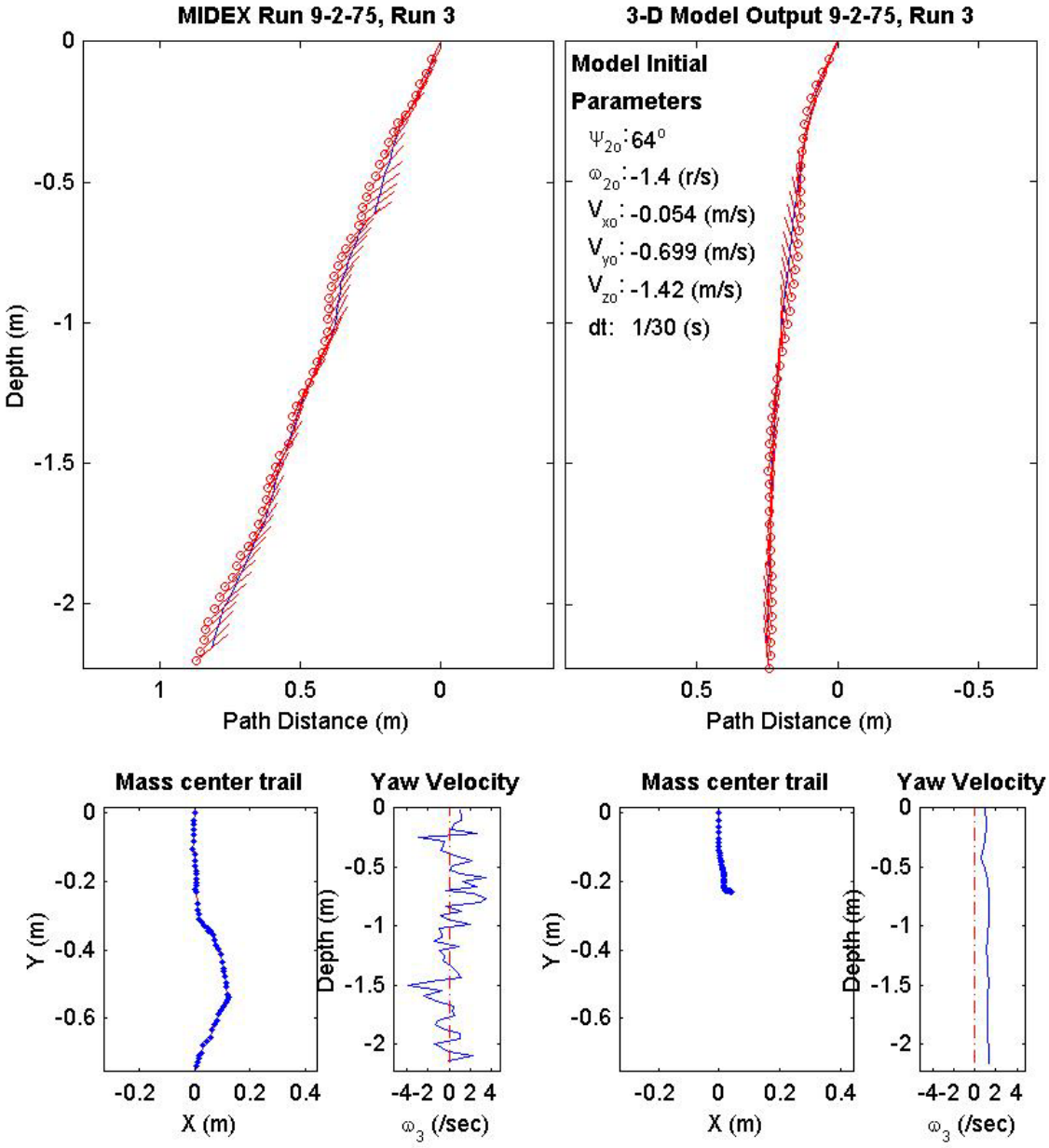

Final Drop
Parameters (75/9-2496)

time: 1.57(s)
xy_{fe}: 0.101(m)
V_{xfe}: 0.375(m/s)
V_{yfe}: 0.267(m/s)
V_{zfe}: -1.13(m/s)
Ψ_{fe}: 57.3°
depth: 2.22(m)

Mine Shape
Parameters (75/9-2496)

d: 0.04(m)
L: 0.0912(m)
m: 0.215(m)
J_1: 2.35e-005(kg*m^2)
J_2: 0.000156(kg*m^2)
J_3: 0.000156(kg*m^2)
χ: 0.005796(m)

Final Model
Parameters (75/9-2496)

time: 1.53(s)
xy_{fm}: 0.181(m)
V_{xfm}: 0.00489(m/s)
V_{yfm}: 3.77e-018(m/s)
V_{zfm}: -1.4(m/s)
Ψ_{fm}: 82.94°
depth: 2.25(m)

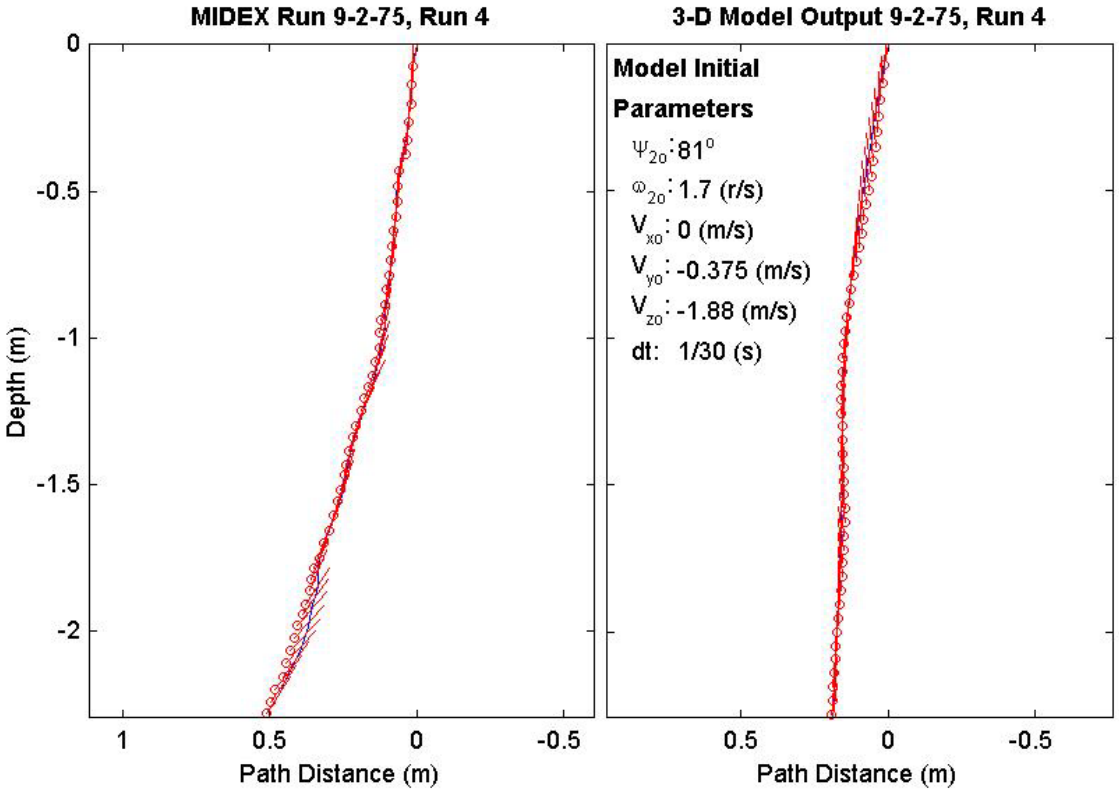

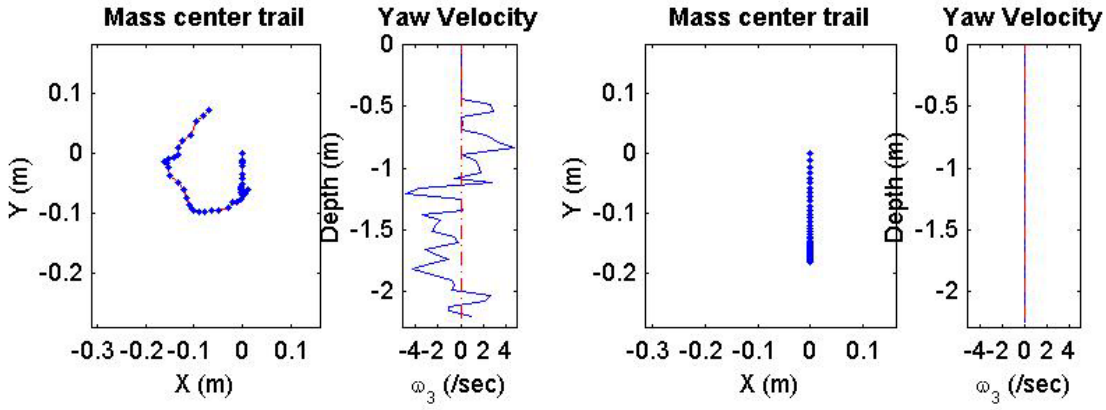

Final Drop
Parameters (15/15-1040)

time: 1.63(s)
xy_{fe}: 0.274(m)
V_{xfe}: -0.429(m/s)
V_{yfe}: 0.48(m/s)
V_{zfe}: -1.02(m/s)
Ψ_{fe}: 36.8°
depth: 2.17(m)

Mine Shape
Parameters (15/15-1040)

d: 0.04(m)
L: 0.152(m)
m: 0.323(m)
J_1: 3.3e-005(kg*m^2)
J_2: 0.000578(kg*m^2)
J_3: 0.000578(kg*m^2)
χ: 0.007411(m)

Final Model
Parameters (15/15-1040)

time: 1.43(s)
xy_{fm}: 0.43(m)
V_{xfm}: 0.0334(m/s)
V_{yfm}: 0.0312(m/s)
V_{zfm}: -1.52(m/s)
Ψ_{fm}: 92.47°
depth: 2.21(m)

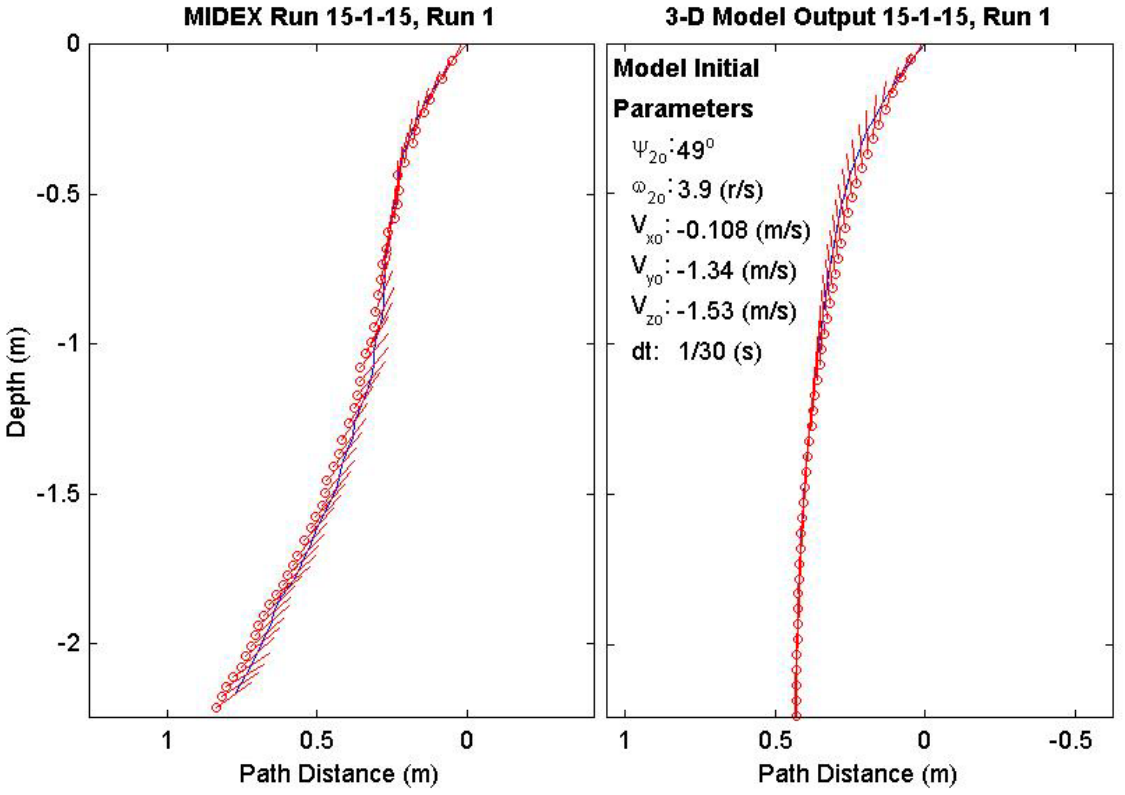

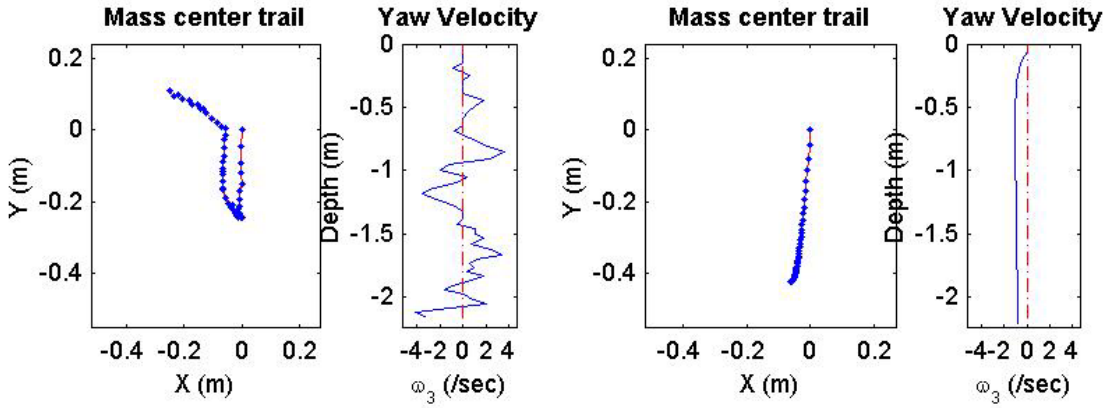

Final Drop Parameters (15/15-1059)

time: 1.4(s)
xy_{fe}: 0.67(m)
V_{xfe}: -0.75(m/s)
V_{yfe}: -0.267(m/s)
V_{zfe}: -1.26(m/s)
Ψ_{fe}: 47.8°
depth: 1.4(m)

Mine Shape Parameters (15/15-1059)

d: 0.04(m)
L: 0.152(m)
m: 0.323(m)
J_1: 3.3e-005(kg*m^2)
J_2: 0.000578(kg*m^2)
J_3: 0.000578(kg*m^2)
χ: 0.007411(m)

Final Model Parameters (15/15-1059)

time: 1.03(s)
xy_{fm}: 0.255(m)
V_{xfm}: -0.0177(m/s)
V_{yfm}: 0.0497(m/s)
V_{zfm}: -1.53(m/s)
Ψ_{fm}: 93.87°
depth: 1.43(m)

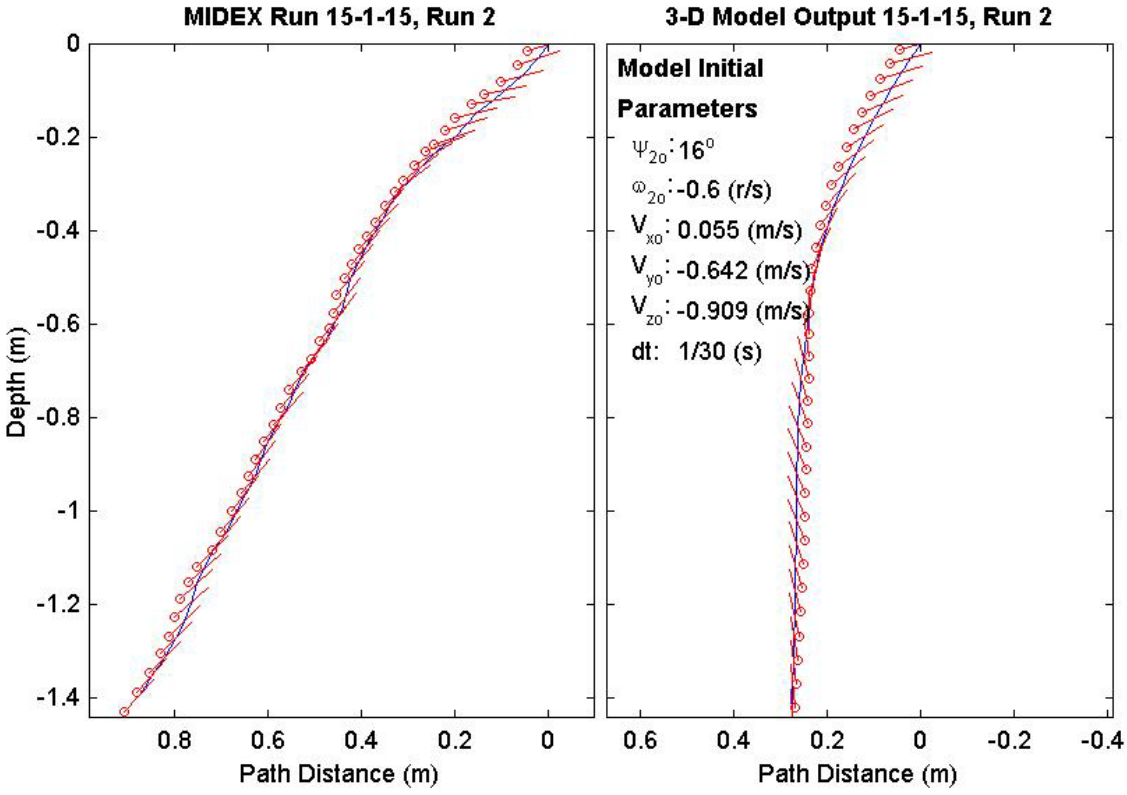

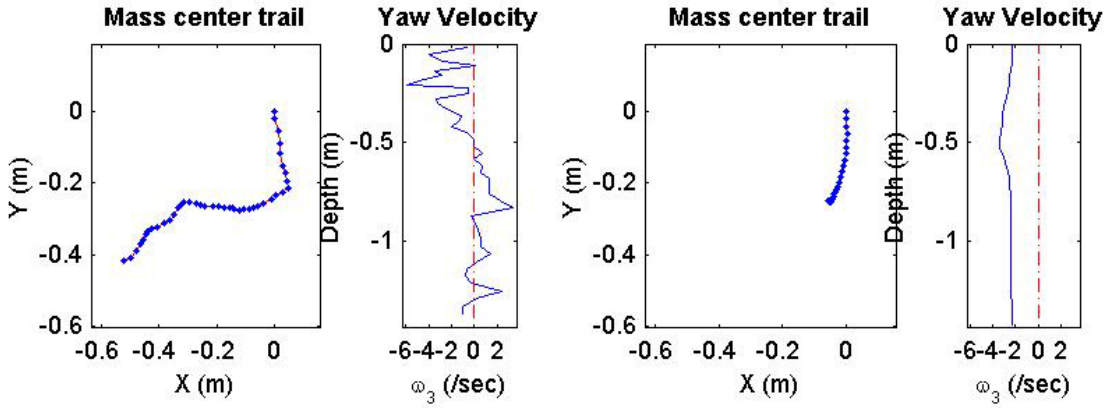

Final Drop Parameters (15/15-2332)

time: 1.17(s)
xy_{fe}: 0.799(m)
V_{xfe}: -0.804(m/s)
V_{yfe}: -0.055(m/s)
V_{zfe}: -1.34(m/s)
Ψ_{fe}: 42.3°
depth: 1.69(m)

Mine Shape Parameters (15/15-2332)

d: 0.04(m)
L: 0.152(m)
m: 0.323(m)
J_1: 3.3e-005(kg*m^2)
J_2: 0.000578(kg*m^2)
J_3: 0.000578(kg*m^2)
χ: 0.007411(m)

Final Model Parameters (15/15-2332)

time: 1.17(s)
xy_{fm}: 0.603(m)
V_{xfm}: 0.13(m/s)
V_{yfm}: -0.00367(m/s)
V_{zfm}: -1.51(m/s)
Ψ_{fm}: 87.58°
depth: 1.72(m)

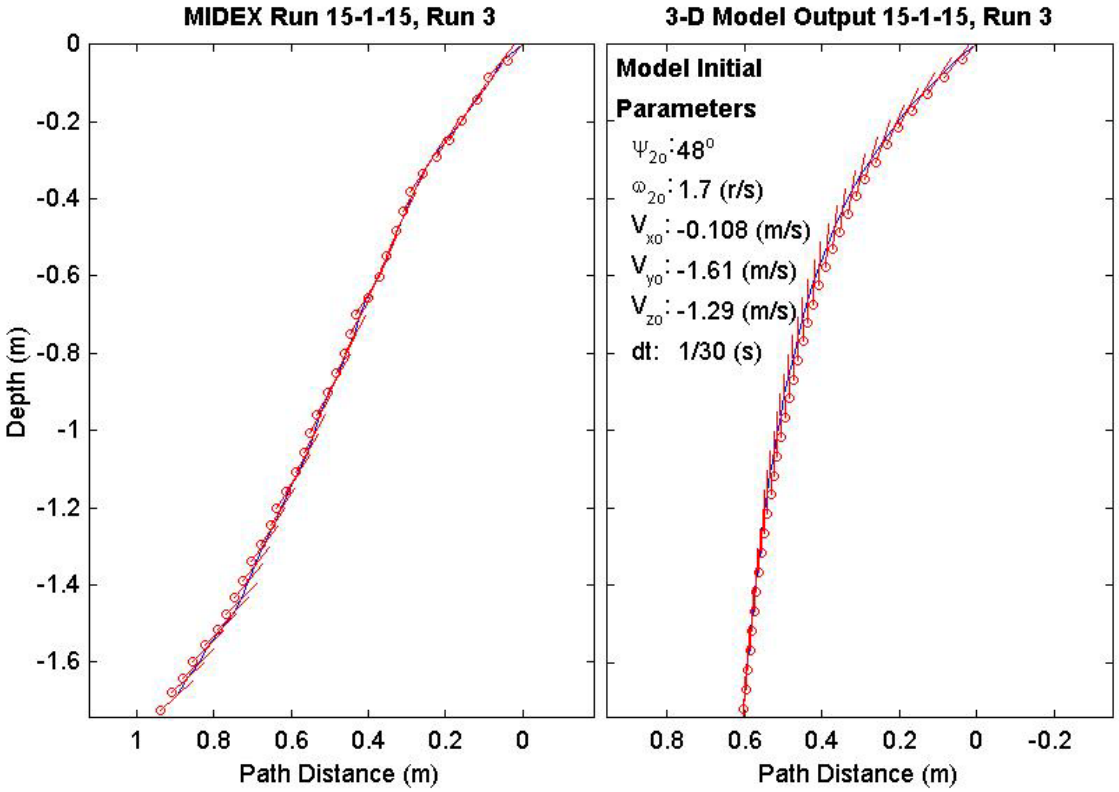

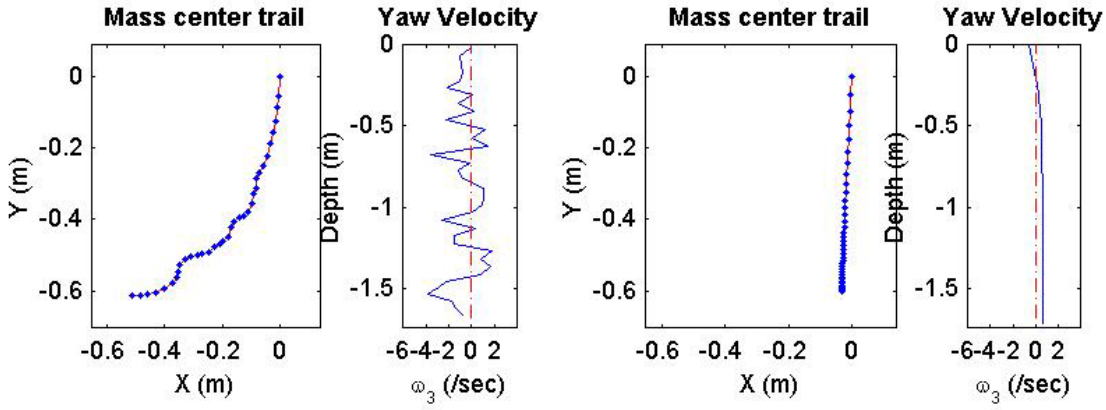

Final Drop
Parameters (15/12-1212)

time: 2.17(s)
xy_{fe}: 0.591(m)
V_{xfe}: 0.159(m/s)
V_{yfe}: 0.429(m/s)
V_{zfe}: -0.99(m/s)
Ψ_{fe}: 54.8°
depth: 2.2(m)

Mine Shape
Parameters (15/12-1212)

d: 0.04(m)
L: 0.121(m)
m: 0.254(m)
J_1: 2.71e-005(kg*m^2)
J_2: 0.000321(kg*m^2)
J_3: 0.000321(kg*m^2)
χ: 0.005307(m)

Final Model
Parameters (15/12-1212)

time: 1.63(s)
xy_{fm}: 0.383(m)
V_{xfm}: -0.0185(m/s)
V_{yfm}: 0.0294(m/s)
V_{zfm}: -1.37(m/s)
Ψ_{fm}: 94.31°
depth: 2.24(m)

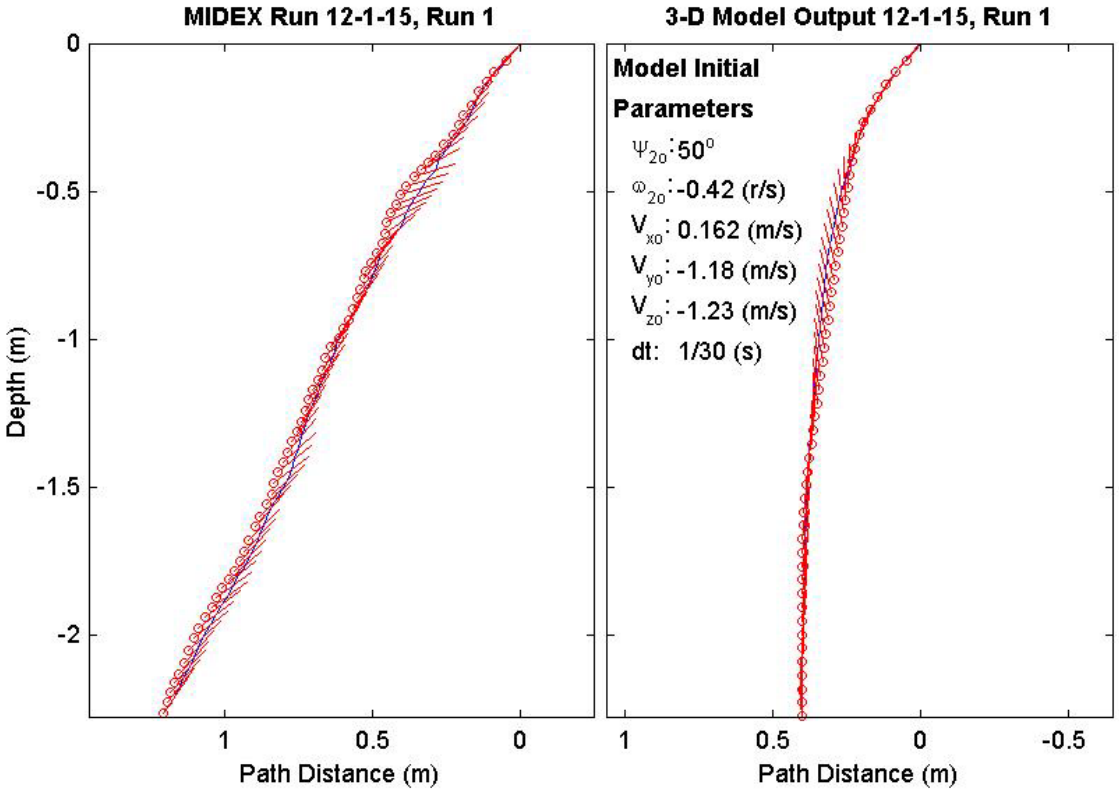

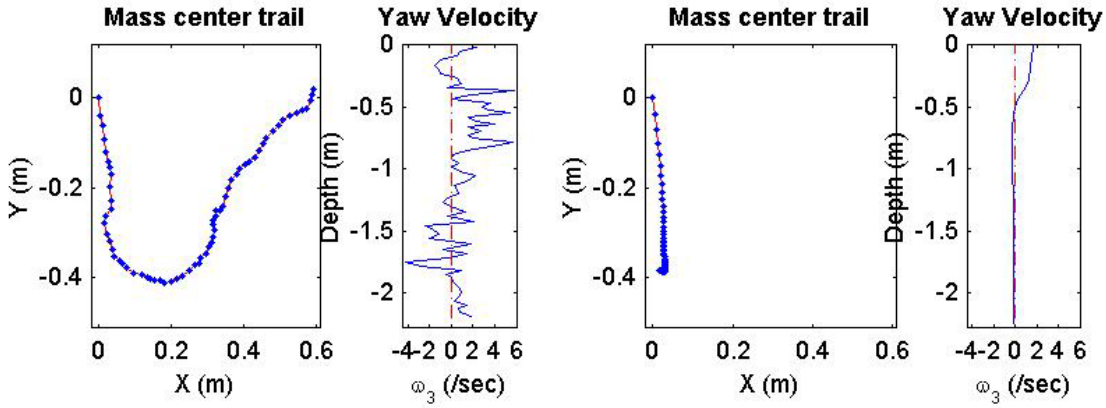

Final Drop

Parameters (15/12-1118)

time: 2.2(s)
xy_{fe}: 0.552(m)
V_{xfe}: -0.375(m/s)
V_{yfe}: -0.054(m/s)
V_{zfe}: -0.992(m/s)
Ψ_{fe}: 54.9°
depth: 1.94(m)

Mine Shape

Parameters (15/12-1118)

d: 0.04(m)
L: 0.121(m)
m: 0.254(m)
J_1: 2.71e-005(kg*m^2)
J_2: 0.000321(kg*m^2)
J_3: 0.000321(kg*m^2)
χ: 0.005307(m)

Final Model

Parameters (15/12-1118)

time: 1.57(s)
xy_{fm}: 0.37(m)
V_{xfm}: 0.00042(m/s)
V_{yfm}: -0.00151(m/s)
V_{zfm}: -1.38(m/s)
Ψ_{fm}: 79.44°
depth: 1.96(m)

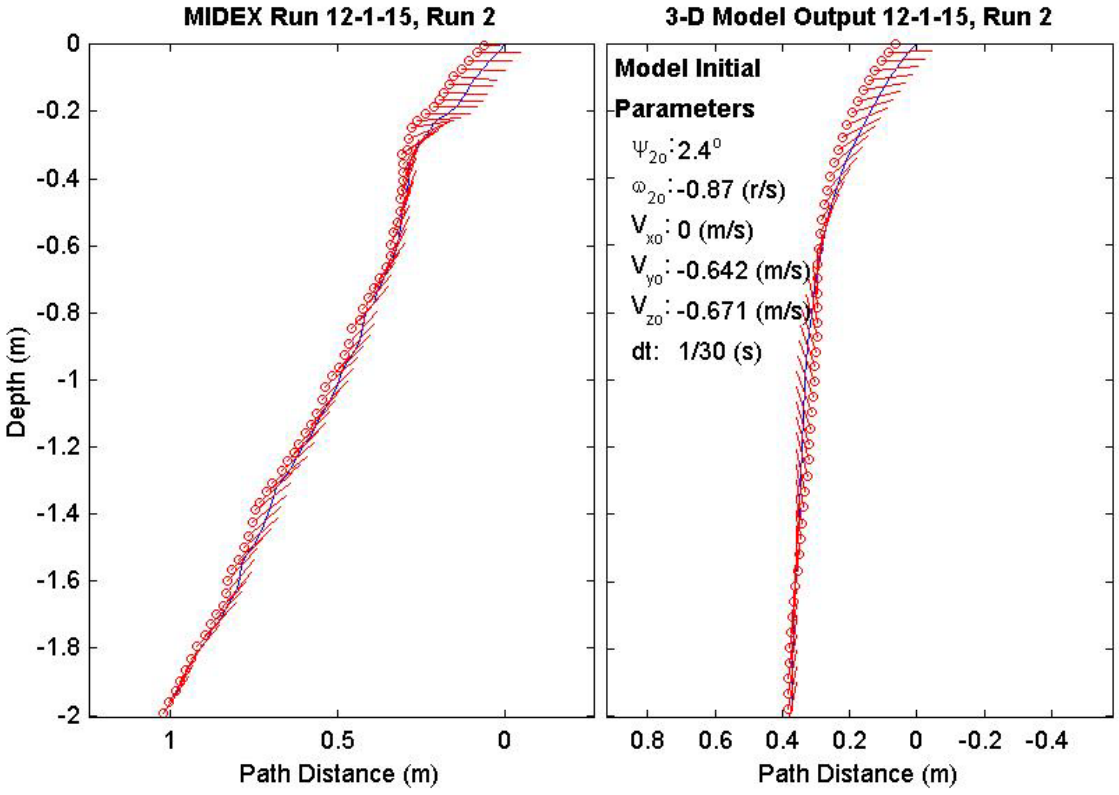

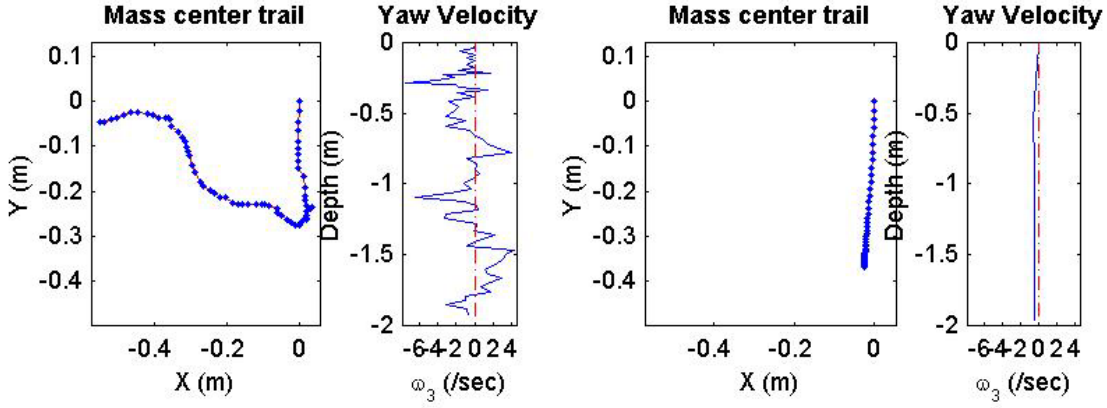

Final Drop Parameters (15/12-1894)

time: 2.1(s)
xy_{fe}: 1.08(m)
V_{xfe}: -0.162(m/s)
V_{yfe}: -0.588(m/s)
V_{zfe}: -0.99(m/s)
Ψ_{fe}: 45.7°
depth: 2.1(m)

Mine Shape Parameters (15/12-1894)

d: 0.04(m)
L: 0.121(m)
m: 0.254(m)
J_1: 2.71e-005($kg*m^2$)
J_2: 0.000321($kg*m^2$)
J_3: 0.000321($kg*m^2$)
χ: 0.005307(m)

Final Model Parameters (15/12-1894)

time: 1.53(s)
xy_{fm}: 0.233(m)
V_{xfm}: -0.0331(m/s)
V_{yfm}: 0.0138(m/s)
V_{zfm}: -1.37(m/s)
Ψ_{fm}: 93.48°
depth: 2.11(m)

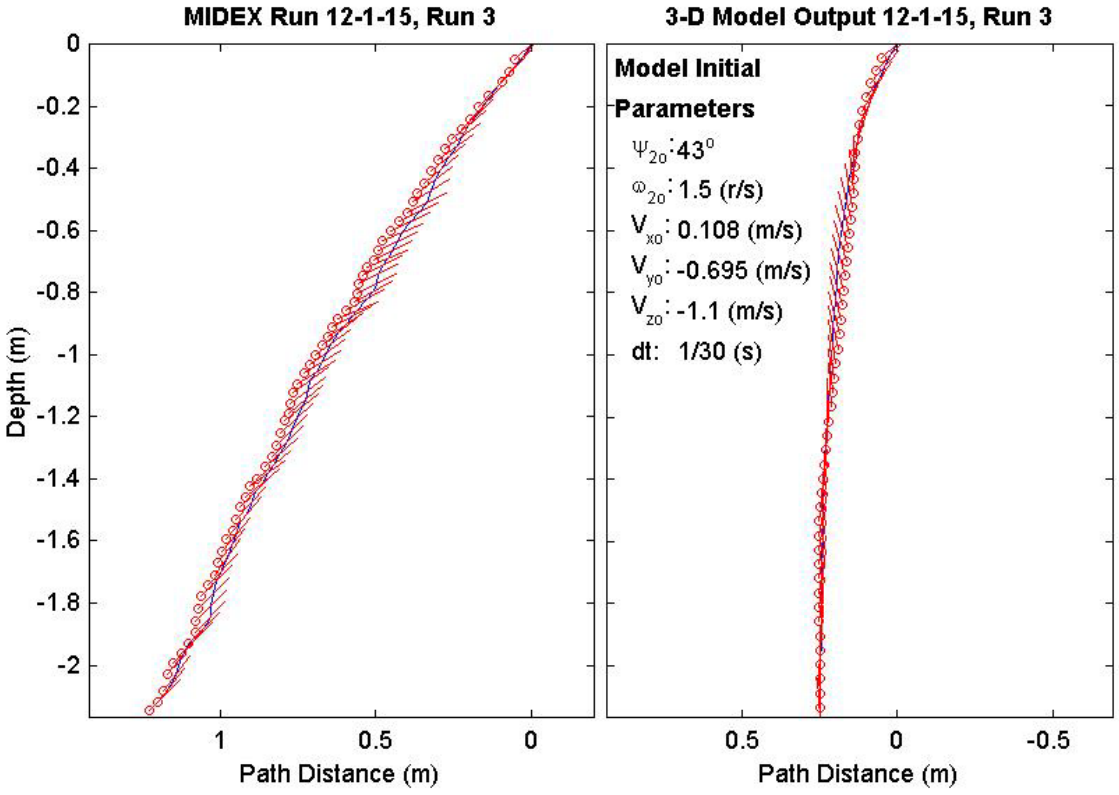

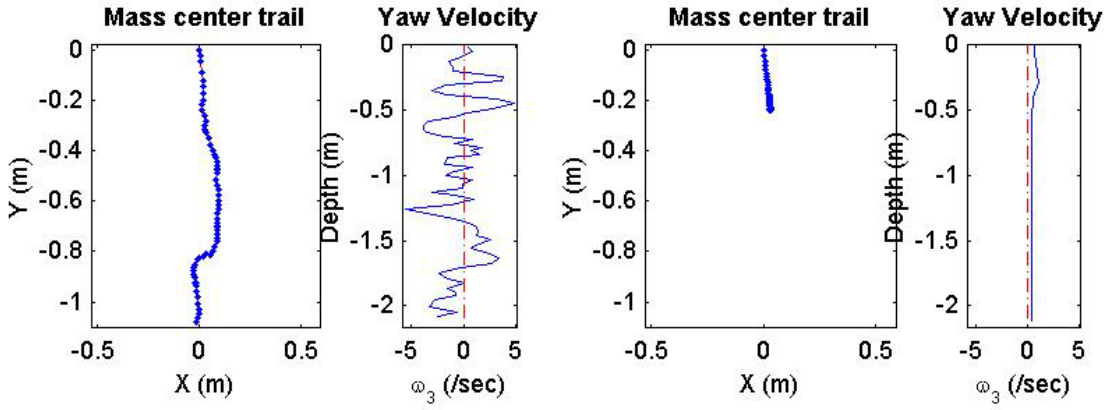

Final Drop

Parameters (15/9-1510)

time: 1.93(s)
xy_{fe}: 0.458(m)
V_{xfe}: 0.375(m/s)
V_{yfe}: -0.321(m/s)
V_{zfe}: -0.749(m/s)
Ψ_{fe}: 38.1°
depth: 2.13(m)

Mine Shape

Parameters (15/9-1510)

d: 0.04(m)
L: 0.0912(m)
m: 0.215(m)
J_1: 2.35e-005(kg*m^2)
J_2: 0.000158(kg*m^2)
J_3: 0.000158(kg*m^2)
χ: 0.002911(m)

Final Model

Parameters (15/9-1510)

time: 1.47(s)
xy_{fm}: 0.268(m)
V_{xfm}: -0.0373(m/s)
V_{yfm}: -0.017(m/s)
V_{zfm}: -1.41(m/s)
Ψ_{fm}: 83.49°
depth: 2.13(m)

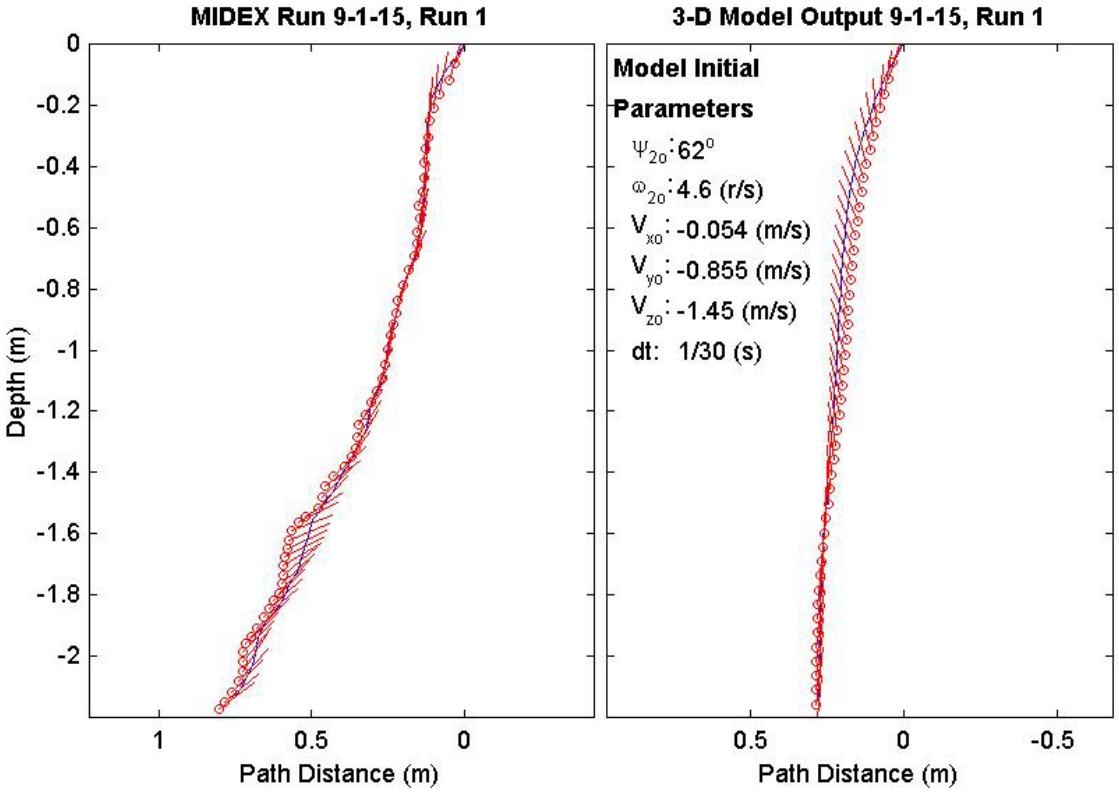

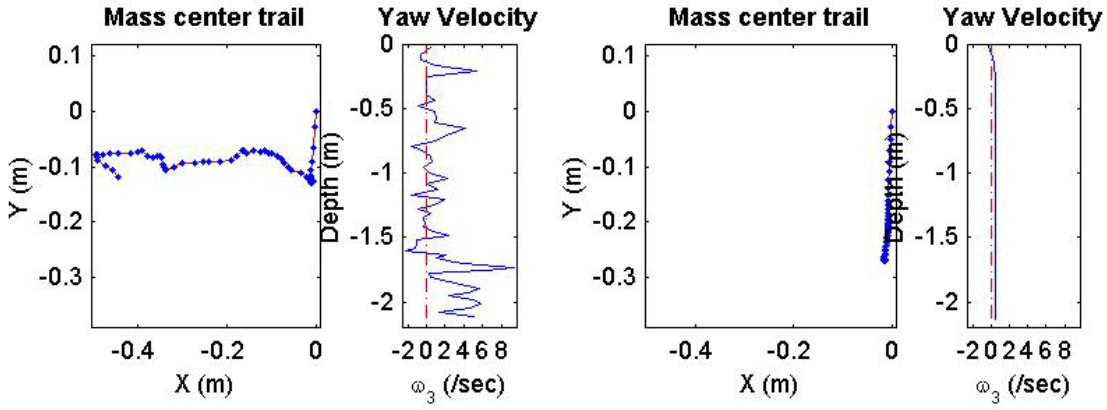

Final Drop
Parameters (15/9-1709)

time:	2.47(s)
xy_{fe}:	0.314(m)
V_{xfe}:	-0.645(m/s)
V_{yfe}:	-0.054(m/s)
V_{zfe}:	-0.671(m/s)
Ψ_{fe}:	-29.4°
depth:	2.28(m)

Mine Shape
Parameters (15/9-1709)

d:	0.04(m)
L:	0.0912(m)
m:	0.215(m)
J_1:	2.35e-005(kg*m^2)
J_2:	0.000158(kg*m^2)
J_3:	0.000158(kg*m^2)
χ:	0.002911(m)

Final Model
Parameters (15/9-1709)

time:	1.63(s)
xy_{fm}:	0.395(m)
V_{xfm}:	0.0145(m/s)
V_{yfm}:	-0.00412(m/s)
V_{zfm}:	-1.4(m/s)
Ψ_{fm}:	81.66°
depth:	2.3(m)

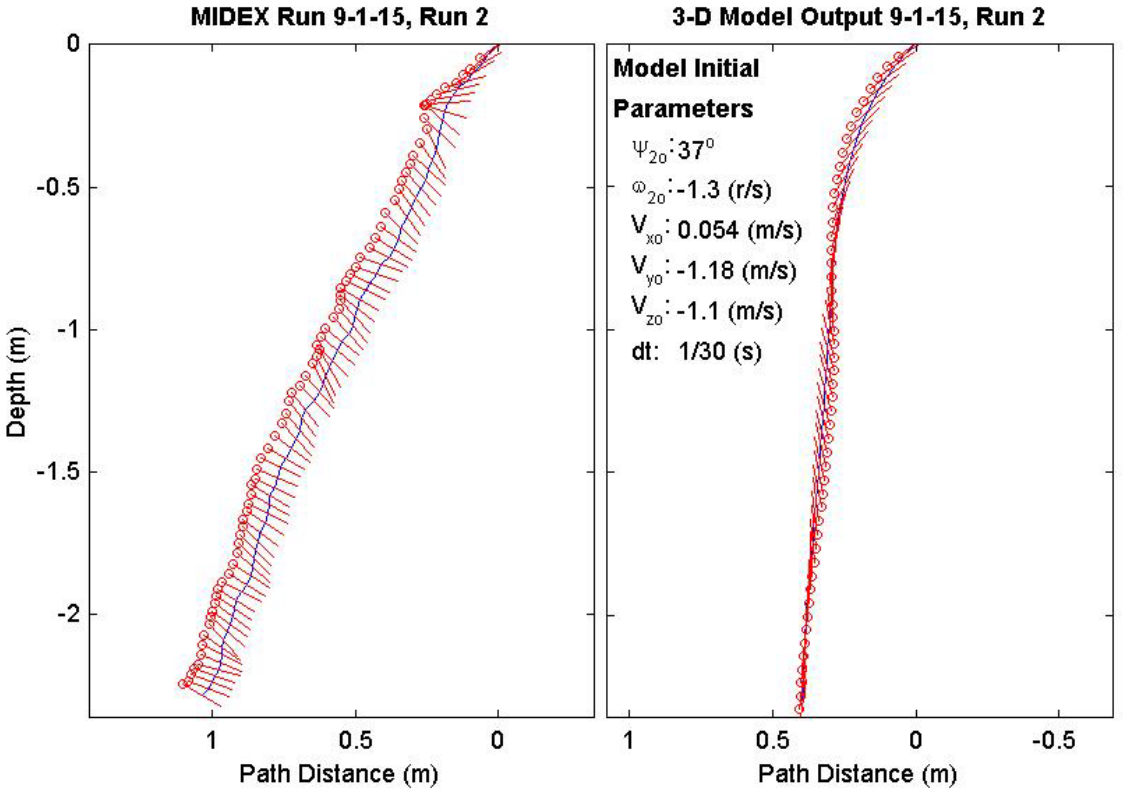

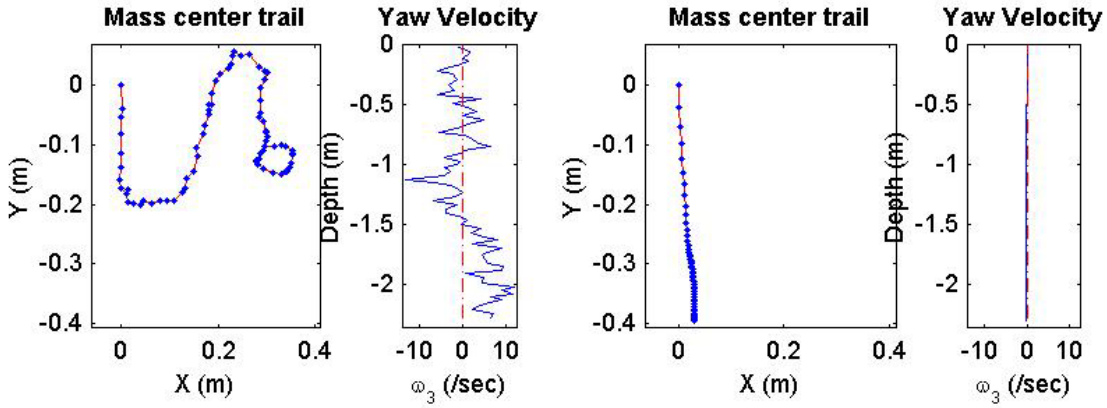

Final Drop
Parameters (15/9-1880)

time: 2.33(s)
xy_{fe}: 0.111(m)
V_{xfe}: 0(m/s)
V_{yfe}: -0.054(m/s)
V_{zfe}: -0.858(m/s)
Ψ_{fe}: 45.5°
depth: 2.19(m)

Mine Shape
Parameters (15/9-1880)

d: 0.04(m)
L: 0.0912(m)
m: 0.215(m)
J_1: 2.35e-005(kg*m^2)
J_2: 0.000158(kg*m^2)
J_3: 0.000158(kg*m^2)
χ: 0.002911(m)

Final Model
Parameters (15/9-1880)

time: 1.53(s)
xy_{fm}: 0.289(m)
V_{xfm}: -0.0223(m/s)
V_{yfm}: 0.0161(m/s)
V_{zfm}: -1.4(m/s)
Ψ_{fm}: 84.64°
depth: 2.24(m)

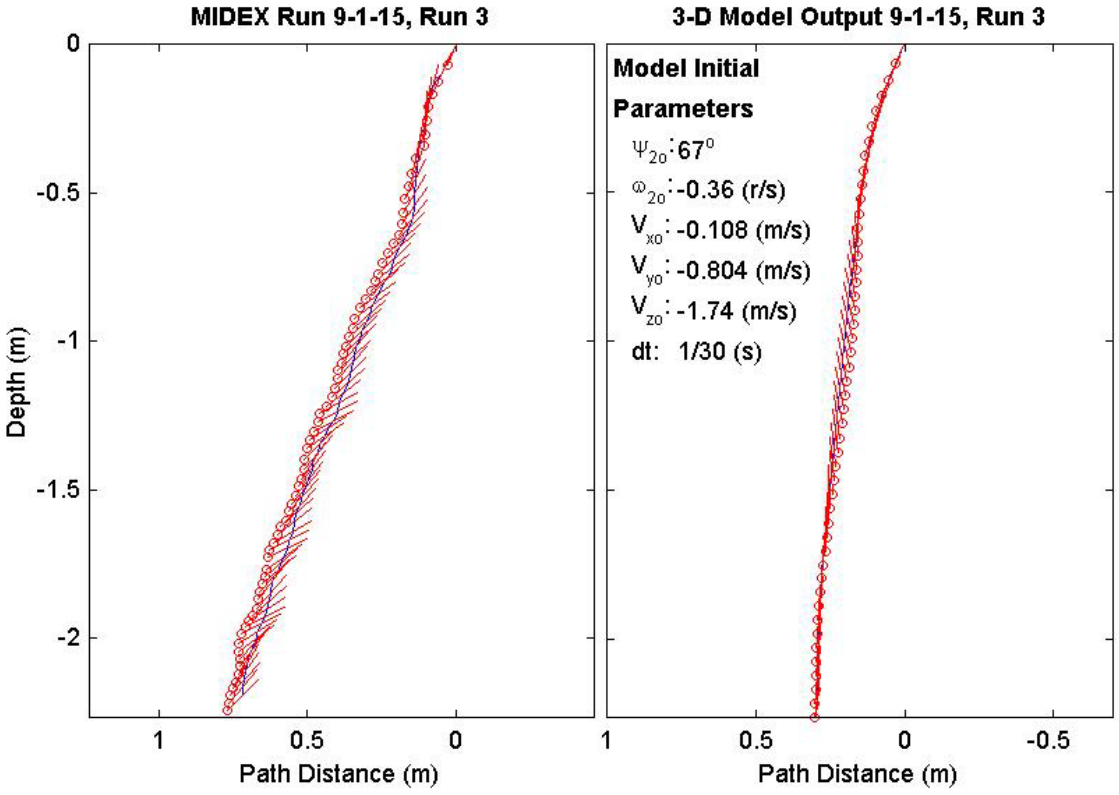

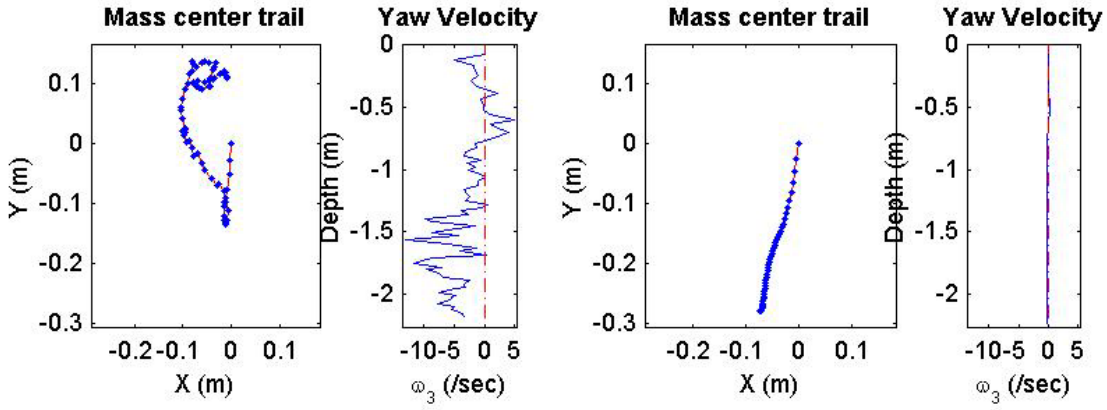

Final Drop Parameters (30/15-3079)

time: 1.73(s)
xy_{fe}: 0.473(m)
V_{xfe}: 0.375(m/s)
V_{yfe}: 0.267(m/s)
V_{zfe}: -1.02(m/s)
Ψ_{fe}: 42.6°
depth: 2.2(m)

Mine Shape Parameters (30/15-3079)

d: 0.04(m)
L: 0.152(m)
m: 0.323(m)
J_1: 3.3e-005(kg*m^2)
J_2: 0.000578(kg*m^2)
J_3: 0.000578(kg*m^2)
χ: 0.007411(m)

Final Model Parameters (30/15-3079)

time: 1.43(s)
xy_{fm}: 0.573(m)
V_{xfm}: 0.0939(m/s)
V_{yfm}: -0.0549(m/s)
V_{zfm}: -1.52(m/s)
Ψ_{fm}: 92.96°
depth: 2.25(m)

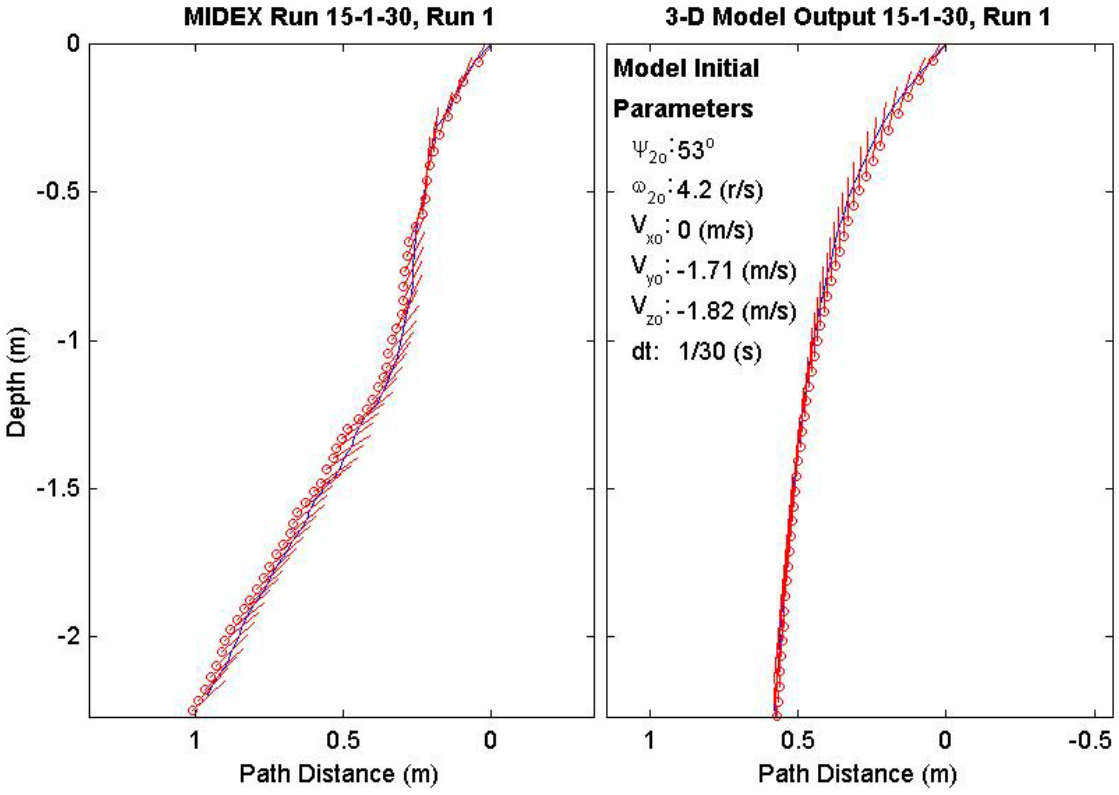

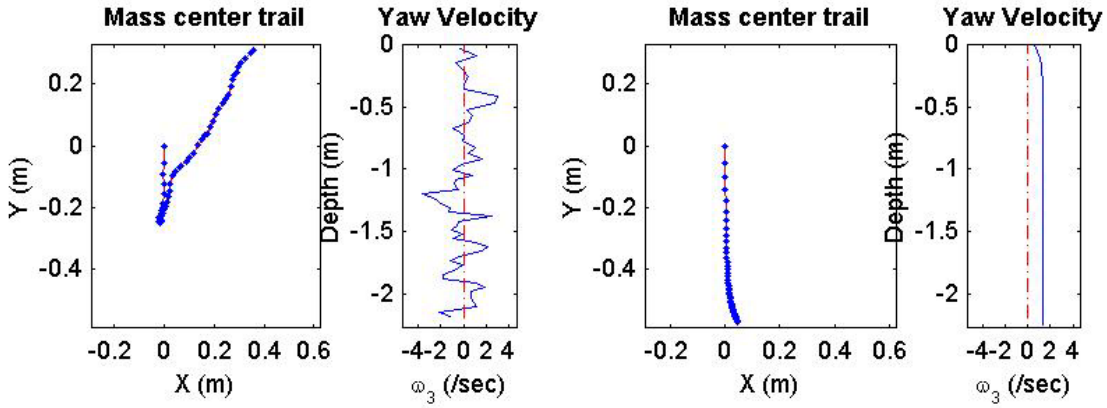

Final Drop Parameters (30/15-1871)

time: 1.47(s)
xy_{fe}: 0.928(m)
V_{xfe}: 0(m/s)
V_{yfe}: -0.48(m/s)
V_{zfe}: -1.02(m/s)
Ψ_{fe}: 44.5°
depth: 2.06(m)

Mine Shape Parameters (30/15-1871)

d: 0.04(m)
L: 0.152(m)
m: 0.323(m)
J_1: 3.3e-005(kg*m^2)
J_2: 0.000578(kg*m^2)
J_3: 0.000578(kg*m^2)
χ: 0.007411(m)

Final Model Parameters (30/15-1871)

time: 1.33(s)
xy_{fm}: 0.313(m)
V_{xfm}: 0.000244(m/s)
V_{yfm}: -0.0151(m/s)
V_{zfm}: -1.53(m/s)
Ψ_{fm}: 83.73°
depth: 2.08(m)

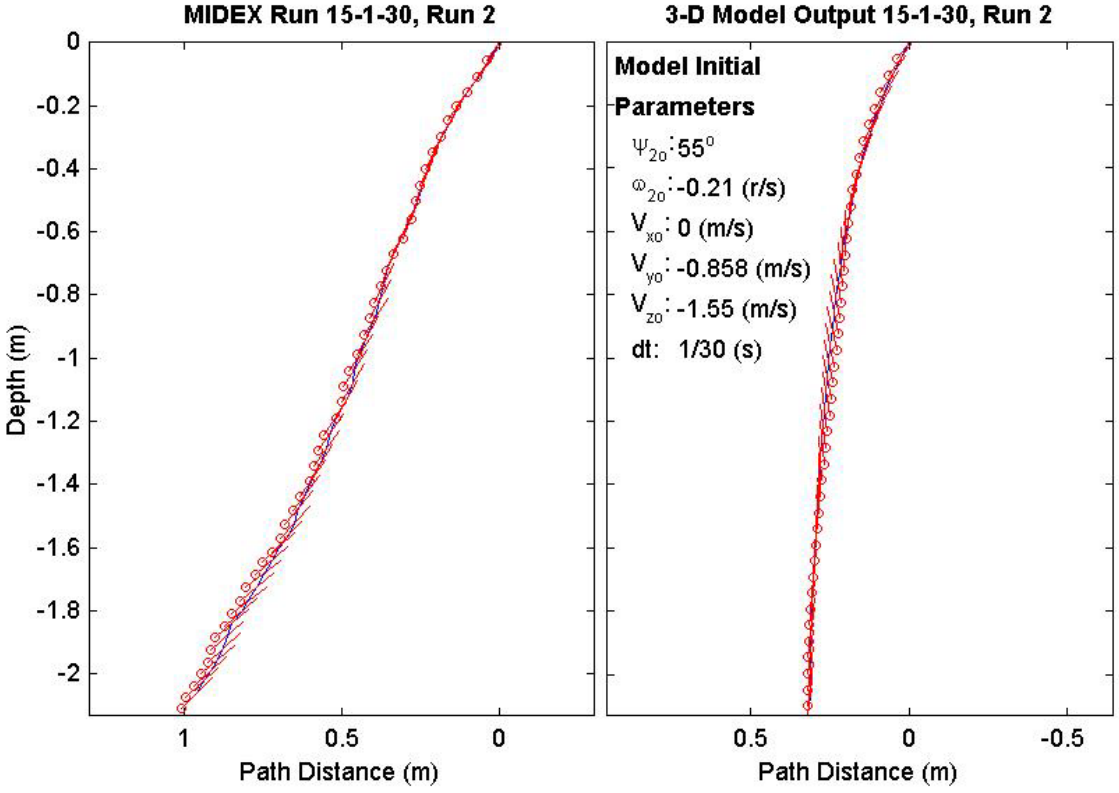

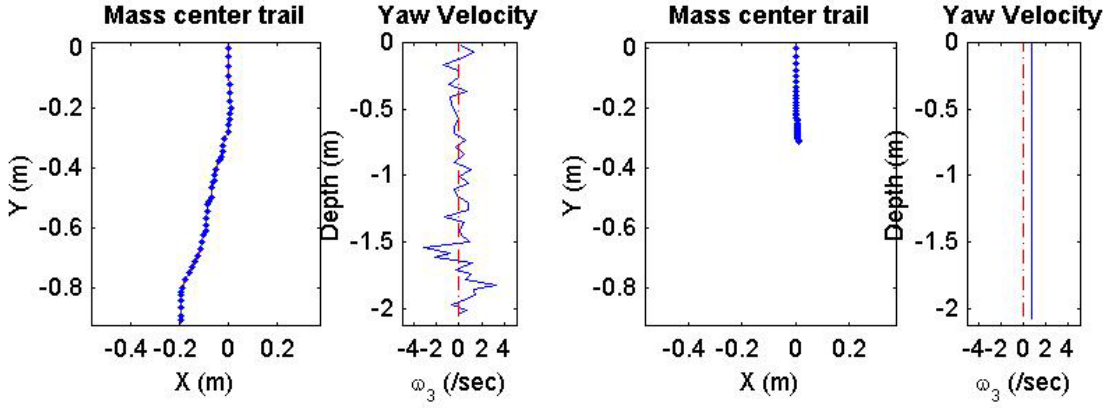

Final Drop
Parameters (30/15-1920)

time: 1.23(s)
xy_{fe}: 0.55(m)
V_{xfe}: 0(m/s)
V_{yfe}: -0.163(m/s)
V_{zfe}: -1.58(m/s)
Ψ_{fe}: 85.7°
depth: 2.05(m)

Mine Shape
Parameters (30/15-1920)

d: 0.04(m)
L: 0.152(m)
m: 0.323(m)
J_1: 3.3e-005(kg*m^2)
J_2: 0.000578(kg*m^2)
J_3: 0.000578(kg*m^2)
χ: 0.007411(m)

Final Model
Parameters (30/15-1920)

time: 1.37(s)
xy_{fm}: 0.254(m)
V_{xfm}: -0.023(m/s)
V_{yfm}: -0.0223(m/s)
V_{zfm}: -1.53(m/s)
Ψ_{fm}: 87.26°
depth: 2.1(m)

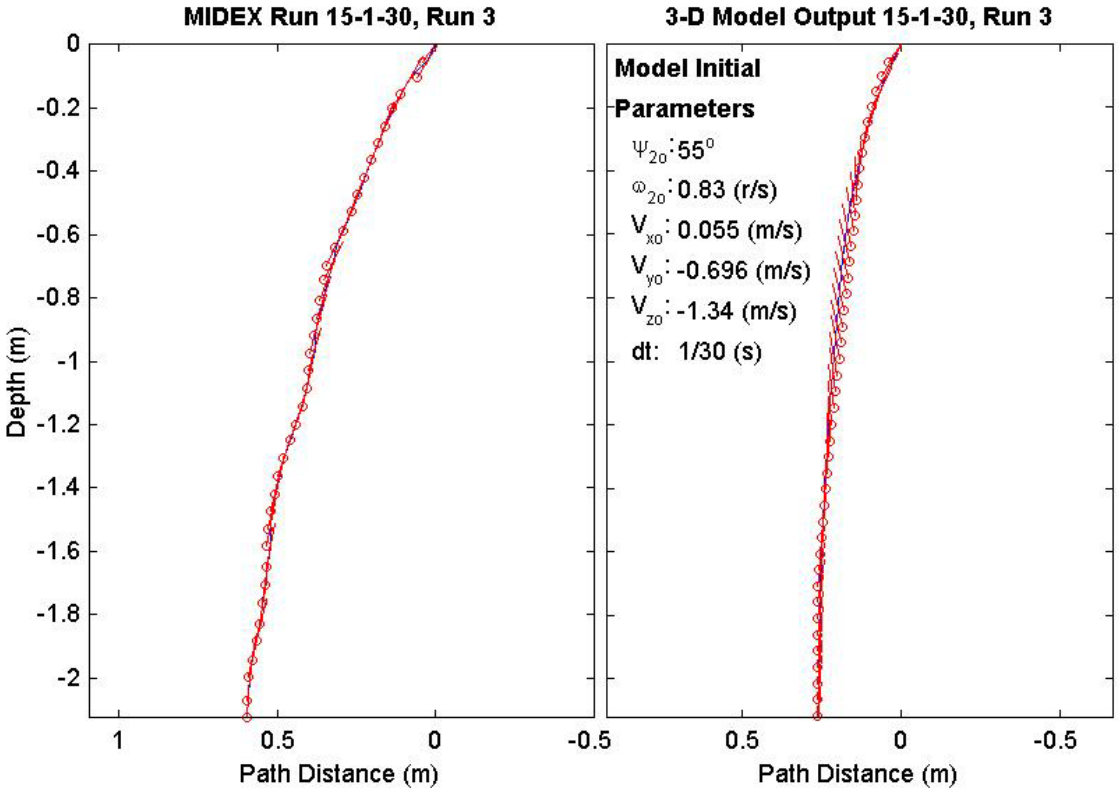

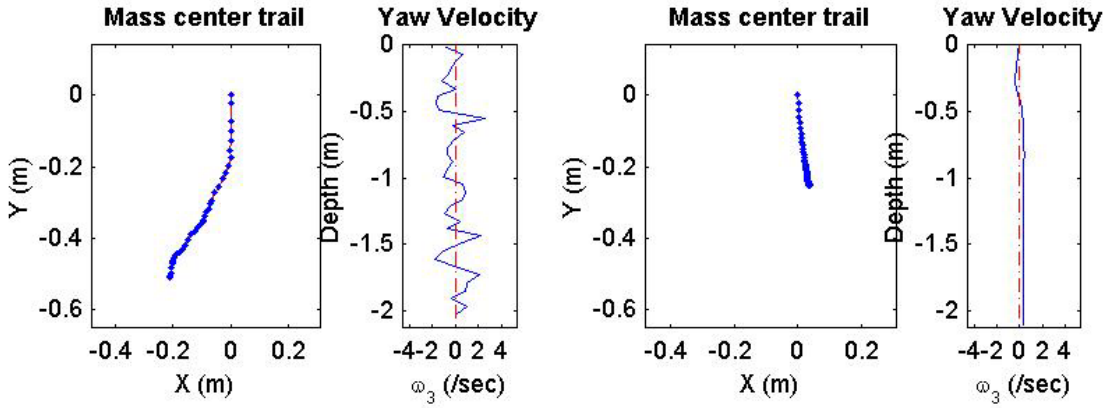

Final Drop Parameters (30/15-1347)

time: 1.97(s)
xy_{fe}: 0.997(m)
V_{xfe}: 0.375(m/s)
V_{yfe}: -0.267(m/s)
V_{zfe}: -1.18(m/s)
Ψ_{fe}: 54.5°
depth: 2.15(m)

Mine Shape Parameters (30/15-1347)

d: 0.04(m)
L: 0.152(m)
m: 0.323(m)
J_1: 3.3e-005(kg*m^2)
J_2: 0.000578(kg*m^2)
J_3: 0.000578(kg*m^2)
χ: 0.007411(m)

Final Model Parameters (30/15-1347)

time: 1.43(s)
xy_{fm}: 0.387(m)
V_{xfm}: -0.0218(m/s)
V_{yfm}: 0.021(m/s)
V_{zfm}: -1.52(m/s)
Ψ_{fm}: 88.39°
depth: 2.18(m)

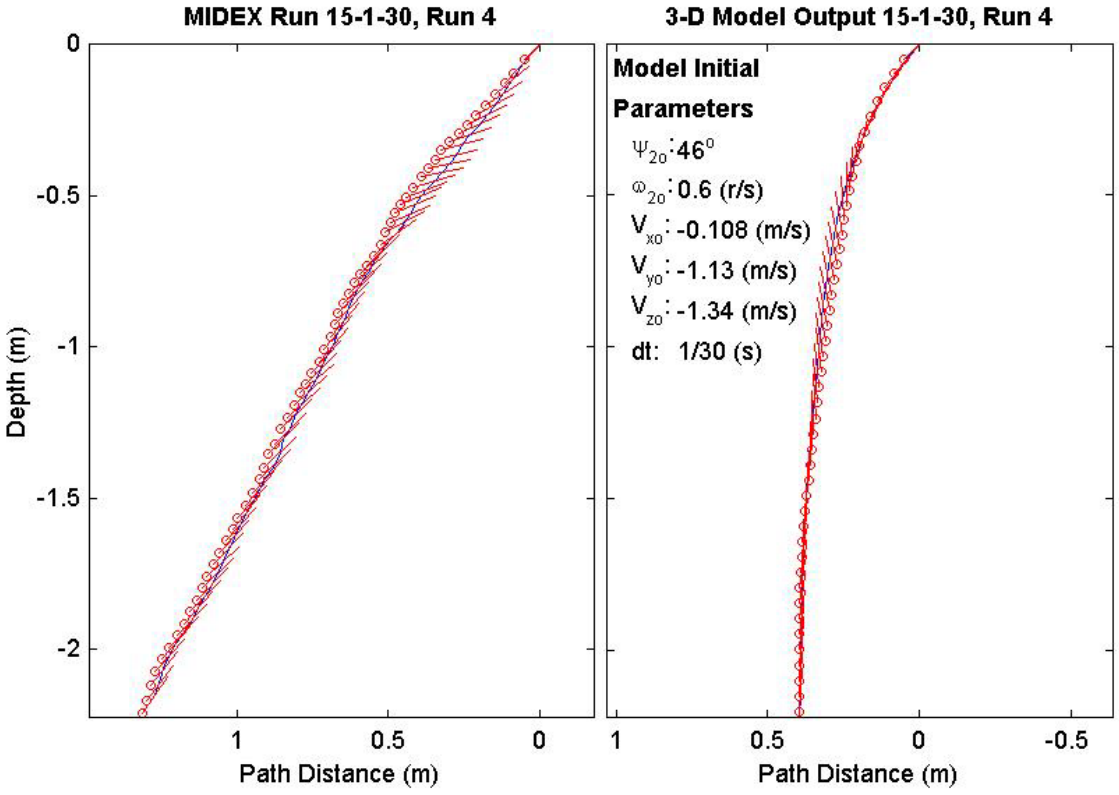

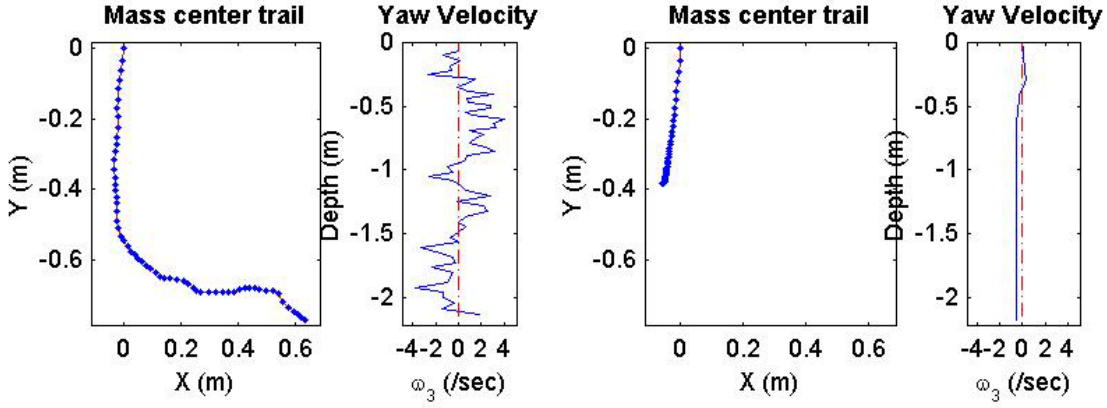

Final Drop
Parameters (30/15-917)

time: 1.53(s)
xy_{fe}: 0.896(m)
V_{xfe}: -0.321(m/s)
V_{yfe}: -0.055(m/s)
V_{zfe}: -1.13(m/s)
Ψ_{fe}: 43.9°
depth: 1.47(m)

Mine Shape
Parameters (30/15-917)

d: 0.04(m)
L: 0.152(m)
m: 0.323(m)
J_1: 3.3e-005(kg*m^2)
J_2: 0.000578(kg*m^2)
J_3: 0.000578(kg*m^2)
χ: 0.007411(m)

Final Model
Parameters (30/15-917)

time: 1.03(s)
xy_{fm}: 0.403(m)
V_{xfm}: 0.0772(m/s)
V_{yfm}: 0.00594(m/s)
V_{zfm}: -1.54(m/s)
Ψ_{fm}: 95.02°
depth: 1.47(m)

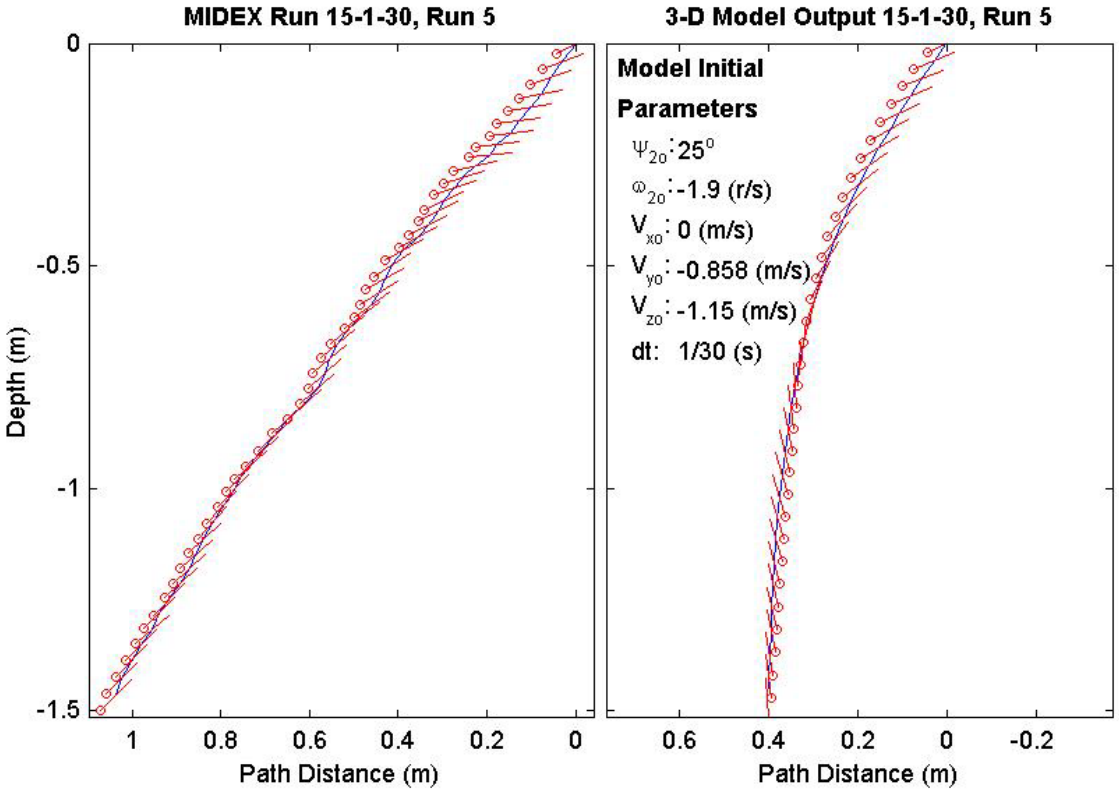

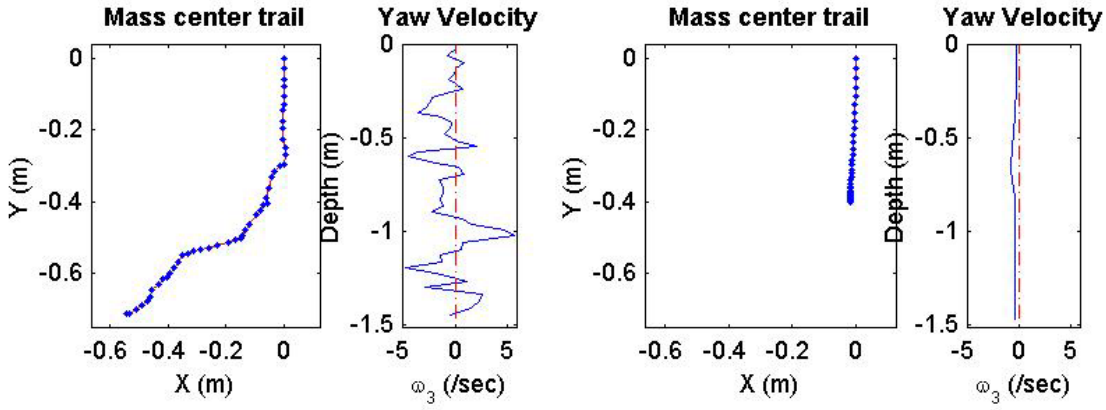

Final Drop Parameters (30/12-2719)

time: 2.03(s)
xy_{fe}: 0.711(m)
V_{xfe}: 0.429(m/s)
V_{yfe}: -0.321(m/s)
V_{zfe}: -0.966(m/s)
Ψ_{fe}: 48.5°
depth: 2.15(m)

Mine Shape Parameters (30/12-2719)

d: 0.04(m)
L: 0.121(m)
m: 0.254(m)
J_1: 2.71e-005(kg*m^2)
J_2: 0.000321(kg*m^2)
J_3: 0.000321(kg*m^2)
χ: 0.005307(m)

Final Model Parameters (30/12-2719)

time: 1.5(s)
xy_{fm}: 0.362(m)
V_{xfm}: 0.0345(m/s)
V_{yfm}: 0.00267(m/s)
V_{zfm}: -1.37(m/s)
Ψ_{fm}: 95.34°
depth: 2.17(m)

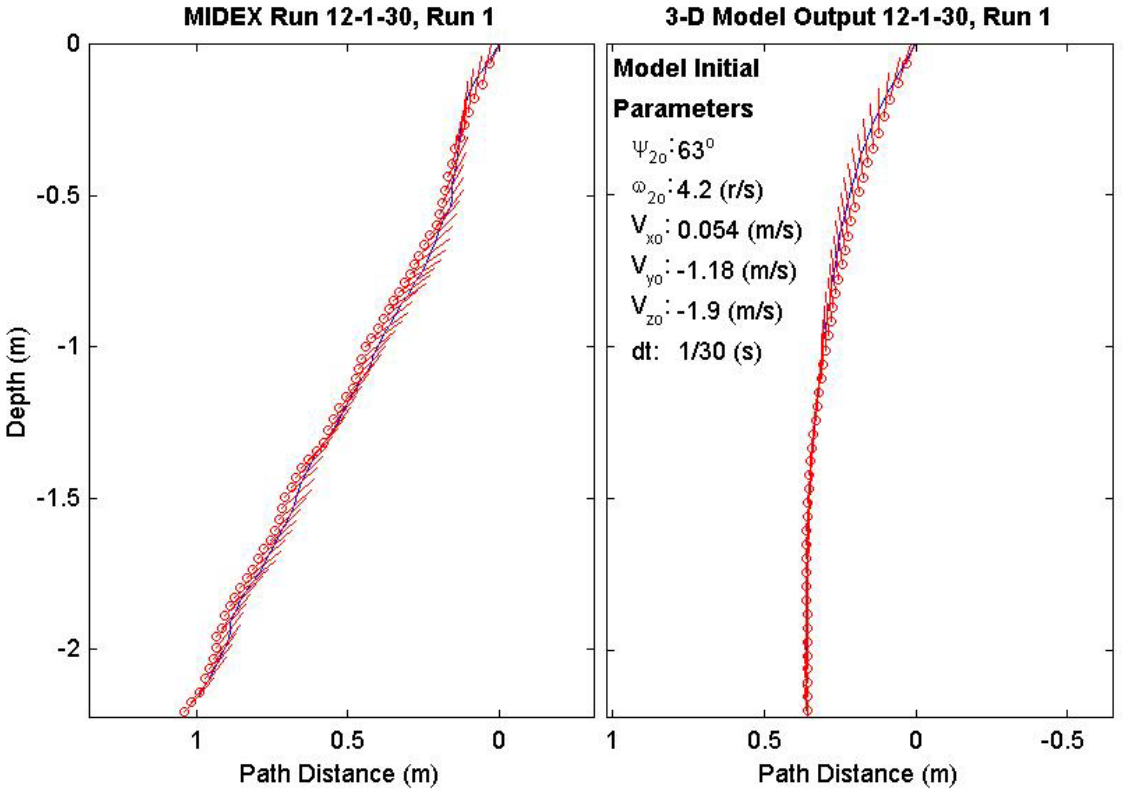

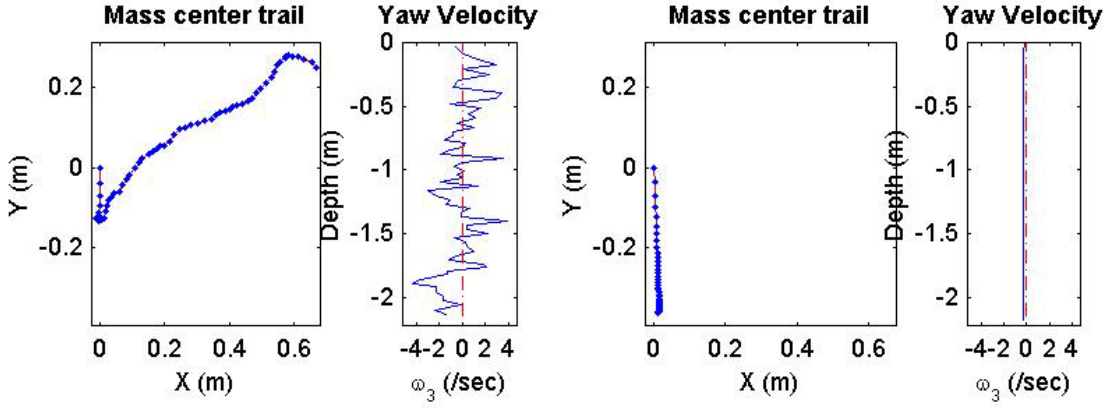

Final Drop Parameters (30/12-1778)

time: 1.93(s)
xy_{fe}: 0.949(m)
V_{xfe}: 0.213(m/s)
V_{yfe}: -0.108(m/s)
V_{zfe}: -1.07(m/s)
Ψ_{fe}: 40.3°
depth: 2.1(m)

Mine Shape Parameters (30/12-1778)

d: 0.04(m)
L: 0.121(m)
m: 0.254(m)
J_1: 2.71e-005(kg*m^2)
J_2: 0.000321(kg*m^2)
J_3: 0.000321(kg*m^2)
χ: 0.005307(m)

Final Model Parameters (30/12-1778)

time: 1.53(s)
xy_{fm}: 0.394(m)
V_{xfm}: -0.0193(m/s)
V_{yfm}: -0.029(m/s)
V_{zfm}: -1.38(m/s)
Ψ_{fm}: 86.42°
depth: 2.13(m)

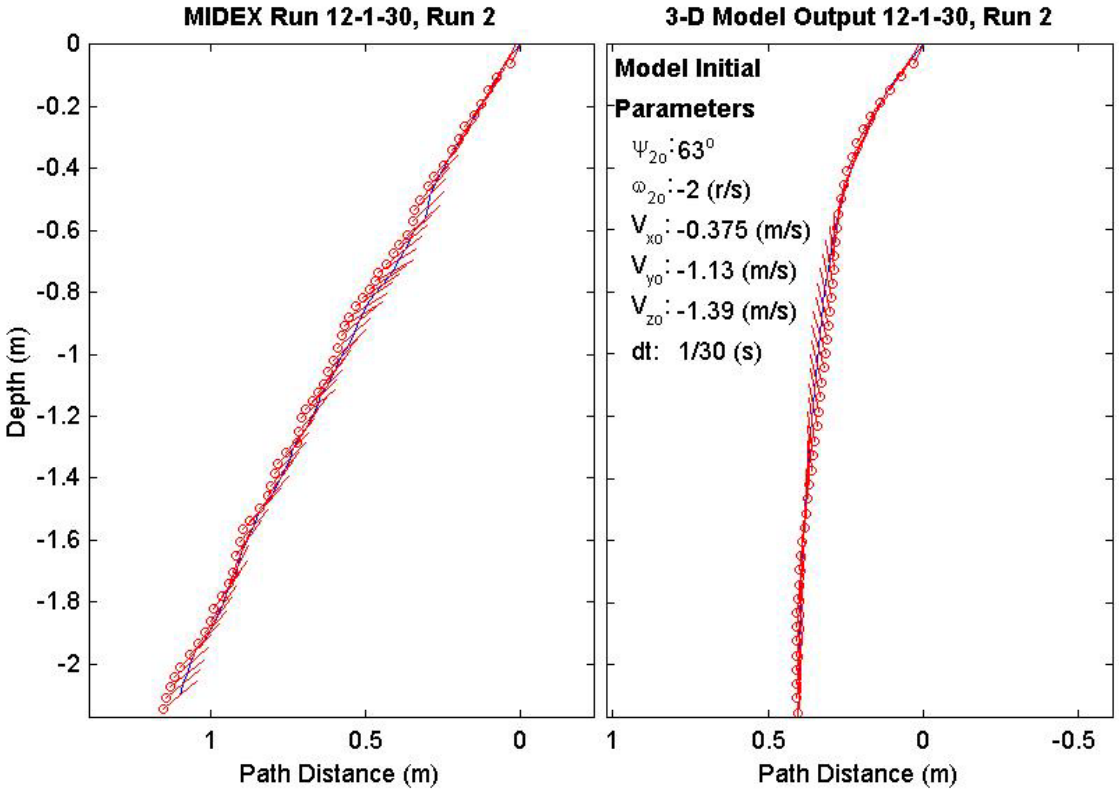

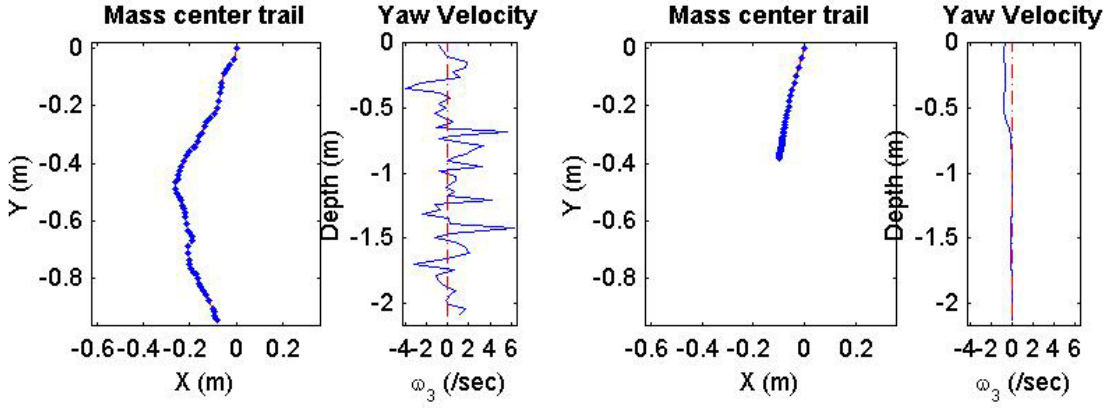

Final Drop Parameters (30/12-1795)

time: 1.57(s)
xy_{fe}: 0.0763(m)
V_{xfe}: 0.108(m/s)
V_{yfe}: 0.375(m/s)
V_{zfe}: -1.02(m/s)
Ψ_{fe}: 38.4°
depth: 2.17(m)

Mine Shape Parameters (30/12-1795)

d: 0.04(m)
L: 0.121(m)
m: 0.254(m)
J_1: 2.71e-005($kg*m^2$)
J_2: 0.000321($kg*m^2$)
J_3: 0.000321($kg*m^2$)
χ: 0.005307(m)

Final Model Parameters (30/12-1795)

time: 1.57(s)
xy_{fm}: 0.303(m)
V_{xfm}: 0.021(m/s)
V_{yfm}: 0.012(m/s)
V_{zfm}: -1.37(m/s)
Ψ_{fm}: 93.3°
depth: 2.18(m)

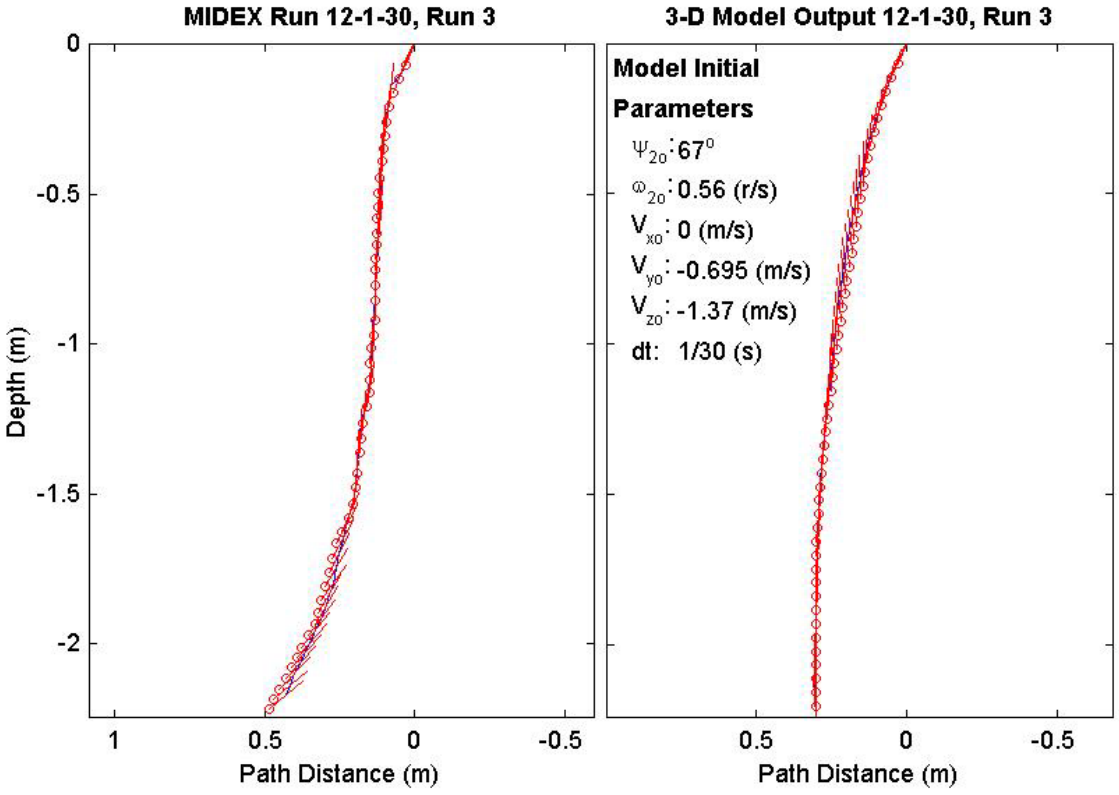

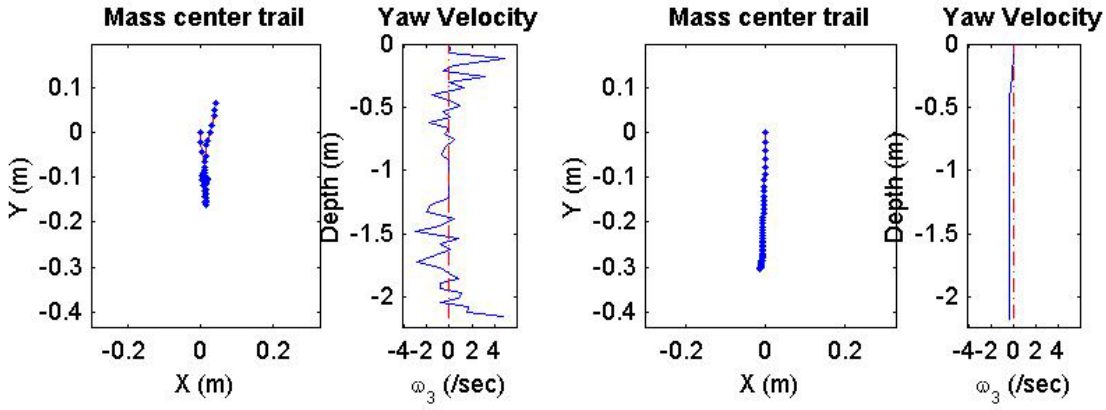

Final Drop Parameters (30/12-1604)

time: 2(s)
xy_{fe}: 0.966(m)
V_{xfe}: -0.159(m/s)
V_{yfe}: -0.695(m/s)
V_{zfe}: -1.58(m/s)
Ψ_{fe}: 51.9°
depth: 2.12(m)

Mine Shape Parameters (30/12-1604)

d: 0.04(m)
L: 0.121(m)
m: 0.254(m)
J_1: 2.71e-005(kg*m^2)
J_2: 0.000321(kg*m^2)
J_3: 0.000321(kg*m^2)
χ: 0.005307(m)

Final Model Parameters (30/12-1604)

time: 1.5(s)
xy_{fm}: 0.329(m)
V_{xfm}: -0.0214(m/s)
V_{yfm}: -0.0185(m/s)
V_{zfm}: -1.38(m/s)
Ψ_{fm}: 85.08°
depth: 2.12(m)

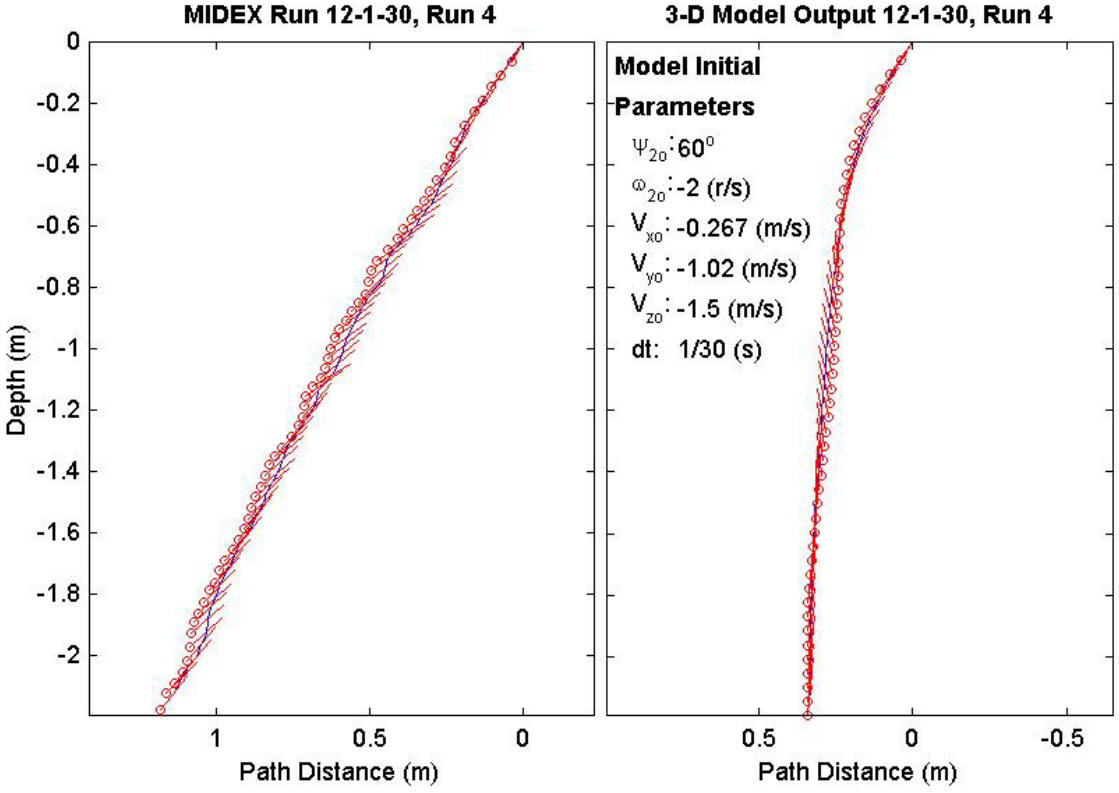

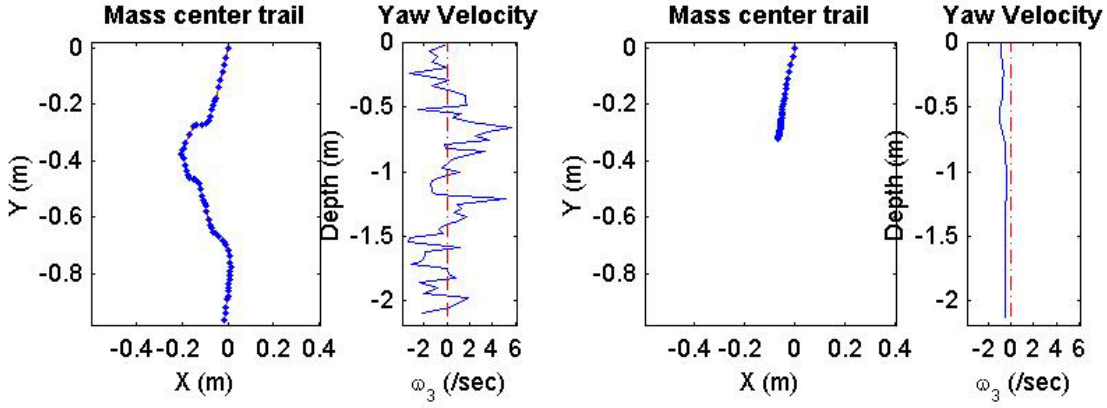

Final Drop Parameters (30/12-1238)

time: 2.27(s)
xy_{fe}: 0.625(m)
V_{xfe}: 0.213(m/s)
V_{yfe}: 0.537(m/s)
V_{zfe}: -1.05(m/s)
Ψ_{fe}: 41.3°
depth: 2.23(m)

Mine Shape Parameters (30/12-1238)

d: 0.04(m)
L: 0.121(m)
m: 0.254(m)
J_1: 2.71e-005(kg*m^2)
J_2: 0.000321(kg*m^2)
J_3: 0.000321(kg*m^2)
χ: 0.005307(m)

Final Model Parameters (30/12-1238)

time: 1.67(s)
xy_{fm}: 0.216(m)
V_{xfm}: -0.0459(m/s)
V_{yfm}: -0.00463(m/s)
V_{zfm}: -1.37(m/s)
Ψ_{fm}: 90.48°
depth: 2.25(m)

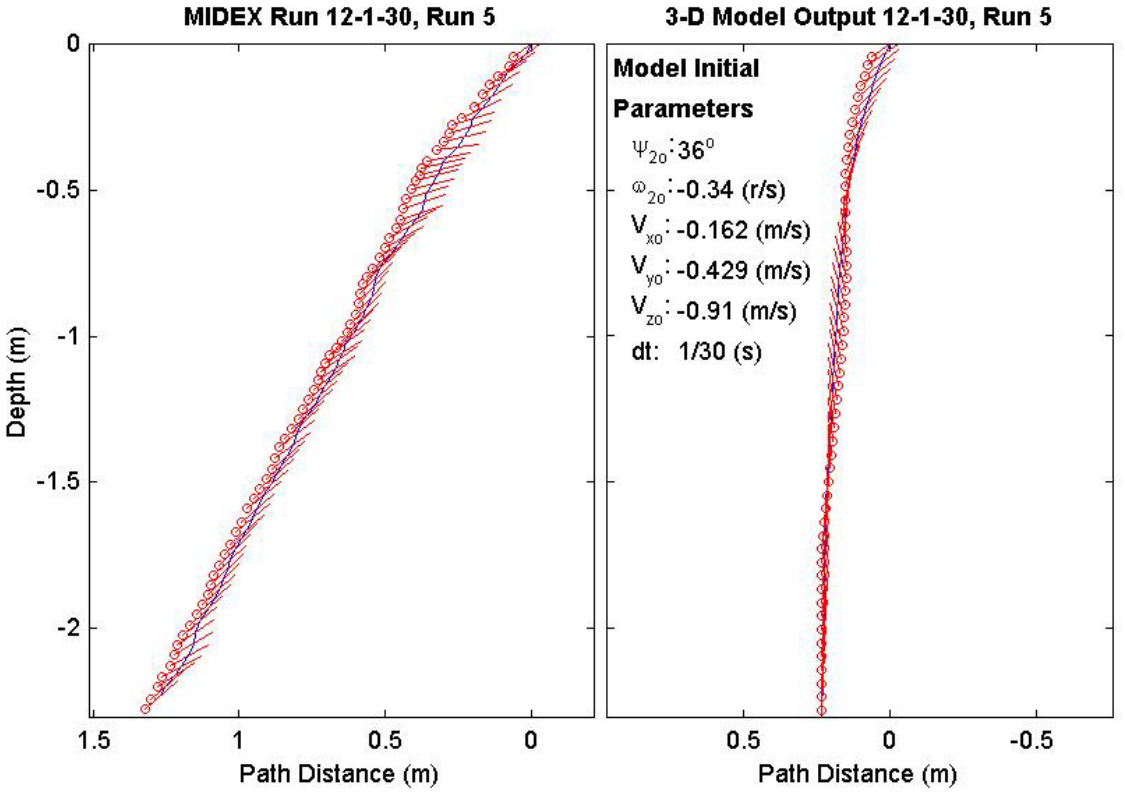

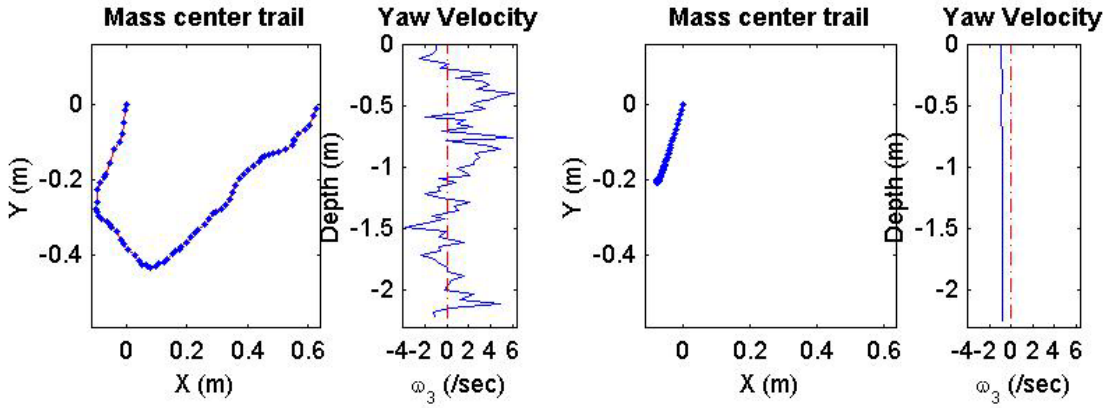

Final Drop

Parameters (30/9-2980)

time: 2.3(s)
xy_{fe}: 0.329(m)
V_{xfe}: 0(m/s)
V_{yfe}: -0.213(m/s)
V_{zfe}: -0.752(m/s)
Ψ_{fe}: 47.8°
depth: 2.25(m)

Mine Shape

Parameters (30/9-2980)

d: 0.04(m)
L: 0.0912(m)
m: 0.215(m)
J_1: 2.35e-005(kg*m^2)
J_2: 0.000158(kg*m^2)
J_3: 0.000158(kg*m^2)
χ: 0.002911(m)

Final Model

Parameters (30/9-2980)

time: 1.53(s)
xy_{fm}: 0.201(m)
V_{xfm}: -0.0437(m/s)
V_{yfm}: -0.00673(m/s)
V_{zfm}: -1.41(m/s)
Ψ_{fm}: 82.59°
depth: 2.26(m)

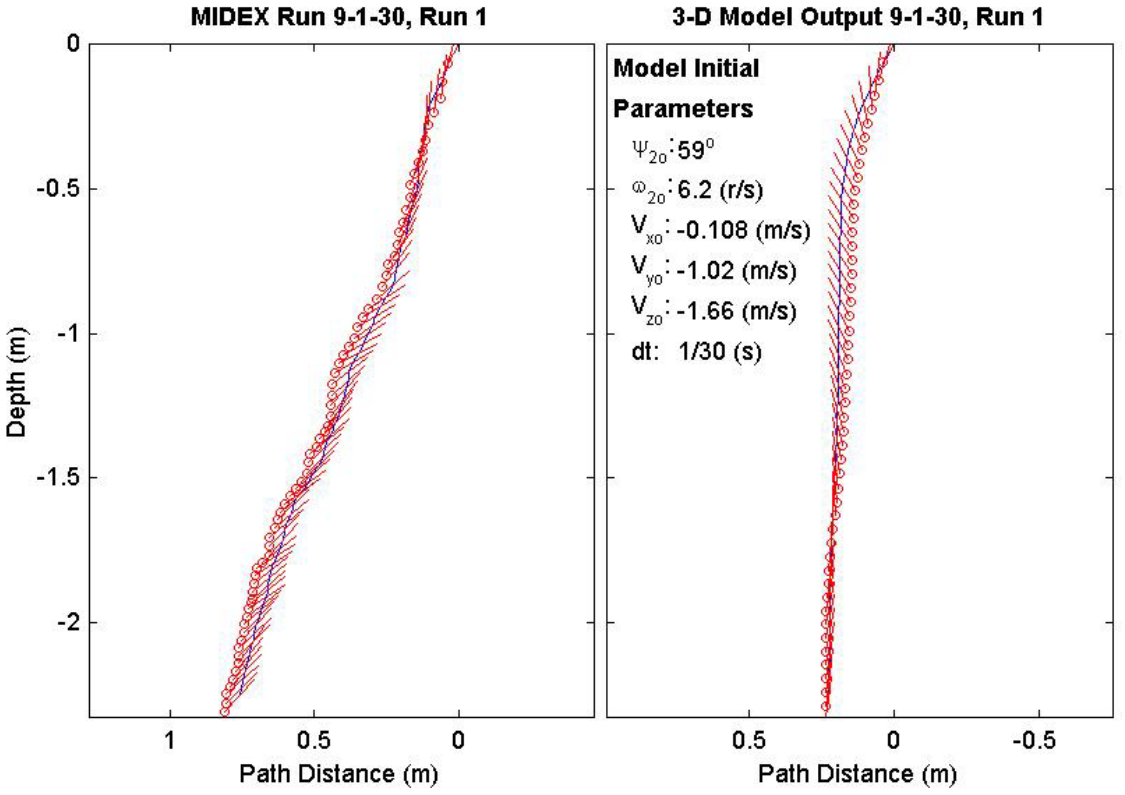

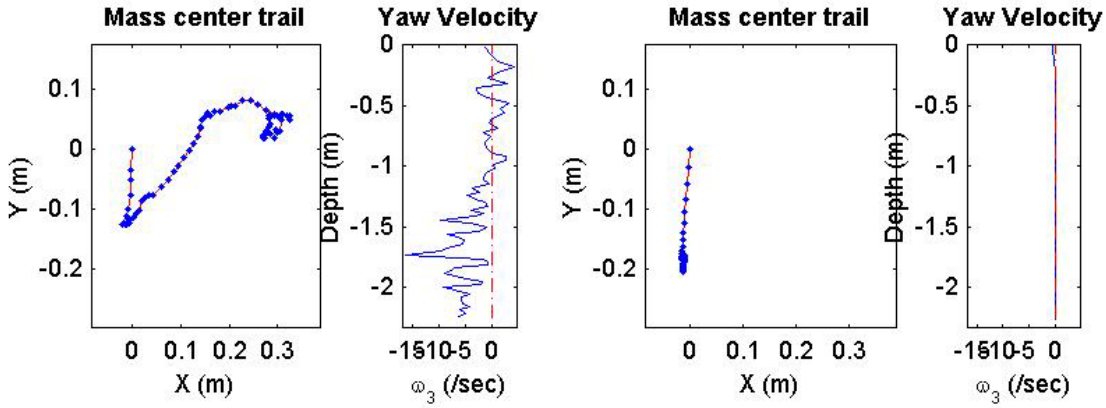

Final Drop

Parameters (30/9-1984)

time: 2.27(s)
xy_{fe}: 0.27(m)
V_{xfe}: -0.108(m/s)
V_{yfe}: 0.375(m/s)
V_{zfe}: -0.804(m/s)
Ψ_{fe}: 40.5^0
depth: 2.17(m)

Mine Shape

Parameters (30/9-1984)

d: 0.04(m)
L: 0.0912(m)
m: 0.215(m)
J_1: 2.35e-005($kg*m^2$)
J_2: 0.000158($kg*m^2$)
J_3: 0.000158($kg*m^2$)
χ: 0.002911(m)

Final Model

Parameters (30/9-1984)

time: 1.53(s)
xy_{fm}: 0.193(m)
V_{xfm}: 0.03(m/s)
V_{yfm}: 0.0234(m/s)
V_{zfm}: -1.4(m/s)
Ψ_{fm}: 79.09^0
depth: 2.21(m)

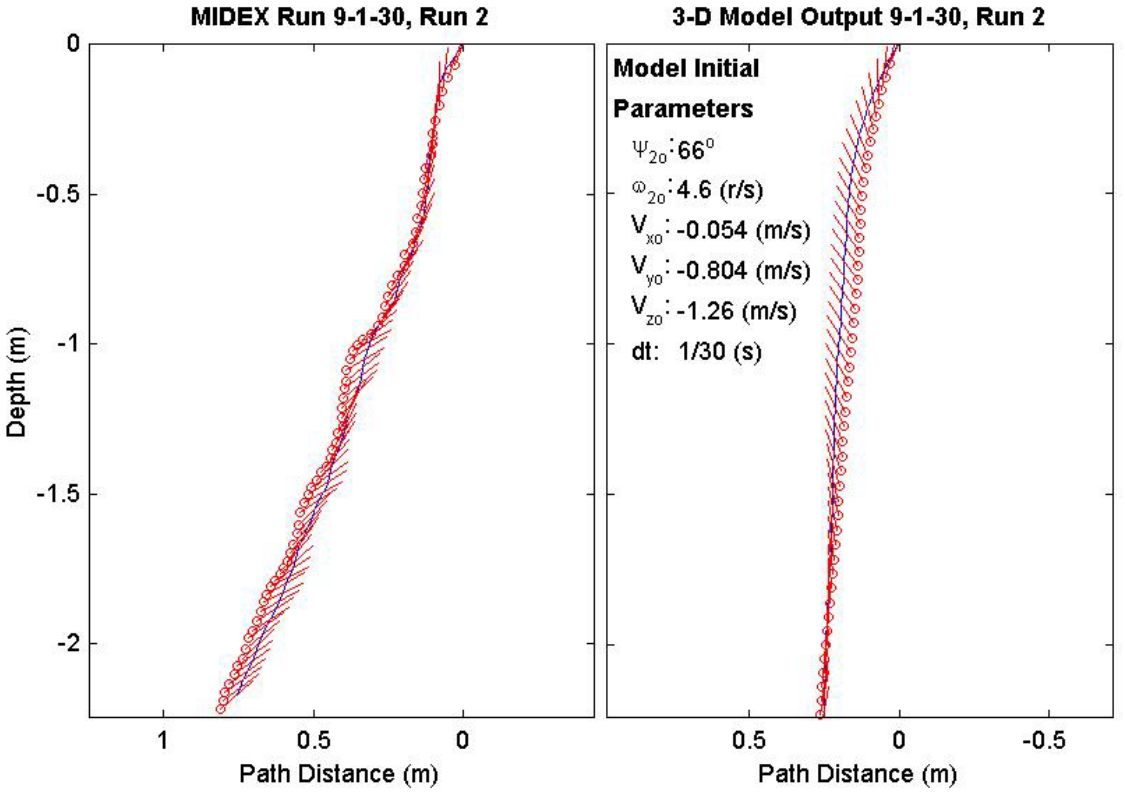

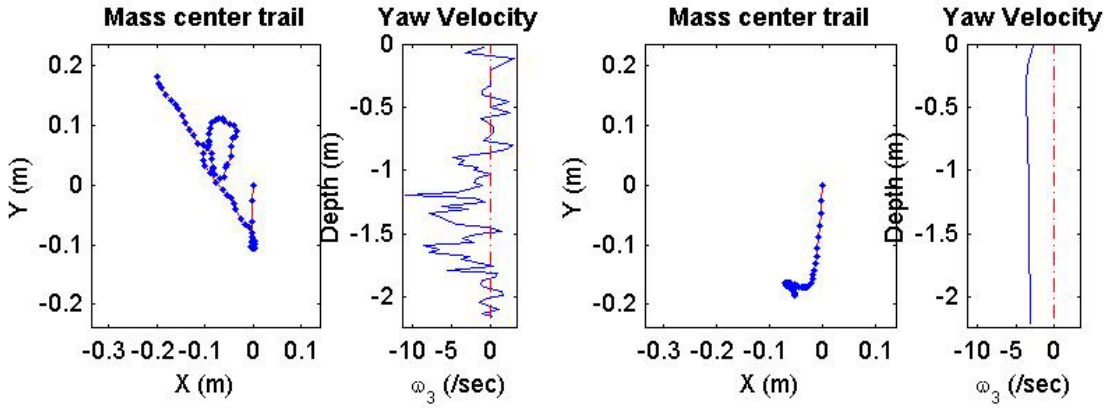

Final Drop

Parameters (30/9-1771)

time: 2.07(s)
xy_{fe}: 0.29(m)
V_{xfe}: -0.375(m/s)
V_{yfe}: -0.159(m/s)
V_{zfe}: -0.857(m/s)
Ψ_{fe}: 31.1°
depth: 2.17(m)

Mine Shape

Parameters (30/9-1771)

d: 0.04(m)
L: 0.0912(m)
m: 0.215(m)
J_1: 2.35e-005(kg*m^2)
J_2: 0.000158(kg*m^2)
J_3: 0.000158(kg*m^2)
χ: 0.002911(m)

Final Model

Parameters (30/9-1771)

time: 1.5(s)
xy_{fm}: 0.152(m)
V_{xfm}: -0.0376(m/s)
V_{yfm}: 0.0309(m/s)
V_{zfm}: -1.41(m/s)
Ψ_{fm}: 83.08°
depth: 2.21(m)

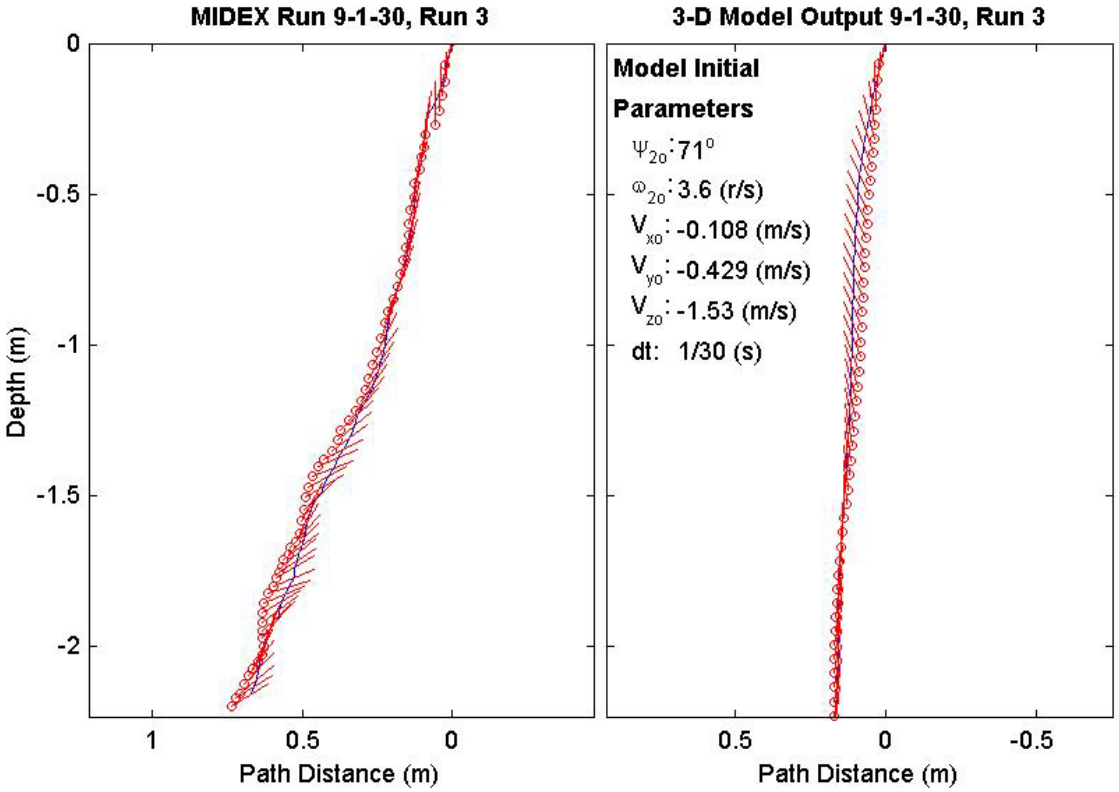

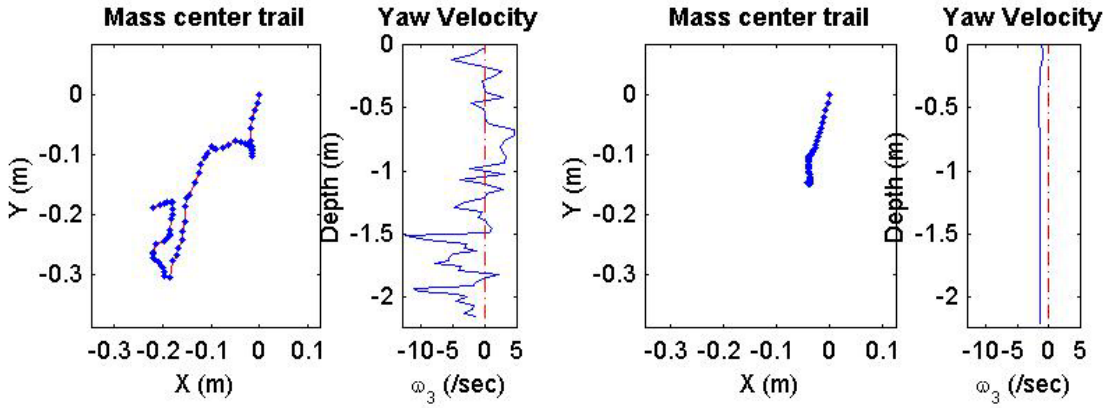

Final Drop
Parameters (30/9-1586)

time: 2.1(s)
xy_{fe}: 0.616(m)
V_{xfe}: -0.162(m/s)
V_{yfe}: 0.054(m/s)
V_{zfe}: -0.938(m/s)
Ψ_{fe}: 34.6°
depth: 2.17(m)

Mine Shape
Parameters (30/9-1586)

d: 0.04(m)
L: 0.0912(m)
m: 0.215(m)
J_1: 2.35e-005(kg*m^2)
J_2: 0.000158(kg*m^2)
J_3: 0.000158(kg*m^2)
χ: 0.002911(m)

Final Model
Parameters (30/9-1586)

time: 1.5(s)
xy_{fm}: 0.163(m)
V_{xfm}: -0.0103(m/s)
V_{yfm}: 0.00473(m/s)
V_{zfm}: -1.39(m/s)
Ψ_{fm}: 92.79°
depth: 2.18(m)

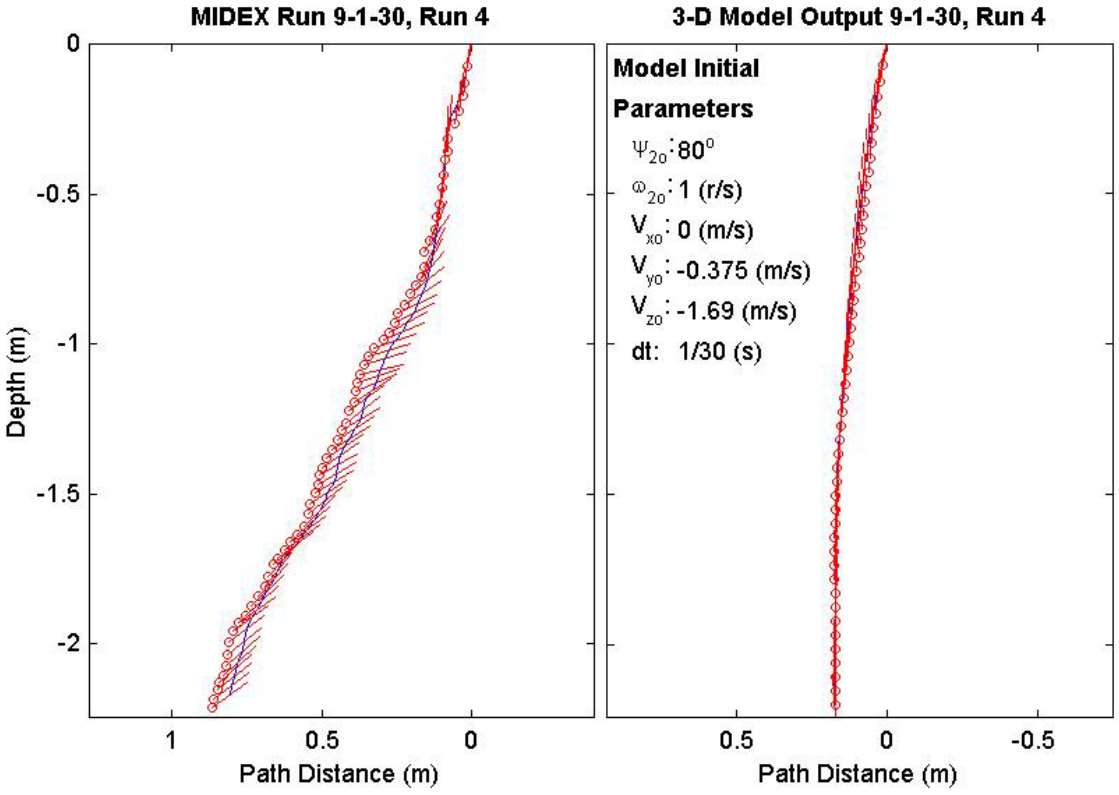

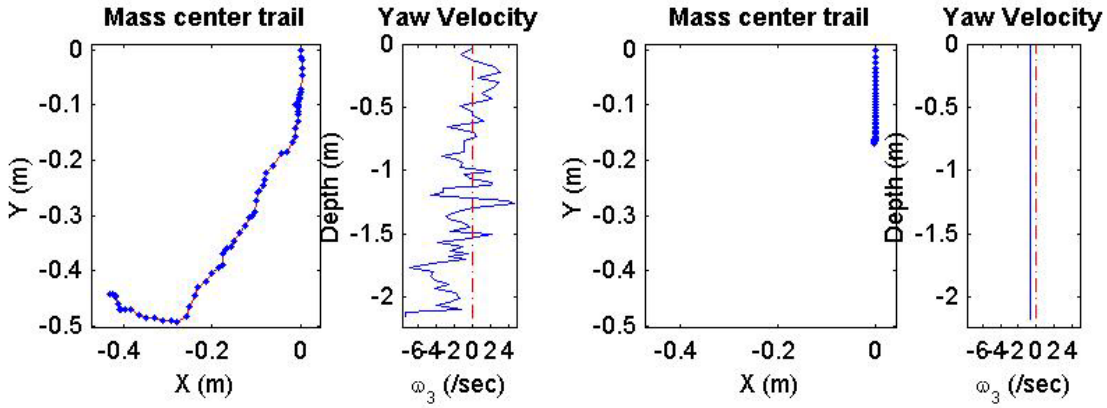

Final Drop

Parameters (30/9-1204)

time: 2.43(s)
xy_{fe}: 0.343(m)
V_{xfe}: -0.375(m/s)
V_{yfe}: 0(m/s)
V_{zfe}: -0.858(m/s)
Ψ_{fe}: 42.2°
depth: 2.17(m)

Mine Shape

Parameters (30/9-1204)

d: 0.04(m)
L: 0.0912(m)
m: 0.215(m)
J_1: 2.35e-005(kg*m^2)
J_2: 0.000158(kg*m^2)
J_3: 0.000158(kg*m^2)
χ: 0.002911(m)

Final Model

Parameters (30/9-1204)

time: 1.53(s)
xy_{fm}: 0.236(m)
V_{xfm}: -0.0514(m/s)
V_{yfm}: -0.00364(m/s)
V_{zfm}: -1.4(m/s)
Ψ_{fm}: 86.13°
depth: 2.21(m)

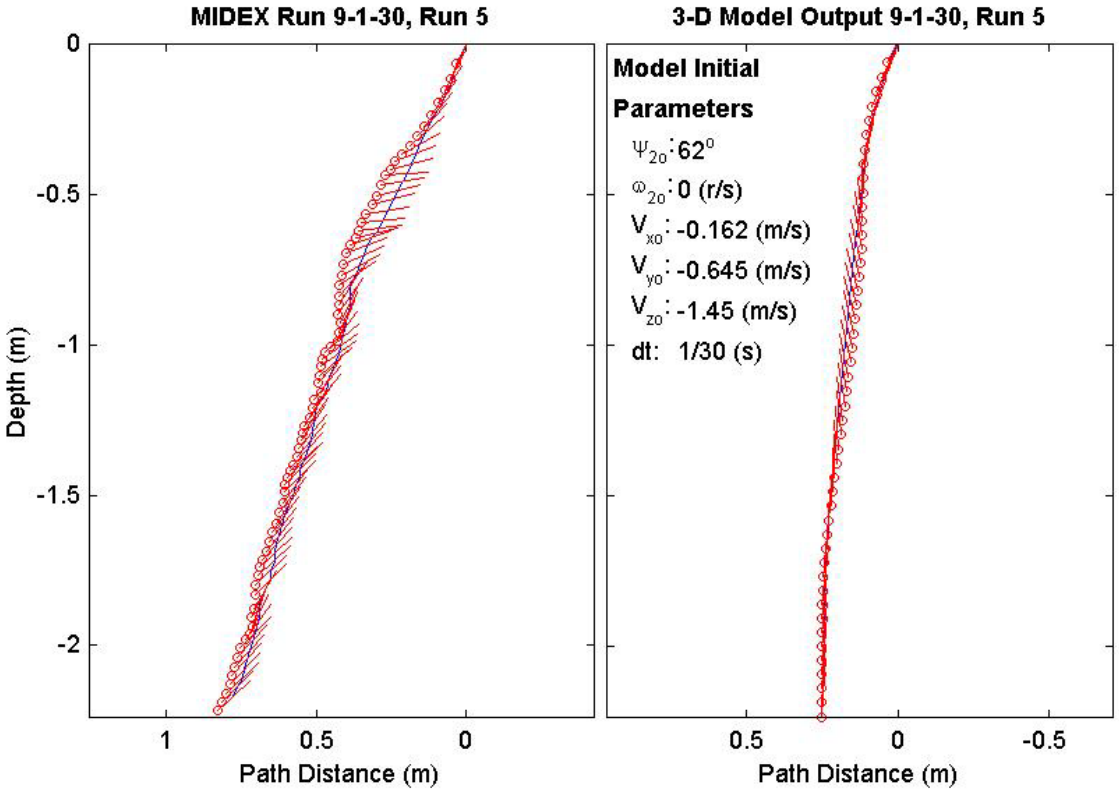

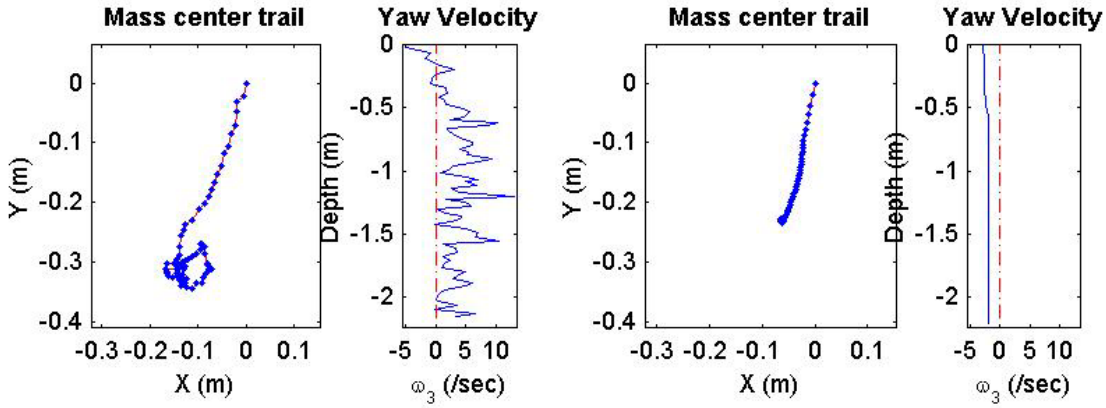

Final Drop

Parameters (45/15-2945)

time: 1.6(s)
xy_{fe}: 0.378(m)
V_{xfe}: -0.163(m/s)
V_{yfe}: 0.429(m/s)
V_{zfe}: -0.883(m/s)
Ψ_{fe}: 32.8°
depth: 2.17(m)

Mine Shape

Parameters (45/15-2945)

d: 0.04(m)
L: 0.152(m)
m: 0.323(m)
J_1: 3.3e-005(kg*m^2)
J_2: 0.000578(kg*m^2)
J_3: 0.000578(kg*m^2)
χ: 0.007411(m)

Final Model

Parameters (45/15-2945)

time: 1.33(s)
xy_{fm}: 0.347(m)
V_{xfm}: 0.0361(m/s)
V_{yfm}: -0.0213(m/s)
V_{zfm}: -1.52(m/s)
Ψ_{fm}: 89.66°
depth: 2.22(m)

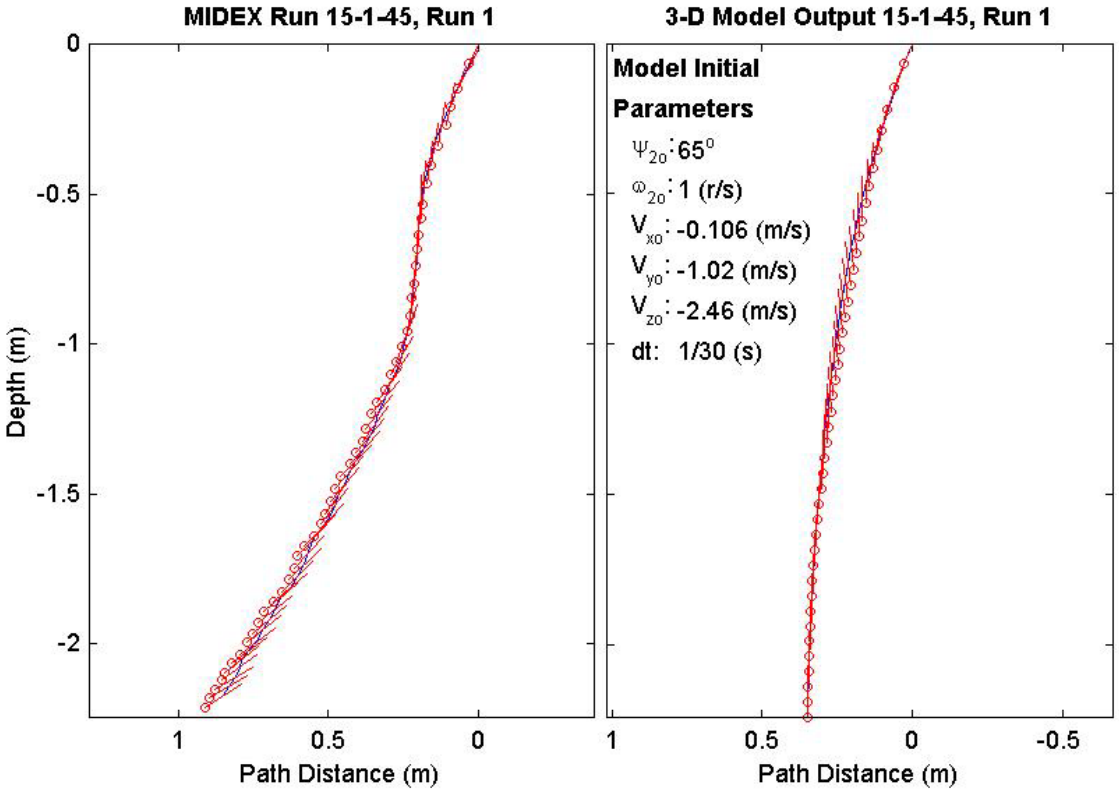

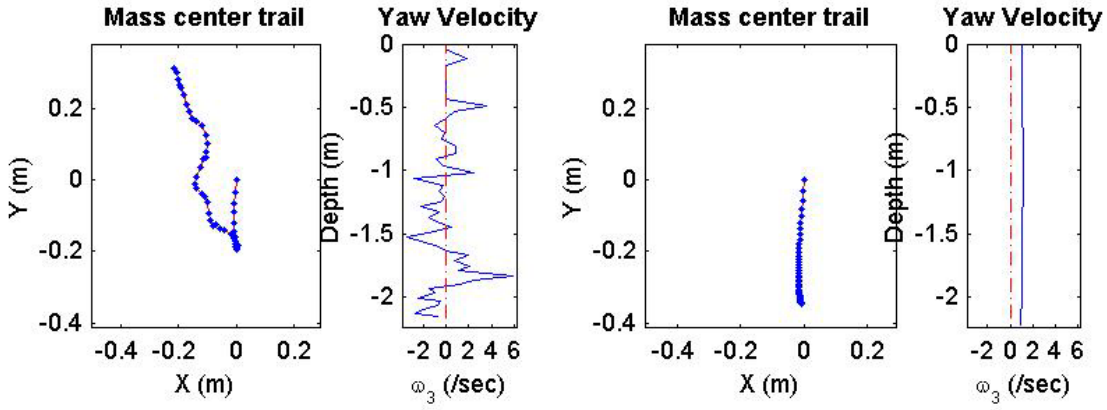

Final Drop

Parameters (45/15-2623)

time: 1.43(s)
xy_{fe}: 0.121(m)
V_{xfe}: -0.321(m/s)
V_{yfe}: 0.591(m/s)
V_{zfe}: -0.99(m/s)
Ψ_{fe}: 44.2°
depth: 2.15(m)

Mine Shape

Parameters (45/15-2623)

d: 0.04(m)
L: 0.152(m)
m: 0.323(m)
J_1: 3.3e-005(kg*m^2)
J_2: 0.000578(kg*m^2)
J_3: 0.000578(kg*m^2)
χ: 0.007411(m)

Final Model

Parameters (45/15-2623)

time: 1.33(s)
xy_{fm}: 0.31(m)
V_{xfm}: -0.00474(m/s)
V_{yfm}: -3.21e-017(m/s)
V_{zfm}: -1.52(m/s)
Ψ_{fm}: 90.61°
depth: 2.16(m)

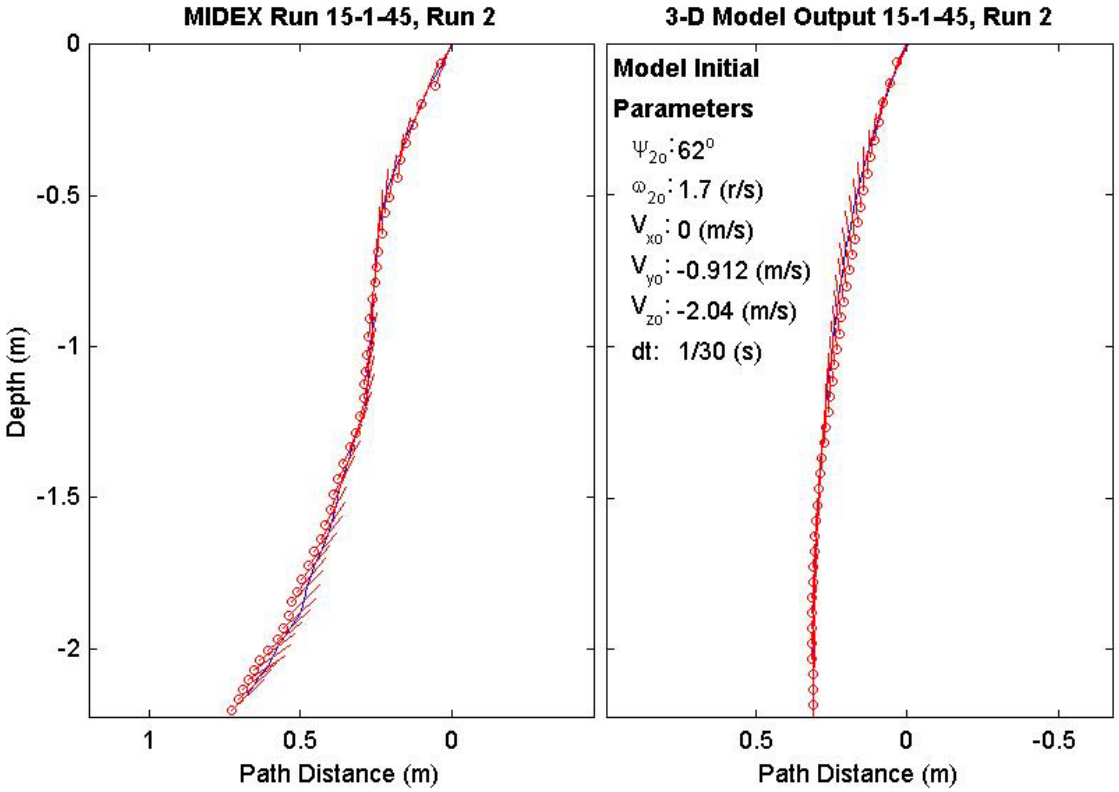

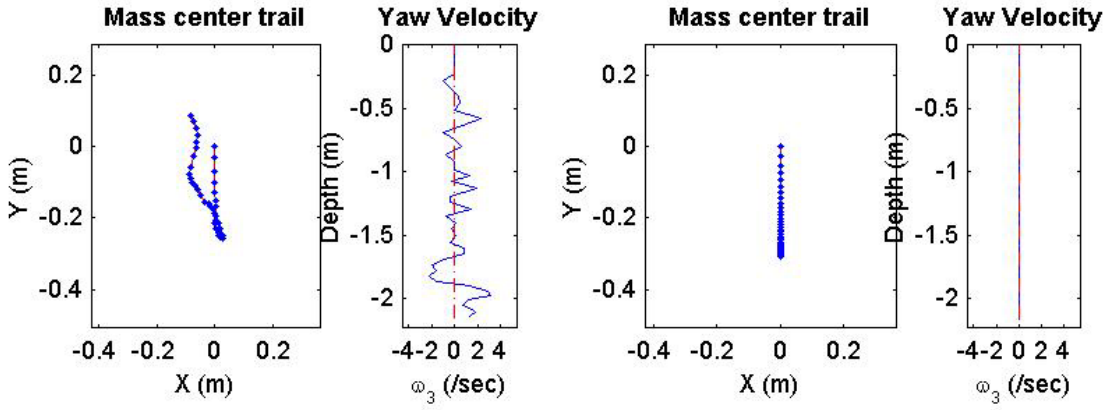

Final Drop

Parameters (45/15-2203)

time: 1.27(s)
xy_{fe}: 0.0488(m)
V_{xfe}: -0.055(m/s)
V_{yfe}: 0.163(m/s)
V_{zfe}: -1.5(m/s)
Ψ_{fe}: 78°
depth: 2.12(m)

Mine Shape

Parameters (45/15-2203)

d: 0.04(m)
L: 0.152(m)
m: 0.323(m)
J_1: 3.3e-005(kg*m^2)
J_2: 0.000578(kg*m^2)
J_3: 0.000578(kg*m^2)
χ: 0.007411(m)

Final Model

Parameters (45/15-2203)

time: 1.37(s)
xy_{fm}: 0.33(m)
V_{xfm}: 0.0027(m/s)
V_{yfm}: 0.0035(m/s)
V_{zfm}: -1.52(m/s)
Ψ_{fm}: 92.21°
depth: 2.17(m)

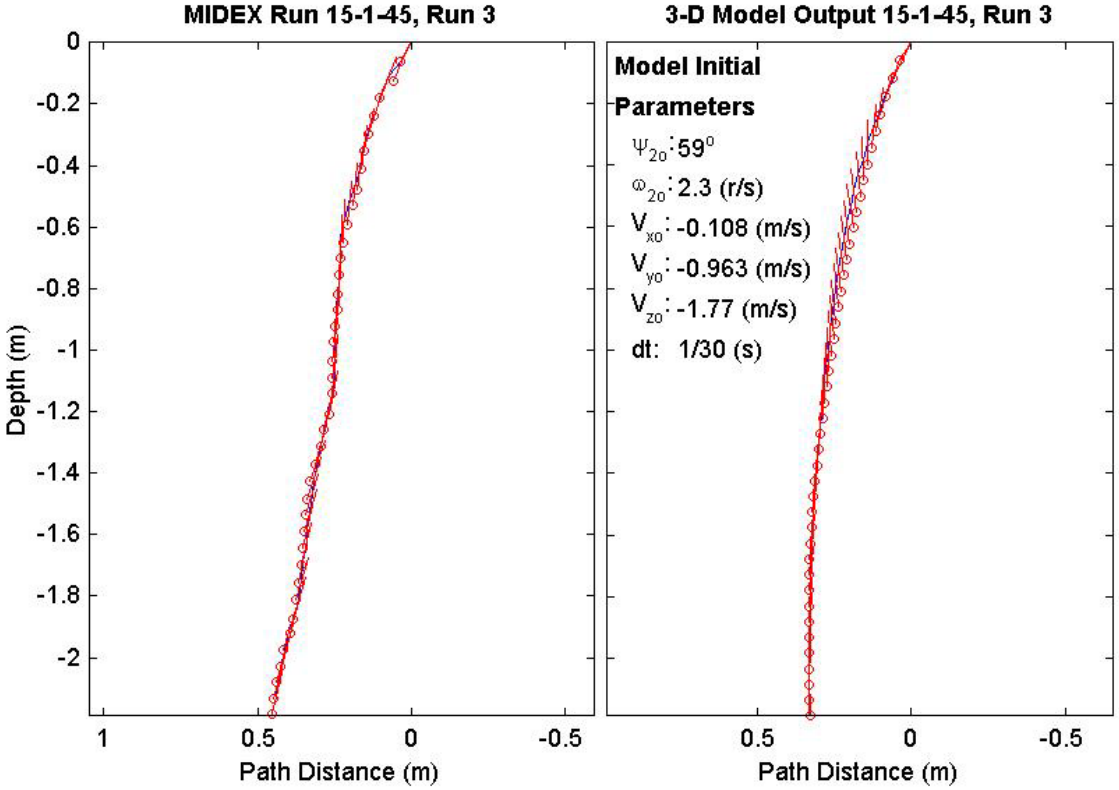

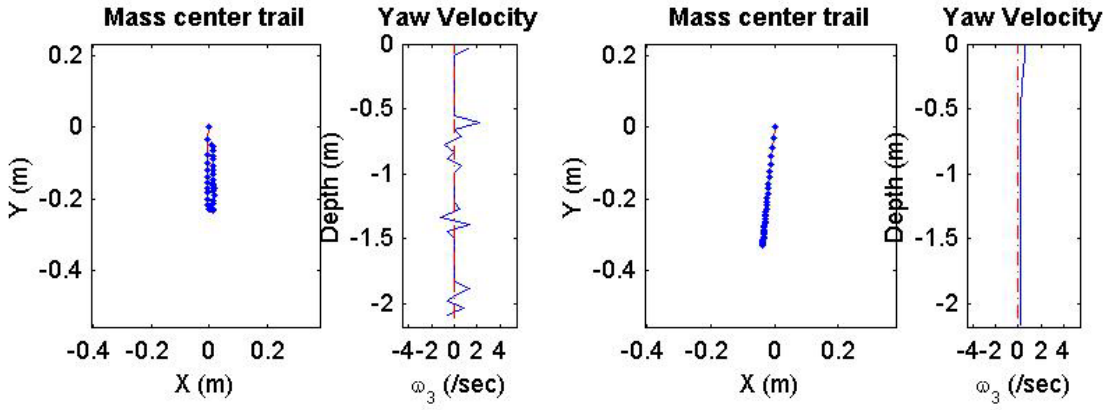

Final Drop Parameters (45/15-1703)

time: 1.23(s)
xy_{fe}: 0.264(m)
V_{xfe}: -0.055(m/s)
V_{yfe}: -0.055(m/s)
V_{zfe}: -1.71(m/s)
Ψ_{fe}: 84.5°
depth: 2.15(m)

Mine Shape Parameters (45/15-1703)

d: 0.04(m)
L: 0.152(m)
m: 0.323(m)
J_1: 3.3e-005(kg*m^2)
J_2: 0.000578(kg*m^2)
J_3: 0.000578(kg*m^2)
χ: 0.007411(m)

Final Model Parameters (45/15-1703)

time: 1.33(s)
xy_{fm}: 0.512(m)
V_{xfm}: 0.0823(m/s)
V_{yfm}: -0.038(m/s)
V_{zfm}: -1.52(m/s)
Ψ_{fm}: 90.06°
depth: 2.2(m)

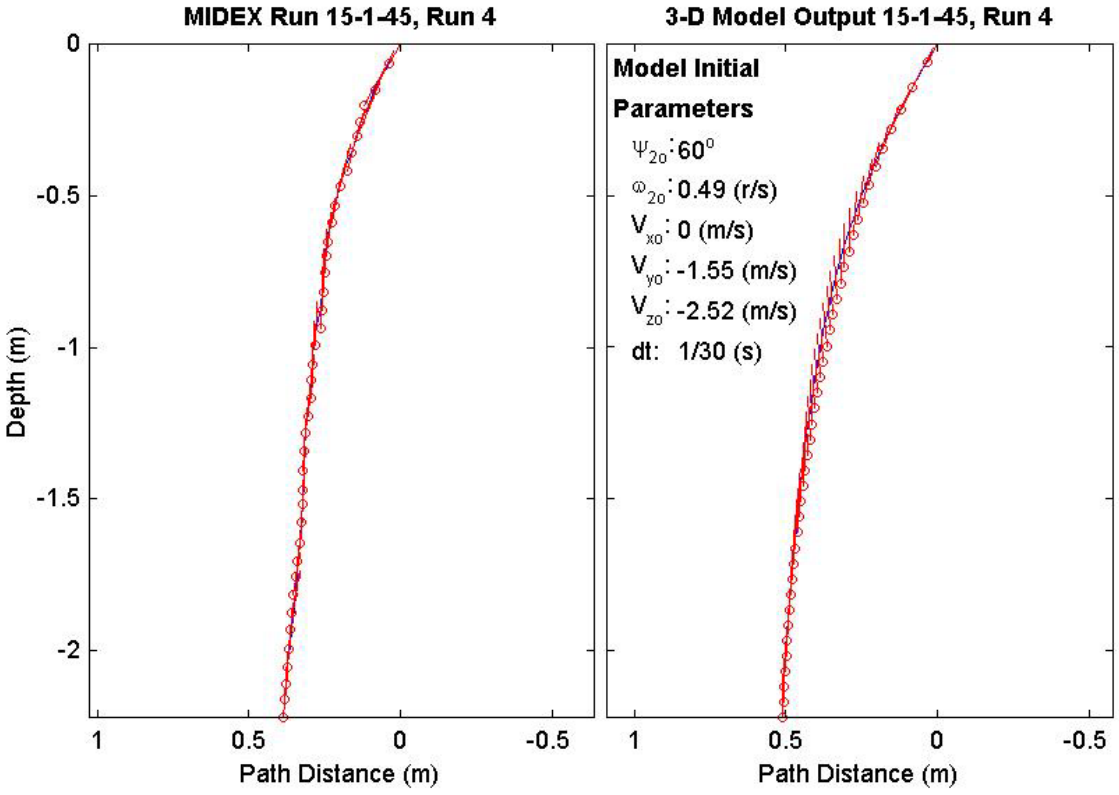

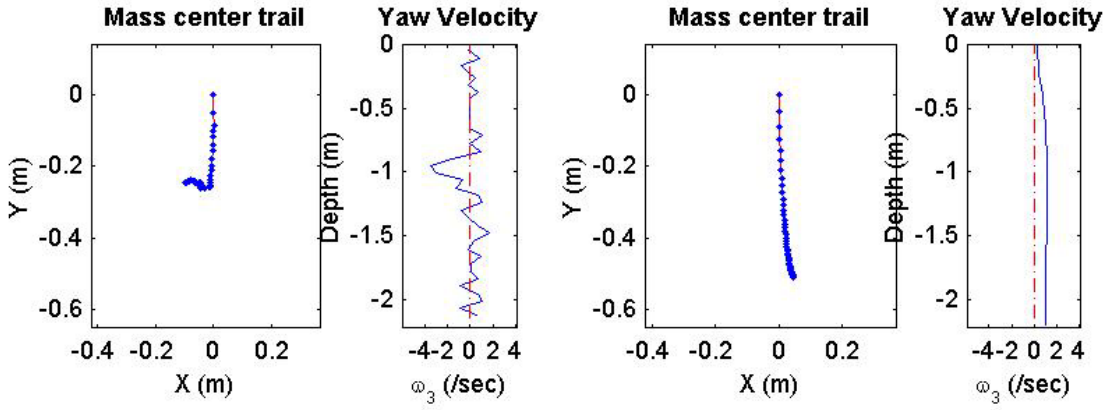

Final Drop
Parameters (45/15-1460)

time: 1.63(s)
xy_{fe}: 0.988(m)
V_{xfe}: 0.429(m/s)
V_{yfe}: -0.588(m/s)
V_{zfe}: -1.34(m/s)
Ψ_{fe}: 45.8°
depth: 2.1(m)

Mine Shape
Parameters (45/15-1460)

d: 0.04(m)
L: 0.152(m)
m: 0.323(m)
J_1: 3.3e-005(kg*m^2)
J_2: 0.000578(kg*m^2)
J_3: 0.000578(kg*m^2)
χ: 0.007411(m)

Final Model
Parameters (45/15-1460)

time: 1.37(s)
xy_{fm}: 0.27(m)
V_{xfm}: -0.0249(m/s)
V_{yfm}: 6.63e-018(m/s)
V_{zfm}: -1.52(m/s)
Ψ_{fm}: 89.14°
depth: 2.12(m)

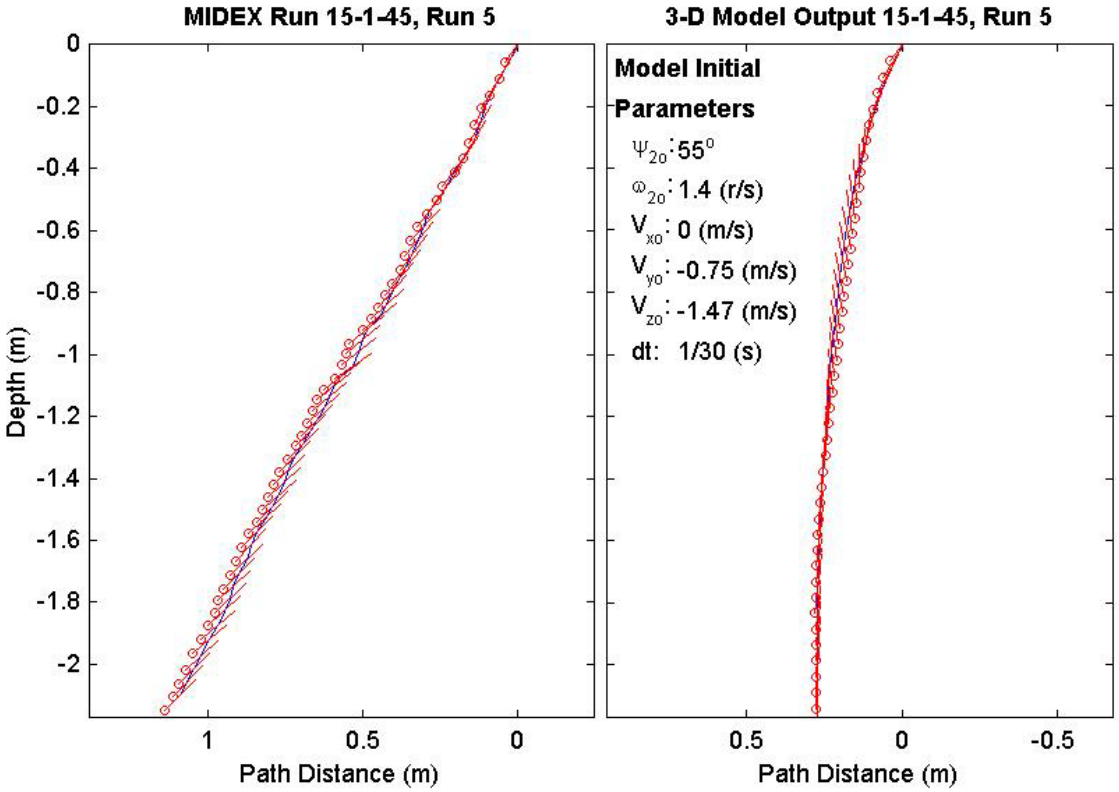

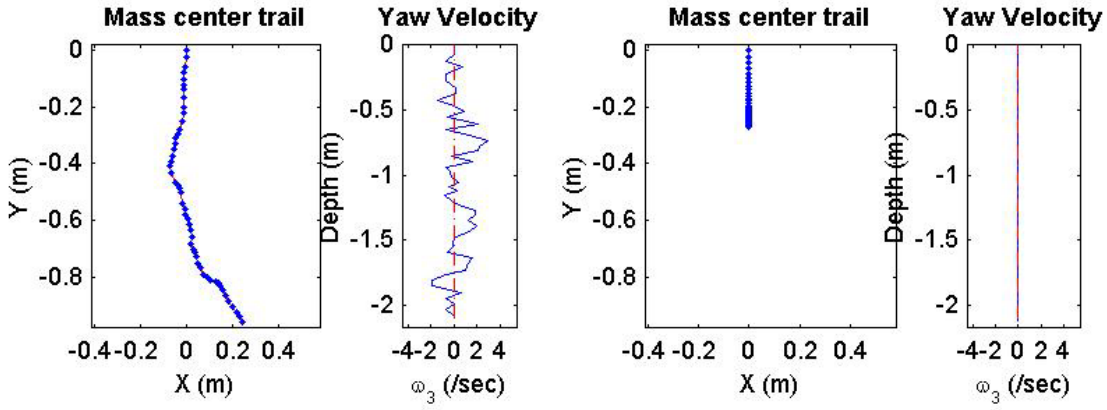

Final Drop

Parameters (45/12-2788)

time: 2(s)
xy_{fe}: 0.657(m)
V_{xfe}: 0.483(m/s)
V_{yfe}: 0.213(m/s)
V_{zfe}: -0.885(m/s)
Ψ_{fe}: 42.4°
depth: 2.16(m)

Mine Shape

Parameters (45/12-2788)

d: 0.04(m)
L: 0.121(m)
m: 0.254(m)
J_1: 2.71e-005(kg*m^2)
J_2: 0.000321(kg*m^2)
J_3: 0.000321(kg*m^2)
χ: 0.005307(m)

Final Model

Parameters (45/12-2788)

time: 1.53(s)
xy_{fm}: 0.329(m)
V_{xfm}: 0.0486(m/s)
V_{yfm}: -0.00916(m/s)
V_{zfm}: -1.37(m/s)
Ψ_{fm}: 94.1°
depth: 2.19(m)

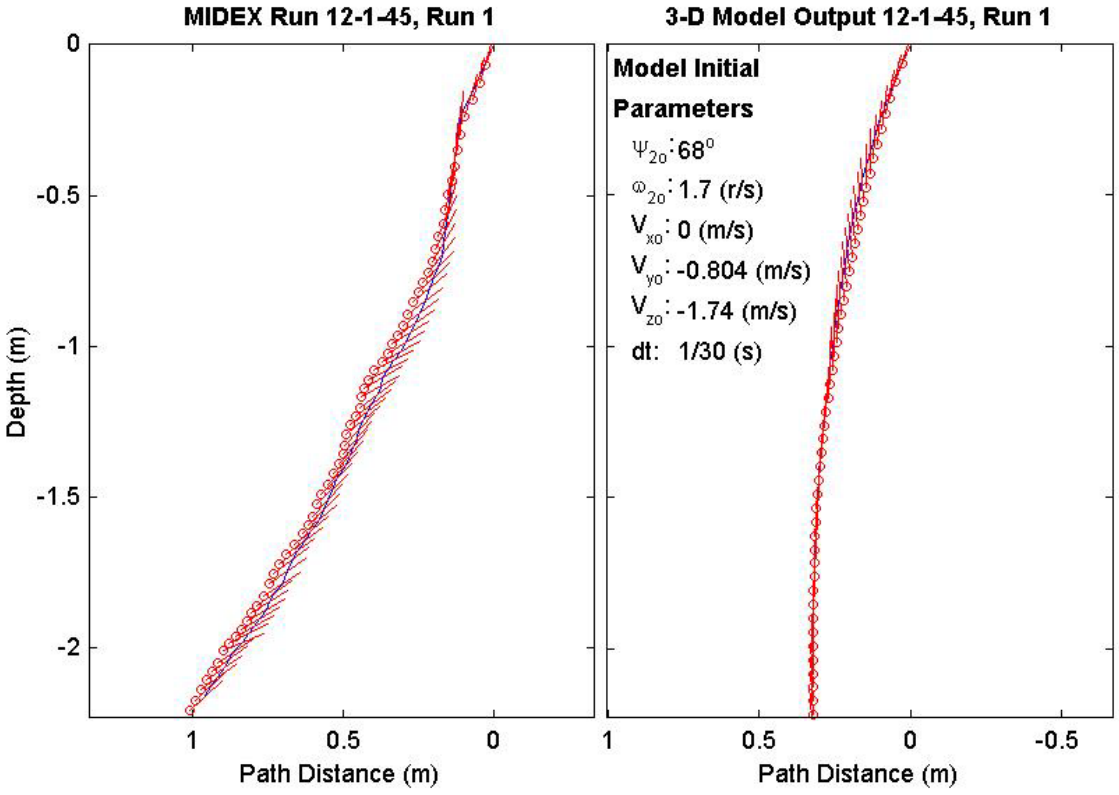

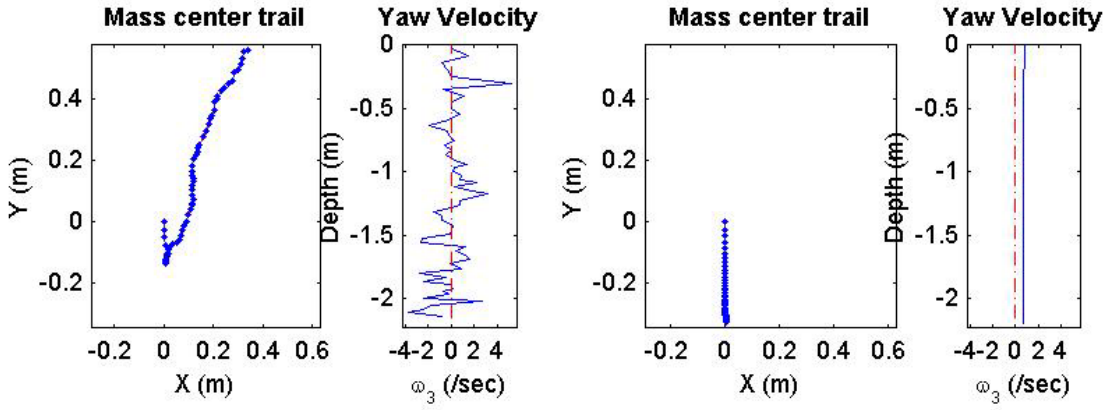

Final Drop

Parameters (45/12-2803)

time: 2.03(s)
xy_{fe}: 0.488(m)
V_{xfe}: -0.159(m/s)
V_{yfe}: 0.267(m/s)
V_{zfe}: -0.909(m/s)
Ψ_{fe}: 46.9°
depth: 2.16(m)

Mine Shape

Parameters (45/12-2803)

d: 0.04(m)
L: 0.121(m)
m: 0.254(m)
J_1: 2.71e-005($kg*m^2$)
J_2: 0.000321($kg*m^2$)
J_3: 0.000321($kg*m^2$)
χ: 0.005307(m)

Final Model

Parameters (45/12-2803)

time: 1.5(s)
xy_{fm}: 0.255(m)
V_{xfm}: 0.00726(m/s)
V_{yfm}: 0.0135(m/s)
V_{zfm}: -1.37(m/s)
Ψ_{fm}: 96.24°
depth: 2.17(m)

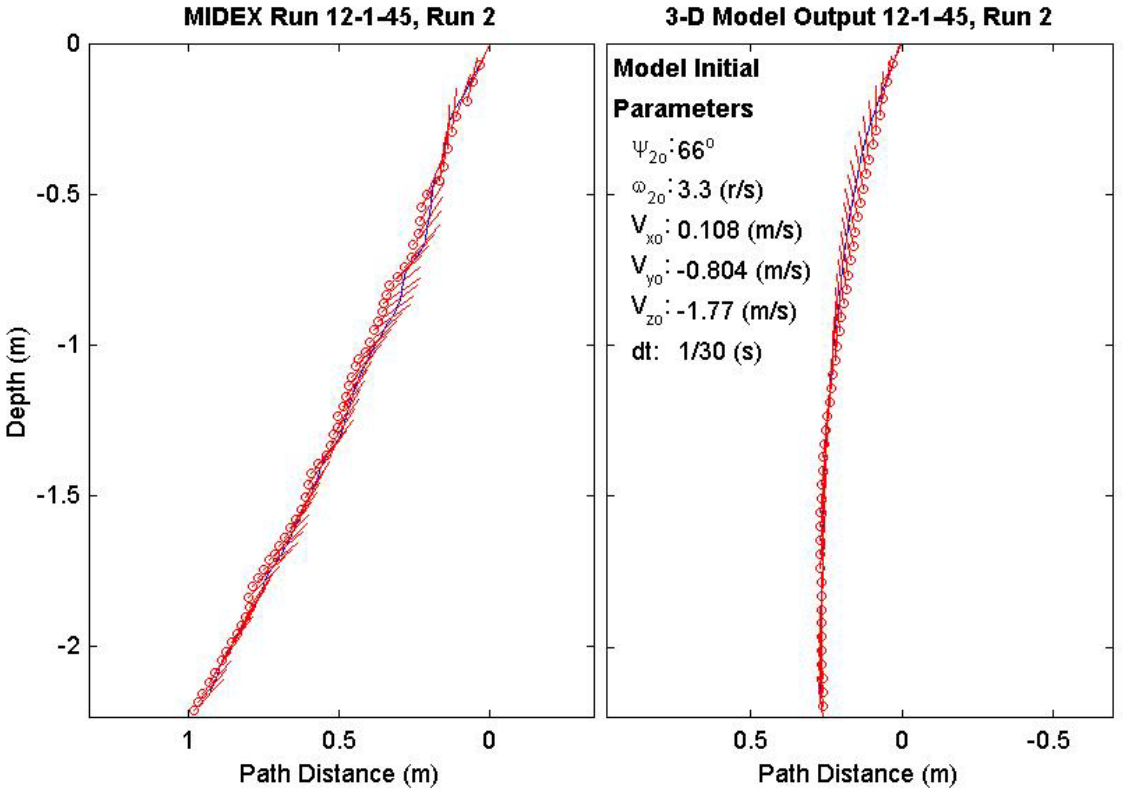

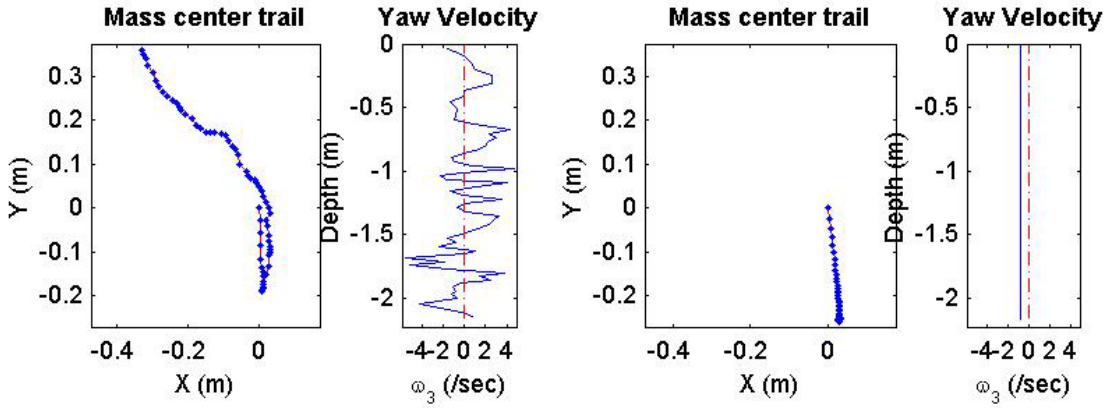

Final Drop Parameters (45/12-2305)

time: 1.43(s)
xy_{fe}: 0.189(m)
V_{xfe}: 0.321(m/s)
V_{yfe}: 0.105(m/s)
V_{zfe}: -1.58(m/s)
Ψ_{fe}: 86.2°
depth: 2.16(m)

Mine Shape Parameters (45/12-2305)

d: 0.04(m)
L: 0.121(m)
m: 0.254(m)
J_1: 2.71e-005(kg*m^2)
J_2: 0.000321(kg*m^2)
J_3: 0.000321(kg*m^2)
χ: 0.005307(m)

Final Model Parameters (45/12-2305)

time: 1.5(s)
xy_{fm}: 0.31(m)
V_{xfm}: -0.00394(m/s)
V_{yfm}: -0.0298(m/s)
V_{zfm}: -1.37(m/s)
Ψ_{fm}: 94.25°
depth: 2.16(m)

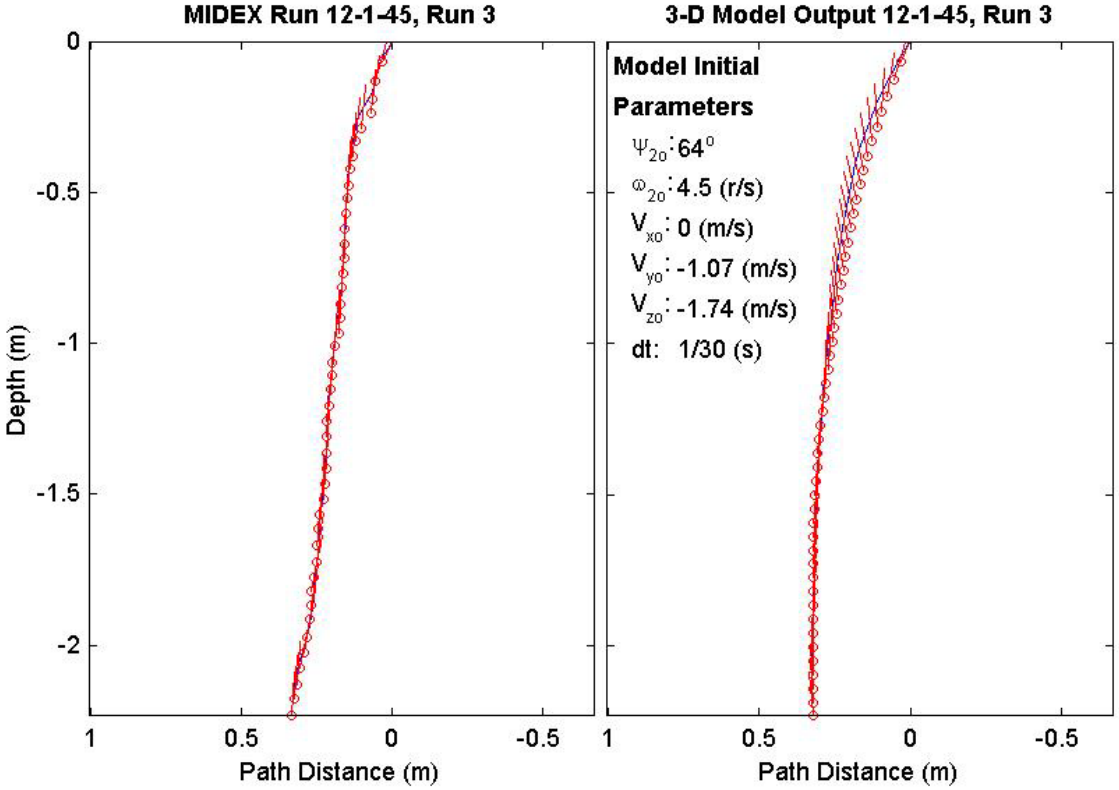

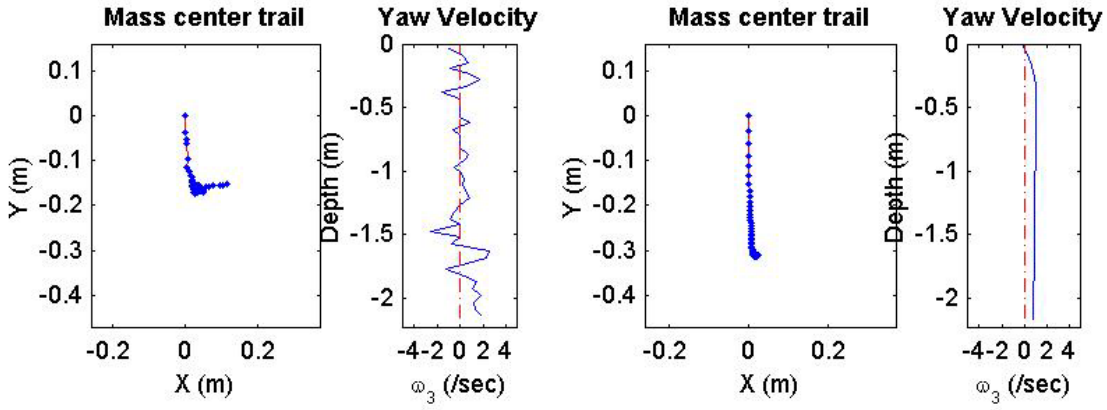

Final Drop

Parameters (45/12-2093)

time: 2(s)
xy_{fe}: 0.583(m)
V_{xfe}: -0.75(m/s)
V_{yfe}: 0.162(m/s)
V_{zfe}: -0.883(m/s)
Ψ_{fe}: 49.9°
depth: 2.17(m)

Mine Shape

Parameters (45/12-2093)

d: 0.04(m)
L: 0.121(m)
m: 0.254(m)
J_1: 2.71e-005(kg*m^2)
J_2: 0.000321(kg*m^2)
J_3: 0.000321(kg*m^2)
χ: 0.005307(m)

Final Model

Parameters (45/12-2093)

time: 1.53(s)
xy_{fm}: 0.15(m)
V_{xfm}: -0.0506(m/s)
V_{yfm}: 0.0363(m/s)
V_{zfm}: -1.37(m/s)
Ψ_{fm}: 89.98°
depth: 2.18(m)

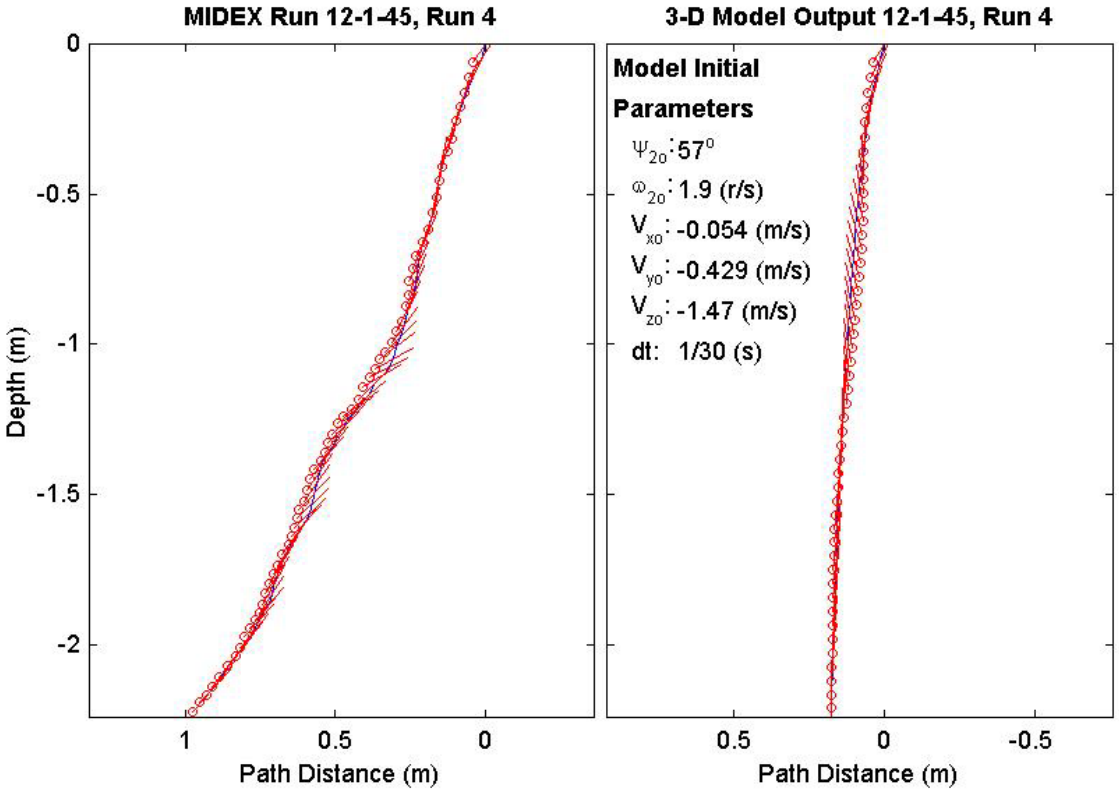

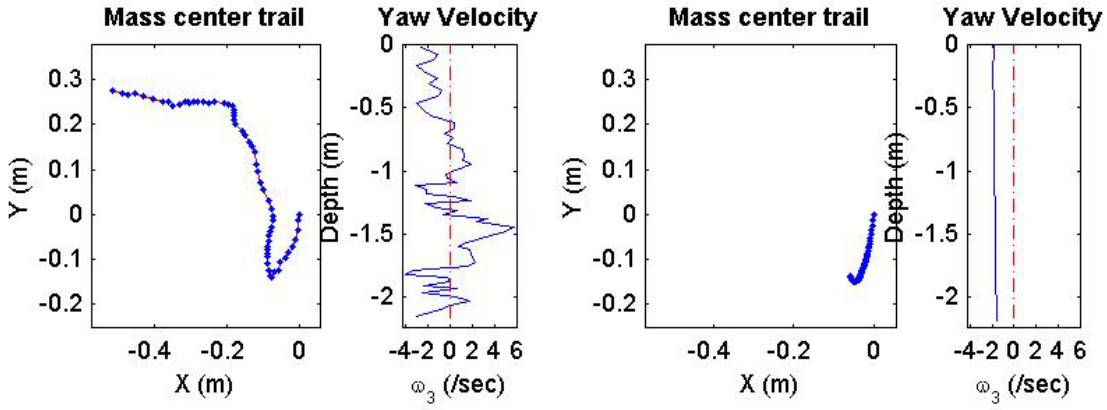

Final Drop

Parameters (45/12-1483)

time: 2.03(s)
xy_{fe}: 1.02(m)
V_{xfe}: -0.162(m/s)
V_{yfe}: 0.267(m/s)
V_{zfe}: -0.992(m/s)
Ψ_{fe}: 61.6°
depth: 2.09(m)

Mine Shape

Parameters (45/12-1483)

d: 0.04(m)
L: 0.121(m)
m: 0.254(m)
J_1: 2.71e-005(kg*m^2)
J_2: 0.000321(kg*m^2)
J_3: 0.000321(kg*m^2)
χ: 0.005307(m)

Final Model

Parameters (45/12-1483)

time: 1.5(s)
xy_{fm}: 0.202(m)
V_{xfm}: -0.0323(m/s)
V_{yfm}: 0.0261(m/s)
V_{zfm}: -1.38(m/s)
Ψ_{fm}: 83.78°
depth: 2.13(m)

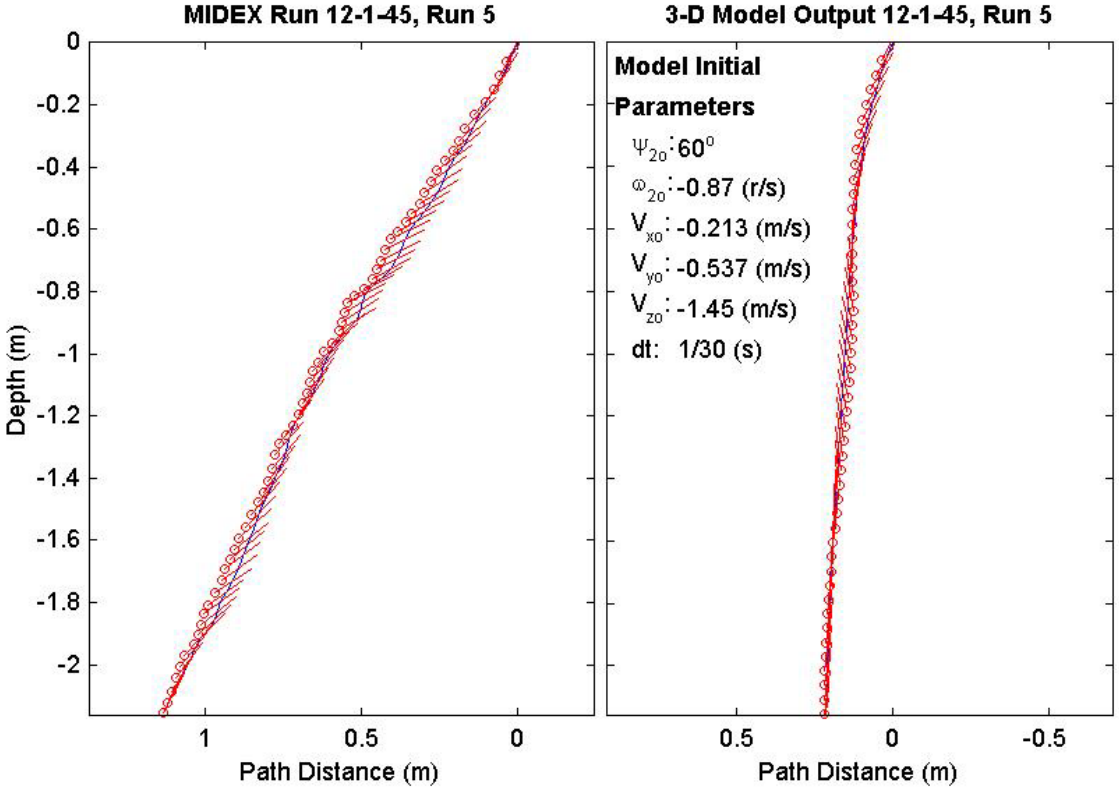

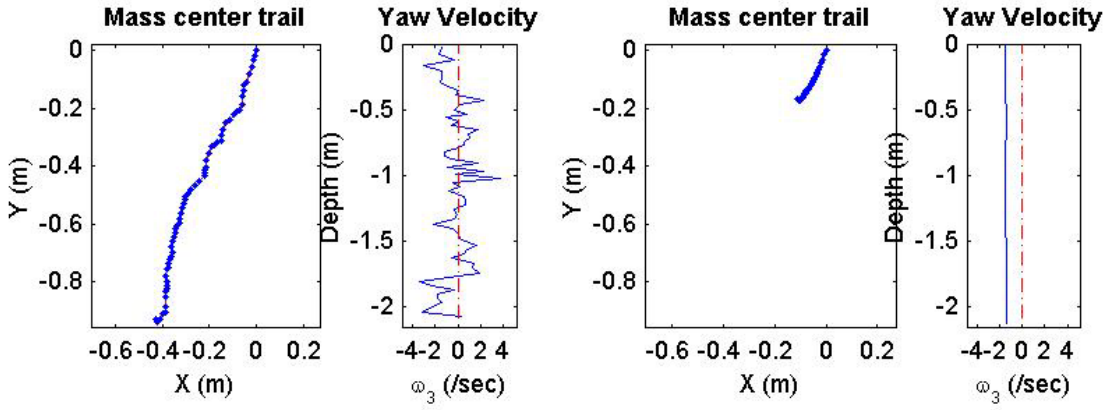

Final Drop

Parameters (45/9-3128)

time: 2.23(s)
xy_{fe}: 0.397(m)
V_{xfe}: 0(m/s)
V_{yfe}: 0.159(m/s)
V_{zfe}: -0.642(m/s)
Ψ_{fe}: 54.3°
depth: 2.11(m)

Mine Shape

Parameters (45/9-3128)

d: 0.04(m)
L: 0.0912(m)
m: 0.215(m)
J_1: 2.35e-005(kg*m^2)
J_2: 0.000158(kg*m^2)
J_3: 0.000158(kg*m^2)
χ: 0.002911(m)

Final Model

Parameters (45/9-3128)

time: 1.43(s)
xy_{fm}: 0.318(m)
V_{xfm}: -0.0359(m/s)
V_{yfm}: 0.00823(m/s)
V_{zfm}: -1.4(m/s)
Ψ_{fm}: 86°
depth: 2.13(m)

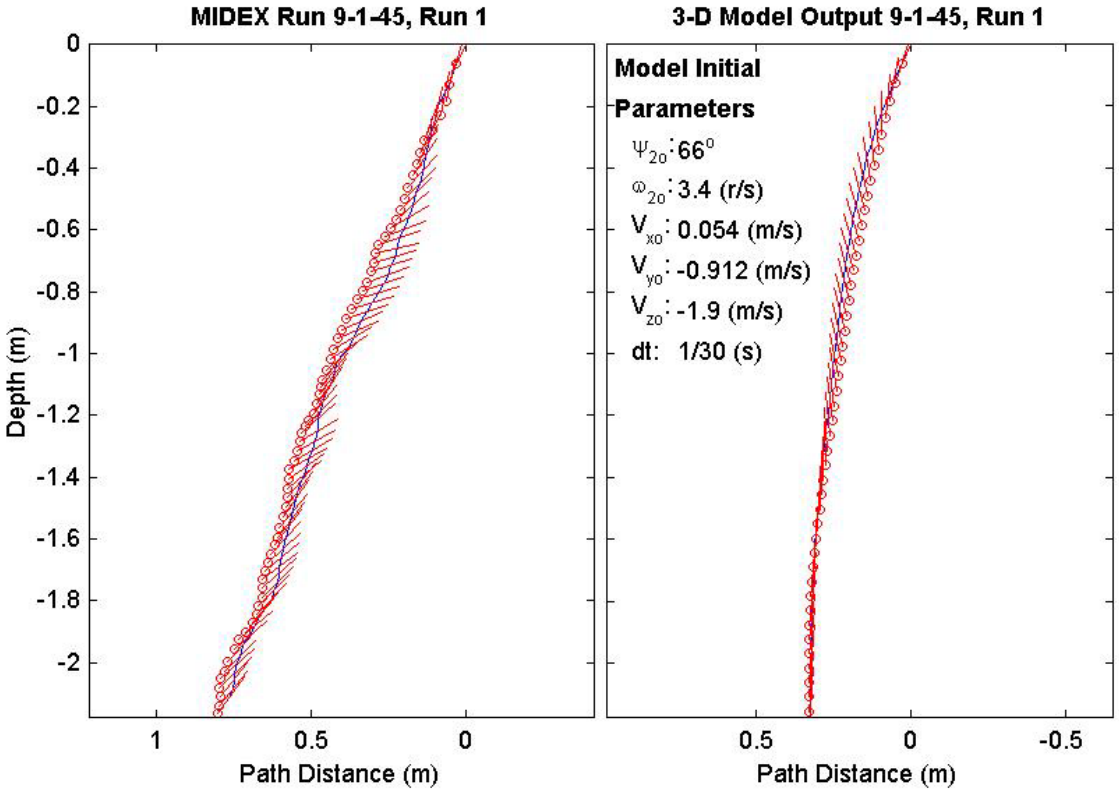

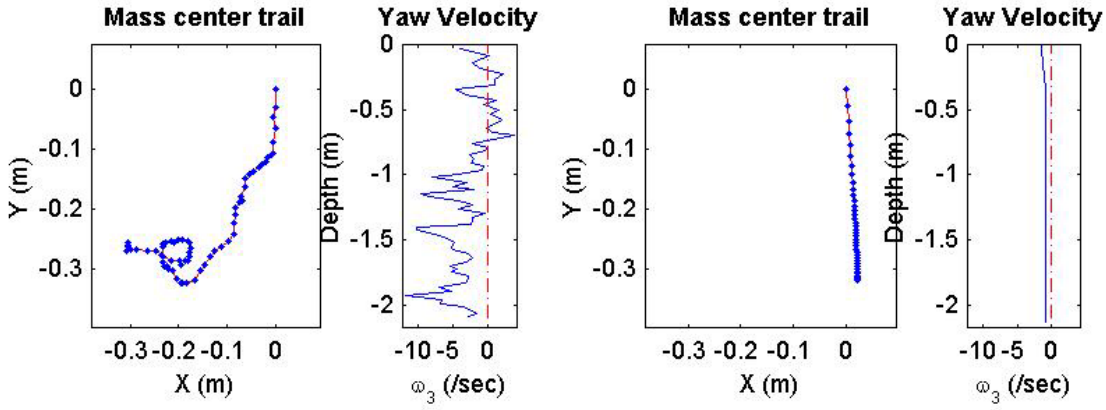

Final Drop

Parameters (45/9-2740)

time: 1.97(s)
xy_{fe}: 0.195(m)
V_{xfe}: 0.375(m/s)
V_{yfe}: 0(m/s)
V_{zfe}: -1.13(m/s)
Ψ_{fe}: 57.5°
depth: 2.24(m)

Mine Shape

Parameters (45/9-2740)

d: 0.04(m)
L: 0.0912(m)
m: 0.215(m)
J_1: 2.35e-005(kg*m^2)
J_2: 0.000158(kg*m^2)
J_3: 0.000158(kg*m^2)
χ: 0.002911(m)

Final Model

Parameters (45/9-2740)

time: 1.53(s)
xy_{fm}: 0.288(m)
V_{xfm}: -0.0219(m/s)
V_{yfm}: 0.0366(m/s)
V_{zfm}: -1.4(m/s)
Ψ_{fm}: 84.26°
depth: 2.28(m)

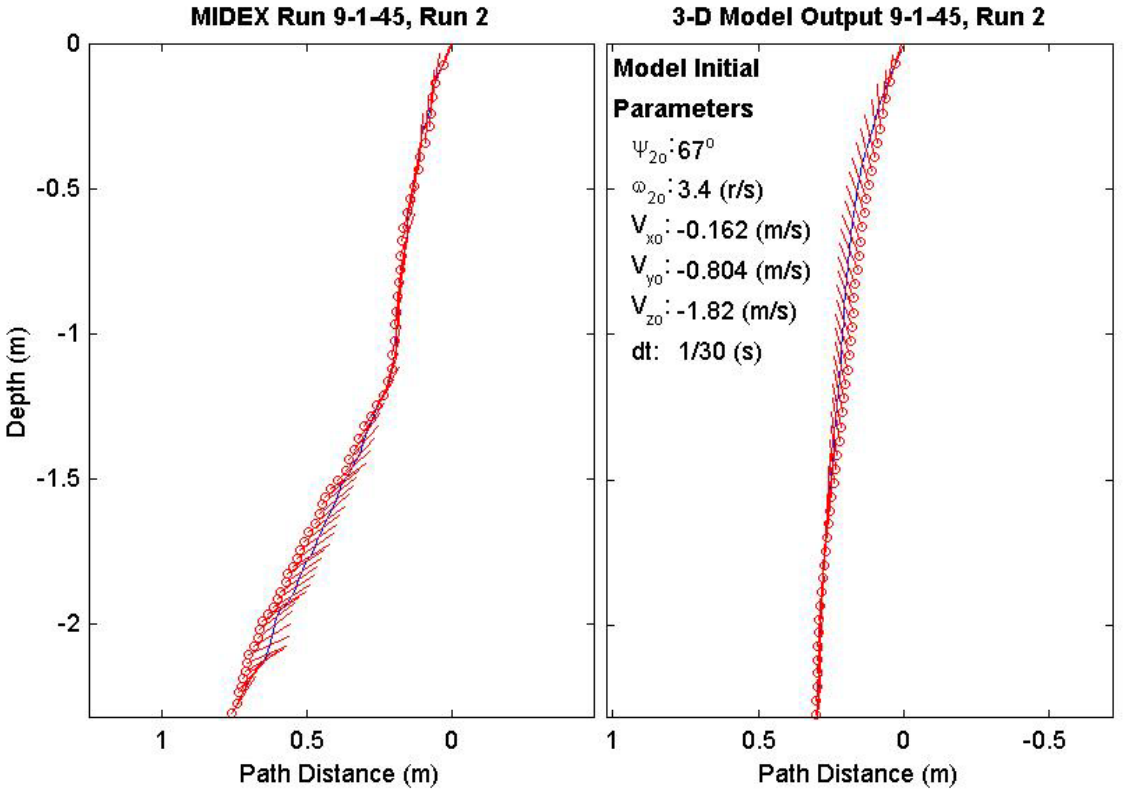

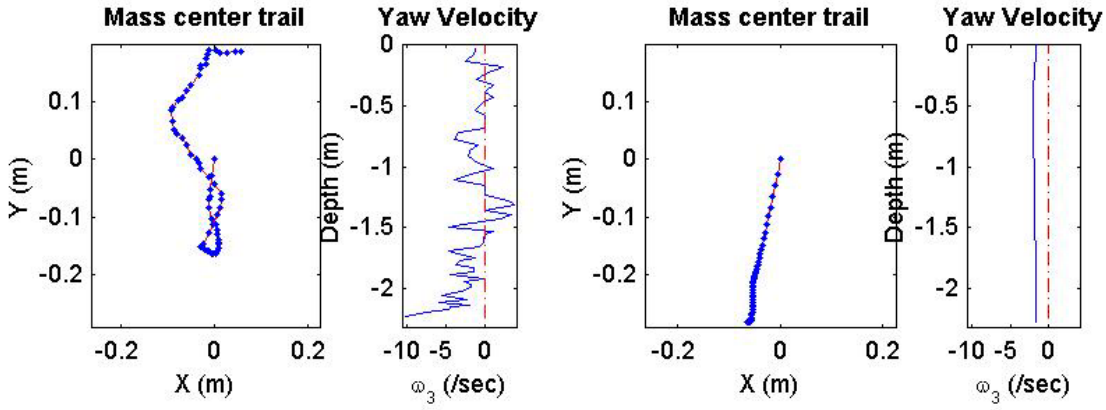

Final Drop

Parameters (45/9-2397)

time: 2.13(s)
xy_{fe}: 0.418(m)
V_{xfe}: -0.159(m/s)
V_{yfe}: 0.108(m/s)
V_{zfe}: -0.91(m/s)
Ψ_{fe}: 51°
depth: 2.19(m)

Mine Shape

Parameters (45/9-2397)

d: 0.04(m)
L: 0.0912(m)
m: 0.215(m)
J_1: 2.35e-005(kg*m^2)
J_2: 0.000158(kg*m^2)
J_3: 0.000158(kg*m^2)
χ: 0.002911(m)

Final Model

Parameters (45/9-2397)

time: 1.5(s)
xy_{fm}: 0.332(m)
V_{xfm}: -0.0102(m/s)
V_{yfm}: 0.0287(m/s)
V_{zfm}: -1.39(m/s)
Ψ_{fm}: 87.27°
depth: 2.2(m)

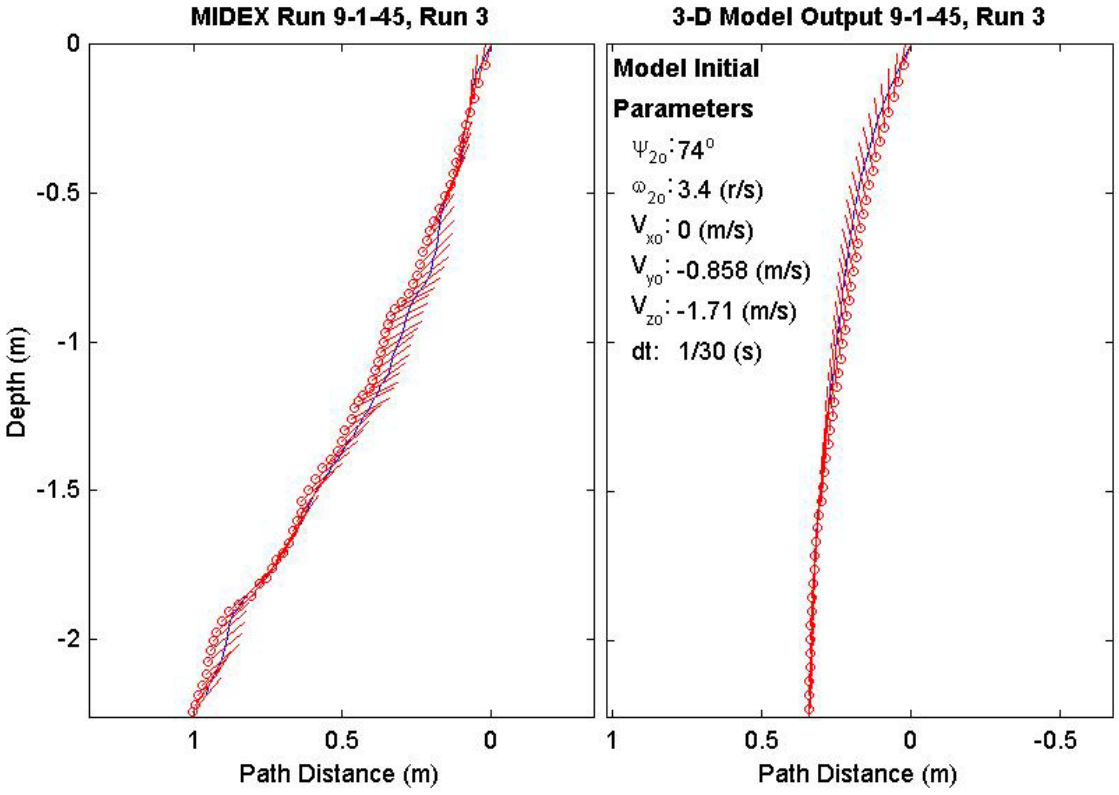

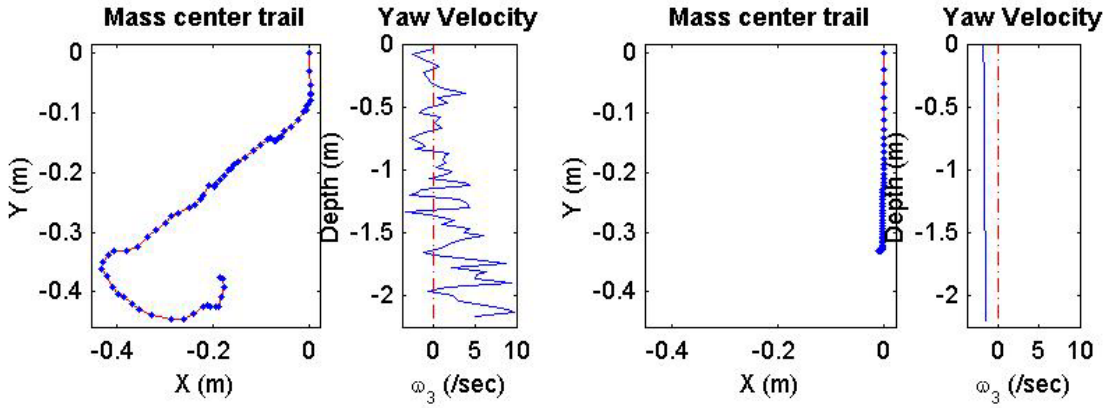

Final Drop

Parameters (45/9-2033)

time: 1.8(s)
xy_{fe}: 0.596(m)
V_{xfe}: 0.051(m/s)
V_{yfe}: -0.321(m/s)
V_{zfe}: -0.99(m/s)
Ψ_{fe}: 54.5°
depth: 2.12(m)

Mine Shape

Parameters (45/9-2033)

d: 0.04(m)
L: 0.0912(m)
m: 0.215(m)
J_1: 2.35e-005(kg*m^2)
J_2: 0.000158(kg*m^2)
J_3: 0.000158(kg*m^2)
χ: 0.002911(m)

Final Model

Parameters (45/9-2033)

time: 1.5(s)
xy_{fm}: 0.38(m)
V_{xfm}: -0.000396(m/s)
V_{yfm}: 0.0119(m/s)
V_{zfm}: -1.39(m/s)
Ψ_{fm}: 90.18°
depth: 2.14(m)

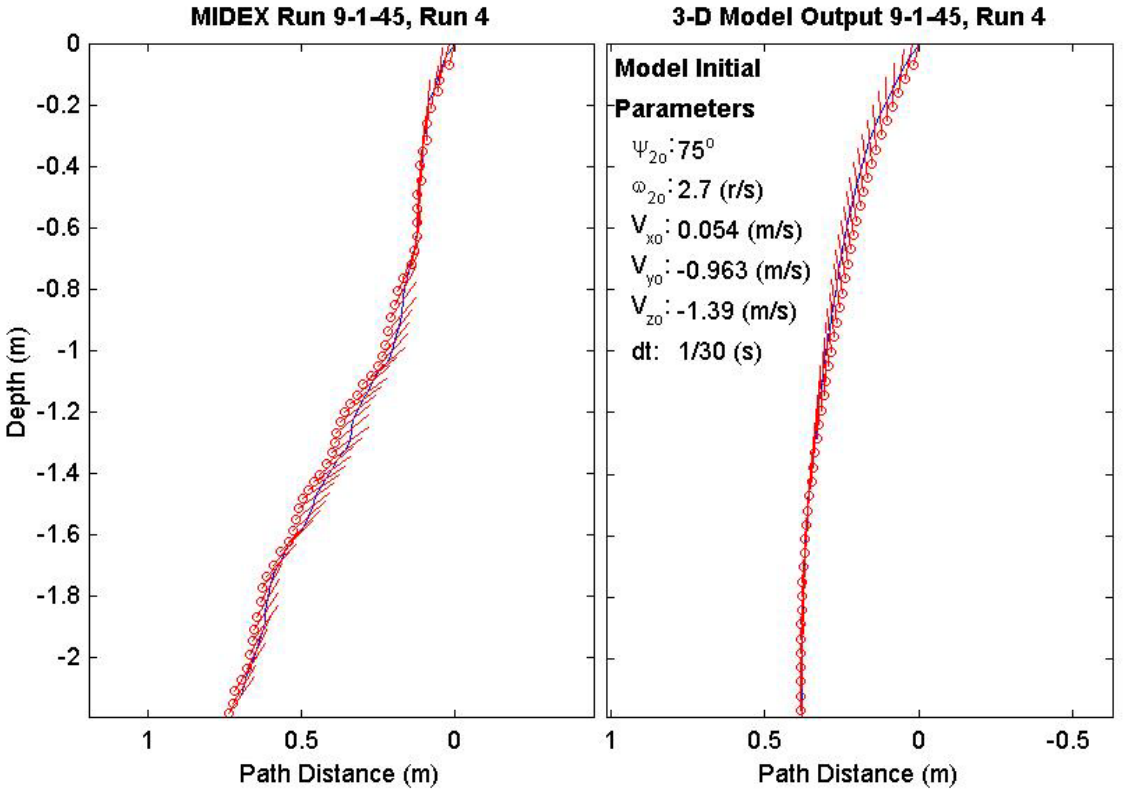

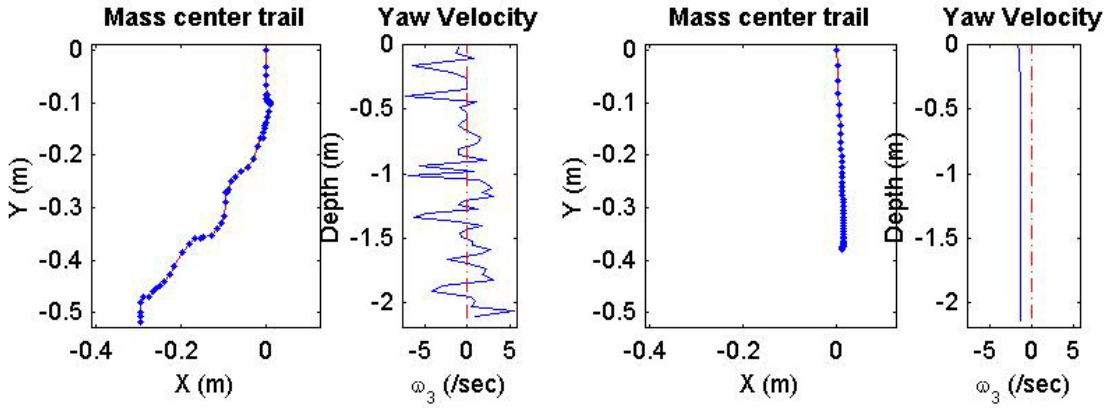

Final Drop

Parameters (45/9-1553)

time: 2.27(s)
xy_{fe}: 0.255(m)
V_{xfe}: 0.321(m/s)
V_{yfe}: -0.108(m/s)
V_{zfe}: -0.696(m/s)
Ψ_{fe}: 34.6°
depth: 2.2(m)

Mine Shape

Parameters (45/9-1553)

d: 0.04(m)
L: 0.0912(m)
m: 0.215(m)
J_1: 2.35e-005(kg*m^2)
J_2: 0.000158(kg*m^2)
J_3: 0.000158(kg*m^2)
χ: 0.002911(m)

Final Model

Parameters (45/9-1553)

time: 1.57(s)
xy_{fm}: 0.19(m)
V_{xfm}: -0.0301(m/s)
V_{yfm}: -0.0241(m/s)
V_{zfm}: -1.4(m/s)
Ψ_{fm}: 85.48°
depth: 2.21(m)

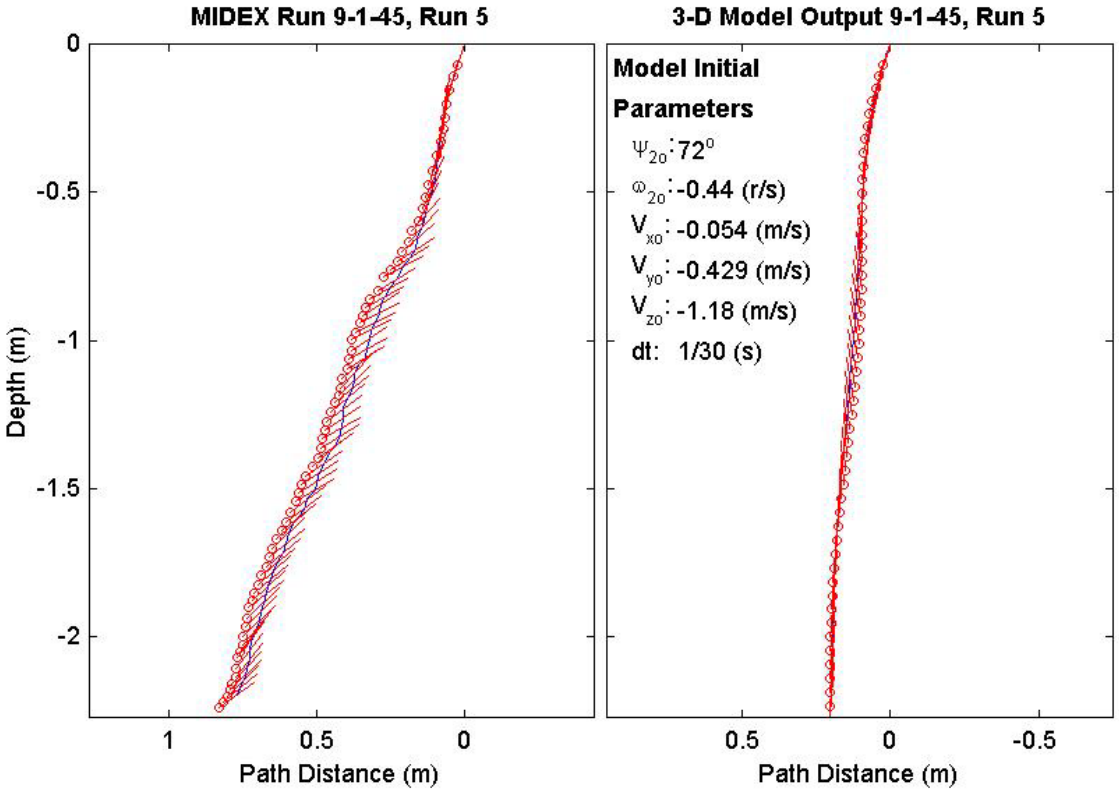

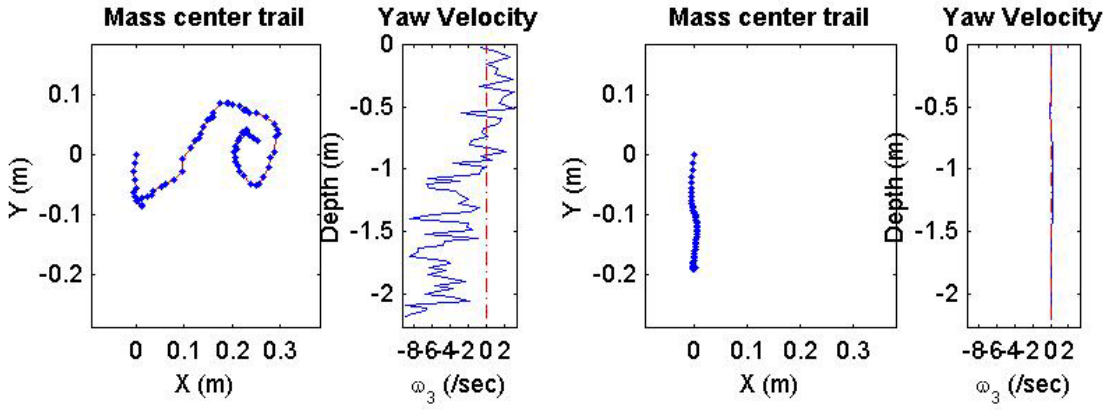

Final Drop

Parameters (60/15-3568)

time: 1.47(s)
xy_{fe}: 0.303(m)
V_{xfe}: 0.163(m/s)
V_{yfe}: 0.375(m/s)
V_{zfe}: -0.911(m/s)
Ψ_{fe}: 43.1°
depth: 2.17(m)

Mine Shape

Parameters (60/15-3568)

d: 0.04(m)
L: 0.152(m)
m: 0.323(m)
J_1: 3.3e-005(kg*m^2)
J_2: 0.000578(kg*m^2)
J_3: 0.000578(kg*m^2)
χ: 0.007411(m)

Final Model

Parameters (60/15-3568)

time: 1.3(s)
xy_{fm}: 0.515(m)
V_{xfm}: 0.107(m/s)
V_{yfm}: -0.0366(m/s)
V_{zfm}: -1.52(m/s)
Ψ_{fm}: 89.51°
depth: 2.18(m)

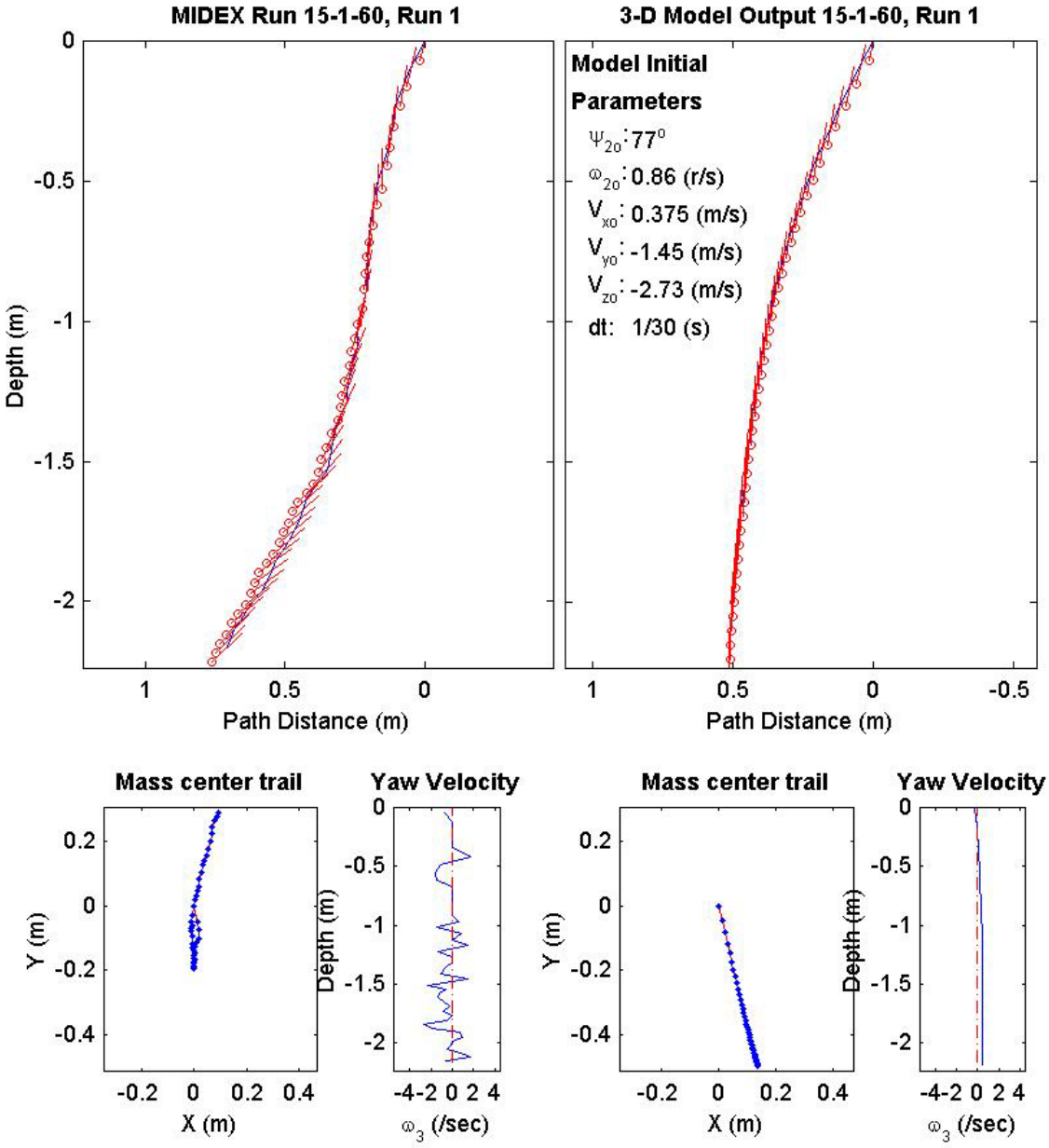

Final Drop Parameters (60/15-2984)

time: 1.4(s)
xy_{fe}: 0.274(m)
V_{xfe}: 0.213(m/s)
V_{yfe}: 0.75(m/s)
V_{zfe}: -0.882(m/s)
Ψ_{fe}: 42.8°
depth: 2.13(m)

Mine Shape Parameters (60/15-2984)

d: 0.04(m)
L: 0.152(m)
m: 0.323(m)
J_1: 3.3e-005(kg*m^2)
J_2: 0.000578(kg*m^2)
J_3: 0.000578(kg*m^2)
χ: 0.007411(m)

Final Model Parameters (60/15-2984)

time: 1.33(s)
xy_{fm}: 0.392(m)
V_{xfm}: 0.098(m/s)
V_{yfm}: -0.0198(m/s)
V_{zfm}: -1.52(m/s)
Ψ_{fm}: 90.51°
depth: 2.16(m)

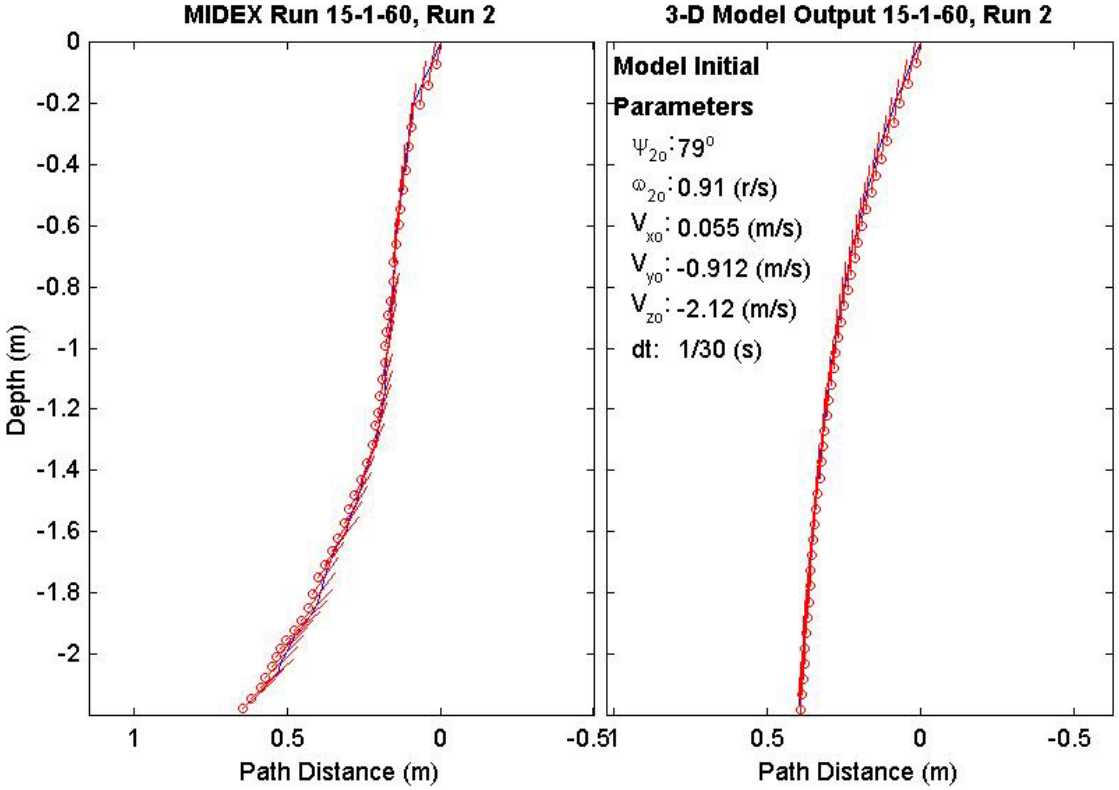

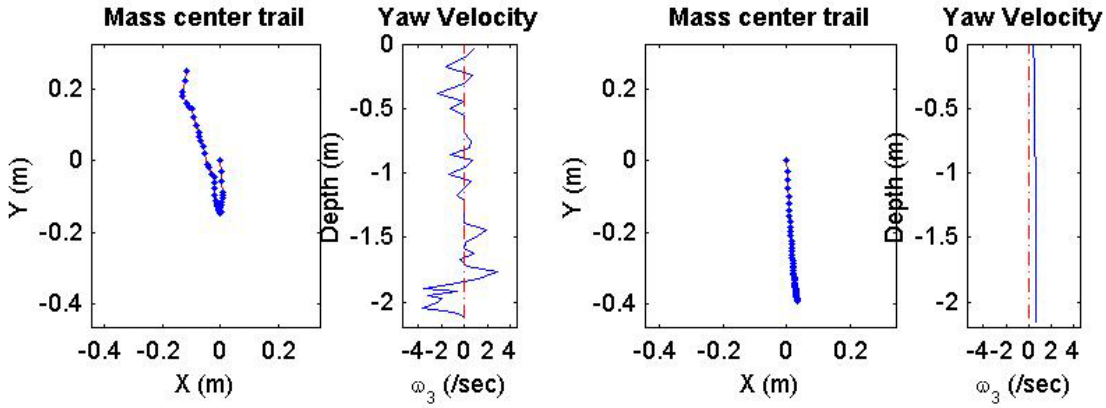

Final Drop Parameters (60/15-2912)

time: 1.43(s)
xy_{fe}: 0.246(m)
V_{xfe}: 0.321(m/s)
V_{yfe}: 0.483(m/s)
V_{zfe}: -0.964(m/s)
Ψ_{fe}: 34.5°
depth: 2.19(m)

Mine Shape Parameters (60/15-2912)

d: 0.04(m)
L: 0.152(m)
m: 0.323(m)
J_1: 3.3e-005(kg*m^2)
J_2: 0.000578(kg*m^2)
J_3: 0.000578(kg*m^2)
χ: 0.007411(m)

Final Model Parameters (60/15-2912)

time: 1.37(s)
xy_{fm}: 0.423(m)
V_{xfm}: 0.0905(m/s)
V_{yfm}: 0.0156(m/s)
V_{zfm}: -1.52(m/s)
Ψ_{fm}: 88.95°
depth: 2.21(m)

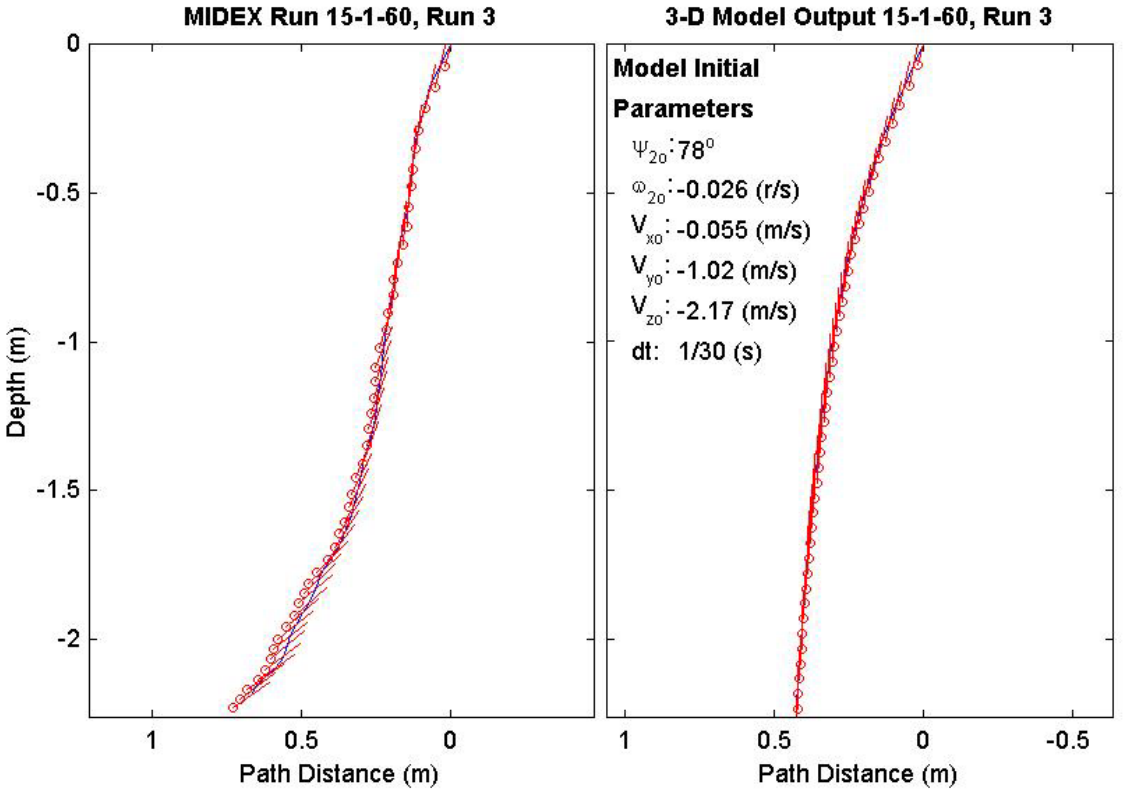

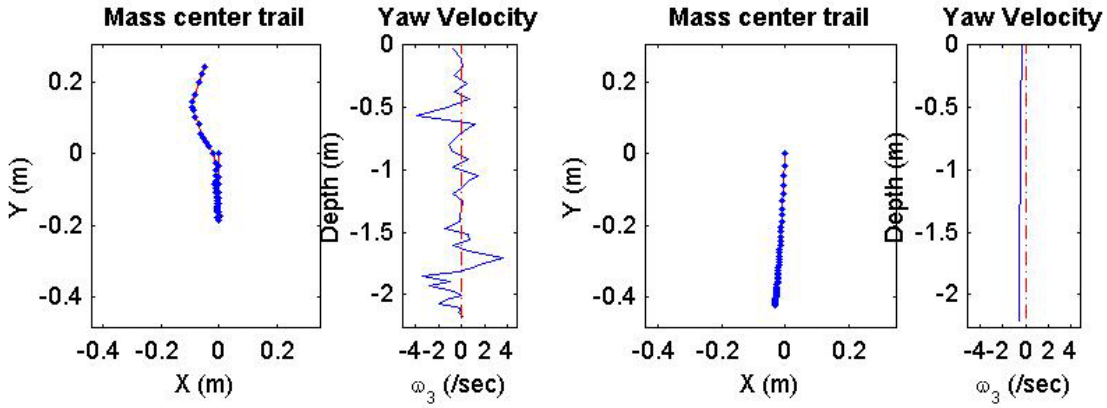

Final Drop

Parameters (60/15-2415)

time: 1.57(s)
xy_{fe}: 0.361(m)
V_{xfe}: 0.055(m/s)
V_{yfe}: 0.48(m/s)
V_{zfe}: -0.883(m/s)
Ψ_{fe}: 48.8°
depth: 2.2(m)

Mine Shape

Parameters (60/15-2415)

d: 0.04(m)
L: 0.152(m)
m: 0.323(m)
J_1: 3.3e-005(kg*m^2)
J_2: 0.000578(kg*m^2)
J_3: 0.000578(kg*m^2)
χ: 0.007411(m)

Final Model

Parameters (60/15-2415)

time: 1.37(s)
xy_{fm}: 0.299(m)
V_{xfm}: 0.0514(m/s)
V_{yfm}: 0.00276(m/s)
V_{zfm}: -1.52(m/s)
Ψ_{fm}: 92.41°
depth: 2.2(m)

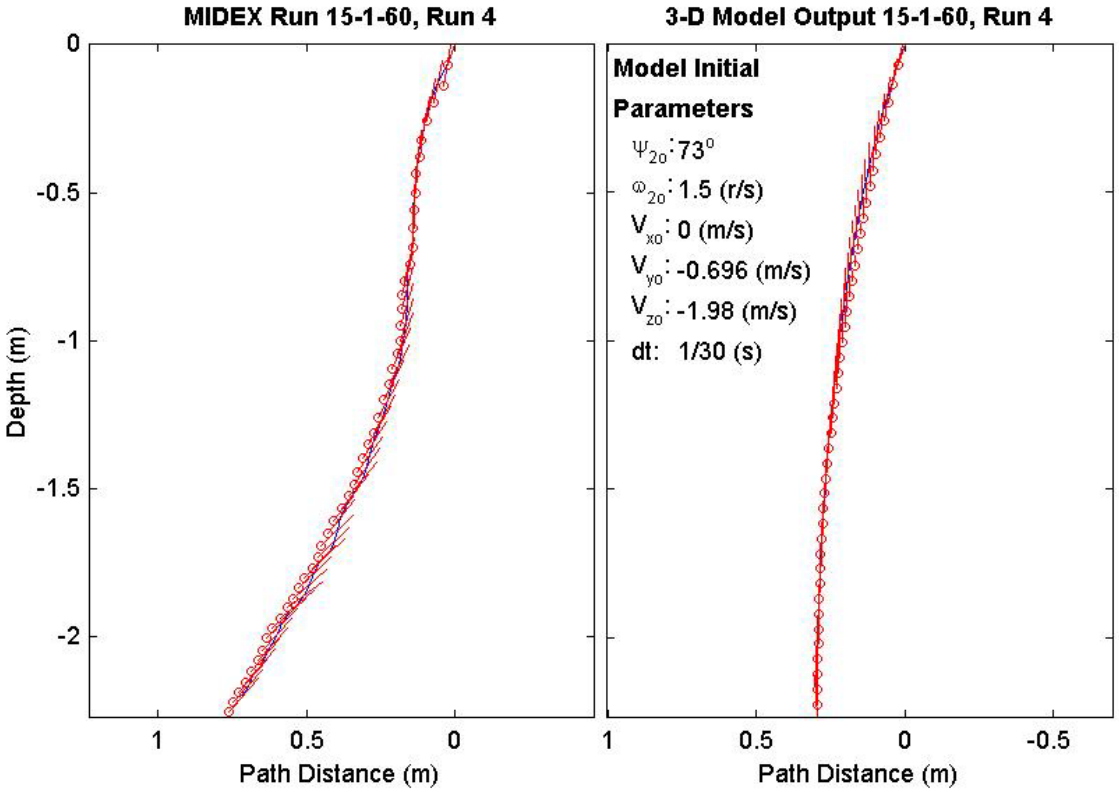

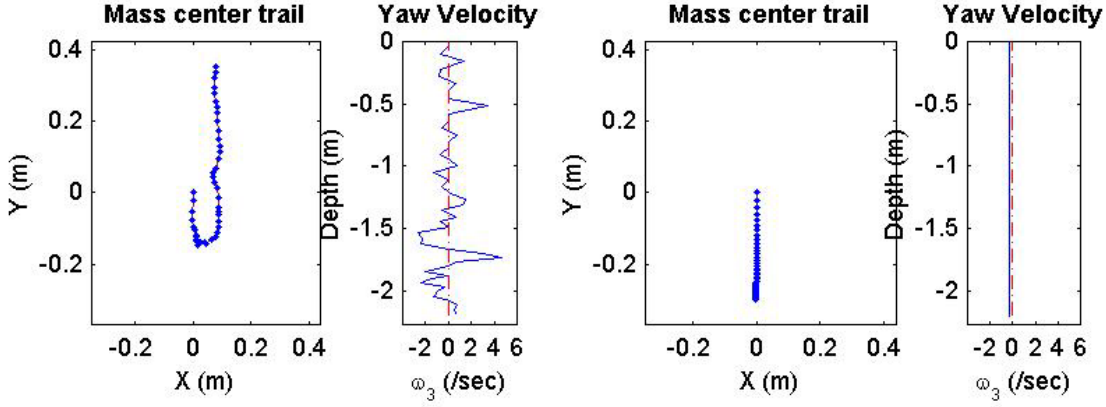

Final Drop

Parameters (60/15-1800)

time: 1.23(s)
xy_{fe}: 0.108(m)
V_{xfe}: 0.055(m/s)
V_{yfe}: 0(m/s)
V_{zfe}: -1.82(m/s)
Ψ_{fe}: 88.2°
depth: 2.13(m)

Mine Shape

Parameters (60/15-1800)

d: 0.04(m)
L: 0.152(m)
m: 0.323(m)
J_1: 3.3e-005(kg*m^2)
J_2: 0.000578(kg*m^2)
J_3: 0.000578(kg*m^2)
χ: 0.007411(m)

Final Model

Parameters (60/15-1800)

time: 1.37(s)
xy_{fm}: 0.105(m)
V_{xfm}: -0.0278(m/s)
V_{yfm}: 0.0227(m/s)
V_{zfm}: -1.53(m/s)
Ψ_{fm}: 85.62°
depth: 2.14(m)

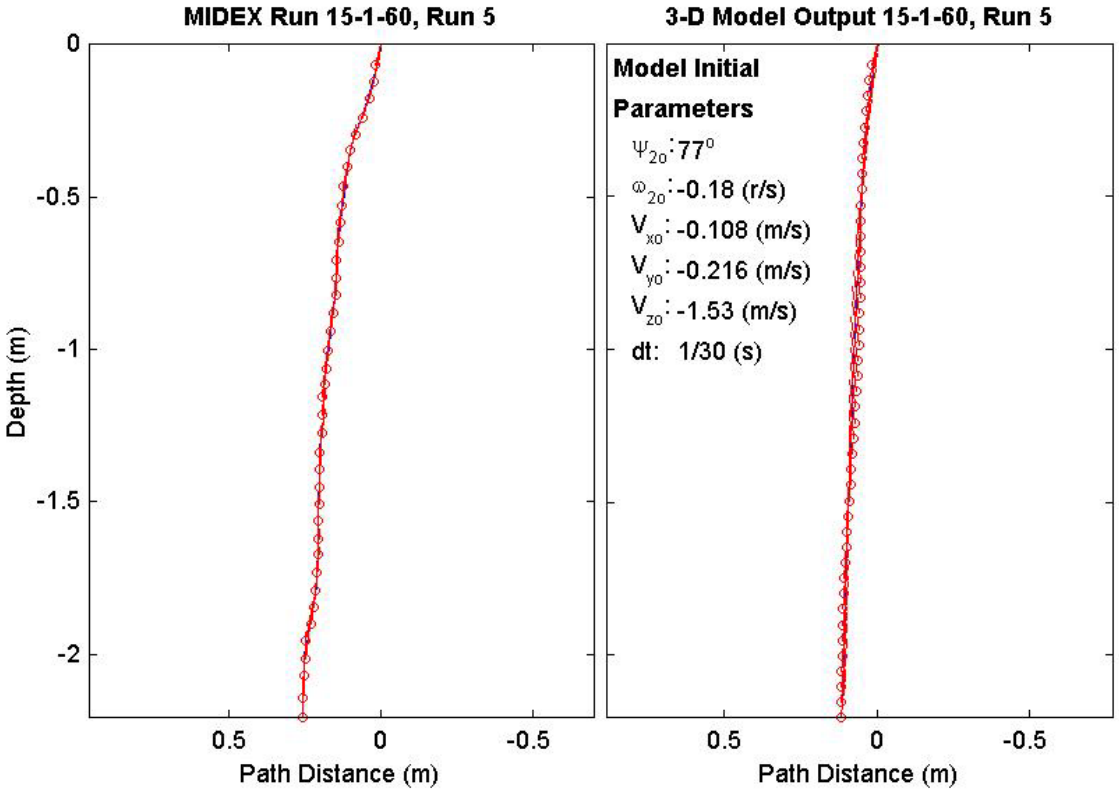

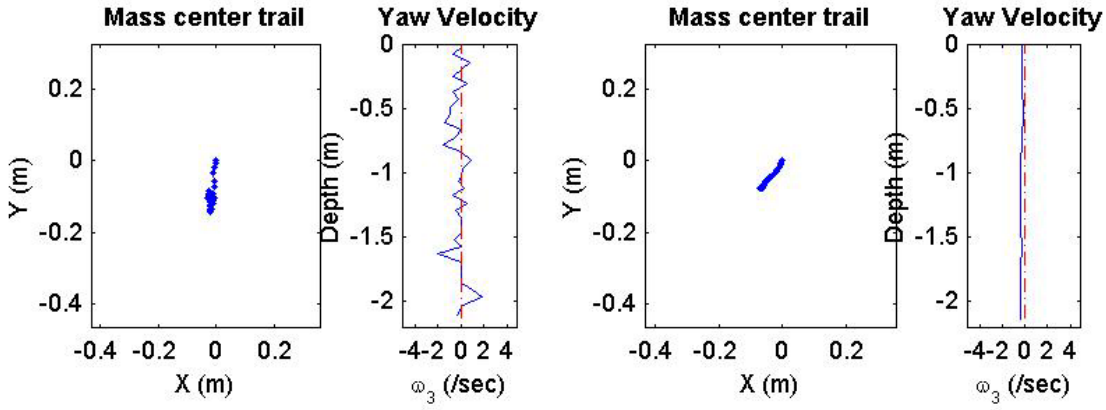

Final Drop Parameters (60/12-3497)

time: 1.37(s)
xy_{fe}: 0.276(m)
V_{xfe}: -0.267(m/s)
V_{yfe}: 0.054(m/s)
V_{zfe}: -1.58(m/s)
Ψ_{fe}: 69.1°
depth: 2.11(m)

Mine Shape Parameters (60/12-3497)

d: 0.04(m)
L: 0.121(m)
m: 0.254(m)
J_1: 2.71e-005(kg*m^2)
J_2: 0.000321(kg*m^2)
J_3: 0.000321(kg*m^2)
χ: 0.005307(m)

Final Model Parameters (60/12-3497)

time: 1.43(s)
xy_{fm}: 0.178(m)
V_{xfm}: -0.0212(m/s)
V_{yfm}: -0.0205(m/s)
V_{zfm}: -1.38(m/s)
Ψ_{fm}: 84.09°
depth: 2.12(m)

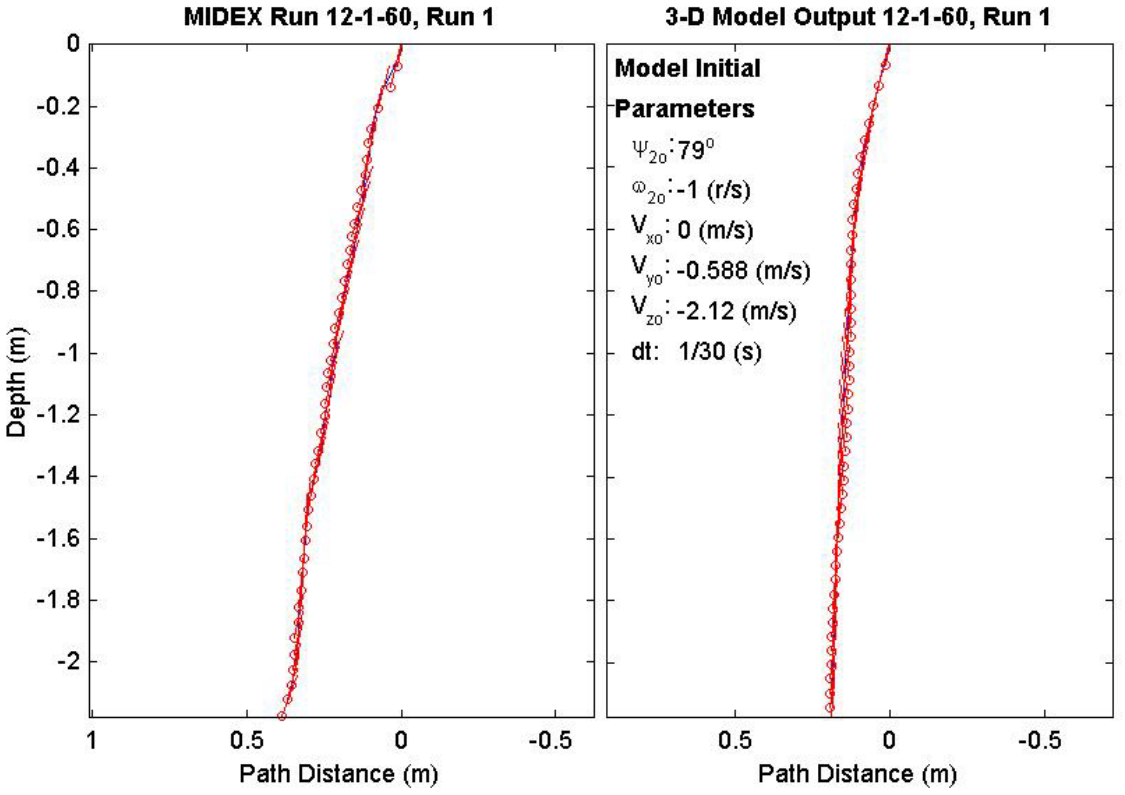

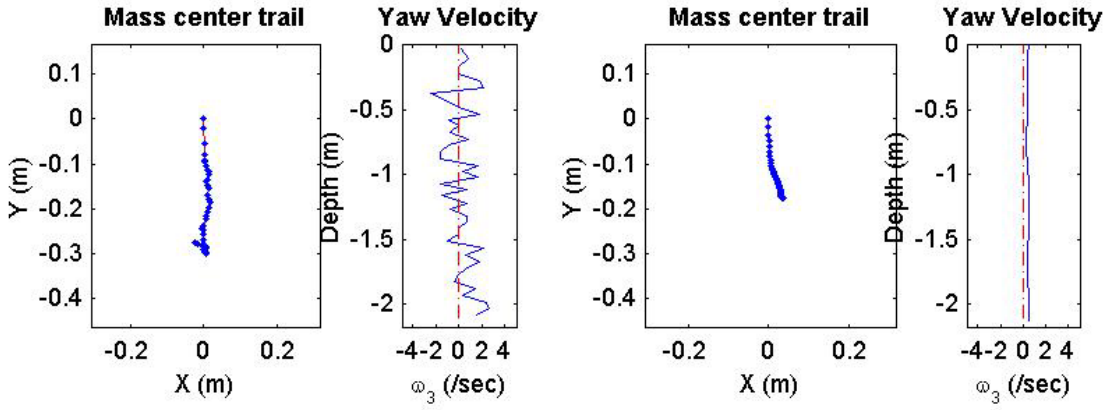

Final Drop Parameters (60/12-3686)

time: 1.7(s)
xy_{fe}: 0.516(m)
V_{xfe}: 0.642(m/s)
V_{yfe}: 0.429(m/s)
V_{zfe}: -1.1(m/s)
Ψ_{fe}: 46.3°
depth: 2.15(m)

Mine Shape Parameters (60/12-3686)

d: 0.04(m)
L: 0.121(m)
m: 0.254(m)
J_1: 2.71e-005(kg*m^2)
J_2: 0.000321(kg*m^2)
J_3: 0.000321(kg*m^2)
χ: 0.005307(m)

Final Model Parameters (60/12-3686)

time: 1.47(s)
xy_{fm}: 0.389(m)
V_{xfm}: 0.066(m/s)
V_{yfm}: 5.49e-018(m/s)
V_{zfm}: -1.37(m/s)
Ψ_{fm}: 88.65°
depth: 2.17(m)

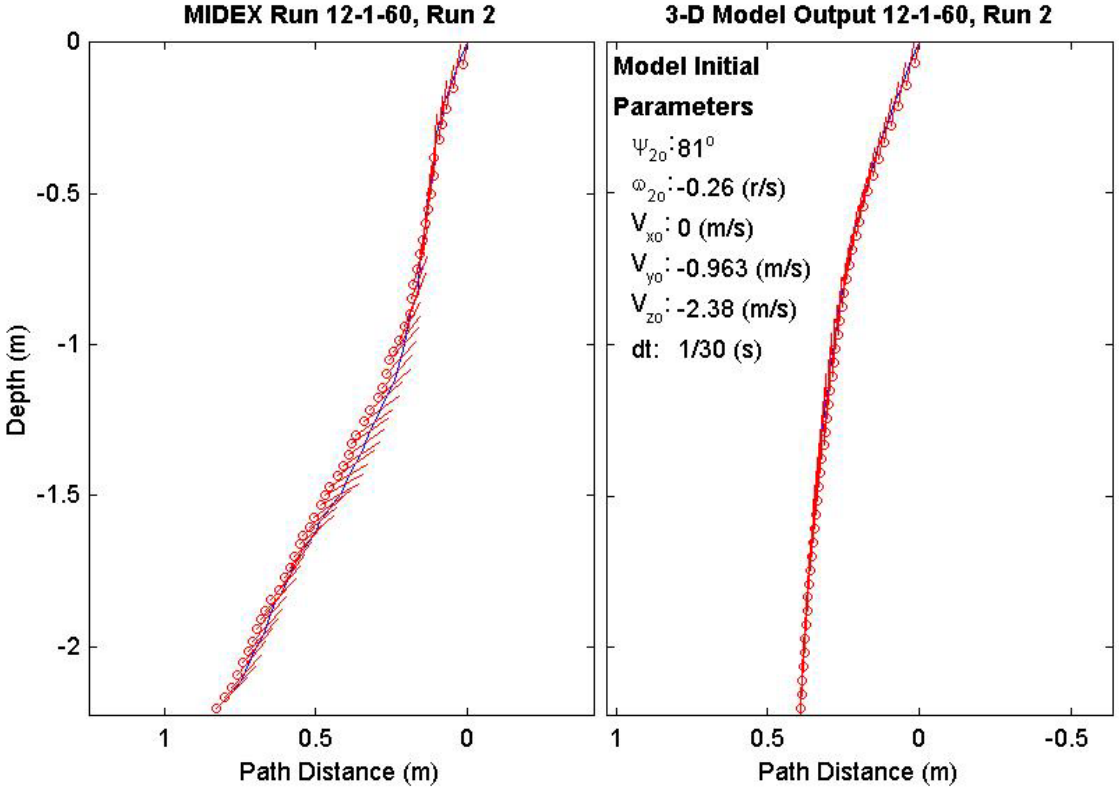

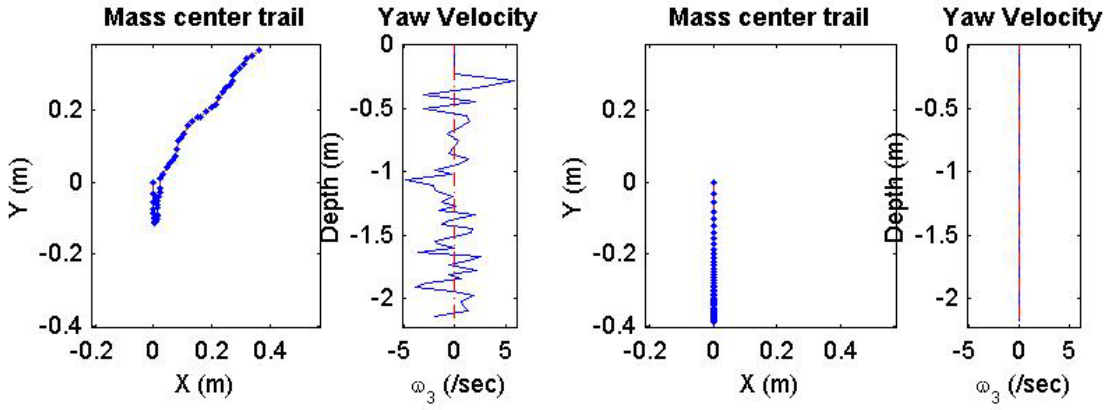

Final Drop

Parameters (60/12-2929)

time: 1.4(s)
xy_{fe}: 0.248(m)
V_{xfe}: -0.324(m/s)
V_{yfe}: -0.162(m/s)
V_{zfe}: -1.26(m/s)
Ψ_{fe}: 56.6°
depth: 2.16(m)

Mine Shape

Parameters (60/12-2929)

d: 0.04(m)
L: 0.121(m)
m: 0.254(m)
J_1: 2.71e-005(kg*m^2)
J_2: 0.000321(kg*m^2)
J_3: 0.000321(kg*m^2)
χ: 0.005307(m)

Final Model

Parameters (60/12-2929)

time: 1.5(s)
xy_{fm}: 0.0874(m)
V_{xfm}: -0.0125(m/s)
V_{yfm}: 0.0323(m/s)
V_{zfm}: -1.37(m/s)
Ψ_{fm}: 83.29°
depth: 2.2(m)

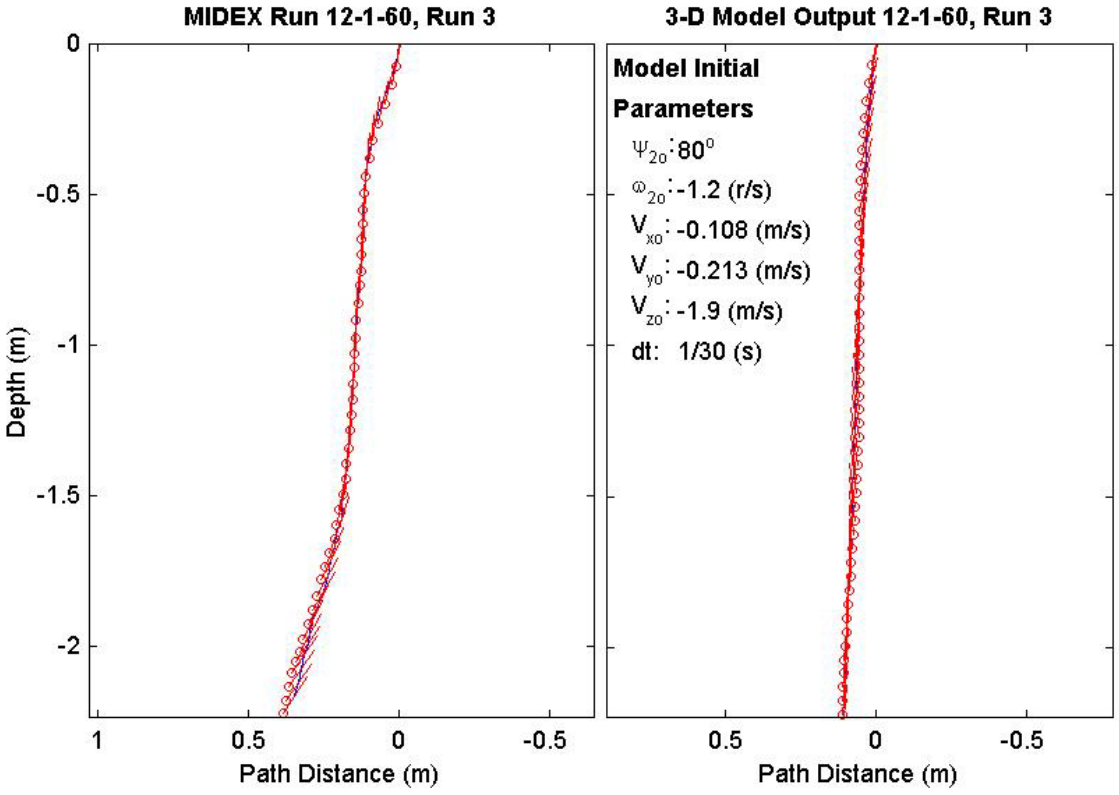

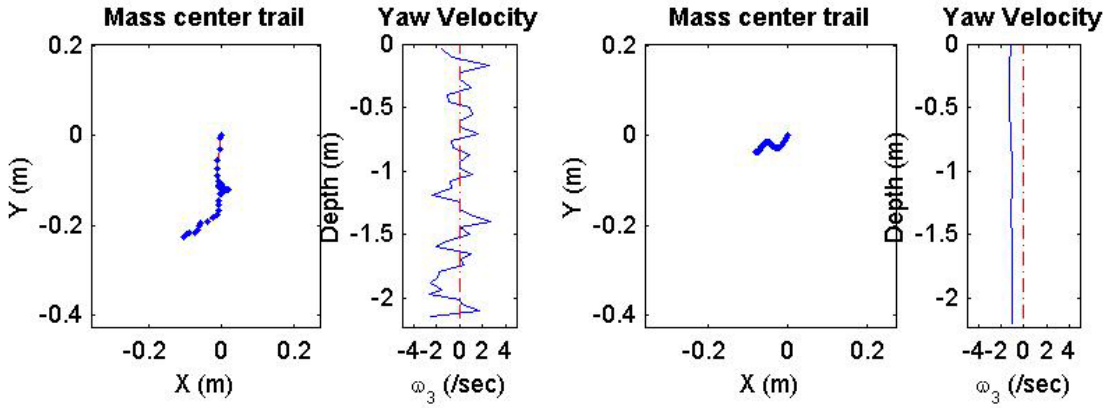

Final Drop Parameters (60/12-2494)

time: 1.4(s)
xy_{fe}: 0.158(m)
V_{xfe}: 0.159(m/s)
V_{yfe}: 0.162(m/s)
V_{zfe}: -1.31(m/s)
Ψ_{fe}: 81.2°
depth: 2.11(m)

Mine Shape Parameters (60/12-2494)

d: 0.04(m)
L: 0.121(m)
m: 0.254(m)
J_1: 2.71e-005(kg*m^2)
J_2: 0.000321(kg*m^2)
J_3: 0.000321(kg*m^2)
χ: 0.005307(m)

Final Model Parameters (60/12-2494)

time: 1.43(s)
xy_{fm}: 0.12(m)
V_{xfm}: -0.0198(m/s)
V_{yfm}: 0.0185(m/s)
V_{zfm}: -1.38(m/s)
Ψ_{fm}: 82.26°
depth: 2.12(m)

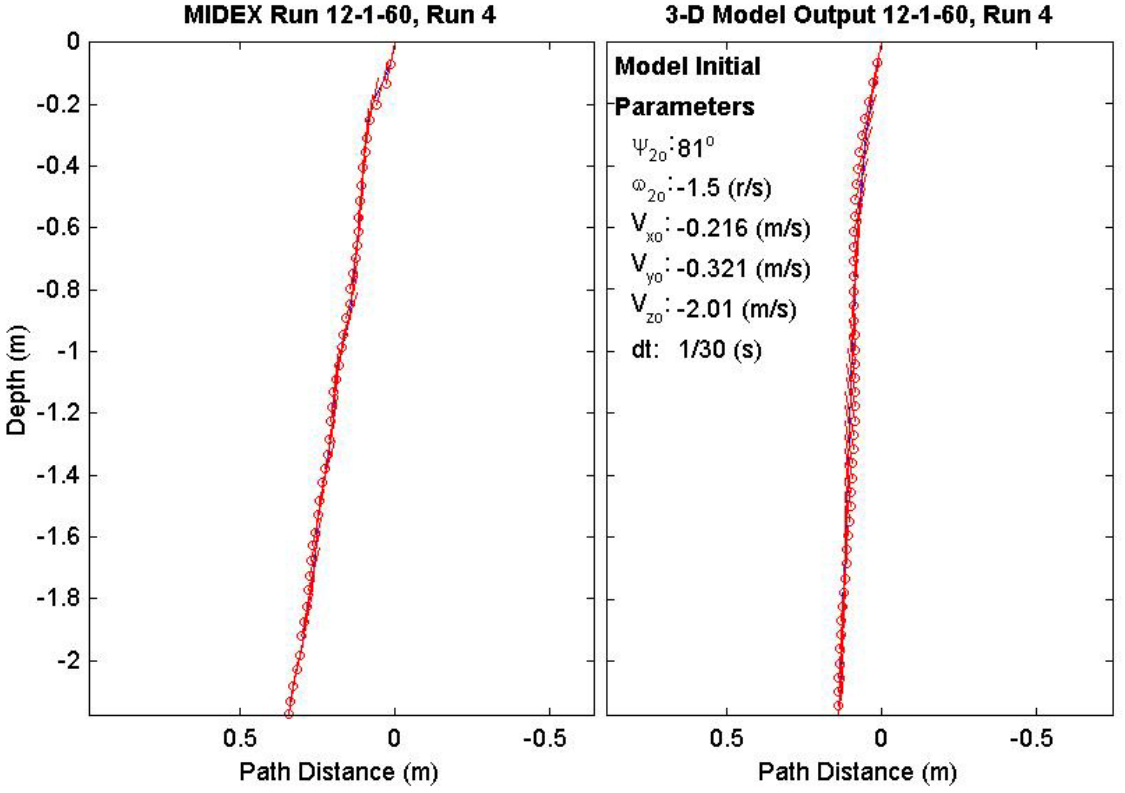

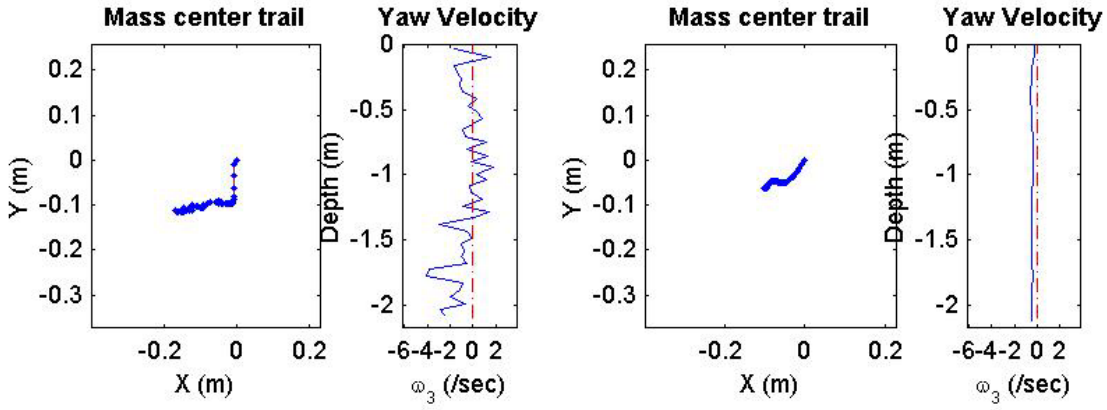

Final Drop

Parameters (60/12-1865)

time: 1.47(s)
xy_{fe}: 0.317(m)
V_{xfe}: -0.162(m/s)
V_{yfe}: -0.321(m/s)
V_{zfe}: -1.29(m/s)
Ψ_{fe}: 51°
depth: 2.17(m)

Mine Shape

Parameters (60/12-1865)

d: 0.04(m)
L: 0.121(m)
m: 0.254(m)
J_1: 2.71e-005(kg*m^2)
J_2: 0.000321(kg*m^2)
J_3: 0.000321(kg*m^2)
χ: 0.005307(m)

Final Model

Parameters (60/12-1865)

time: 1.53(s)
xy_{fm}: 0.208(m)
V_{xfm}: -0.00114(m/s)
V_{yfm}: -0.03(m/s)
V_{zfm}: -1.37(m/s)
Ψ_{fm}: 94.09°
depth: 2.21(m)

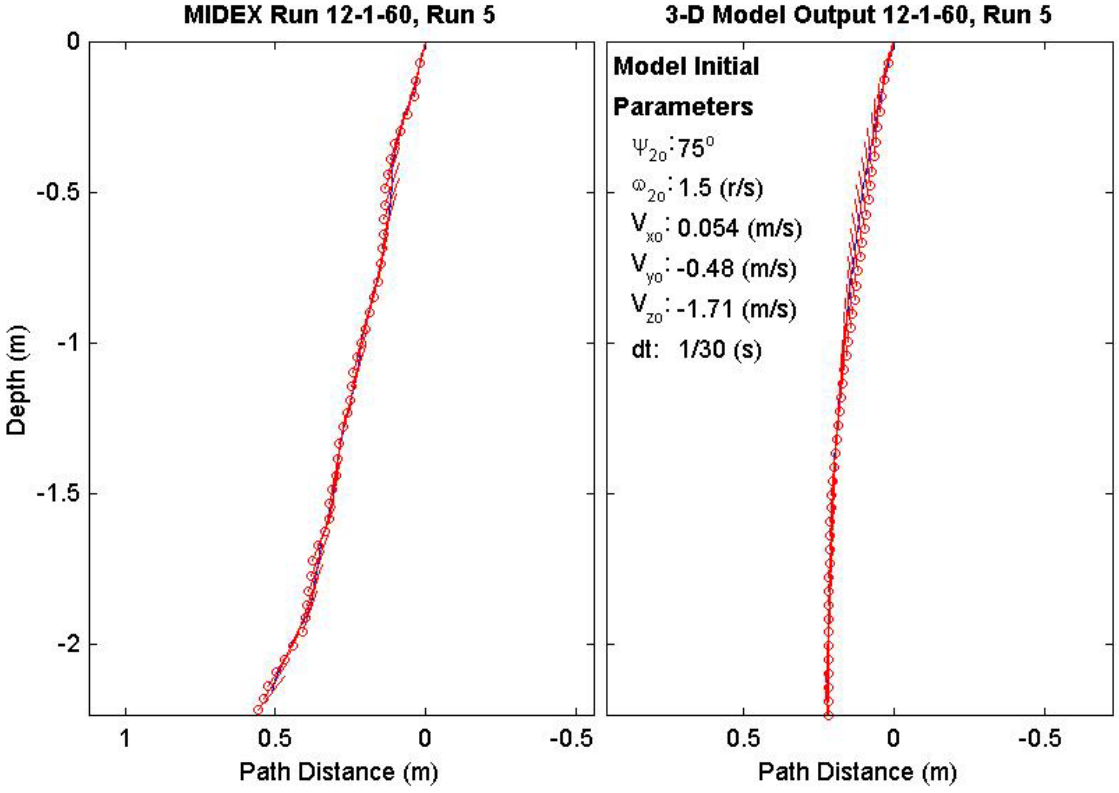

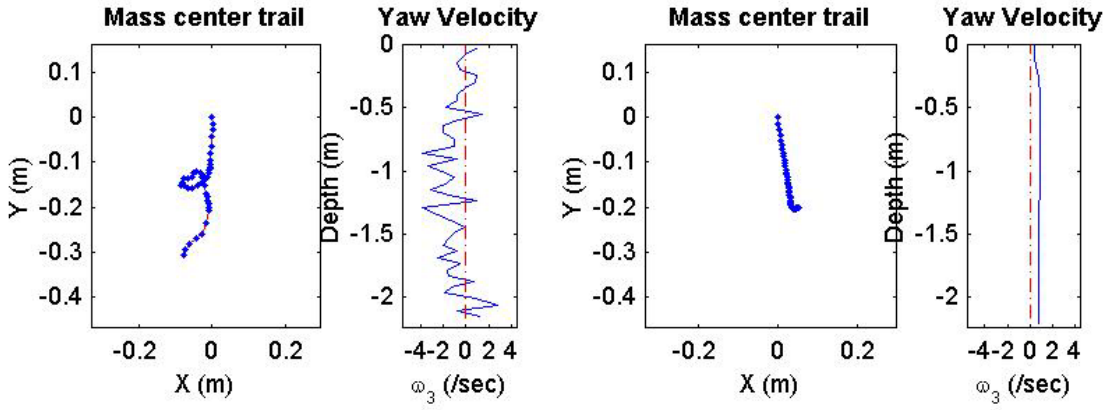

Final Drop
Parameters (60/9-3710)

time: 1.7(s)
xy_{fe}: 0.283(m)
V_{xfe}: 0.105(m/s)
V_{yfe}: -0.375(m/s)
V_{zfe}: -0.964(m/s)
Ψ_{fe}: 51.3°
depth: 2.17(m)

Mine Shape
Parameters (60/9-3710)

d: 0.04(m)
L: 0.0912(m)
m: 0.215(m)
J_1: 2.35e-005(kg*m^2)
J_2: 0.000158(kg*m^2)
J_3: 0.000158(kg*m^2)
χ: 0.002911(m)

Final Model
Parameters (60/9-3710)

time: 1.47(s)
xy_{fm}: 0.372(m)
V_{xfm}: 0.0377(m/s)
V_{yfm}: 0.0307(m/s)
V_{zfm}: -1.39(m/s)
Ψ_{fm}: 85.93°
depth: 2.18(m)

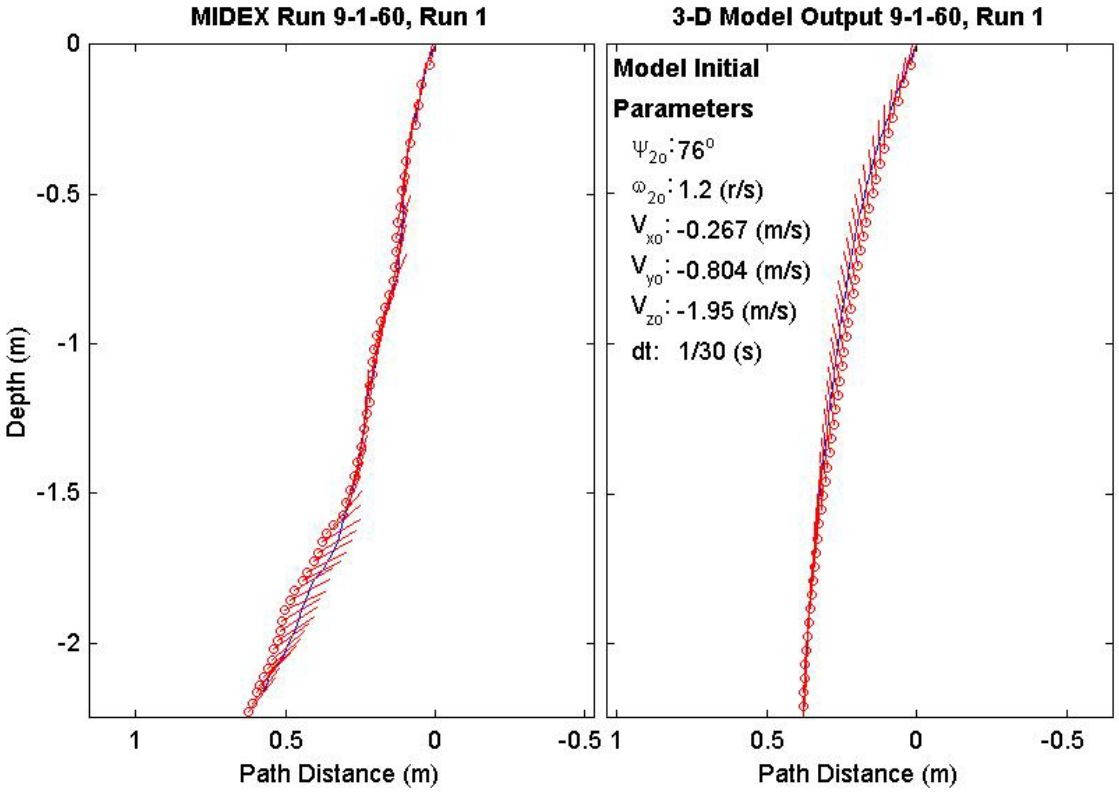

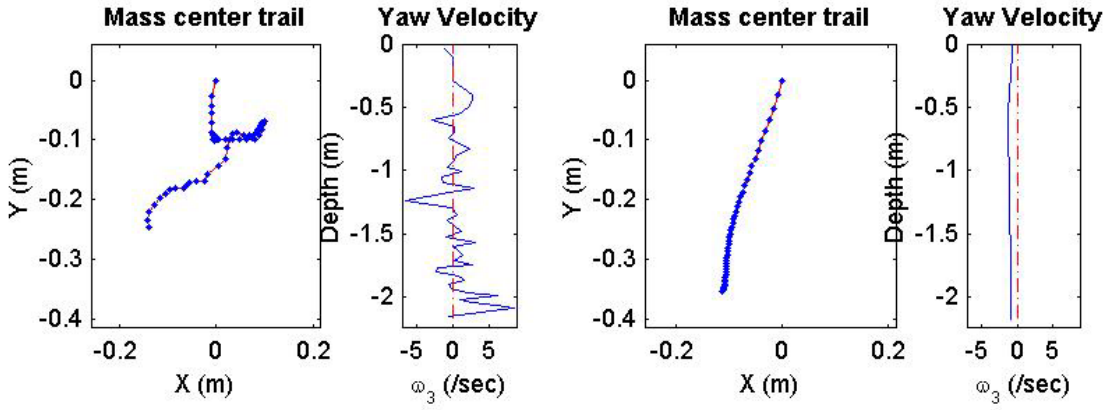

Final Drop
Parameters (60/9-3289)

time:	2.23(s)
xy_{fe}:	0.144(m)
V_{xfe}:	-0.588(m/s)
V_{yfe}:	-0.108(m/s)
V_{zfe}:	-0.83(m/s)
Ψ_{fe}:	51.3^{o}
depth:	2.16(m)

Mine Shape
Parameters (60/9-3289)

d:	0.04(m)
L:	0.0912(m)
m:	0.215(m)
J_1:	2.35e-005($kg*m^2$)
J_2:	0.000158($kg*m^2$)
J_3:	0.000158($kg*m^2$)
χ:	0.002911(m)

Final Model
Parameters (60/9-3289)

time:	1.5(s)
xy_{fm}:	0.207(m)
V_{xfm}:	0.032(m/s)
V_{yfm}:	0.0178(m/s)
V_{zfm}:	-1.39(m/s)
Ψ_{fm}:	83.51^{o}
depth:	2.17(m)

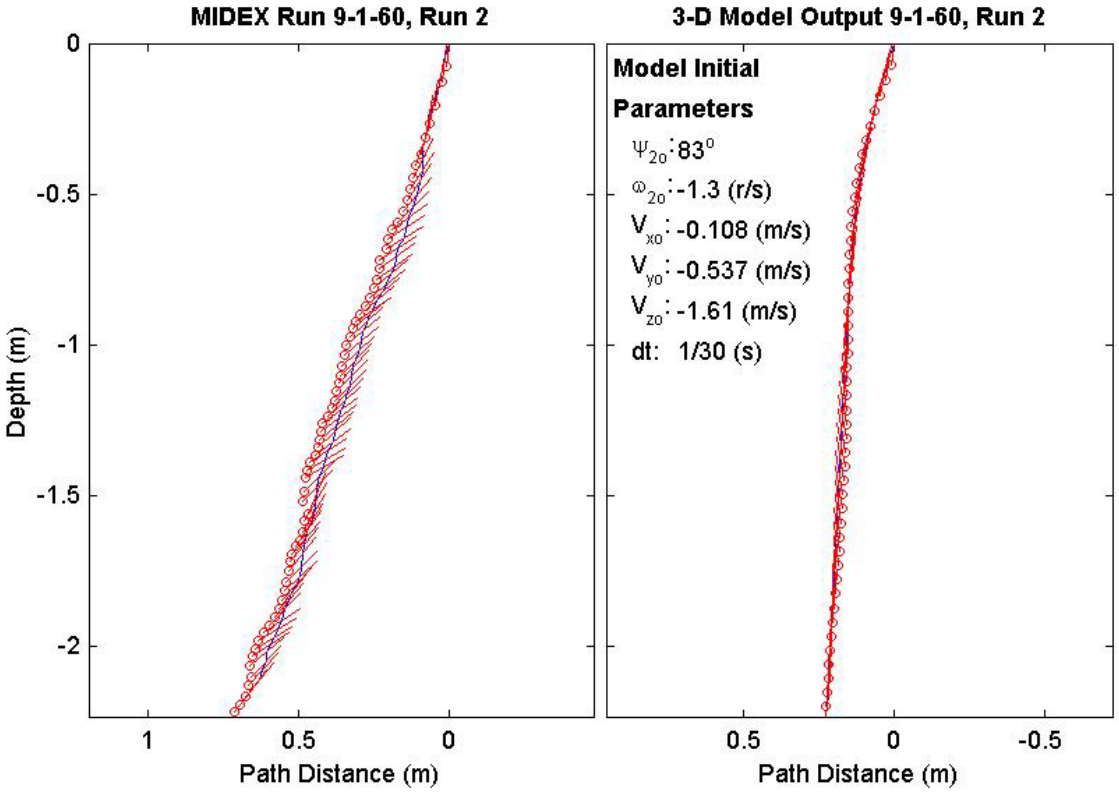

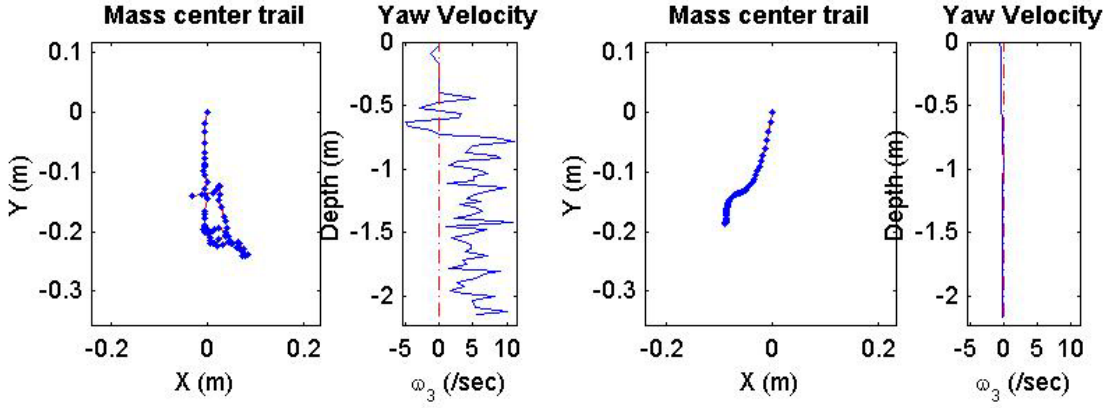

Final Drop
Parameters (60/9-2932)

time: 1.97(s)
xy_{fe}: 0.361(m)
V_{xfe}: 0(m/s)
V_{yfe}: -0.426(m/s)
V_{zfe}: -0.857(m/s)
Ψ_{fe}: 33.1°
depth: 2.21(m)

Mine Shape
Parameters (60/9-2932)

d: 0.04(m)
L: 0.0912(m)
m: 0.215(m)
J_1: 2.35e-005(kg*m^2)
J_2: 0.000158(kg*m^2)
J_3: 0.000158(kg*m^2)
χ: 0.002911(m)

Final Model
Parameters (60/9-2932)

time: 1.53(s)
xy_{fm}: 0.213(m)
V_{xfm}: -0.0262(m/s)
V_{yfm}: 6.15e-018(m/s)
V_{zfm}: -1.39(m/s)
Ψ_{fm}: 92.31°
depth: 2.23(m)

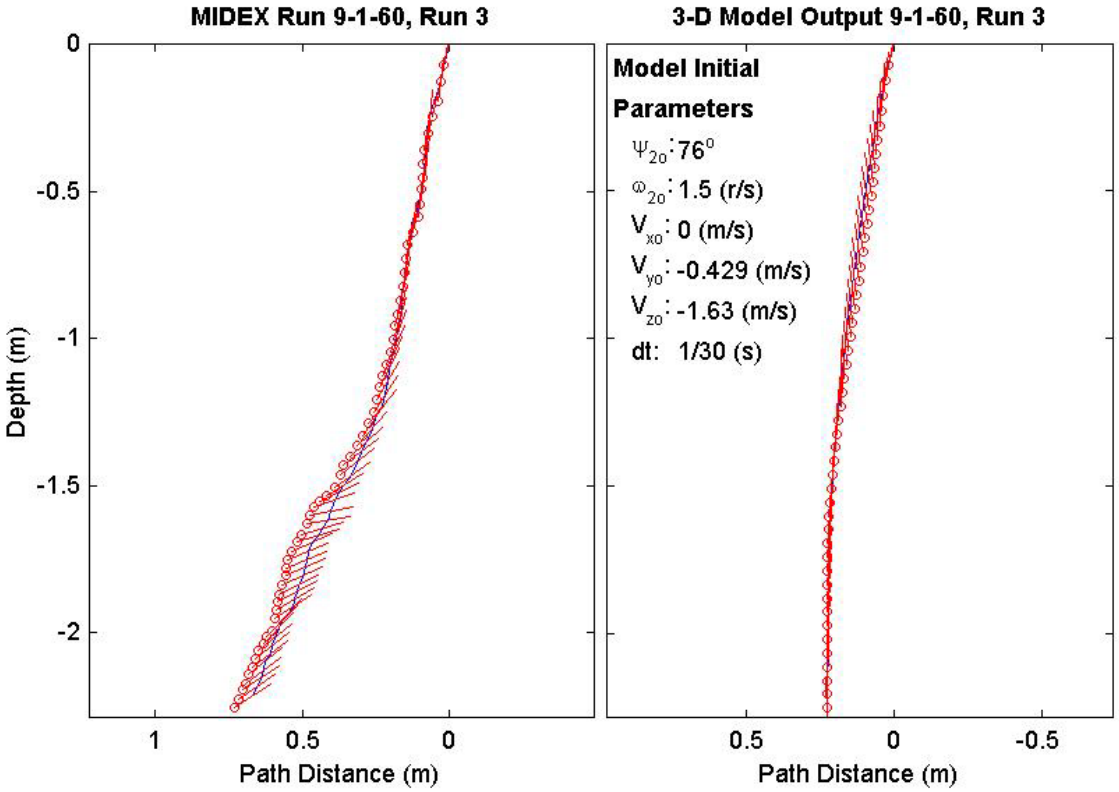

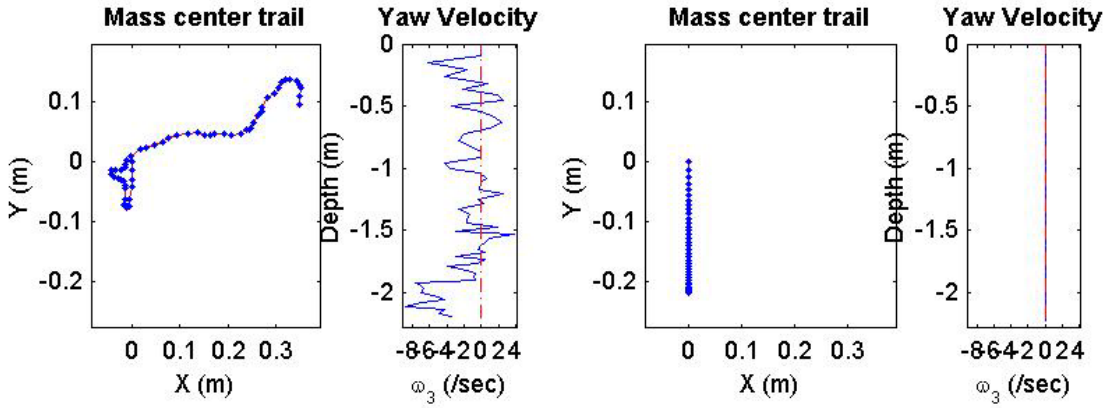

Final Drop

Parameters (60/9-2479)

time: 2.03(s)
xy_{fe}: 0.344(m)
V_{xfe}: 0.267(m/s)
V_{yfe}: 0.537(m/s)
V_{zfe}: -0.723(m/s)
Ψ_{fe}: 57.1°
depth: 2.15(m)

Mine Shape

Parameters (60/9-2479)

d: 0.04(m)
L: 0.0912(m)
m: 0.215(m)
J_1: 2.35e-005(kg*m^2)
J_2: 0.000158(kg*m^2)
J_3: 0.000158(kg*m^2)
χ: 0.002911(m)

Final Model

Parameters (60/9-2479)

time: 1.5(s)
xy_{fm}: 0.176(m)
V_{xfm}: -0.0518(m/s)
V_{yfm}: -0.000307(m/s)
V_{zfm}: -1.39(m/s)
Ψ_{fm}: 91.34°
depth: 2.2(m)

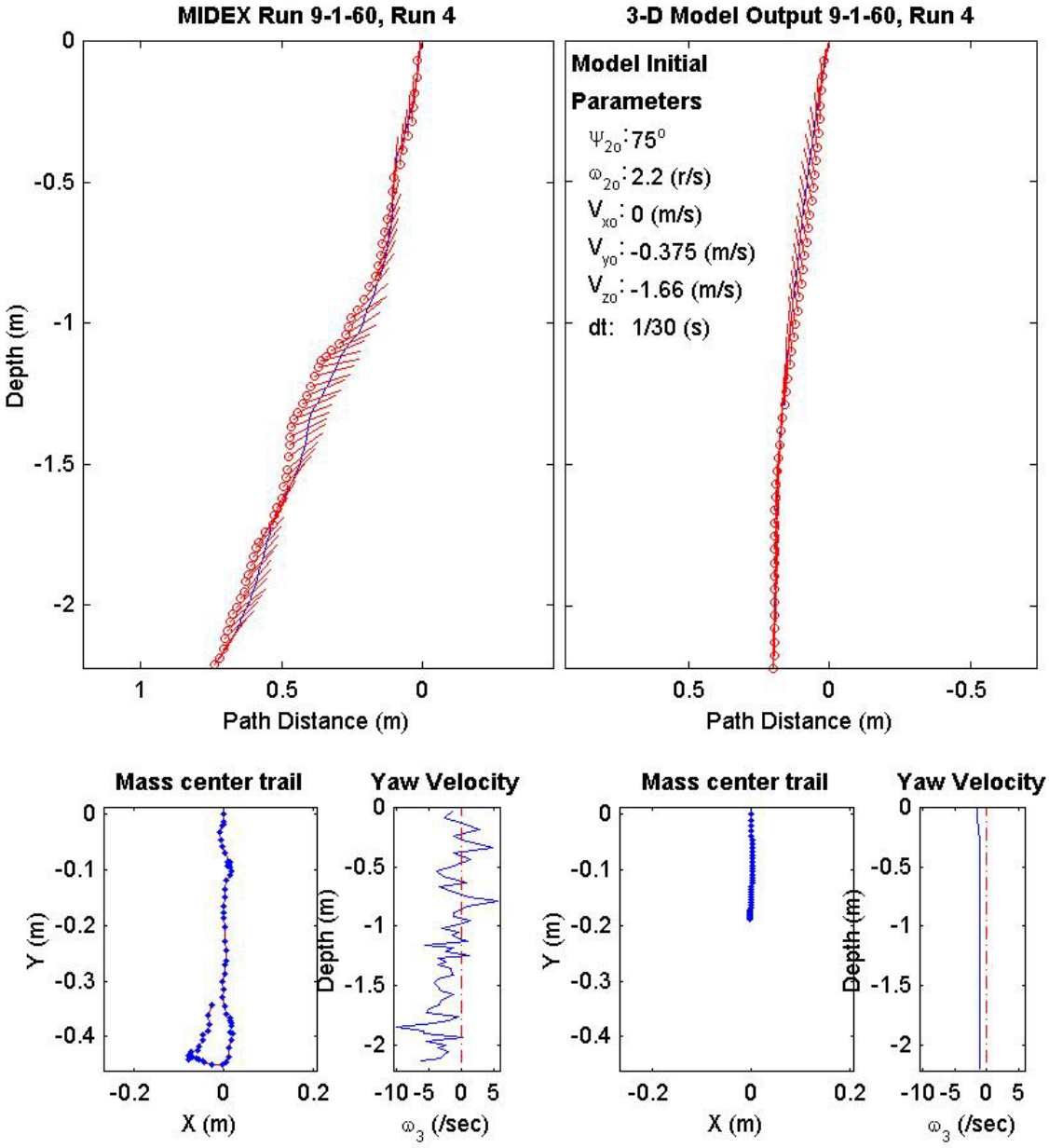

Final Drop
Parameters (60/9-1946)

time: 2.43(s)
xy_{fe}: 0.198(m)
V_{xfe}: 0.054(m/s)
V_{yfe}: 0.105(m/s)
V_{zfe}: -0.938(m/s)
Ψ_{fe}: 49.4°
depth: 2.17(m)

Mine Shape
Parameters (60/9-1946)

d: 0.04(m)
L: 0.0912(m)
m: 0.215(m)
J_1: 2.35e-005(kg*m^2)
J_2: 0.000158(kg*m^2)
J_3: 0.000158(kg*m^2)
χ: 0.002911(m)

Final Model
Parameters (60/9-1946)

time: 1.5(s)
xy_{fm}: 0.214(m)
V_{xfm}: -0.0507(m/s)
V_{yfm}: -0.0304(m/s)
V_{zfm}: -1.4(m/s)
Ψ_{fm}: 87.29°
depth: 2.2(m)

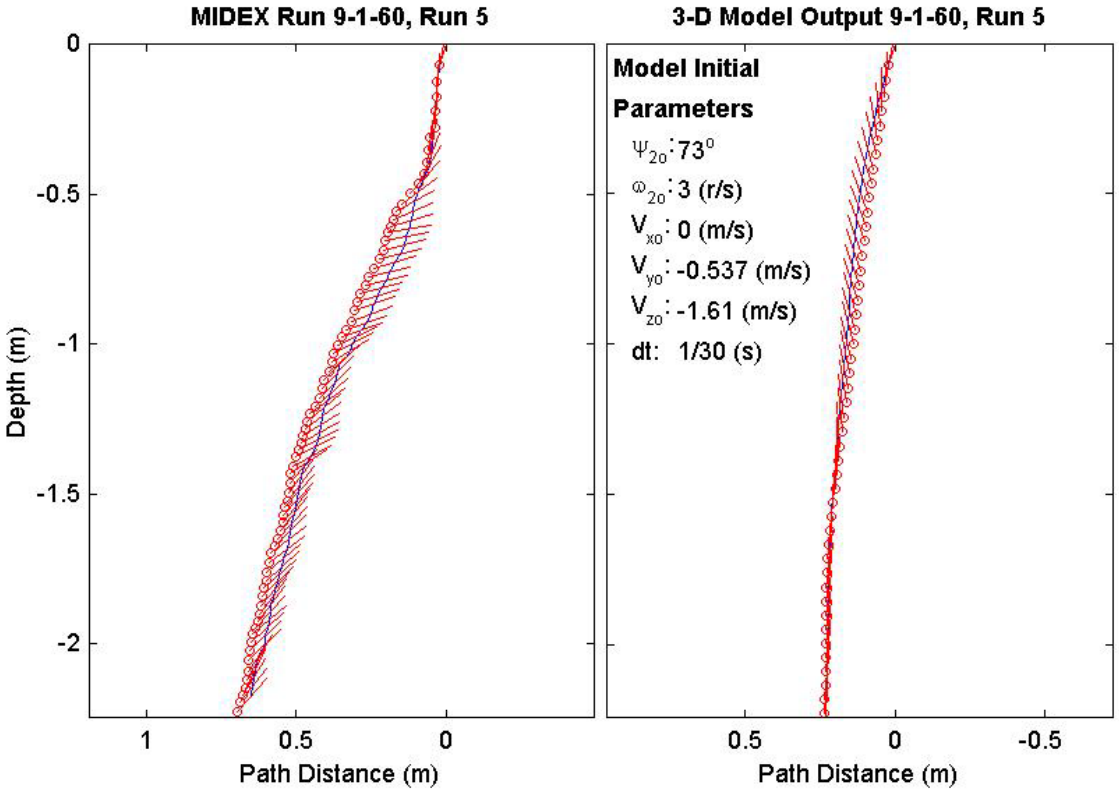

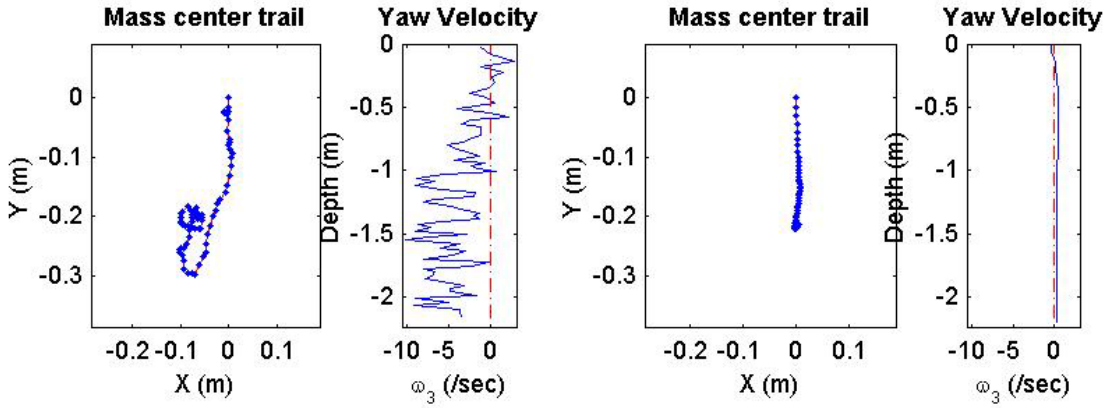

Final Drop Parameters (75/15-3815)

time: 1.07(s)
xy_{fe}: 0.173(m)
V_{xfe}: -0.055(m/s)
V_{yfe}: -0.108(m/s)
V_{zfe}: -1.85(m/s)
Ψ_{fe}: 82.4°
depth: 2.05(m)

Mine Shape Parameters (75/15-3815)

d: 0.04(m)
L: 0.152(m)
m: 0.323(m)
J_1: 3.3e-005(kg*m^2)
J_2: 0.000578(kg*m^2)
J_3: 0.000578(kg*m^2)
χ: 0.007411(m)

Final Model Parameters (75/15-3815)

time: 1.23(s)
xy_{fm}: 0.336(m)
V_{xfm}: 0.101(m/s)
V_{yfm}: 0.00912(m/s)
V_{zfm}: -1.52(m/s)
Ψ_{fm}: 91.15°
depth: 2.09(m)

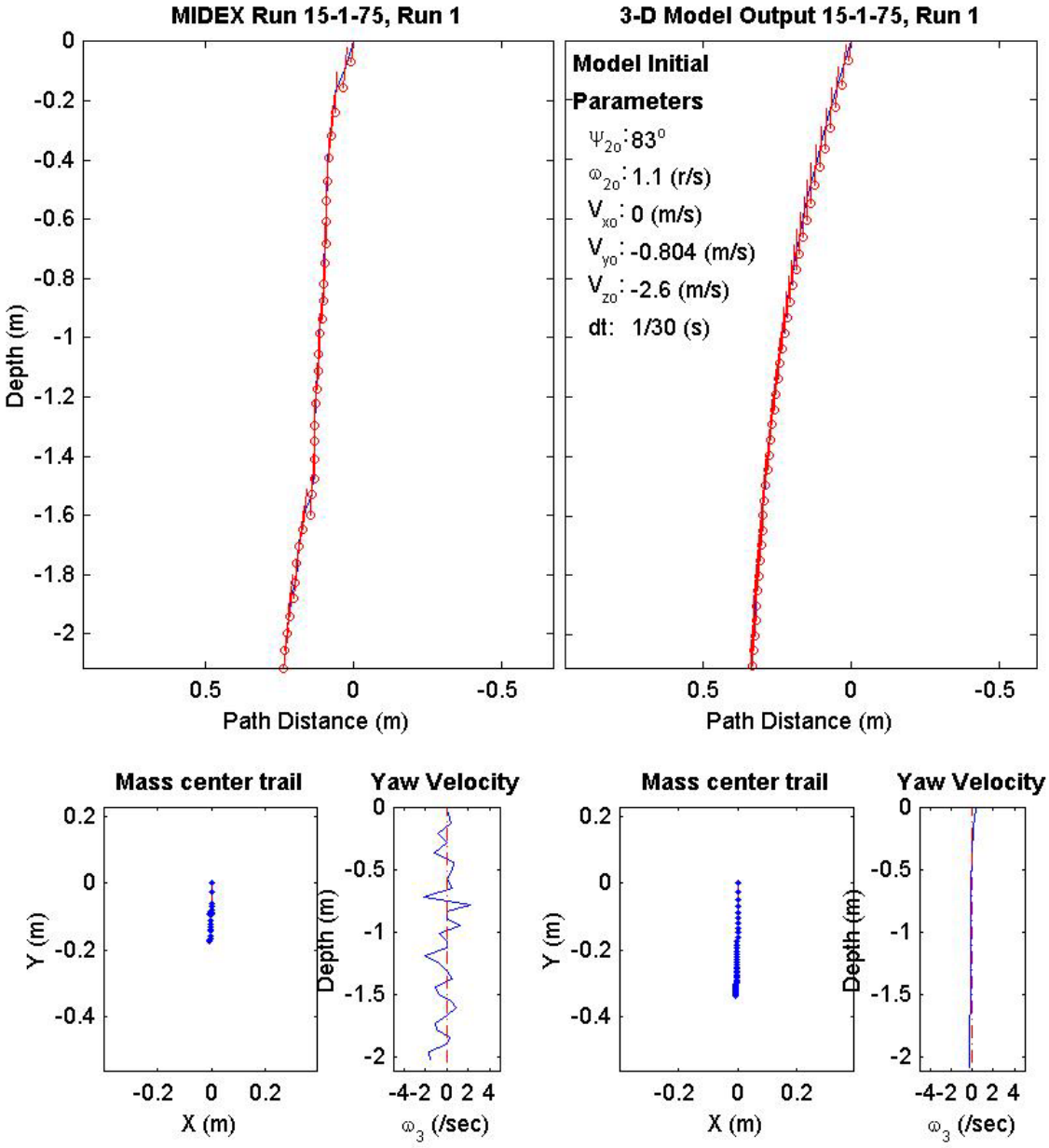

Final Drop Parameters (75/15-3238)

time: 1.1(s)
xy_{fe}: 0.188(m)
V_{xfe}: 0.267(m/s)
V_{yfe}: -0.051(m/s)
V_{zfe}: -1.46(m/s)
Ψ_{fe}: 88.2°
depth: 2.02(m)

Mine Shape Parameters (75/15-3238)

d: 0.04(m)
L: 0.152(m)
m: 0.323(m)
J_1: 3.3e-005(kg*m^2)
J_2: 0.000578(kg*m^2)
J_3: 0.000578(kg*m^2)
χ: 0.007411(m)

Final Model Parameters (75/15-3238)

time: 1.23(s)
xy_{fm}: 0.298(m)
V_{xfm}: 0.0652(m/s)
V_{yfm}: 0.0257(m/s)
V_{zfm}: -1.52(m/s)
Ψ_{fm}: 85.59°
depth: 2.05(m)

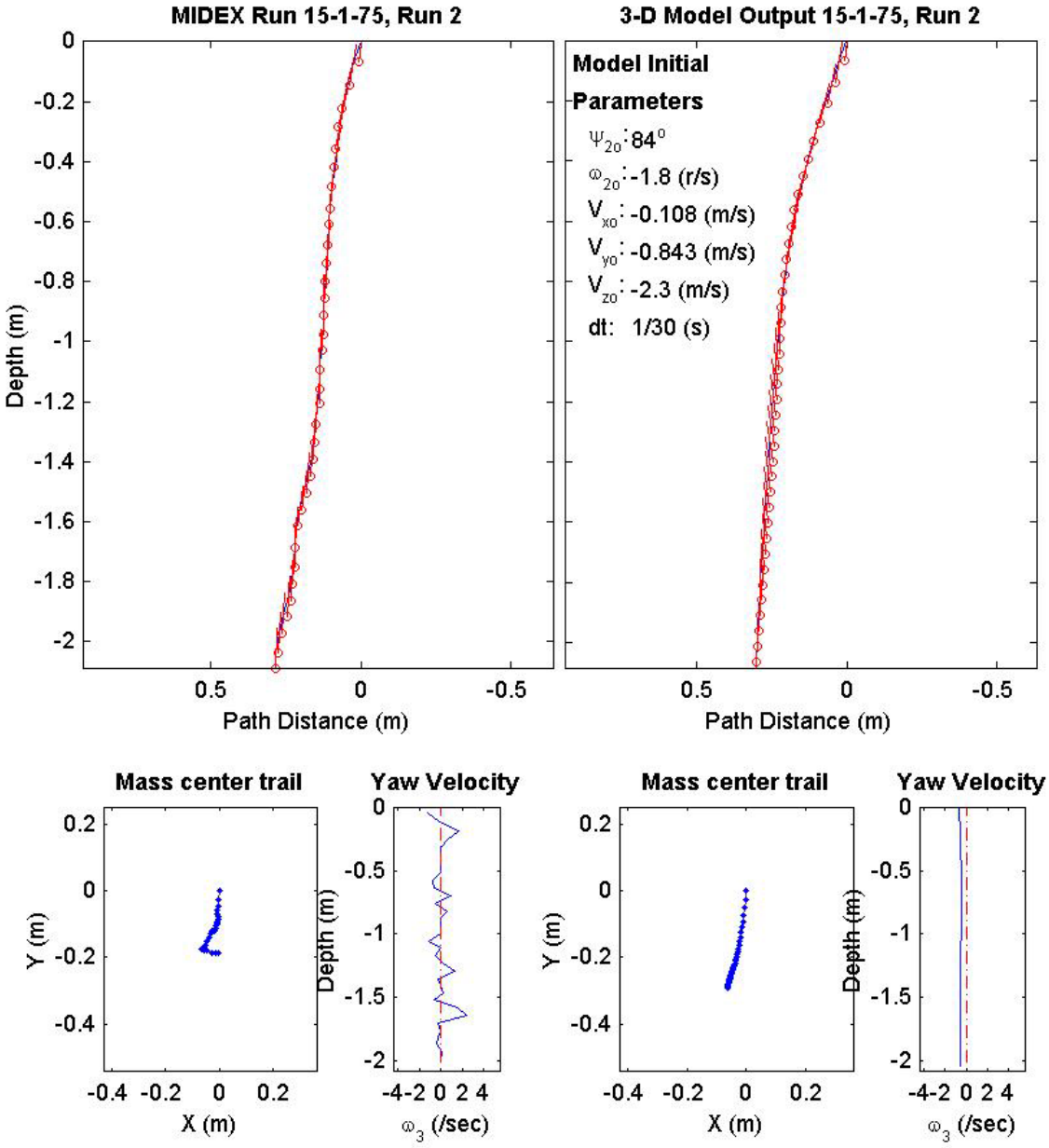

Final Drop Parameters (75/15-2358)

time: 1.2(s)
xy_{fe}: 0.173(m)
V_{xfe}: -0.163(m/s)
V_{yfe}: 0.055(m/s)
V_{zfe}: -1.45(m/s)
Ψ_{fe}: 85.5°
depth: 2.17(m)

Mine Shape Parameters (75/15-2358)

d: 0.04(m)
L: 0.152(m)
m: 0.323(m)
J_1: 3.3e-005(kg*m^2)
J_2: 0.000578(kg*m^2)
J_3: 0.000578(kg*m^2)
χ: 0.007411(m)

Final Model Parameters (75/15-2358)

time: 1.3(s)
xy_{fm}: 0.223(m)
V_{xfm}: 0.0298(m/s)
V_{yfm}: 0.00159(m/s)
V_{zfm}: -1.52(m/s)
Ψ_{fm}: 83.29°
depth: 2.19(m)

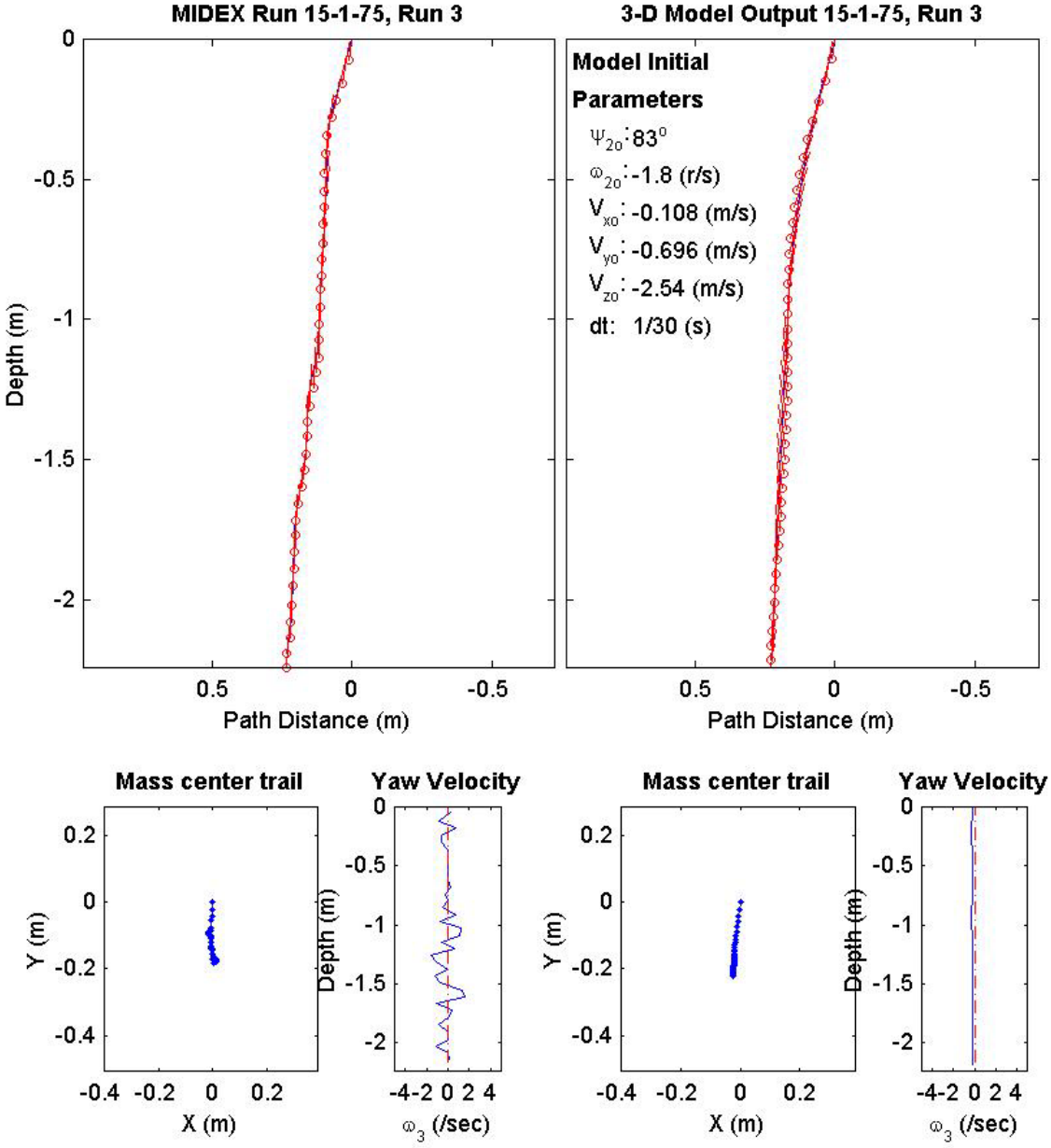

Final Drop

Parameters (75/12-3908)

time: 1.37(s)
xy_{fe}: 0.196(m)
V_{xfe}: 0.213(m/s)
V_{yfe}: -0.054(m/s)
V_{zfe}: -1.39(m/s)
Ψ_{fe}: 75.9°
depth: 2.16(m)

Mine Shape

Parameters (75/12-3908)

d: 0.04(m)
L: 0.121(m)
m: 0.254(m)
J_1: 2.71e-005(kg*m^2)
J_2: 0.000321(kg*m^2)
J_3: 0.000321(kg*m^2)
χ: 0.005307(m)

Final Model

Parameters (75/12-3908)

time: 1.47(s)
xy_{fm}: 0.191(m)
V_{xfm}: 0.0216(m/s)
V_{yfm}: -0.00675(m/s)
V_{zfm}: -1.37(m/s)
Ψ_{fm}: 89.29°
depth: 2.17(m)

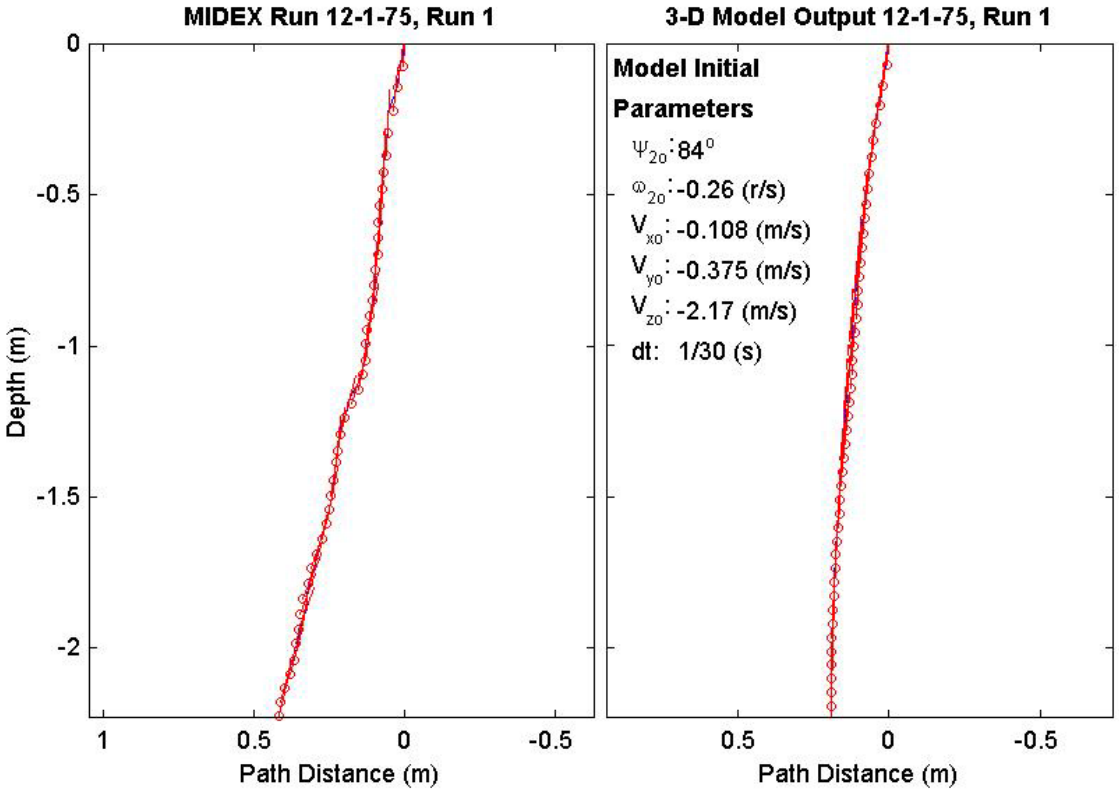

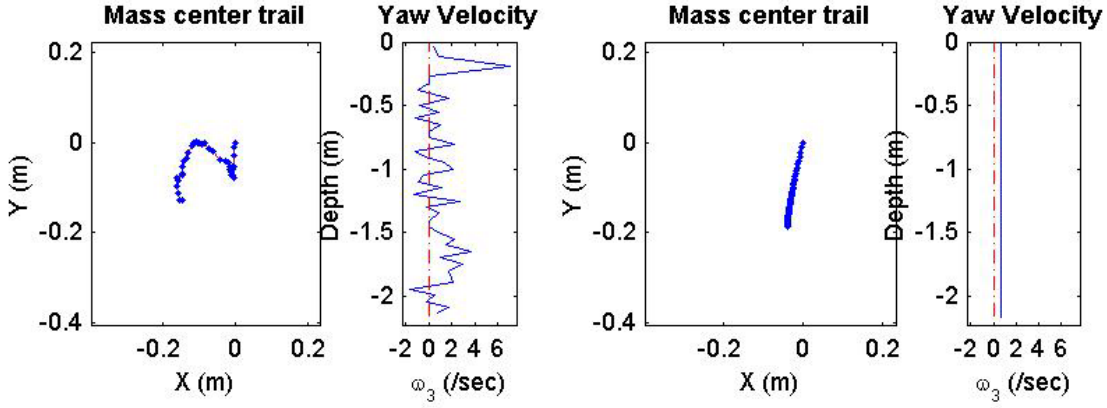

Final Drop

Parameters (75/12-3351)

time: 1.37(s)
xy_{fe}: 0.178(m)
V_{xfe}: 0.537(m/s)
V_{yfe}: -0.213(m/s)
V_{zfe}: -1.31(m/s)
Ψ_{fe}: 57.9°
depth: 2.13(m)

Mine Shape

Parameters (75/12-3351)

d: 0.04(m)
L: 0.121(m)
m: 0.254(m)
J_1: 2.71e-005(kg*m^2)
J_2: 0.000321(kg*m^2)
J_3: 0.000321(kg*m^2)
χ: 0.005307(m)

Final Model

Parameters (75/12-3351)

time: 1.47(s)
xy_{fm}: 0.178(m)
V_{xfm}: -0.0154(m/s)
V_{yfm}: 0.00413(m/s)
V_{zfm}: -1.37(m/s)
Ψ_{fm}: 88.19°
depth: 2.15(m)

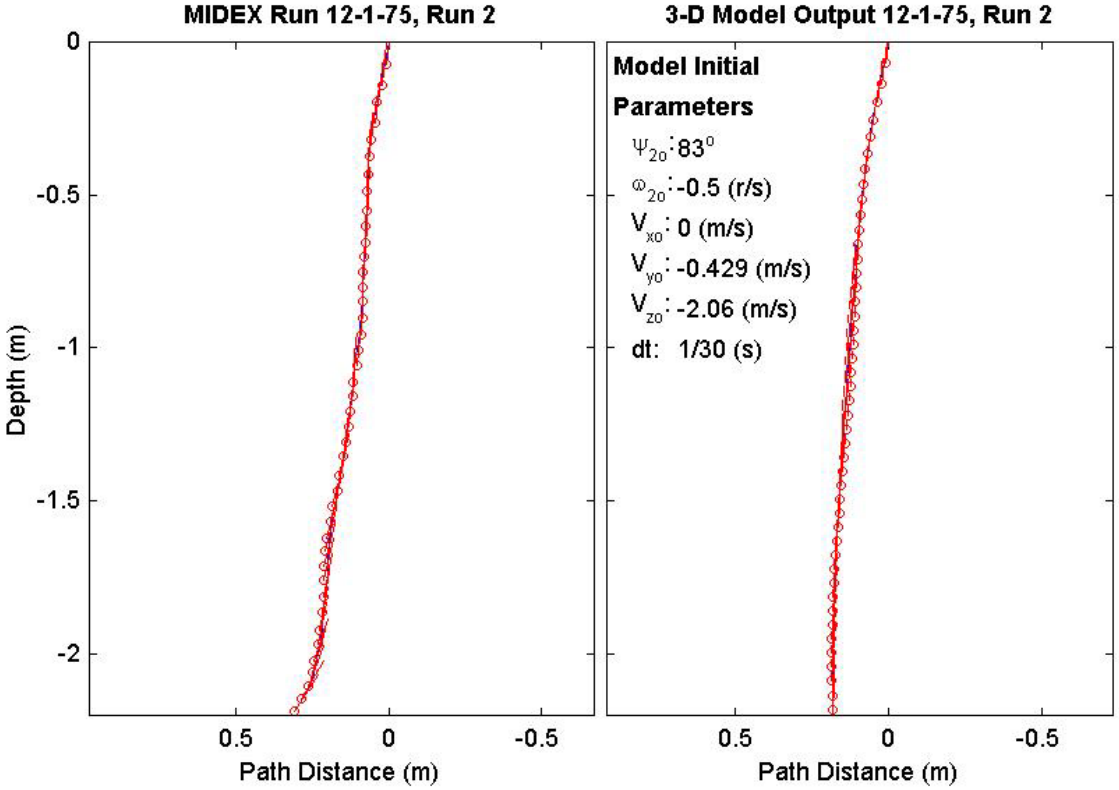

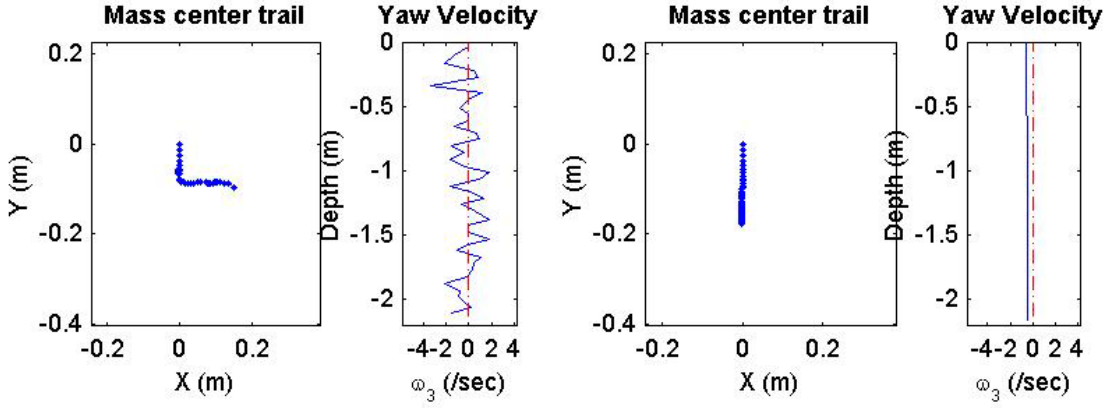

Final Drop
Parameters (75/12-2484)

time: 1.33(s)
xy_{fe}: 0.0861(m)
V_{xfe}: 0.162(m/s)
V_{yfe}: 0.108(m/s)
V_{zfe}: -1.63(m/s)
Ψ_{fe}: 81.4°
depth: 2.12(m)

Mine Shape
Parameters (75/12-2484)

d: 0.04(m)
L: 0.121(m)
m: 0.254(m)
J_1: 2.71e-005(kg*m^2)
J_2: 0.000321(kg*m^2)
J_3: 0.000321(kg*m^2)
χ: 0.005307(m)

Final Model
Parameters (75/12-2484)

time: 1.5(s)
xy_{fm}: 0.223(m)
V_{xfm}: 0.0223(m/s)
V_{yfm}: -0.0285(m/s)
V_{zfm}: -1.37(m/s)
Ψ_{fm}: 89.03°
depth: 2.14(m)

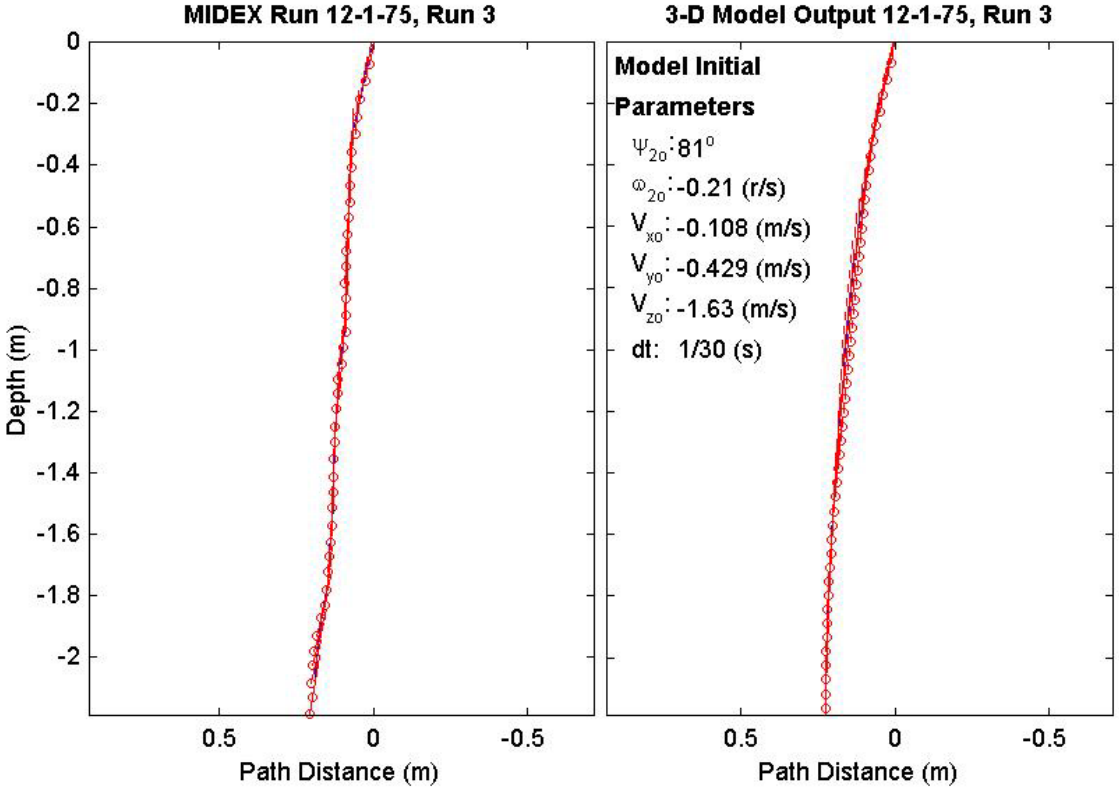

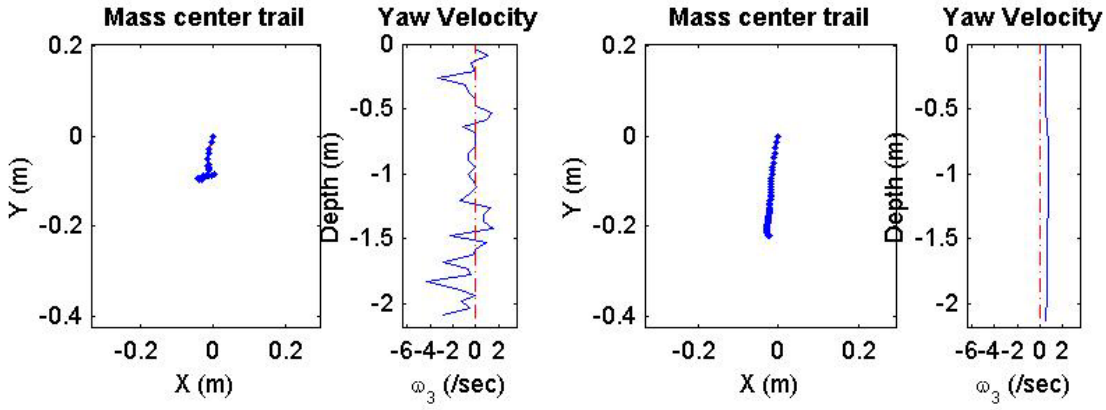

Final Drop

Parameters (75/9-4014)

time: 1.8(s)
xy_{fe}: 0.529(m)
V_{xfe}: -0.051(m/s)
V_{yfe}: -0.051(m/s)
V_{zfe}: -1.04(m/s)
Ψ_{fe}: 34.4°
depth: 2.05(m)

Mine Shape

Parameters (75/9-4014)

d: 0.04(m)
L: 0.0912(m)
m: 0.215(m)
J_1: 2.35e-005(kg*m^2)
J_2: 0.000158(kg*m^2)
J_3: 0.000158(kg*m^2)
χ: 0.002911(m)

Final Model

Parameters (75/9-4014)

time: 1.4(s)
xy_{fm}: 0.129(m)
V_{xfm}: -0.0411(m/s)
V_{yfm}: 5.45e-018(m/s)
V_{zfm}: -1.39(m/s)
Ψ_{fm}: 91.16°
depth: 2.09(m)

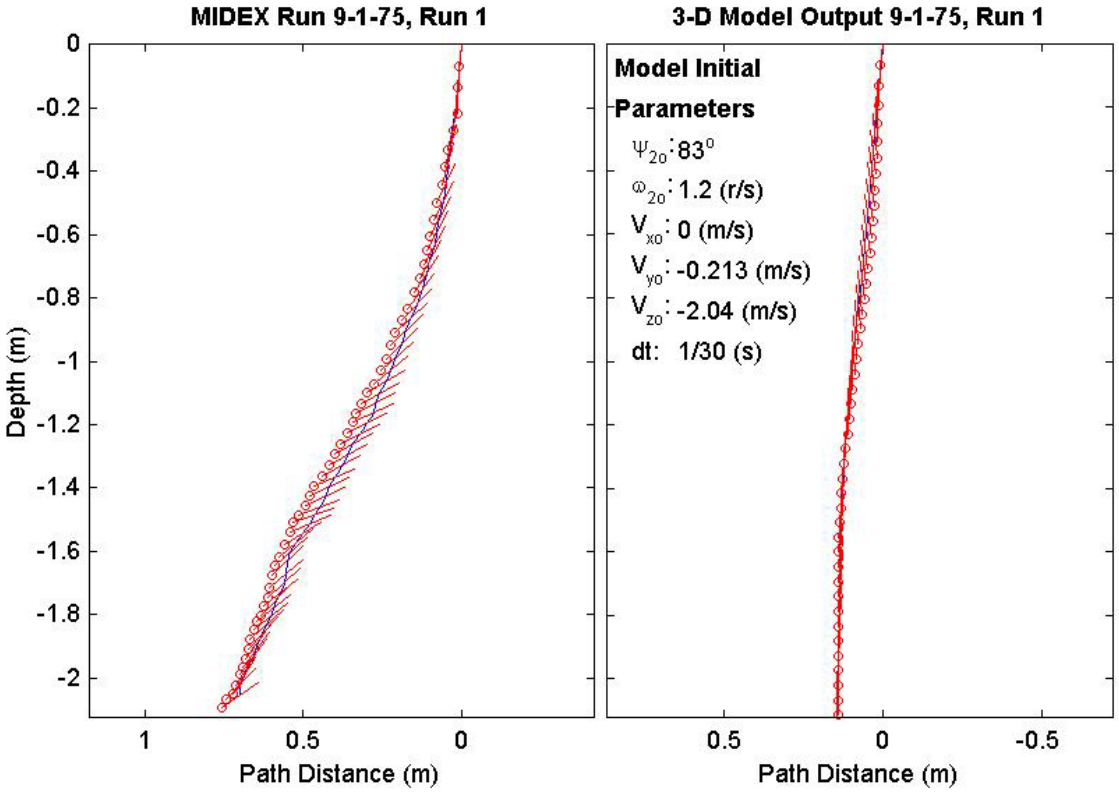

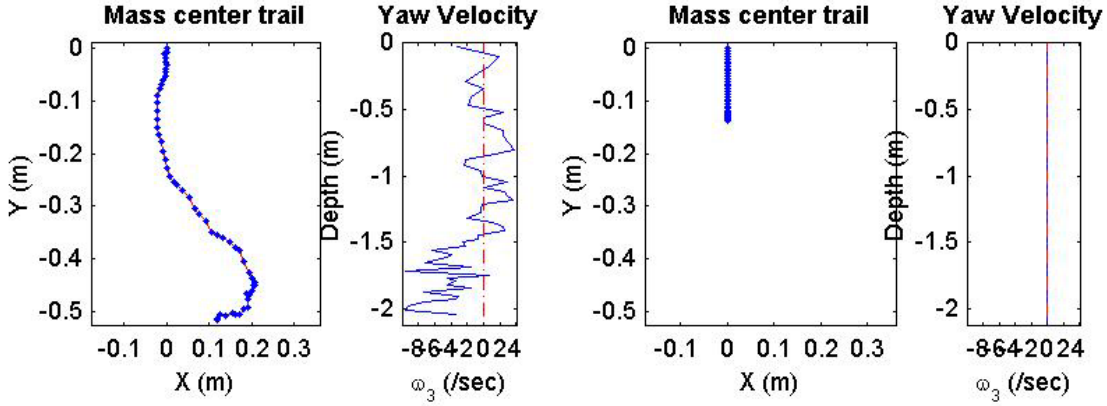

Final Drop

Parameters (75/9-3275)

time: 2.07(s)
xy_{fe}: 0.147(m)
V_{xfe}: -0.216(m/s)
V_{yfe}: 0.321(m/s)
V_{zfe}: -0.669(m/s)
Ψ_{fe}: 46°
depth: 2.19(m)

Mine Shape

Parameters (75/9-3275)

d: 0.04(m)
L: 0.0912(m)
m: 0.215(m)
J_1: 2.35e-005(kg*m^2)
J_2: 0.000158(kg*m^2)
J_3: 0.000158(kg*m^2)
χ: 0.002911(m)

Final Model

Parameters (75/9-3275)

time: 1.5(s)
xy_{fm}: 0.125(m)
V_{xfm}: 0.0267(m/s)
V_{yfm}: 0.0211(m/s)
V_{zfm}: -1.39(m/s)
Ψ_{fm}: 85.43°
depth: 2.21(m)

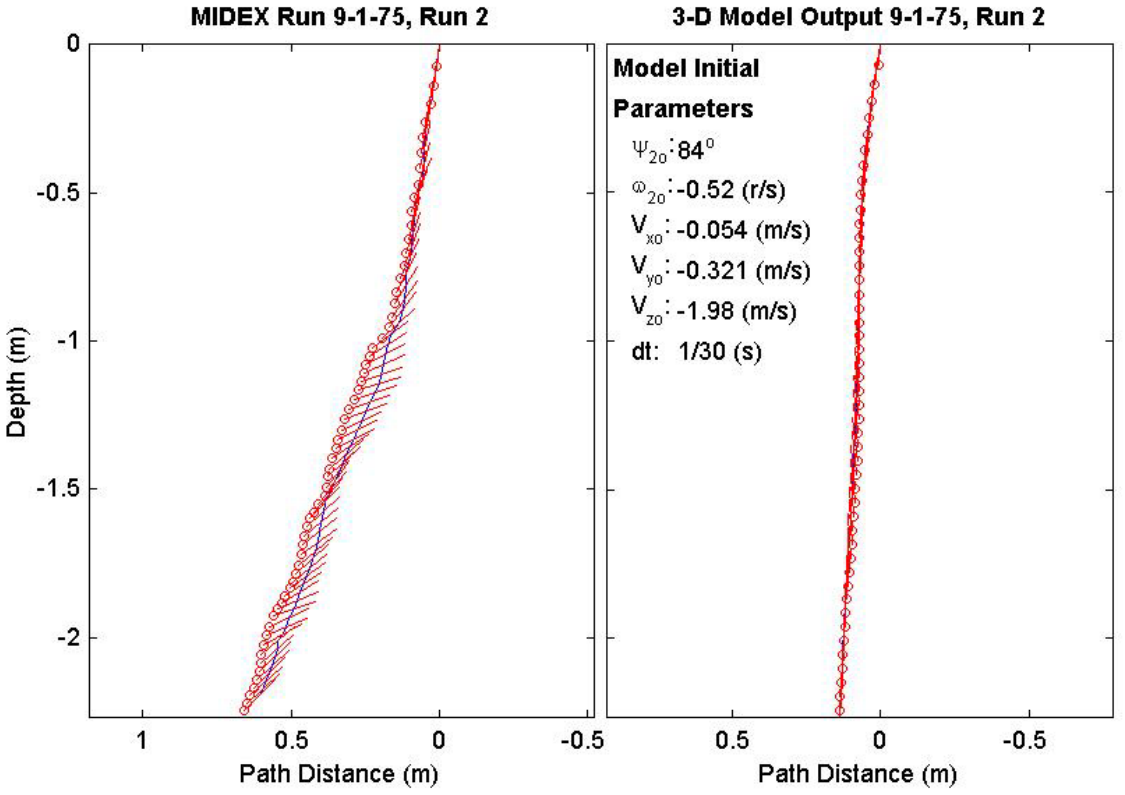

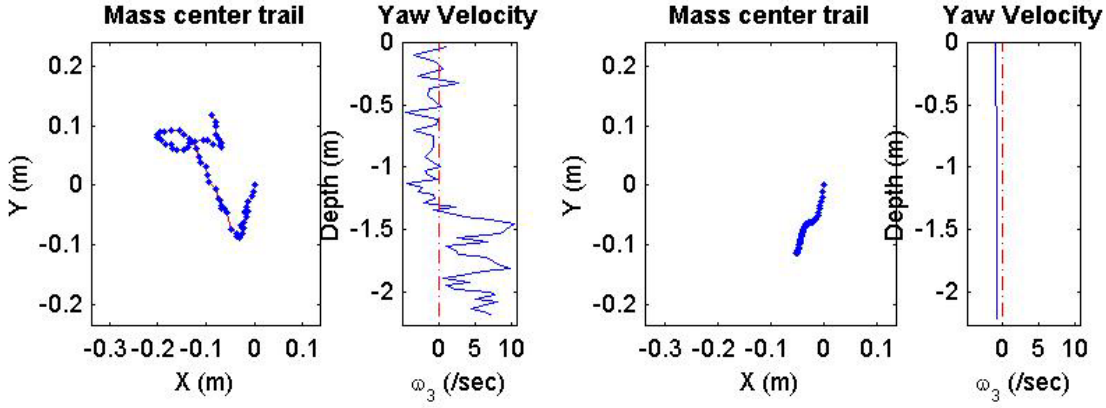

Final Drop

Parameters (75/9-2428)

time: 2.23(s)
xy_{fe}: 0.109(m)
V_{xfe}: 0.216(m/s)
V_{yfe}: 0(m/s)
V_{zfe}: -0.696(m/s)
Ψ_{fe}: 37.3°
depth: 2.28(m)

Mine Shape

Parameters (75/9-2428)

d: 0.04(m)
L: 0.0912(m)
m: 0.215(m)
J_1: 2.35e-005(kg*m^2)
J_2: 0.000158(kg*m^2)
J_3: 0.000158(kg*m^2)
χ: 0.002911(m)

Final Model

Parameters (75/9-2428)

time: 1.57(s)
xy_{fm}: 0.154(m)
V_{xfm}: -0.0336(m/s)
V_{yfm}: -0.0124(m/s)
V_{zfm}: -1.39(m/s)
Ψ_{fm}: 93.8°
depth: 2.31(m)

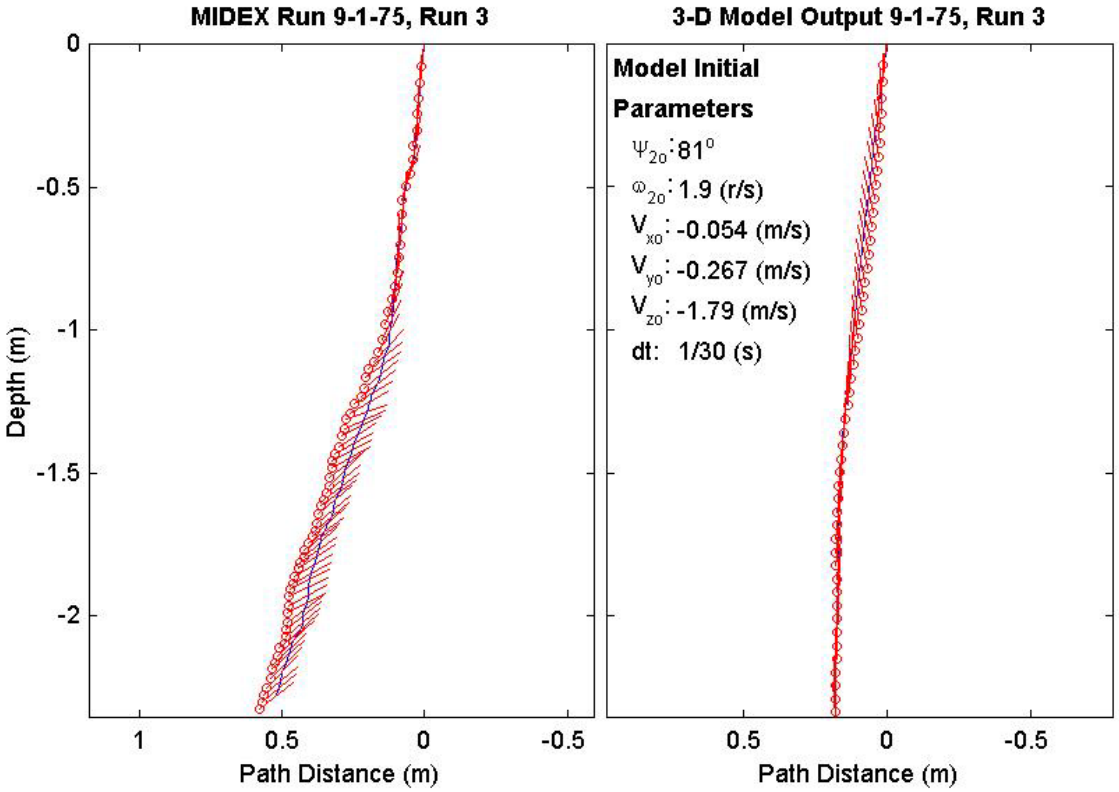

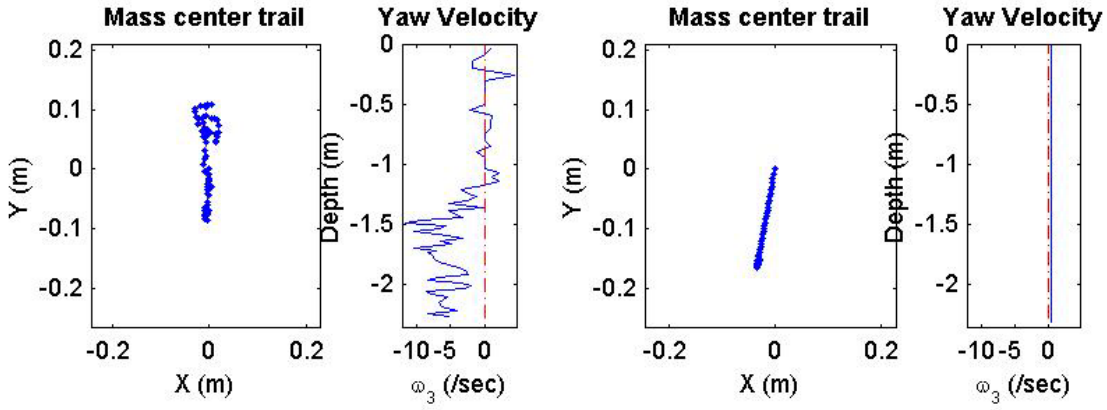

Final Drop Parameters (15/15-1384)

time: 3.2(s)
xy_{fe}: 0.323(m)
V_{xfe}: 0(m/s)
V_{yfe}: -0.163(m/s)
V_{zfe}: -0.723(m/s)
Ψ_{fe}: -21°
depth: 2.24(m)

Mine Shape Parameters (15/15-1384)

d: 0.04(m)
L: 0.152(m)
m: 0.323(m)
J_1: 3.3e-005(kg*m^2)
J_2: 0.000609(kg*m^2)
J_3: 0.000609(kg*m^2)
χ: 4.6e-005(m)

Final Model Parameters (15/15-1384)

time: 1.83(s)
xy_{fm}: 0.247(m)
V_{xfm}: 0.00588(m/s)
V_{yfm}: 0.0359(m/s)
V_{zfm}: -1.53(m/s)
Ψ_{fm}: -85.43°
depth: 2.27(m)

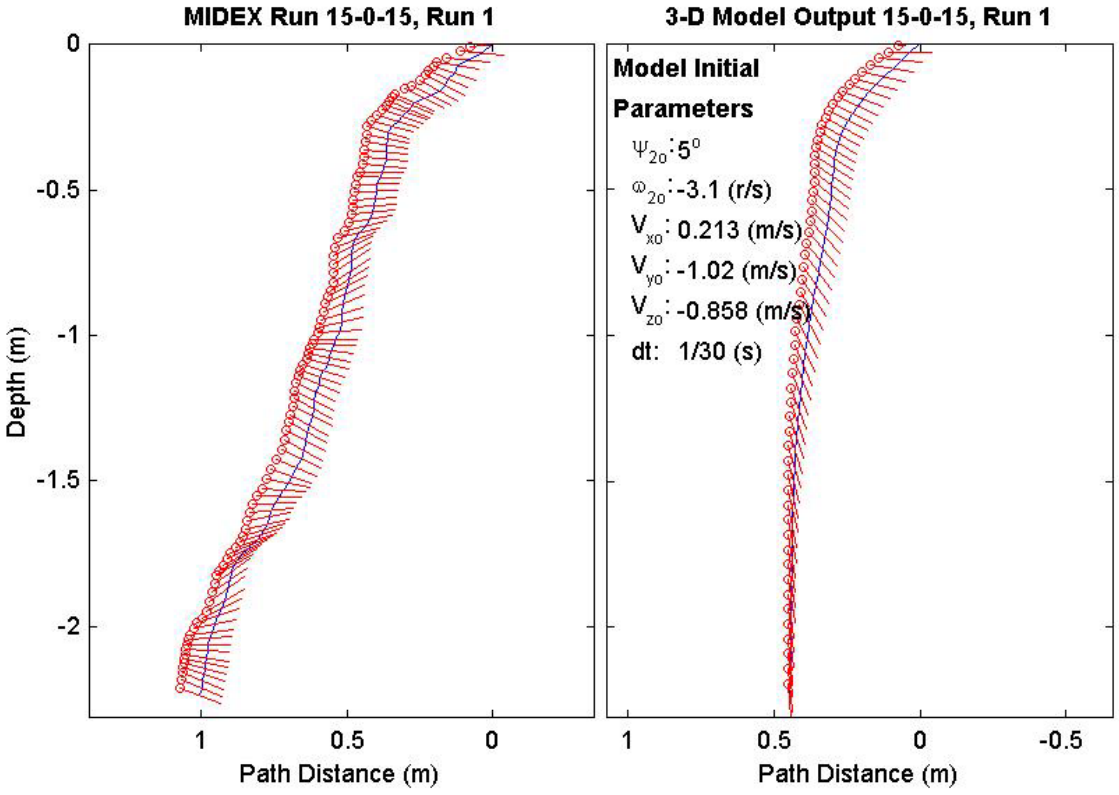

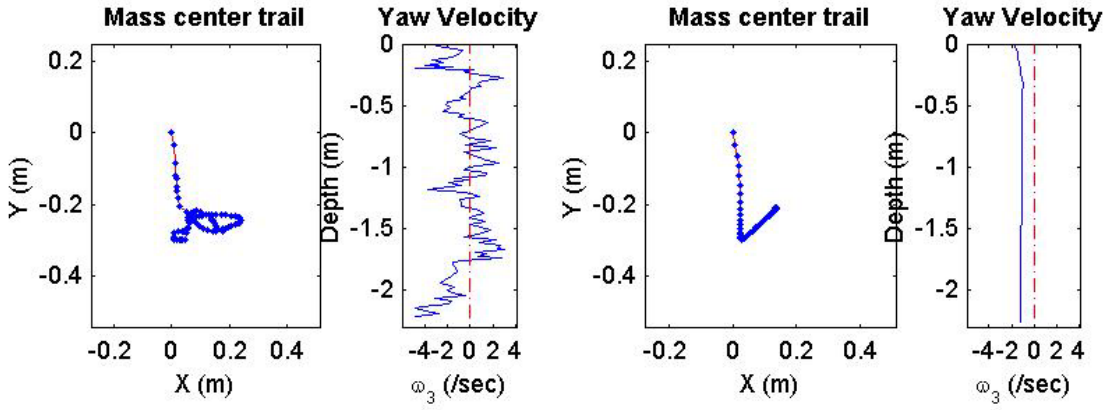

Final Drop Parameters (15/15-1379)

time: 2.9(s)
xy_{fe}: 0.0187(m)
V_{xfe}: -0.106(m/s)
V_{yfe}: -0.163(m/s)
V_{zfe}: -0.75(m/s)
Ψ_{fe}: 3.3°
depth: 2.25(m)

Mine Shape Parameters (15/15-1379)

d: 0.04(m)
L: 0.152(m)
m: 0.323(m)
J_1: 3.3e-005(kg*m^2)
J_2: 0.000609(kg*m^2)
J_3: 0.000609(kg*m^2)
χ: 4.6e-005(m)

Final Model Parameters (15/15-1379)

time: 1.8(s)
xy_{fm}: 0.252(m)
V_{xfm}: 0.0459(m/s)
V_{yfm}: 0.0258(m/s)
V_{zfm}: -1.53(m/s)
Ψ_{fm}: -85.91°
depth: 2.25(m)

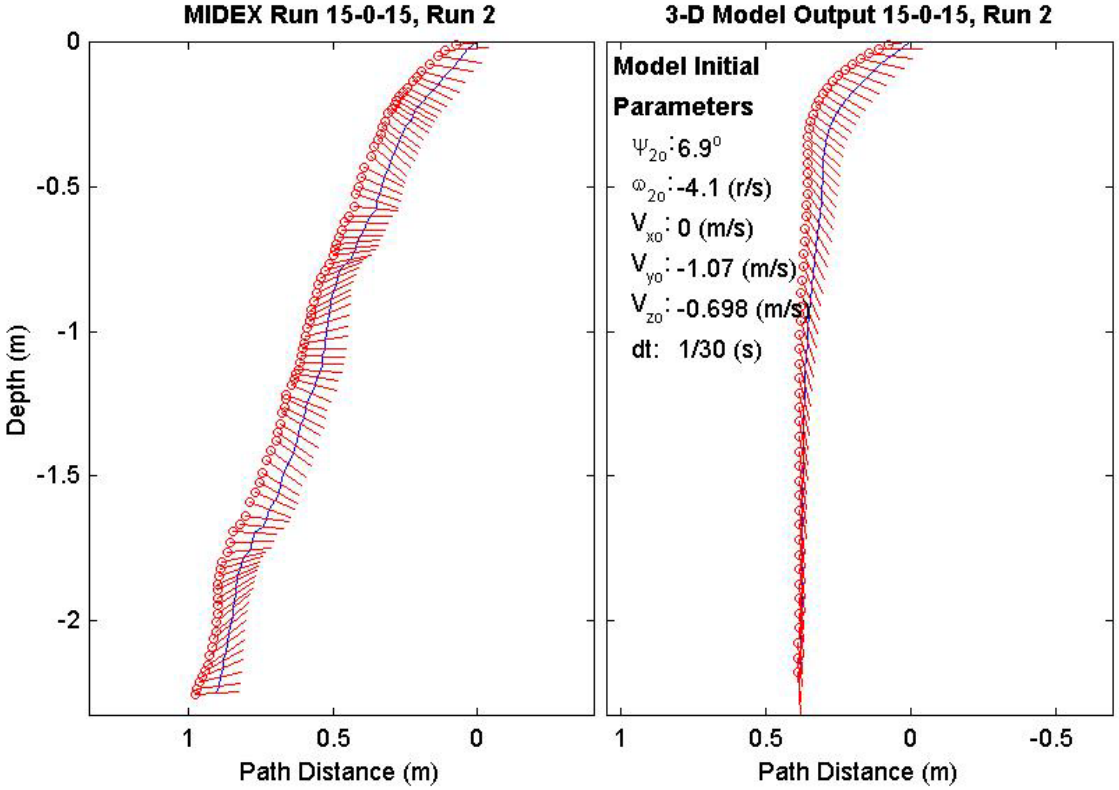

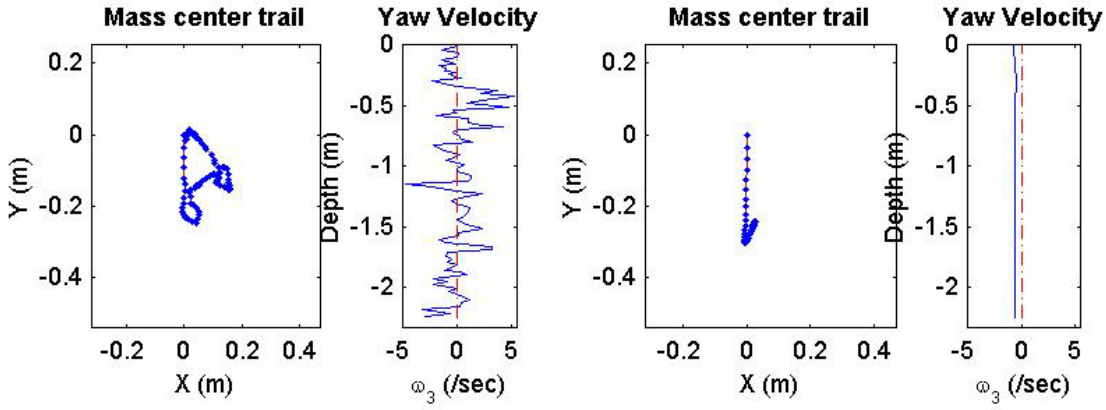

Final Drop Parameters (15/15-2180)

time: 2.77(s)
xy_{fe}: 0.475(m)
V_{xfe}: -0.106(m/s)
V_{yfe}: 0(m/s)
V_{zfe}: -0.883(m/s)
Ψ_{fe}: 0^{o}
depth: 2.21(m)

Mine Shape Parameters (15/15-2180)

d: 0.04(m)
L: 0.152(m)
m: 0.323(m)
J_1: 3.3e-005($kg*m^2$)
J_2: 0.000609($kg*m^2$)
J_3: 0.000609($kg*m^2$)
χ: 4.6e-005(m)

Final Model Parameters (15/15-2180)

time: 1.83(s)
xy_{fm}: 0.431(m)
V_{xfm}: -0.0253(m/s)
V_{yfm}: -0.016(m/s)
V_{zfm}: -1.53(m/s)
Ψ_{fm}: -78.9^{o}
depth: 2.22(m)

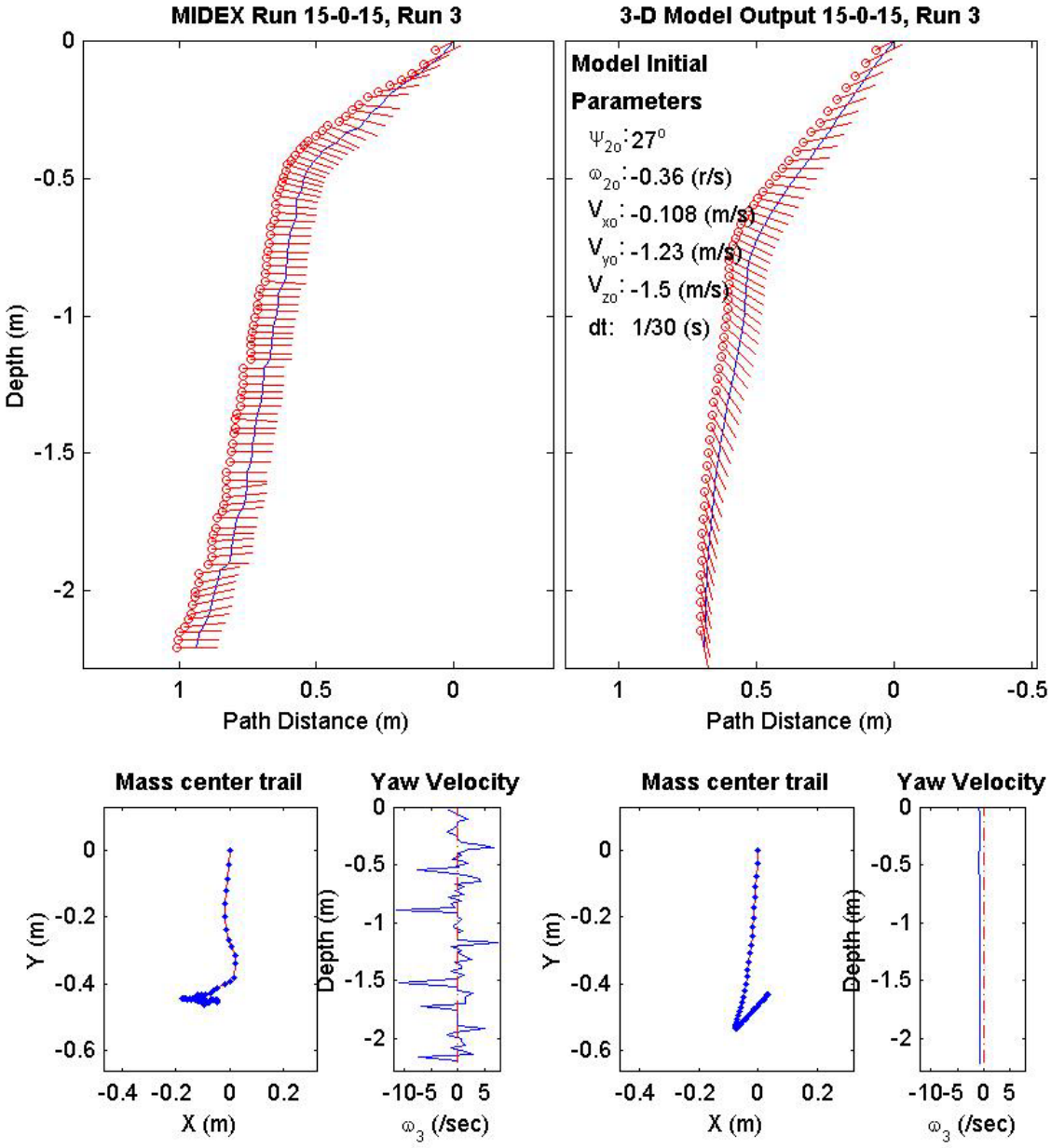

Final Drop Parameters (15/15-1918)

time: 2.87(s)
xy_{fe}: 0.371(m)
V_{xfe}: 0.055(m/s)
V_{yfe}: -0.163(m/s)
V_{zfe}: -0.938(m/s)
Ψ_{fe}: 4.3°
depth: 2.24(m)

Mine Shape Parameters (15/15-1918)

d: 0.04(m)
L: 0.152(m)
m: 0.323(m)
J_1: 3.3e-005(kg*m^2)
J_2: 0.000609(kg*m^2)
J_3: 0.000609(kg*m^2)
χ: 4.6e-005(m)

Final Model Parameters (15/15-1918)

time: 2.07(s)
xy_{fm}: 0.649(m)
V_{xfm}: 0.00509(m/s)
V_{yfm}: 0.0686(m/s)
V_{zfm}: -1.52(m/s)
Ψ_{fm}: -89.91°
depth: 2.27(m)

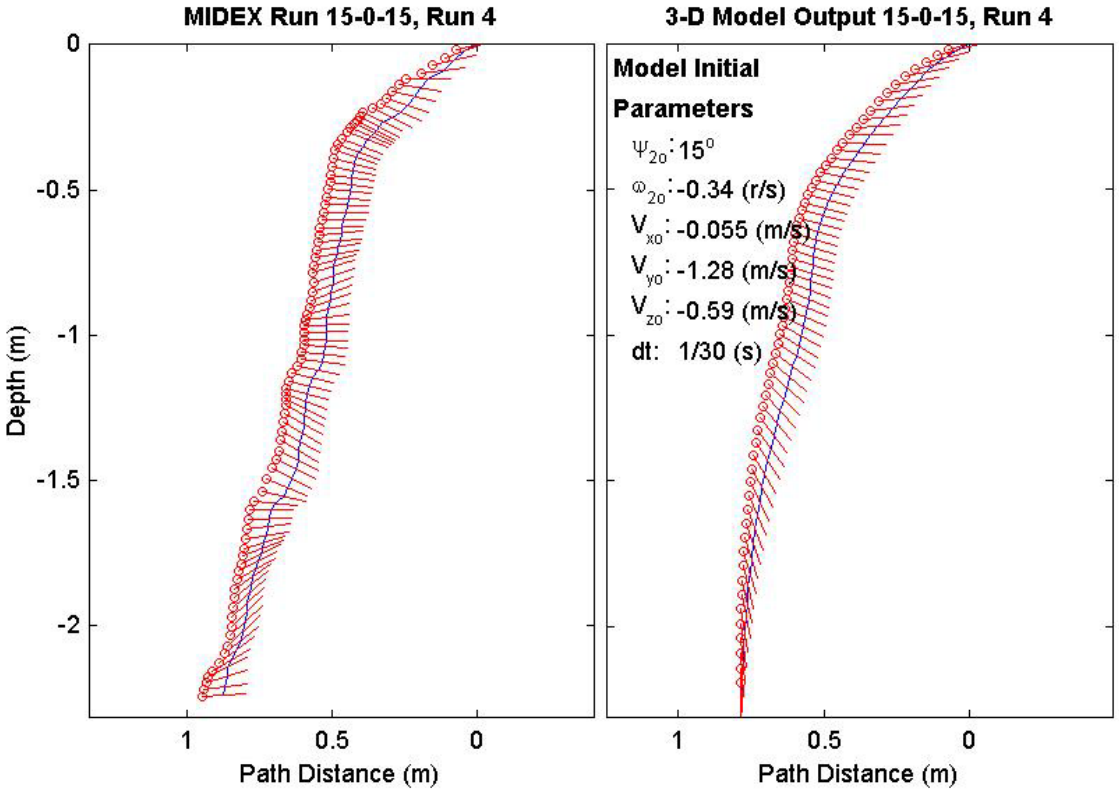

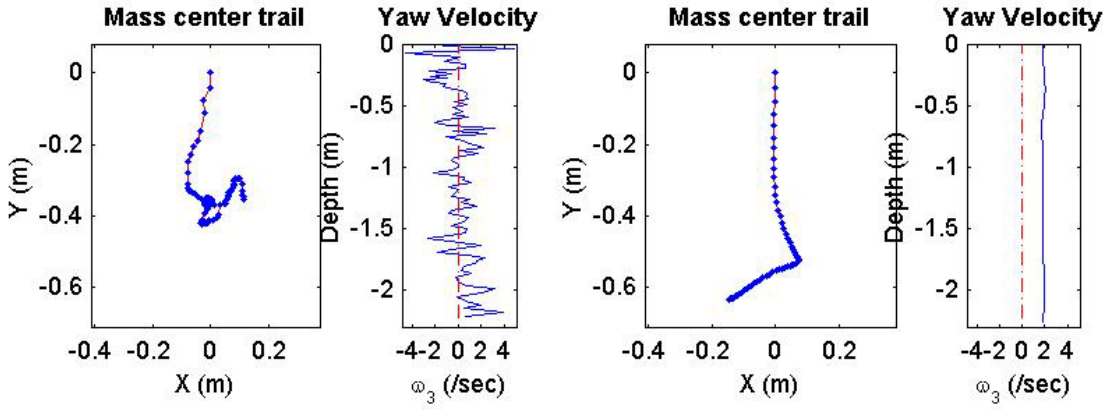

Final Drop

Parameters (15/12-1563)

time: 2.97(s)
xy_{fe}: 0.223(m)
V_{xfe}: -0.321(m/s)
V_{yfe}: 0.105(m/s)
V_{zfe}: -0.752(m/s)
Ψ_{fe}: 0^{o}
depth: 2.29(m)

Mine Shape

Parameters (15/12-1563)

d: 0.04(m)
L: 0.121(m)
m: 0.254(m)
J_1: 2.71e-005($kg*m^2$)
J_2: 0.000343($kg*m^2$)
J_3: 0.000343($kg*m^2$)
χ: 0.000644(m)

Final Model

Parameters (15/12-1563)

time: 1.9(s)
xy_{fm}: 0.0853(m)
V_{xfm}: 0.0875(m/s)
V_{yfm}: -5.46e-018(m/s)
V_{zfm}: -1.4(m/s)
Ψ_{fm}: -80.77^{o}
depth: 2.29(m)

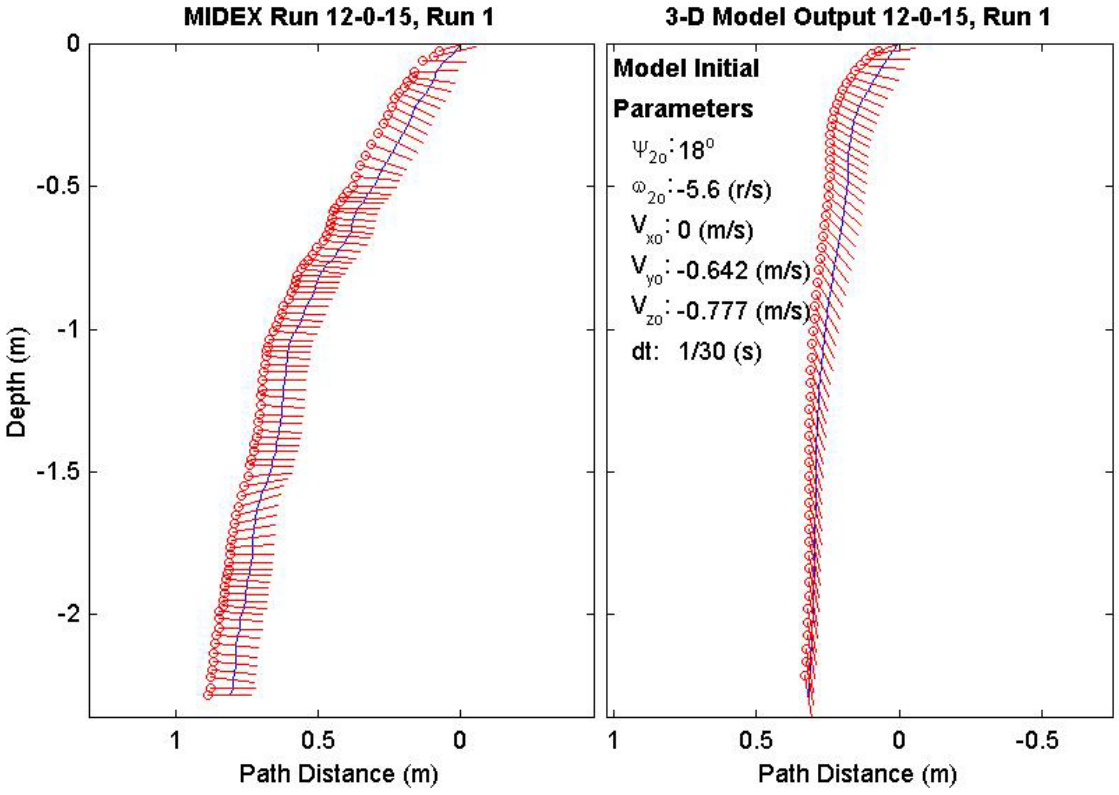

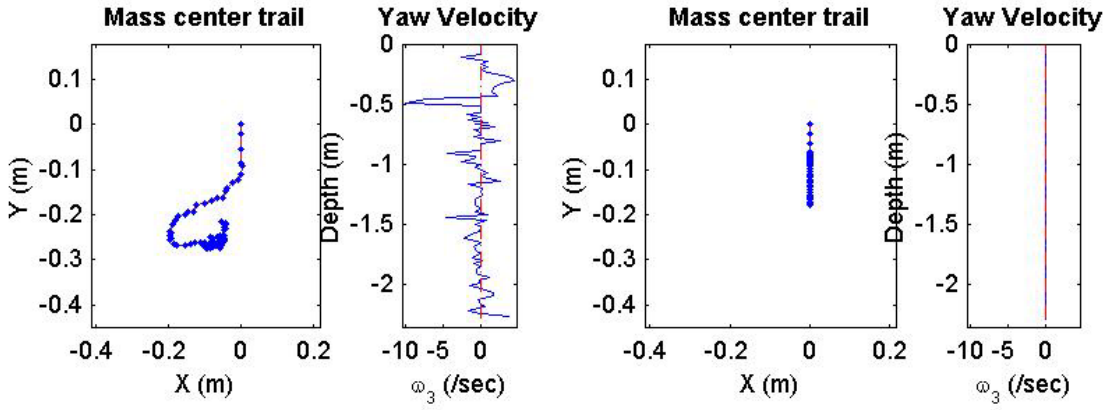

Final Drop

Parameters (15/12-2175)

time: 2.43(s)
xy_{fe}: 0.215(m)
V_{xfe}: 0.108(m/s)
V_{yfe}: 0.159(m/s)
V_{zfe}: -0.99(m/s)
Ψ_{fe}: 51.6°
depth: 2.23(m)

Mine Shape

Parameters (15/12-2175)

d: 0.04(m)
L: 0.121(m)
m: 0.254(m)
J_1: 2.71e-005(kg*m^2)
J_2: 0.000343(kg*m^2)
J_3: 0.000343(kg*m^2)
χ: 0.000644(m)

Final Model

Parameters (15/12-2175)

time: 2.07(s)
xy_{fm}: 0.0805(m)
V_{xfm}: 0.296(m/s)
V_{yfm}: -0.116(m/s)
V_{zfm}: -1.12(m/s)
Ψ_{fm}: -140.5°
depth: 2.26(m)

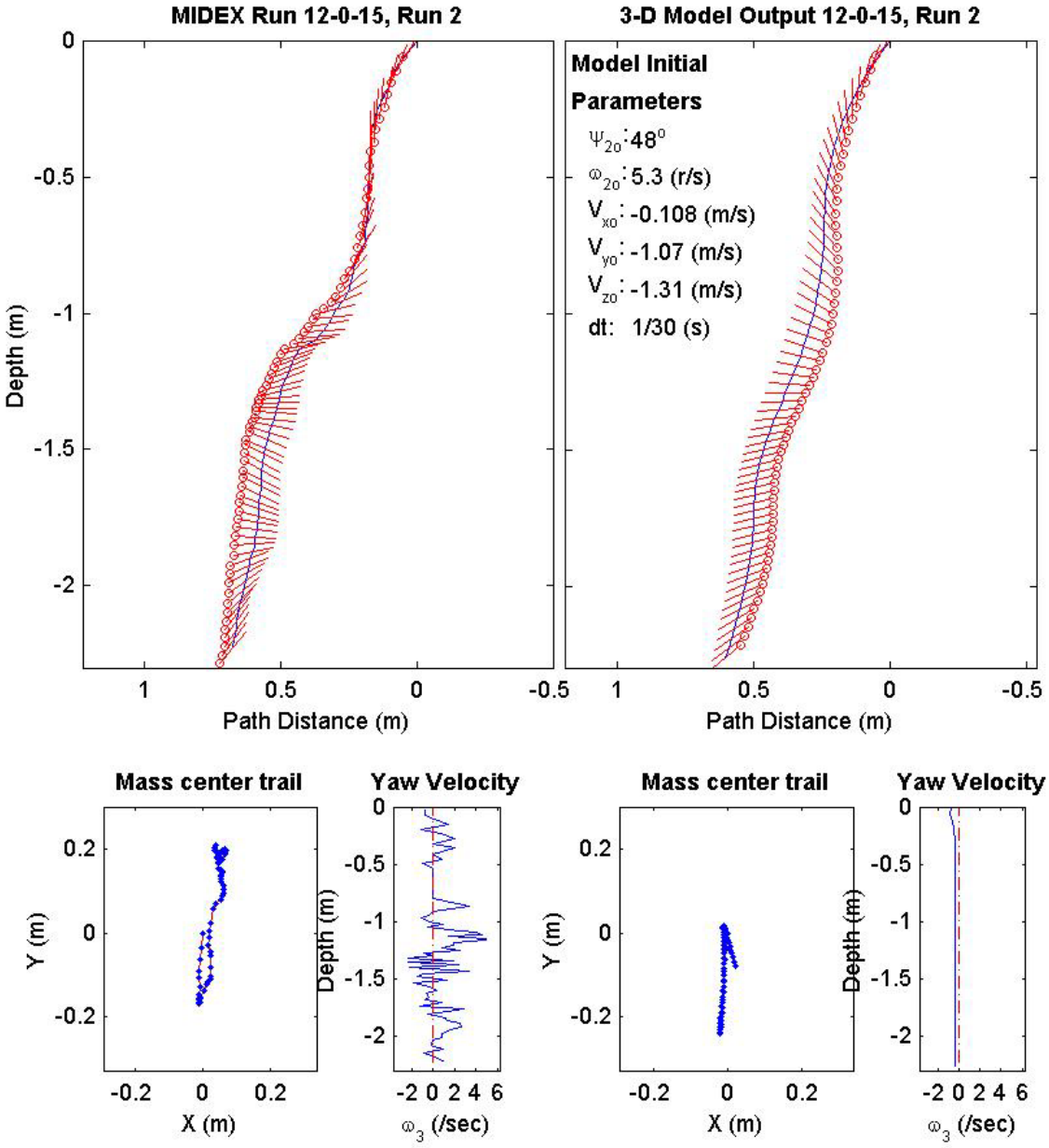

Final Drop Parameters (15/12-2102)

time: 2.47(s)
xy_{fe}: 0.385(m)
V_{xfe}: -0.051(m/s)
V_{yfe}: 0.054(m/s)
V_{zfe}: -0.779(m/s)
Ψ_{fe}: 25°
depth: 2.09(m)

Mine Shape Parameters (15/12-2102)

d: 0.04(m)
L: 0.121(m)
m: 0.254(m)
J_1: 2.71e-005(kg*m^2)
J_2: 0.000343(kg*m^2)
J_3: 0.000343(kg*m^2)
χ: 0.000644(m)

Final Model Parameters (15/12-2102)

time: 1.9(s)
xy_{fm}: 0.581(m)
V_{xfm}: -0.0448(m/s)
V_{yfm}: -0.289(m/s)
V_{zfm}: -1.04(m/s)
Ψ_{fm}: -32.48°
depth: 2.12(m)

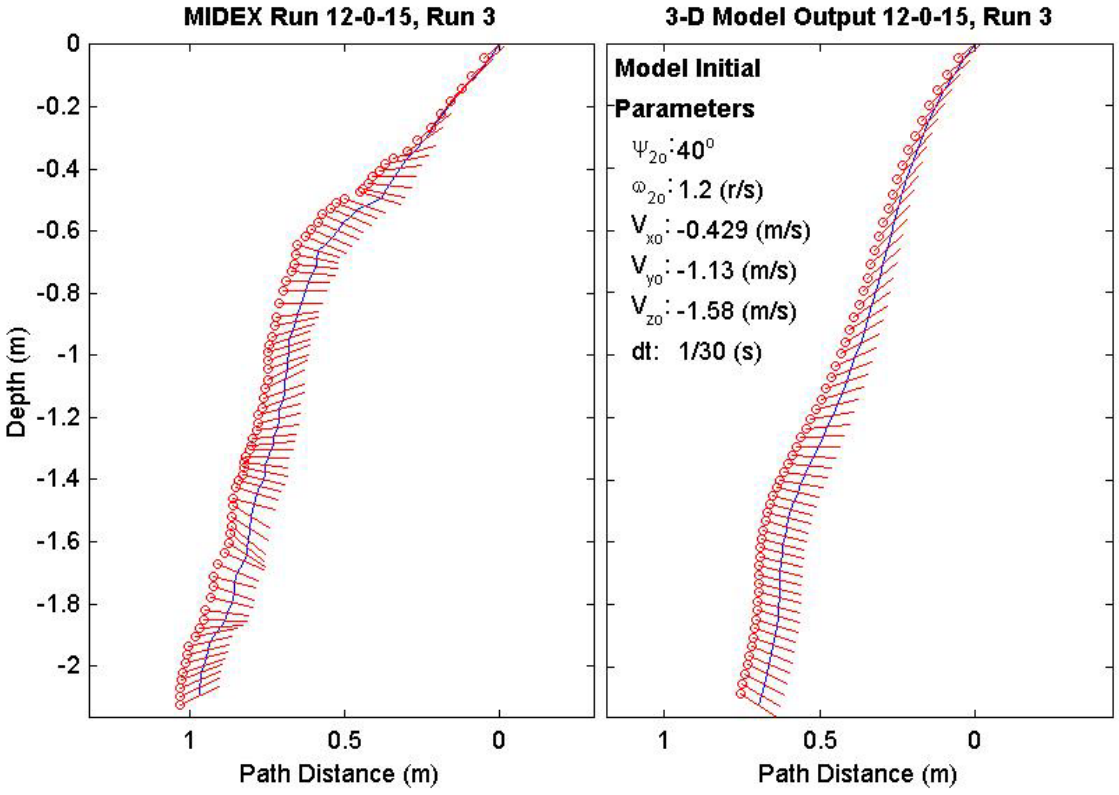

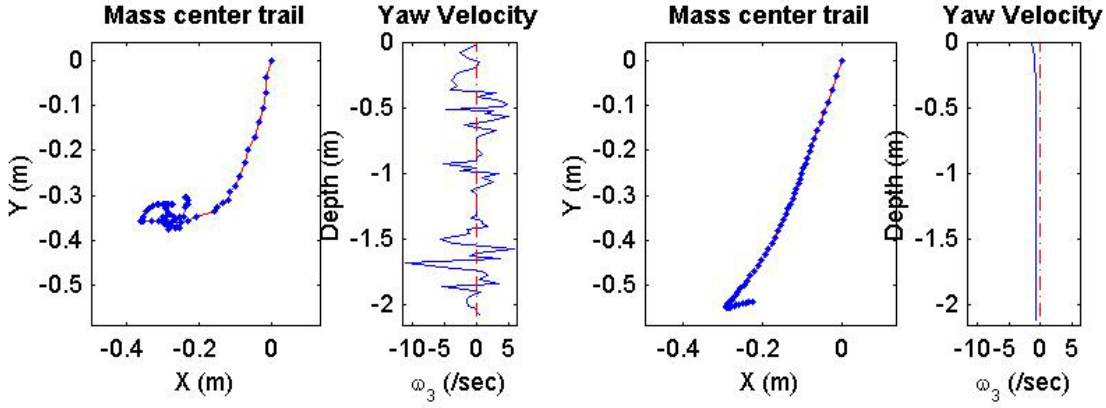

Final Drop Parameters (15/12-1893)

time: 2.77(s)
xy_{fe}: 0.366(m)
V_{xfe}: 0.108(m/s)
V_{yfe}: 0(m/s)
V_{zfe}: -0.937(m/s)
Ψ_{fe}: 0°
depth: 2.23(m)

Mine Shape Parameters (15/12-1893)

d: 0.04(m)
L: 0.121(m)
m: 0.254(m)
J_1: 2.71e-005(kg*m^2)
J_2: 0.000343(kg*m^2)
J_3: 0.000343(kg*m^2)
χ: 0.000644(m)

Final Model Parameters (15/12-1893)

time: 1.97(s)
xy_{fm}: 0.303(m)
V_{xfm}: -0.00198(m/s)
V_{yfm}: -0.0149(m/s)
V_{zfm}: -1.41(m/s)
Ψ_{fm}: -74.94°
depth: 2.25(m)

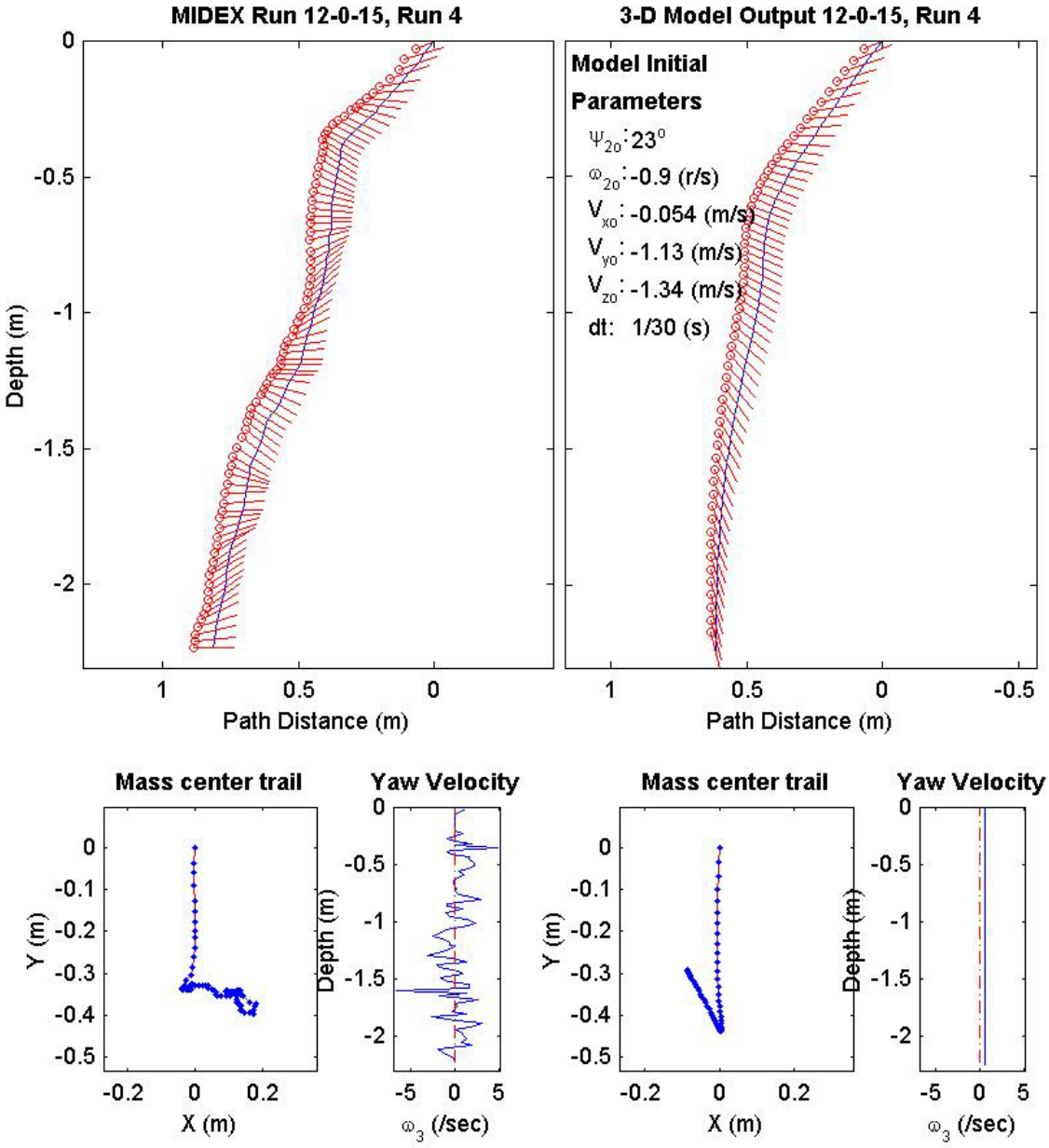

Final Drop

Parameters (15/9-1555)

time: 2.4(s)
xy_{fe}: 0.243(m)
V_{xfe}: 0.159(m/s)
V_{yfe}: -0.054(m/s)
V_{zfe}: -0.938(m/s)
Ψ_{fe}: -51°
depth: 2.23(m)

Mine Shape

Parameters (15/9-1555)

d: 0.04(m)
L: 0.0912(m)
m: 0.215(m)
J_1: 2.35e-005(kg*m^2)
J_2: 0.00017(kg*m^2)
J_3: 0.00017(kg*m^2)
χ: 2.9e-005(m)

Final Model

Parameters (15/9-1555)

time: 1.77(s)
xy_{fm}: 0.129(m)
V_{xfm}: -0.114(m/s)
V_{yfm}: -0.0506(m/s)
V_{zfm}: -1.43(m/s)
Ψ_{fm}: -99.48°
depth: 2.25(m)

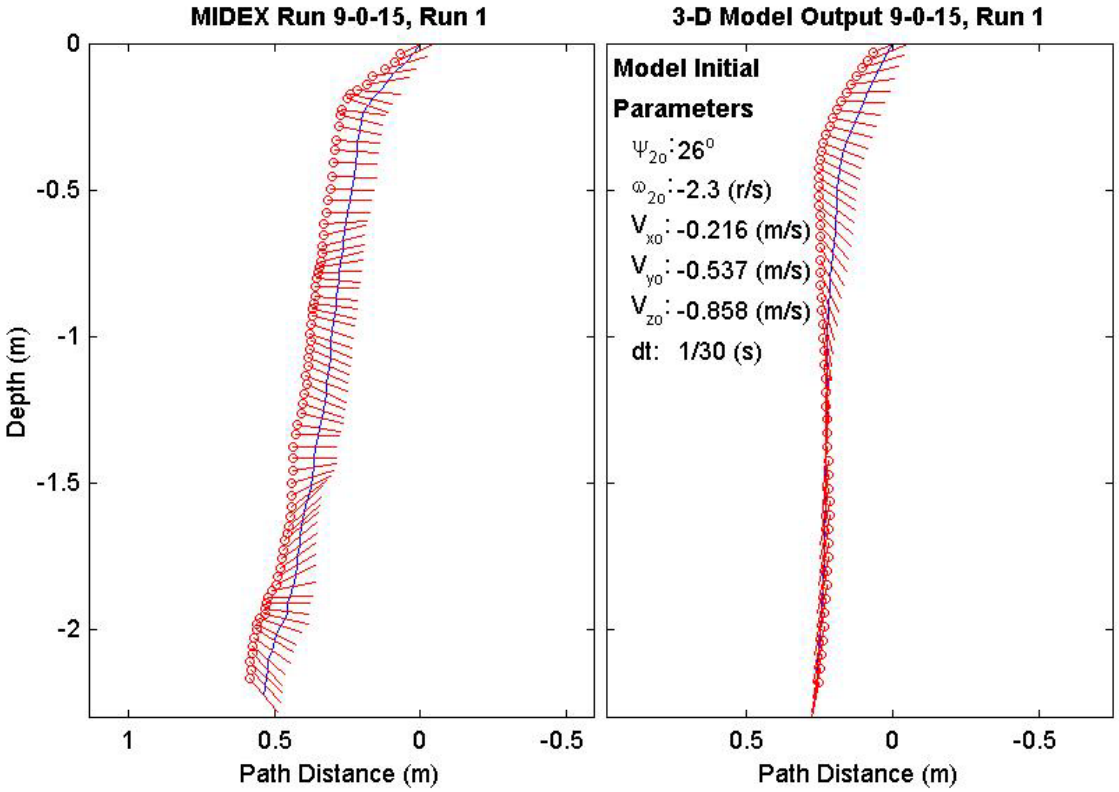

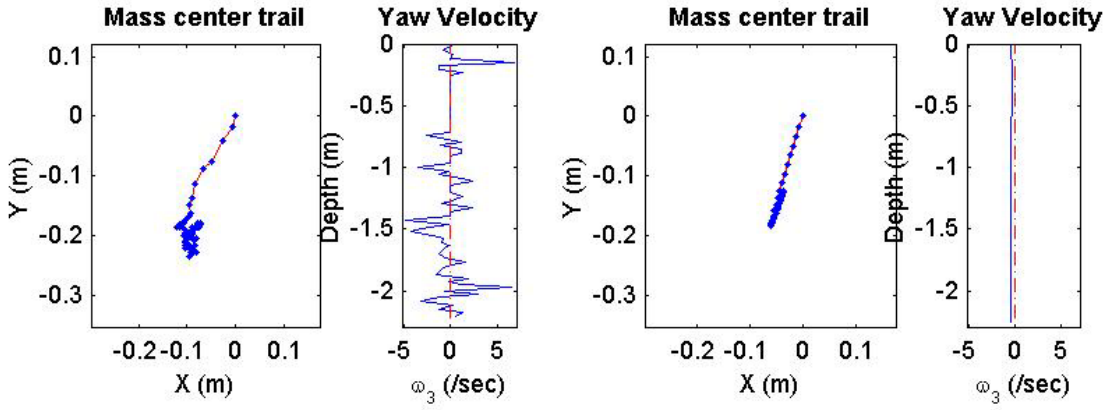

Final Drop

Parameters (15/9-1657)

time: 2.37(s)
xy_{fe}: 0.305(m)
V_{xfe}: -0.267(m/s)
V_{yfe}: -0.213(m/s)
V_{zfe}: -1.21(m/s)
Ψ_{fe}: 39.6°
depth: 2.22(m)

Mine Shape

Parameters (15/9-1657)

d: 0.04(m)
L: 0.0912(m)
m: 0.215(m)
J_1: 2.35e-005(kg*m^2)
J_2: 0.00017(kg*m^2)
J_3: 0.00017(kg*m^2)
χ: 2.9e-005(m)

Final Model

Parameters (15/9-1657)

time: 1.7(s)
xy_{fm}: 0.261(m)
V_{xfm}: -0.0883(m/s)
V_{yfm}: -0.00478(m/s)
V_{zfm}: -1.43(m/s)
Ψ_{fm}: -103.8°
depth: 2.26(m)

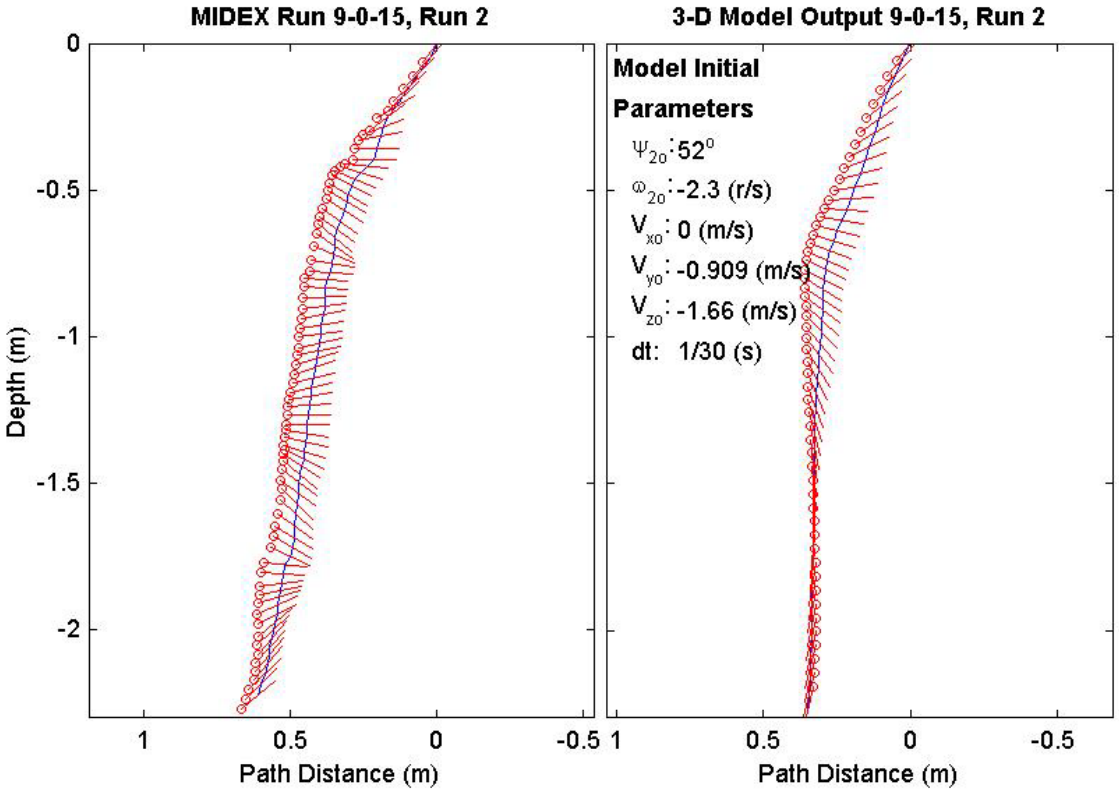

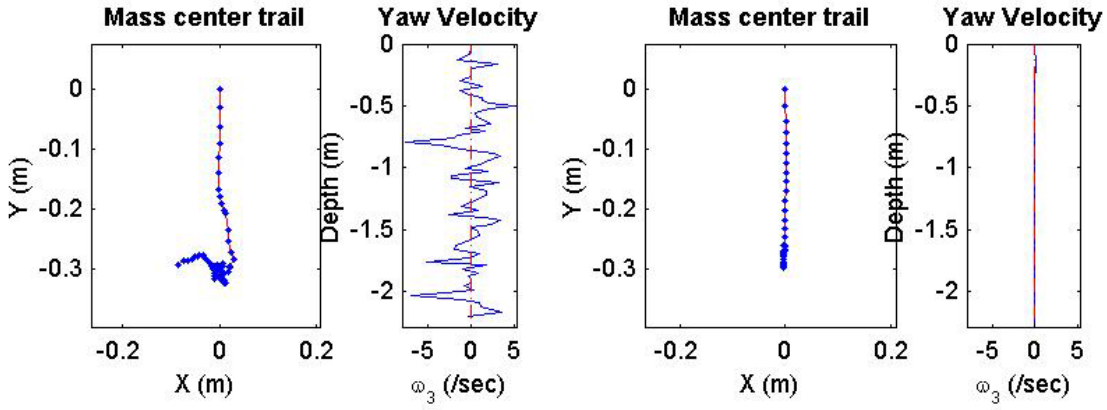

Final Drop
Parameters (15/9-2520)

time: 2.4(s)
xy_{fe}: 0.0439(m)
V_{xfe}: 0(m/s)
V_{yfe}: 0.105(m/s)
V_{zfe}: -0.802(m/s)
Ψ_{fe}: 3.6°
depth: 2.25(m)

Mine Shape
Parameters (15/9-2520)

d: 0.04(m)
L: 0.0912(m)
m: 0.215(m)
J_1: 2.35e-005(kg*m^2)
J_2: 0.00017(kg*m^2)
J_3: 0.00017(kg*m^2)
χ: 2.9e-005(m)

Final Model
Parameters (15/9-2520)

time: 1.77(s)
xy_{fm}: 0.323(m)
V_{xfm}: 0.0213(m/s)
V_{yfm}: 0.0036(m/s)
V_{zfm}: -1.4(m/s)
Ψ_{fm}: -81.45°
depth: 2.26(m)

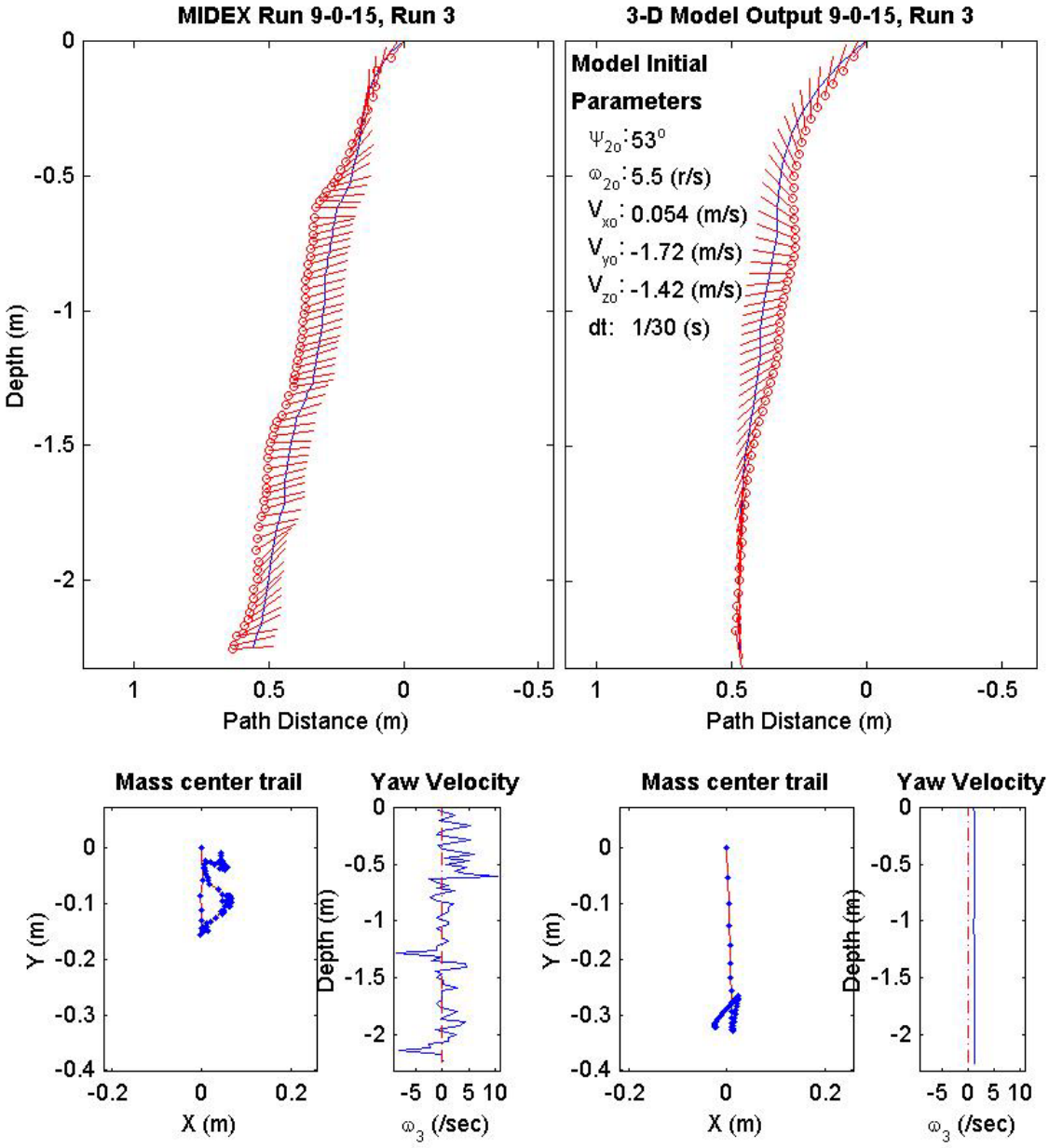

Final Drop

Parameters (15/9-1520)

time: 2.37(s)
xy_{fe}: 0.319(m)
V_{xfe}: -0.051(m/s)
V_{yfe}: -0.213(m/s)
V_{zfe}: -0.696(m/s)
Ψ_{fe}: -5.4°
depth: 2.23(m)

Mine Shape

Parameters (15/9-1520)

d: 0.04(m)
L: 0.0912(m)
m: 0.215(m)
J_1: 2.35e-005(kg*m^2)
J_2: 0.00017(kg*m^2)
J_3: 0.00017(kg*m^2)
χ: 2.9e-005(m)

Final Model

Parameters (15/9-1520)

time: 1.73(s)
xy_{fm}: 0.252(m)
V_{xfm}: -0.103(m/s)
V_{yfm}: 6.72e-018(m/s)
V_{zfm}: -1.43(m/s)
Ψ_{fm}: -102.4°
depth: 2.23(m)

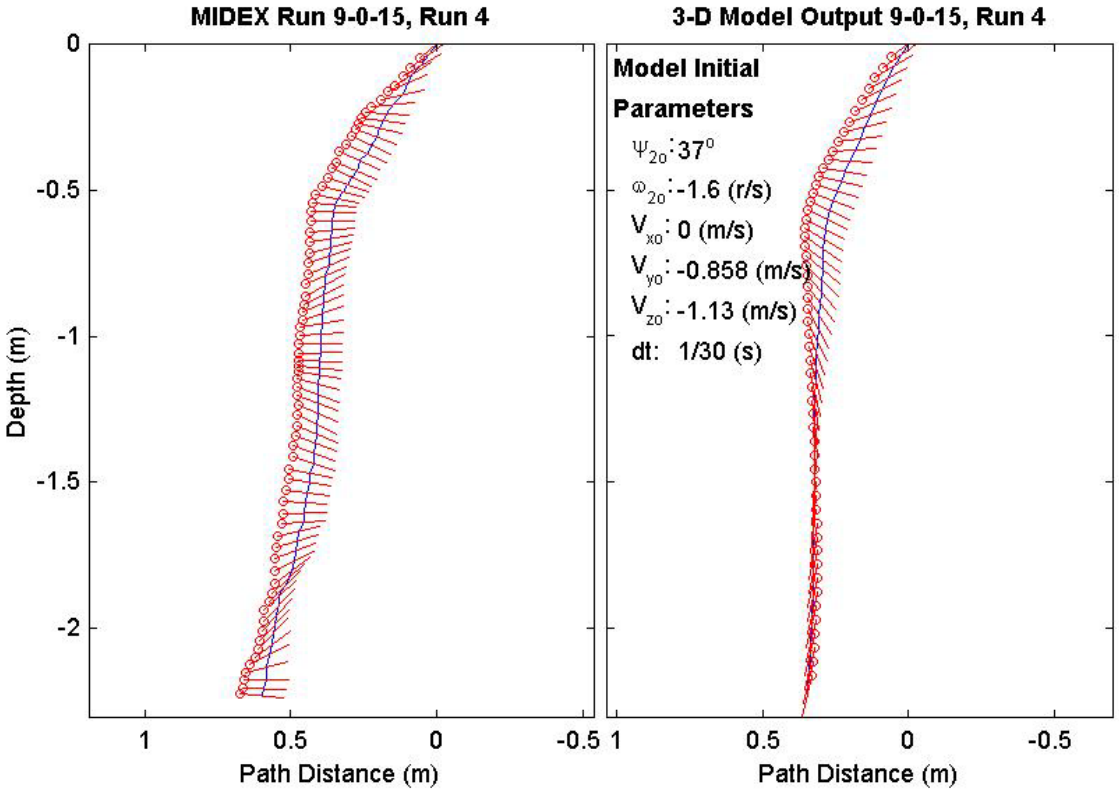

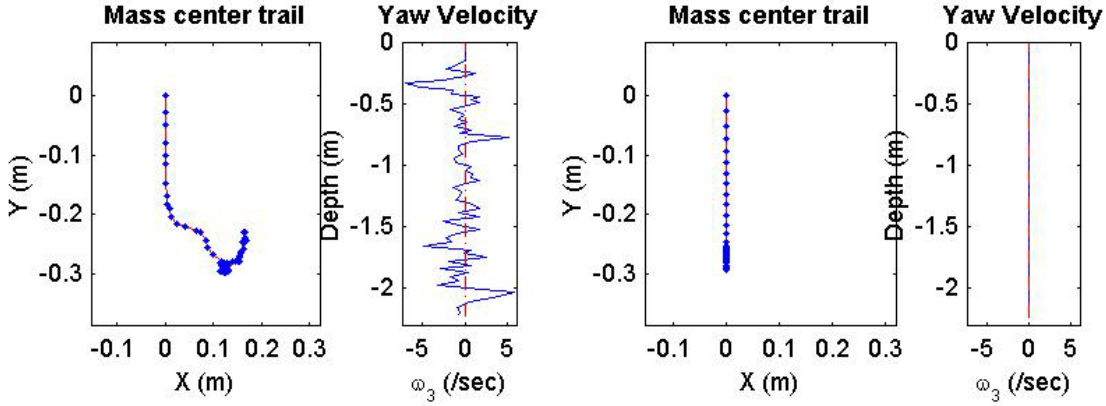

Final Drop

Parameters (30/15-2280)

time: 2.67(s)
xy_{fe}: 0.401(m)
V_{xfe}: 0.055(m/s)
V_{yfe}: 0(m/s)
V_{zfe}: -0.883(m/s)
Ψ_{fe}: -3.4°
depth: 2.17(m)

Mine Shape

Parameters (30/15-2280)

d: 0.04(m)
L: 0.152(m)
m: 0.323(m)
J_1: 3.3e-005(kg*m^2)
J_2: 0.000609(kg*m^2)
J_3: 0.000609(kg*m^2)
χ: 4.6e-005(m)

Final Model

Parameters (30/15-2280)

time: 1.47(s)
xy_{fm}: 0.665(m)
V_{xfm}: 0.131(m/s)
V_{yfm}: -0.0103(m/s)
V_{zfm}: -1.53(m/s)
Ψ_{fm}: 57.53°
depth: 2.2(m)

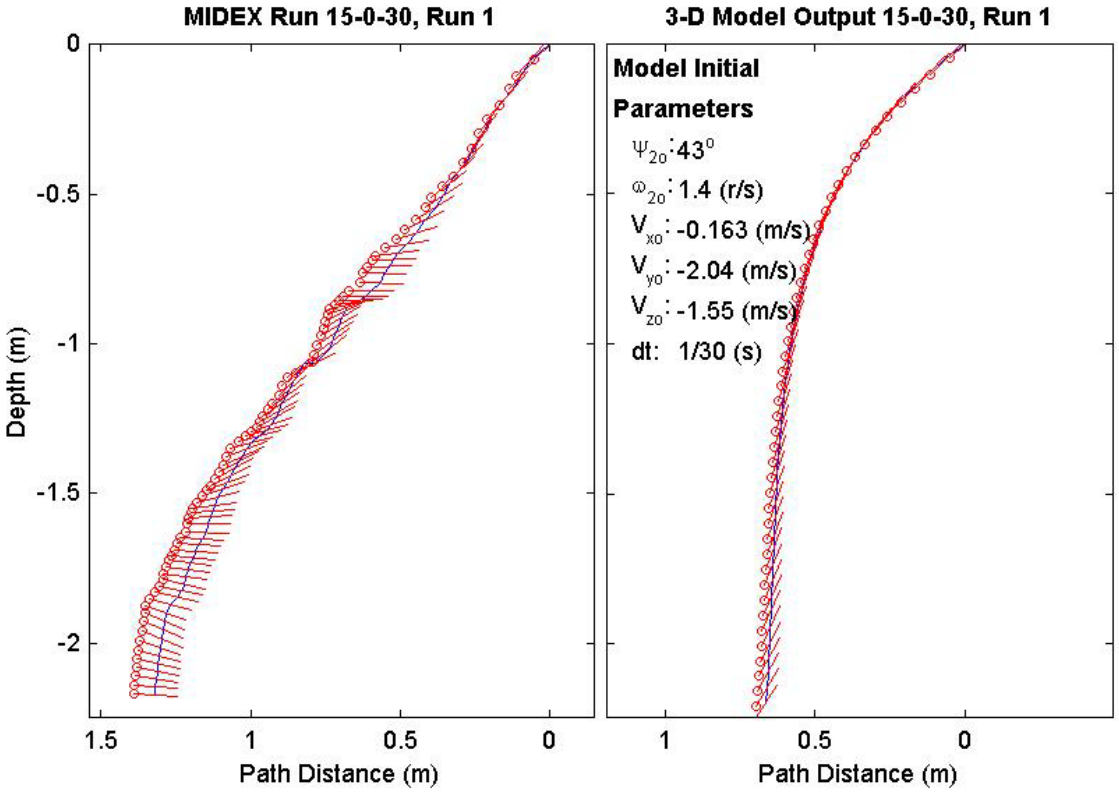

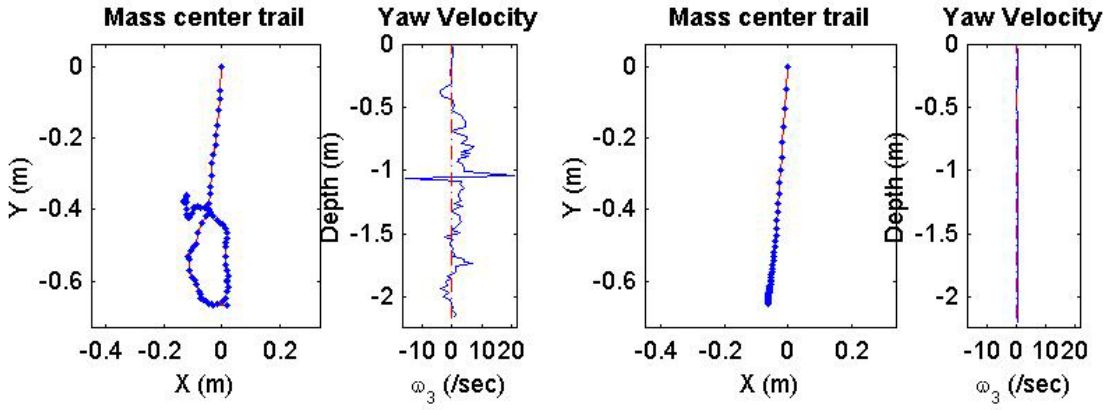

Final Drop Parameters (15/15-1379)

time: 2.9(s)
xy_{fe}: 0.0187(m)
V_{xfe}: -0.106(m/s)
V_{yfe}: -0.163(m/s)
V_{zfe}: -0.75(m/s)
Ψ_{fe}: 3.3°
depth: 2.25(m)

Mine Shape Parameters (15/15-1379)

d: 0.04(m)
L: 0.152(m)
m: 0.323(m)
J_1: 3.3e-005(kg*m^2)
J_2: 0.000609(kg*m^2)
J_3: 0.000609(kg*m^2)
χ: 4.6e-005(m)

Final Model Parameters (15/15-1379)

time: 1.8(s)
xy_{fm}: 0.252(m)
V_{xfm}: 0.0459(m/s)
V_{yfm}: 0.0258(m/s)
V_{zfm}: -1.53(m/s)
Ψ_{fm}: -85.91°
depth: 2.25(m)

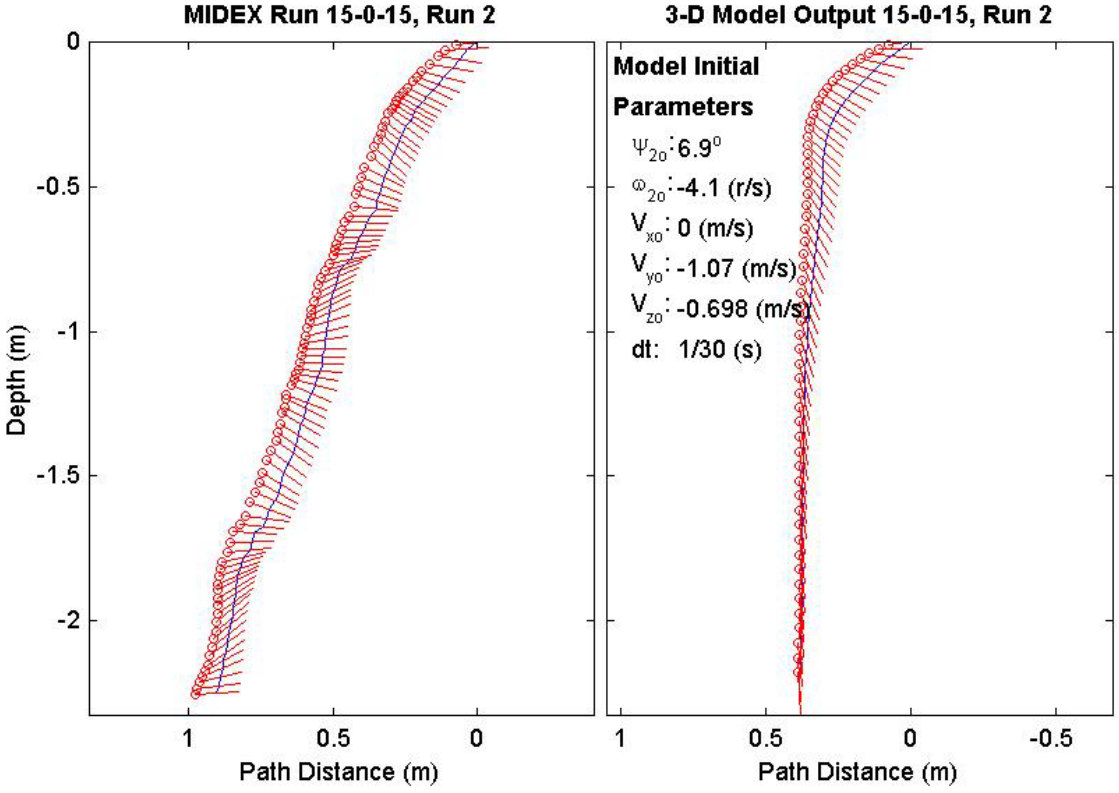

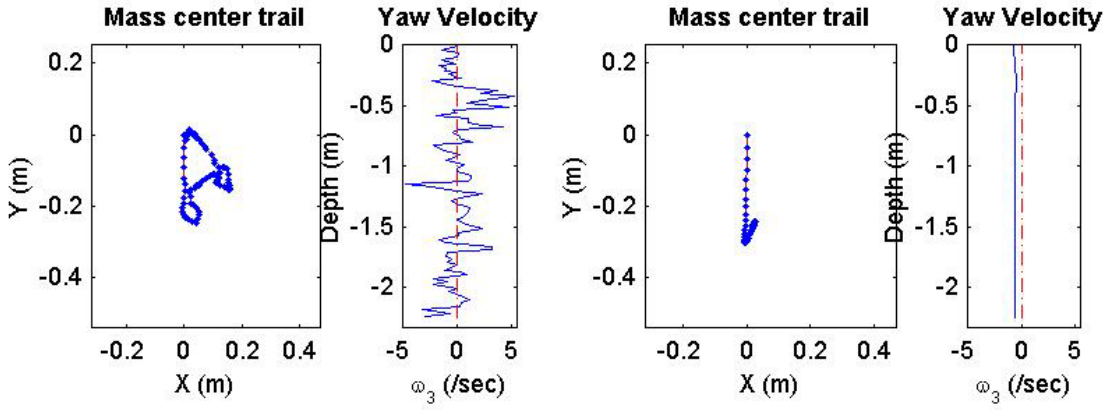

Final Drop
Parameters (30/15-1070)

time: 2.97(s)
xy_{fe}: 0.198(m)
V_{xfe}: -0.055(m/s)
V_{yfe}: -0.051(m/s)
V_{zfe}: -0.803(m/s)
Ψ_{fe}: 1.6°
depth: 2.27(m)

Mine Shape
Parameters (30/15-1070)

d: 0.04(m)
L: 0.152(m)
m: 0.323(m)
J_1: 3.3e-005(kg*m^2)
J_2: 0.000609(kg*m^2)
J_3: 0.000609(kg*m^2)
χ: 4.6e-005(m)

Final Model
Parameters (30/15-1070)

time: 1.93(s)
xy_{fm}: 0.426(m)
V_{xfm}: 0.0516(m/s)
V_{yfm}: 0.049(m/s)
V_{zfm}: -1.55(m/s)
Ψ_{fm}: -100.2°
depth: 2.32(m)

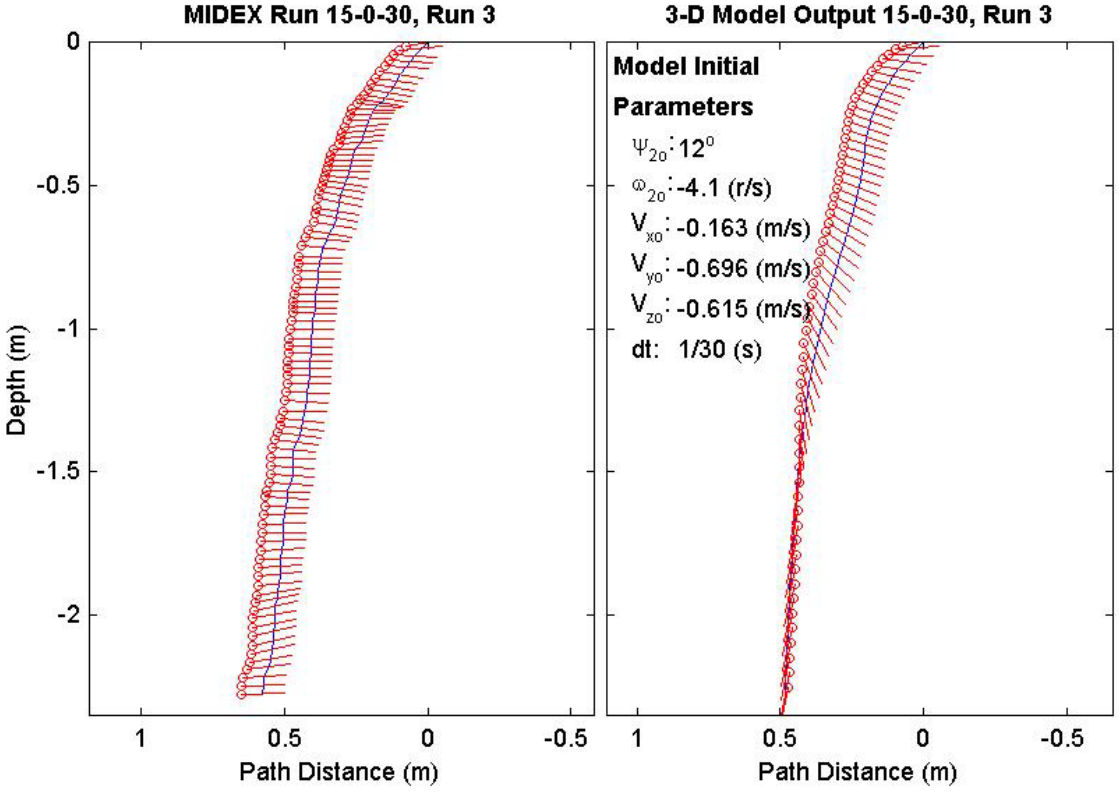

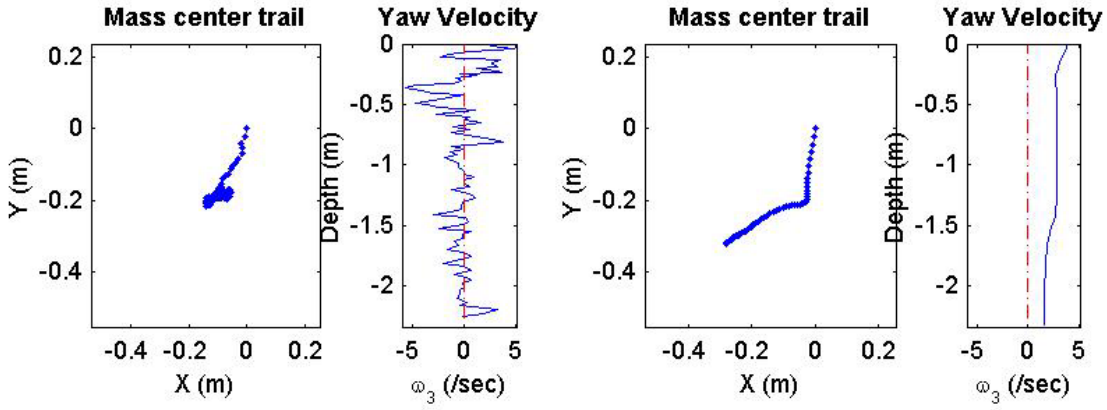

Final Drop Parameters (30/15-1289)

time: 3.03(s)
xy_{fe}: 0.195(m)
V_{xfe}: 0.375(m/s)
V_{yfe}: -0.055(m/s)
V_{zfe}: -0.75(m/s)
Ψ_{fe}: 0^{o}
depth: 2.26(m)

Mine Shape Parameters (30/15-1289)

d: 0.04(m)
L: 0.152(m)
m: 0.323(m)
J_1: 3.3e-005($kg*m^2$)
J_2: 0.000609($kg*m^2$)
J_3: 0.000609($kg*m^2$)
χ: 4.6e-005(m)

Final Model Parameters (30/15-1289)

time: 1.83(s)
xy_{fm}: 0.388(m)
V_{xfm}: 0.0523(m/s)
V_{yfm}: 0.00154(m/s)
V_{zfm}: -1.53(m/s)
Ψ_{fm}: -86.04^{o}
depth: 2.28(m)

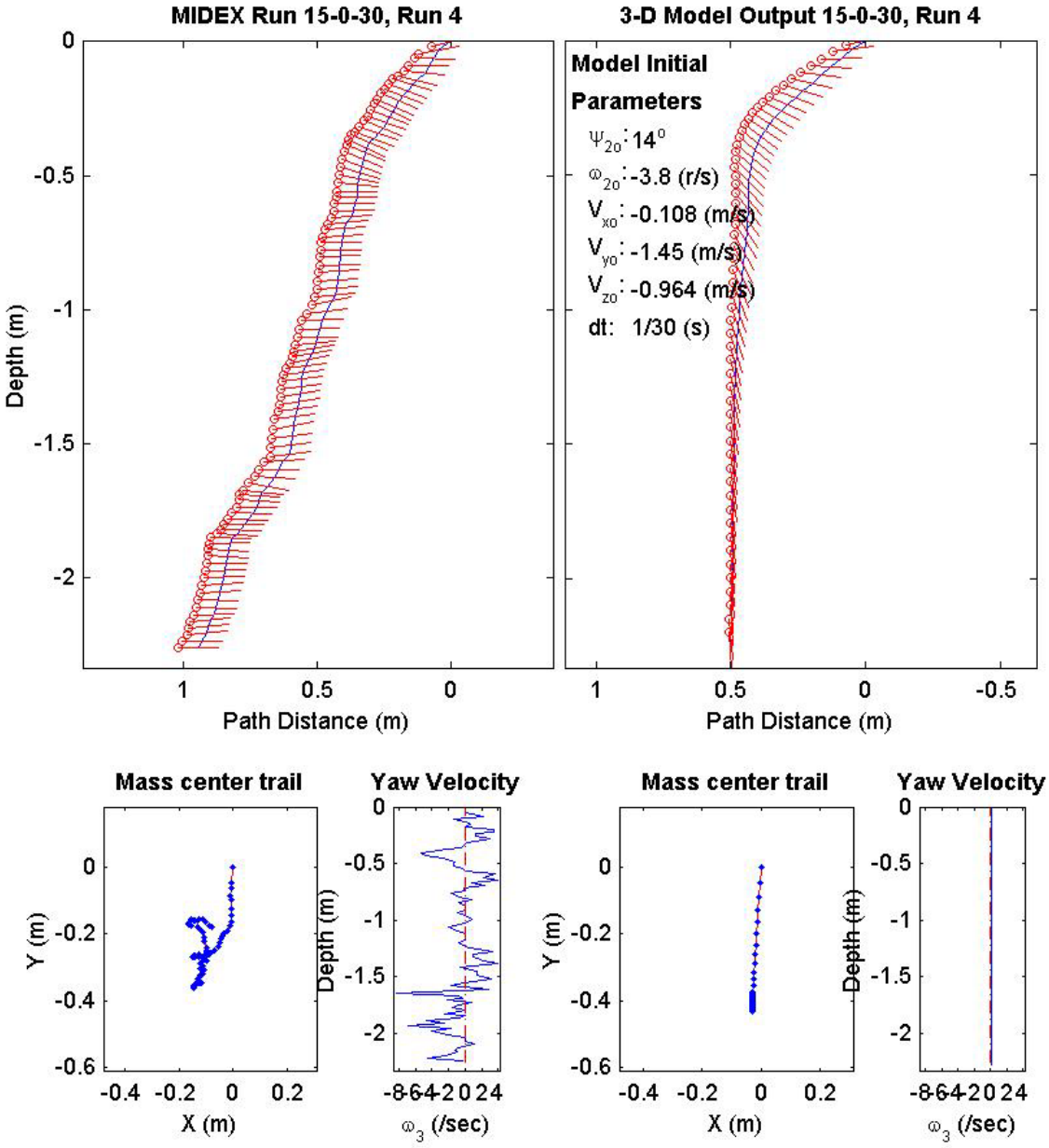

Final Drop

Parameters (30/15-573)

time: 2.93(s)
xy_{fe}: 0.197(m)
V_{xfe}: -0.108(m/s)
V_{yfe}: -0.055(m/s)
V_{zfe}: -0.67(m/s)
Ψ_{fe}: 19.3°
depth: 2.26(m)

Mine Shape

Parameters (30/15-573)

d: 0.04(m)
L: 0.152(m)
m: 0.323(m)
J_1: 3.3e-005(kg*m^2)
J_2: 0.000609(kg*m^2)
J_3: 0.000609(kg*m^2)
χ: 4.6e-005(m)

Final Model

Parameters (30/15-573)

time: 1.9(s)
xy_{fm}: 0.141(m)
V_{xfm}: 0.0127(m/s)
V_{yfm}: 0.000695(m/s)
V_{zfm}: -1.53(m/s)
Ψ_{fm}: -82.29°
depth: 2.28(m)

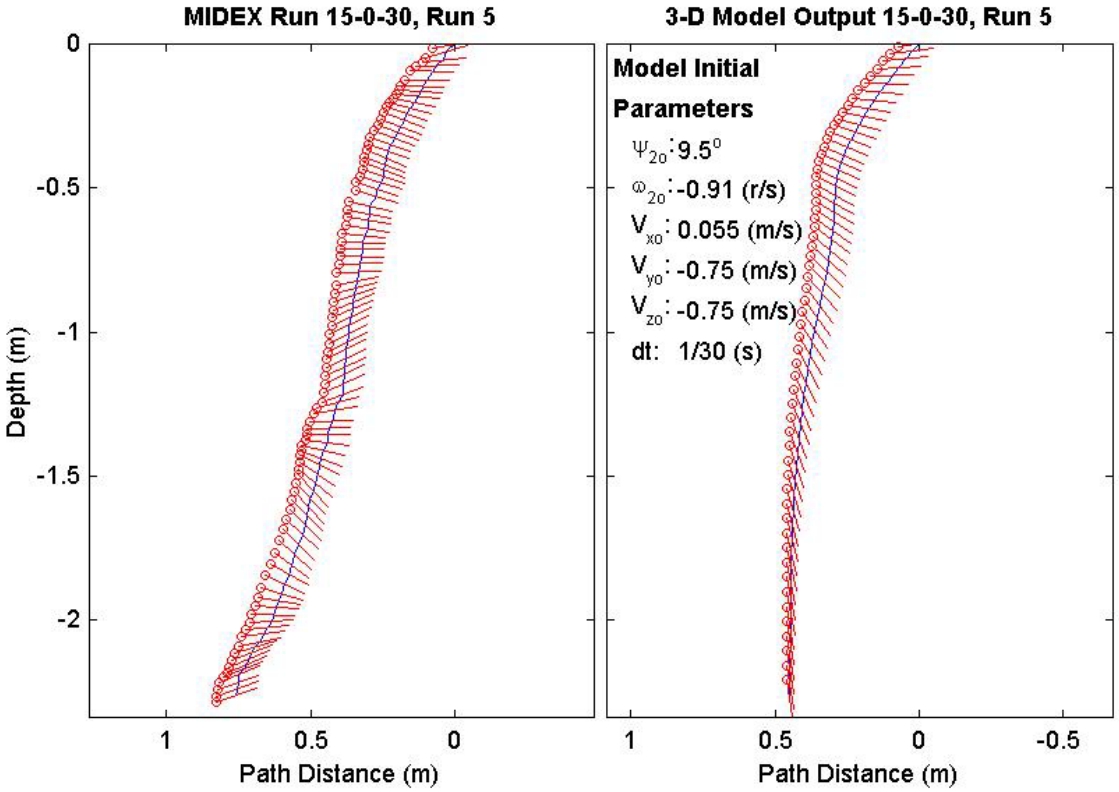

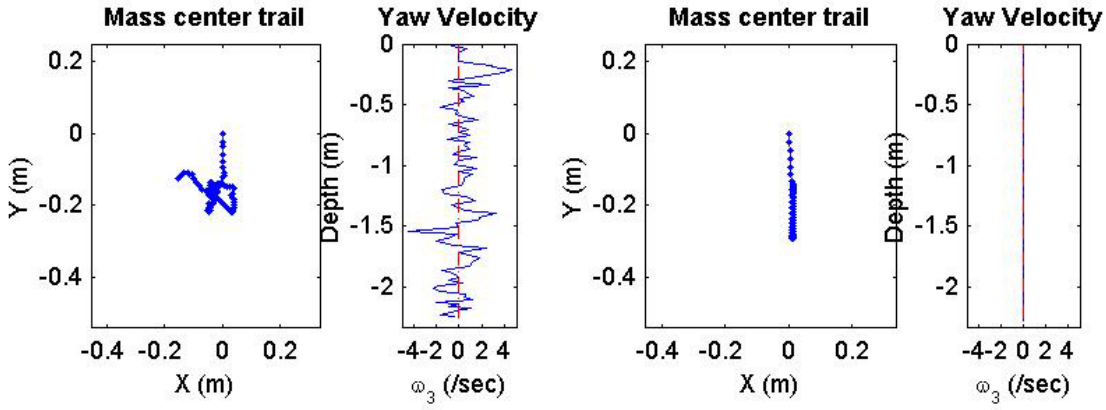

Final Drop

Parameters (30/12-2658)

time: 2.5(s)
xy_{fe}: 0.114(m)
V_{xfe}: -0.216(m/s)
V_{yfe}: -0.159(m/s)
V_{zfe}: -0.91(m/s)
Ψ_{fe}: -28.5°
depth: 2.2(m)

Mine Shape

Parameters (30/12-2658)

d: 0.04(m)
L: 0.121(m)
m: 0.254(m)
J_1: 2.71e-005(kg*m^2)
J_2: 0.000343(kg*m^2)
J_3: 0.000343(kg*m^2)
χ: 0.000644(m)

Final Model

Parameters (30/12-2658)

time: 1.57(s)
xy_{fm}: 0.373(m)
V_{xfm}: 0.0341(m/s)
V_{yfm}: -0.00187(m/s)
V_{zfm}: -1.41(m/s)
Ψ_{fm}: 112.9°
depth: 2.21(m)

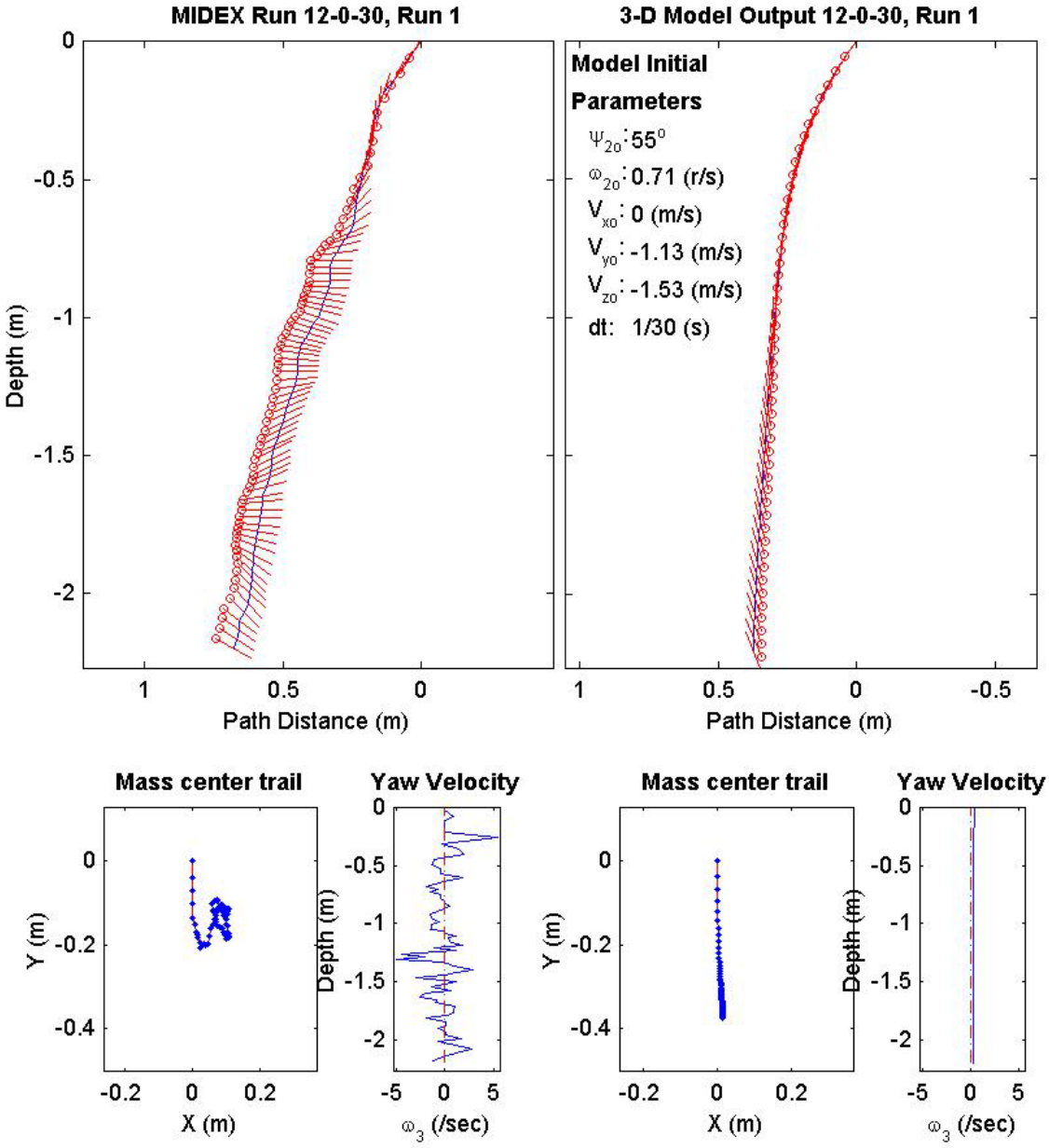

Final Drop Parameters (30/12-1964)

time: 2.5(s)
xy_{fe}: 0.349(m)
V_{xfe}: 0(m/s)
V_{yfe}: 0.054(m/s)
V_{zfe}: -0.749(m/s)
Ψ_{fe}: 0^{o}
depth: 2.19(m)

Mine Shape Parameters (30/12-1964)

d: 0.04(m)
L: 0.121(m)
m: 0.254(m)
J_1: 2.71e-005($kg*m^2$)
J_2: 0.000343($kg*m^2$)
J_3: 0.000343($kg*m^2$)
χ: 0.000644(m)

Final Model Parameters (30/12-1964)

time: 1.67(s)
xy_{fm}: 0.086(m)
V_{xfm}: -0.349(m/s)
V_{yfm}: -0.183(m/s)
V_{zfm}: -0.894(m/s)
Ψ_{fm}: -174.3^{o}
depth: 2.2(m)

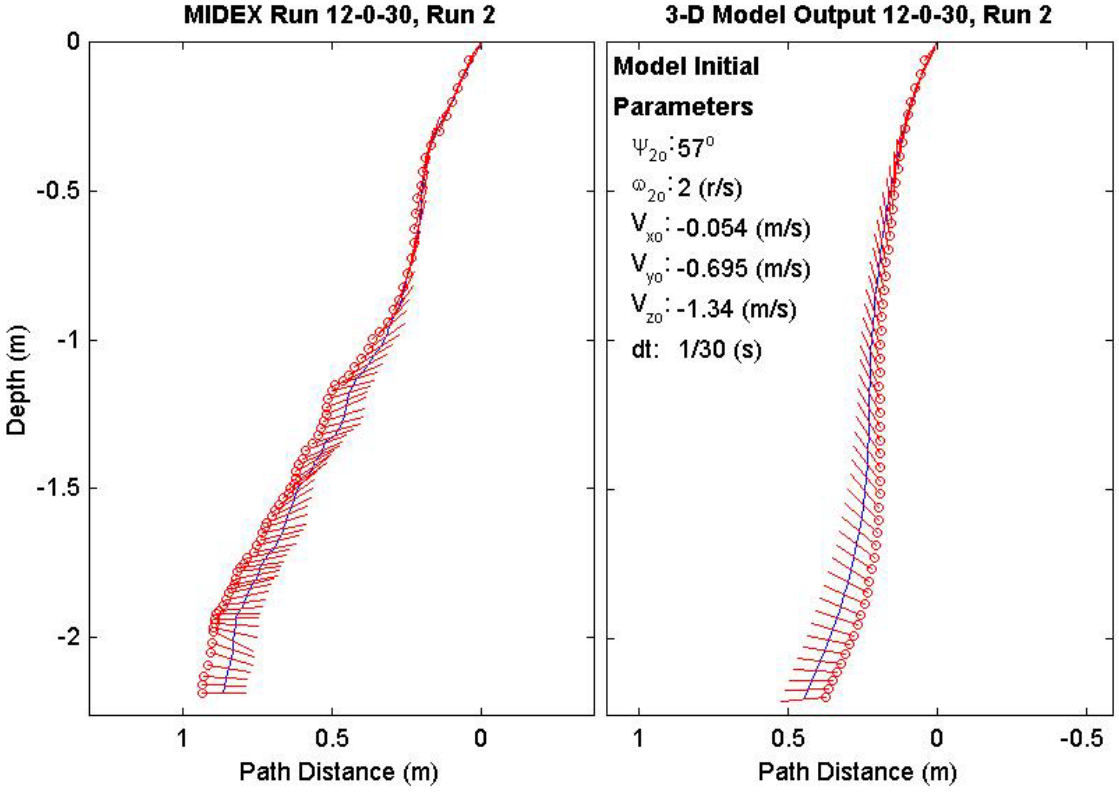

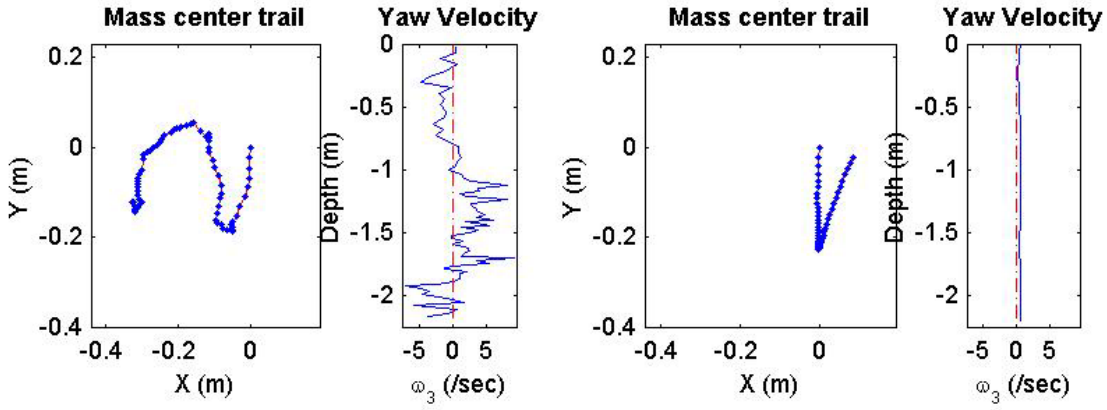

Final Drop

Parameters (30/12-1672)

time: 2.6(s)
xy_{fe}: 0.39(m)
V_{xfe}: 0.051(m/s)
V_{yfe}: 0(m/s)
V_{zfe}: -0.723(m/s)
Ψ_{fe}: 19.4°
depth: 2.2(m)

Mine Shape

Parameters (30/12-1672)

d: 0.04(m)
L: 0.121(m)
m: 0.254(m)
J_1: 2.71e-005($kg*m^2$)
J_2: 0.000343($kg*m^2$)
J_3: 0.000343($kg*m^2$)
χ: 0.000644(m)

Final Model

Parameters (30/12-1672)

time: 2.03(s)
xy_{fm}: 0.488(m)
V_{xfm}: -0.281(m/s)
V_{yfm}: 1.73e-017(m/s)
V_{zfm}: -1.25(m/s)
Ψ_{fm}: -50.82°
depth: 2.23(m)

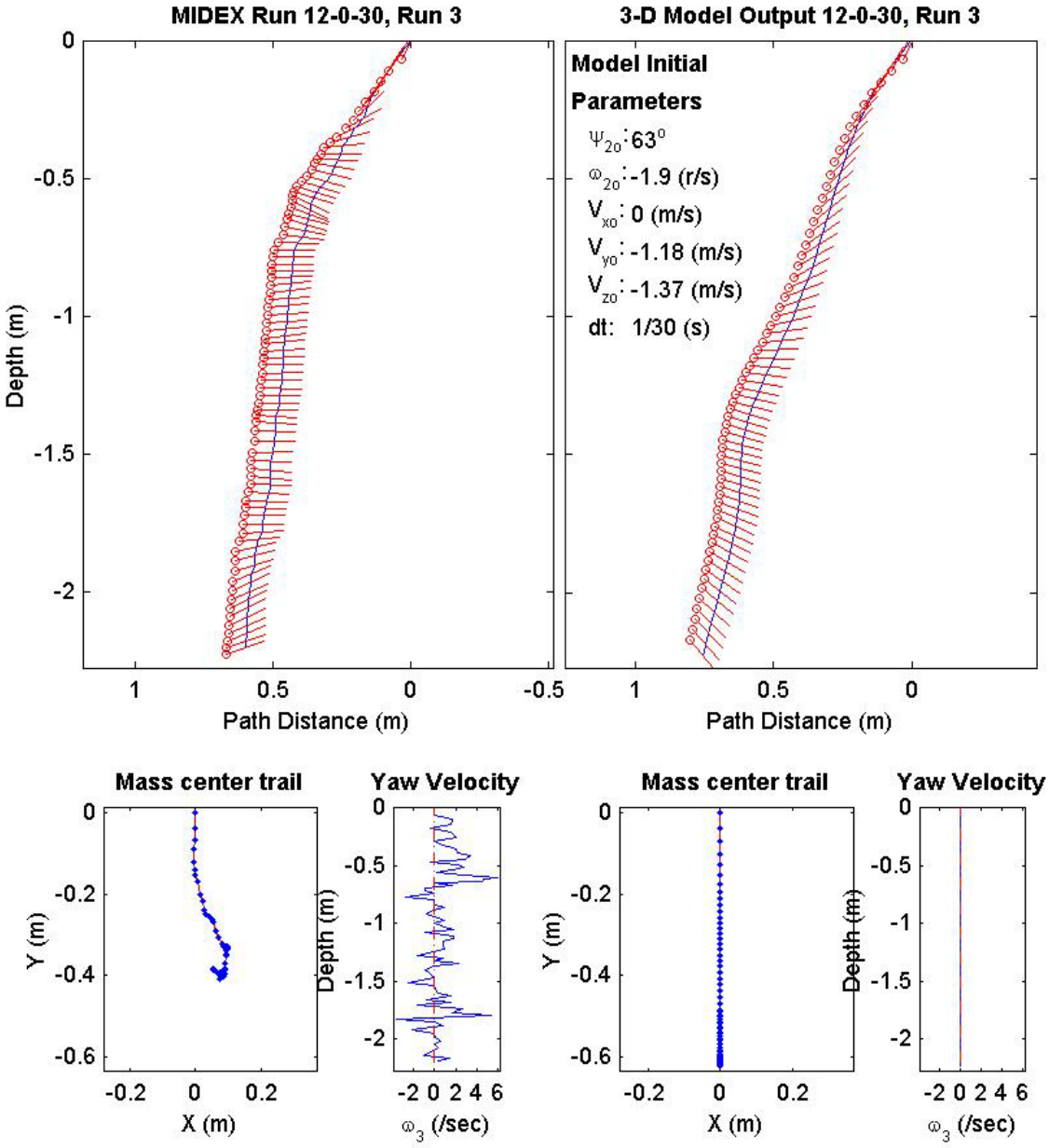

Final Drop Parameters (30/12-1479)

time: 2.77(s)
xy_{fe}: 0.42(m)
V_{xfe}: 0.054(m/s)
V_{yfe}: 0.054(m/s)
V_{zfe}: -0.669(m/s)
Ψ_{fe}: -23.5°
depth: 2.22(m)

Mine Shape Parameters (30/12-1479)

d: 0.04(m)
L: 0.121(m)
m: 0.254(m)
J_1: 2.71e-005(kg*m^2)
J_2: 0.000343(kg*m^2)
J_3: 0.000343(kg*m^2)
χ: 0.000644(m)

Final Model Parameters (30/12-1479)

time: 1.67(s)
xy_{fm}: 0.199(m)
V_{xfm}: -0.426(m/s)
V_{yfm}: 0.0825(m/s)
V_{zfm}: -1.03(m/s)
Ψ_{fm}: 172.4°
depth: 2.23(m)

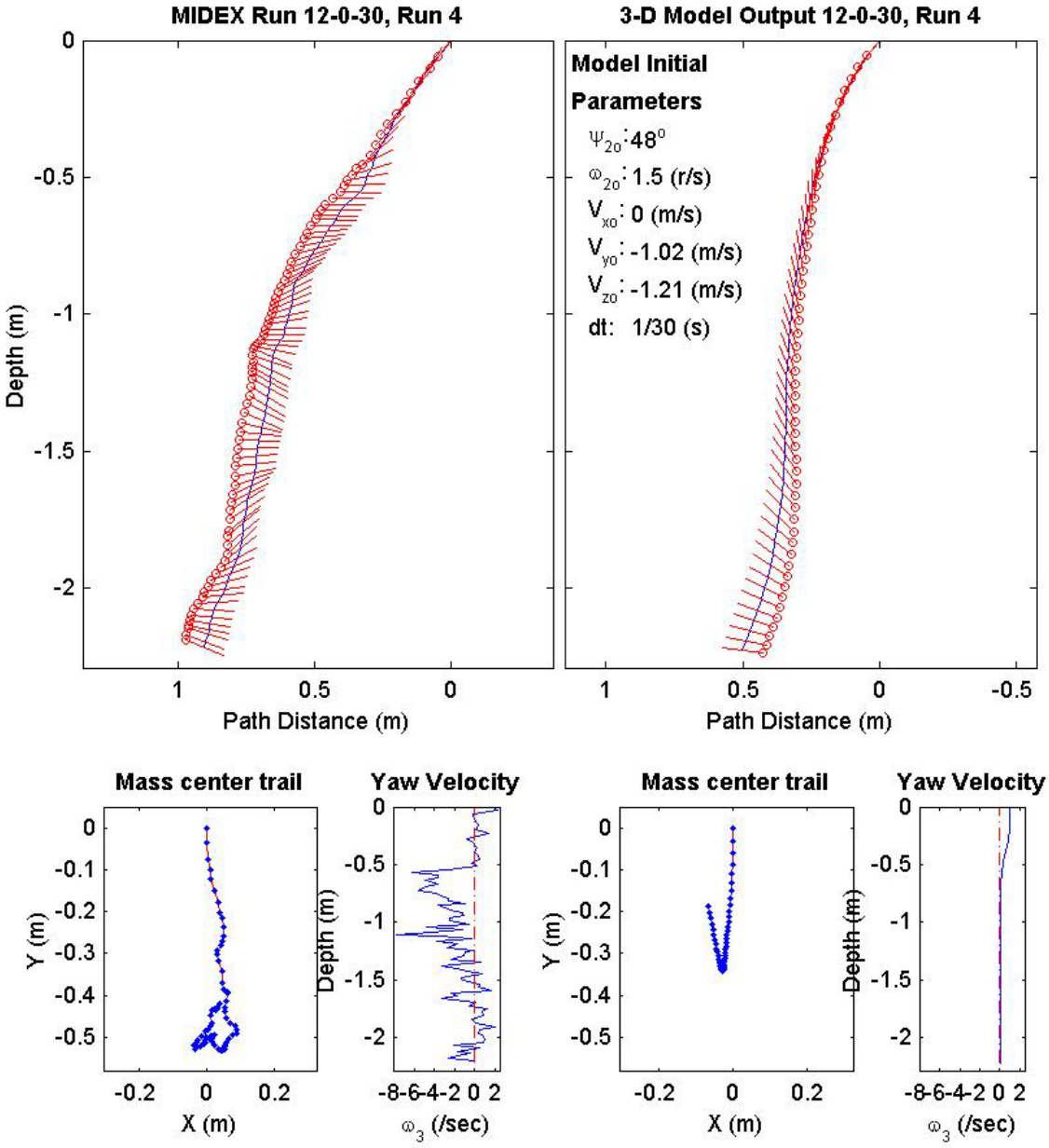

Final Drop

Parameters (30/12-812)

time: 2.9(s)
xy_{fe}: 0.221(m)
V_{xfe}: 0.105(m/s)
V_{yfe}: -0.105(m/s)
V_{zfe}: -0.803(m/s)
Ψ_{fe}: 0^{o}
depth: 2.28(m)

Mine Shape

Parameters (30/12-812)

d: 0.04(m)
L: 0.121(m)
m: 0.254(m)
J_1: 2.71e-005($kg*m^2$)
J_2: 0.000343($kg*m^2$)
J_3: 0.000343($kg*m^2$)
χ: 0.000644(m)

Final Model

Parameters (30/12-812)

time: 2.07(s)
xy_{fm}: 0.269(m)
V_{xfm}: 0.036(m/s)
V_{yfm}: 0.00756(m/s)
V_{zfm}: -1.41(m/s)
Ψ_{fm}: -76.63^{o}
depth: 2.32(m)

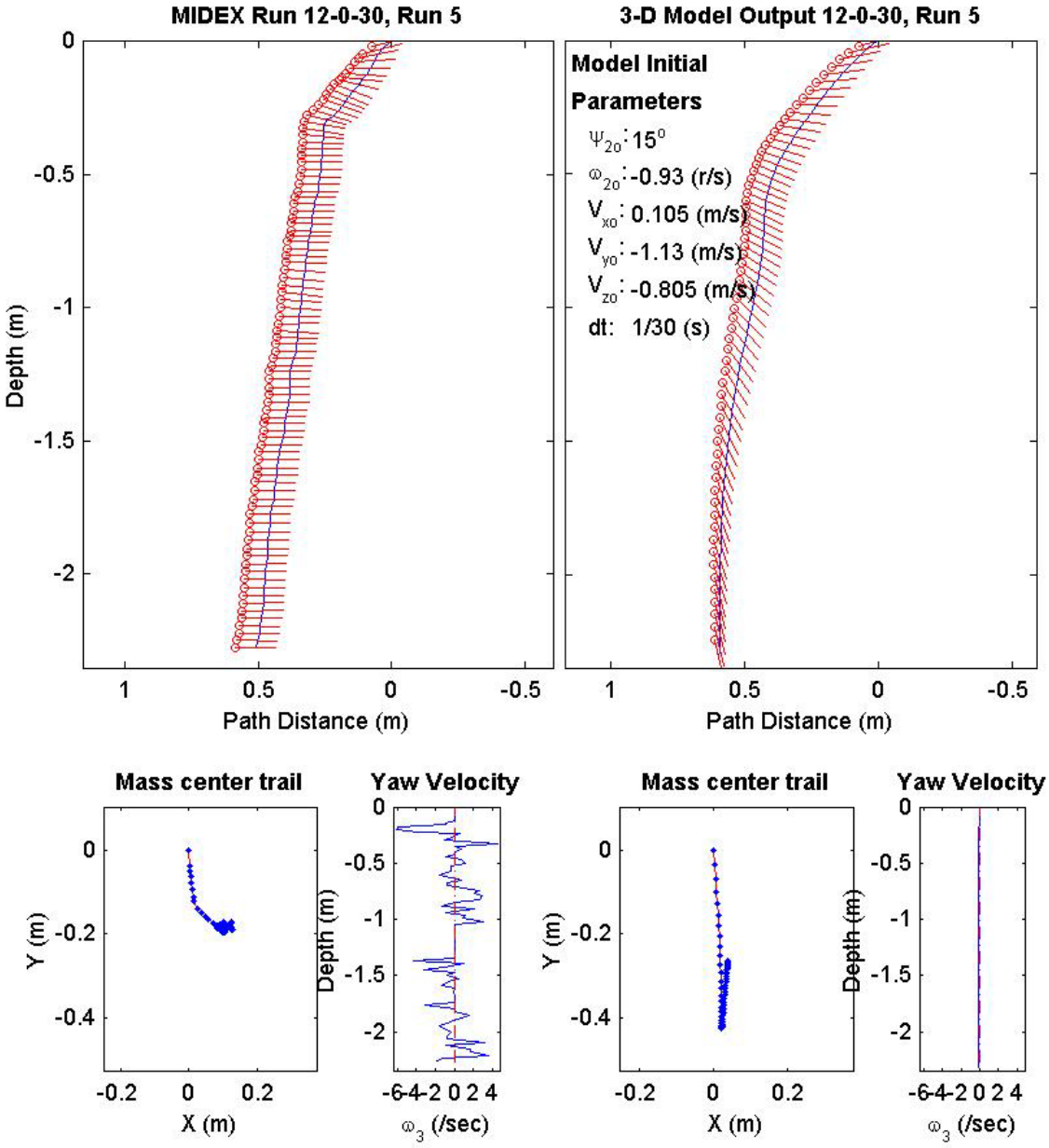

Final Drop
Parameters (30/9-2446)

time: 2.43(s)
xy_{fe}: 0.0644(m)
V_{xfe}: 0(m/s)
V_{yfe}: 0.051(m/s)
V_{zfe}: -0.966(m/s)
Ψ_{fe}: 10.2^{o}
depth: 2.29(m)

Mine Shape
Parameters (30/9-2446)

d: 0.04(m)
L: 0.0912(m)
m: 0.215(m)
J_1: 2.35e-005($kg*m^2$)
J_2: 0.00017($kg*m^2$)
J_3: 0.00017($kg*m^2$)
χ: 2.9e-005(m)

Final Model
Parameters (30/9-2446)

time: 1.77(s)
xy_{fm}: 0.194(m)
V_{xfm}: -0.00747(m/s)
V_{yfm}: -0.0139(m/s)
V_{zfm}: -1.4(m/s)
Ψ_{fm}: -85.84^{o}
depth: 2.32(m)

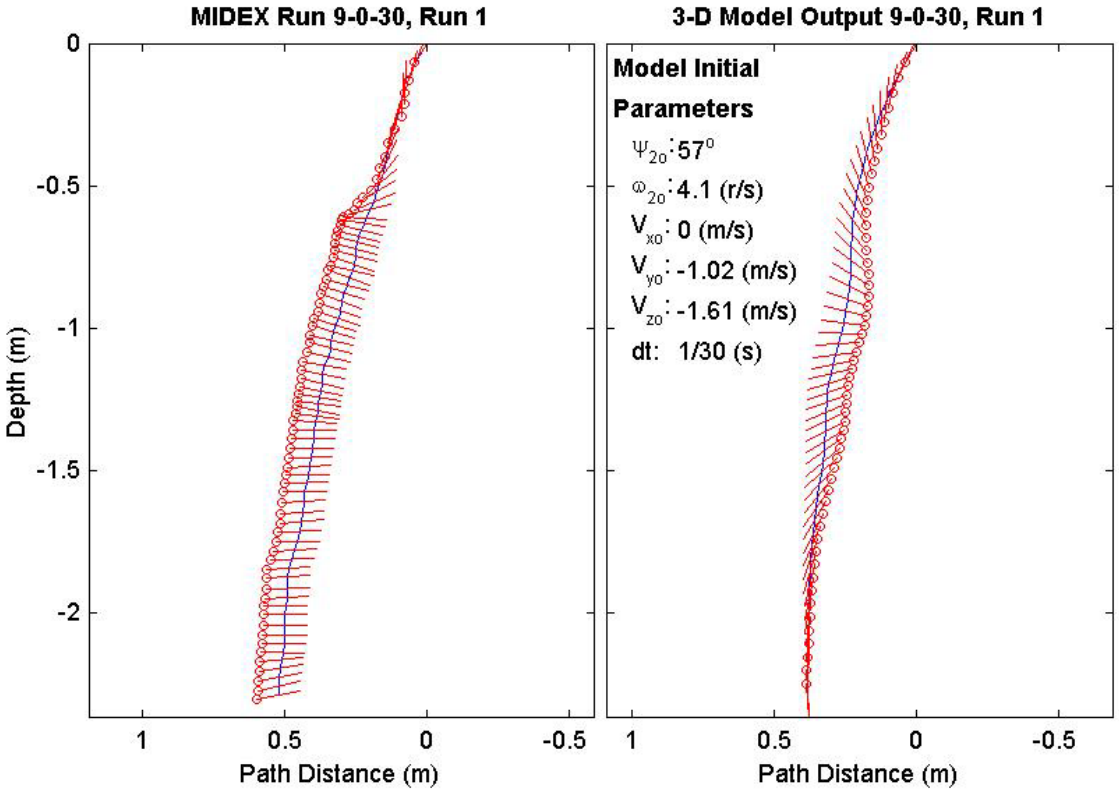

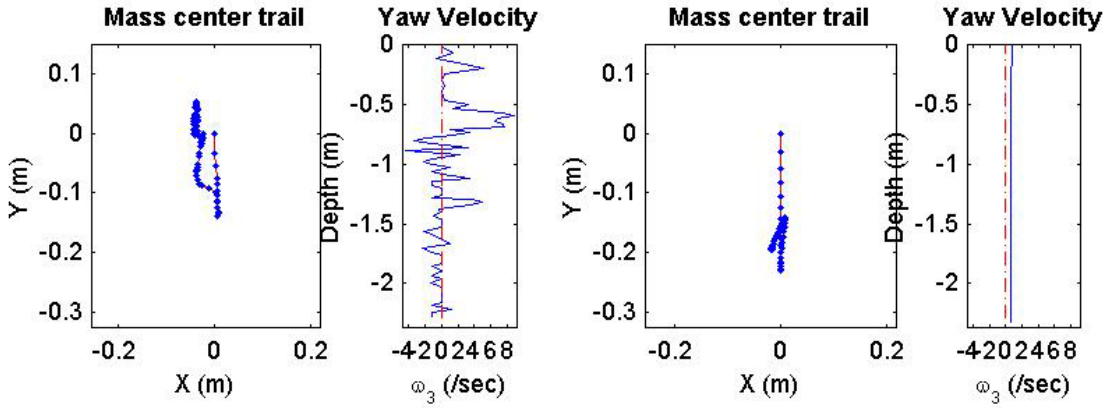

Final Drop
Parameters (30/9-1836)

time: 2.37(s)
xy_{fe}: 0.184(m)
V_{xfe}: 0(m/s)
V_{yfe}: 0(m/s)
V_{zfe}: -0.804(m/s)
Ψ_{fe}: 14.1°
depth: 2.26(m)

Mine Shape
Parameters (30/9-1836)

d: 0.04(m)
L: 0.0912(m)
m: 0.215(m)
J_1: 2.35e-005(kg*m^2)
J_2: 0.00017(kg*m^2)
J_3: 0.00017(kg*m^2)
χ: 2.9e-005(m)

Final Model
Parameters (30/9-1836)

time: 1.6(s)
xy_{fm}: 0.271(m)
V_{xfm}: -0.183(m/s)
V_{yfm}: -0.0306(m/s)
V_{zfm}: -1.37(m/s)
Ψ_{fm}: 149.6°
depth: 2.28(m)

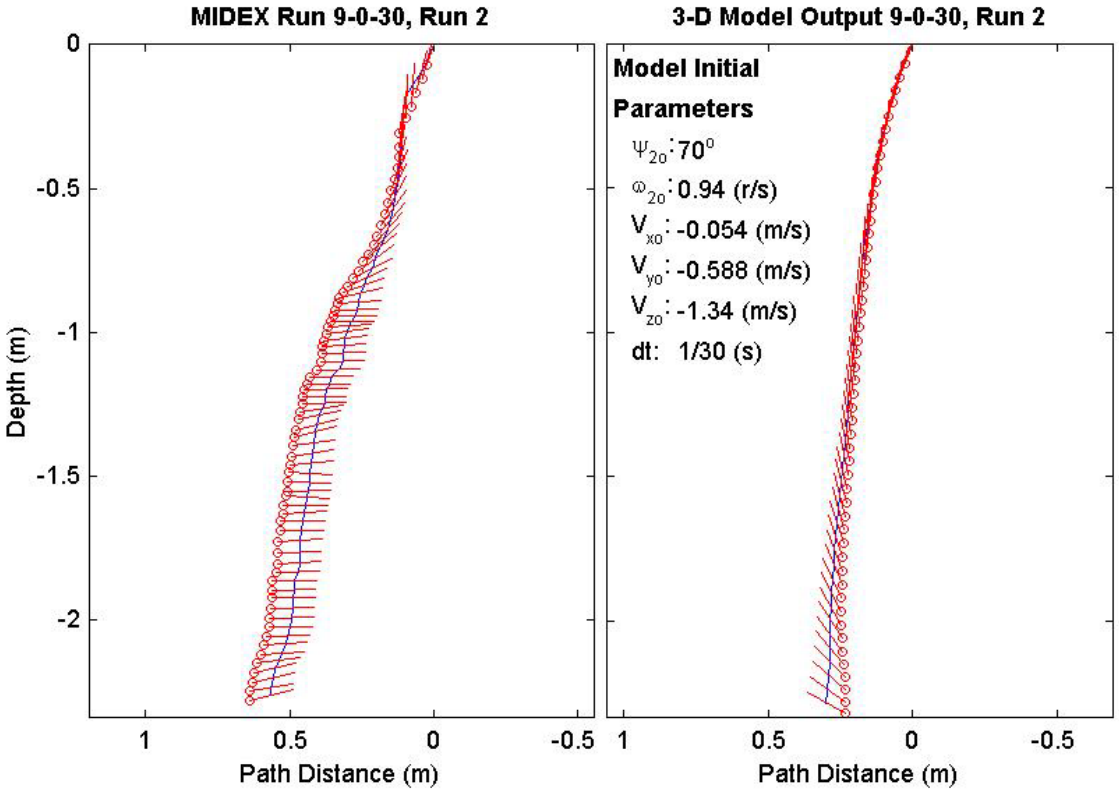

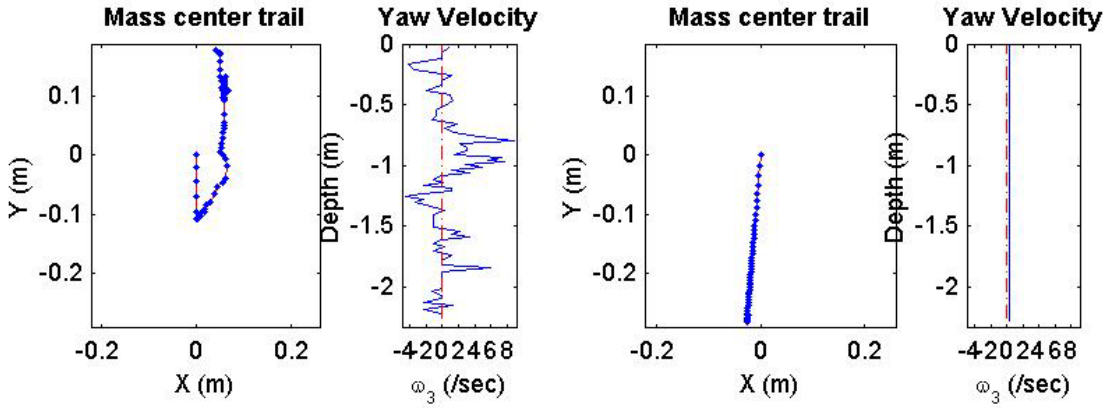

Final Drop
Parameters (30/9-1828)

time: 2.3(s)
xy_{fe}: 0.0896(m)
V_{xfe}: 0(m/s)
V_{yfe}: 0.108(m/s)
V_{zfe}: -1.07(m/s)
Ψ_{fe}: 4.5°
depth: 2.24(m)

Mine Shape
Parameters (30/9-1828)

d: 0.04(m)
L: 0.0912(m)
m: 0.215(m)
J_1: 2.35e-005(kg*m^2)
J_2: 0.00017(kg*m^2)
J_3: 0.00017(kg*m^2)
χ: 2.9e-005(m)

Final Model
Parameters (30/9-1828)

time: 1.63(s)
xy_{fm}: 0.155(m)
V_{xfm}: -0.246(m/s)
V_{yfm}: 0.0155(m/s)
V_{zfm}: -1.01(m/s)
Ψ_{fm}: -164.8°
depth: 2.25(m)

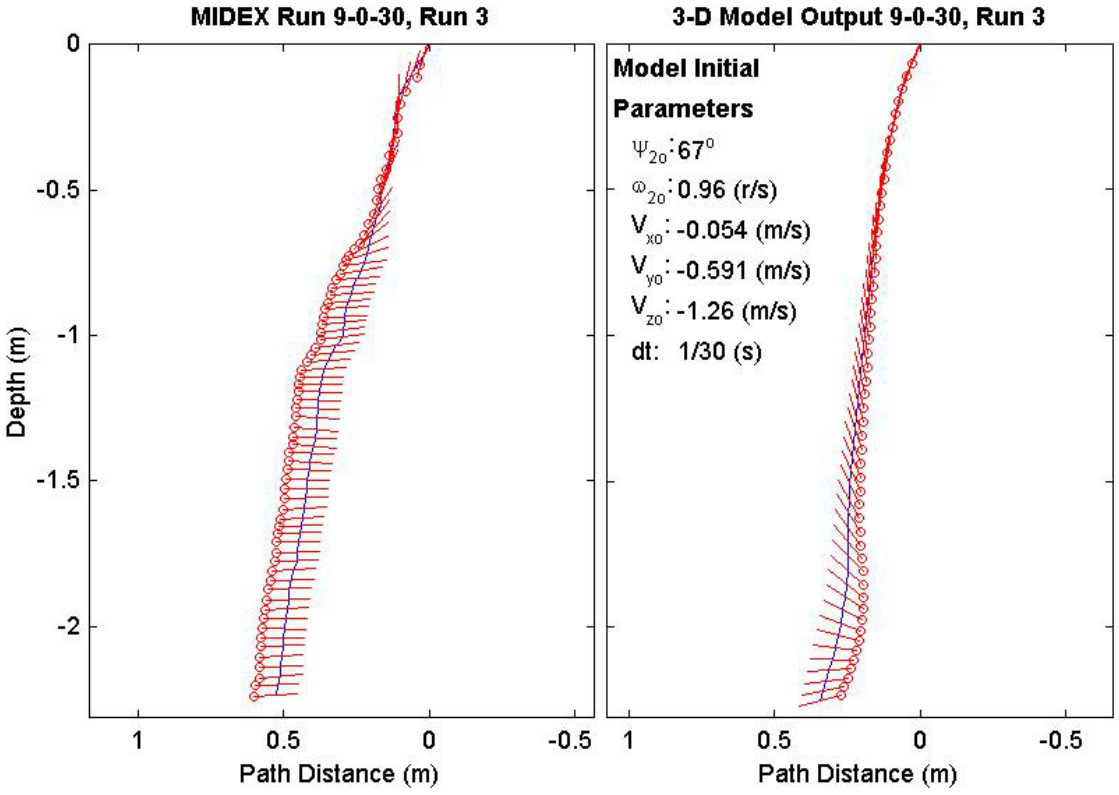

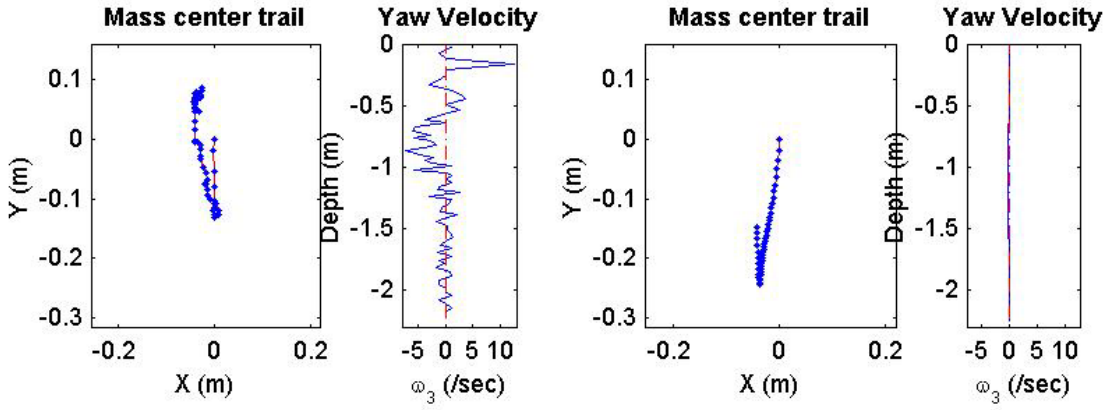

Final Drop

Parameters (30/9-1569)

time: 2.33(s)
xy_{fe}: 0.0604(m)
V_{xfe}: 0.108(m/s)
V_{yfe}: -0.213(m/s)
V_{zfe}: -0.991(m/s)
Ψ_{fe}: 2.4^{o}
depth: 2.29(m)

Mine Shape

Parameters (30/9-1569)

d: 0.04(m)
L: 0.0912(m)
m: 0.215(m)
J_1: 2.35e-005($kg*m^2$)
J_2: 0.00017($kg*m^2$)
J_3: 0.00017($kg*m^2$)
χ: 2.9e-005(m)

Final Model

Parameters (30/9-1569)

time: 1.8(s)
xy_{fm}: 0.187(m)
V_{xfm}: 0.0076(m/s)
V_{yfm}: -0.022(m/s)
V_{zfm}: -1.4(m/s)
Ψ_{fm}: -90^{o}
depth: 2.3(m)

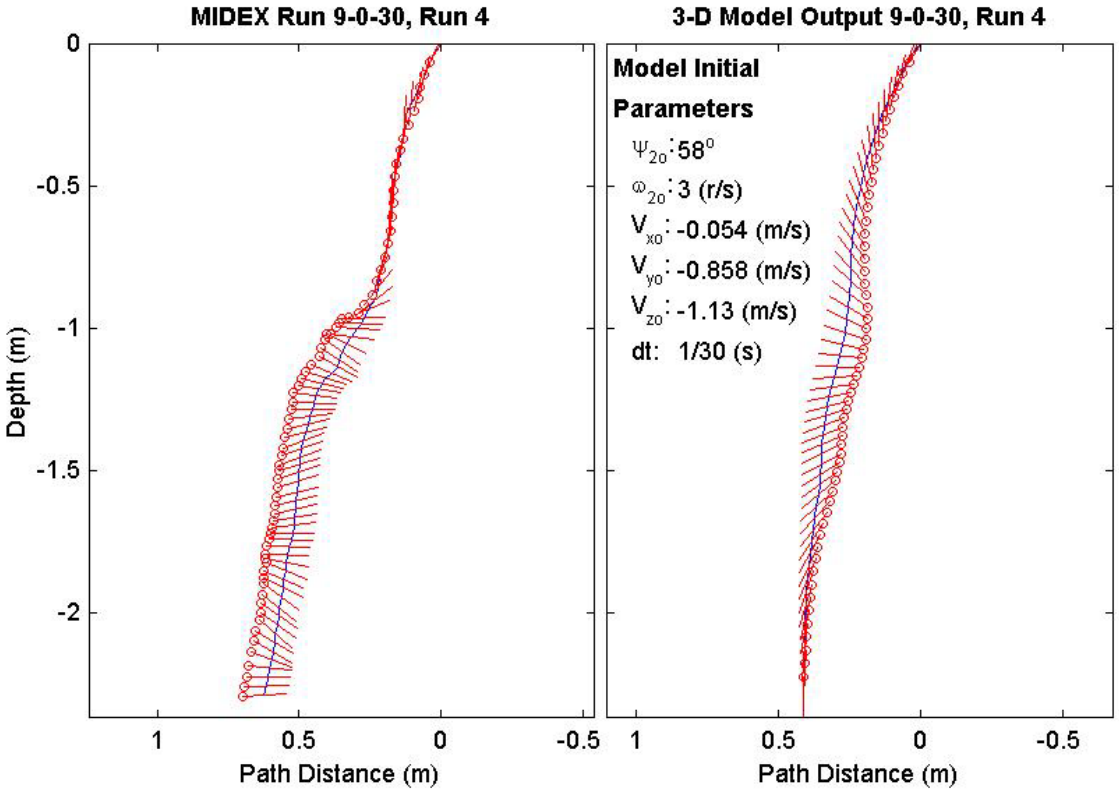

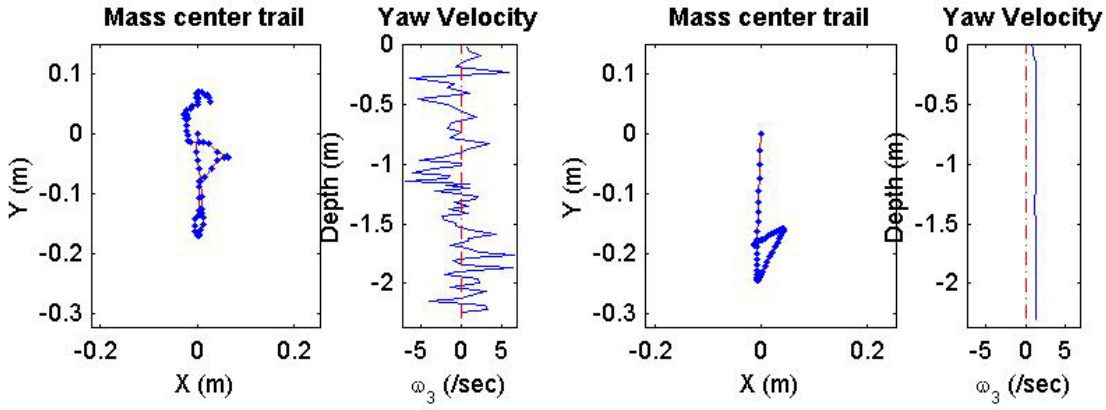

Final Drop

Parameters (30/9-1028)

time: 2.5(s)
xy_{fe}: 0.189(m)
V_{xfe}: -0.321(m/s)
V_{yfe}: -0.159(m/s)
V_{zfe}: -0.963(m/s)
Ψ_{fe}: 4.5°
depth: 2.23(m)

Mine Shape

Parameters (30/9-1028)

d: 0.04(m)
L: 0.0912(m)
m: 0.215(m)
J_1: 2.35e-005(kg*m^2)
J_2: 0.00017(kg*m^2)
J_3: 0.00017(kg*m^2)
χ: 2.9e-005(m)

Final Model

Parameters (30/9-1028)

time: 1.77(s)
xy_{fm}: 0.203(m)
V_{xfm}: -0.0421(m/s)
V_{yfm}: 0.0944(m/s)
V_{zfm}: -1.43(m/s)
Ψ_{fm}: -102.2°
depth: 2.23(m)

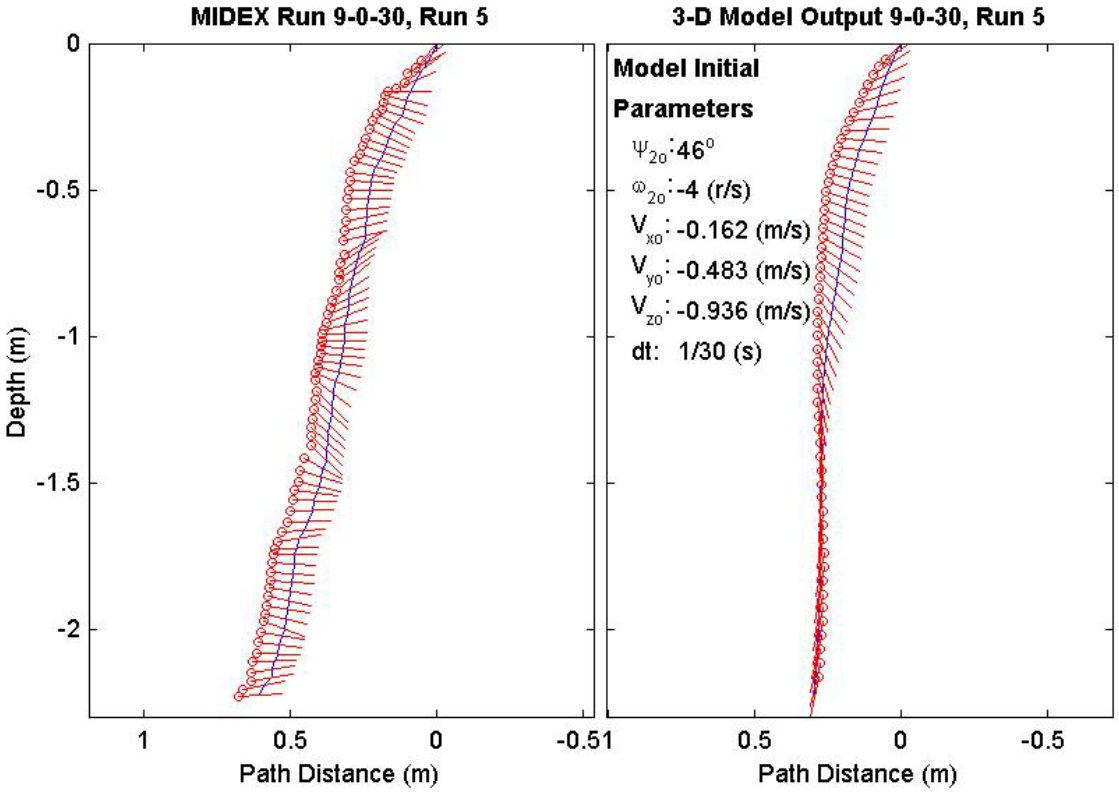

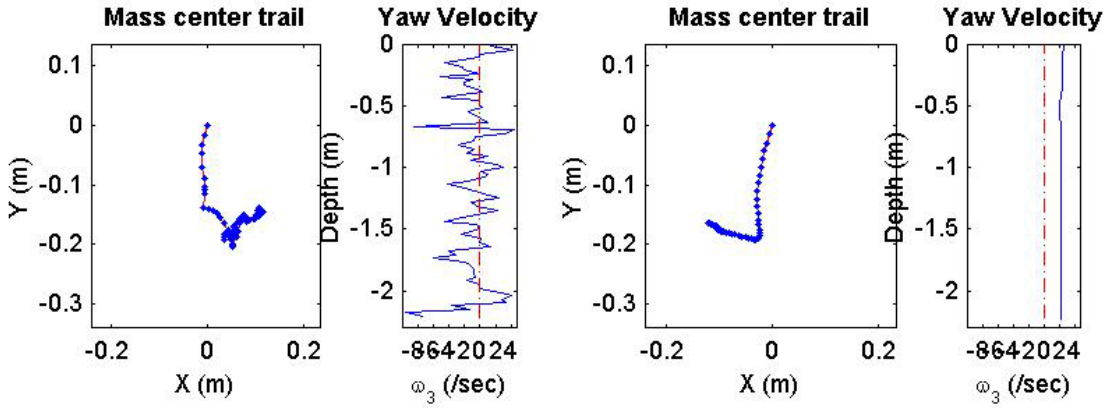

Final Drop

Parameters (45/15-2847)

time: 2.17(s)
xy_{fe}: 0.525(m)
V_{xfe}: 0.108(m/s)
V_{yfe}: 0(m/s)
V_{zfe}: -0.858(m/s)
Ψ_{fe}: -7.8°
depth: 2.14(m)

Mine Shape

Parameters (45/15-2847)

d: 0.04(m)
L: 0.152(m)
m: 0.323(m)
J_1: 3.3e-005(kg*m^2)
J_2: 0.000609(kg*m^2)
J_3: 0.000609(kg*m^2)
χ: 4.6e-005(m)

Final Model

Parameters (45/15-2847)

time: 1.37(s)
xy_{fm}: 0.454(m)
V_{xfm}: 0.374(m/s)
V_{yfm}: 0.0907(m/s)
V_{zfm}: -1.38(m/s)
Ψ_{fm}: 34.38°
depth: 2.18(m)

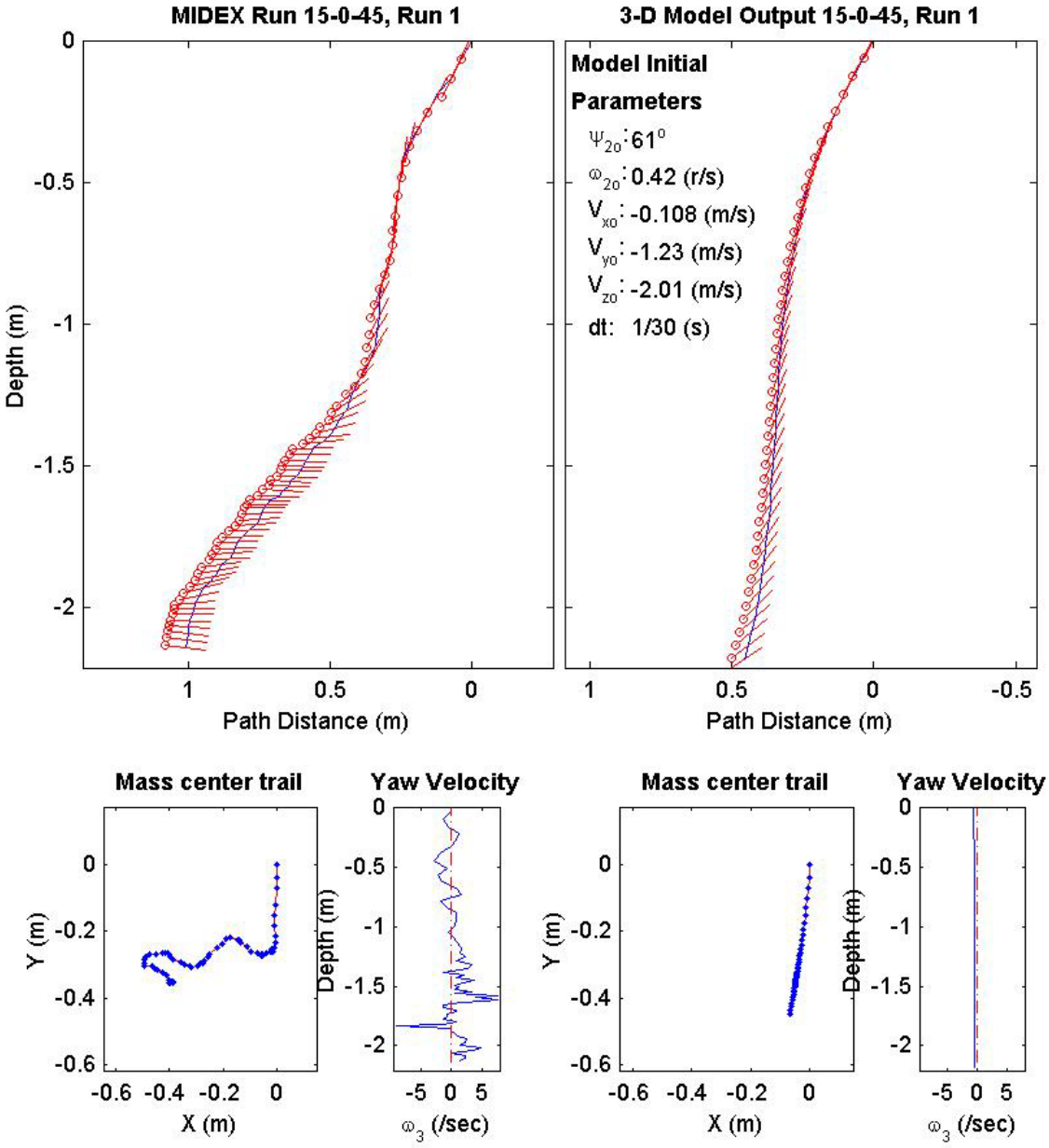

Final Drop

Parameters (45/15-2783)

time: 2.1(s)
xy_{fe}: 0.0797(m)
V_{xfe}: 0.055(m/s)
V_{yfe}: 0.159(m/s)
V_{zfe}: -0.804(m/s)
Ψ_{fe}: 42.8°
depth: 2.2(m)

Mine Shape

Parameters (45/15-2783)

d: 0.04(m)
L: 0.152(m)
m: 0.323(m)
J_1: 3.3e-005(kg*m^2)
J_2: 0.000609(kg*m^2)
J_3: 0.000609(kg*m^2)
χ: 4.6e-005(m)

Final Model

Parameters (45/15-2783)

time: 1.4(s)
xy_{fm}: 0.59(m)
V_{xfm}: 0.015(m/s)
V_{yfm}: -0.0268(m/s)
V_{zfm}: -1.52(m/s)
Ψ_{fm}: 87.27°
depth: 2.23(m)

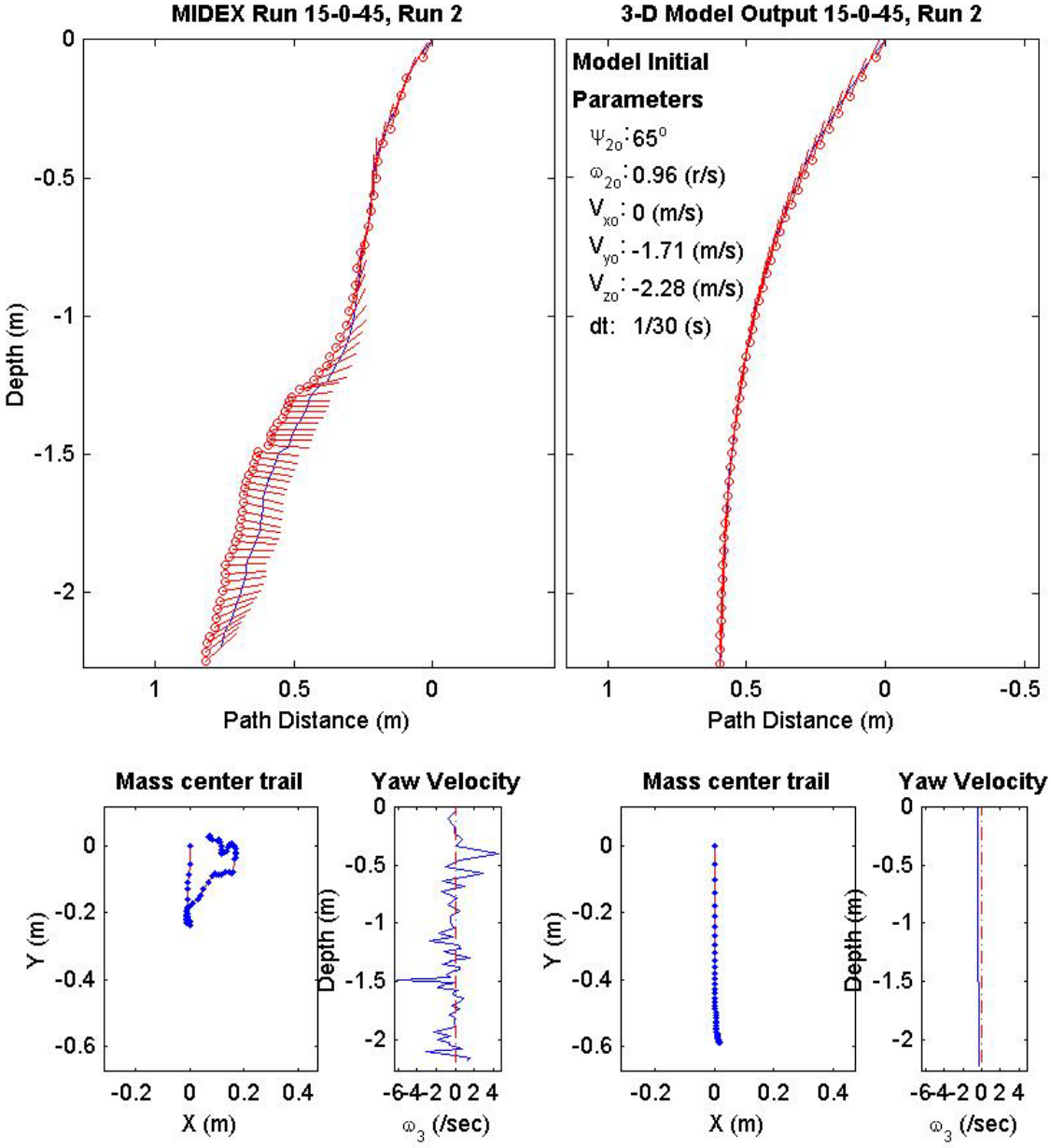

Final Drop

Parameters (45/15-2254)

time: 1.27(s)
xy_{fe}: 0.55(m)
V_{xfe}: -0.106(m/s)
V_{yfe}: 0.051(m/s)
V_{zfe}: -1.66(m/s)
Ψ_{fe}: 60.8°
depth: 2.1(m)

Mine Shape

Parameters (45/15-2254)

d: 0.04(m)
L: 0.152(m)
m: 0.323(m)
J_1: 3.3e-005(kg*m^2)
J_2: 0.000609(kg*m^2)
J_3: 0.000609(kg*m^2)
χ: 4.6e-005(m)

Final Model

Parameters (45/15-2254)

time: 1.47(s)
xy_{fm}: 0.603(m)
V_{xfm}: 0.483(m/s)
V_{yfm}: -0.122(m/s)
V_{zfm}: -0.931(m/s)
Ψ_{fm}: -4.389°
depth: 2.12(m)

MIDEX Run 15-0-45, Run 3

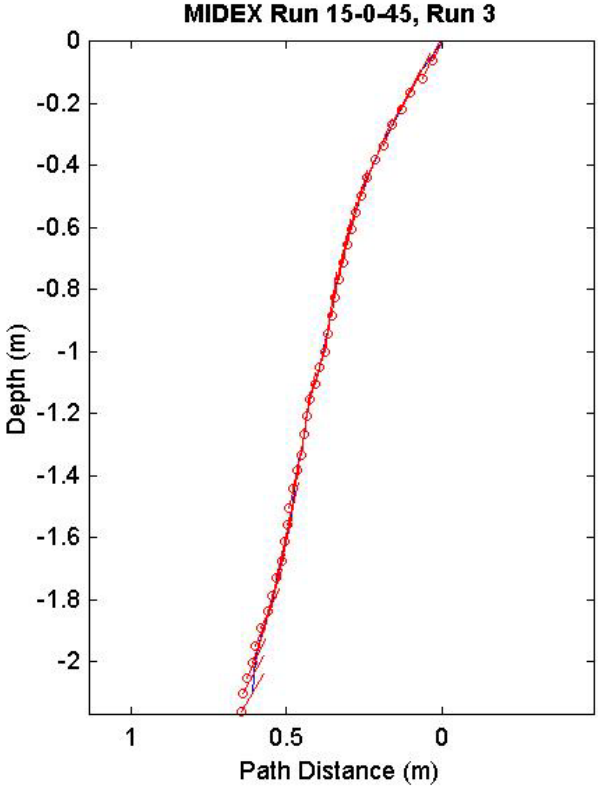

3-D Model Output 15-0-45, Run 3

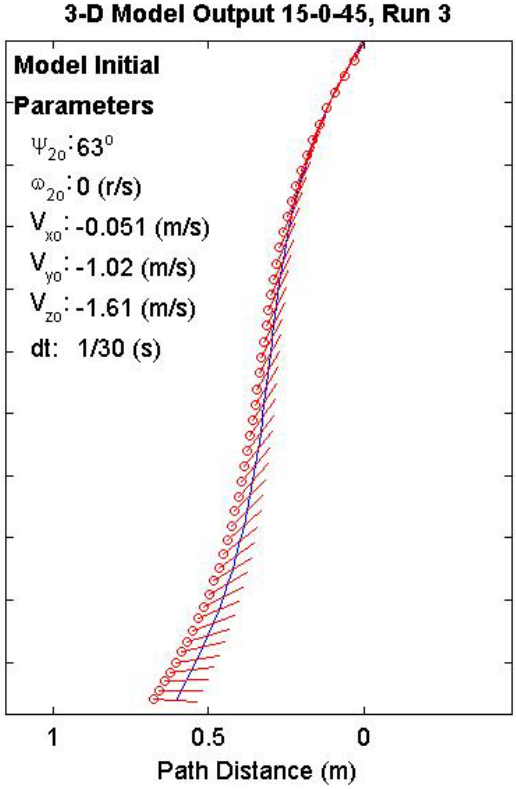

Mass center trail

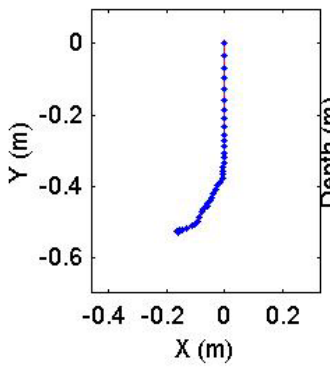

Yaw Velocity

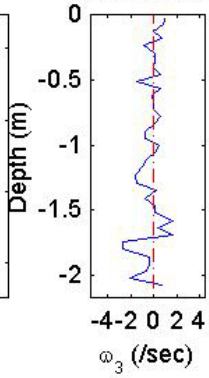

Mass center trail

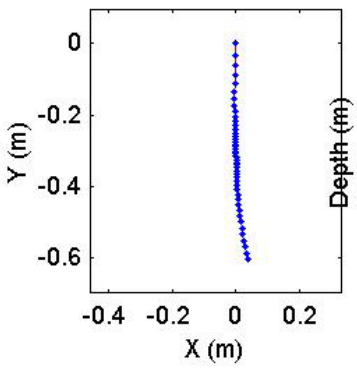

Yaw Velocity

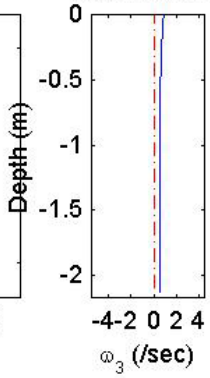

Final Drop Parameters (45/15-2026)

time: 2.57(s)
xy_{fe}: 0.458(m)
V_{xfe}: 0(m/s)
V_{yfe}: 0.588(m/s)
V_{zfe}: -0.831(m/s)
Ψ_{fe}: 20.7°
depth: 2.19(m)

Mine Shape Parameters (45/15-2026)

d: 0.04(m)
L: 0.152(m)
m: 0.323(m)
J_1: 3.3e-005(kg*m^2)
J_2: 0.000609(kg*m^2)
J_3: 0.000609(kg*m^2)
χ: 4.6e-005(m)

Final Model Parameters (45/15-2026)

time: 1.9(s)
xy_{fm}: 0.617(m)
V_{xfm}: -0.223(m/s)
V_{yfm}: 1.37e-017(m/s)
V_{zfm}: -1.42(m/s)
Ψ_{fm}: -62.5°
depth: 2.22(m)

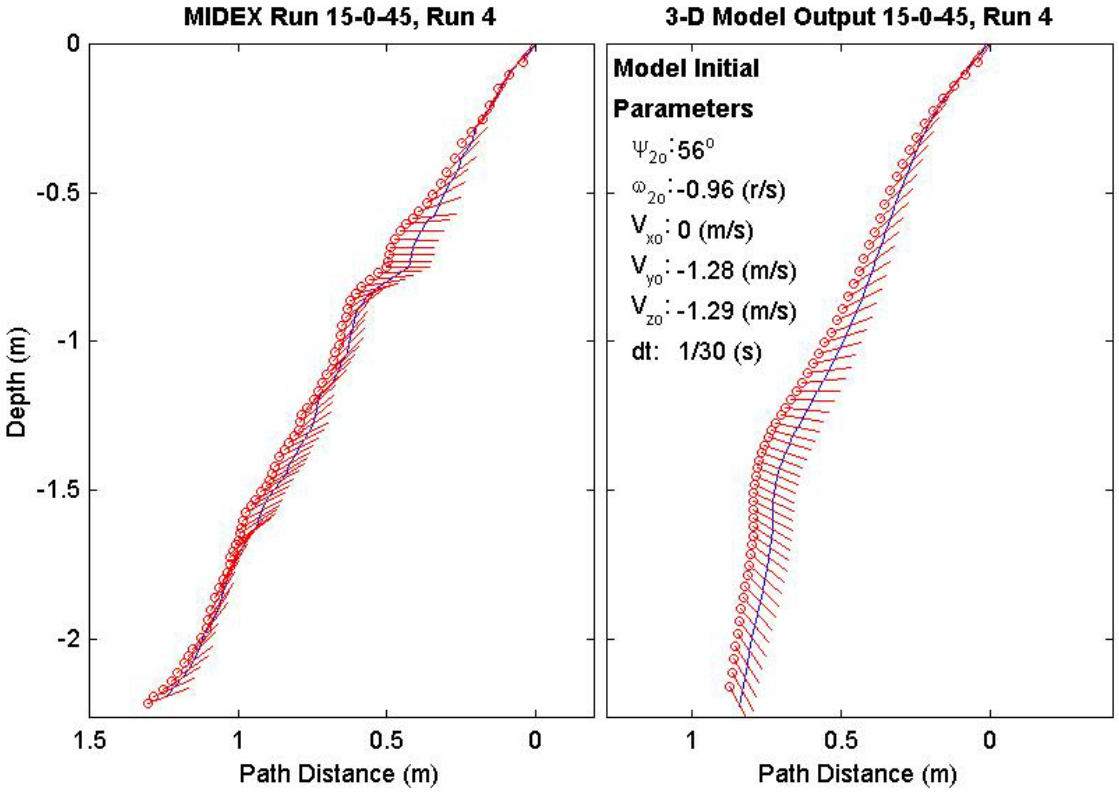

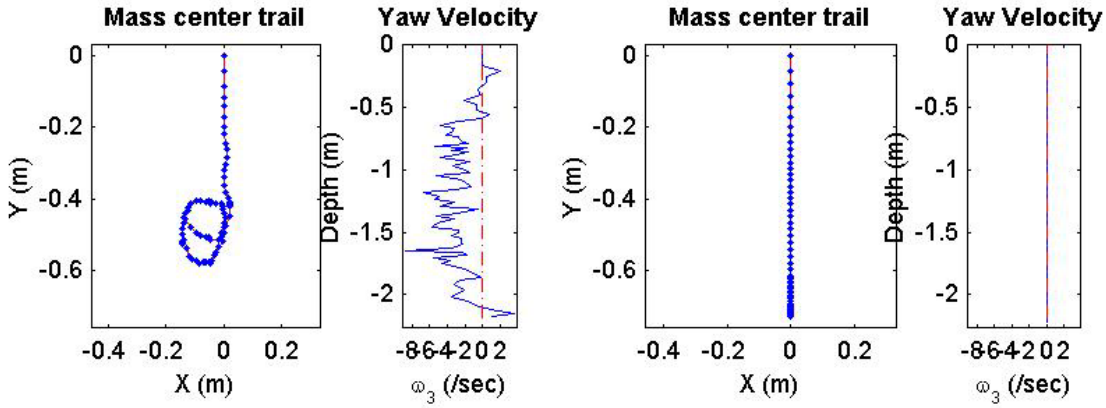

Final Drop

Parameters (45/12-3222)

time: 2.53(s)
xy_{fe}: 0.0659(m)
V_{xfe}: 0.054(m/s)
V_{yfe}: -0.054(m/s)
V_{zfe}: -0.643(m/s)
Ψ_{fe}: 23.5°
depth: 2.24(m)

Mine Shape

Parameters (45/12-3222)

d: 0.04(m)
L: 0.121(m)
m: 0.254(m)
J_1: 2.71e-005($kg*m^2$)
J_2: 0.000343($kg*m^2$)
J_3: 0.000343($kg*m^2$)
χ: 0.000644(m)

Final Model

Parameters (45/12-3222)

time: 1.57(s)
xy_{fm}: 0.48(m)
V_{xfm}: 0.098(m/s)
V_{yfm}: -0.00336(m/s)
V_{zfm}: -1.37(m/s)
Ψ_{fm}: 91.08°
depth: 2.24(m)

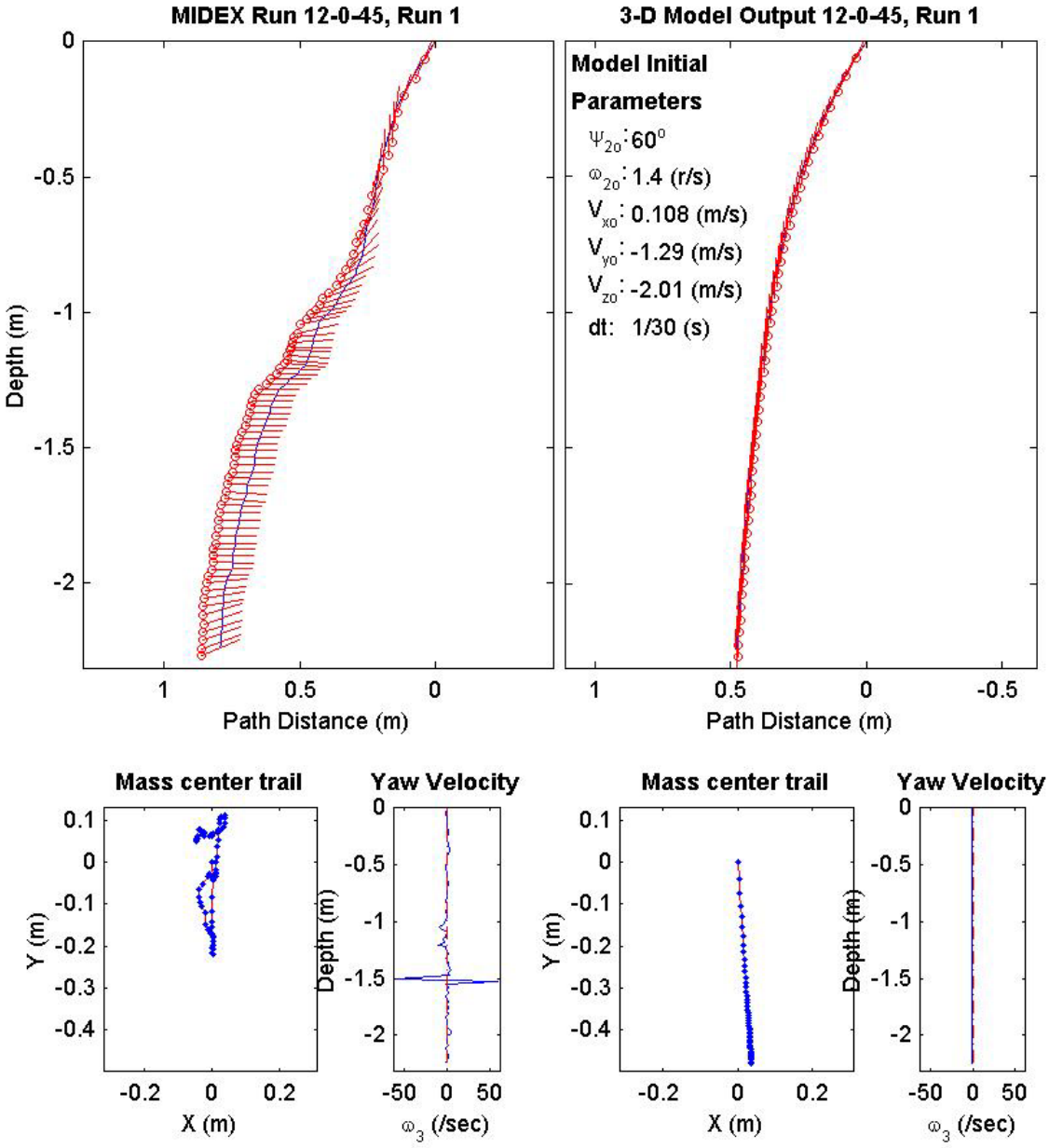

Final Drop

Parameters (45/12-2675)

time: 2.53(s)
xy_{fe}: 0.0103(m)
V_{xfe}: 0.054(m/s)
V_{yfe}: 0(m/s)
V_{zfe}: -0.803(m/s)
Ψ_{fe}: -39.8°
depth: 2.23(m)

Mine Shape

Parameters (45/12-2675)

d: 0.04(m)
L: 0.121(m)
m: 0.254(m)
J_1: 2.71e-005(kg*m^2)
J_2: 0.000343(kg*m^2)
J_3: 0.000343(kg*m^2)
χ: 0.000644(m)

Final Model

Parameters (45/12-2675)

time: 1.6(s)
xy_{fm}: 0.131(m)
V_{xfm}: -0.368(m/s)
V_{yfm}: 0.0294(m/s)
V_{zfm}: -1.2(m/s)
Ψ_{fm}: 155.5°
depth: 2.25(m)

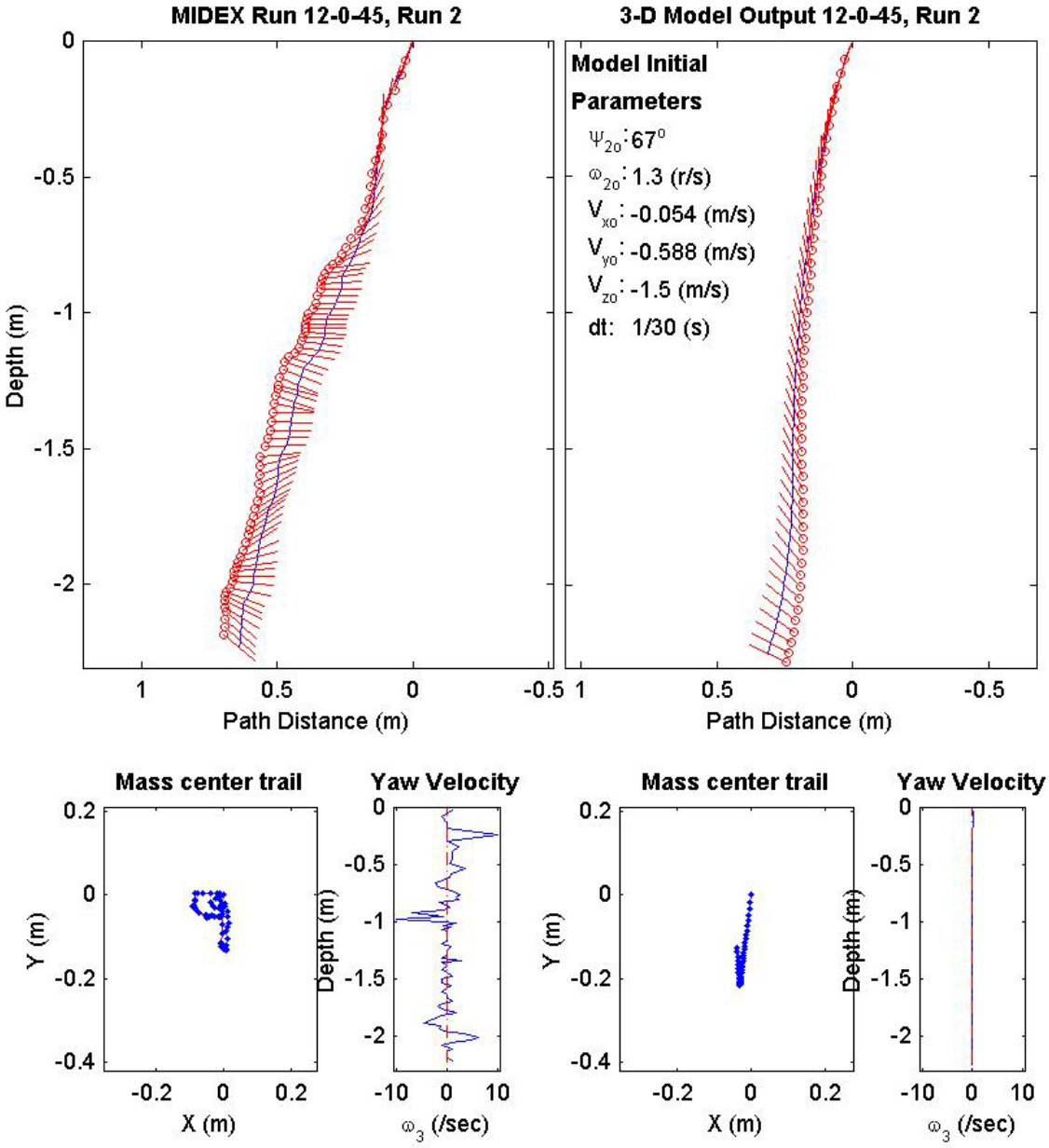

Final Drop

Parameters (45/12-2348)

time: 1.63(s)
xy_{fe}: 0.433(m)
V_{xfe}: -0.054(m/s)
V_{yfe}: -0.054(m/s)
V_{zfe}: -0.804(m/s)
Ψ_{fe}: 2.7°
depth: 2.24(m)

Mine Shape

Parameters (45/12-2348)

d: 0.04(m)
L: 0.121(m)
m: 0.254(m)
J_1: 2.71e-005(kg*m^2)
J_2: 0.000343(kg*m^2)
J_3: 0.000343(kg*m^2)
χ: 0.000644(m)

Final Model

Parameters (45/12-2348)

time: 1.63(s)
xy_{fm}: 0.246(m)
V_{xfm}: -0.417(m/s)
V_{yfm}: 0.109(m/s)
V_{zfm}: -1.05(m/s)
Ψ_{fm}: 170.1°
depth: 2.27(m)

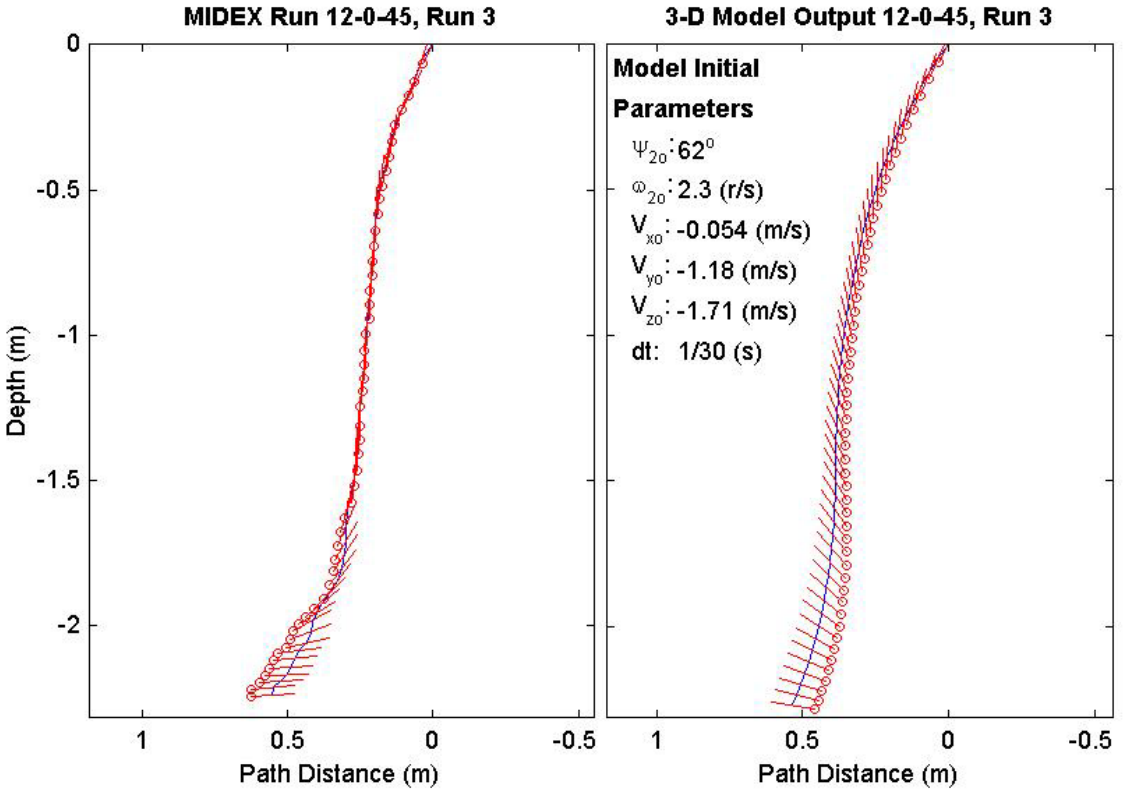

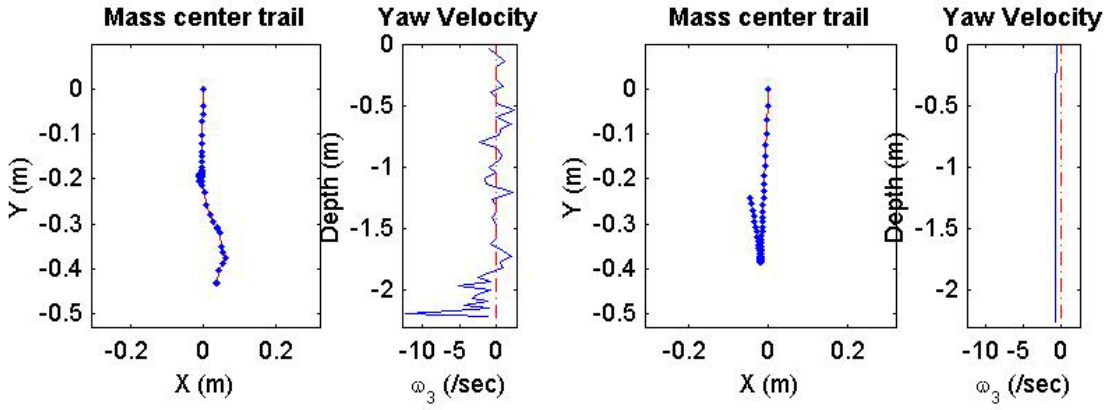

Final Drop

Parameters (45/12-1841)

time: 1.63(s)
xy_{fe}: 0.48(m)
V_{xfe}: 0(m/s)
V_{yfe}: 0.159(m/s)
V_{zfe}: -0.562(m/s)
Ψ_{fe}: -7.9°
depth: 2.2(m)

Mine Shape

Parameters (45/12-1841)

d: 0.04(m)
L: 0.121(m)
m: 0.254(m)
J_1: 2.71e-005($kg*m^2$)
J_2: 0.000343($kg*m^2$)
J_3: 0.000343($kg*m^2$)
χ: 0.000644(m)

Final Model

Parameters (45/12-1841)

time: 1.77(s)
xy_{fm}: 0.63(m)
V_{xfm}: 0.11(m/s)
V_{yfm}: 0.00341(m/s)
V_{zfm}: -0.846(m/s)
Ψ_{fm}: -15.47°
depth: 2.22(m)

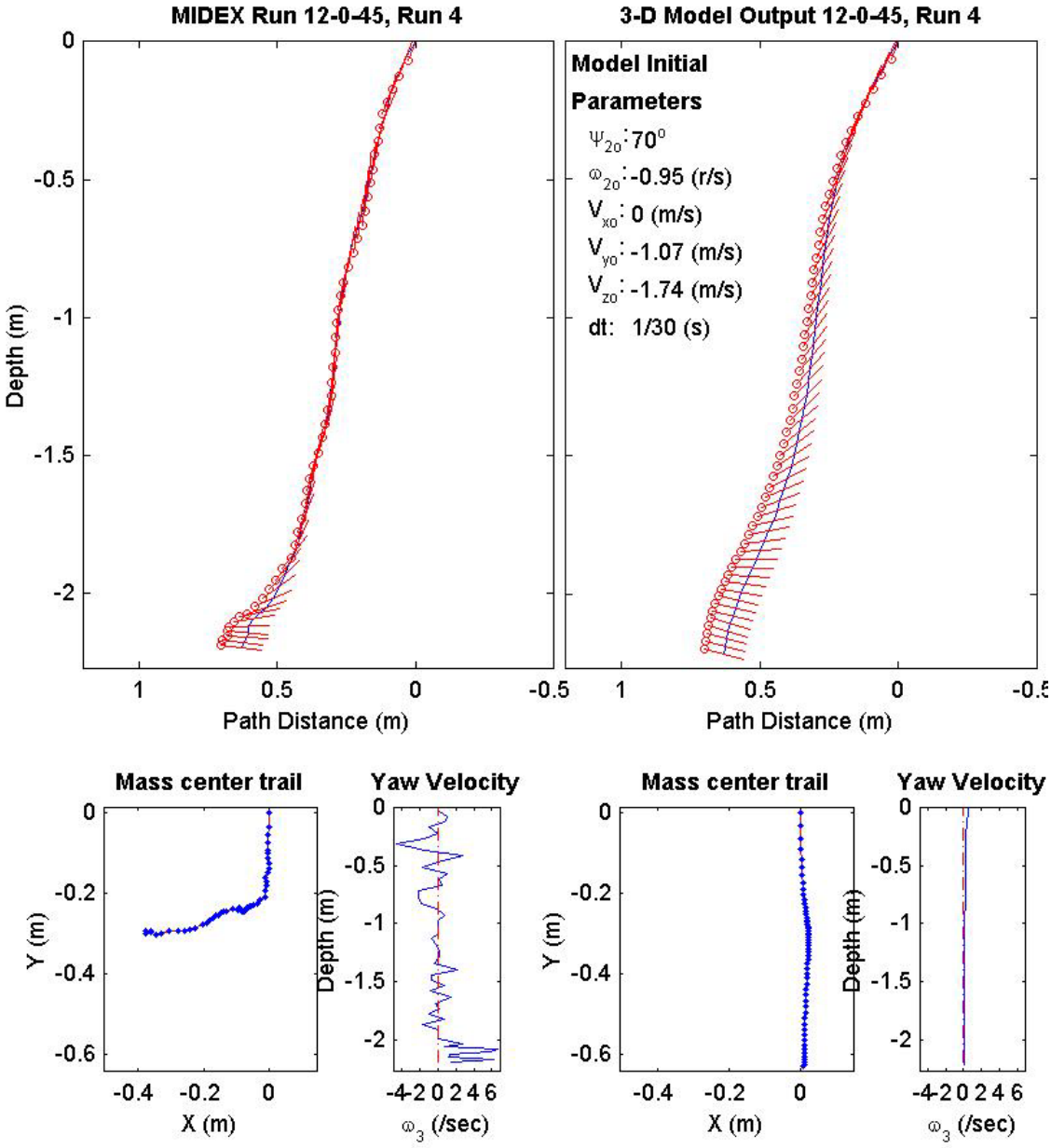

Final Drop Parameters (45/12-1376)

time: 2.63(s)
xy_{fe}: 0.329(m)
V_{xfe}: 0.591(m/s)
V_{yfe}: 0.054(m/s)
V_{zfe}: -0.589(m/s)
Ψ_{fe}: -10°
depth: 2.2(m)

Mine Shape Parameters (45/12-1376)

d: 0.04(m)
L: 0.121(m)
m: 0.254(m)
J_1: 2.71e-005(kg*m^2)
J_2: 0.000343(kg*m^2)
J_3: 0.000343(kg*m^2)
χ: 0.000644(m)

Final Model Parameters (45/12-1376)

time: 1.83(s)
xy_{fm}: 0.693(m)
V_{xfm}: 0.0065(m/s)
V_{yfm}: -0.00886(m/s)
V_{zfm}: -0.869(m/s)
Ψ_{fm}: -15.35°
depth: 2.2(m)

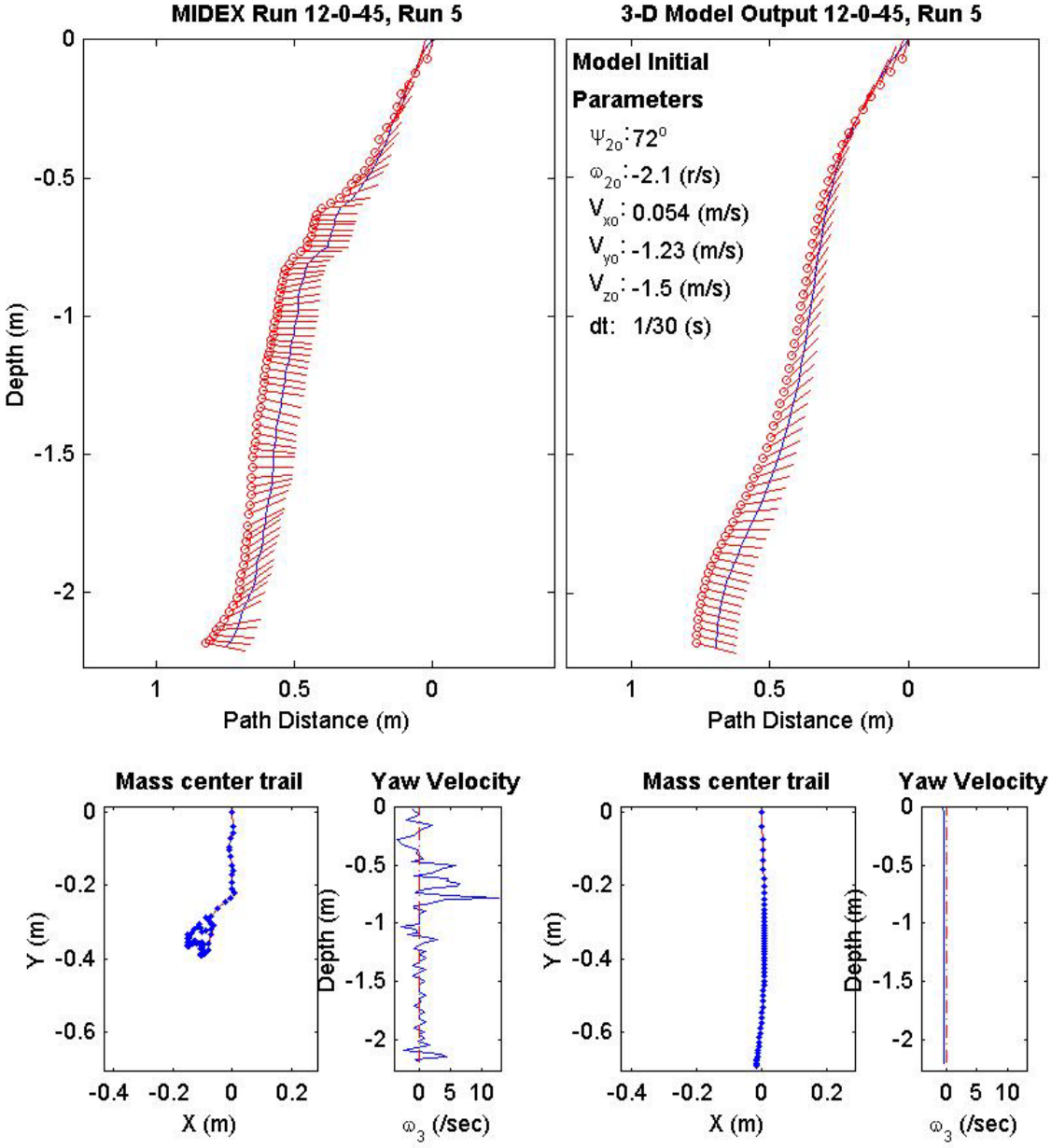

Final Drop

Parameters (45/9-3434)

time: 2.07(s)
xy_{fe}: 0.362(m)
V_{xfe}: 0.213(m/s)
V_{yfe}: 0.108(m/s)
V_{zfe}: -0.802(m/s)
Ψ_{fe}: -10.8°
depth: 2.18(m)

Mine Shape

Parameters (45/9-3434)

d: 0.04(m)
L: 0.0912(m)
m: 0.215(m)
J_1: 2.35e-005(kg*m^2)
J_2: 0.00017(kg*m^2)
J_3: 0.00017(kg*m^2)
χ: 2.9e-005(m)

Final Model

Parameters (45/9-3434)

time: 1.67(s)
xy_{fm}: 0.229(m)
V_{xfm}: -0.0101(m/s)
V_{yfm}: 0.0205(m/s)
V_{zfm}: -1.4(m/s)
Ψ_{fm}: -89.36°
depth: 2.21(m)

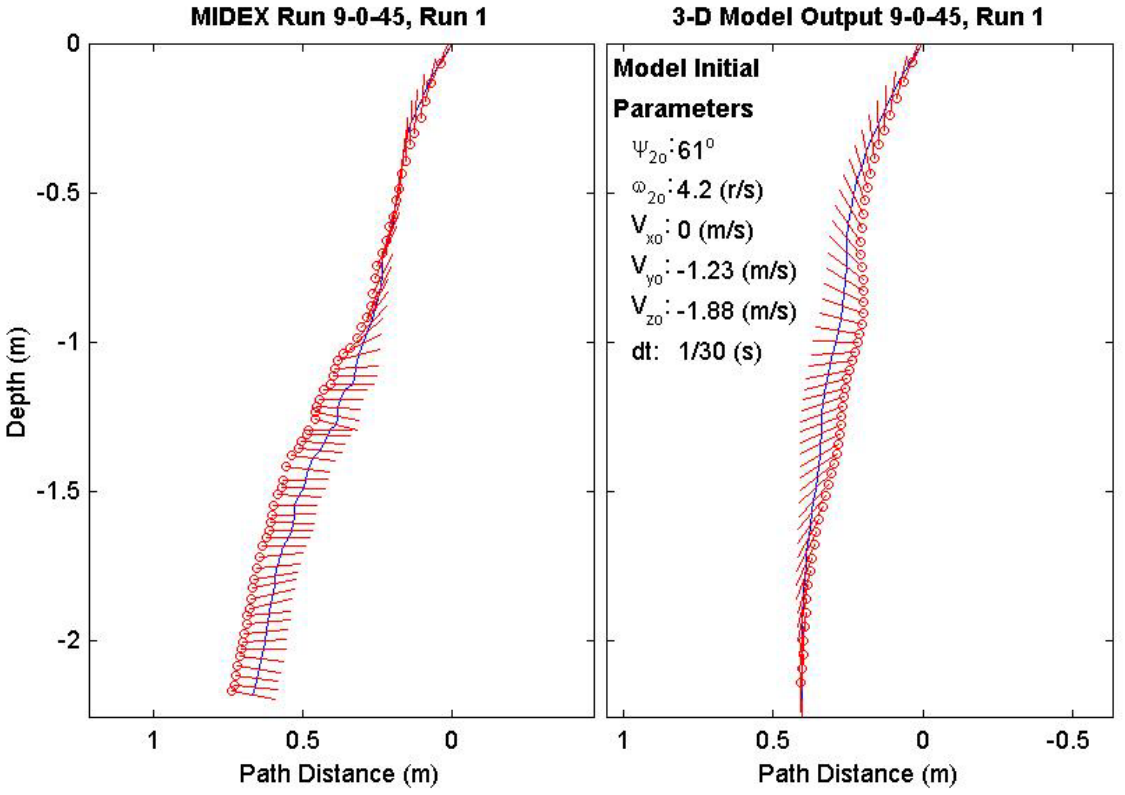

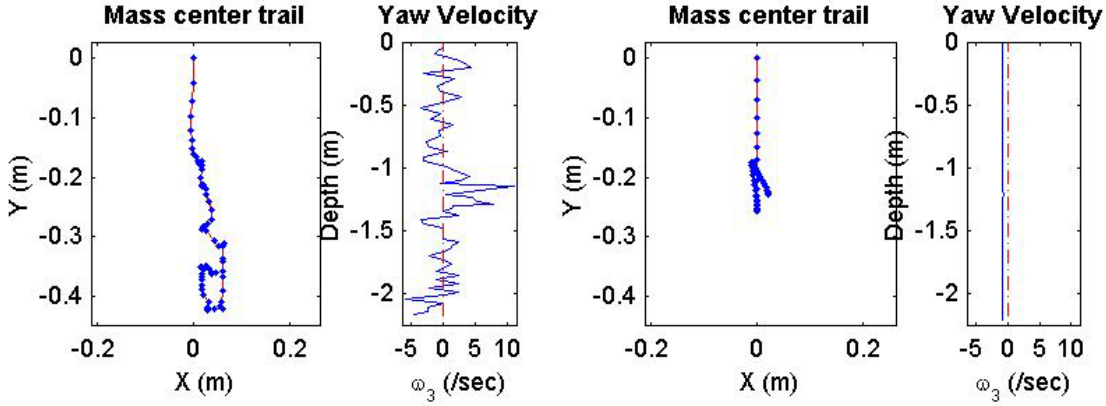

Final Drop

Parameters (45/9-2956)

time: 2.23(s)
xy_{fe}: 0.527(m)
V_{xfe}: -0.162(m/s)
V_{yfe}: 0.108(m/s)
V_{zfe}: -1.1(m/s)
Ψ_{fe}: 17°
depth: 2.17(m)

Mine Shape

Parameters (45/9-2956)

d: 0.04(m)
L: 0.0912(m)
m: 0.215(m)
J_1: 2.35e-005(kg*m^2)
J_2: 0.00017(kg*m^2)
J_3: 0.00017(kg*m^2)
χ: 2.9e-005(m)

Final Model

Parameters (45/9-2956)

time: 1.67(s)
xy_{fm}: 0.207(m)
V_{xfm}: 0.0741(m/s)
V_{yfm}: -4.42e-018(m/s)
V_{zfm}: -1.39(m/s)
Ψ_{fm}: -107.5°
depth: 2.21(m)

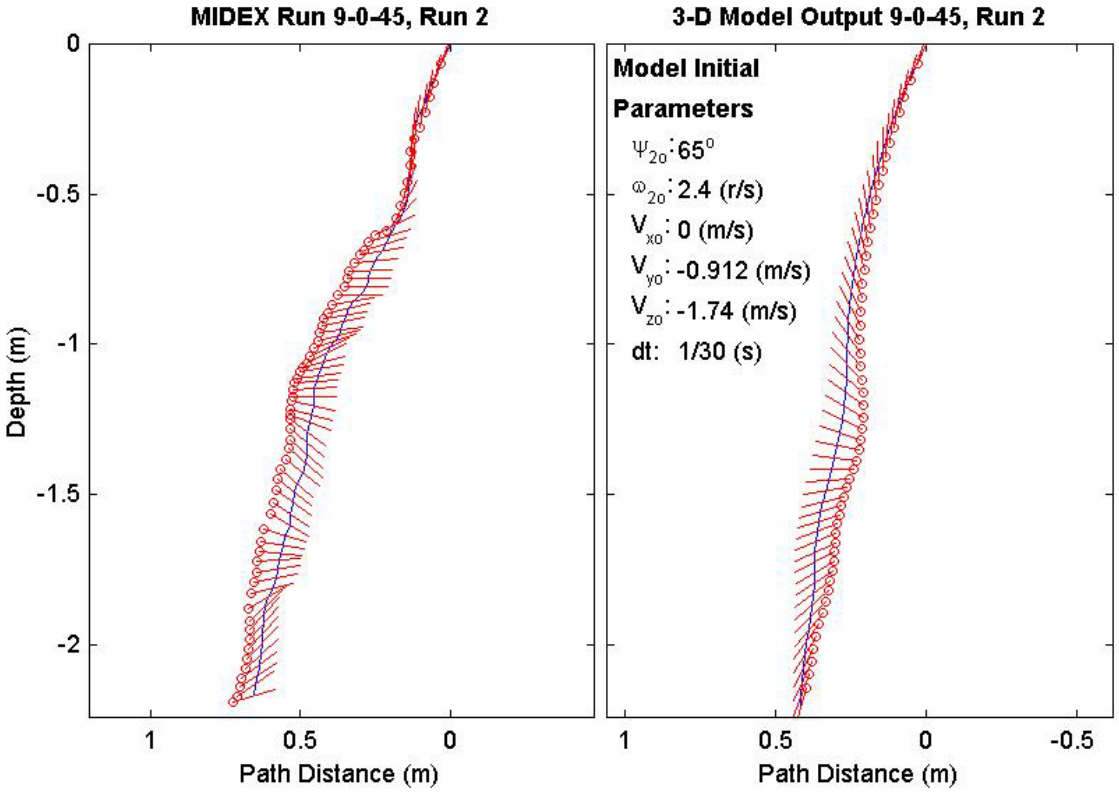

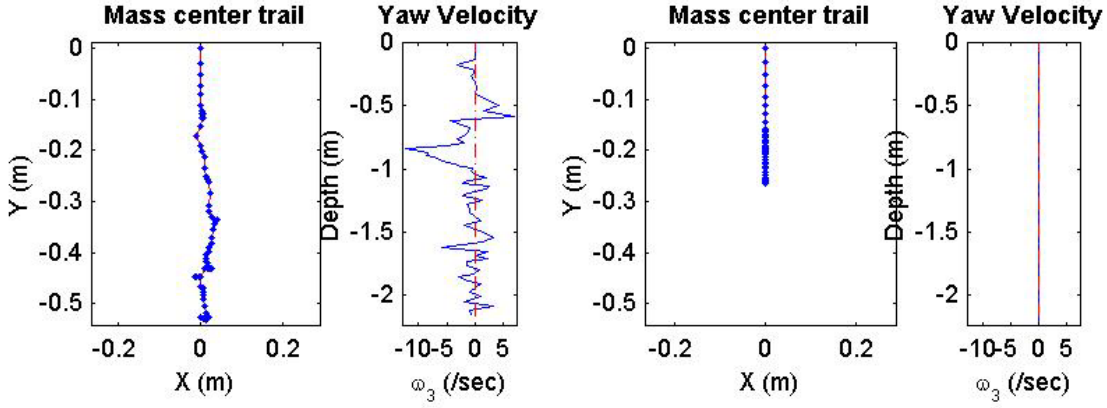

Final Drop

Parameters (45/9-2273)

time: 2.07(s)
xy_{fe}: 0.25(m)
V_{xfe}: 0(m/s)
V_{yfe}: 0(m/s)
V_{zfe}: -0.991(m/s)
Ψ_{fe}: -1.4°
depth: 2.23(m)

Mine Shape

Parameters (45/9-2273)

d: 0.04(m)
L: 0.0912(m)
m: 0.215(m)
J_1: 2.35e-005(kg*m^2)
J_2: 0.00017(kg*m^2)
J_3: 0.00017(kg*m^2)
χ: 2.9e-005(m)

Final Model

Parameters (45/9-2273)

time: 1.73(s)
xy_{fm}: 0.0847(m)
V_{xfm}: -0.0836(m/s)
V_{yfm}: 0.0188(m/s)
V_{zfm}: -1.45(m/s)
Ψ_{fm}: -76.27°
depth: 2.24(m)

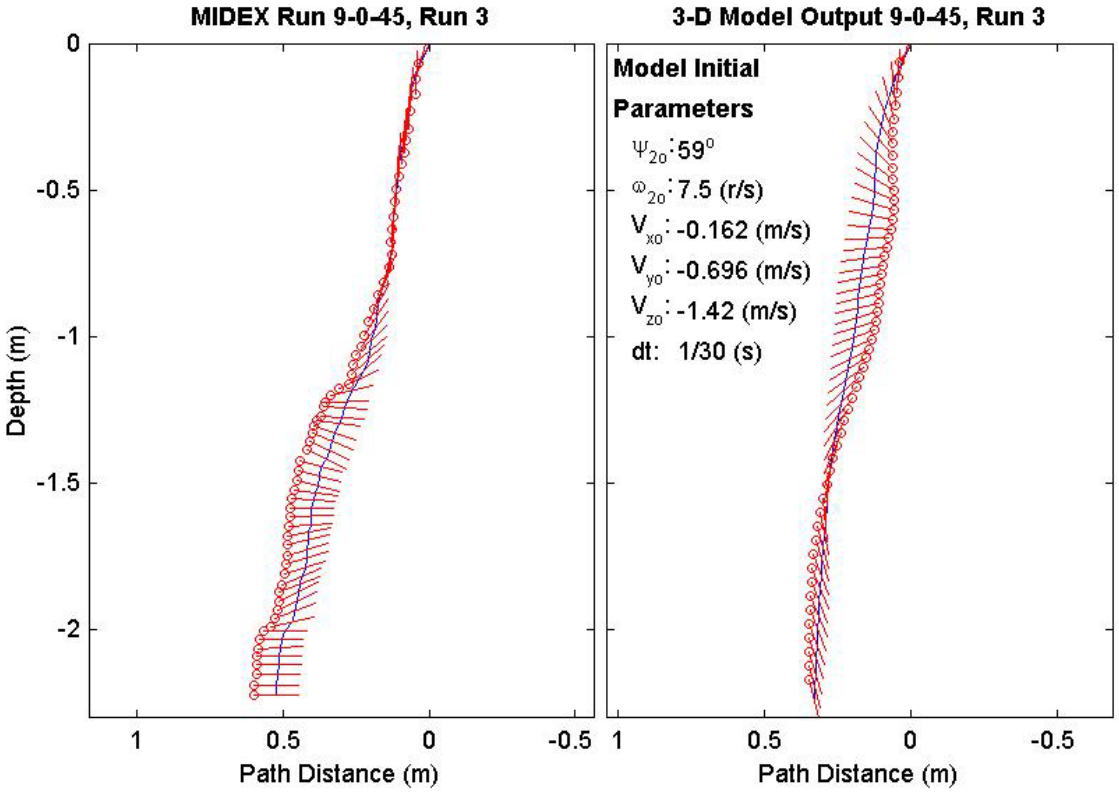

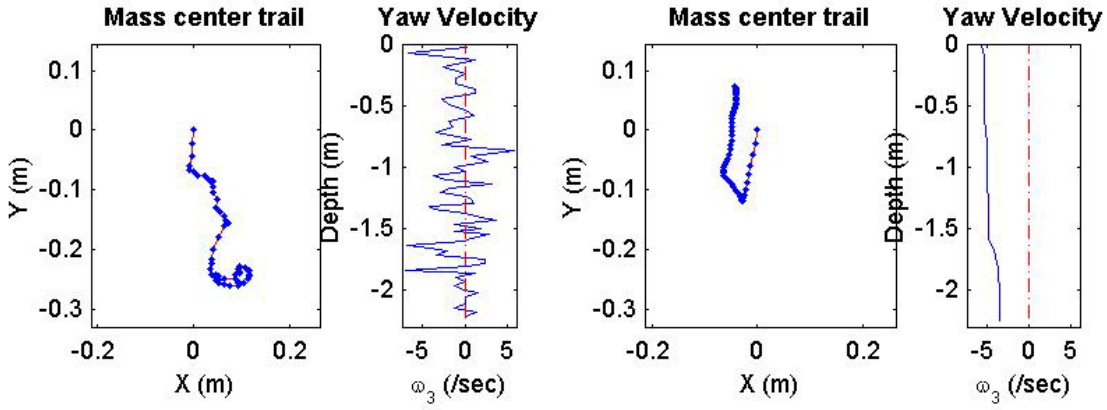

Final Drop

Parameters (45/9-2123)

time: 2.1(s)
xy_{fe}: 0.291(m)
V_{xfe}: 0.108(m/s)
V_{yfe}: -0.054(m/s)
V_{zfe}: -0.883(m/s)
Ψ_{fe}: -12.1°
depth: 2.24(m)

Mine Shape

Parameters (45/9-2123)

d: 0.04(m)
L: 0.0912(m)
m: 0.215(m)
J_1: 2.35e-005(kg*m^2)
J_2: 0.00017(kg*m^2)
J_3: 0.00017(kg*m^2)
χ: 2.9e-005(m)

Final Model

Parameters (45/9-2123)

time: 1.73(s)
xy_{fm}: 0.123(m)
V_{xfm}: 0.00591(m/s)
V_{yfm}: -0.00318(m/s)
V_{zfm}: -1.4(m/s)
Ψ_{fm}: -83.49°
depth: 2.27(m)

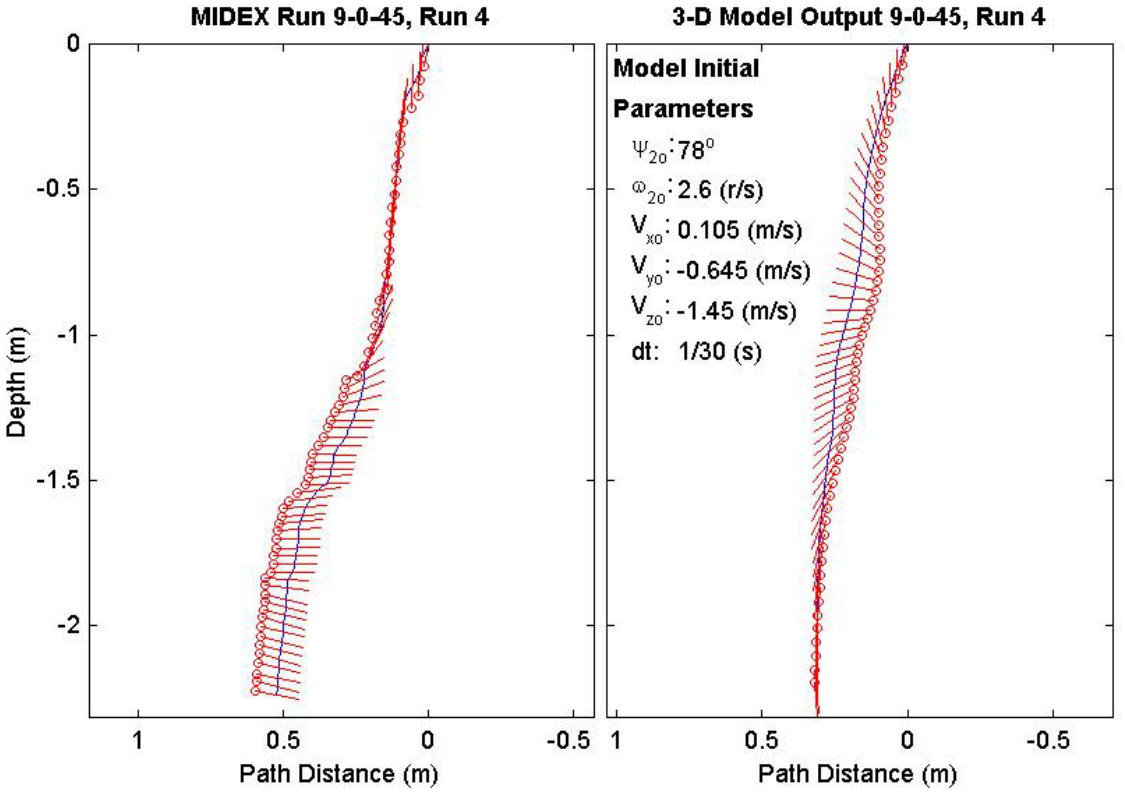

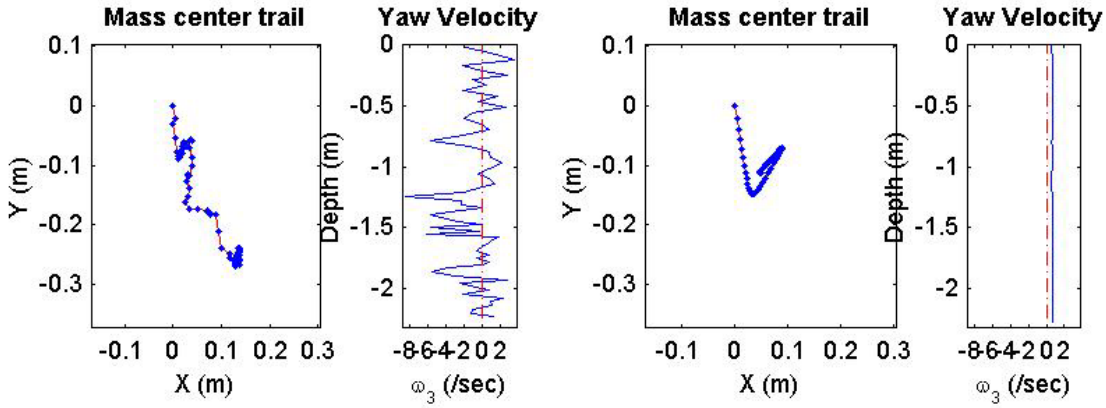

Final Drop

Parameters (45/9-1563)

time: 2.17(s)
xy_{fe}: 0.28(m)
V_{xfe}: -0.108(m/s)
V_{yfe}: 0(m/s)
V_{zfe}: -0.883(m/s)
Ψ_{fe}: 53.4°
depth: 2.16(m)

Mine Shape

Parameters (45/9-1563)

d: 0.04(m)
L: 0.0912(m)
m: 0.215(m)
J_1: 2.35e-005(kg*m^2)
J_2: 0.00017(kg*m^2)
J_3: 0.00017(kg*m^2)
χ: 2.9e-005(m)

Final Model

Parameters (45/9-1563)

time: 1.67(s)
xy_{fm}: 0.0688(m)
V_{xfm}: 0.00676(m/s)
V_{yfm}: -0.0182(m/s)
V_{zfm}: -1.4(m/s)
Ψ_{fm}: -93.12°
depth: 2.19(m)

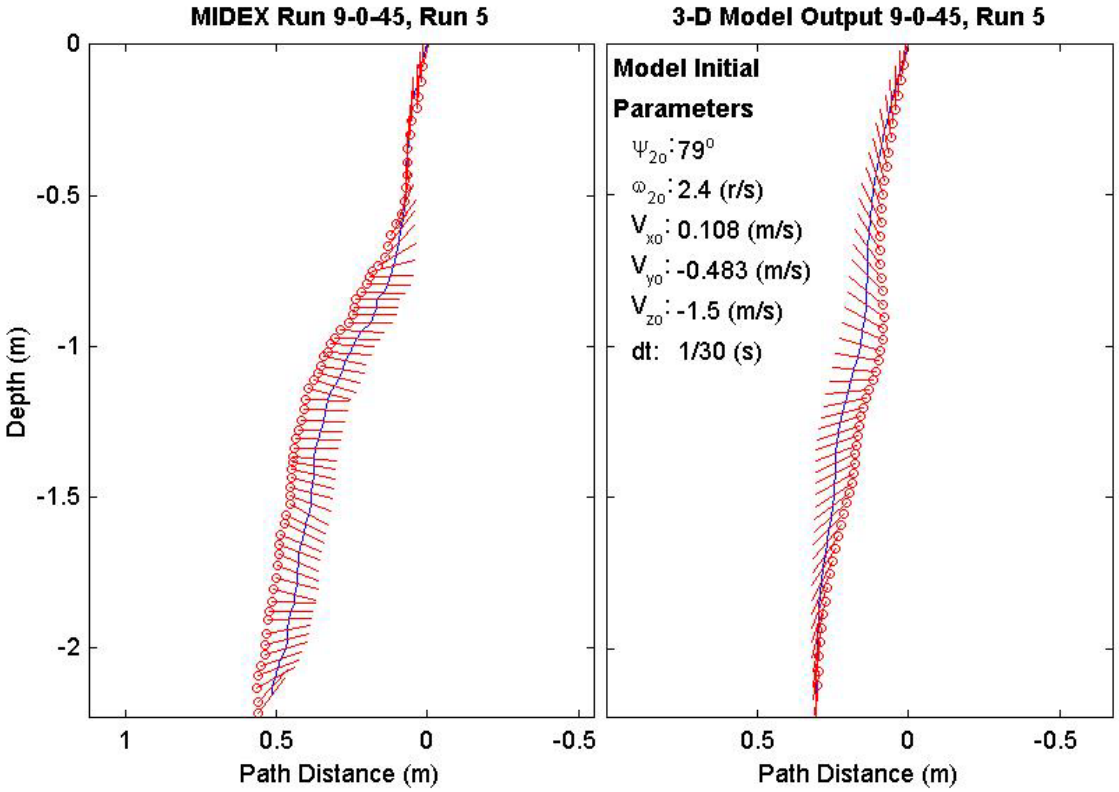

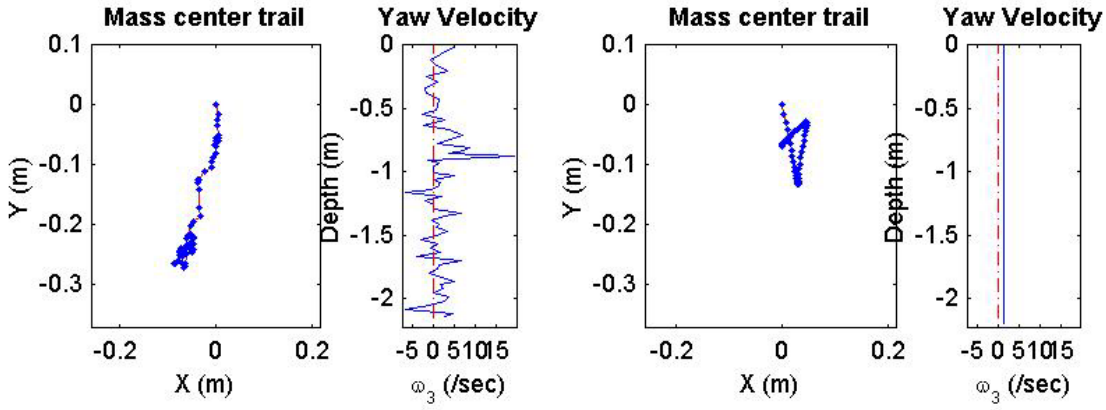

Final Drop Parameters (60/15-3471)

time: 1.83(s)
xy_{fe}: 0.216(m)
V_{xfe}: 0.321(m/s)
V_{yfe}: -0.108(m/s)
V_{zfe}: -0.695(m/s)
Ψ_{fe}: 39.3°
depth: 2.19(m)

Mine Shape Parameters (60/15-3471)

d: 0.04(m)
L: 0.152(m)
m: 0.323(m)
J_1: 3.3e-005(kg*m^2)
J_2: 0.000609(kg*m^2)
J_3: 0.000609(kg*m^2)
χ: 4.6e-005(m)

Final Model Parameters (60/15-3471)

time: 1.63(s)
xy_{fm}: 0.702(m)
V_{xfm}: 0.0237(m/s)
V_{yfm}: -0.00787(m/s)
V_{zfm}: -0.89(m/s)
Ψ_{fm}: -25.58°
depth: 2.2(m)

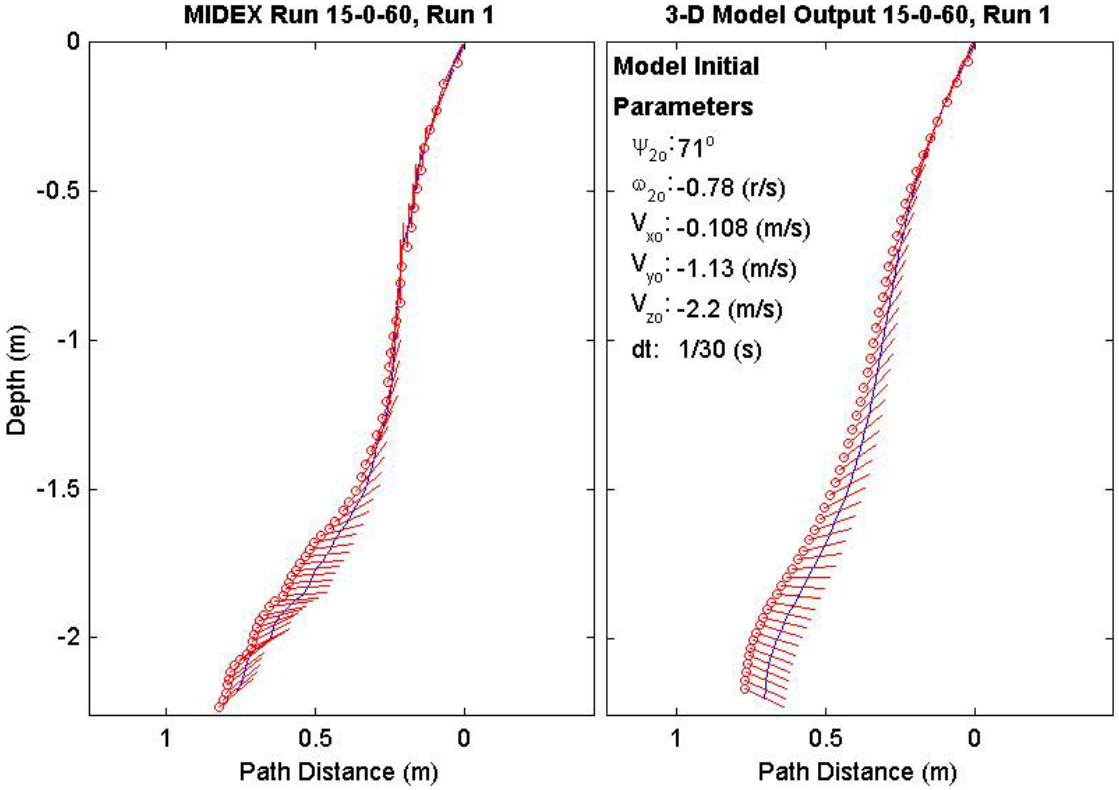

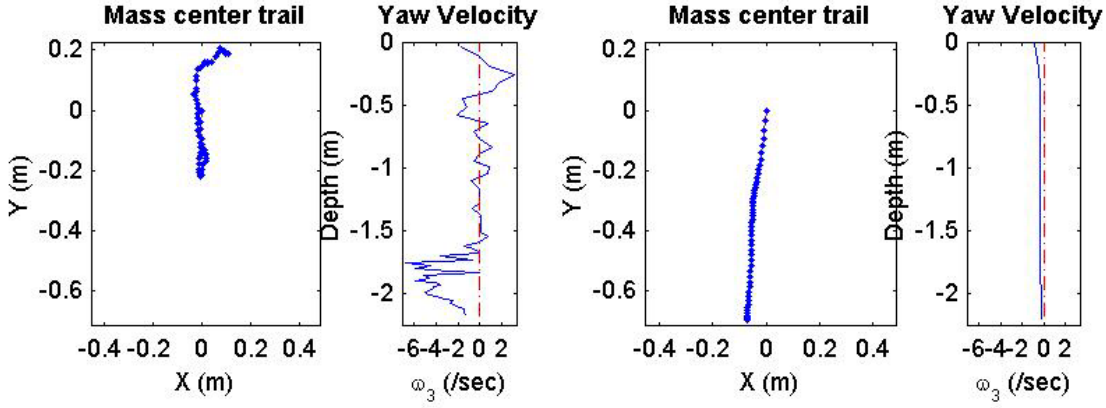

Final Drop
Parameters (60/15-3001)

time: 2.27(s)
xy_{fe}: 0.289(m)
V_{xfe}: 0(m/s)
V_{yfe}: -0.106(m/s)
V_{zfe}: -0.642(m/s)
Ψ_{fe}: -17.8°
depth: 2.15(m)

Mine Shape
Parameters (60/15-3001)

d: 0.04(m)
L: 0.152(m)
m: 0.323(m)
J_1: 3.3e-005(kg*m^2)
J_2: 0.000609(kg*m^2)
J_3: 0.000609(kg*m^2)
χ: 4.6e-005(m)

Final Model
Parameters (60/15-3001)

time: 1.33(s)
xy_{fm}: 0.468(m)
V_{xfm}: -0.00819(m/s)
V_{yfm}: 3.33e-018(m/s)
V_{zfm}: -1.55(m/s)
Ψ_{fm}: 114.6°
depth: 2.18(m)

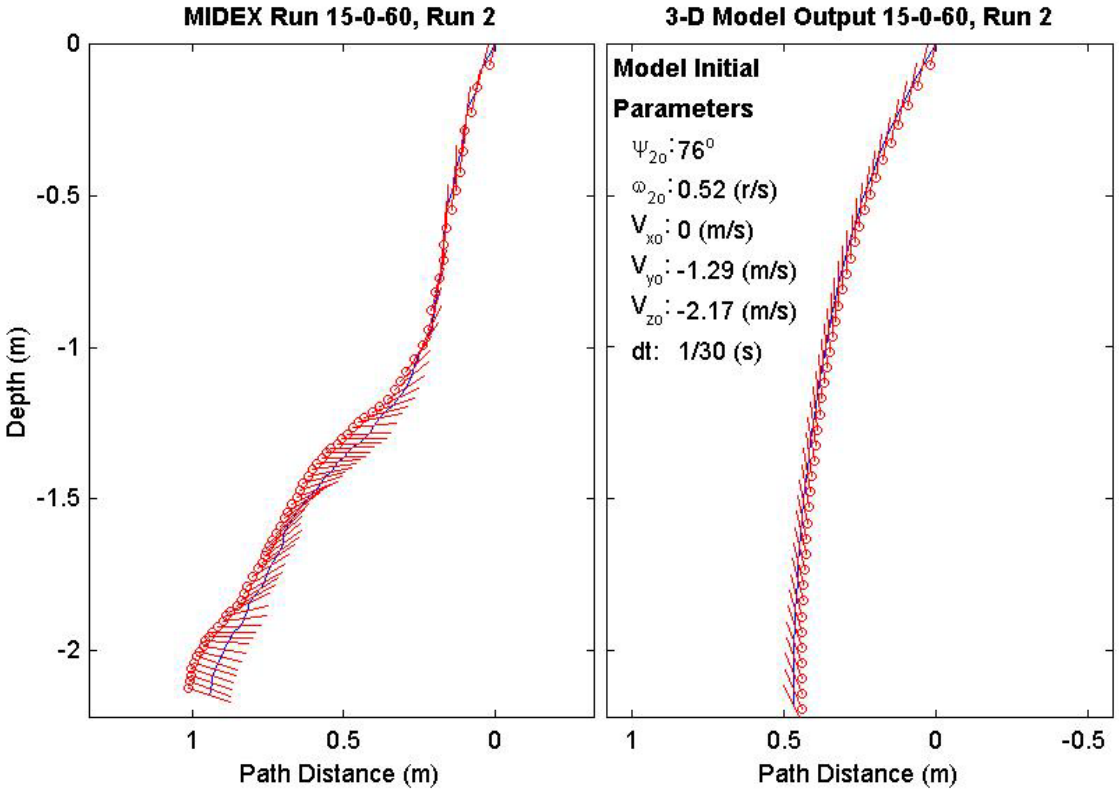

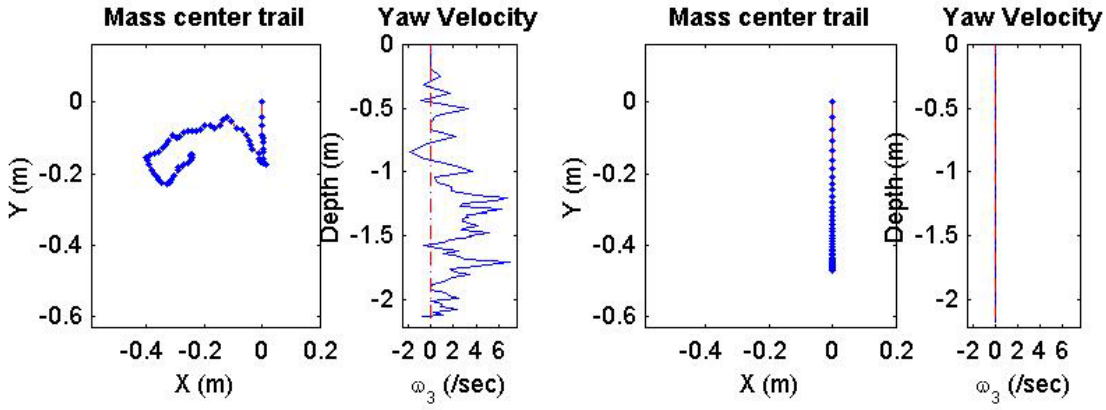

Final Drop Parameters (60/15-2634)

time: 1.77(s)
xy_{fe}: 0.281(m)
V_{xfe}: -0.534(m/s)
V_{yfe}: 0.108(m/s)
V_{zfe}: -0.642(m/s)
Ψ_{fe}: 41.5°
depth: 2.17(m)

Mine Shape Parameters (60/15-2634)

d: 0.04(m)
L: 0.152(m)
m: 0.323(m)
J_1: 3.3e-005(kg*m^2)
J_2: 0.000609(kg*m^2)
J_3: 0.000609(kg*m^2)
χ: 4.6e-005(m)

Final Model Parameters (60/15-2634)

time: 1.33(s)
xy_{fm}: 0.348(m)
V_{xfm}: 0.0747(m/s)
V_{yfm}: -0.0135(m/s)
V_{zfm}: -1.52(m/s)
Ψ_{fm}: 93.91°
depth: 2.18(m)

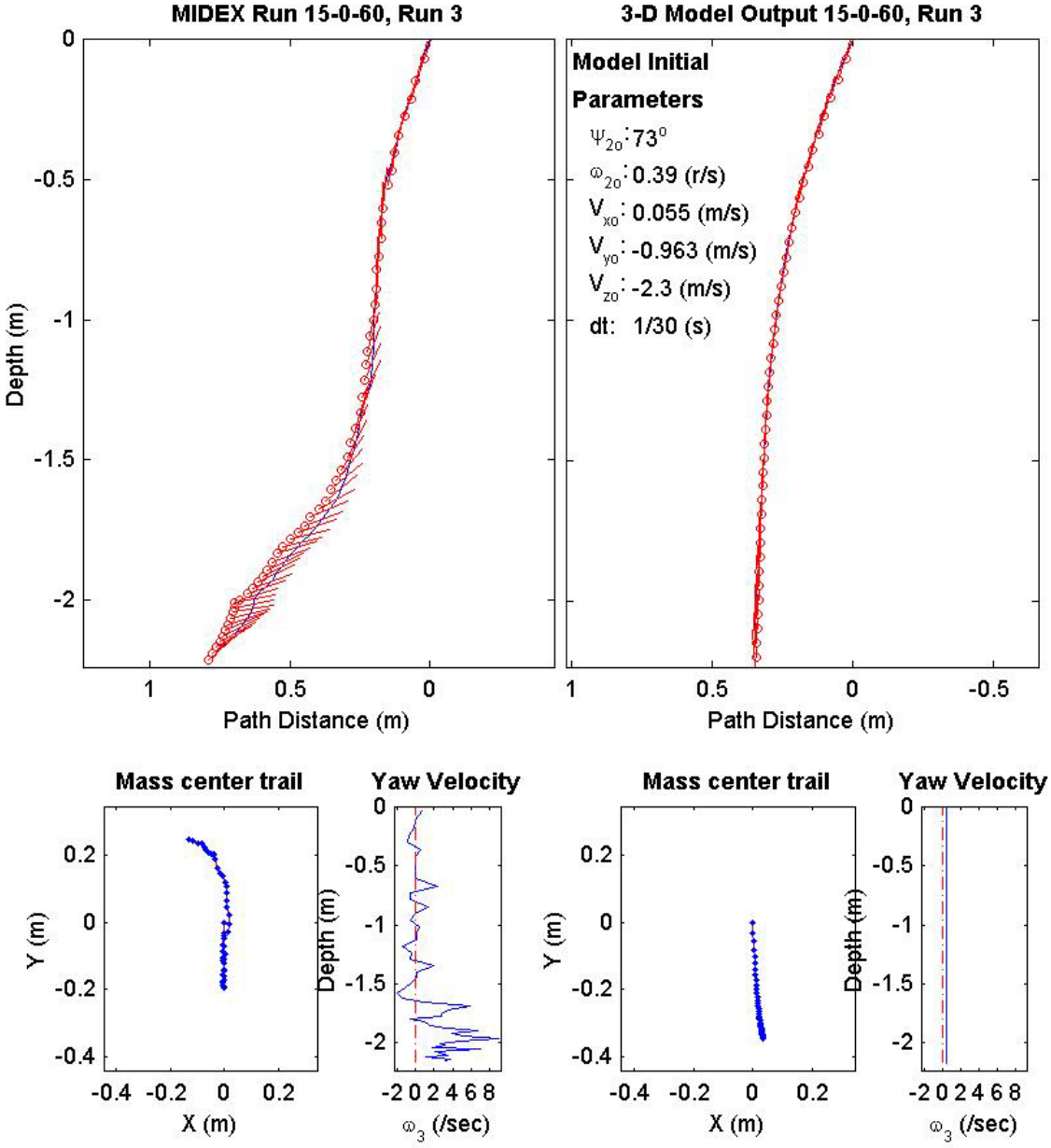

Final Drop

Parameters (60/15-2260)

time: 1.57(s)
xy_{fe}: 0.236(m)
V_{xfe}: -0.159(m/s)
V_{yfe}: 0.267(m/s)
V_{zfe}: -0.642(m/s)
Ψ_{fe}: -3.5°
depth: 2.23(m)

Mine Shape

Parameters (60/15-2260)

d: 0.04(m)
L: 0.152(m)
m: 0.323(m)
J_1: 3.3e-005(kg*m^2)
J_2: 0.000609(kg*m^2)
J_3: 0.000609(kg*m^2)
χ: 4.6e-005(m)

Final Model

Parameters (60/15-2260)

time: 1.63(s)
xy_{fm}: 0.512(m)
V_{xfm}: 0.162(m/s)
V_{yfm}: -0.03(m/s)
V_{zfm}: -0.841(m/s)
Ψ_{fm}: -21.9°
depth: 2.24(m)

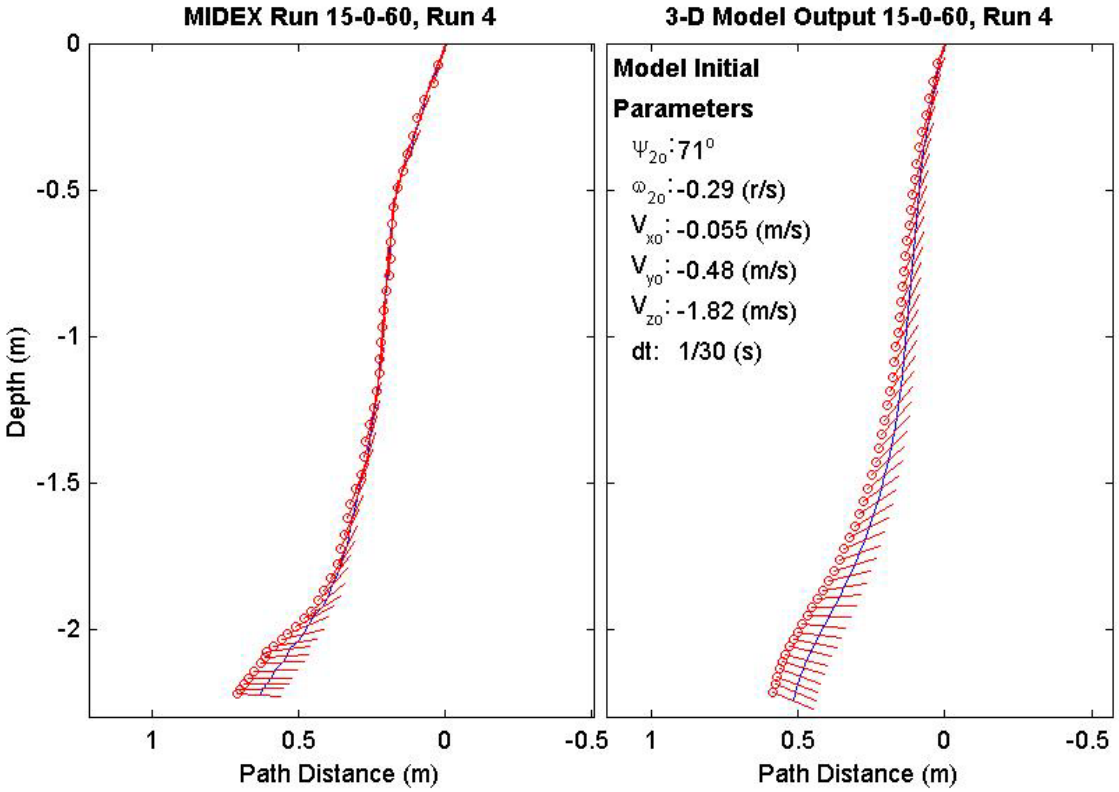

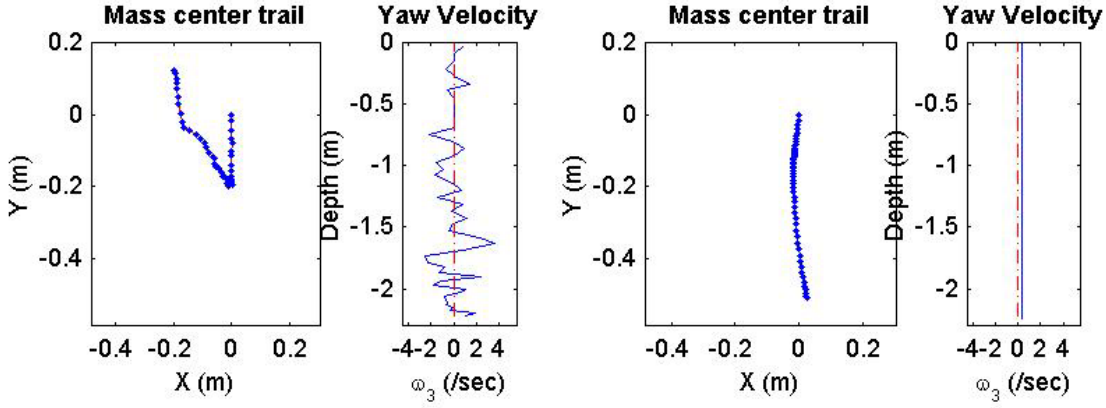

Final Drop Parameters (60/15-1422)

time: 2.57(s)
xy_{fe}: 0.377(m)
V_{xfe}: 0.159(m/s)
V_{yfe}: -0.321(m/s)
V_{zfe}: -0.535(m/s)
Ψ_{fe}: 0.7°
depth: 2.16(m)

Mine Shape Parameters (60/15-1422)

d: 0.04(m)
L: 0.152(m)
m: 0.323(m)
J_1: 3.3e-005(kg*m^2)
J_2: 0.000609(kg*m^2)
J_3: 0.000609(kg*m^2)
χ: 4.6e-005(m)

Final Model Parameters (60/15-1422)

time: 1.73(s)
xy_{fm}: 0.546(m)
V_{xfm}: -0.206(m/s)
V_{yfm}: 0.105(m/s)
V_{zfm}: -1.09(m/s)
Ψ_{fm}: -40.64°
depth: 2.16(m)

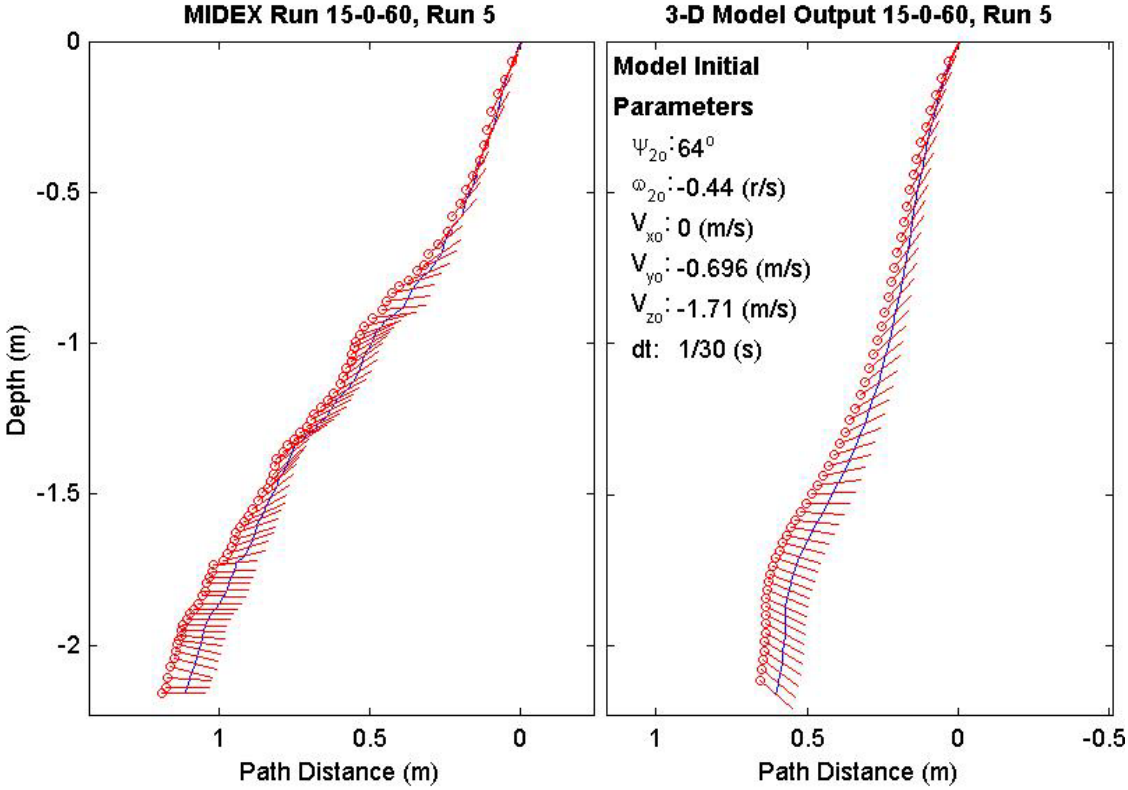

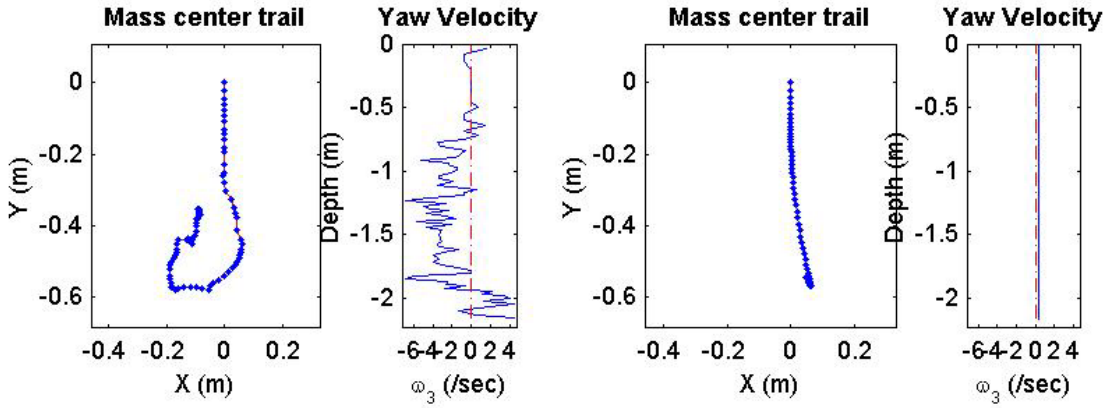

Final Drop Parameters (60/15-3362)

time: 2(s)
xy_{fe}: 0.166(m)
V_{xfe}: 0.055(m/s)
V_{yfe}: -0.483(m/s)
V_{zfe}: -0.509(m/s)
Ψ_{fe}: 14.4°
depth: 2.21(m)

Mine Shape Parameters (60/15-3362)

d: 0.04(m)
L: 0.152(m)
m: 0.323(m)
J_1: 3.3e-005(kg*m^2)
J_2: 0.000609(kg*m^2)
J_3: 0.000609(kg*m^2)
χ: 4.6e-005(m)

Final Model Parameters (60/15-3362)

time: 1.33(s)
xy_{fm}: 0.354(m)
V_{xfm}: 0.0695(m/s)
V_{yfm}: -0.00186(m/s)
V_{zfm}: -1.55(m/s)
Ψ_{fm}: 104.6°
depth: 2.22(m)

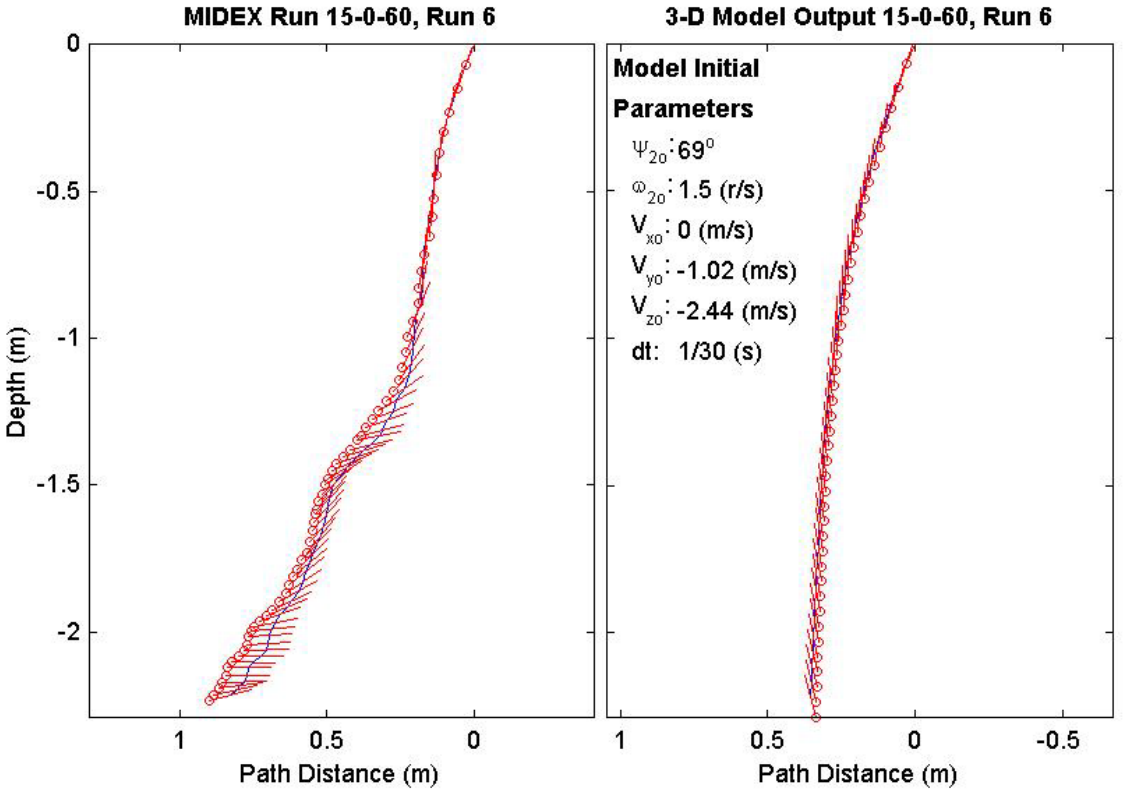

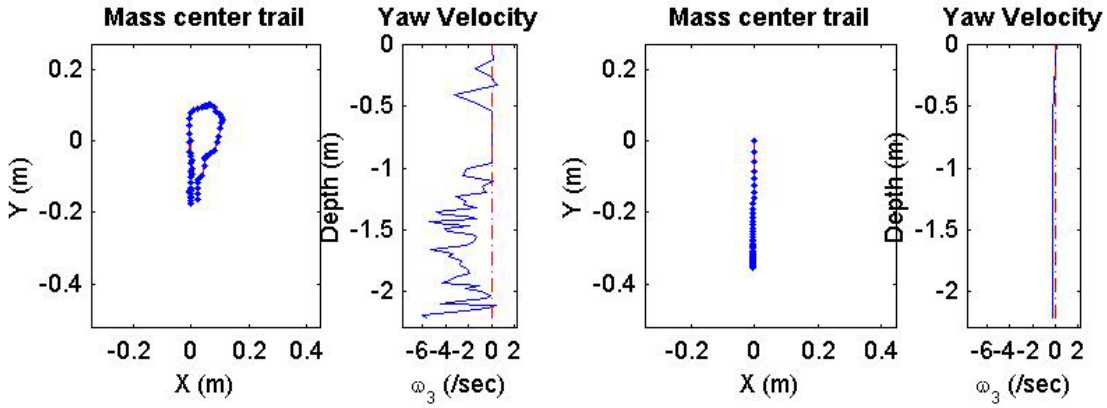

Final Drop Parameters (60/12-3464)

time: 2.37(s)
xy_{fe}: 0.139(m)
V_{xfe}: 0(m/s)
V_{yfe}: -0.267(m/s)
V_{zfe}: -0.75(m/s)
Ψ_{fe}: 49.2°
depth: 2.13(m)

Mine Shape Parameters (60/12-3464)

d: 0.04(m)
L: 0.121(m)
m: 0.254(m)
J_1: 2.71e-005(kg*m^2)
J_2: 0.000343(kg*m^2)
J_3: 0.000343(kg*m^2)
χ: 0.000644(m)

Final Model Parameters (60/12-3464)

time: 1.5(s)
xy_{fm}: 0.456(m)
V_{xfm}: 0.0938(m/s)
V_{yfm}: 0.00343(m/s)
V_{zfm}: -1.37(m/s)
Ψ_{fm}: 95.08°
depth: 2.18(m)

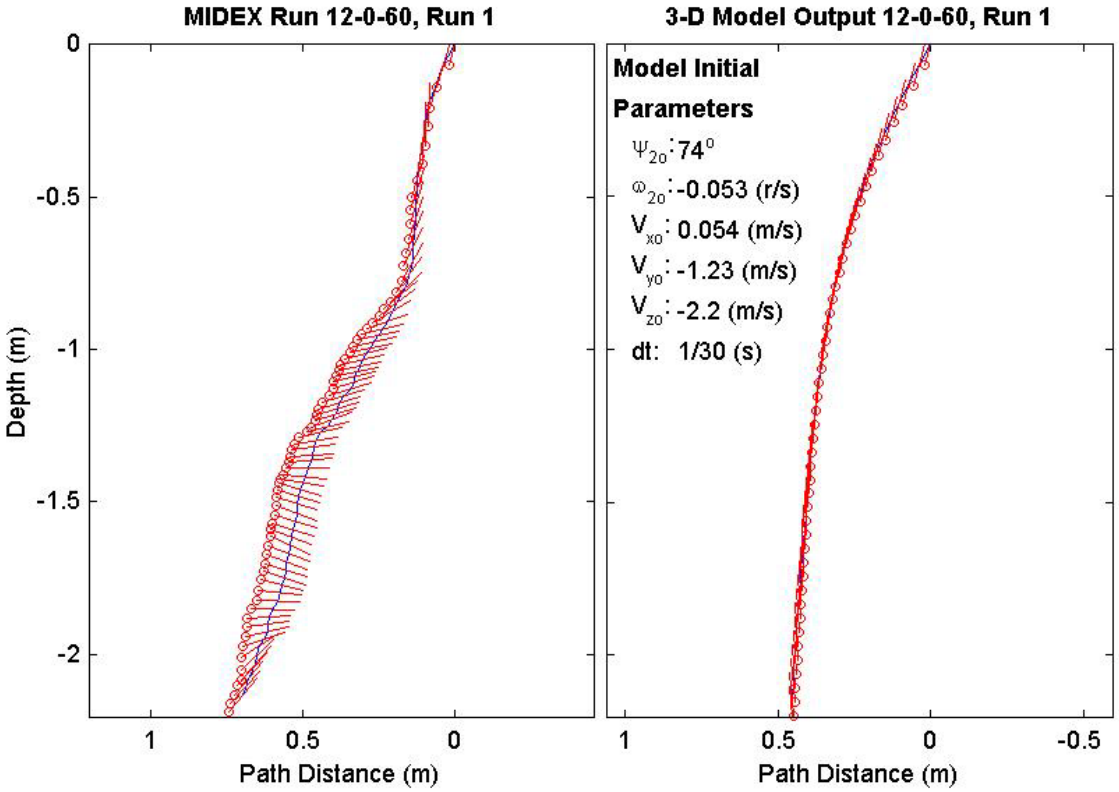

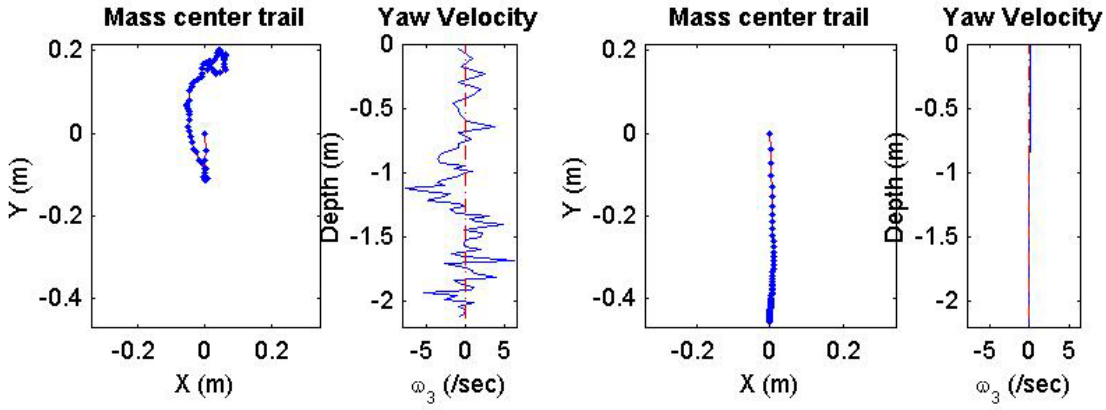

Final Drop

Parameters (60/12-3025)

time: 2.33(s)
xy_{fe}: 0.194(m)
V_{xfe}: -0.054(m/s)
V_{yfe}: -0.213(m/s)
V_{zfe}: -0.909(m/s)
Ψ_{fe}: -1°
depth: 2.22(m)

Mine Shape

Parameters (60/12-3025)

d: 0.04(m)
L: 0.121(m)
m: 0.254(m)
J_1: 2.71e-005($kg*m^2$)
J_2: 0.000343($kg*m^2$)
J_3: 0.000343($kg*m^2$)
χ: 0.000644(m)

Final Model

Parameters (60/12-3025)

time: 1.53(s)
xy_{fm}: 0.125(m)
V_{xfm}: -0.358(m/s)
V_{yfm}: 0.0878(m/s)
V_{zfm}: -1.2(m/s)
Ψ_{fm}: 155.4°
depth: 2.24(m)

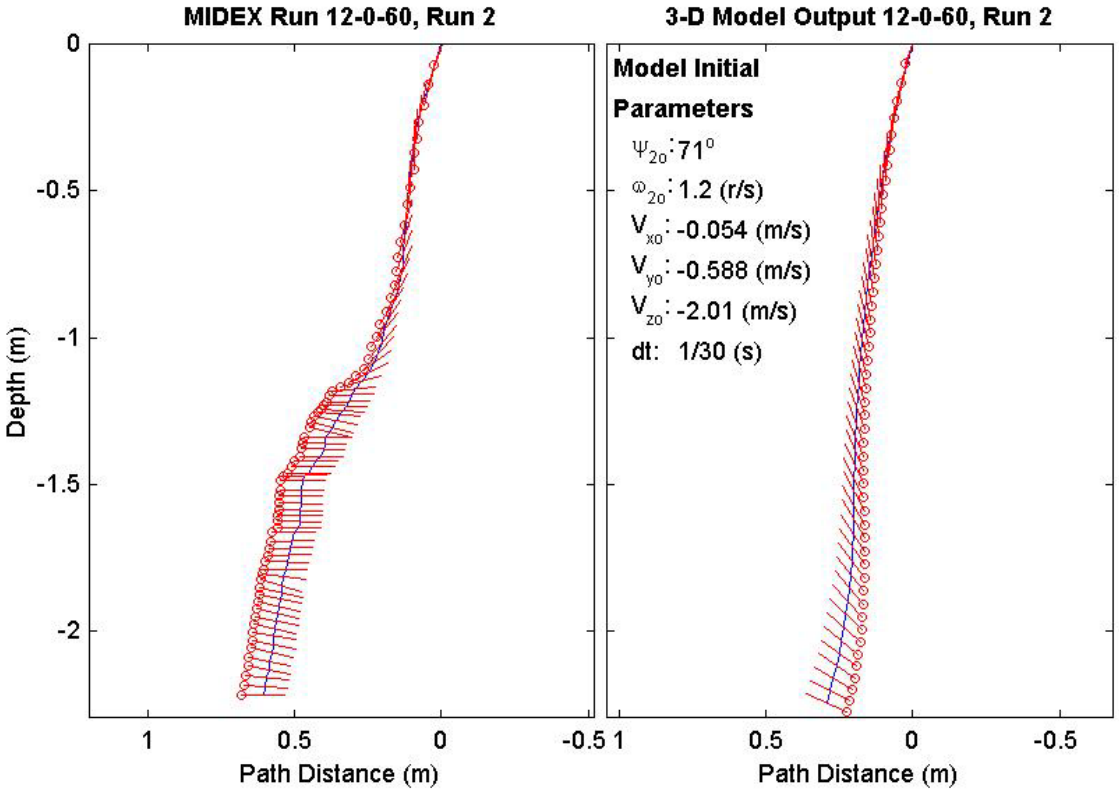

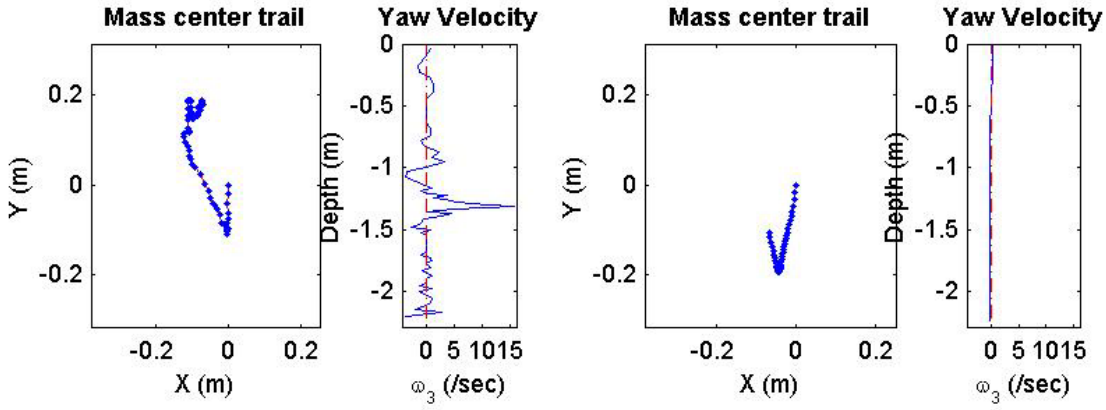

Final Drop

Parameters (60/12-2693)

time: 1.43(s)
xy_{fe}: 0.332(m)
V_{xfe}: -0.429(m/s)
V_{yfe}: -0.591(m/s)
V_{zfe}: -0.803(m/s)
Ψ_{fe}: 41.5°
depth: 2.17(m)

Mine Shape

Parameters (60/12-2693)

d: 0.04(m)
L: 0.121(m)
m: 0.254(m)
J_1: 2.71e-005(kg*m^2)
J_2: 0.000343(kg*m^2)
J_3: 0.000343(kg*m^2)
χ: 0.000644(m)

Final Model

Parameters (60/12-2693)

time: 1.5(s)
xy_{fm}: 0.224(m)
V_{xfm}: -0.206(m/s)
V_{yfm}: 1.37e-017(m/s)
V_{zfm}: -1.35(m/s)
Ψ_{fm}: 136.8°
depth: 2.2(m)

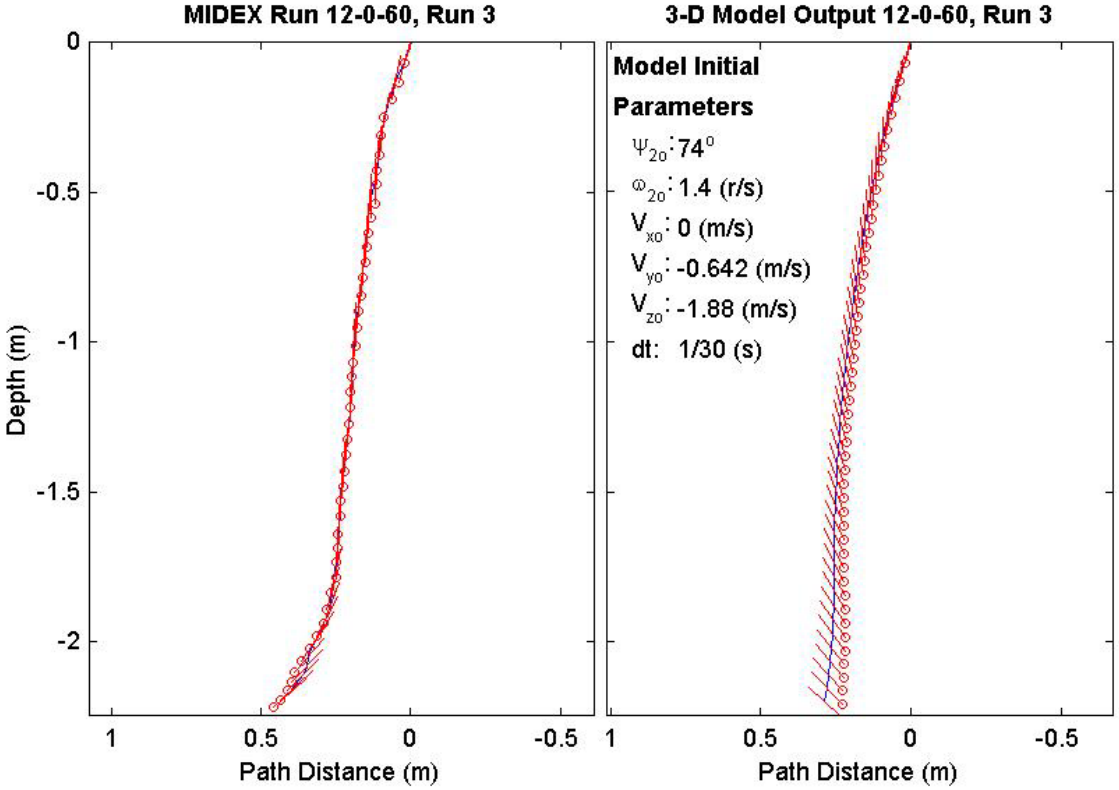

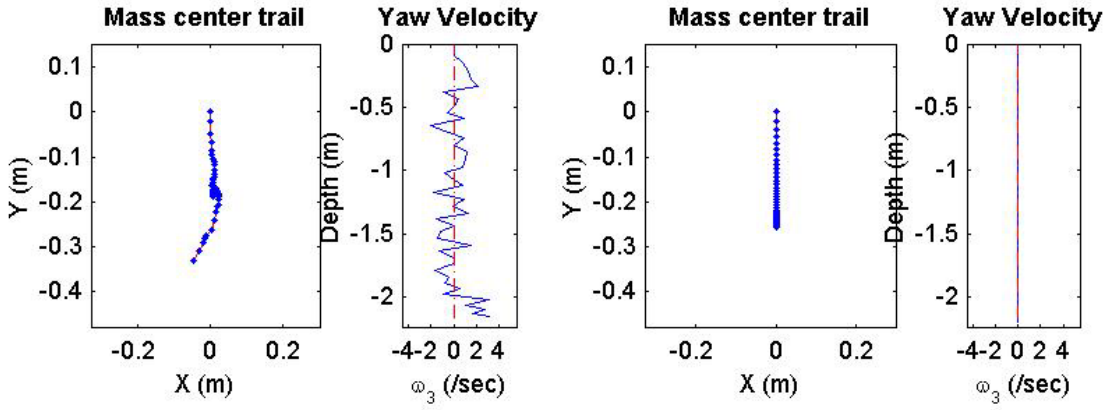

Final Drop

Parameters (60/12-2189)

time: 2.17(s)
xy_{fe}: 0.509(m)
V_{xfe}: 0(m/s)
V_{yfe}: 0.051(m/s)
V_{zfe}: -0.777(m/s)
Ψ_{fe}: -17.3°
depth: 2.2(m)

Mine Shape

Parameters (60/12-2189)

d: 0.04(m)
L: 0.121(m)
m: 0.254(m)
J_1: 2.71e-005(kg*m^2)
J_2: 0.000343(kg*m^2)
J_3: 0.000343(kg*m^2)
χ: 0.000644(m)

Final Model

Parameters (60/12-2189)

time: 1.53(s)
xy_{fm}: 0.153(m)
V_{xfm}: -0.0682(m/s)
V_{yfm}: -0.0135(m/s)
V_{zfm}: -1.41(m/s)
Ψ_{fm}: 74.17°
depth: 2.23(m)

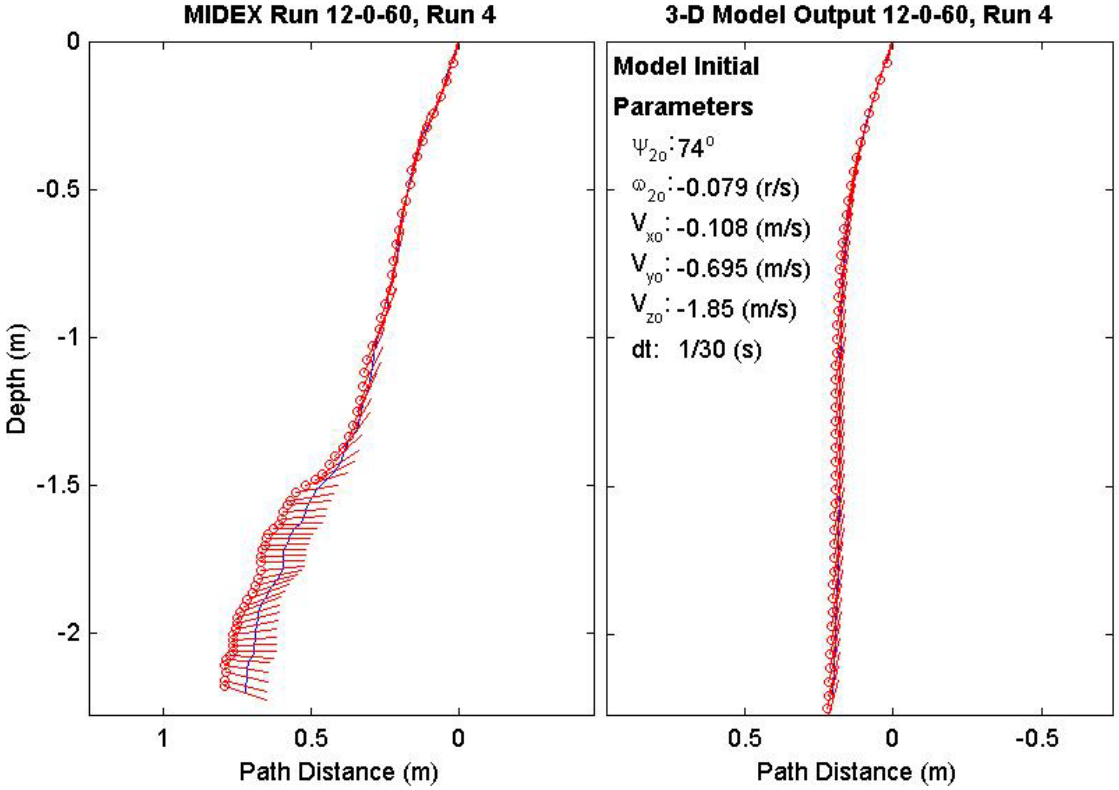

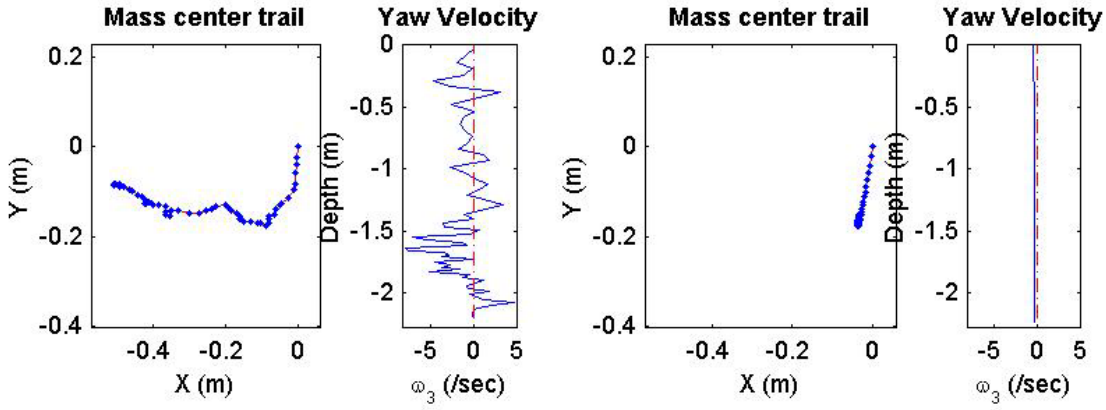

Final Drop

Parameters (60/12-1588)

time: 2.5(s)
xy_{fe}: 0.334(m)
V_{xfe}: -0.267(m/s)
V_{yfe}: 0.054(m/s)
V_{zfe}: -0.858(m/s)
Ψ_{fe}: 34.8°
depth: 2.2(m)

Mine Shape

Parameters (60/12-1588)

d: 0.04(m)
L: 0.121(m)
m: 0.254(m)
J_1: 2.71e-005(kg*m^2)
J_2: 0.000343(kg*m^2)
J_3: 0.000343(kg*m^2)
χ: 0.000644(m)

Final Model

Parameters (60/12-1588)

time: 1.8(s)
xy_{fm}: 0.368(m)
V_{xfm}: -0.132(m/s)
V_{yfm}: -0.138(m/s)
V_{zfm}: -0.839(m/s)
Ψ_{fm}: -6.16°
depth: 2.21(m)

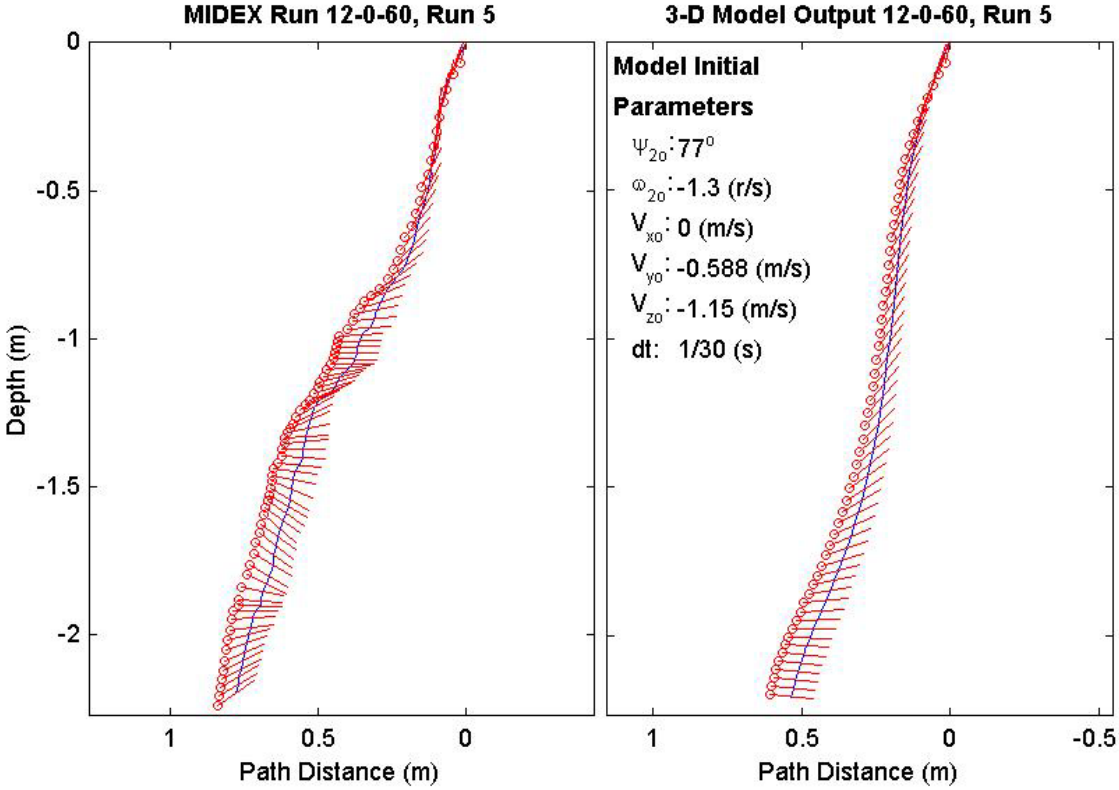

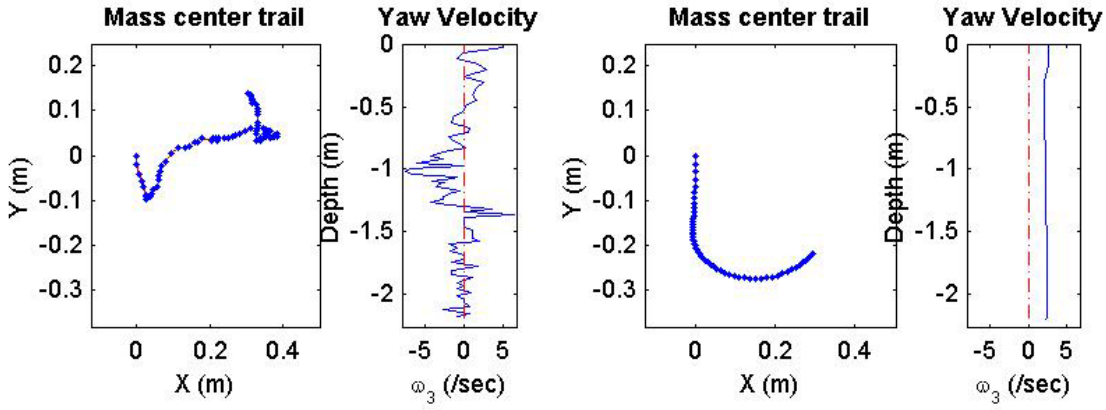

Final Drop Parameters (60/12-3347)

time: 2.3(s)
xy_{fe}: 0.331(m)
V_{xfe}: -0.216(m/s)
V_{yfe}: -0.054(m/s)
V_{zfe}: -0.536(m/s)
Ψ_{fe}: 38.1^{o}
depth: 2.12(m)

Mine Shape Parameters (60/12-3347)

d: 0.04(m)
L: 0.121(m)
m: 0.254(m)
J_1: 2.71e-005($kg*m^2$)
J_2: 0.000343($kg*m^2$)
J_3: 0.000343($kg*m^2$)
χ: 0.000644(m)

Final Model Parameters (60/12-3347)

time: 1.47(s)
xy_{fm}: 0.26(m)
V_{xfm}: -0.386(m/s)
V_{yfm}: 2.45e-017(m/s)
V_{zfm}: -1.17(m/s)
Ψ_{fm}: 158.6^{o}
depth: 2.15(m)

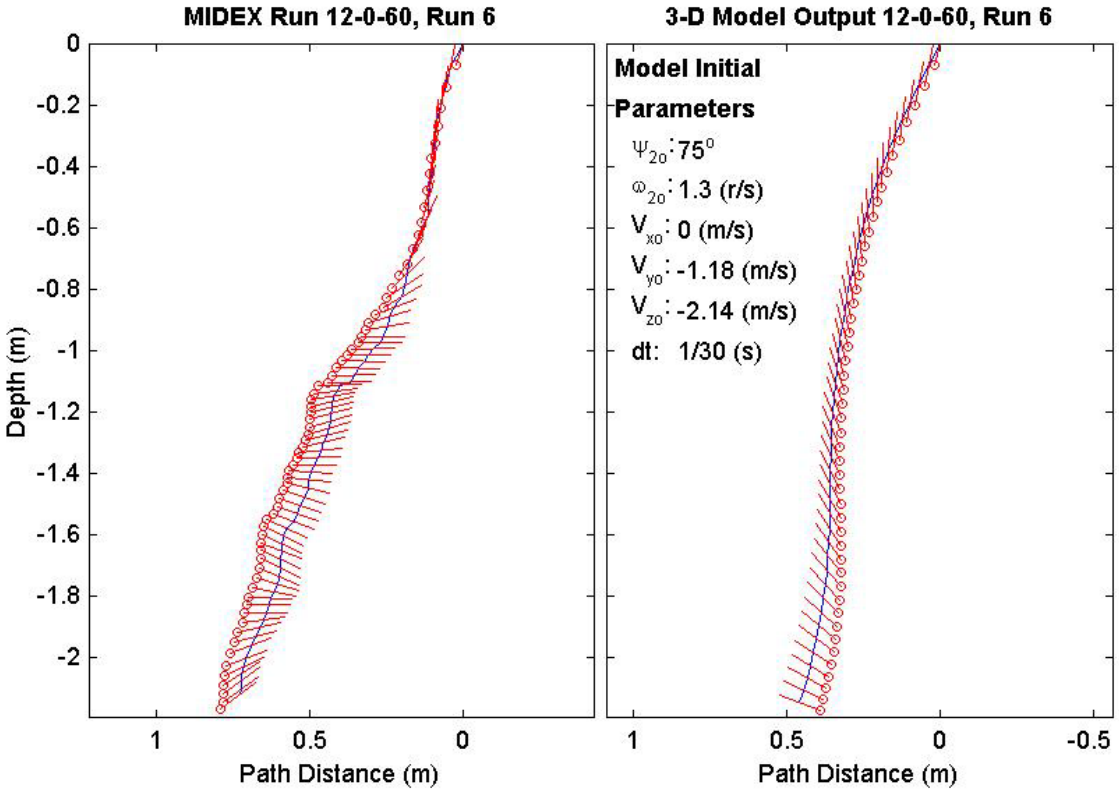

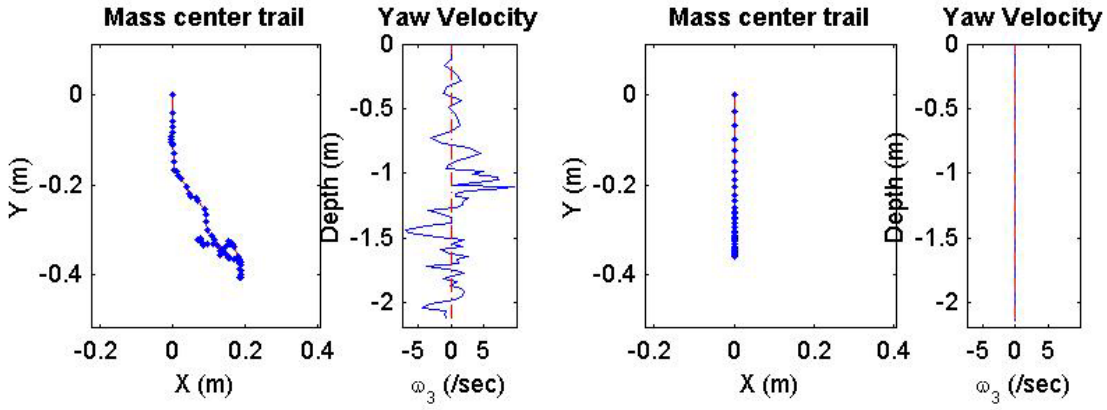

Final Drop
Parameters (60/9-3654)

time: 2.13(s)
xy_{fe}: 0.235(m)
V_{xfe}: 0.108(m/s)
V_{yfe}: 0.108(m/s)
V_{zfe}: -1.1(m/s)
Ψ_{fe}: 12.5°
depth: 2.16(m)

Mine Shape
Parameters (60/9-3654)

d: 0.04(m)
L: 0.0912(m)
m: 0.215(m)
J_1: 2.35e-005(kg*m^2)
J_2: 0.00017(kg*m^2)
J_3: 0.00017(kg*m^2)
χ: 2.9e-005(m)

Final Model
Parameters (60/9-3654)

time: 1.6(s)
xy_{fm}: 0.232(m)
V_{xfm}: 0.109(m/s)
V_{yfm}: -0.047(m/s)
V_{zfm}: -1.36(m/s)
Ψ_{fm}: -113.6°
depth: 2.16(m)

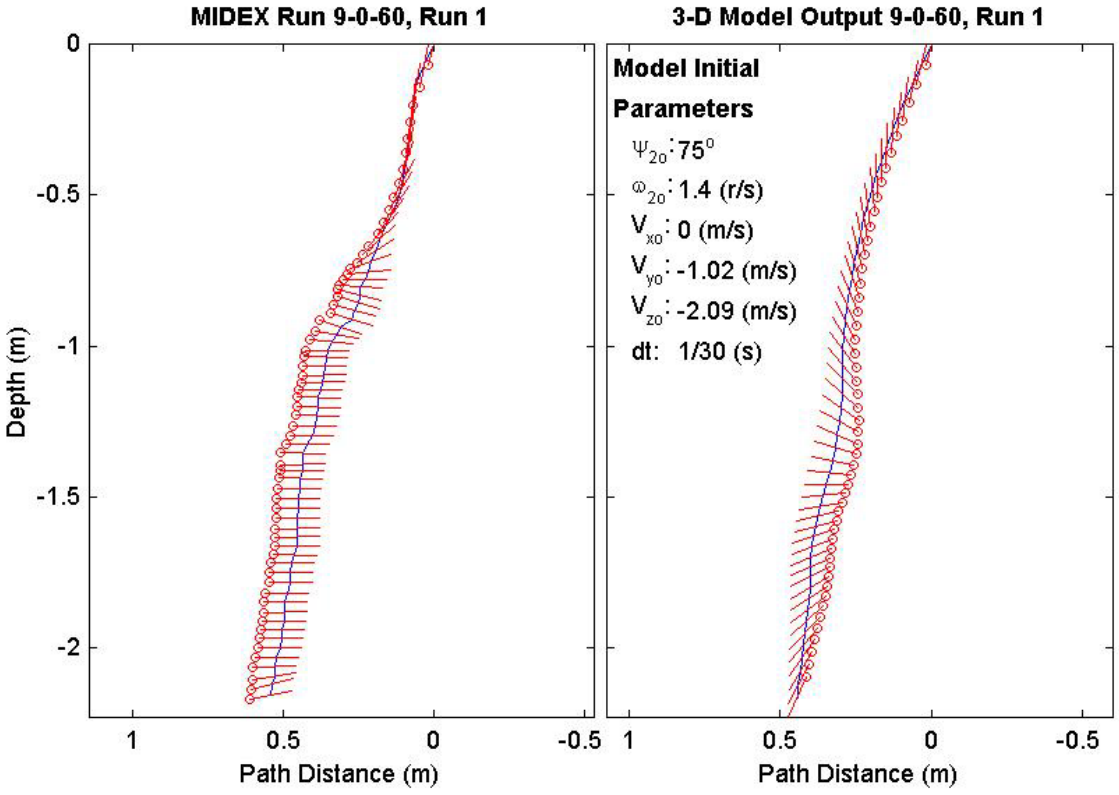

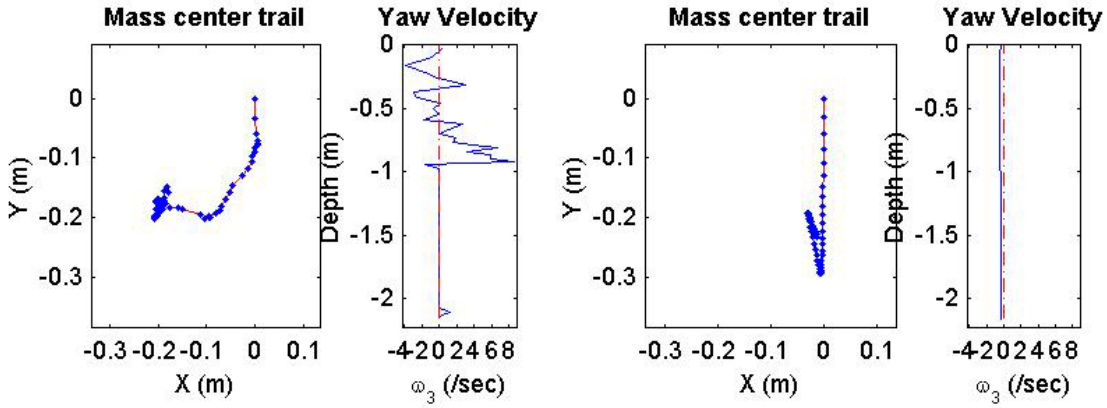

Final Drop

Parameters (60/9-3128)

time: 2.17(s)
xy_{fe}: 0.263(m)
V_{xfe}: 0.054(m/s)
V_{yfe}: 0(m/s)
V_{zfe}: -0.91(m/s)
Ψ_{fe}: -17.4°
depth: 2.24(m)

Mine Shape

Parameters (60/9-3128)

d: 0.04(m)
L: 0.0912(m)
m: 0.215(m)
J_1: 2.35e-005(kg*m^2)
J_2: 0.00017(kg*m^2)
J_3: 0.00017(kg*m^2)
χ: 2.9e-005(m)

Final Model

Parameters (60/9-3128)

time: 1.67(s)
xy_{fm}: 0.104(m)
V_{xfm}: 0.024(m/s)
V_{yfm}: -0.00127(m/s)
V_{zfm}: -1.4(m/s)
Ψ_{fm}: -99.32°
depth: 2.26(m)

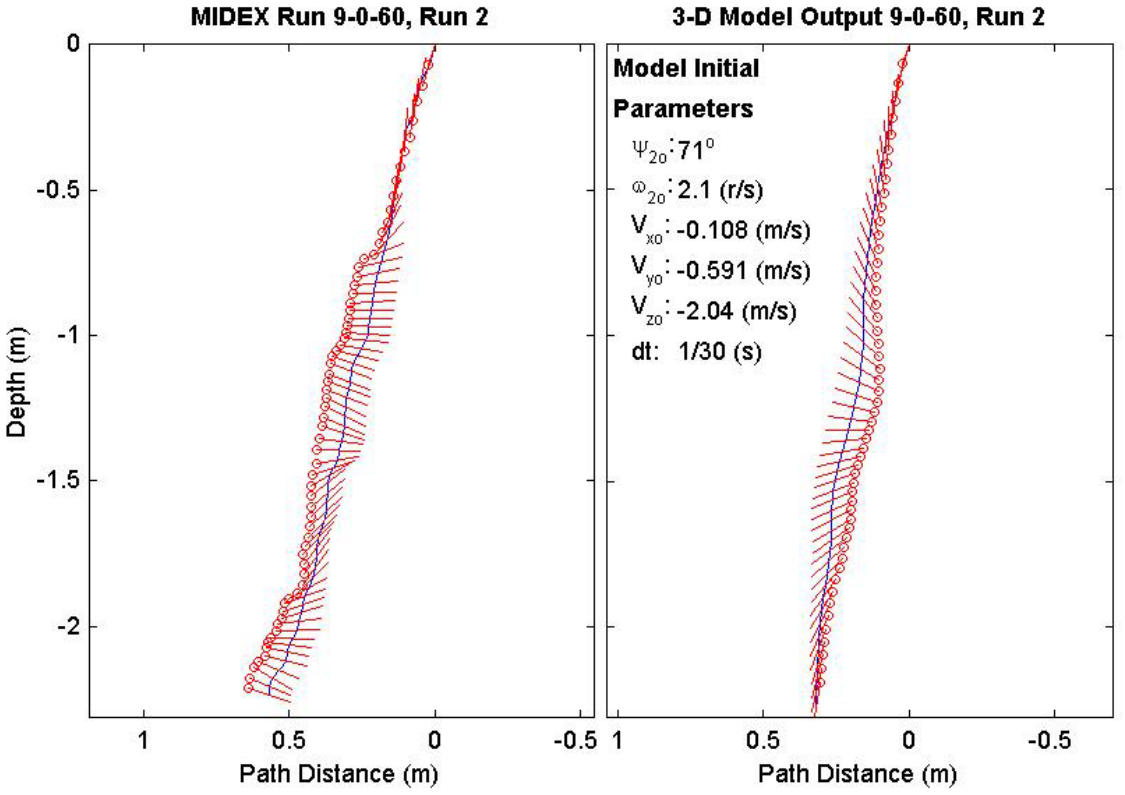

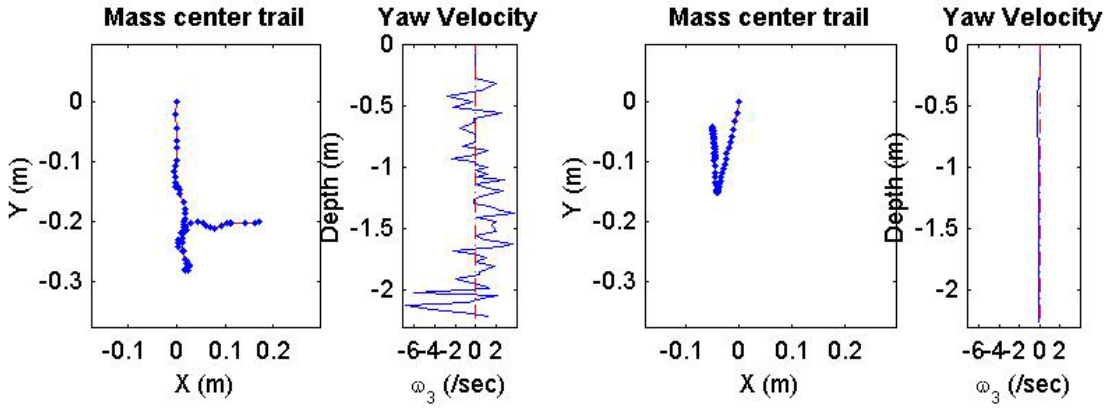

Final Drop

Parameters (60/9-2714)

time: 2.1(s)
xy_{fe}: 0.164(m)
V_{xfe}: 0.054(m/s)
V_{yfe}: 0.216(m/s)
V_{zfe}: -0.991(m/s)
Ψ_{fe}: -53.4°
depth: 2.21(m)

Mine Shape

Parameters (60/9-2714)

d: 0.04(m)
L: 0.0912(m)
m: 0.215(m)
J_1: 2.35e-005(kg*m^2)
J_2: 0.00017(kg*m^2)
J_3: 0.00017(kg*m^2)
χ: 2.9e-005(m)

Final Model

Parameters (60/9-2714)

time: 1.7(s)
xy_{fm}: 0.0773(m)
V_{xfm}: -0.00752(m/s)
V_{yfm}: -0.00407(m/s)
V_{zfm}: -1.4(m/s)
Ψ_{fm}: -85.02°
depth: 2.25(m)

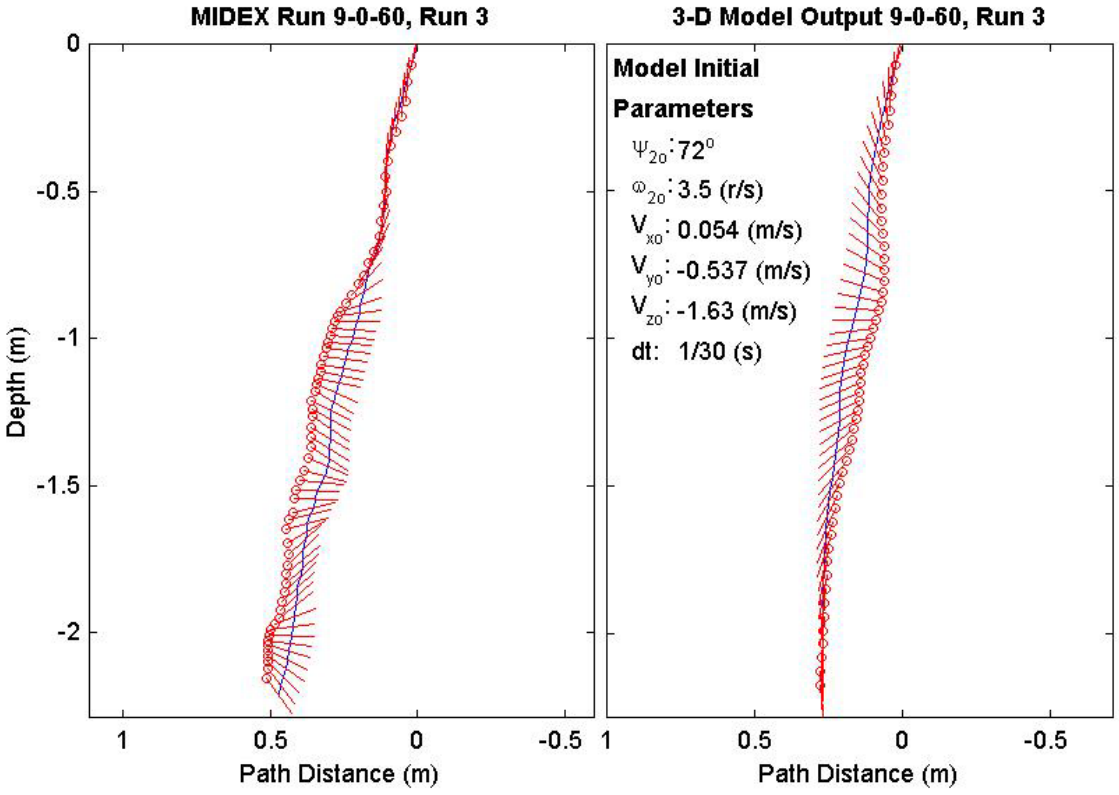

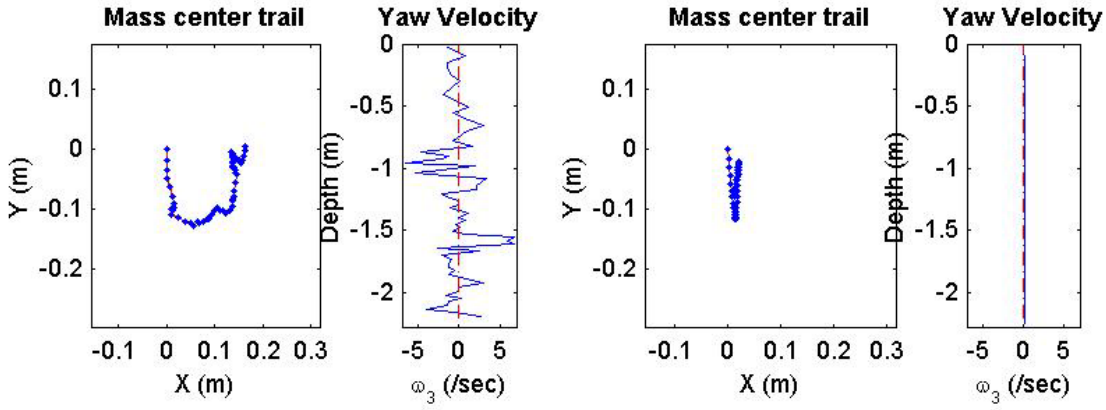

Final Drop

Parameters (60/9-2350)

time: 2.13(s)
xy_{fe}: 0.388(m)
V_{xfe}: 0(m/s)
V_{yfe}: 0.054(m/s)
V_{zfe}: -0.883(m/s)
Ψ_{fe}: -28.3°
depth: 2.21(m)

Mine Shape

Parameters (60/9-2350)

d: 0.04(m)
L: 0.0912(m)
m: 0.215(m)
J_1: 2.35e-005(kg*m^2)
J_2: 0.00017(kg*m^2)
J_3: 0.00017(kg*m^2)
χ: 2.9e-005(m)

Final Model

Parameters (60/9-2350)

time: 1.7(s)
xy_{fm}: 0.046(m)
V_{xfm}: 0.0191(m/s)
V_{yfm}: 0.00436(m/s)
V_{zfm}: -1.4(m/s)
Ψ_{fm}: -98.88°
depth: 2.25(m)

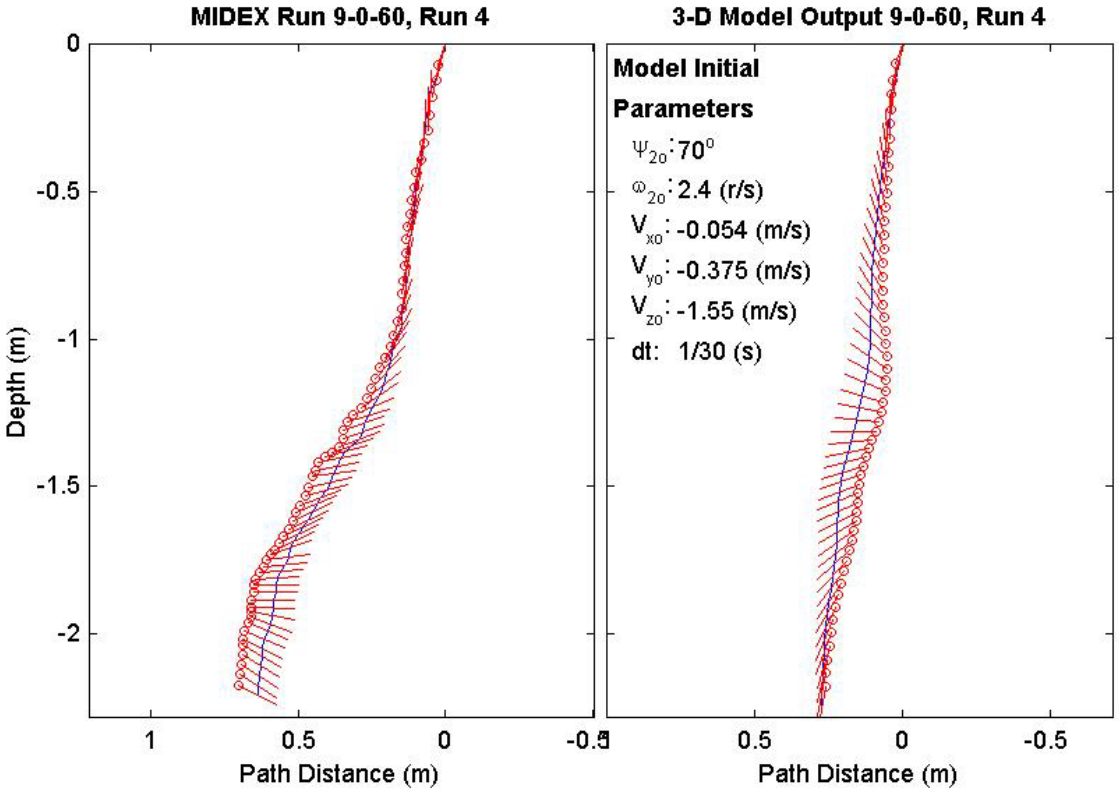

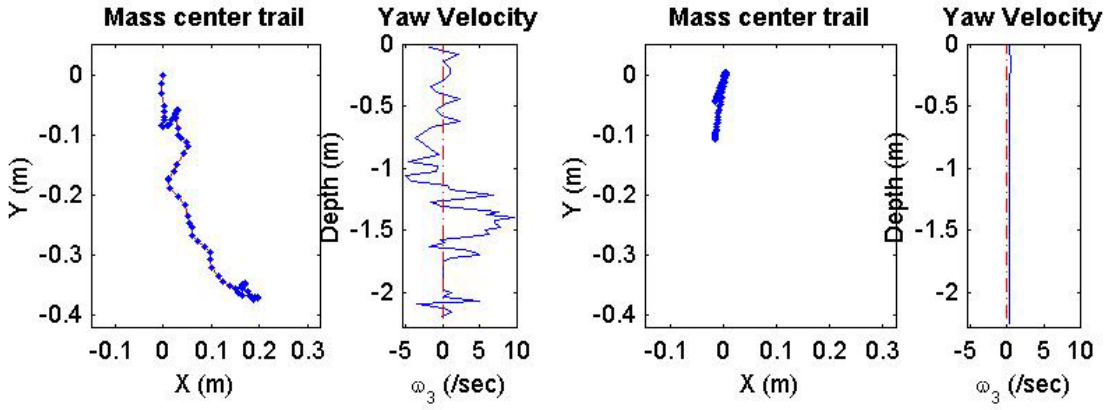

Final Drop
Parameters (60/9-1790)

time: 2.1(s)
xy_{fe}: 0.308(m)
V_{xfe}: -0.216(m/s)
V_{yfe}: -0.108(m/s)
V_{zfe}: -0.91(m/s)
Ψ_{fe}: -12.8°
depth: 2.19(m)

Mine Shape
Parameters (60/9-1790)

d: 0.04(m)
L: 0.0912(m)
m: 0.215(m)
J_1: 2.35e-005(kg*m^2)
J_2: 0.00017(kg*m^2)
J_3: 0.00017(kg*m^2)
χ: 2.9e-005(m)

Final Model
Parameters (60/9-1790)

time: 1.7(s)
xy_{fm}: 0.0468(m)
V_{xfm}: 0.06(m/s)
V_{yfm}: -0.0286(m/s)
V_{zfm}: -1.39(m/s)
Ψ_{fm}: -106.7°
depth: 2.23(m)

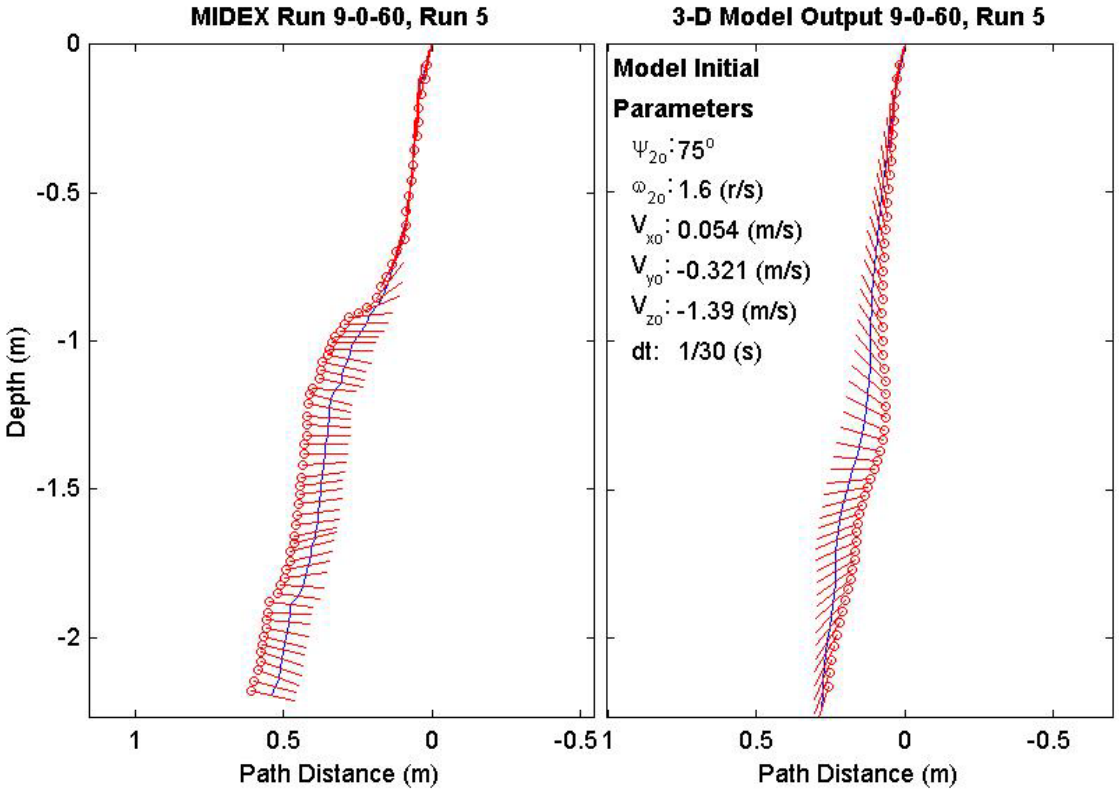

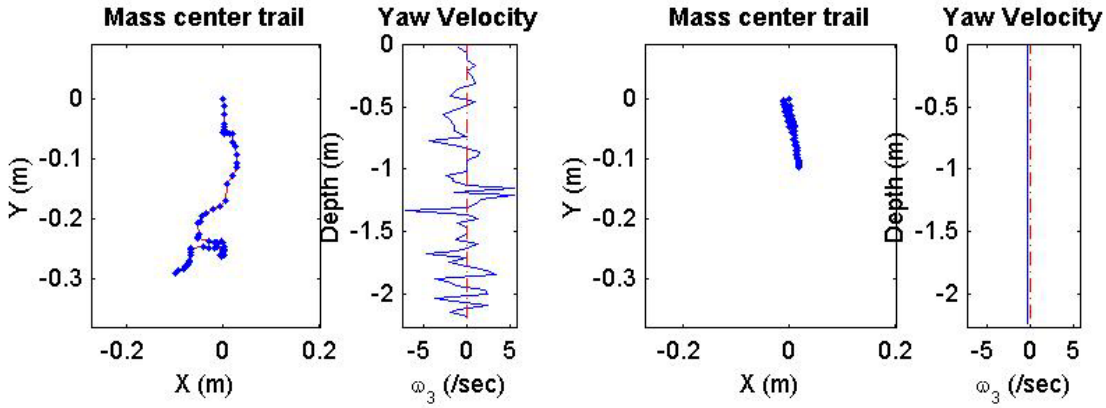

Final Drop

Parameters (60/9-3698)

time: 2.07(s)
xy_{fe}: 0.208(m)
V_{xfe}: -0.054(m/s)
V_{yfe}: 0(m/s)
V_{zfe}: -0.964(m/s)
Ψ_{fe}: 55.7°
depth: 2.15(m)

Mine Shape

Parameters (60/9-3698)

d: 0.04(m)
L: 0.0912(m)
m: 0.215(m)
J_1: 2.35e-005(kg*m^2)
J_2: 0.00017(kg*m^2)
J_3: 0.00017(kg*m^2)
χ: 2.9e-005(m)

Final Model

Parameters (60/9-3698)

time: 1.63(s)
xy_{fm}: 0.118(m)
V_{xfm}: 0.00146(m/s)
V_{yfm}: 0.0213(m/s)
V_{zfm}: -1.4(m/s)
Ψ_{fm}: -91.58°
depth: 2.19(m)

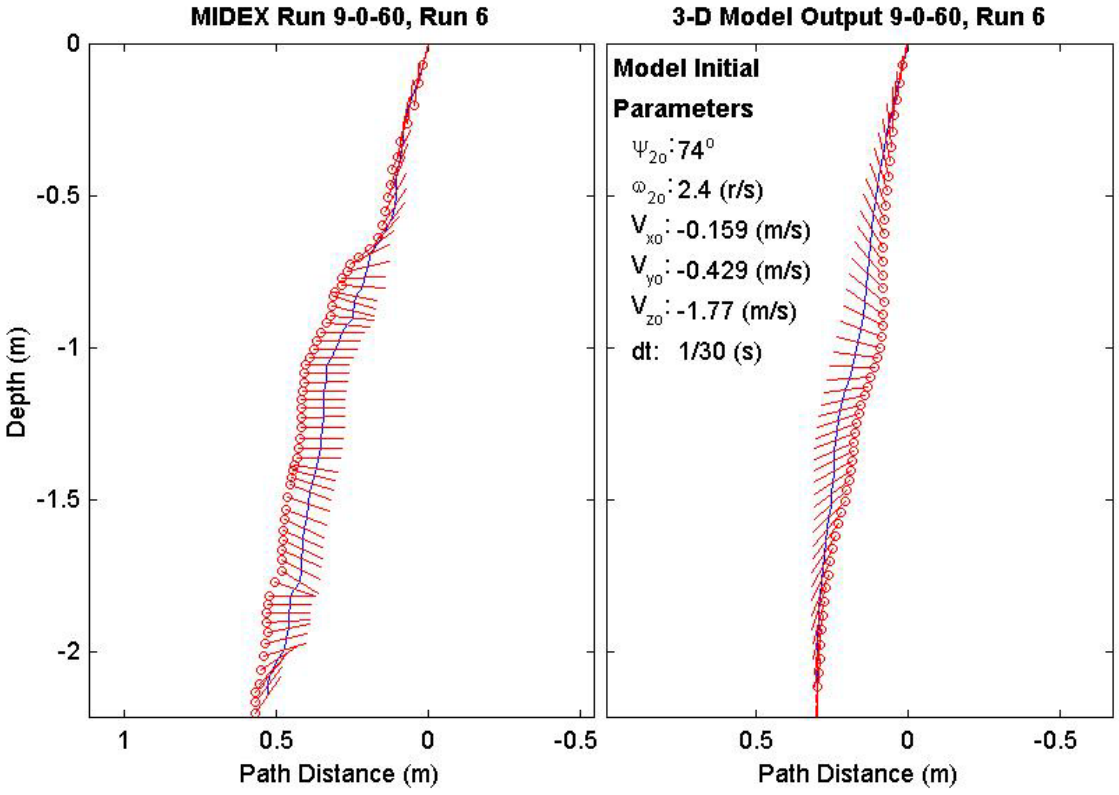

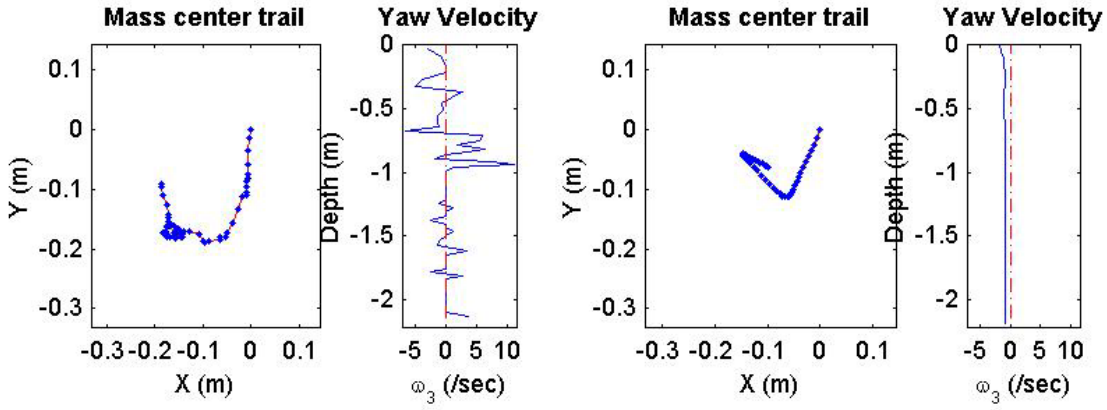

Final Drop

Parameters (75/15-1403)

time: 1.8(s)
xy_{fe}: 0.166(m)
V_{xfe}: 0.106(m/s)
V_{yfe}: -0.588(m/s)
V_{zfe}: -0.778(m/s)
Ψ_{fe}: 10.2^{o}
depth: 2.15(m)

Mine Shape

Parameters (75/15-1403)

d: 0.04(m)
L: 0.152(m)
m: 0.323(m)
J_1: 3.3e-005($kg*m^2$)
J_2: 0.000609($kg*m^2$)
J_3: 0.000609($kg*m^2$)
χ: 4.6e-005(m)

Final Model

Parameters (75/15-1403)

time: 1.33(s)
xy_{fm}: 0.0926(m)
V_{xfm}: -0.468(m/s)
V_{yfm}: -0.234(m/s)
V_{zfm}: -1.02(m/s)
Ψ_{fm}: 176.3^{o}
depth: 2.15(m)

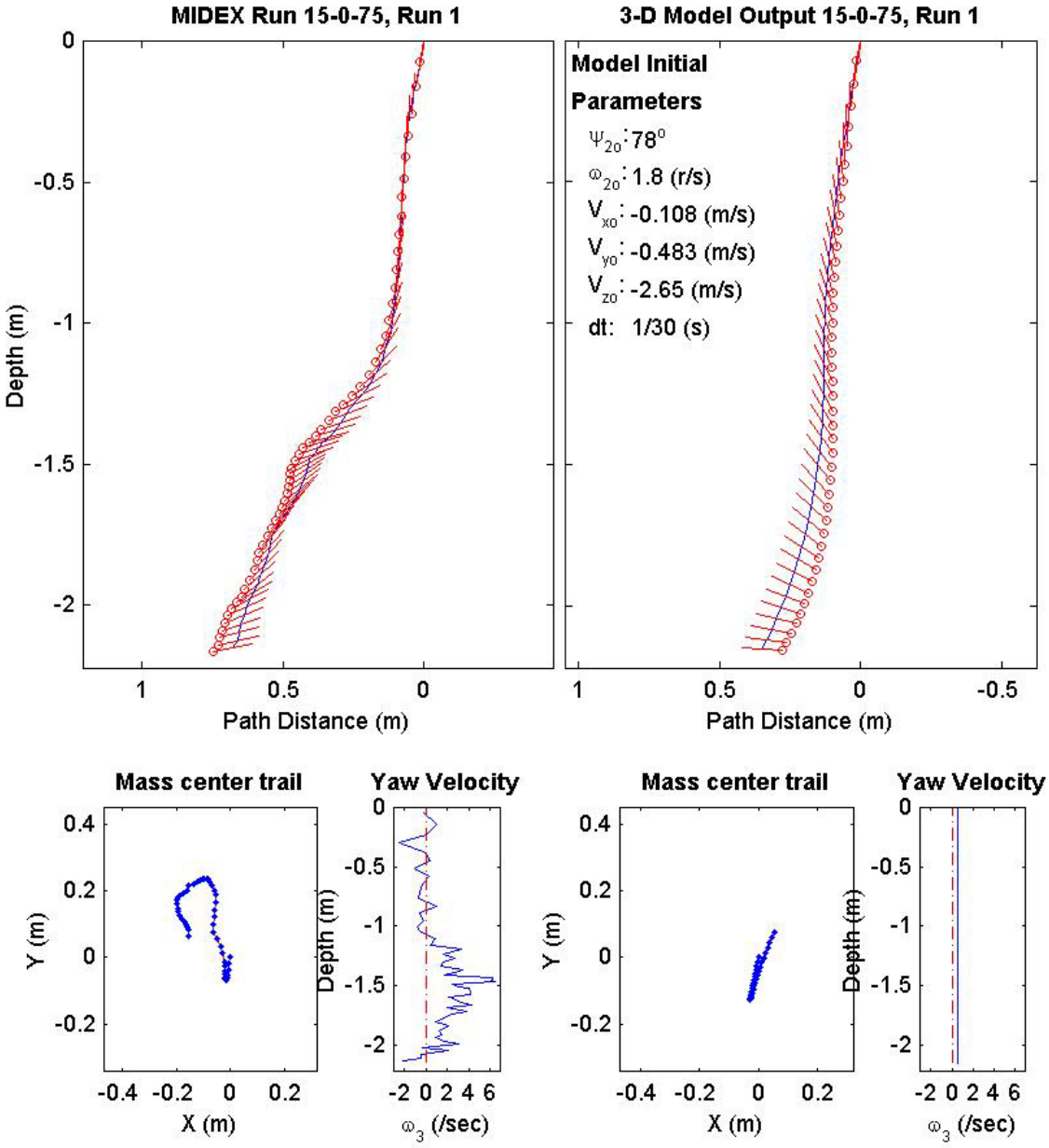

Final Drop
Parameters (75/15-1500)

time: 2.1(s)
xy_{fe}: 0.252(m)
V_{xfe}: 0.429(m/s)
V_{yfe}: 0.483(m/s)
V_{zfe}: -0.966(m/s)
Ψ_{fe}: 38.3°
depth: 2.14(m)

Mine Shape
Parameters (75/15-1500)

d: 0.04(m)
L: 0.152(m)
m: 0.323(m)
J_1: 3.3e-005(kg*m^2)
J_2: 0.000609(kg*m^2)
J_3: 0.000609(kg*m^2)
χ: 4.6e-005(m)

Final Model
Parameters (75/15-1500)

time: 1.4(s)
xy_{fm}: 0.146(m)
V_{xfm}: -0.357(m/s)
V_{yfm}: 0.337(m/s)
V_{zfm}: -0.948(m/s)
Ψ_{fm}: -178.4°
depth: 2.17(m)

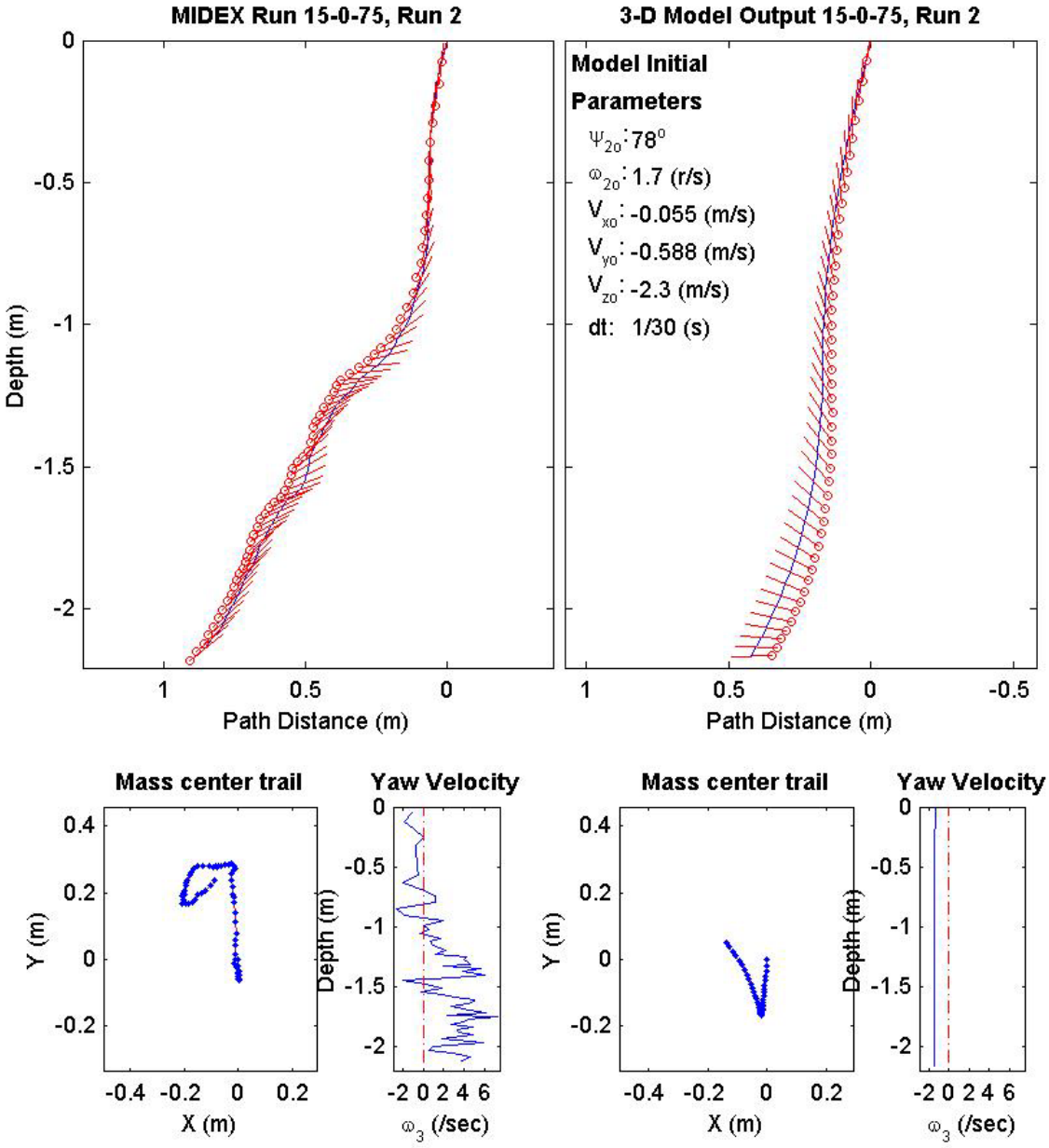

Final Drop Parameters (75/12-3934)

time: 1.27(s)
xy_{fe}: 0.133(m)
V_{xfe}: -0.051(m/s)
V_{yfe}: -0.162(m/s)
V_{zfe}: -1.18(m/s)
Ψ_{fe}: 57.3°
depth: 2.15(m)

Mine Shape Parameters (75/12-3934)

d: 0.04(m)
L: 0.121(m)
m: 0.254(m)
J_1: 2.71e-005(kg*m^2)
J_2: 0.000343(kg*m^2)
J_3: 0.000343(kg*m^2)
χ: 0.000644(m)

Final Model Parameters (75/12-3934)

time: 1.63(s)
xy_{fm}: 0.213(m)
V_{xfm}: -0.0473(m/s)
V_{yfm}: 0.106(m/s)
V_{zfm}: -0.843(m/s)
Ψ_{fm}: -171.3°
depth: 2.16(m)

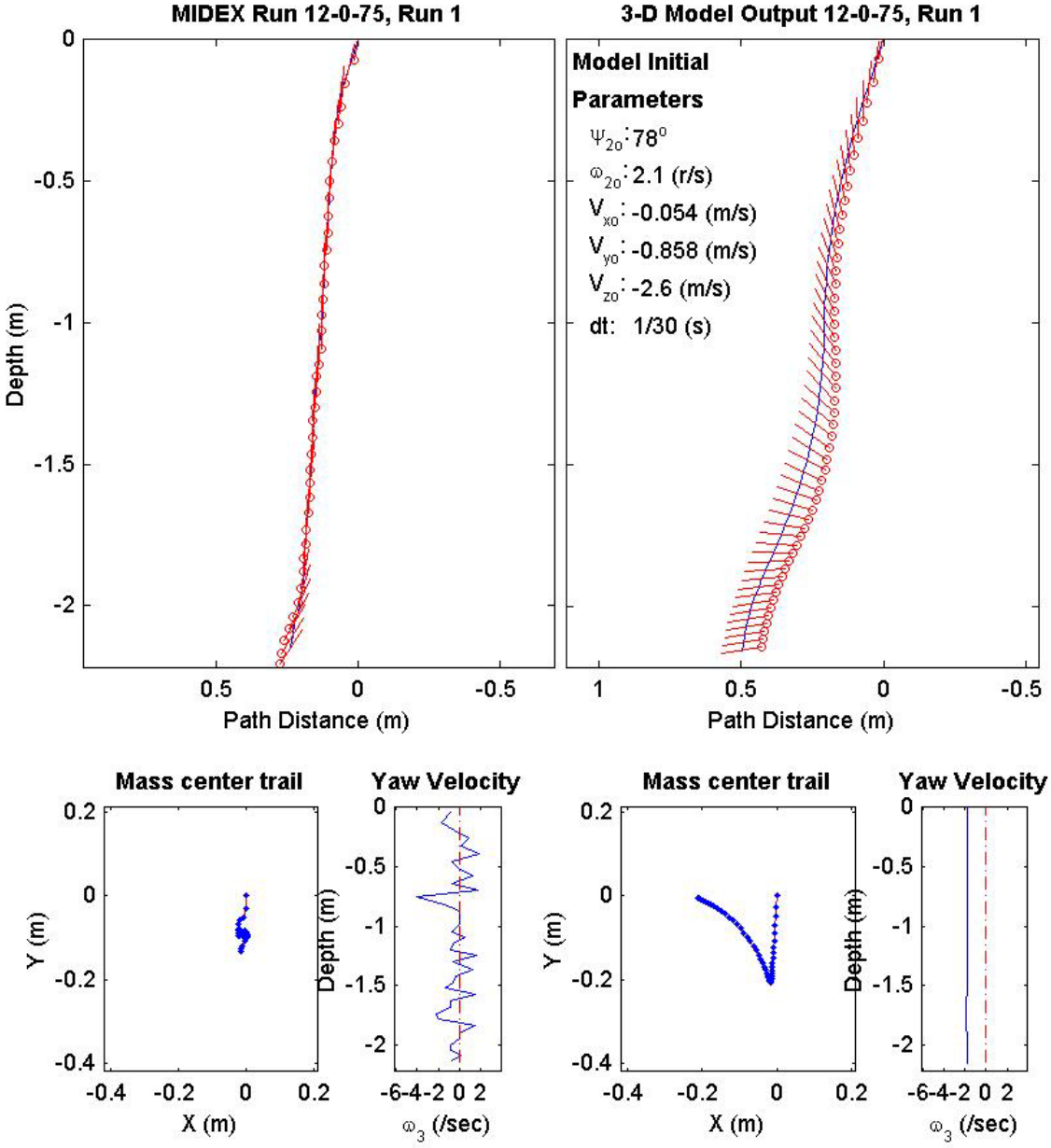

Final Drop Parameters (75/12-3171)

time: 1.8(s)
xy_{fe}: 0.268(m)
V_{xfe}: 0.054(m/s)
V_{yfe}: -0.054(m/s)
V_{zfe}: -0.883(m/s)
Ψ_{fe}: -16.9°
depth: 2.18(m)

Mine Shape Parameters (75/12-3171)

d: 0.04(m)
L: 0.121(m)
m: 0.254(m)
J_1: 2.71e-005(kg*m^2)
J_2: 0.000343(kg*m^2)
J_3: 0.000343(kg*m^2)
χ: 0.000644(m)

Final Model Parameters (75/12-3171)

time: 1.47(s)
xy_{fm}: 0.303(m)
V_{xfm}: 0.0456(m/s)
V_{yfm}: 0.0236(m/s)
V_{zfm}: -1.41(m/s)
Ψ_{fm}: 111.4°
depth: 2.22(m)

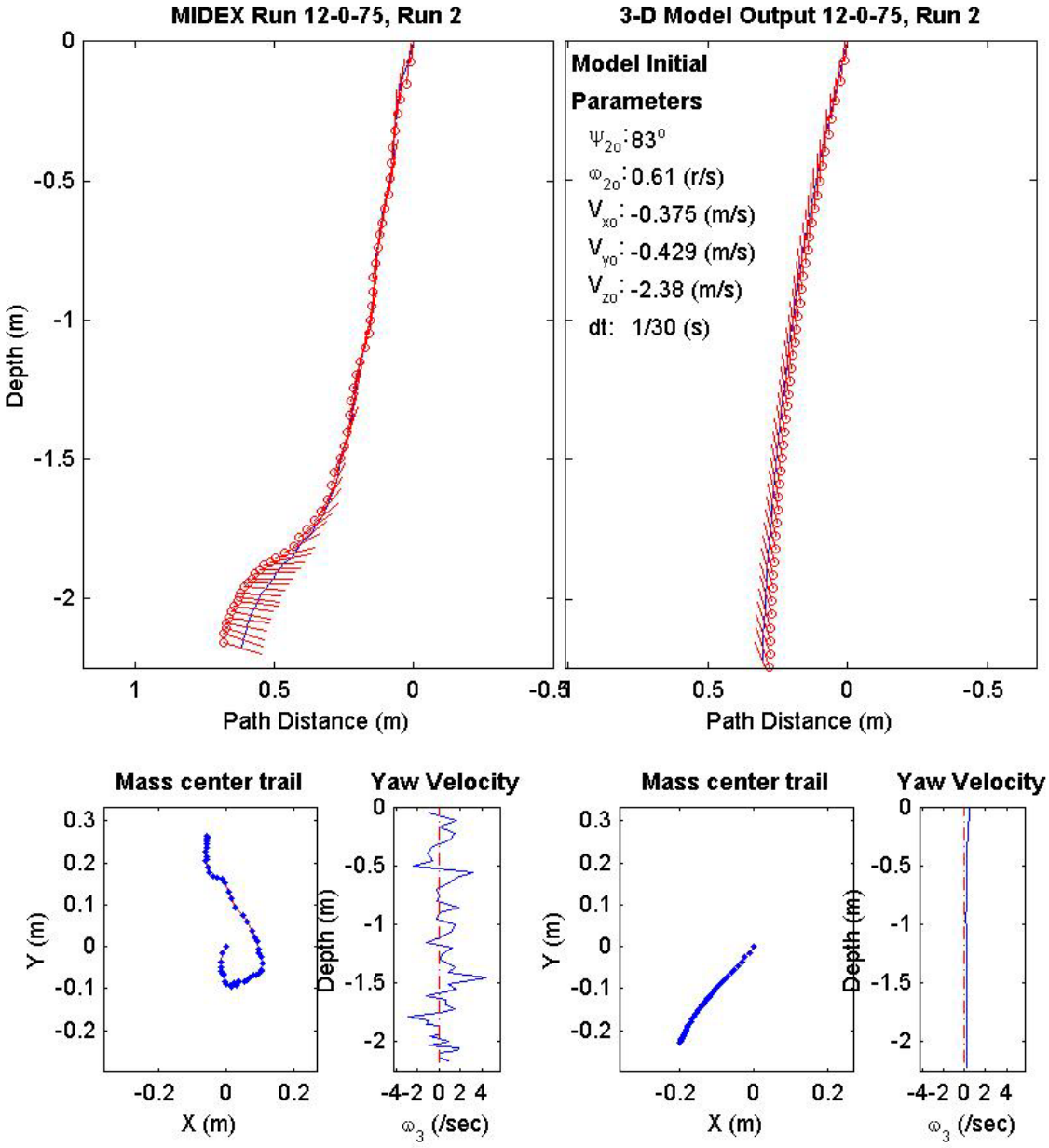

Final Drop

Parameters (75/9-4155)

time: 1.93(s)
xy_{fe}: 0.164(m)
V_{xfe}: 0.159(m/s)
V_{yfe}: 0.054(m/s)
V_{zfe}: -0.91(m/s)
Ψ_{fe}: 0^{o}
depth: 2.21(m)

Mine Shape

Parameters (75/9-4155)

d: 0.04(m)
L: 0.0912(m)
m: 0.215(m)
J_1: 2.35e-005($kg*m^2$)
J_2: 0.00017($kg*m^2$)
J_3: 0.00017($kg*m^2$)
χ: 2.9e-005(m)

Final Model

Parameters (75/9-4155)

time: 1.47(s)
xy_{fm}: 0.101(m)
V_{xfm}: 0.0489(m/s)
V_{yfm}: 0.0226(m/s)
V_{zfm}: -1.44(m/s)
Ψ_{fm}: 46.55^{o}
depth: 2.25(m)

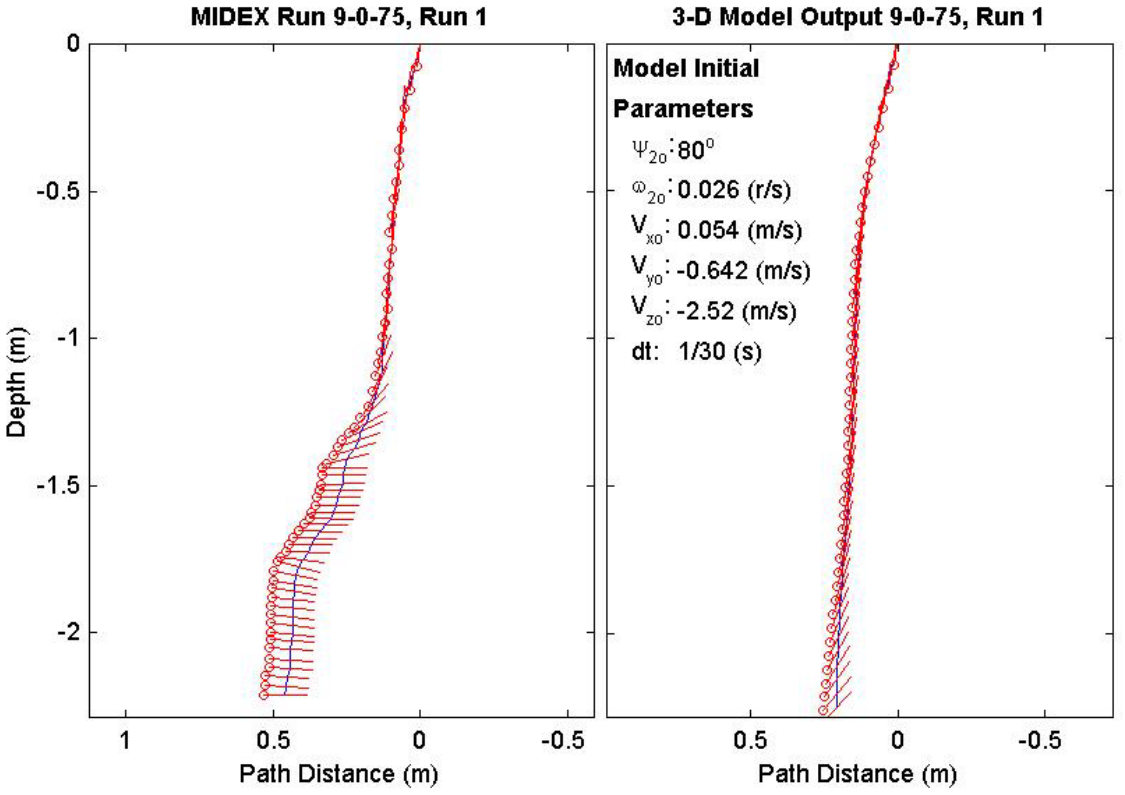

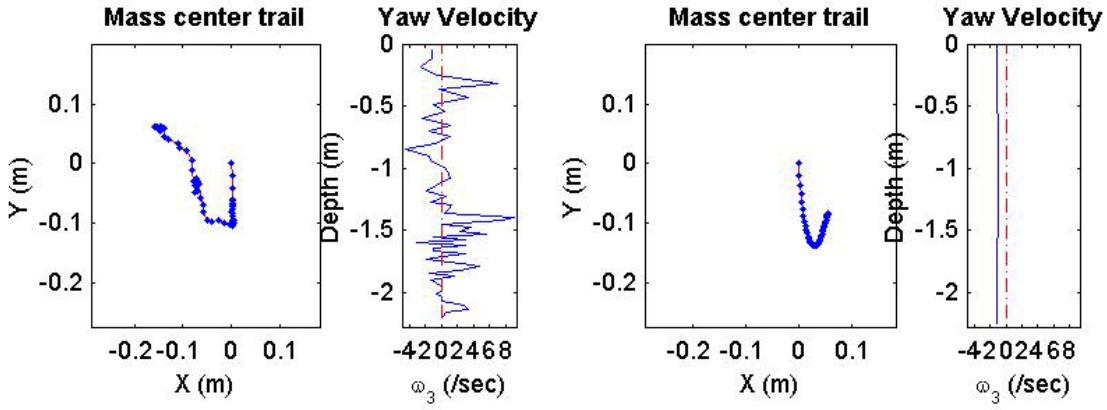

Final Drop

Parameters (75/9-3312)

time: 2.07(s)
xy_{fe}: 0.152(m)
V_{xfe}: -0.054(m/s)
V_{yfe}: -0.159(m/s)
V_{zfe}: -0.616(m/s)
Ψ_{fe}: 2.2°
depth: 2.24(m)

Mine Shape

Parameters (75/9-3312)

d: 0.04(m)
L: 0.0912(m)
m: 0.215(m)
J_1: 2.35e-005(kg*m^2)
J_2: 0.00017(kg*m^2)
J_3: 0.00017(kg*m^2)
χ: 2.9e-005(m)

Final Model

Parameters (75/9-3312)

time: 1.53(s)
xy_{fm}: 0.246(m)
V_{xfm}: 0.0805(m/s)
V_{yfm}: 4.94e-018(m/s)
V_{zfm}: -1.39(m/s)
Ψ_{fm}: 91.8°
depth: 2.27(m)

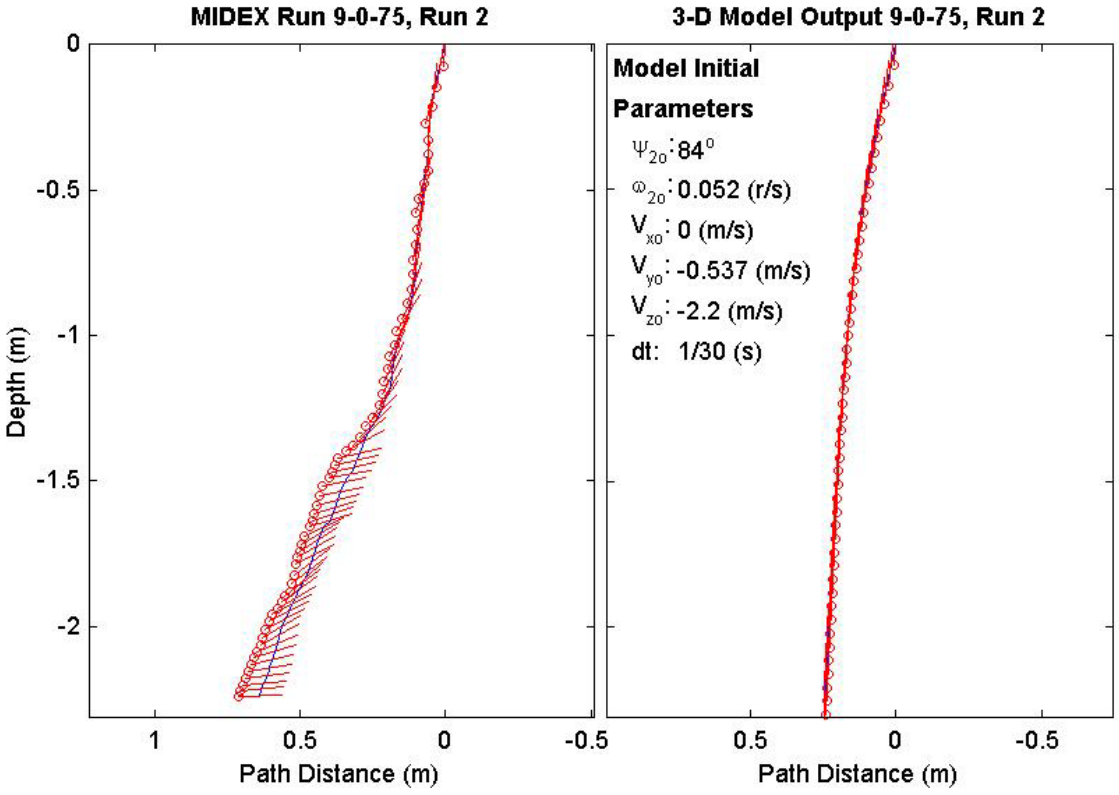

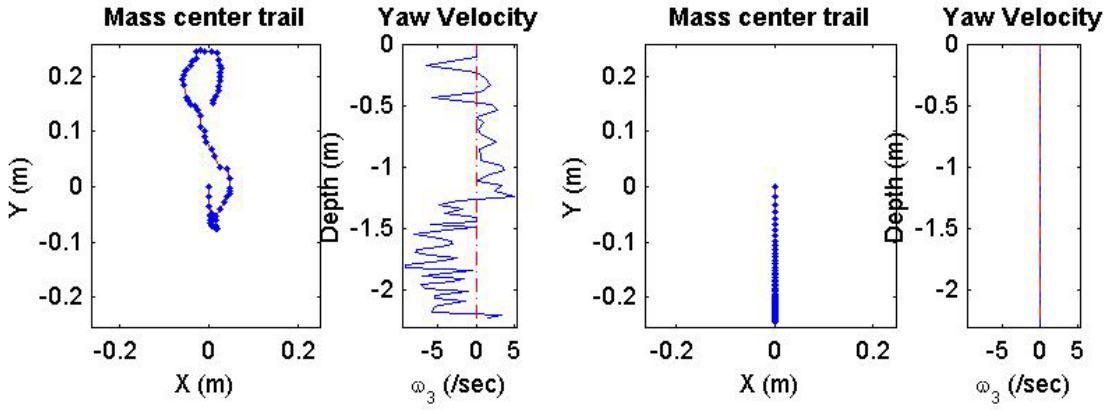

Final Drop Parameters (30/15-2307)

time: 1.77(s)
xy_{fe}: 0.909(m)
V_{xfe}: -0.267(m/s)
V_{yfe}: -0.429(m/s)
V_{zfe}: -0.936(m/s)
Ψ_{fe}: -48.2°
depth: 1.9(m)

Mine Shape Parameters (30/15-2307)

d: 0.04(m)
L: 0.152(m)
m: 0.323(m)
J_1: 3.3e-005(kg*m^2)
J_2: 0.000578(kg*m^2)
J_3: 0.000578(kg*m^2)
χ: -0.007411(m)

Final Model Parameters (30/15-2307)

time: 1.4(s)
xy_{fm}: 0.295(m)
V_{xfm}: 0.0503(m/s)
V_{yfm}: -0.000478(m/s)
V_{zfm}: -1.54(m/s)
Ψ_{fm}: -82.95°
depth: 1.94(m)

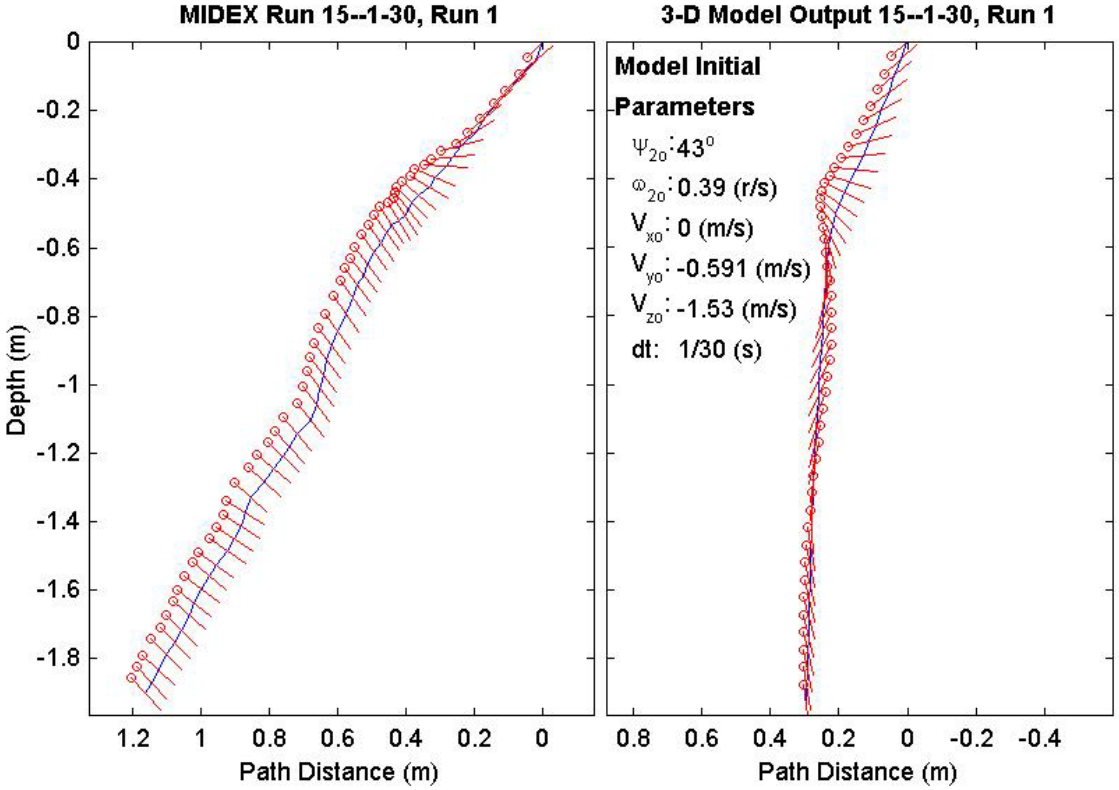

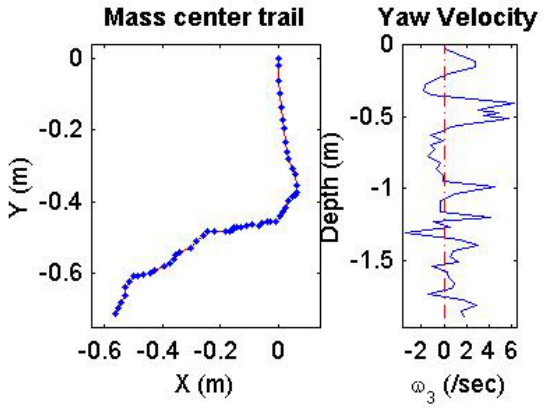

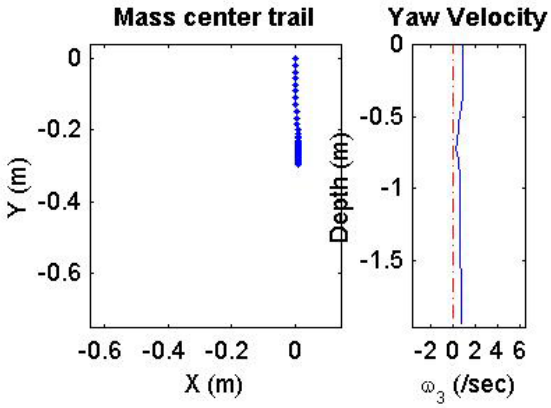

Final Drop

Parameters (30/15-1552)

time: 1.67(s)
xy_{fe}: 0.568(m)
V_{xfe}: -0.055(m/s)
V_{yfe}: 0.055(m/s)
V_{zfe}: -1.18(m/s)
Ψ_{fe}: -60.8°
depth: 1.86(m)

Mine Shape

Parameters (30/15-1552)

d: 0.04(m)
L: 0.152(m)
m: 0.323(m)
J_1: 3.3e-005(kg*m^2)
J_2: 0.000578(kg*m^2)
J_3: 0.000578(kg*m^2)
χ: 0.007411(m)

Final Model

Parameters (30/15-1552)

time: 1.47(s)
xy_{fm}: 0.404(m)
V_{xfm}: -0.0613(m/s)
V_{yfm}: -0.0634(m/s)
V_{zfm}: -1.52(m/s)
Ψ_{fm}: 86.85°
depth: 1.9(m)

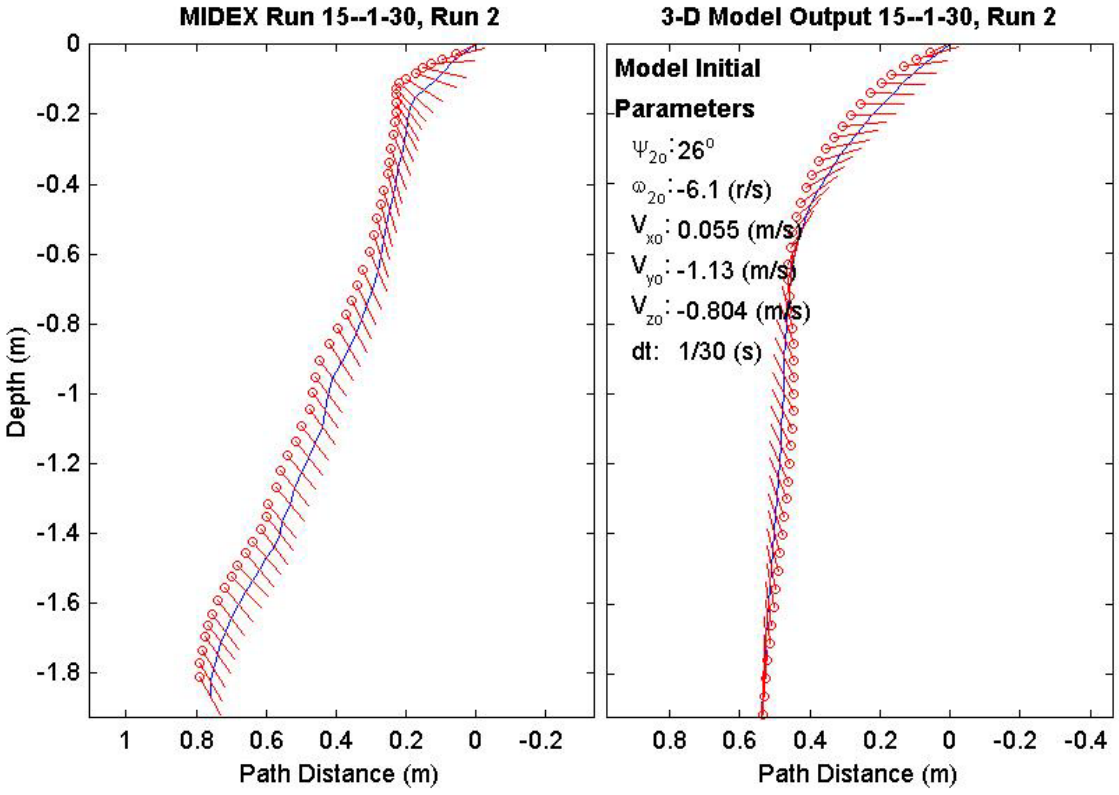

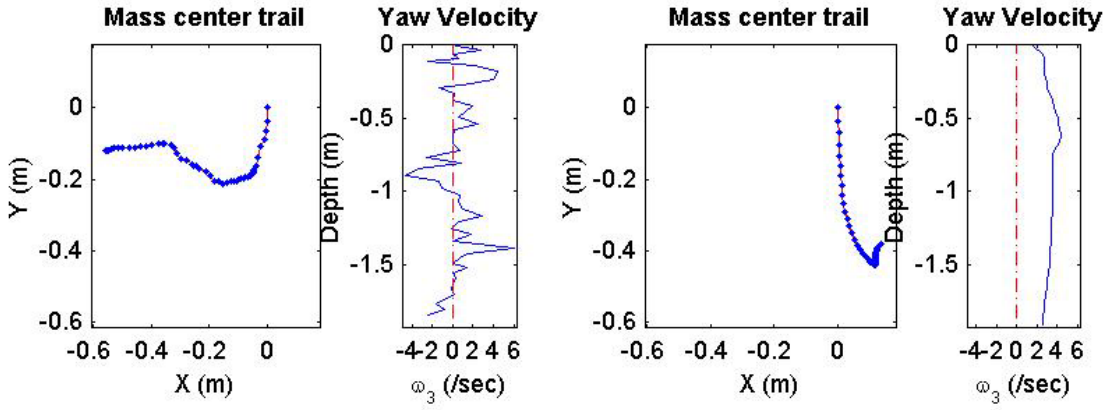

Final Drop

Parameters (30/12-2448)

time: 1.77(s)
xy_{fe}: 0.24(m)
V_{xfe}: 0.054(m/s)
V_{yfe}: -0.162(m/s)
V_{zfe}: -1.31(m/s)
Ψ_{fe}: -82.6°
depth: 2.22(m)

Mine Shape

Parameters (30/12-2448)

d: 0.04(m)
L: 0.121(m)
m: 0.254(m)
J_1: 2.71e-005(kg*m^2)
J_2: 0.000321(kg*m^2)
J_3: 0.000321(kg*m^2)
χ: -0.005307(m)

Final Model

Parameters (30/12-2448)

time: 1.7(s)
xy_{fm}: 0.409(m)
V_{xfm}: 0.0531(m/s)
V_{yfm}: -0.011(m/s)
V_{zfm}: -1.4(m/s)
Ψ_{fm}: -77.86°
depth: 2.25(m)

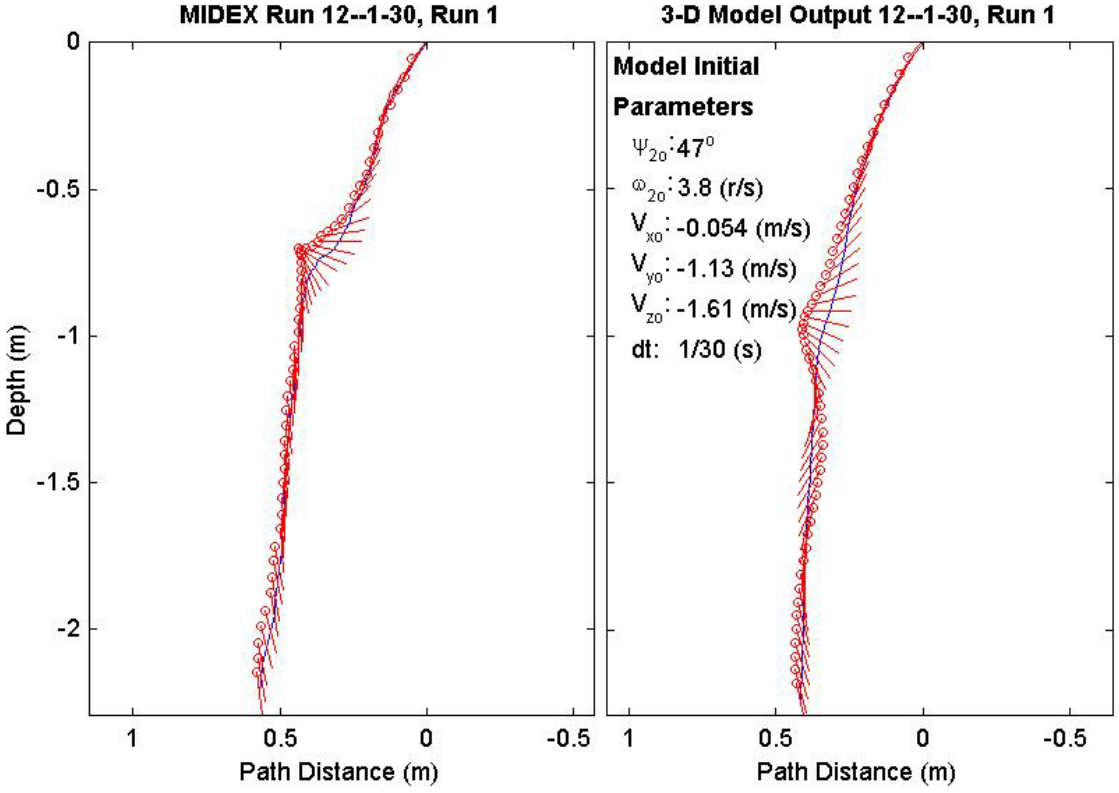

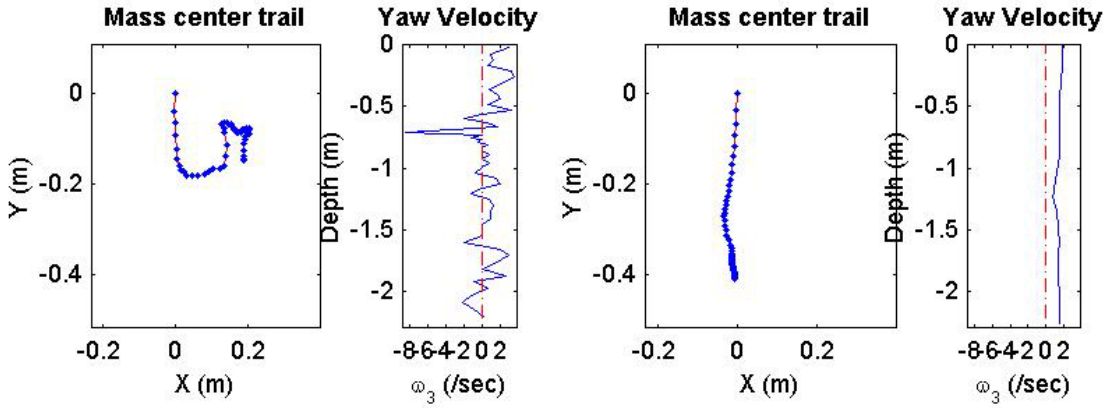

Final Drop
Parameters (30/12-1828)

time: 2.27(s)
xy_{fe}: 0.501(m)
V_{xfe}: 0.054(m/s)
V_{yfe}: 0.375(m/s)
V_{zfe}: -0.91(m/s)
ψ_{fe}: -39.8°
depth: 2.25(m)

Mine Shape
Parameters (30/12-1828)

d: 0.04(m)
L: 0.121(m)
m: 0.254(m)
J_1: 2.71e-005(kg*m^2)
J_2: 0.000321(kg*m^2)
J_3: 0.000321(kg*m^2)
χ: 0.005307(m)

Final Model
Parameters (30/12-1828)

time: 1.6(s)
xy_{fm}: 0.299(m)
V_{xfm}: 0.00191(m/s)
V_{yfm}: 0.0097(m/s)
V_{zfm}: -1.37(m/s)
ψ_{fm}: 96.63°
depth: 2.27(m)

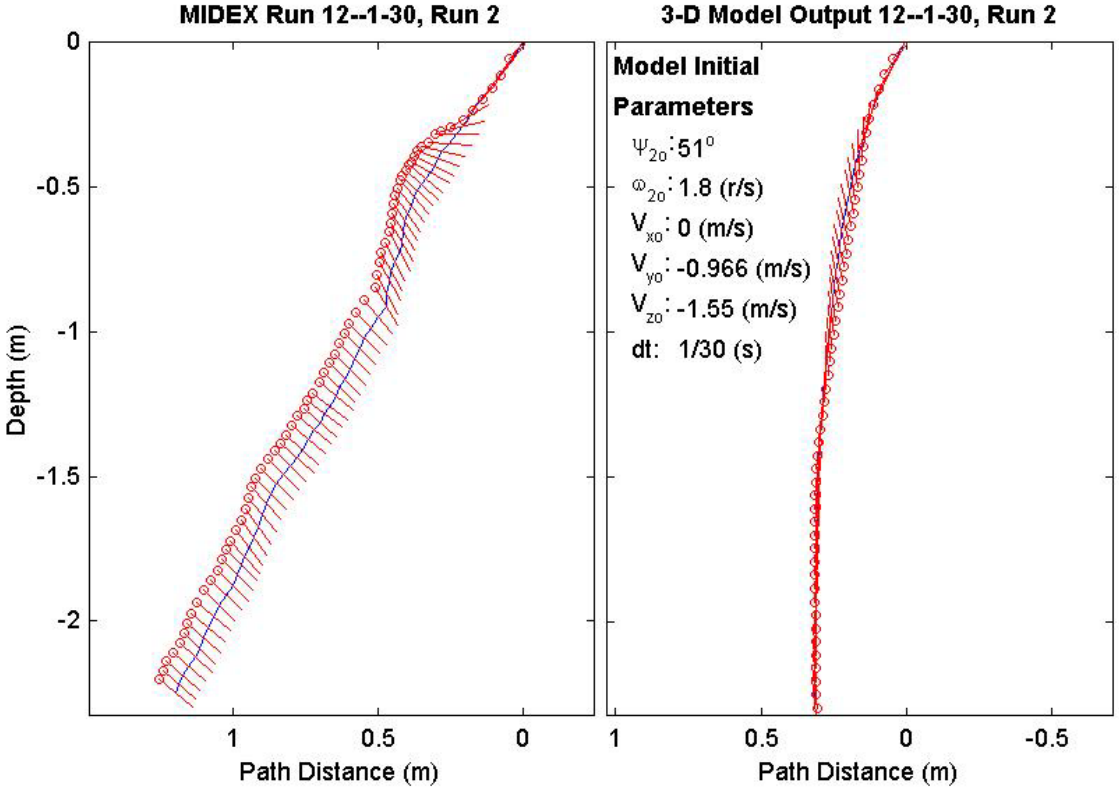

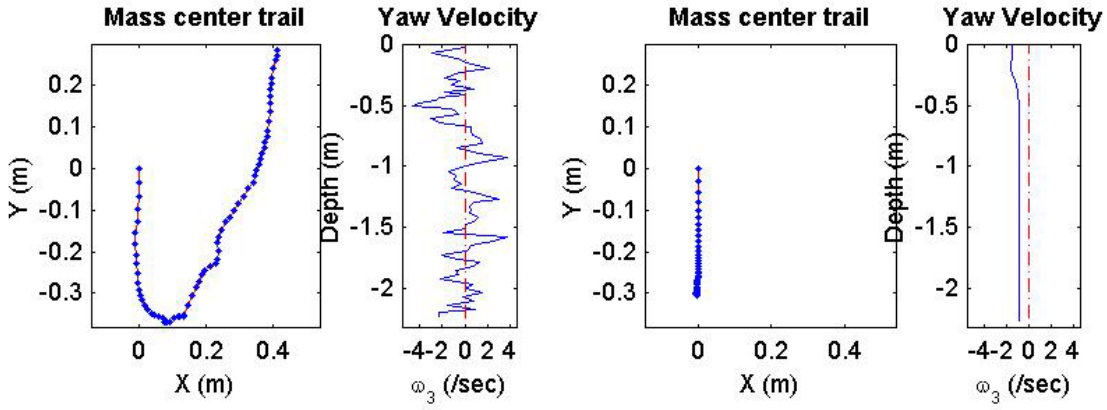

Final Drop
Parameters (30/9-2258)

time:	2.23(s)
xy_{fe}:	0.302(m)
V_{xfe}:	0.321(m/s)
V_{yfe}:	-0.321(m/s)
V_{zfe}:	-0.91(m/s)
Ψ_{fe}:	-53.2°
depth:	2.23(m)

Mine Shape
Parameters (30/9-2258)

d:	0.04(m)
L:	0.0912(m)
m:	0.215(m)
J_1:	2.35e-005(kg*m^2)
J_2:	0.000158(kg*m^2)
J_3:	0.000158(kg*m^2)
χ:	-0.002911(m)

Final Model
Parameters (30/9-2258)

time:	1.6(s)
xy_{fm}:	0.199(m)
V_{xfm}:	-0.075(m/s)
V_{yfm}:	-0.0193(m/s)
V_{zfm}:	-1.41(m/s)
Ψ_{fm}:	-85.49°
depth:	2.23(m)

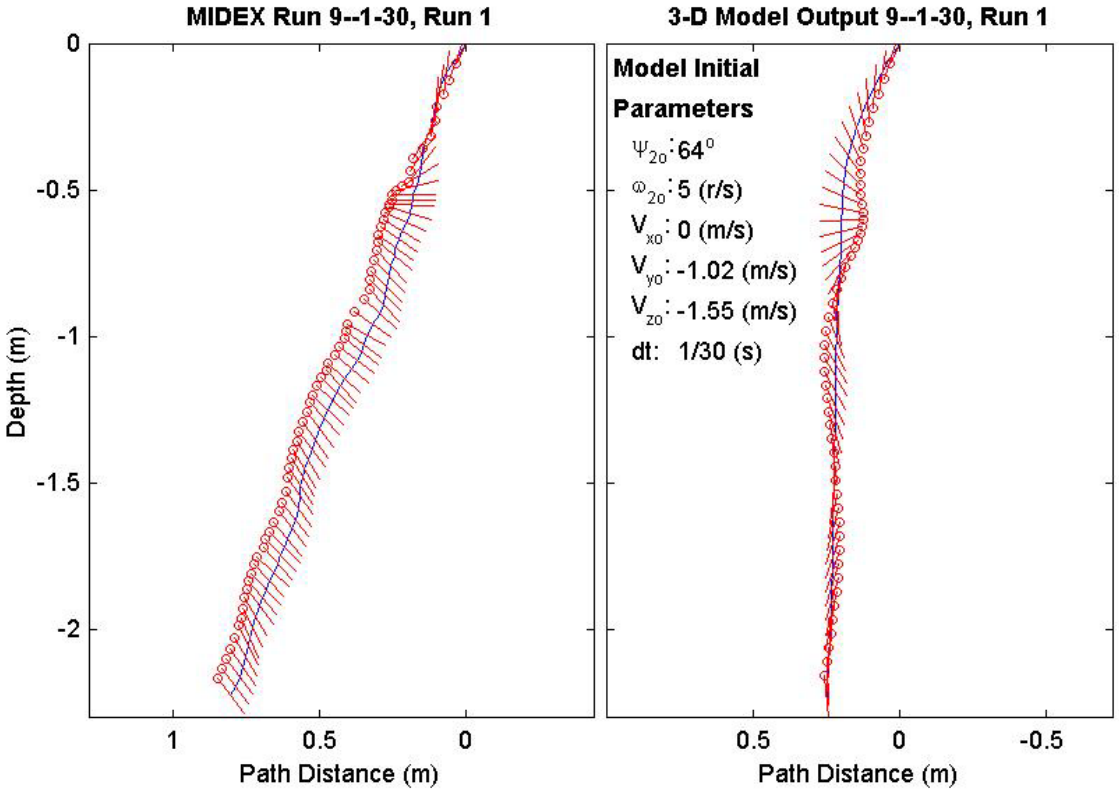

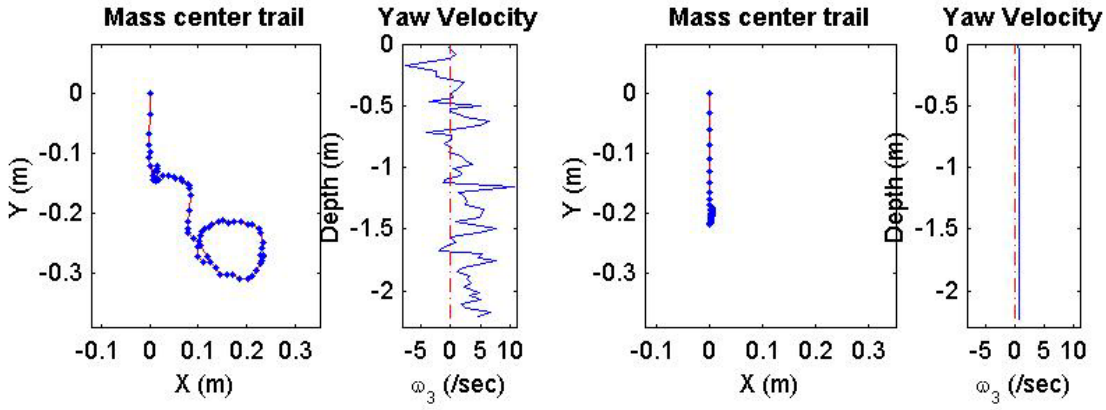

Final Drop

Parameters (30/9-1815)

time: 2.17(s)
xy_{fe}: 0.375(m)
V_{xfe}: -0.375(m/s)
V_{yfe}: 0(m/s)
V_{zfe}: -0.858(m/s)
Ψ_{fe}: -35.1°
depth: 2.25(m)

Mine Shape

Parameters (30/9-1815)

d: 0.04(m)
L: 0.0912(m)
m: 0.215(m)
J_1: 2.35e-005(kg*m^2)
J_2: 0.000158(kg*m^2)
J_3: 0.000158(kg*m^2)
χ: 0.002911(m)

Final Model

Parameters (30/9-1815)

time: 1.57(s)
xy_{fm}: 0.336(m)
V_{xfm}: -0.0468(m/s)
V_{yfm}: 0.0208(m/s)
V_{zfm}: -1.4(m/s)
Ψ_{fm}: 86.02°
depth: 2.26(m)

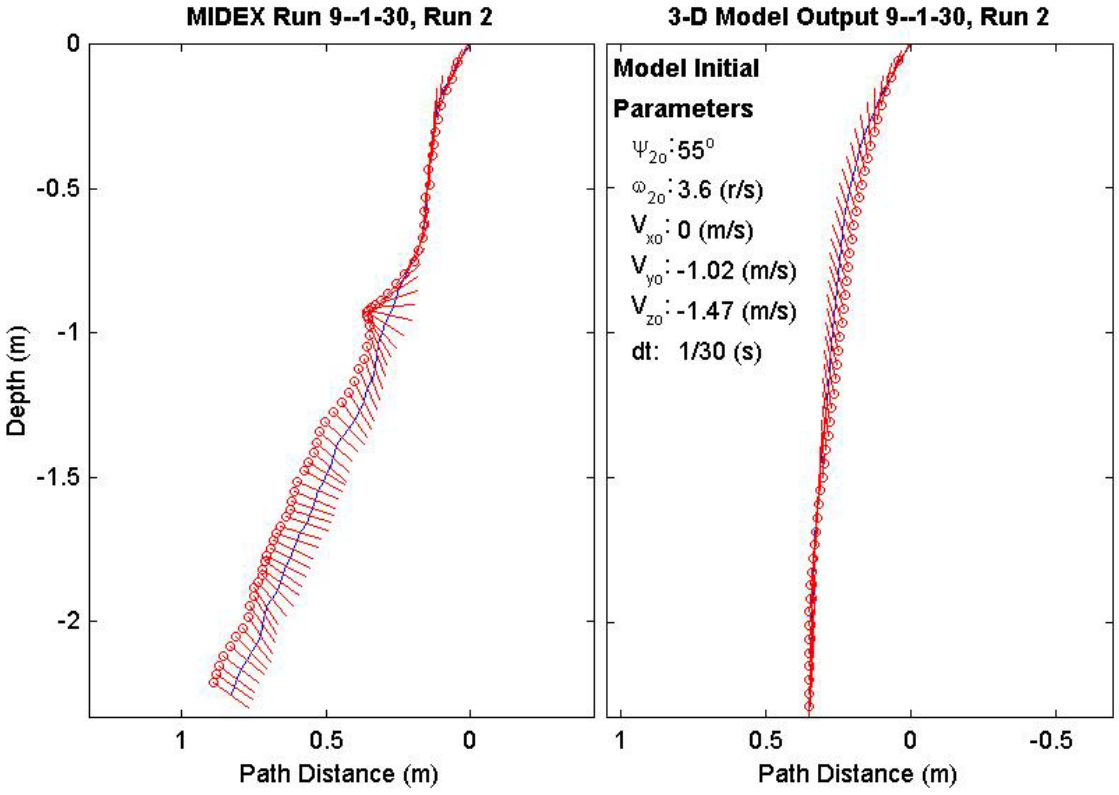

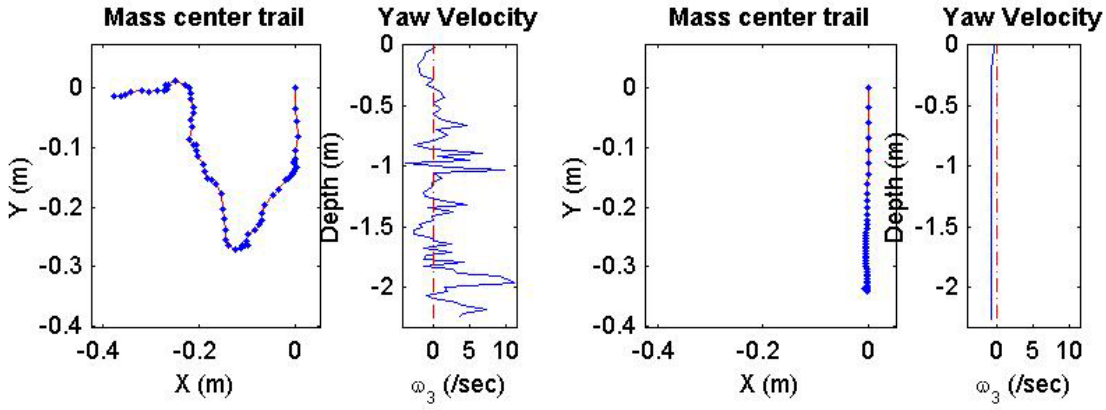

Final Drop Parameters (45/15-3006)

time: 1.67(s)
xy_{fe}: 0.679(m)
V_{xfe}: -0.163(m/s)
V_{yfe}: -0.48(m/s)
V_{zfe}: -1.15(m/s)
Ψ_{fe}: -45.2°
depth: 1.8(m)

Mine Shape Parameters (45/15-3006)

d: 0.04(m)
L: 0.152(m)
m: 0.323(m)
J_1: 3.3e-005(kg*m^2)
J_2: 0.000578(kg*m^2)
J_3: 0.000578(kg*m^2)
χ: -0.007411(m)

Final Model Parameters (45/15-3006)

time: 1.37(s)
xy_{fm}: 0.503(m)
V_{xfm}: 0.0602(m/s)
V_{yfm}: 0.000502(m/s)
V_{zfm}: -1.54(m/s)
Ψ_{fm}: -80.46°
depth: 1.83(m)

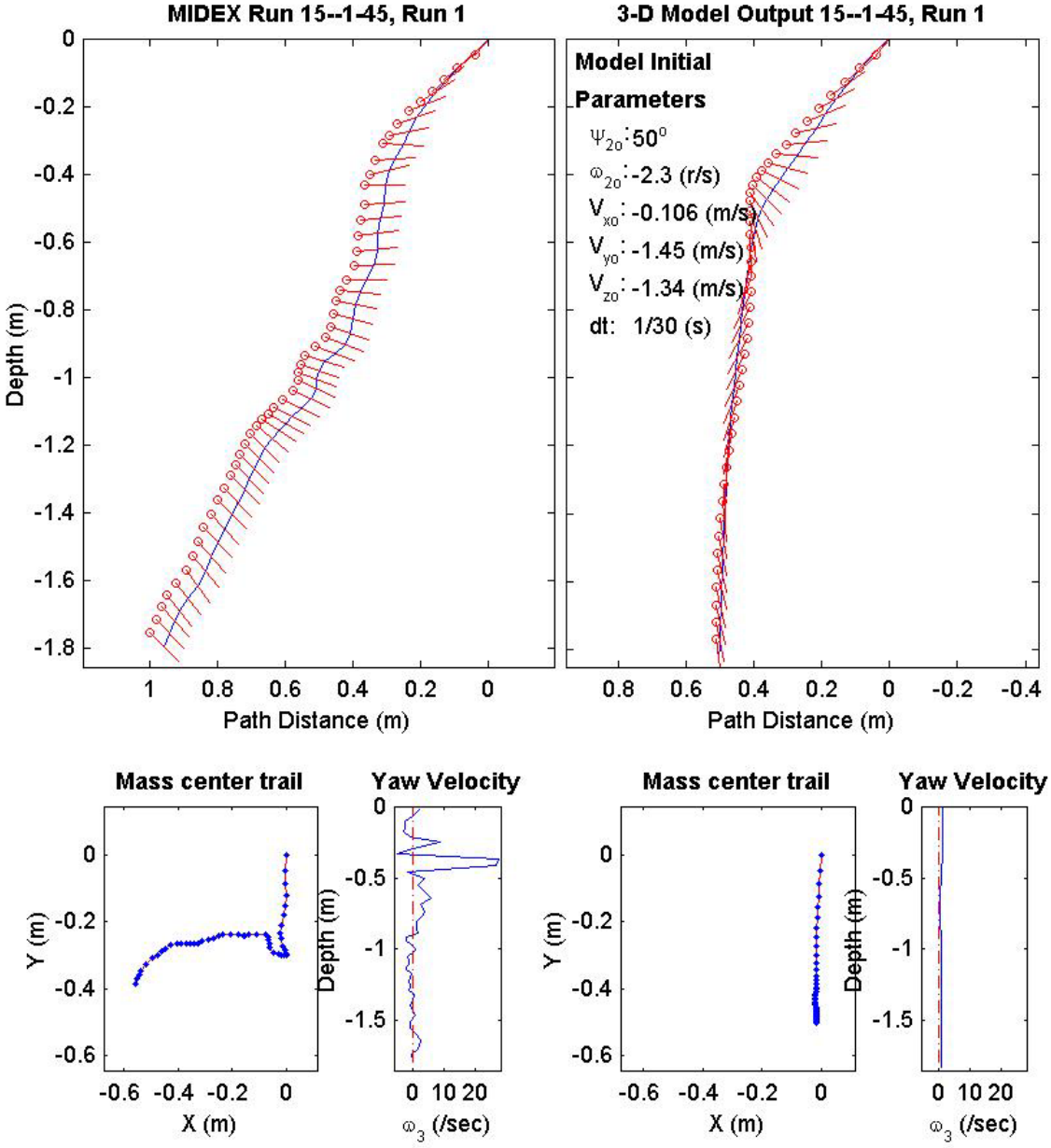

Final Drop
Parameters (45/15-2339)

time: 1.77(s)
xy_{fe}: 0.405(m)
V_{xfe}: -0.216(m/s)
V_{yfe}: 0.375(m/s)
V_{zfe}: -1.15(m/s)
Ψ_{fe}: -62.5°
depth: 1.95(m)

Mine Shape
Parameters (45/15-2339)

d: 0.04(m)
L: 0.152(m)
m: 0.323(m)
J_1: 3.3e-005(kg*m^2)
J_2: 0.000578(kg*m^2)
J_3: 0.000578(kg*m^2)
χ: 0.007411(m)

Final Model
Parameters (45/15-2339)

time: 1.27(s)
xy_{fm}: 0.509(m)
V_{xfm}: 0.0909(m/s)
V_{yfm}: -0.00454(m/s)
V_{zfm}: -1.52(m/s)
Ψ_{fm}: 88.66°
depth: 1.96(m)

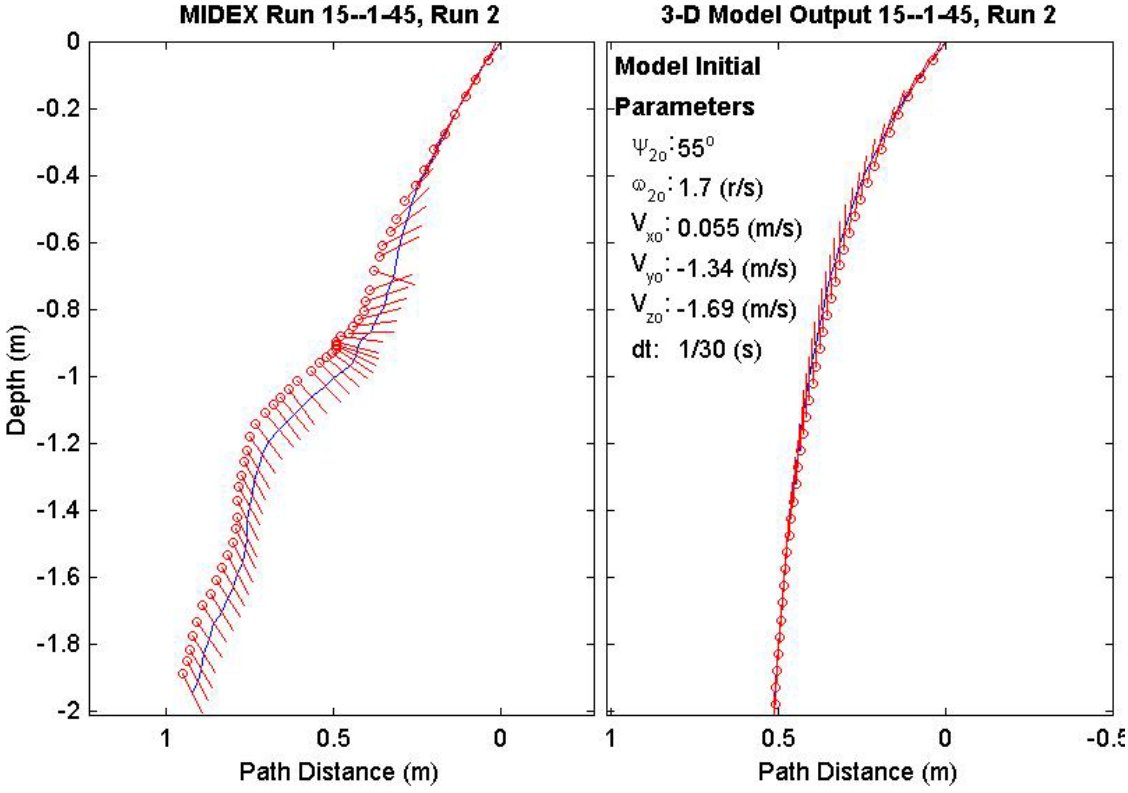

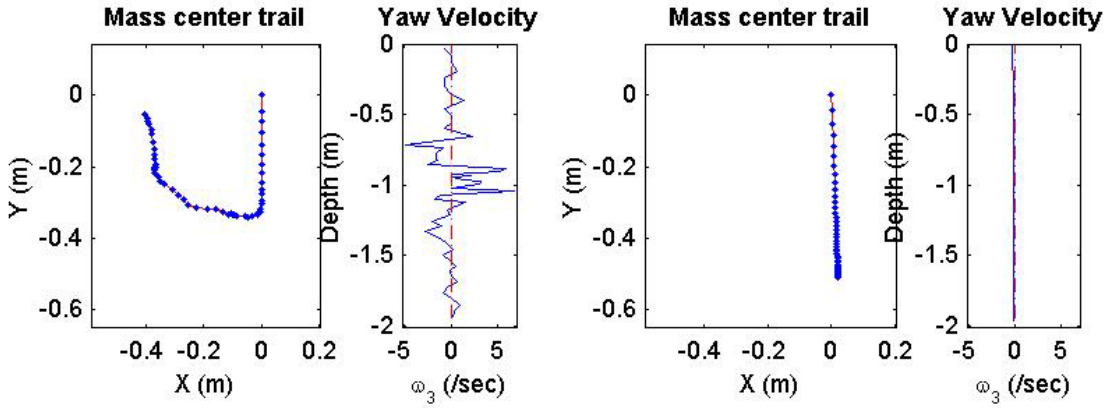

Final Drop

Parameters (45/12-3224)

time: 2.27(s)
xy_{fe}: 1.01(m)
V_{xfe}: 0.429(m/s)
V_{yfe}: -0.375(m/s)
V_{zfe}: -0.856(m/s)
Ψ_{fe}: -36.4°
depth: 2.19(m)

Mine Shape

Parameters (45/12-3224)

d: 0.04(m)
L: 0.121(m)
m: 0.254(m)
J_1: 2.71e-005(kg*m^2)
J_2: 0.000321(kg*m^2)
J_3: 0.000321(kg*m^2)
χ: -0.005307(m)

Final Model

Parameters (45/12-3224)

time: 1.7(s)
xy_{fm}: 0.405(m)
V_{xfm}: 0.0559(m/s)
V_{yfm}: 0.00154(m/s)
V_{zfm}: -1.4(m/s)
Ψ_{fm}: -83.66°
depth: 2.19(m)

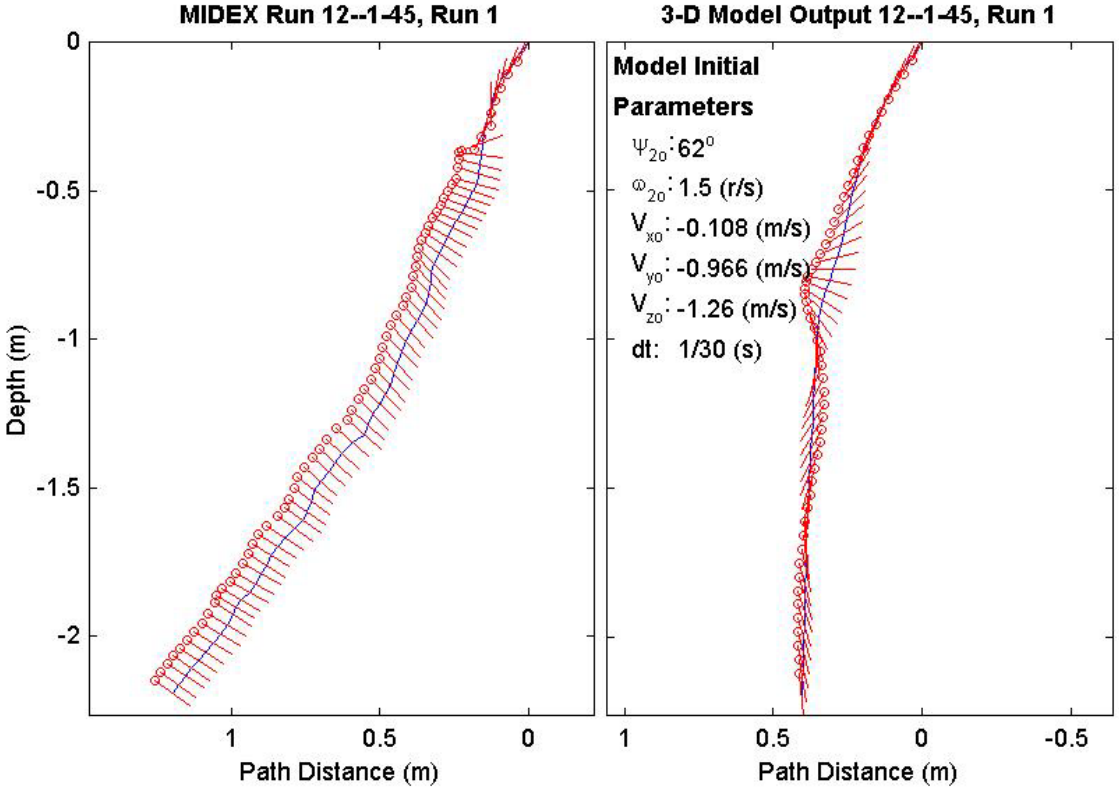

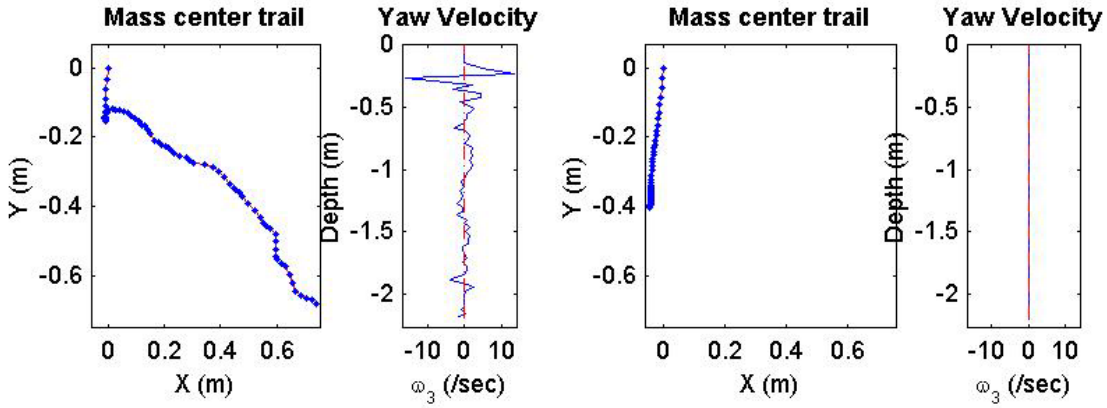

Final Drop

Parameters (45/12-2461)

time: 2.07(s)
xy_{fe}: 0.592(m)
V_{xfe}: -0.054(m/s)
V_{yfe}: -0.483(m/s)
V_{zfe}: -0.859(m/s)
Ψ_{fe}: -49.9°
depth: 2.19(m)

Mine Shape

Parameters (45/12-2461)

d: 0.04(m)
L: 0.121(m)
m: 0.254(m)
J_1: 2.71e-005(kg*m^2)
J_2: 0.000321(kg*m^2)
J_3: 0.000321(kg*m^2)
χ: 0.005307(m)

Final Model

Parameters (45/12-2461)

time: 1.53(s)
xy_{fm}: 0.176(m)
V_{xfm}: -0.0403(m/s)
V_{yfm}: 7.9e-018(m/s)
V_{zfm}: -1.37(m/s)
Ψ_{fm}: 89.74°
depth: 2.23(m)

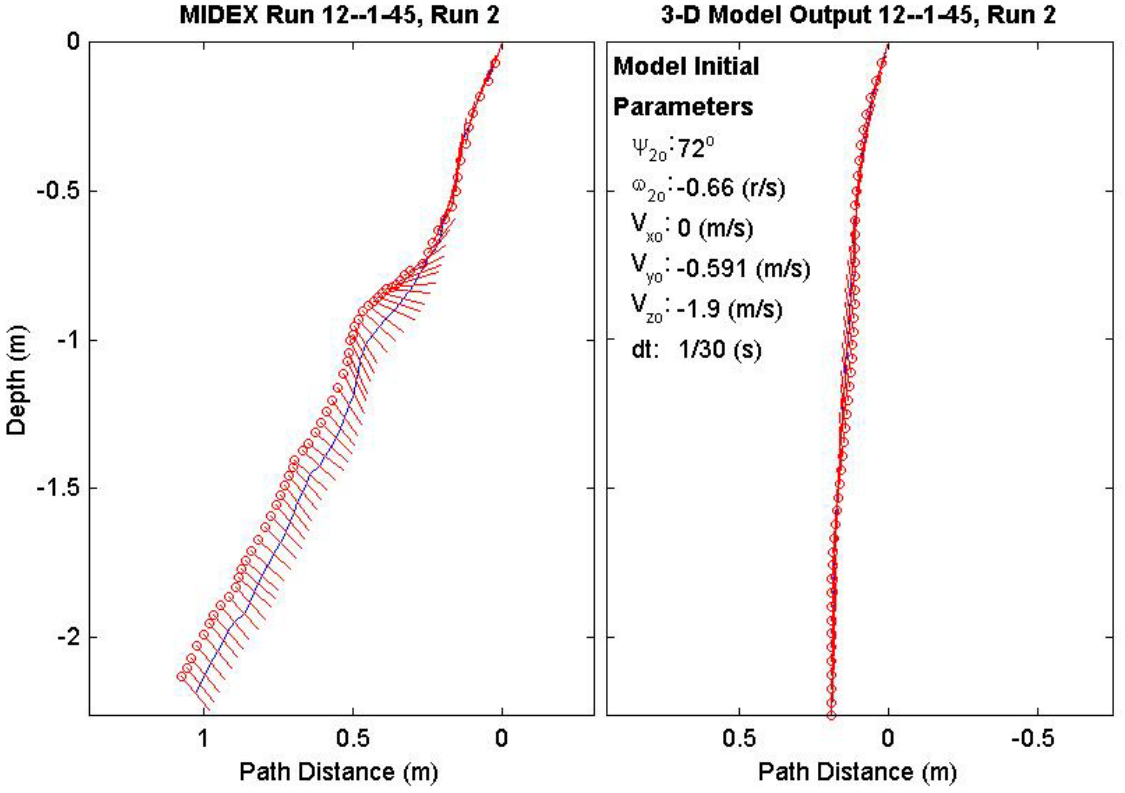

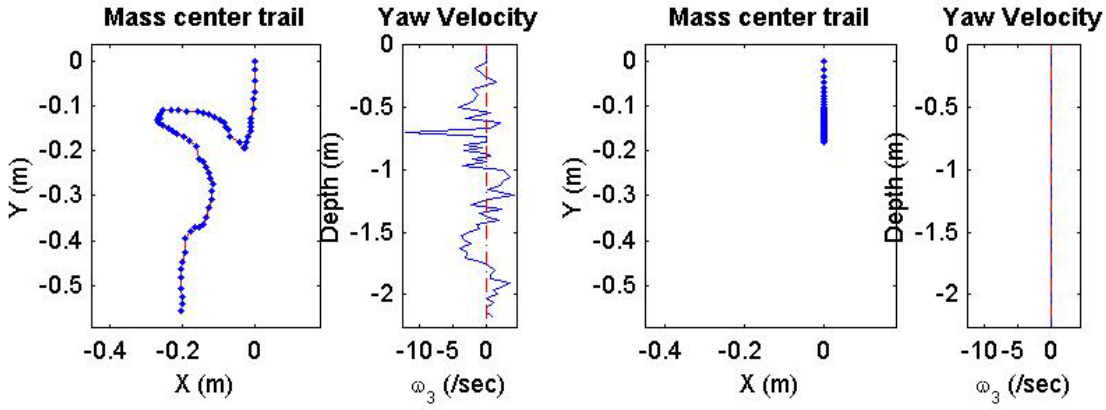

Final Drop

Parameters (45/9-3030)

time: 2.2(s)
xy_{fe}: 0.253(m)
V_{xfe}: 0.162(m/s)
V_{yfe}: -0.159(m/s)
V_{zfe}: -0.589(m/s)
Ψ_{fe}: -55.5°
depth: 2.14(m)

Mine Shape

Parameters (45/9-3030)

d: 0.04(m)
L: 0.0912(m)
m: 0.215(m)
J_1: 2.35e-005(kg*m^2)
J_2: 0.000158(kg*m^2)
J_3: 0.000158(kg*m^2)
χ: -0.002911(m)

Final Model

Parameters (45/9-3030)

time: 1.57(s)
xy_{fm}: 0.145(m)
V_{xfm}: -0.0777(m/s)
V_{yfm}: -0.00211(m/s)
V_{zfm}: -1.44(m/s)
Ψ_{fm}: -98.08°
depth: 2.19(m)

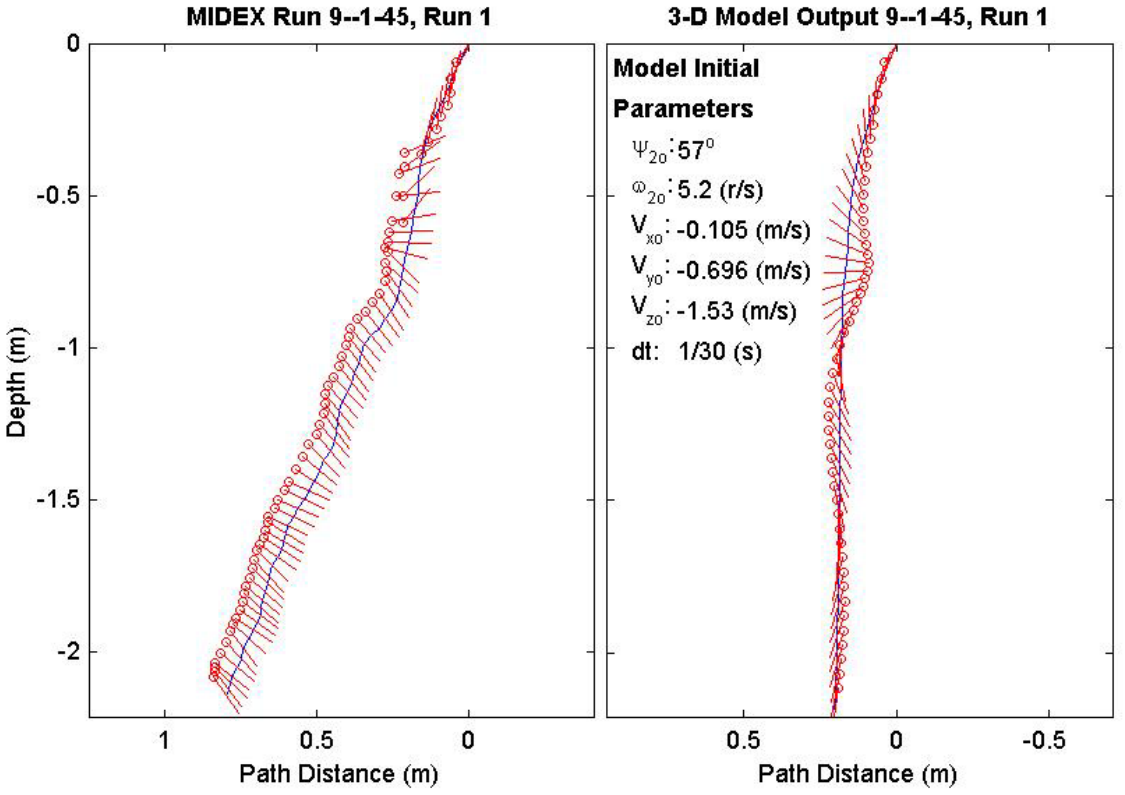

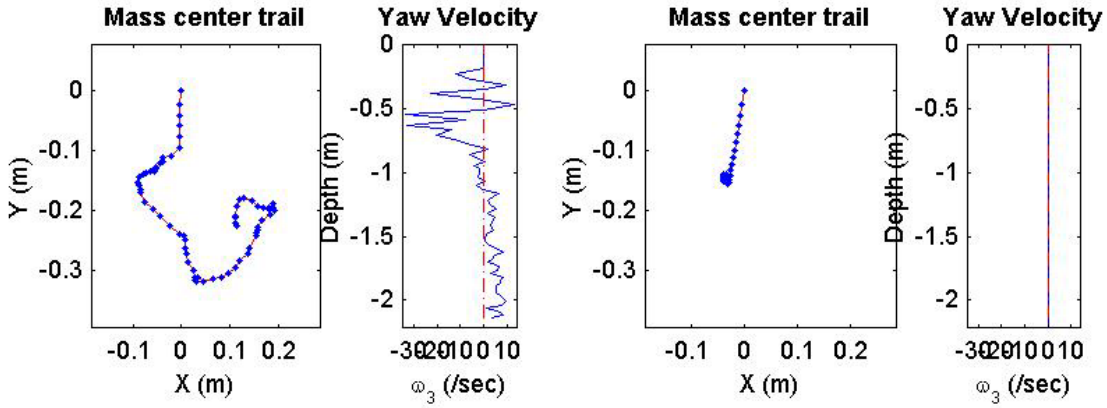

Final Drop

Parameters (45/9-2318)

time: 2.07(s)
xy_{fe}: 0.0649(m)
V_{xfe}: 0.213(m/s)
V_{yfe}: -0.108(m/s)
V_{zfe}: -1.07(m/s)
Ψ_{fe}: -52.2°
depth: 2.05(m)

Mine Shape

Parameters (45/9-2318)

d: 0.04(m)
L: 0.0912(m)
m: 0.215(m)
J_1: 2.35e-005(kg*m^2)
J_2: 0.000158(kg*m^2)
J_3: 0.000158(kg*m^2)
χ: 0.002911(m)

Final Model

Parameters (45/9-2318)

time: 1.47(s)
xy_{fm}: 0.266(m)
V_{xfm}: -0.0435(m/s)
V_{yfm}: 0.0149(m/s)
V_{zfm}: -1.4(m/s)
Ψ_{fm}: 85.3°
depth: 2.09(m)

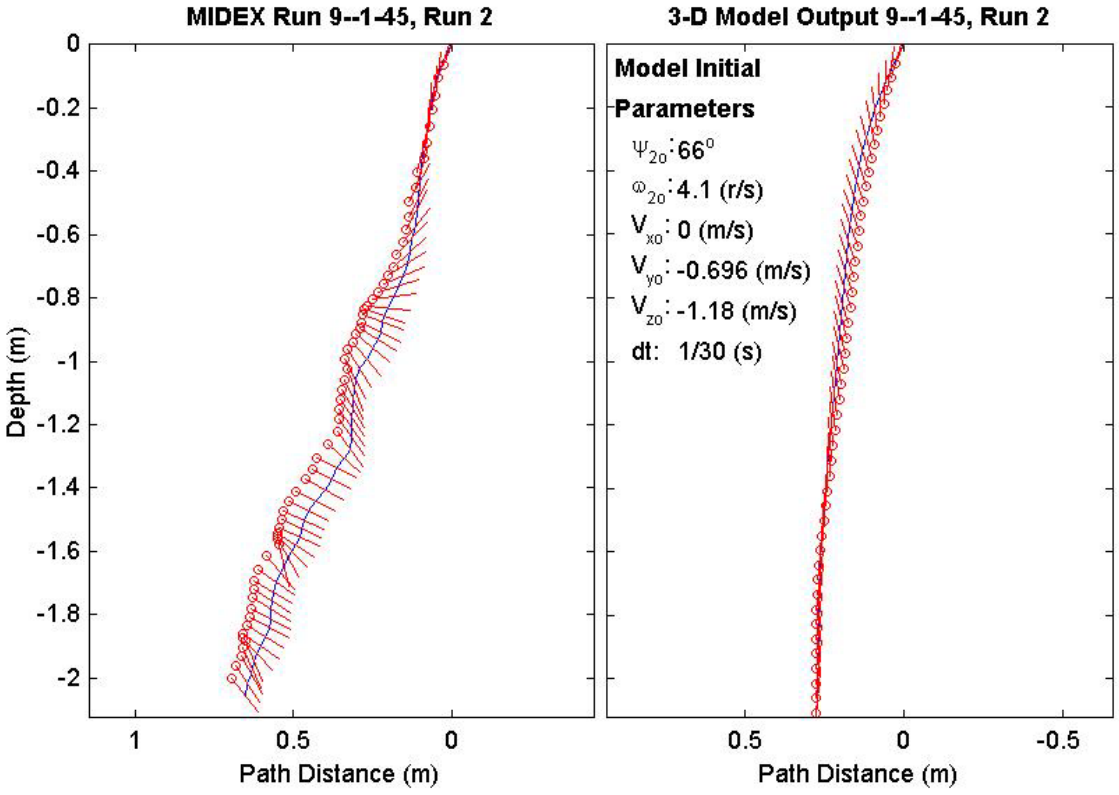

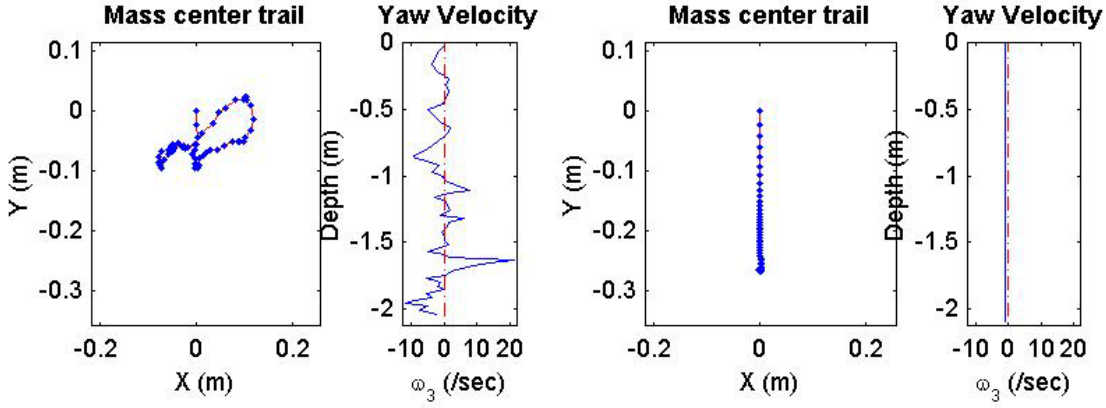

Final Drop Parameters (60/15-3359)

time: 1.67(s)
xy_{fe}: 0.614(m)
V_{xfe}: -0.055(m/s)
V_{yfe}: -0.213(m/s)
V_{zfe}: -1.26(m/s)
Ψ_{fe}: -58.4°
depth: 1.92(m)

Mine Shape Parameters (60/15-3359)

d: 0.04(m)
L: 0.152(m)
m: 0.323(m)
J_1: 3.3e-005(kg*m^2)
J_2: 0.000578(kg*m^2)
J_3: 0.000578(kg*m^2)
χ: -0.007411(m)

Final Model Parameters (60/15-3359)

time: 1.33(s)
xy_{fm}: 0.25(m)
V_{xfm}: -0.0665(m/s)
V_{yfm}: -0.00864(m/s)
V_{zfm}: -1.46(m/s)
Ψ_{fm}: -69.54°
depth: 1.93(m)

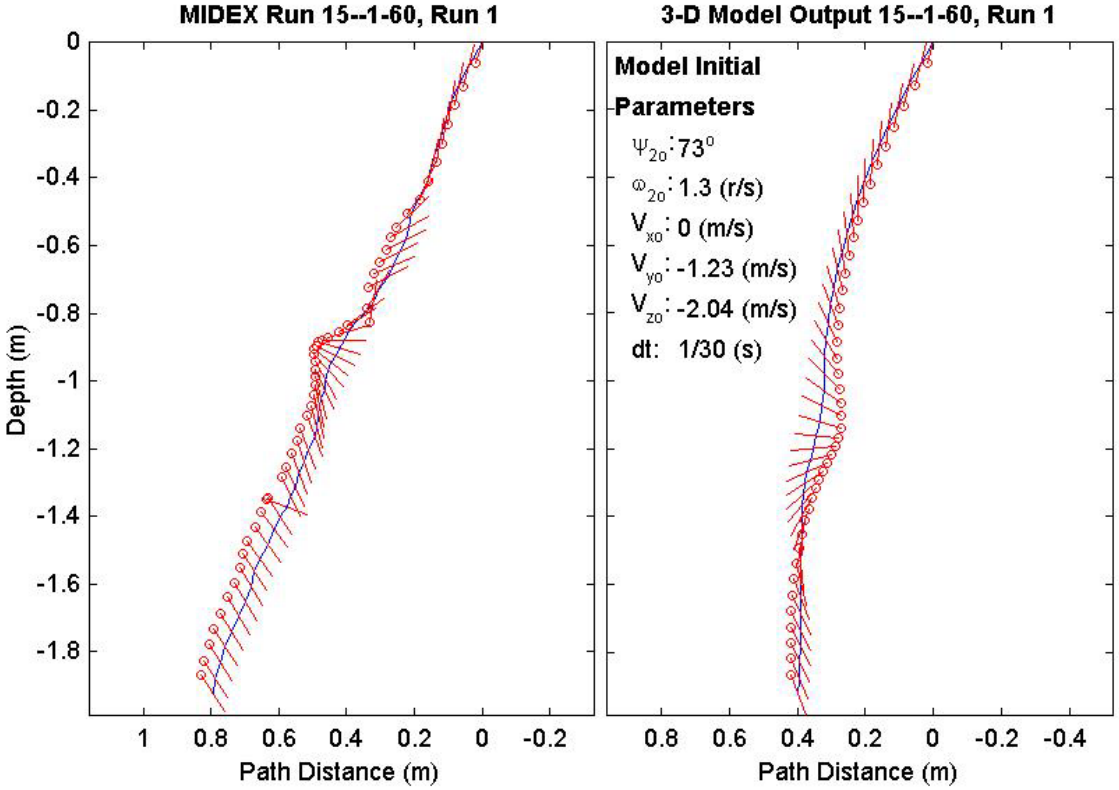

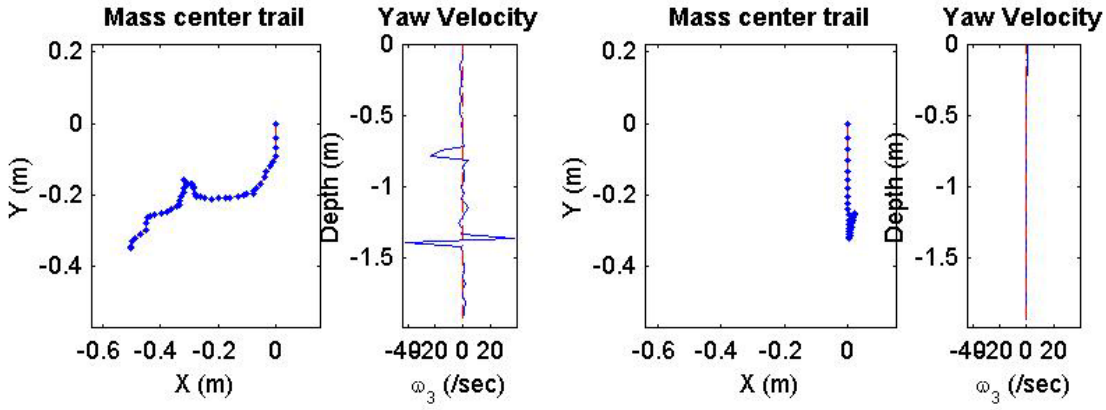

Final Drop Parameters (60/15-2961)

time: 1.67(s)
xy_{fe}: 0.559(m)
V_{xfe}: 0.858(m/s)
V_{yfe}: -0.213(m/s)
V_{zfe}: -1.26(m/s)
Ψ_{fe}: -38°
depth: 2.02(m)

Mine Shape Parameters (60/15-2961)

d: 0.04(m)
L: 0.152(m)
m: 0.323(m)
J_1: 3.3e-005(kg*m^2)
J_2: 0.000578(kg*m^2)
J_3: 0.000578(kg*m^2)
χ: 0.007411(m)

Final Model Parameters (60/15-2961)

time: 1.3(s)
xy_{fm}: 0.497(m)
V_{xfm}: 0.102(m/s)
V_{yfm}: -0.014(m/s)
V_{zfm}: -1.52(m/s)
Ψ_{fm}: 89.45°
depth: 2.03(m)

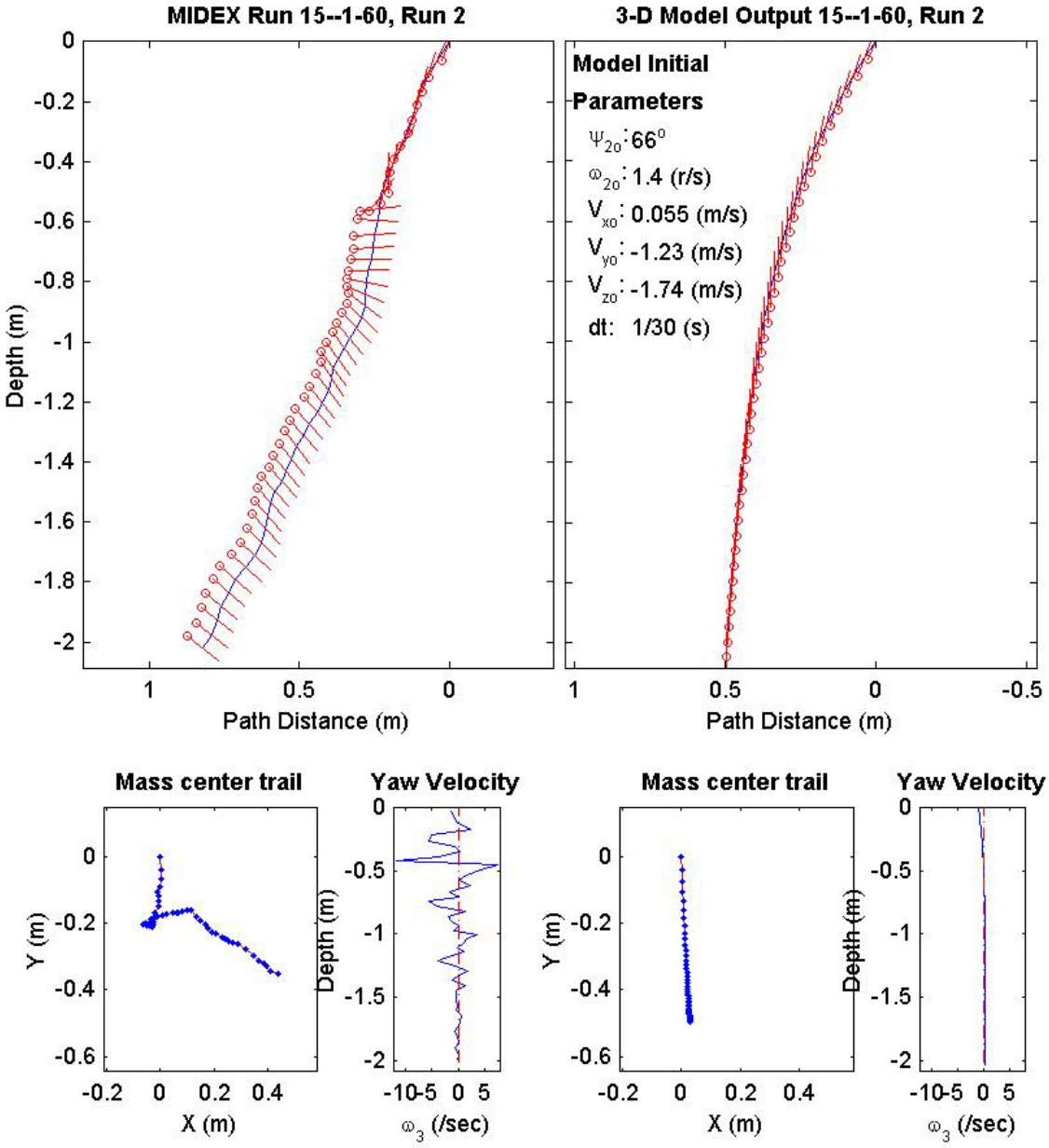

Final Drop Parameters (60/12-3794)

time: 1.93(s)
xy_{fe}: 0.575(m)
V_{xfe}: 0(m/s)
V_{yfe}: -0.644(m/s)
V_{zfe}: -0.966(m/s)
Ψ_{fe}: -45.8°
depth: 2.14(m)

Mine Shape Parameters (60/12-3794)

d: 0.04(m)
L: 0.121(m)
m: 0.254(m)
J_1: 2.71e-005(kg*m^2)
J_2: 0.000321(kg*m^2)
J_3: 0.000321(kg*m^2)
χ: -0.005307(m)

Final Model Parameters (60/12-3794)

time: 1.57(s)
xy_{fm}: 0.413(m)
V_{xfm}: 0.0264(m/s)
V_{yfm}: -0.000912(m/s)
V_{zfm}: -1.37(m/s)
Ψ_{fm}: -87.96°
depth: 2.14(m)

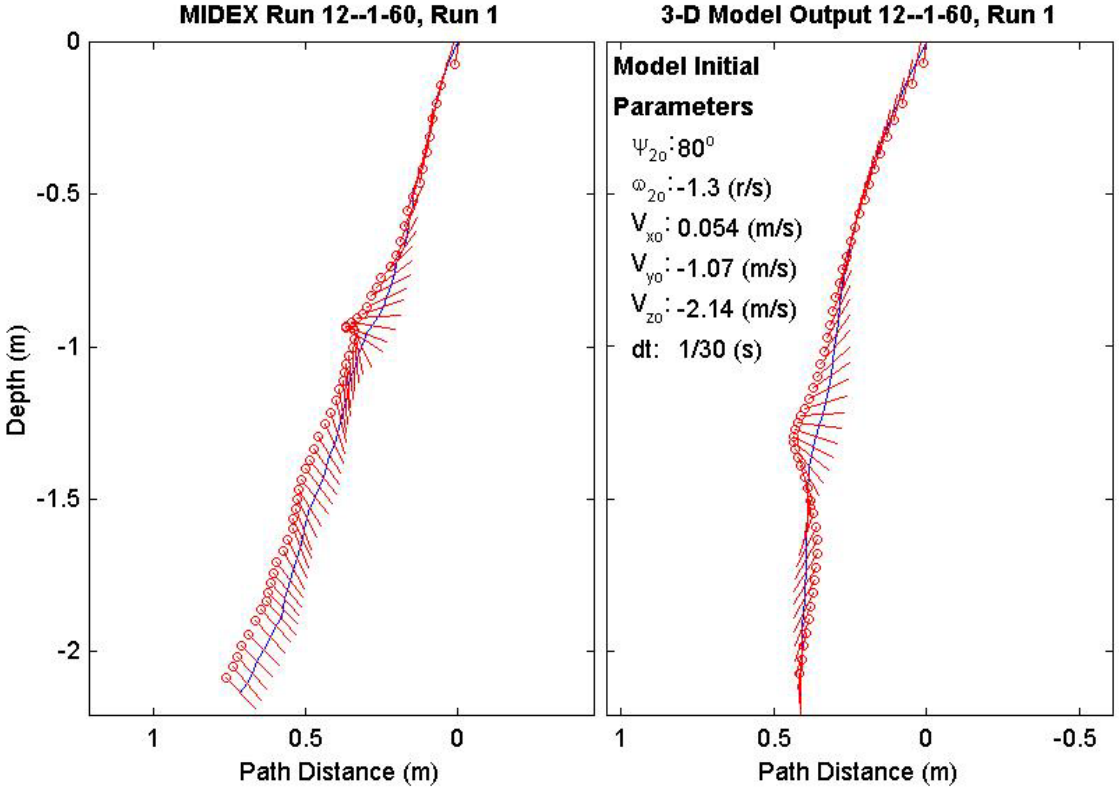

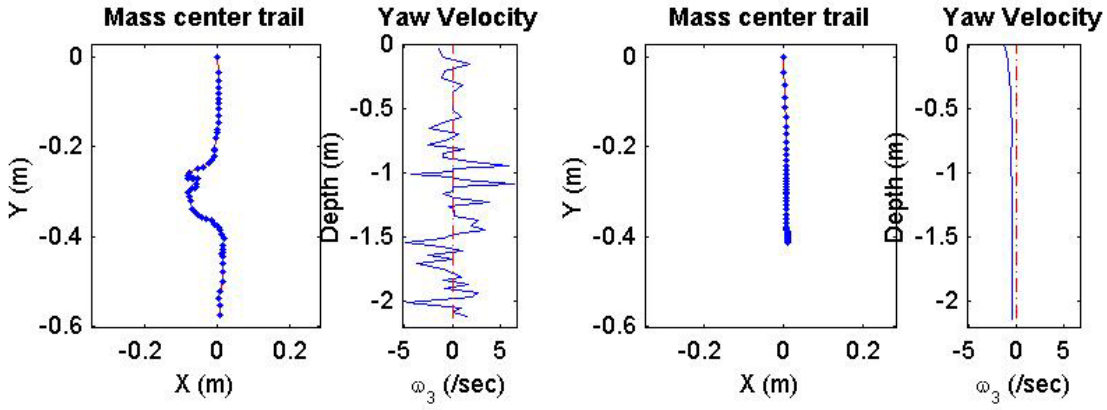

Final Drop

Parameters (60/12-2789)

time: 1.83(s)
xy_{fe}: 0.595(m)
V_{xfe}: -0.483(m/s)
V_{yfe}: -0.804(m/s)
V_{zfe}: -0.901(m/s)
Ψ_{fe}: -36.6°
depth: 1.95(m)

Mine Shape

Parameters (60/12-2789)

d: 0.04(m)
L: 0.121(m)
m: 0.254(m)
J_1: 2.71e-005(kg*m^2)
J_2: 0.000321(kg*m^2)
J_3: 0.000321(kg*m^2)
χ: 0.005307(m)

Final Model

Parameters (60/12-2789)

time: 1.4(s)
xy_{fm}: 0.275(m)
V_{xfm}: 0.0393(m/s)
V_{yfm}: -0.00442(m/s)
V_{zfm}: -1.37(m/s)
Ψ_{fm}: 92.58°
depth: 1.95(m)

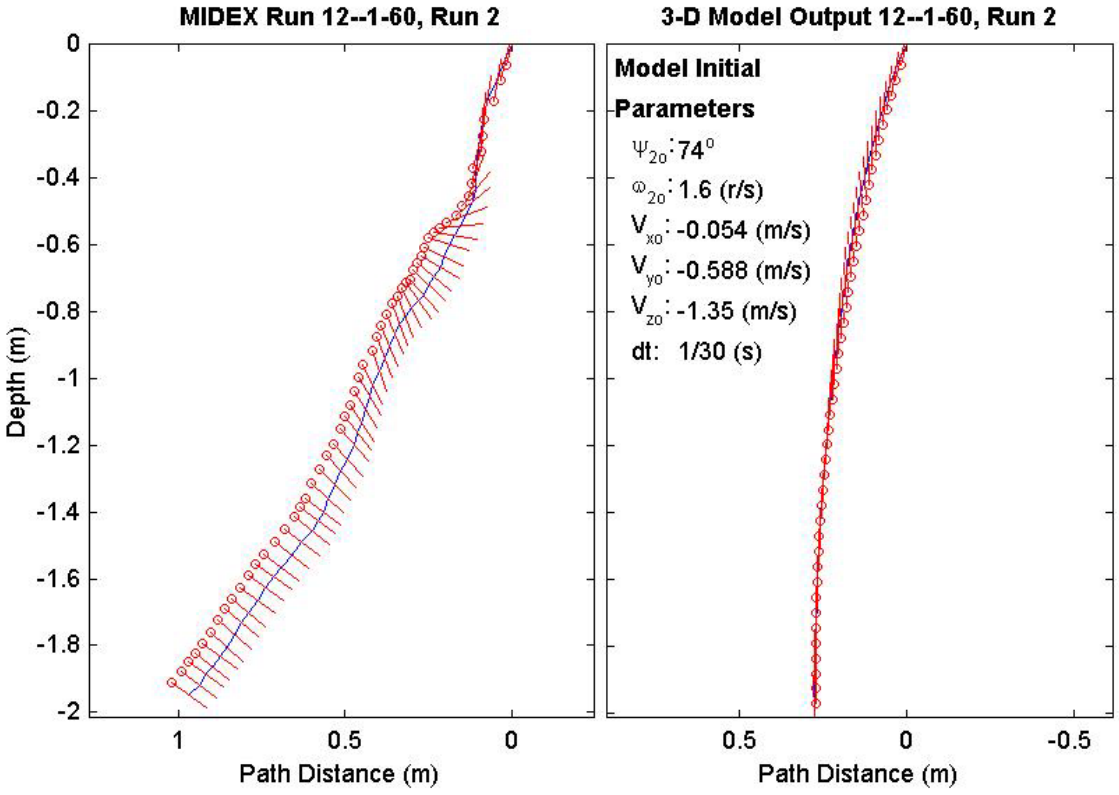

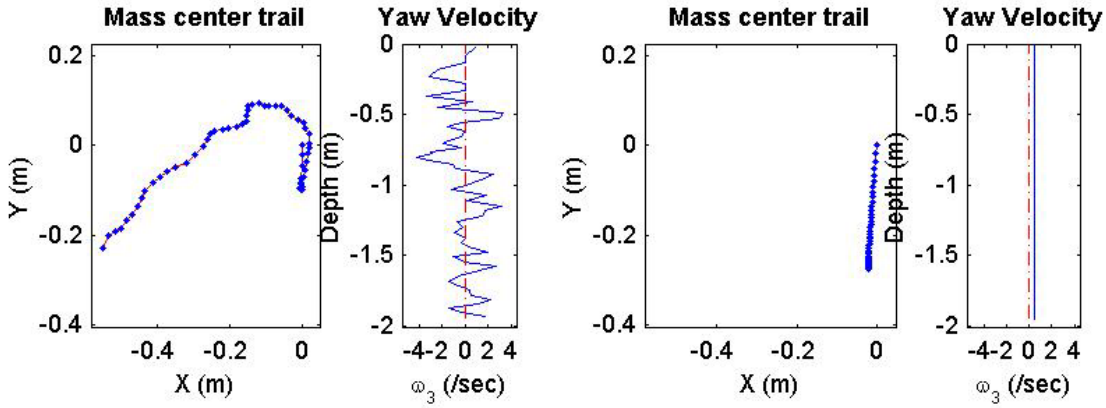

Final Drop
Parameters (60/9-3810)

time: 2.27(s)
xy_{fe}: 0.296(m)
V_{xfe}: -0.162(m/s)
V_{yfe}: 0.108(m/s)
V_{zfe}: -0.696(m/s)
Ψ_{fe}: -35.5°
depth: 2.16(m)

Mine Shape
Parameters (60/9-3810)

d: 0.04(m)
L: 0.0912(m)
m: 0.215(m)
J_1: 2.35e-005(kg*m^2)
J_2: 0.000158(kg*m^2)
J_3: 0.000158(kg*m^2)
χ: -0.002911(m)

Final Model
Parameters (60/9-3810)

time: 1.53(s)
xy_{fm}: 0.195(m)
V_{xfm}: 0.0804(m/s)
V_{yfm}: 0.00761(m/s)
V_{zfm}: -1.44(m/s)
Ψ_{fm}: -81.6°
depth: 2.17(m)

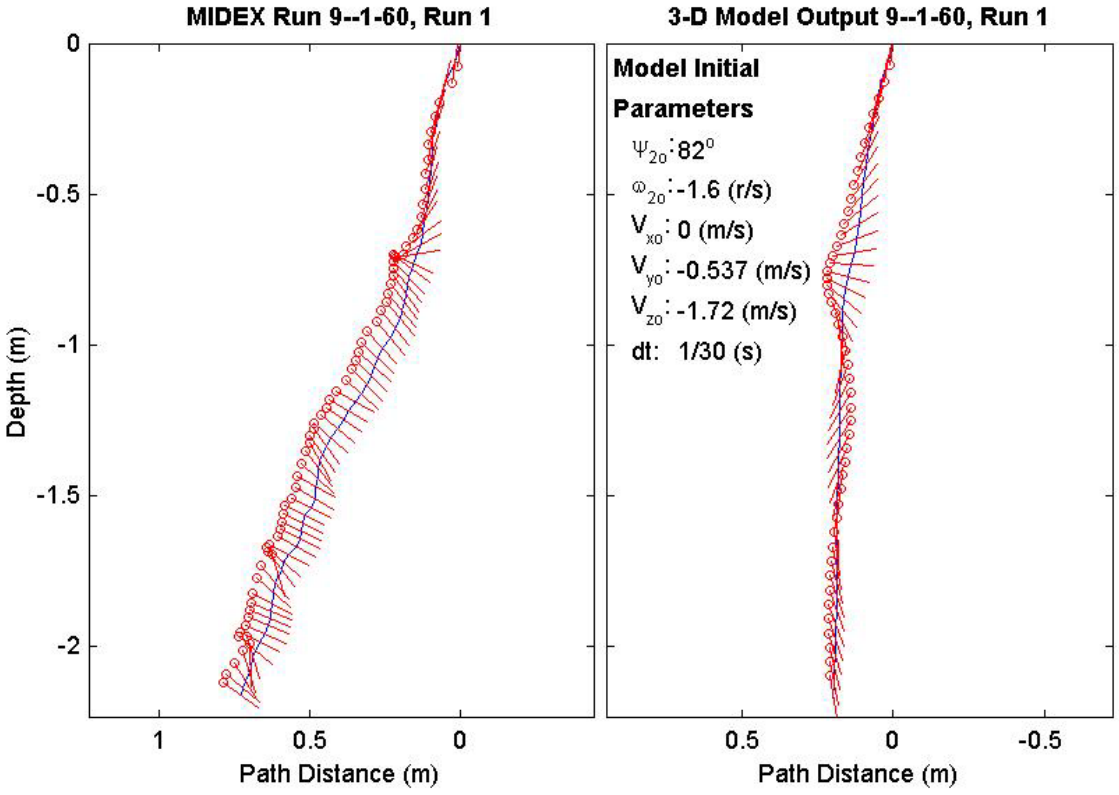

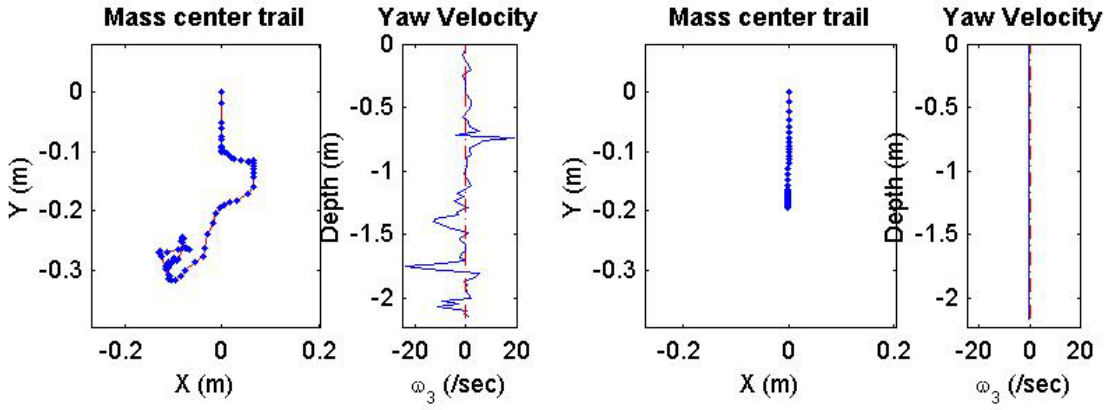

Final Drop

Parameters (60/9-2942)

time: 2.27(s)
xy_{fe}: 0.182(m)
V_{xfe}: -0.105(m/s)
V_{yfe}: 0(m/s)
V_{zfe}: -0.936(m/s)
Ψ_{fe}: -31.9°
depth: 2.22(m)

Mine Shape

Parameters (60/9-2942)

d: 0.04(m)
L: 0.0912(m)
m: 0.215(m)
J_1: 2.35e-005(kg*m^2)
J_2: 0.000158(kg*m^2)
J_3: 0.000158(kg*m^2)
χ: 0.002911(m)

Final Model

Parameters (60/9-2942)

time: 1.53(s)
xy_{fm}: 0.247(m)
V_{xfm}: -0.0308(m/s)
V_{yfm}: -0.00398(m/s)
V_{zfm}: -1.39(m/s)
Ψ_{fm}: 91.33°
depth: 2.24(m)

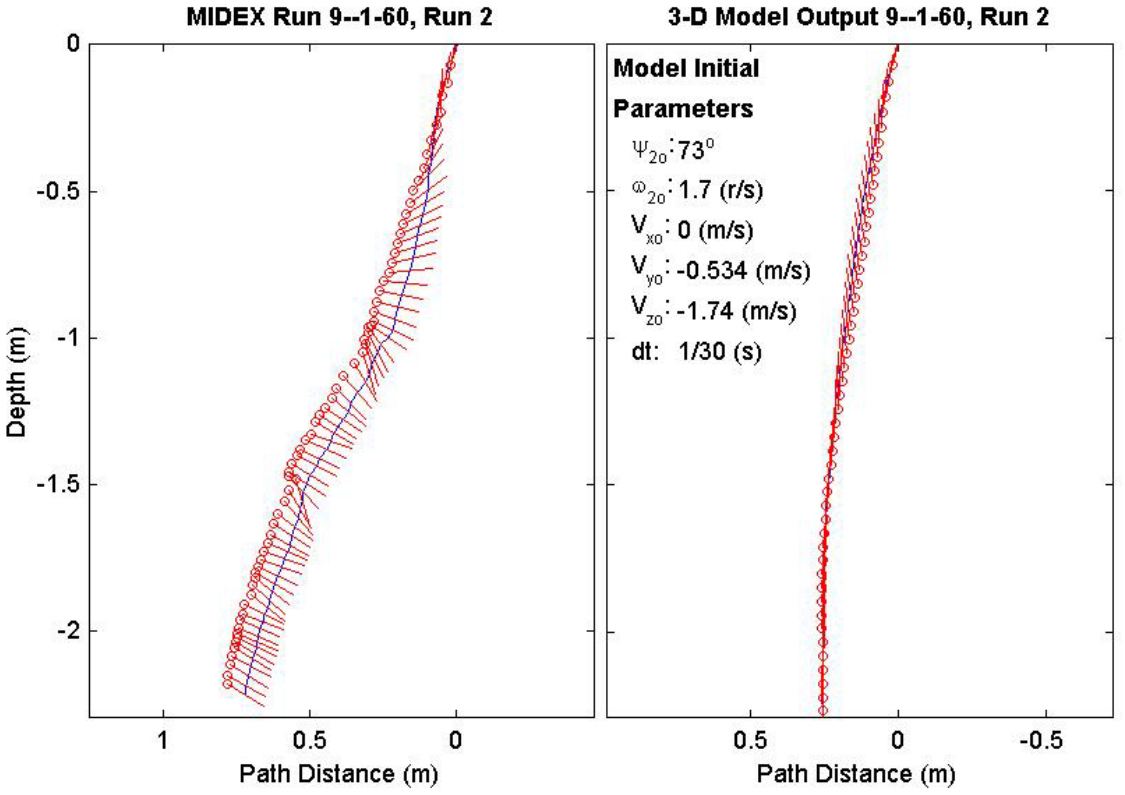

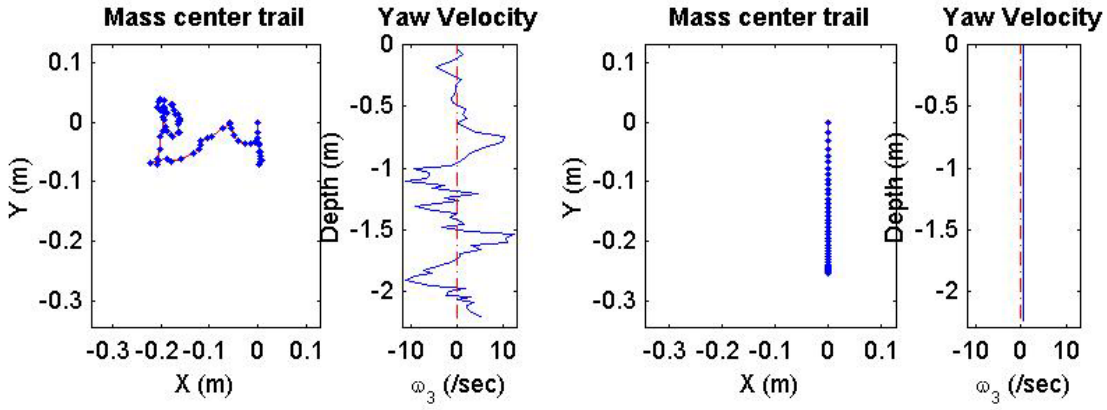

Final Drop Parameters (30/15-2390)

time: 1.53(s)
xy_{fe}: 0.437(m)
V_{xfe}: 0(m/s)
V_{yfe}: 0.108(m/s)
V_{zfe}: -1.58(m/s)
Ψ_{fe}: -87.9°
depth: 2.14(m)

Mine Shape Parameters (30/15-2390)

d: 0.04(m)
L: 0.152(m)
m: 0.323(m)
J_1: 3.3e-005(kg*m^2)
J_2: 0.000623(kg*m^2)
J_3: 0.000623(kg*m^2)
χ: -0.01477(m)

Final Model Parameters (30/15-2390)

time: 1.6(s)
xy_{fm}: 0.549(m)
V_{xfm}: 0.014(m/s)
V_{yfm}: -2.13e-019(m/s)
V_{zfm}: -1.53(m/s)
Ψ_{fm}: -78.57°
depth: 2.19(m)

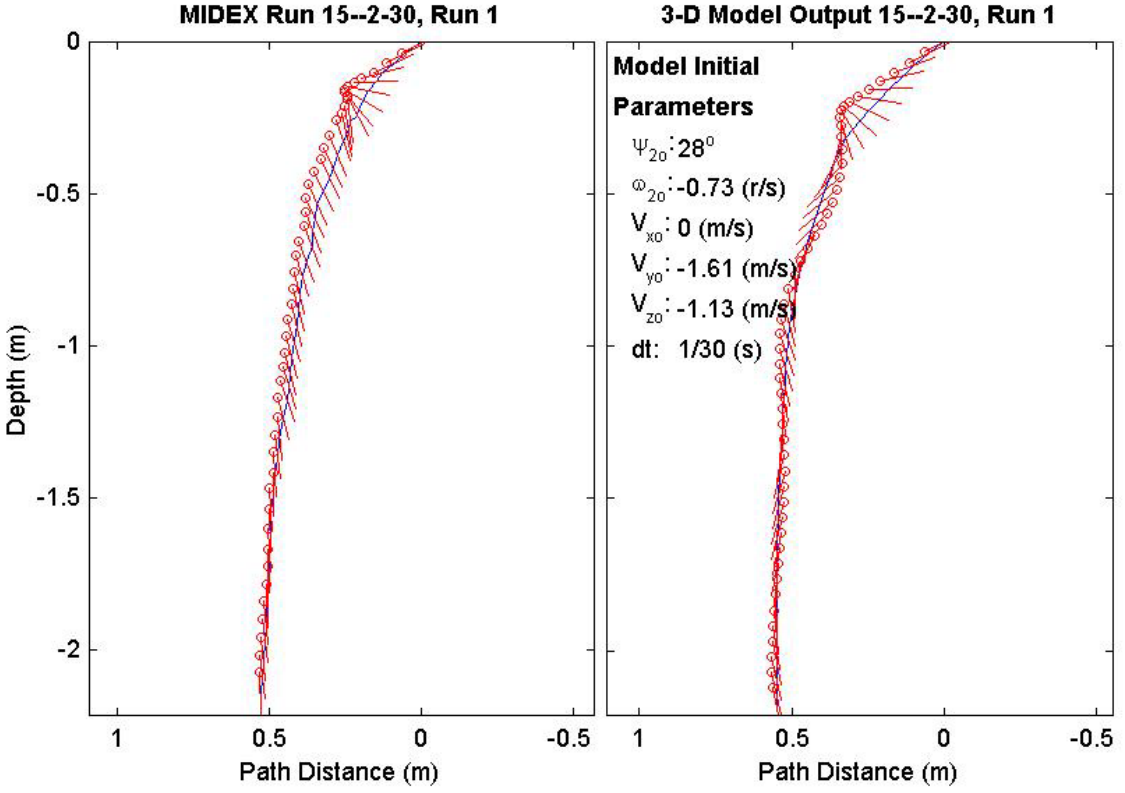

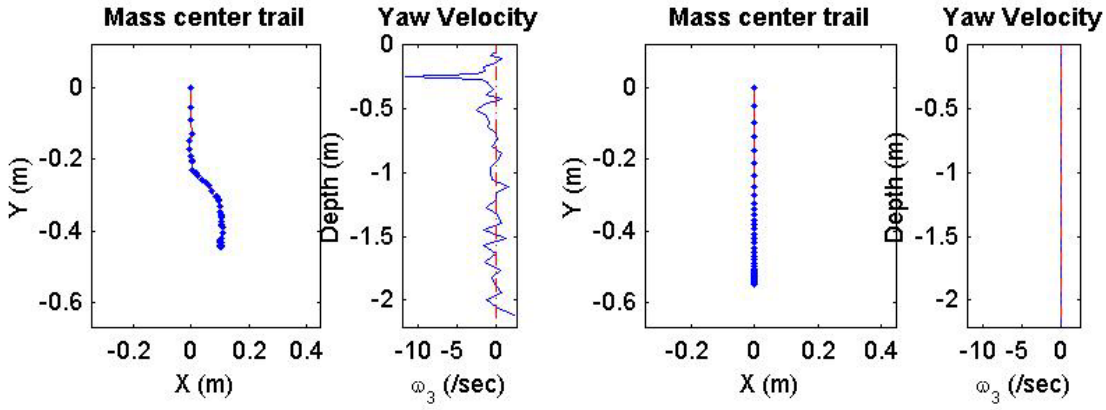

Final Drop

Parameters (30/15-1553)

time: 1.5(s)
xy_{fe}: 0.367(m)
V_{xfe}: 0(m/s)
V_{yfe}: 0(m/s)
V_{zfe}: -1.82(m/s)
Ψ_{fe}: -90°
depth: 2.13(m)

Mine Shape

Parameters (30/15-1553)

d: 0.04(m)
L: 0.152(m)
m: 0.323(m)
J_1: 3.3e-005(kg*m^2)
J_2: 0.000623(kg*m^2)
J_3: 0.000623(kg*m^2)
χ: 0.01477(m)

Final Model

Parameters (30/15-1553)

time: 1.53(s)
xy_{fm}: 0.349(m)
V_{xfm}: 0.0259(m/s)
V_{yfm}: -0.0534(m/s)
V_{zfm}: -1.53(m/s)
Ψ_{fm}: 90.91°
depth: 2.15(m)

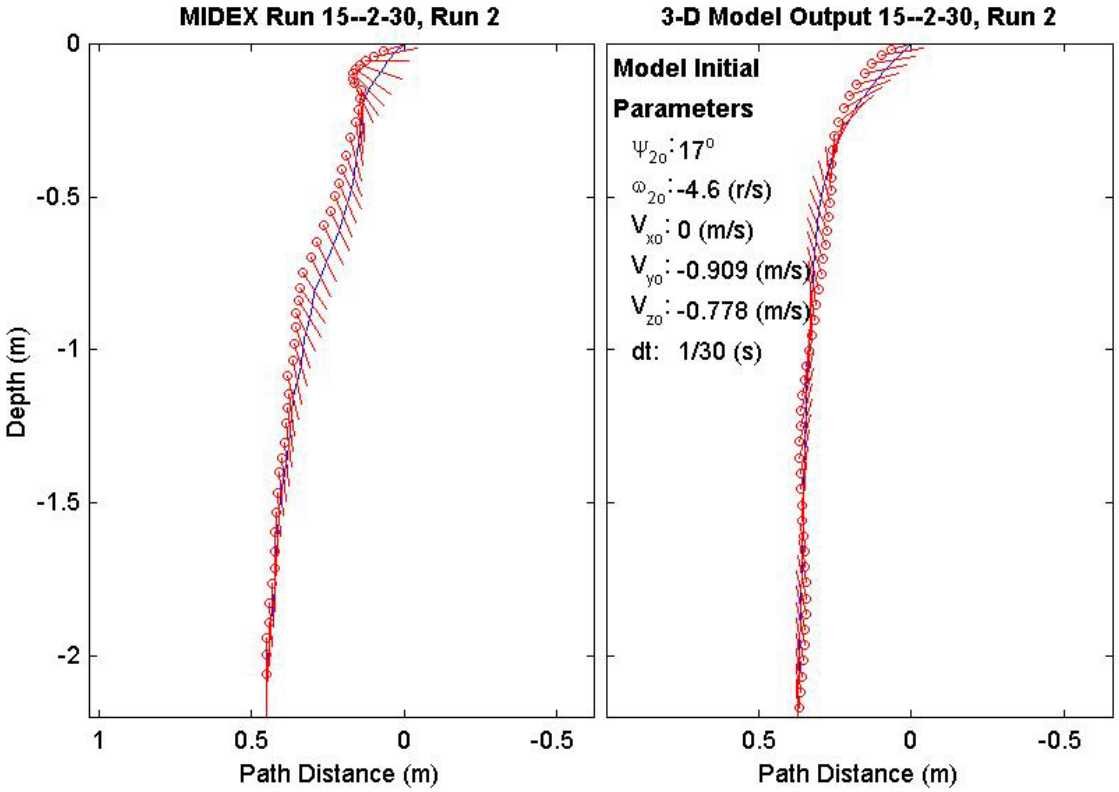

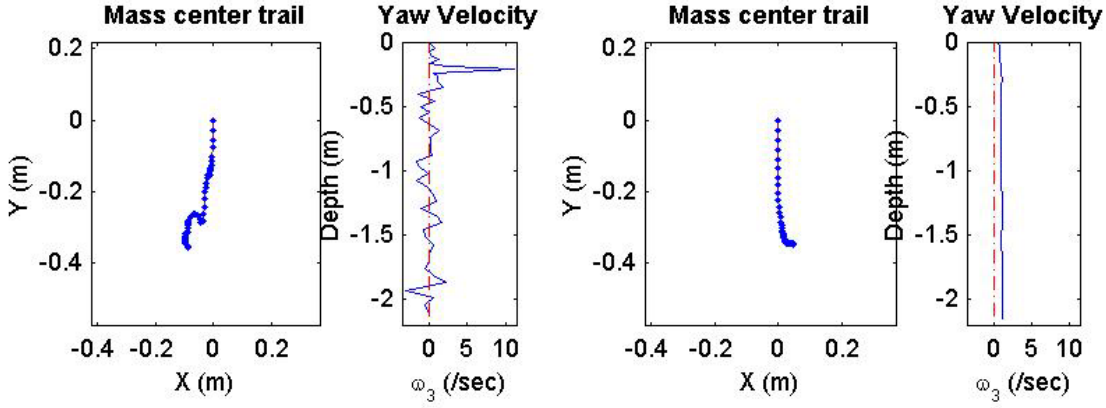

Final Drop

Parameters (30/12-2507)

time: 1.73(s)
xy_{fe}: 0.416(m)
V_{xfe}: 0.054(m/s)
V_{yfe}: 0(m/s)
V_{zfe}: -1.58(m/s)
Ψ_{fe}: -80.6°
depth: 2.19(m)

Mine Shape

Parameters (30/12-2507)

d: 0.04(m)
L: 0.121(m)
m: 0.254(m)
J_1: 2.71e-005(kg*m^2)
J_2: 0.000331(kg*m^2)
J_3: 0.000331(kg*m^2)
χ: -0.00997(m)

Final Model

Parameters (30/12-2507)

time: 1.73(s)
xy_{fm}: 0.461(m)
V_{xfm}: 0.0502(m/s)
V_{yfm}: -0.0086(m/s)
V_{zfm}: -1.39(m/s)
Ψ_{fm}: -91.43°
depth: 2.22(m)

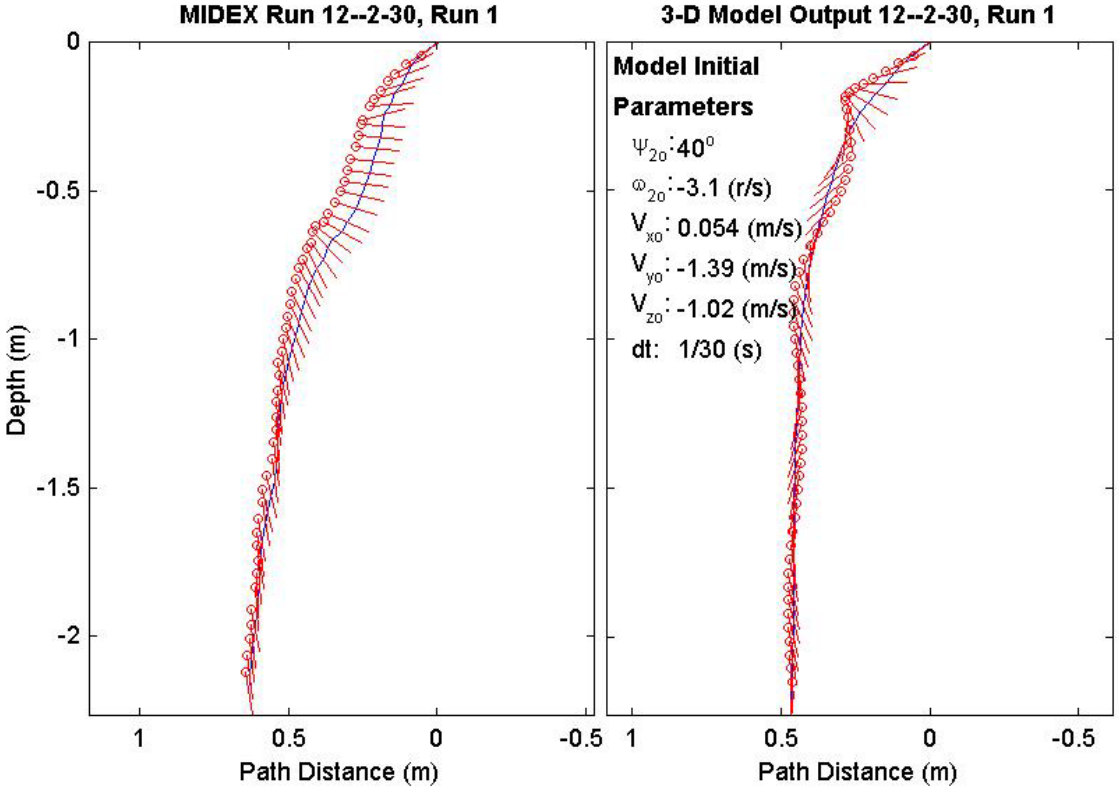

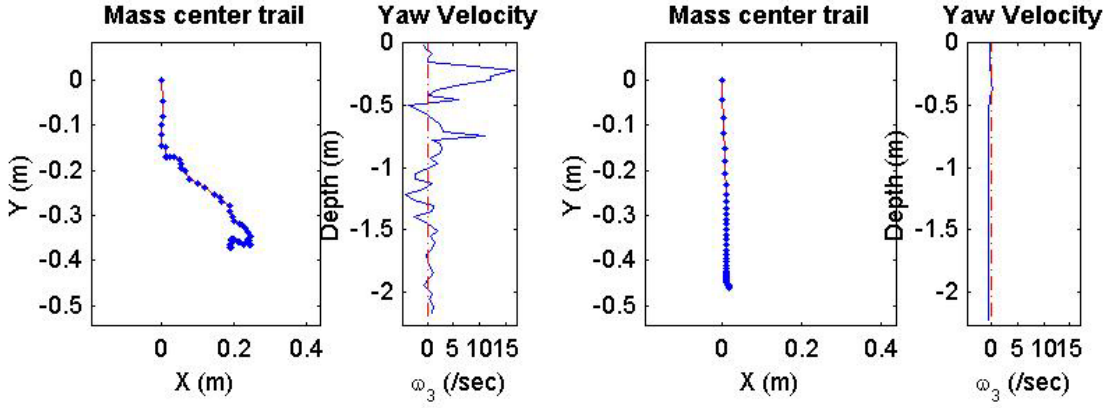

Final Drop Parameters (30/12-1278)

time: 1.73(s)
xy_{fe}: 0.55(m)
V_{xfe}: 0(m/s)
V_{yfe}: -0.162(m/s)
V_{zfe}: -1.45(m/s)
Ψ_{fe}: -88°
depth: 2.09(m)

Mine Shape Parameters (30/12-1278)

d: 0.04(m)
L: 0.121(m)
m: 0.254(m)
J_1: 2.71e-005(kg*m^2)
J_2: 0.000331(kg*m^2)
J_3: 0.000331(kg*m^2)
χ: 0.00997(m)

Final Model Parameters (30/12-1278)

time: 1.63(s)
xy_{fm}: 0.287(m)
V_{xfm}: 0.0425(m/s)
V_{yfm}: -0.00983(m/s)
V_{zfm}: -1.38(m/s)
Ψ_{fm}: 85.27°
depth: 2.11(m)

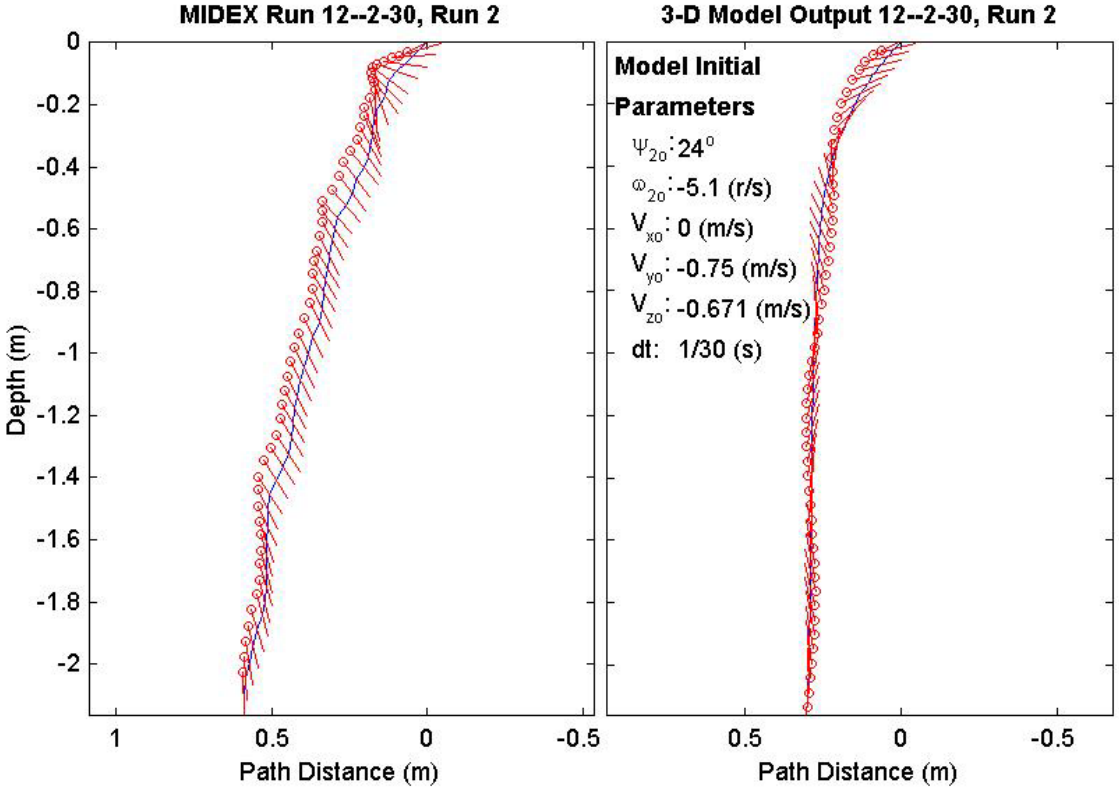

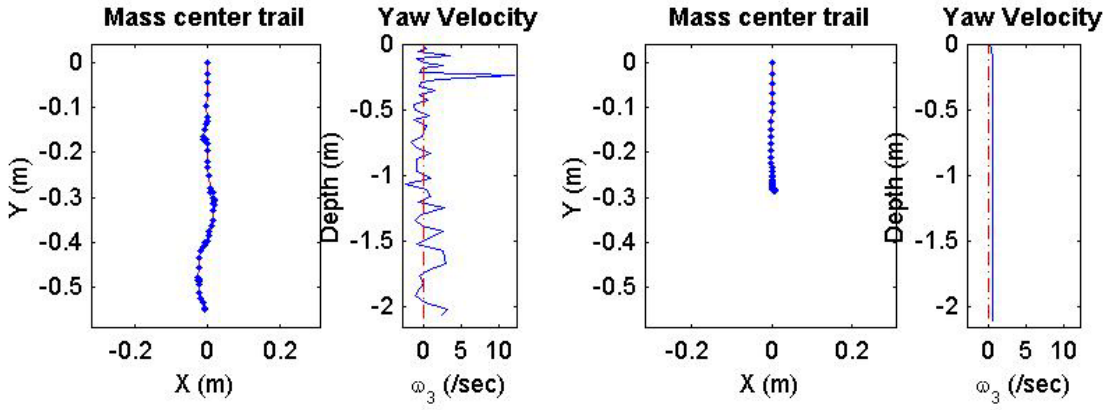

Final Drop
Parameters (30/9-2294)

time:	1.83(s)
xy_{fe}:	0.29(m)
V_{xfe}:	0(m/s)
V_{yfe}:	0.642(m/s)
V_{zfe}:	-1.21(m/s)
Ψ_{fe}:	9.8°
depth:	2.22(m)

Mine Shape
Parameters (30/9-2294)

d:	0.04(m)
L:	0.0912(m)
m:	0.215(m)
J_1:	2.35e-005(kg*m^2)
J_2:	0.000156(kg*m^2)
J_3:	0.000156(kg*m^2)
χ:	-0.005796(m)

Final Model
Parameters (30/9-2294)

time:	1.63(s)
xy_{fm}:	0.293(m)
V_{xfm}:	0.0386(m/s)
V_{yfm}:	-2.02e-018(m/s)
V_{zfm}:	-1.43(m/s)
Ψ_{fm}:	-76.47°
depth:	2.25(m)

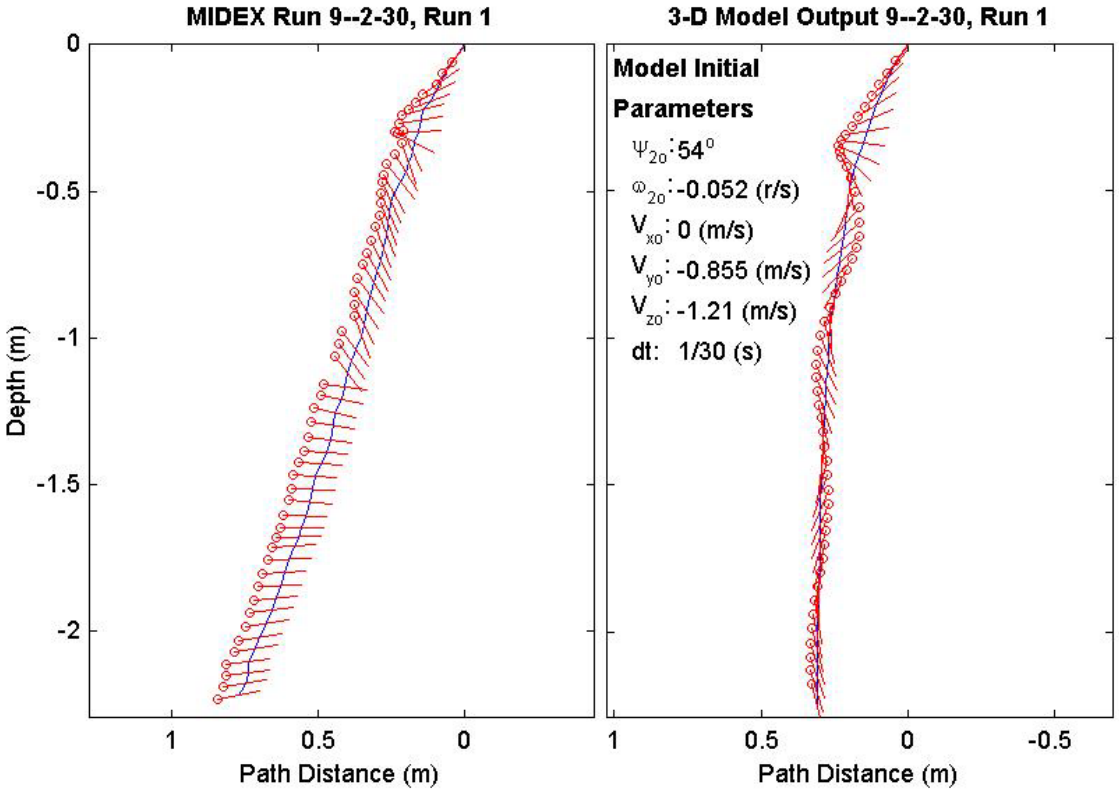

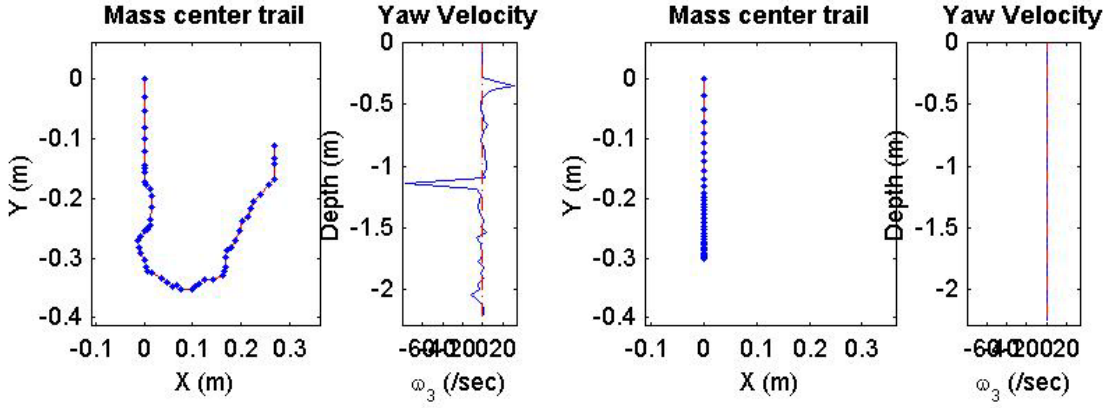

Final Drop

Parameters (30/9-1415)

time: 1.8(s)
xy_{fe}: 0.0471(m)
V_{xfe}: 0.321(m/s)
V_{yfe}: 0.108(m/s)
V_{zfe}: -1.26(m/s)
Ψ_{fe}: -78.2°
depth: 2.25(m)

Mine Shape

Parameters (30/9-1415)

d: 0.04(m)
L: 0.0912(m)
m: 0.215(m)
J_1: 2.35e-005(kg*m^2)
J_2: 0.000156(kg*m^2)
J_3: 0.000156(kg*m^2)
χ: 0.005796(m)

Final Model

Parameters (30/9-1415)

time: 1.63(s)
xy_{fm}: 0.292(m)
V_{xfm}: 0.0421(m/s)
V_{yfm}: -0.00563(m/s)
V_{zfm}: -1.41(m/s)
Ψ_{fm}: 91.12°
depth: 2.26(m)

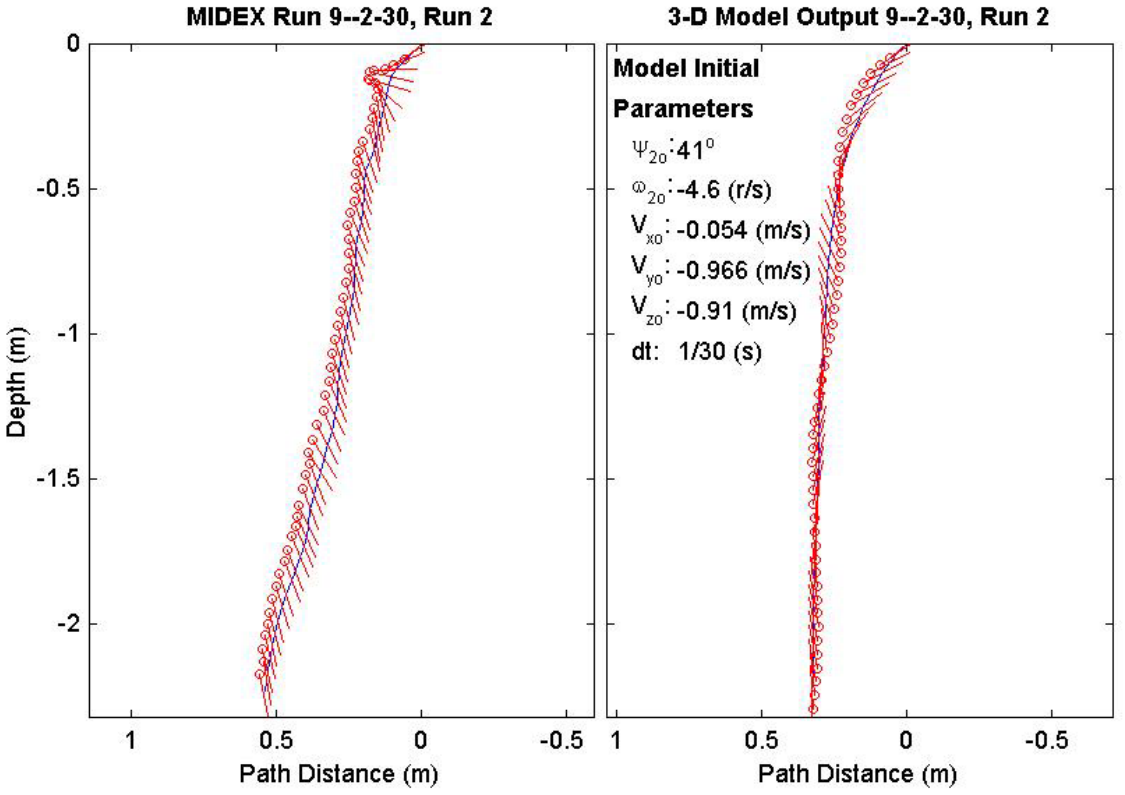

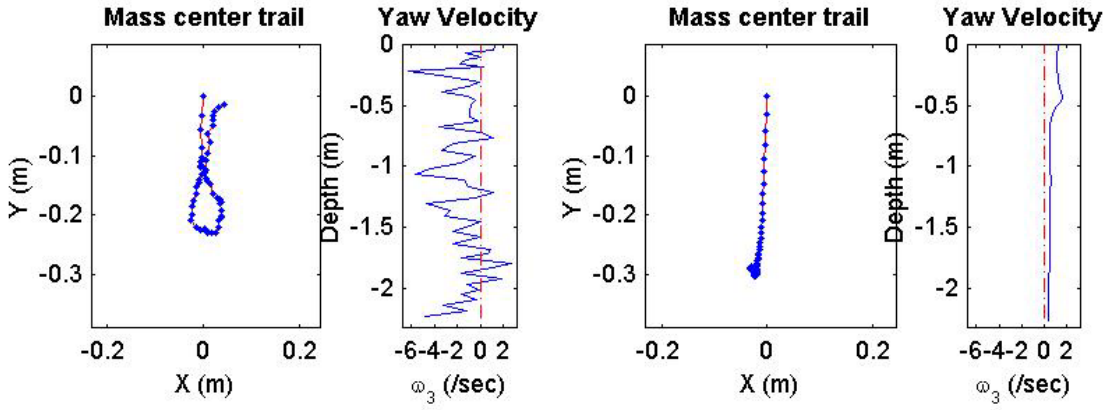

Final Drop

Parameters (45/15-2874)

time: 1.53(s)
xy_{fe}: 0.612(m)
V_{xfe}: 0.051(m/s)
V_{yfe}: 0.055(m/s)
V_{zfe}: -2.46(m/s)
Ψ_{fe}: -88.6°
depth: 2.12(m)

Mine Shape

Parameters (45/15-2874)

d: 0.04(m)
L: 0.152(m)
m: 0.323(m)
J_1: 3.3e-005(kg*m^2)
J_2: 0.000623(kg*m^2)
J_3: 0.000623(kg*m^2)
χ: -0.01477(m)

Final Model

Parameters (45/15-2874)

time: 1.5(s)
xy_{fm}: 0.366(m)
V_{xfm}: -0.0101(m/s)
V_{yfm}: 7.08e-019(m/s)
V_{zfm}: -1.53(m/s)
Ψ_{fm}: -85.12°
depth: 2.15(m)

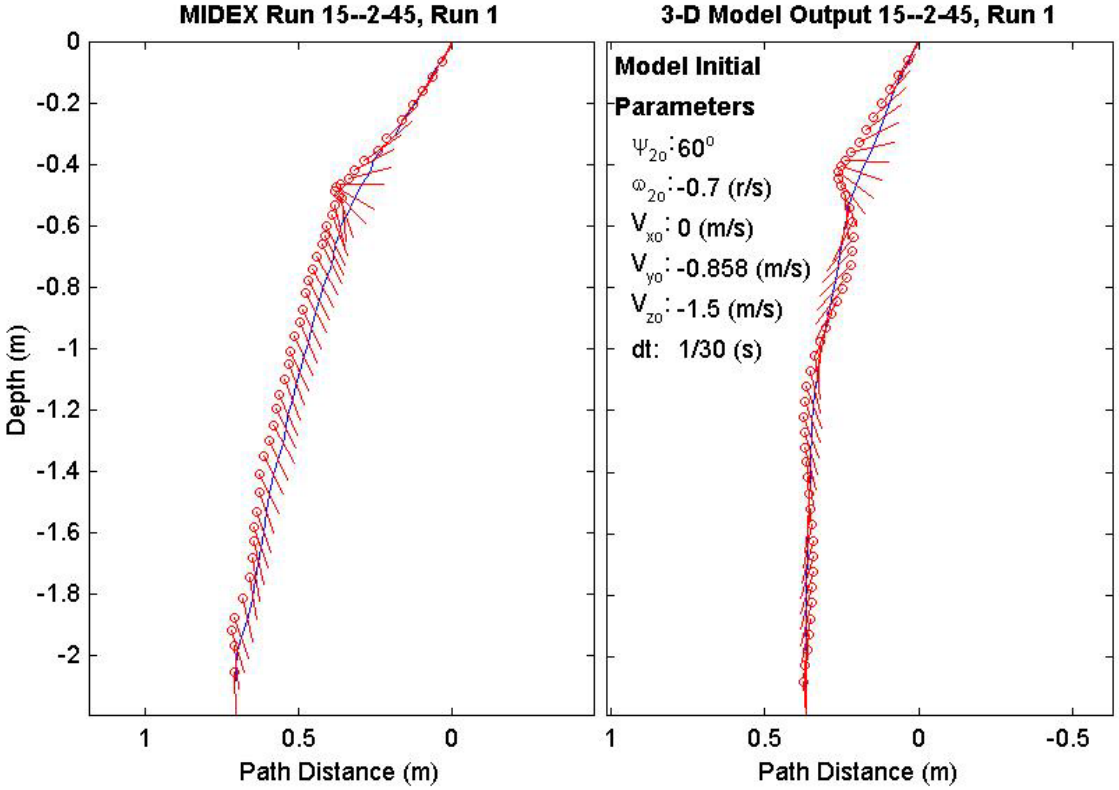

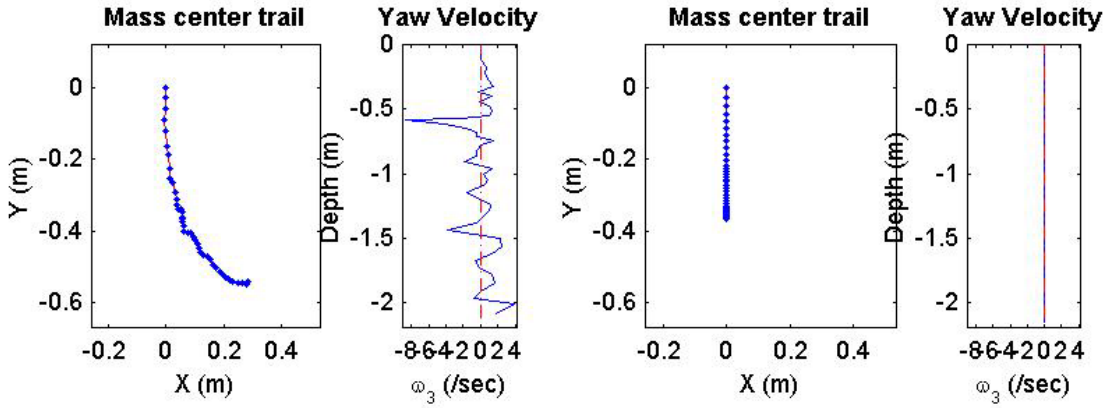

Final Drop
Parameters (45/15-2332)

time: 1.57(s)
xy_{fe}: 0.373(m)
V_{xfe}: 0.108(m/s)
V_{yfe}: 0.055(m/s)
V_{zfe}: -1.42(m/s)
Ψ_{fe}: -86.8°
depth: 2.17(m)

Mine Shape
Parameters (45/15-2332)

d: 0.04(m)
L: 0.152(m)
m: 0.323(m)
J_1: 3.3e-005(kg*m^2)
J_2: 0.000623(kg*m^2)
J_3: 0.000623(kg*m^2)
χ: 0.01477(m)

Final Model
Parameters (45/15-2332)

time: 1.43(s)
xy_{fm}: 0.372(m)
V_{xfm}: 0.0415(m/s)
V_{yfm}: 0.00695(m/s)
V_{zfm}: -1.53(m/s)
Ψ_{fm}: 91.86°
depth: 2.18(m)

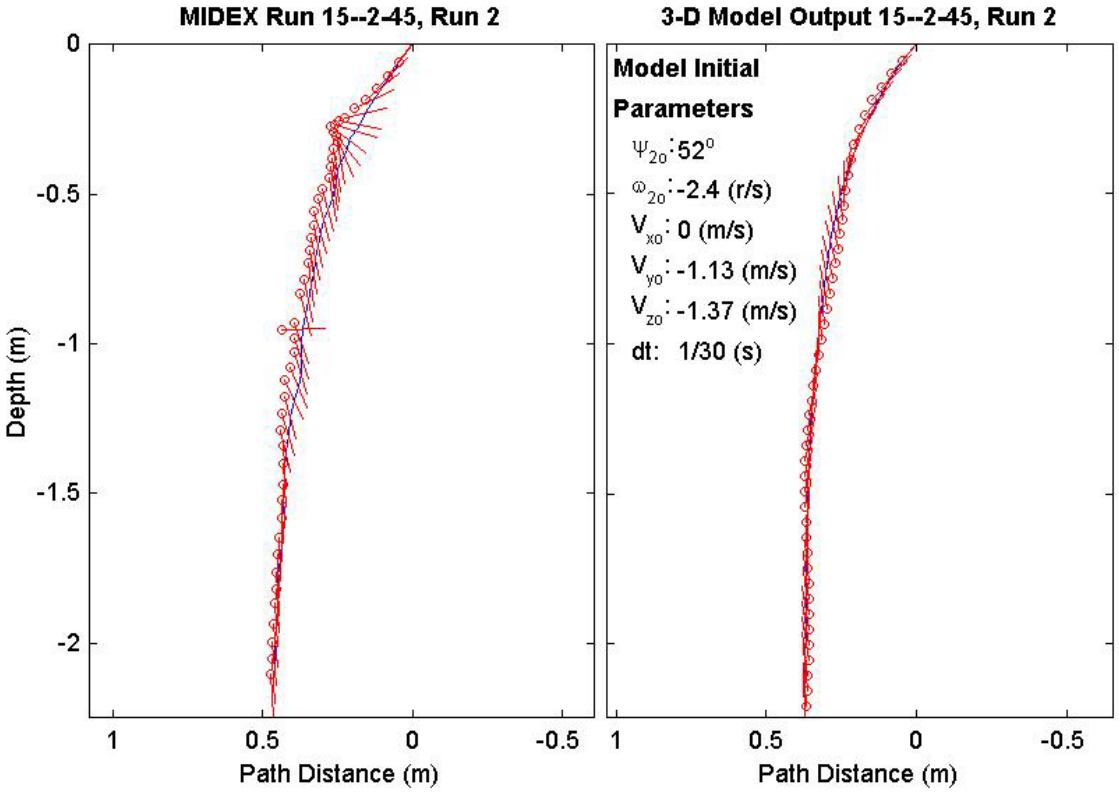

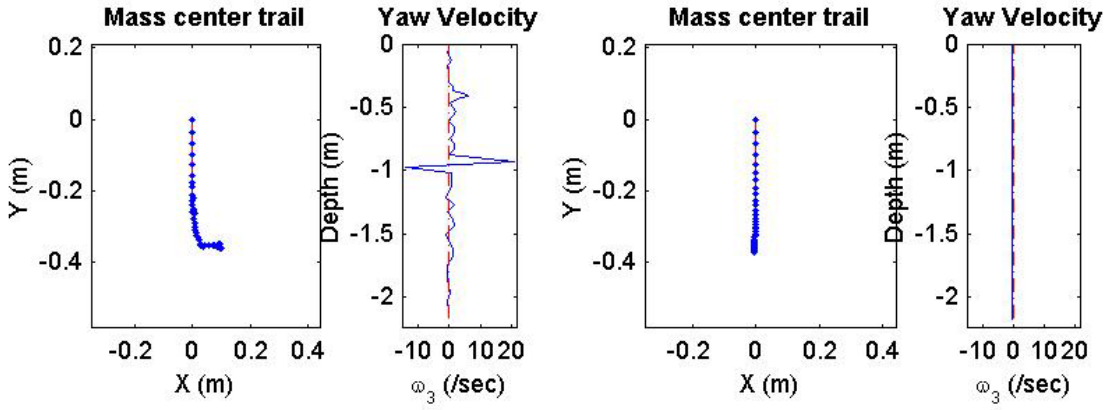

Final Drop

Parameters (45/12-2977)

time: 1.6(s)
xy_{fe}: 0.55(m)
V_{xfe}: -0.051(m/s)
V_{yfe}: 0.108(m/s)
V_{zfe}: -1.37(m/s)
Ψ_{fe}: -84.8°
depth: 2.03(m)

Mine Shape

Parameters (45/12-2977)

d: 0.04(m)
L: 0.121(m)
m: 0.254(m)
J_1: 2.71e-005(kg*m^2)
J_2: 0.000331(kg*m^2)
J_3: 0.000331(kg*m^2)
χ: -0.00997(m)

Final Model

Parameters (45/12-2977)

time: 1.53(s)
xy_{fm}: 0.329(m)
V_{xfm}: -0.014(m/s)
V_{yfm}: 1.32e-018(m/s)
V_{zfm}: -1.38(m/s)
Ψ_{fm}: -78.58°
depth: 2.07(m)

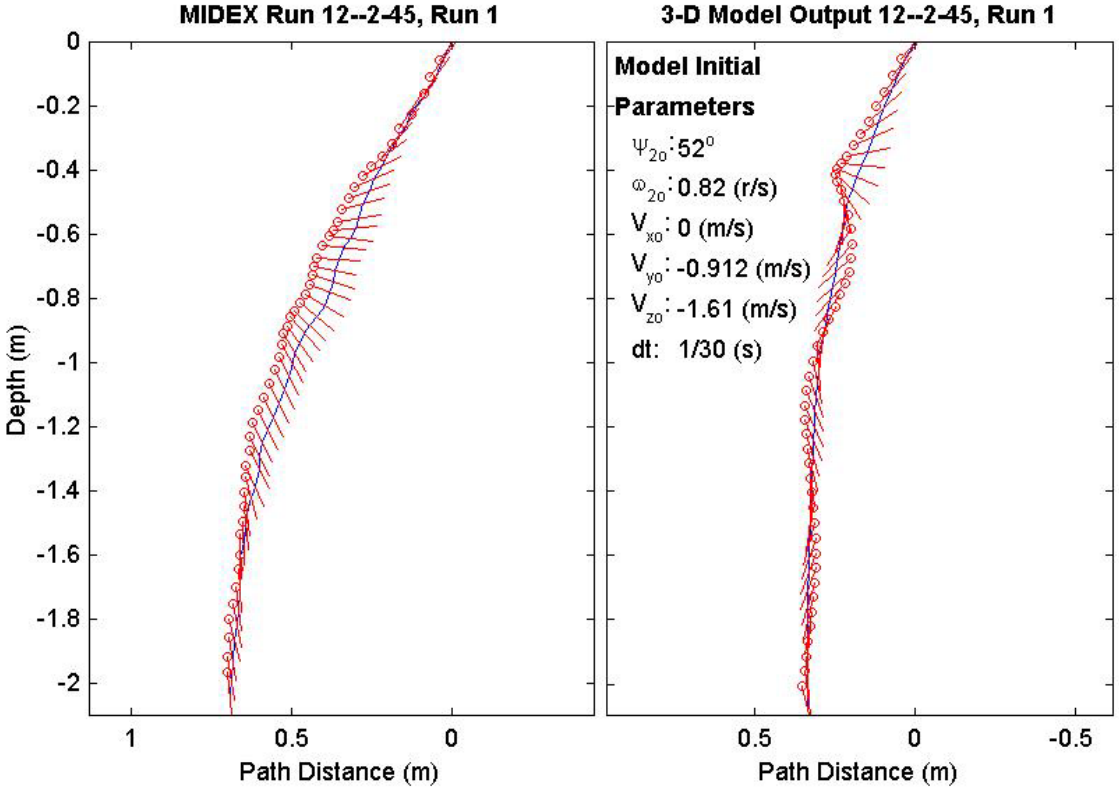

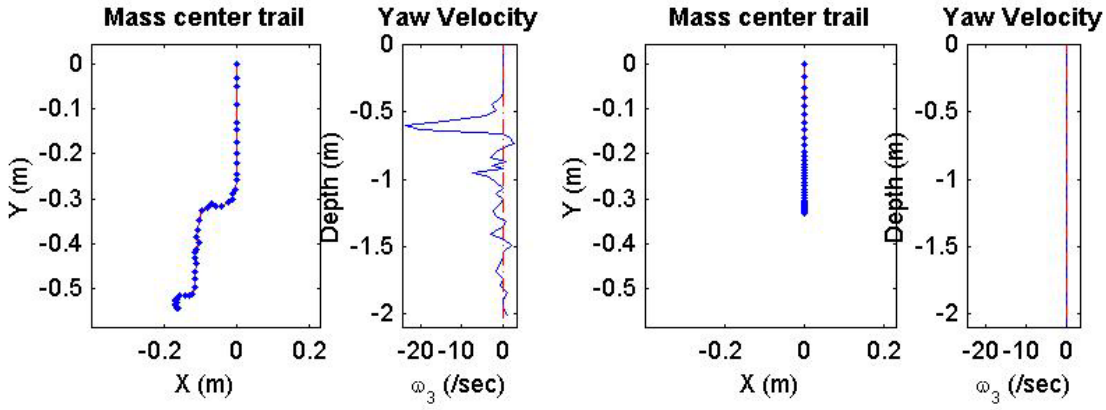

Final Drop
Parameters (45/12-1996)

time: 1.7(s)
xy_{fe}: 0.304(m)
V_{xfe}: 0.051(m/s)
V_{yfe}: -0.108(m/s)
V_{zfe}: -1.23(m/s)
Ψ_{fe}: -78.4°
depth: 2.17(m)

Mine Shape
Parameters (45/12-1996)

d: 0.04(m)
L: 0.121(m)
m: 0.254(m)
J_1: 2.71e-005(kg*m^2)
J_2: 0.000331(kg*m^2)
J_3: 0.000331(kg*m^2)
χ: 0.00997(m)

Final Model
Parameters (45/12-1996)

time: 1.57(s)
xy_{fm}: 0.345(m)
V_{xfm}: 0.0283(m/s)
V_{yfm}: -2.15e-018(m/s)
V_{zfm}: -1.37(m/s)
Ψ_{fm}: 82.49°
depth: 2.21(m)

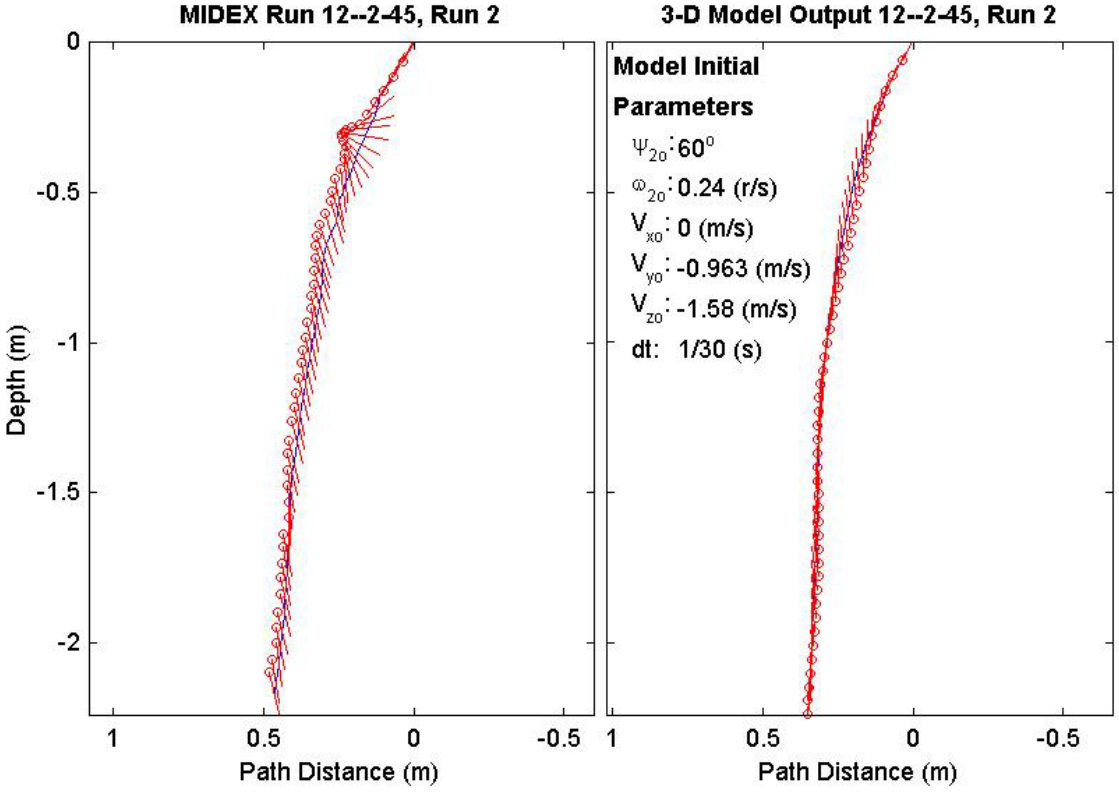

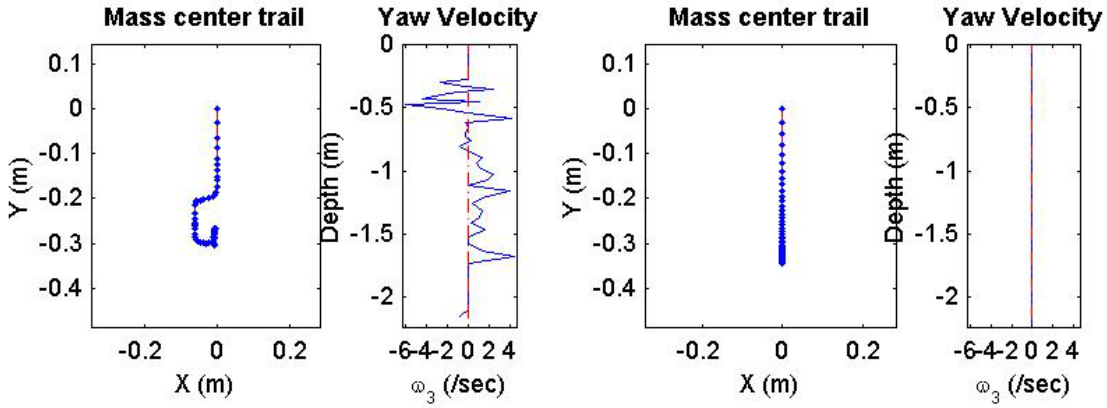

Final Drop

Parameters (45/9-2895)

time: 1.8(s)
xy_{fe}: 0.191(m)
V_{xfe}: 0.054(m/s)
V_{yfe}: 0.105(m/s)
V_{zfe}: -1.23(m/s)
Ψ_{fe}: -63.4°
depth: 2.21(m)

Mine Shape

Parameters (45/9-2895)

d: 0.04(m)
L: 0.0912(m)
m: 0.215(m)
J_1: 2.35e-005(kg*m^2)
J_2: 0.000156(kg*m^2)
J_3: 0.000156(kg*m^2)
χ: -0.005796(m)

Final Model

Parameters (45/9-2895)

time: 1.57(s)
xy_{fm}: 0.268(m)
V_{xfm}: -0.095(m/s)
V_{yfm}: 0.162(m/s)
V_{zfm}: -1.39(m/s)
Ψ_{fm}: -81.29°
depth: 2.22(m)

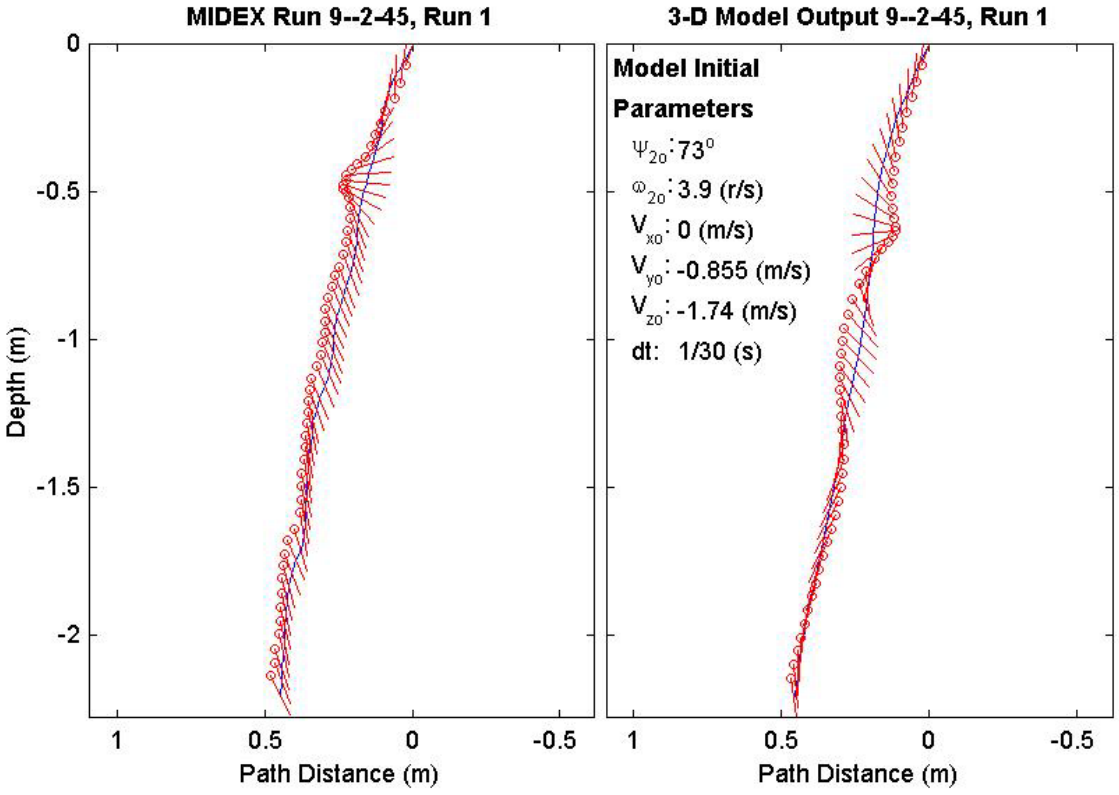

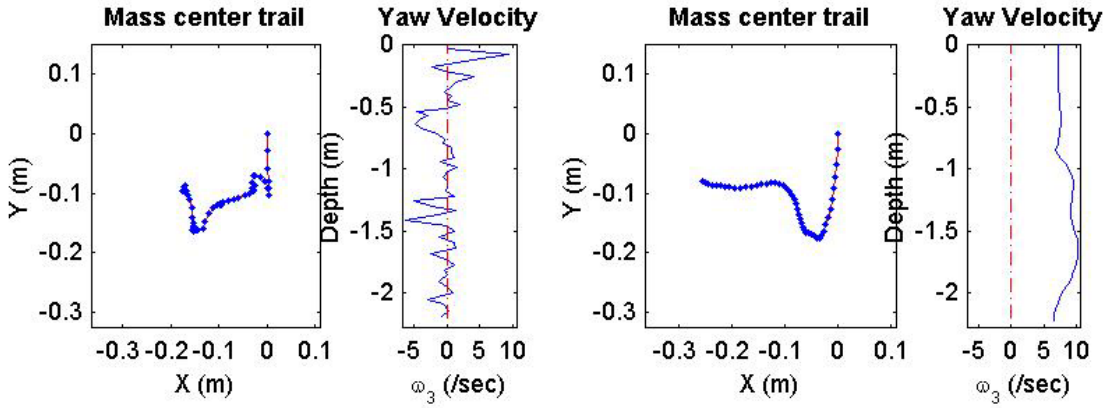

Final Drop

Parameters (45/9-2271)

time: 1.77(s)
xy_{fe}: 0.141(m)
V_{xfe}: 0.588(m/s)
V_{yfe}: 0.375(m/s)
V_{zfe}: -0.964(m/s)
Ψ_{fe}: -51.7°
depth: 2.1(m)

Mine Shape

Parameters (45/9-2271)

d: 0.04(m)
L: 0.0912(m)
m: 0.215(m)
J_1: 2.35e-005(kg*m^2)
J_2: 0.000156(kg*m^2)
J_3: 0.000156(kg*m^2)
χ: 0.005796(m)

Final Model

Parameters (45/9-2271)

time: 1.5(s)
xy_{fm}: 0.232(m)
V_{xfm}: 0.053(m/s)
V_{yfm}: 0.00171(m/s)
V_{zfm}: -1.41(m/s)
Ψ_{fm}: 93.92°
depth: 2.14(m)

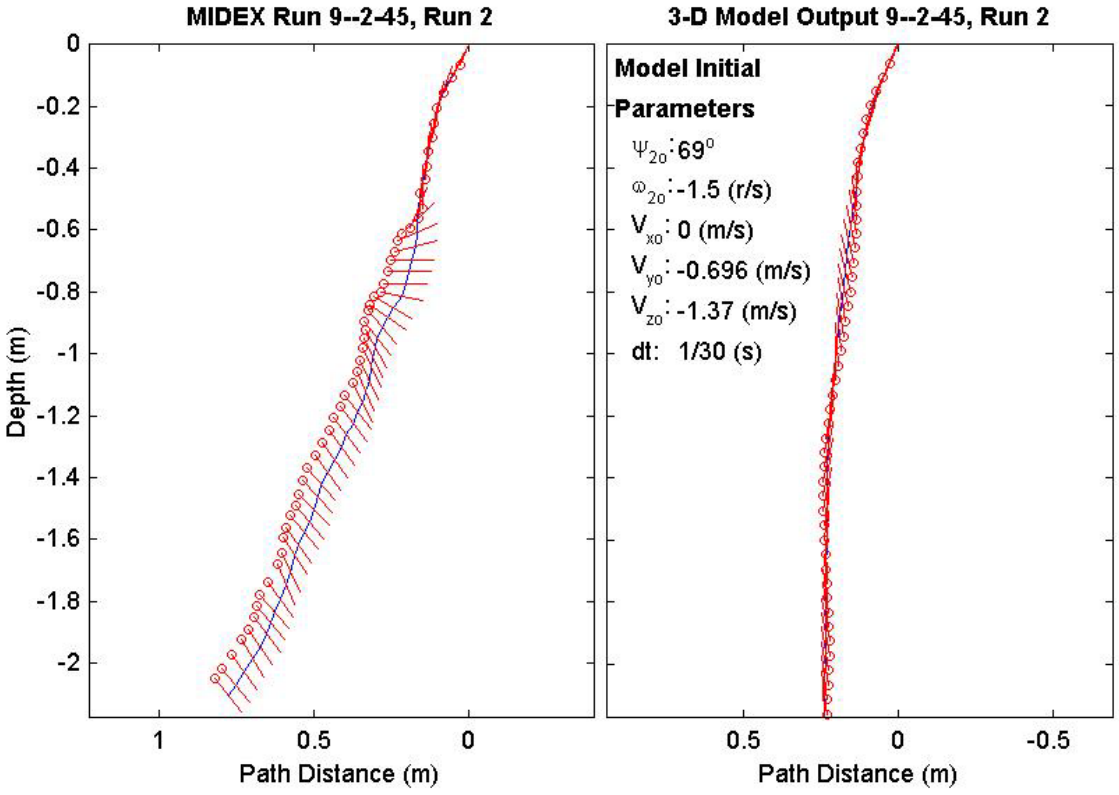

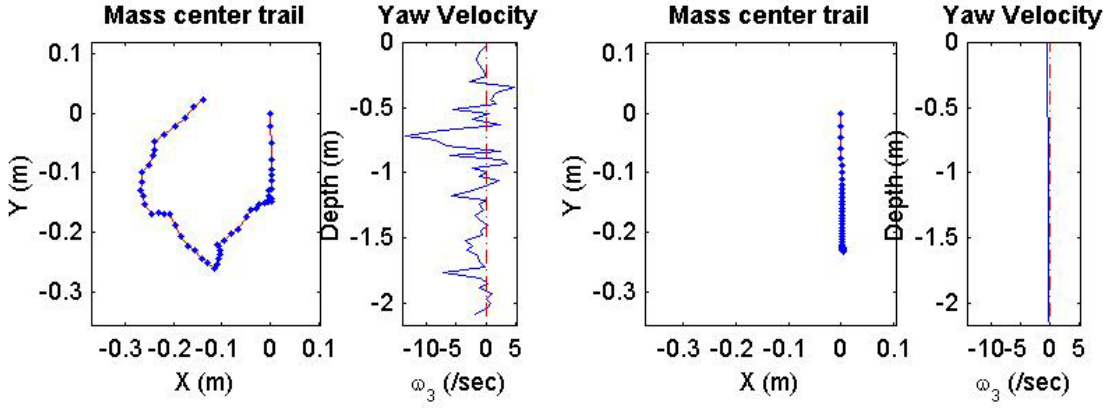

APPENDIX B. MODEL SOURCE CODE

The following subroutines comprise the MATLAB source code for the mine three dimensional Impact Burial Prediction Model. It was developed during May – August 2002 in the Naval Ocean Analysis and Prediction Laboratory (NOAP), Naval Postgraduate School, Monterey CA. These subroutines are called from within the main data retrieval, formatting and presentation code of Appendix C. They return position, angle, linear velocity, and angular velocity vectors and an updated mine body to earth fixed reference frame transformation matrix. Please contact the NOAP lab, Naval Postgraduate School Monterey, CA with questions concerning subroutines and application. The points of contact are Professor Peter C. Chu, chu@nps.navy.mil, or Mr. Chenwu Fan, NPS Oceanographer, fan@nps.navy.mil.

A. SUBROUTINE 1

```
function[Pos,Ang,Vo,Omgm,eRm]=diag1step(m,J,d,L,chi,Pos,Ang,Vo,Omgm,eRm
,dt,rhomn,rhow,Vwater,temp,sea_water,cc);
% function
[Pos,Ang,Vo,Omgm,eRm]=diag1step(m,J,d,L,chi,Pos,Ang,Vo,Omgm,eRm,dt,rhom
n,rhow,Vwater,temp,sea_water,cc);
%
% This main subroutine calls all the other required subroutines to
provide a complete set of solution vectors for each timestep to the
main program.
%
%  inputs:
%  m:   mine mass
%  J:   the moment of inertia of the cylinder J(1:3)
%  d:  mine diameter
%  L:  mine length
%  chi: the distance between volume center and mass center
%  Pos: position of mass center as [xo;yo,zo]
%  Ang: angle position of the mine as [0;fi2;fi3]
%  Vo:  velocity vector of mass center as [u,v,w]
%  Omgm: mine angle velocity base on moving frame as [OMG;omg2;omg3]
%  eRm:  the rotation matrix between earth and moving frame.
```

```
%  dt:   time step
%  rhomn:  mean mine density.
%  rhow: rhow: sea water density (default: 1028)
%  Vwater: sea water velocity (default: [0;0;0] m/s)
%  temp:  water temperature (C)  (default: 20)
%  sea_water:  1-for sea water, 0- not sea water.
%
%  Chenwu Fan,  NOAP,  NPS    7/12/2002
%  Ashley D. Evans, NPS       7/15/2002

if(~exist('rhow')), rhow=1028; Vwater=zeros(3,1); temp=20; sea_water=0;
elseif(~exist('Vwater')), Vwater=zeros(3,1); temp=20; sea_water=0;
elseif(~exist('temp')), temp=20; sea_water=0;
elseif(~exist('sea_water')), sea_water=0; end

if(~exist('cc')), cc=0.1; end

[ABV,ABA]=ODEdiagmtx(m,J,d,L,chi,Ang,Vo,Omgm,eRm,rhomn,rhow,Vwater,temp
,sea_water,cc);

%  solve linear ODE

[Vo,IntV]=ODEdiagsolve(ABV,Vo,dt);
Pos=Pos+IntV;

[Omgm,Intomg]=ODEdiagsolve(ABA,Omgm,dt);

% update eRm
eRm = eRm*ERM(Intomg(2),Intomg(3));

[Ang,eRm] = eRm2ag(eRm,Ang(3));
```

B. SUBROUTINE 2

```
function
[ABV,ABA]=ODEdiagmtx(m,J,d,L,chi,Ang,Vo,Omgm,eRm,rhomn,rhow,Vwater,temp
,sea_water,cc);
% function
[ABV,ABA]=ODEdiagmtx(m,J,d,L,chi,Ang,Vo,Omgm,eRm,rhomn,rhow,Vwater,temp
,sea_water,cc);
%
% This subroutine calculates the forces and moments acting on the solid
body for each time step and returns as outputs, two coefficient
matrices; one for moments and the other for the forces.
%
%  input:
%  m:   mine mass
%  J:   the moment of inertia of the cylinder J(1:3)
%  d:  mine diameter
%  L:  mine length
%  chi: the distance between volume center and mass center
%  Ang: angle position of the mine as [0;fi2;fi3]
%  Vo:  velocity vector of mass center as [u,v,w]
%  Omgm: mine angle velocity base on moving frame as [OMG;omg2;omg3]
%  eRm:  the rotation matrix between earth and moving frame.
%  rhomn:  mean mine density.
```

```
%  rhow: rhow: sea water density (default: 1028)
%  Vwater: sea water velocity (default: [0;0;0] m/s)
%  temp:  water temperature (C)  (default: 20)
%  sea_water:  1-for sea water, 0- not sea water.
%  cc: the maximum non-dimensioal force center gap. cc>=0: added mass
%  output:
%  ABV:  coefficient matrix of V PDE
%  ABA:  coefficient matrix of angle velocity PDE
%        dV/dt = ABV(:,1).*V + ABV(:,2)
%        dOmg/dt = AVA(:,1).*V + ABA(:,2)
%
%  Chenwu Fan,  NOAP,  NPS    7/12/2002
%  Ashley D. Evans, NPS,      7/18/2002

% global cdtb;

if(~exist('rhow')), rhow=1028; Vwater=zeros(3,1); temp=20; sea_water=0;
elseif(~exist('Vwater')), Vwater=zeros(3,1); temp=20; sea_water=0;
elseif(~exist('temp')), temp=20; sea_water=0;
elseif(~exist('sea_water')), sea_water=0; end

g=9.806; idig=[1,5,9]';

V=Vwater-Vo;       % relative water velocity

[eRd,v1,v2]=ERD(eRm,V);   % rotation matrix from drag to earth frame.
mRd=eRm'*eRd;      % rotation matrix from drag to moving frame.

Omgd=mRd'*Omgm;    % drag frame angle velocity.

%  define the end Layer flow coerrect fact
%  if(v2==0), fact=0; else, fact=1-exp(-abs(v1/v2)); end

if(~exist('cc')), cc = 0.05; end
if(cc>=0)
  R=L/d;
  if(R>1), ecc=sqrt(1-1/R^2); else, ecc=0.00001; end
  a = 2*(1-ecc^2)/ecc^3*(0.5*log((1+ecc)/(1-ecc))-ecc);
  B = 1/ecc^2-(1-ecc^2)/(2*ecc^3)*log((1+ecc)/(1-ecc));
  k1=a/(2-a);                % inertial coefficient in axial flow
  k2=B/(2-B);                % inertial coefficient in cross flow
  tp=2/ecc^2-1;
  kdash=1/(tp*(2/(B-a)-tp));   %inertial coefficient for rotation
  fk1=(1+k1*rhow/rhomn);
  fk2=(1+k2*rhow/rhomn);
  JA=J.*[1;(1+kdash*rhow/rhomn);(1+kdash*rhow/rhomn)];
else
  fk1=1; fk2=1;
end


%  creat linear coeficient matrix ABV and ABA:
ABV=zeros(3,2); ABA=ABV;
nu=Nu(temp,sea_water); mu=nu*rhow;
cd1=Cd1(v1,d,L,temp,sea_water); cd2=Cd2(v2,d,L,temp,sea_water);
```

```
%  Along cylindier drag force coefficient
  cf1=cd1*pi*d^2/8*rhow*abs(v1)/fk1;
  A = eRd(:,1)*eRd(:,1)';  AA=A; AA(idig)=0;
  ABV(:,1)= ABV(:,1) - cf1*A(idig);
  ABV(:,2)= ABV(:,2) - cf1*AA*Vo + cf1*A*Vwater;


%  cross cylinder drag force coefficient
   cf2=cd2*d*L*rhow*(abs(v2)/2+chi*Omgd(3))/fk2;
   fcf2=cd2*d*L*rhow*Omgd(3)^2*(chi^2/2+L^2/24)/fk2;
   A = eRd(:,2)*eRd(:,2)'; AA=A; AA(idig)=0;
   ABV(:,1) = ABV(:,1) - cf2*A(idig);
   ABV(:,2)= ABV(:,2) - cf2*AA*Vo + cf2*A*Vwater + fcf2*eRd(:,2);

%  Lift director drag force
  fd3=-cd2*d*rhow*chi*(3*L^2+4*chi^2)*abs(Omgd(2))*Omgd(2)/fk2;
  ABV(:,2) = ABV(:,2) + fd3*eRd(:,3);

%  Lift force
  cfl=Omgm(1)*d^2*L*rhow/2; fcfl=Omgm(1)*d^2*L*rhow*Omgd(3)*chi/2/fk2;
  A = eRd(:,3)*eRd(:,2)'; AA=A; AA(idig)=0;
  ABV(:,1) = ABV(:,1) - cfl*A(idig);
  ABV(:,2)= ABV(:,2) - cfl*AA*Vo + cfl*A*Vwater + fcfl*eRd(:,3);

% two end force: as Falkber-Skan Similarity Solution on two sqrt(pi)*r
% squre.
%  Lr=d/2*sqrt(pi); Ree=sqrt(v2*Lr/nu);
%  [cde1,cde2]=Cde(v1,v2);
%  % disp([cde1,cde2]);
%  if(Ree<1e-6), cfe=0; else
%  cfe=(cde1+cde2)/(2*Ree)*rhow*Lr^2*v2; end
%  A = eRd(:,2)*eRd(:,2)'; AA=A; AA(idig)=0;
%  ABV(:,1) = ABV(:,1) - cfe*A(idig);
%  ABV(:,2) = ABV(:,2) - cfe*AA*Vo;

% divide m and add gravity force;
  ABV=ABV/m; ABV(3,2) = ABV(3,2) -(1-rhow/rhomn)*g;


%  define the gap between the center of force and the center of volume
as
%  fc = L*cc*sin(2*af);       cc is the relative gap, assume is a
contant
%  number.  af is the attack angle.
   af = atan2(v1,v2);
   fc = L*abs(cc)*abs(sin(2*af));  % disp([chi,fc,chi+fc]);

%  Cylind rotation around axis
  ABA(1,1) = ABA(1,1) -pi*mu*L*d^2;

%  Drag force torque around lift axis
  cm3=-
cd2*d*rhow*(v2*L^3/12+v2*L*chi^2+L^3*Omgd(3)*chi/8+L*chi^3*Omgd(3)/2);
  mcm3=-cd2*d*rhow*v2^2*L*(chi-fc)/2;
  A = mRd(:,3)*mRd(:,3)';  AA=A; AA(idig)=0;
  ABA(:,1) = ABA(:,1) + cm3*A(idig);
```

```
  ABA(:,2) = ABA(:,2) + cm3*AA*Omgm + mcm3*mRd(:,3);



%  Drag force torque around cross flow axis
%  cm2=-cd2*d*rhow*(L^4/16+3*L^2*chi^2/2+chi^4)*abs(Omgd(2))/4;
  cm2=-mu*(L^3/3+4*L*chi^2);
  A = mRd(:,2)*mRd(:,2)'; AA=A; AA(idig)=0;
  ABA(:,1) = ABA(:,1) + cm2*A(idig);
  ABA(:,2) = ABA(:,2) + cm2*AA*Omgm;

%  Lift moment (cross axis)
  cml=Omgd(1)*d^2*rhow*L*(L^2/24+chi^2/2);
  mcml=Omgd(1)*d^2*rhow*L*v2*chi/2;
  A = mRd(:,2)*mRd(:,3)'; AA=A; AA(idig)=0;
  ABA(:,1) = ABA(:,1) + cml*A(idig);
  ABA(:,2) = ABA(:,2) + cml*AA*Omgm + mcml*mRd(:,2);

%  two end force torque:  (Falkber-Skan Similarity Solution)
%  if(Ree<1e-6), mcme=0; else,
%  mcme=rhow*Lr^2*(v2^2)/(2*Ree)*(cde1*(L/2-chi)-cde2*(L/2+chi)); end
%  ABA(:,2) = ABA(:,2) + mcme*mRd(:,3);

% divide J and add gravity torque
  ABA=ABA./(JA*ones(1,2));
%  disp(ABA(2,1));
  ABA(2,2)=ABA(2,2)+m*chi*g*rhow*cos(Ang(2))/(rhomn*J(2));
```

C. SUBROUTINE 3

```
function [Q,IntQ] = ODEdiagsolve(AB,Q0,dt);
%function [Q,IntQ] = ODEdiagsolve(AB,Q0,dt);
% function Q = ODEdiagsolve(AB,Q0,dt);
% Solve diagonal ODE as dQ/dt = AB(:,1)*Q + AB(:,2), with the initial
% condition Q0 at time step dt. Q and Q0 can be V and Ang column
% vector.
% Subroutine creates and update each time step the solution for the
% momentum and moment of momentum system of linear ordinary
% differential equations.
%
%   AB: the linear and constant coefficient matrix.
%   Q (Q0): V or Ang colume vector
%   IntQ:  the integration of Q along dt.
%
%  Chenwu Fan,  NOAP,  NPS    7/12/2002
%  Ashley D. Evans,    NPS    7/18/2002

Q=zeros(3,1); IntQ=Q;
for k=1:3
  lm=AB(k,1);
  if(abs(lm)>1e-10)
    ini=-AB(k,2)/lm; c=Q0(k)-ini;
    Q(k)=c*exp(lm*dt)+ini; IntQ(k)=ini*dt+c/lm*(exp(lm*dt)-1);
  else
    Q(k)=Q0(k)+AB(k,2)*dt; IntQ(k)=Q0(k)*dt+AB(k,2)*dt^2/2;
  end
```

```
end
```

D. SUBROUTINE 4

```
function [R,v1,v2] = ERD(eRm,V);
%function [Ri,v1,v2] = ERD(eRm,V);
%
% Subroutine creates and updates the earth fixed to drag lift force
% reference frame transformation matrix.
%
% where eRm, is the rotation matrix from moving to earth frame,
%        V=[u;v;w] relative fluid velocity vector.
%
%  Chenwu Fan,  NOAP,  NPS    7/12/2002
%  Ashley D. Evans,    NPS    7/19/2002

e1=eRm(:,1); v1=V'*e1;
V2=V-v1*e1; v2=sqrt(V2'*V2);
if(v2==0), R=eRm; else
e2=V2/v2; e3=cross(e1,e2); R = [e1,e2,e3]; end
```

E. SUBROUTINE 5

```
function R = ERM(psi2,psi3);
% function R = ERM(psi2,psi3)
%
% Subroutine creates and updates the earth fixed to mine body
% reference frame transformation matrix.
%

%  Chenwu Fan,  NOAP,  NPS    7/12/2002
%  Ashley D. Evans,    NPS    7/19/2002

cp2=cos(psi2); cp3=cos(psi3); sp2=sin(psi2); sp3=sin(psi3);

R = [cp3,-sp3,0;sp3,cp3,0;0,0,1]*[cp2,0,sp2;0,1,0;-sp2,0,cp2];
```

F. SUBROUTINE 6

```
function [ang,R]=eRm2ag(R,ang3);
% function [ang,R]=eRm2ag(R,ang3);
%%
% Subroutine creates and updates the Euler angles for each
% time step.
%
%  Chenwu Fan,  NOAP,  NPS    7/12/2002
%  Ashley D. Evans,    NPS    7/19/2002

 ag2=acos(R(3,3)); ag3=acos(R(2,2));

 if(R(1,2)>0), ag3=2*pi-ag3; end
 if(R(3,1)>0), ag2=2*pi-ag2; end

 if(exist('ang3'))
   while((ag3-ang3)<-pi), ag3=ag3+2*pi; end
```

```
   while((ag3-ang3)>pi), ag3=ag3-2*pi; end
 end

ang=[0;ag2;ag3];

R = ERM(ag2,ag3);
```

G. SUBROUTINE 7

```
function cd1 = Cd1(v,d,L,t,sea_water);
% function cd1 = Cd1(v,d,L,t,sea_water);
%
% Calculates the axial flow drag coefficient.
%
%  Chenwu Fan,  NOAP,  NPS    7/12/2002
%  Ashley D. Evans,    NPS    7/19/2002

if(~exist('t')); t=20; sea_water=0;
elseif(~exist('sea_water')), sea_water=0; end

Re=abs(v)*d/Nu(t,sea_water);  AR=L/d;

if(AR>8)
  cd1=1;
elseif(AR>0.5)
  cd1=0.75+AR/32.1934+0.09612/AR^2;   % cd1=0.75+AR/33.6+0.0962/AR^2;
else
  cd1=1.15;
end
```

H. SUBROUTINE 8

```
function cd2 = Cd2(v,d,L,t,sea_water);
% function cd2 = Cd2(v,d,L,t,sea_water);
%
% Calculates the cross flow drag coefficient.
%
%  Chenwu Fan,  NOAP,  NPS    7/12/2002
%  Ashley D. Evans,    NPS    7/19/2002

if(~exist('t')); t=20; sea_water=0;
elseif(~exist('sea_water')), sea_water=0; end


Re=max(0.001,abs(v)*d/Nu(t,sea_water)); AR=L/d;
% disp(['Re= ',num2str(Re)]);

if(Re<=12)
  cd2=1.9276+8/Re;       % cd2=1.8+8/Re;
elseif(Re<=180)
  cd2=1.261+16/Re;       % cd2=1.26+16/Re;
elseif(Re<=2000)
  cd2=0.8555+89/Re;      % cd2=0.86+89/Re;
elseif(Re<=12000)
  cd2=0.84+0.00003*Re;
elseif(Re<=150000)
```

```
  if(AR>=10), cd2=1.2-4/AR; elseif(AR>=2), cd2=0.835-0.35/AR;
  else, cd2=0.7-0.08/AR; end                %  cd2=1.2;
elseif(Re<=350000)
  cd2=1.875-0.0000045*Re;
else
  cd2=1/(641550/Re+1.5);
end

cd2=1.1*cd2;
```

I. SUBROUTINE 9

```
function  nu = Nu(t,sea_water);
% function  nu = Nu(t,sea_water);
%
% Calculates the kinematic viscosity of water.
%
%  Chenwu Fan,  NOAP,  NPS    7/12/2002
%  Ashley D. Evans,    NPS    7/19/2002

if(~exist('t')); t=20; end

if(t<=10), nu=10^(-5.7471-0.0136*t); else
nu=10^(-5.77592-0.010718*t); end

if(exist('sea_water') & sea_water)
  nu=nu*1.058*(1+0.0000363*t^2);
end
```

APPENDIX C. DATA PRESENTATION CODE

Appendix C contains the MATLAB application presentation code used to output displays of the Carderock data files, the MIDEX data files, and associated three dimensional model outputs to presentation graphics as seen in Appendix A.

A. CARDEROCK DATA CODE

```
% carderock.m, This program computes the position of Carderock
Experimnental
% Drops and plots them to the screen in an S (path) vs Z plot, x-y
% bottom plot and center of mass movement angle plot. The second part
% of the program uses the data initial conditions and runs the Mine
% Burial 3-D model and produces the same set of plots from the 3-D
model
% for comparison.
%
% Ashley D. Evans and Chenwu Fan
% Thesis Program 2002
% NOAP Lab for Peter Chu.
% July 2002
% LCDR/USN

% Part 1: This program asks for a mine drop data file, there are a
total
% of 42 drops at Carderock used in this validation.  Then references
% that file to (0,0,0) in x,y,z. It then plots the center of mass
% position and a small mine shape around it with an identification
% table.

clear all
close all

% General Mine data for the mine shapes used at Carderock. Understand
% the moments of inertia are a 3x3 matrix.
%
%          1          2          3          4          5          6
mi=[     17.2,      22.2,      34.5,      46.3,      45.4,      44.7];
Ji=[   0.0647,    0.0806,    0.1362,    0.1696,    0.1693,
0.1692;...
       0.356,     0.477,       2.9,      3.82,      3.94,      4.57;...
        0.356,     0.477,       2.9,      3.82,      3.94,      4.57];
chii=[0.0002385,  0.001908,  0.001964,  0.008838,  0.045172,
0.076596];
Li = [    0.477,     0.477,     0.982,     0.982,     0.982,
0.982];
```

```
di=0.168*ones(1,6);

minepath % Path to all the required subroutine functions for 3-D model.

% Request for model type input.

icc=input('input case drop number and model mine number number and cc:
','s');

icc=str2num(icc);  ic=icc(2); cas=icc(1);
if(length(icc)==3);
   cc=icc(3);
else
   cc=0.13;
end

% Sets the mine model parameters for the given mine drop in part 1.

ma=mi(ic); J=Ji(:,ic); chi=chii(ic); L=Li(ic); d=di(ic);d2r=pi/180;

% Request for input data file and creates the file as (pos matrix).
% time, x, y, z, pithc angle(around y axis), and yaw angle (around
% the z axis).

dr = 'carderockdata/';

flnm=[int2str(cas),'w-',int2str(ic),'.txt'];
flnmp=[int2str(cas),'w-',int2str(ic)];
fid=fopen([dr,flnm]);
   if(fid<2), break;
   end
pos=fscanf(fid,'%f',[6,inf]);
fclose(fid);

dt1 = 0.008;

% Input files from Carderock are all in cm, and this converts them to
% meter standard.

pos(2,:) = pos(2,:)./100;
pos(3,:) = pos(3,:)./100;
pos(4,:) = pos(4,:)./100;
pos(6,:) = 180+pos(6,:);

 % This section calculates angle 3 and insures they are all
 % < 180 degrees.

   dag3=diff(pos(6,:));
   ii=find(dag3>200);
   if(~isempty(ii));
      for k=1:length(ii);
         pos(6,ii(k)+1:end)=pos(6,ii(k)+1:end)-360;
      end
   end
   ii=find(dag3<-200);
   if(~isempty(ii))
```

```
      for k=1:length(ii)
         pos(6,ii(k)+1:end)=pos(6,ii(k)+1:end)+360;
      end
   end


% This section saves the tilt angles in degrees and converts separately
% to radians for pitch and yaw.

posa(5,:) = pos(5,:);
pos(5,:) = pos(5,:)*pi/180;
pos(6,:) = pos(6,:)*pi/180;
ang2i = pos(5,1);

% If the initial time is not zero this portion calculates the initial
% instantaneous velocity vector to use in the model run portion of
% Part 2. Then calculates an initial mean angular velocity rate based
% on the first 20 time increments of angle2 and angle3.

Vo = [0;0;0];
Omgm=[0;0;0];
nnn=3;
Vo(1) = (pos(2,nnn+1) - pos(2,1))/(nnn*dt1);
Vo(2) = (pos(3,nnn+1) - pos(3,1))/(nnn*dt1);
Vo(3) = (pos(4,nnn+1) - pos(4,1))/(nnn*dt1);
% Vo = Vo';
Omgm=[0;0;0];
Omgm(2) = (pos(5,nnn+1) - pos(5,1))/(nnn*dt1);
Omgm(3) = ((pos(6,nnn+1) - pos(6,1))*cos(pos(5,2)))/(nnn*dt1);

Vxo = Vo(1);
Vyo = Vo(2);
Vzo = Vo(3);
Omgmo = Omgm;

% This section references time and xyz to zero both spatially and
% temporally. This makes the output consistent with the model
% outputs. (Has to wait until after the initial velocity
% calculation as t0 is a check.

pos(1,:) = pos(1,:) - pos(1,1); % time reset.
pos(2,:) = pos(2,:) - pos(2,1); % x displacement.
pos(3,:) = pos(3,:) - pos(3,1); % y displacement.
pos(4,:) = pos(4,:) - pos(4,1); % z displacement.

% Rename the position vectors.

xm = pos(2,:); % x displacement from zero.
ym = pos(3,:); % y displacement from zero.
zm = pos(4,:); % z displacement from zero.

% Calculates the bottom as the last position tracked on the file.

bot = -abs(pos(4,end));

% Creates a short vector used to denote the long axis of the mine.
```

```
dd = abs(bot/30);

% Sets up a new figure for plotting of the given mine data file from
% Carderock.

ftsz = 8;
figure('units','inches','position',[1,.4,8,7],'paperposition',...
   [1.5,1.6,5.5,8],'paperorientation','portrait');
axes('position',[0.1,0.175,0.44,0.67],'xdir','reverse','ylim',...
   [bot-dd,0],'box','on','fontsize',ftsz);
hold on;
axis('equal');
ylabel('Depth (m)');
xlabel('Path Distance (m)');

% Calculate the path length of mine travel.

path = sqrt(diff(ym).^2+diff(xm).^2);
path = [0,path];
path = cumsum(path);
plot(path,zm);

[mm,n] = size(path);
xx(1,:)=path+dd*cos(pos(5,:)); xx(2,:)= path-dd*cos(pos(5,:));
zz(1,:)=zm-dd*sin(pos(5,:)); zz(2,:)=zm+dd*sin(pos(5,:));

% Actual steps to plot mine after calculations are complete.
for i = 1:8:n
   plot(xx(:,i),zz(:,i),'r-');
   % Plots the line for long axis of the mine.
   plot(xx(1,i),zz(1,i),'ro','markersize',3);
   % Plots the head of mine.
end
%plot(pos(2,:),pos(4,:)); %Plots the center of mass position in x,z.
icm = num2str(ic);
casm = num2str(cas);
title(['Carderock Experiment Run: ',casm,'w-
',icm],'fontweight','bold');
hold off

% Calculates the horizontial movement from release center line, impact
% velocity components and impact angle.

xyf = sqrt(xm(end)^2 + ym(end)^2);
Vxf = (pos(2,n)-pos(2,n-10))/(10*dt1);
Vyf = (pos(3,n)-pos(3,n-10))/(10*dt1);
Vzf = (pos(4,n)-pos(4,n-10))/(10*dt1);
angf = posa(5,end);
% Corrects values of angle to 180 to 180.
if angf > 180
   angf = angf - 360;
end
timef = pos(1,end);

% Plot a data card to annotate the final velocity components,impact
% angle time and horizontial movement for respective model drop.
```

```
axes('position',[0.11,0.75,0.2,0.24],'fontsize',ftsz);
axis off;
hold on;

dx=1; x1=0; x2=1;
ddy=1; y2=1; y1 = 0;
x3=x1+0.08*dx; x4=x3+0.3*dx; xm1=(x1+x2)/2;

y=y2-.01*ddy;
text(xm1,y,'Final Drop','HorizontalAlignment','center','fontsize',...
   ftsz,'fontweight','bold');
y=y-.01*ddy; text(xm1,y,'Parameters','HorizontalAlignment','center',...
      'fontsize',ftsz,'fontweight','bold')
y=y-.01*ddy; text(x3,y,'time:','fontsize',ftsz);
text(x4,y,[num2str((timef),3),'(s)'],'fontsize',ftsz);
y=y-.01*ddy; text(x3,y,'xy_f_e:','fontsize',ftsz);
text(x4,y,[num2str(xyf,3),' (m)'],'fontsize',ftsz);
y=y-.01*ddy; text(x3,y,'V_x_f_e:','fontsize',ftsz);
text(x4,y,[num2str(Vxf,3),' (m/s)'],'fontsize',ftsz);
y=y-.01*ddy; text(x3,y,'V_y_f_e:','fontsize',ftsz);
text(x4,y,[num2str(Vyf,3),' (m/s)'],'fontsize',ftsz);
y=y-.01*ddy; text(x3,y,'V_z_f_e:','fontsize',ftsz);
text(x4,y,[num2str(Vzf,3),' (m/s)'],'fontsize',ftsz);
y=y-.01*ddy; text(x3,y,'\psi_2_f_e:','fontsize',ftsz);
text(x4,y,[num2str(angf,3),'^o'],'fontsize',ftsz);
y=y-.01*ddy; text(x3,y,'depth:','fontsize',ftsz);
text(x4,y,[num2str(-(bot),4),' (m)'],'fontsize',ftsz);
y1=y-.01*ddy;

set(gca,'ylim',[y1,y2],'xlim',[x1,x2]);
plot([x1,x2,x2,x1,x1],[y1,y1,y2,y2,y1]);
hold off

%
%########################################################################
% Part 2 of the code runs the initial conditions from the Carderock
case
% using the specified mine shape characteristics and traces out the 3-D
% model results.
%
%########################################################################

m=mi(ic); J=Ji(:,ic); chi=chii(ic); L=Li(ic); d=di(ic);
dt=1/15;
%
% Creates the data card for the mine parameters for the selected mine.
%
axes('position',[0.42,0.75,0.24,0.24],'fontsize',ftsz);
axis off;
hold on
dx=1; x11=0; x22=1;
ddy=1/2; y22=1;
x3=x11+0.08*dx; x4=x3+0.3*dx; xm1=(x11+x22)/2;
%
y=y22-.01*ddy;
```

```
text(xm1,y,'Mine Shape','HorizontalAlignment','center','fontsize',...
   ftsz,'fontweight','bold');
y=y-.01*ddy; text(xm1,y,'Parameters','HorizontalAlignment','center',...
      'fontsize',ftsz,'fontweight','bold')
y=y-.01*ddy; text(x3,y,'d:','fontsize',ftsz);
text(x4,y,[num2str(d,3),' (m)'],'fontsize',ftsz);
y=y-.01*ddy; text(x3,y,'L:','fontsize',ftsz-2);
text(x4,y,[num2str(L,3),' (m)'],'fontsize',ftsz);
y=y-.01*ddy; text(x3,y,'m:','fontsize',ftsz-2);
text(x4,y,[num2str(m,3),' (kg)'],'fontsize',ftsz);
y=y-.01*ddy; text(x3,y,'J_1:','fontsize',ftsz);
text(x4,y,[num2str(J(1),3),' (kg*m^2)'],'fontsize',ftsz);
y=y-.01*ddy; text(x3,y,'J_2:','fontsize',ftsz);
text(x4,y,[num2str(J(2),3),' (kg*m^2)'],'fontsize',ftsz);
y=y-.01*ddy; text(x3,y,'J_3:','fontsize',ftsz);
text(x4,y,[num2str(J(3),3),' (kg*m^2)'],'fontsize',ftsz);
y=y-.01*ddy; text(x3,y,'\chi:','fontsize',ftsz);
text(x4,y,[num2str(chi,4),' (m)'],'fontsize',ftsz);
y11=y-.01*ddy;
%
set(gca,'ylim',[y11,y22],'xlim',[x11,x22]);
plot([x11,x22,x22,x11,x11],[y11,y11,y22,y22,y11]);
%
hold off

% Calculations required for the specified mine shape in the initial
% conditions.

vol=pi*d^2*L/4; rhomn=m/vol;
Pos=[0;0;0];  Ang=[0;ang2i;pos(6,1)];
Vwater=zeros(3,1); temp=21;sea_water=0;

% Water density calculation.

rhow=1028.17 – 0.0742*temp - 0.0048*(temp^2);

eRm=ERM(Ang(2),Ang(3));
pos1=Pos; ang=Ang; omg=Omgm; time=0;
dthdt2=Omgm(3);
for k=1:600
  [Pos,Ang,Vo,Omgm,eRm]=diag1step(m,J,d,L,chi,Pos,Ang,Vo,Omgm,eRm,...
      dt,rhomn,rhow,Vwater,temp,sea_water,cc);
pos1=[pos1,Pos]; ang=[ang,Ang]; omg=[omg,Omgm];
dthdt2=[dthdt2,Omgm(3)];
if(Pos(3)<bot), break;
  end
  time=time+dt;
end

% Calculate the path distance of the mine shape from model output.

ptt = sqrt(diff(pos1(1,:)).^2+diff(pos1(2,:)).^2);
ptt = [0,ptt];
ptt =  cumsum(ptt);

angd=ang*180/pi;
```

```
axes('position',[0.55,0.175,0.44,0.67],'xdir','reverse','ylim',...
   [bot-dd,0],'box','on','fontsize',ftsz);
hold on;
axis('equal');
xlabel('Path Distance (m)');
set(gca,'yticklabel',[]);
plot(ptt,pos1(3,:));

xx1(1,:)=ptt+dd*cos(ang(2,:));
xx1(2,:)=ptt-dd*cos(ang(2,:));
zz1(1,:)=pos1(3,:)-dd*sin(ang(2,:));
zz1(2,:)=pos1(3,:)+dd*sin(ang(2,:));

plot(xx1,zz1,'r-'); plot(xx1(1,:),zz1(1,:),'ro','markersize',3);
title(['3-D Model Solution: 'casm,'w-
'num2str(ic)],'fontweight','bold');

xlm=get(gca,'xlim'); ylm=get(gca,'ylim');

% Prints the card for the initial parameters for the model inside the
% axes of the model figure on the output page.

dx=diff(xlm); dy=diff(ylm);
x1=xlm(2); y1=ylm(2)-0.02*dy;

ddy=0.08*dy;
x3=x1-.05*dx; x4=x3 - .09*dx; y = y1; y=y-.2*ddy;
text(x1-.025,y,'Model Initial','fontsize',ftsz,'fontweight','bold');
y=y-.75*ddy;
text(x1-.025,y,'Parameters','fontsize',ftsz,'fontweight','bold');
y=y-.75*ddy; text(x3,y,'\psi_2_o:','fontsize',8);
text(x4,y,[num2str(ang2i*180/pi,3),'^o'],'fontsize',8);
y=y-.75*ddy; text(x3,y,'\omega_2_o:','fontsize',8);
text(x4,y,[num2str(Omgmo(2),2),' (r/s)'],'fontsize',8);
y=y-.75*ddy; text(x3,y,'V_x_o:','fontsize',8);
text(x4,y,[num2str(Vxo,3),' (m/s)'],'fontsize',8);
y=y-.75*ddy; text(x3,y,'V_y_o:','fontsize',8);
text(x4,y,[num2str(Vyo,3),' (m/s)'],'fontsize',8);
y=y-.75*ddy; text(x3,y,'V_z_o:','fontsize',8);
text(x4,y,[num2str(Vzo,3),' (m/s)'],'fontsize',8);
y=y-.75*ddy; text(x3,y,'dt:','fontsize',8);
text(x4,y,['1/'num2str(1/dt,2),' (s)'],'fontsize',8);
hold off
%
% Calculates and plots xy travel of center of mass of the mine and
% also a center of mass movement angle vs depth.
xm11 = xm; ym11 = ym;
xmax=max(max(xm11),max(pos1(1,:)));
xmin=min(min(xm11),min(pos1(1,:)));
ymax=max(max(ym11),max(pos1(2,:)));
ymin=min(min(ym11),min(pos1(2,:)));
ddxy=max([5*L,(xmax-xmin),(ymax-ymin)])*0.52;
xlm=(xmin+xmax)/2+ddxy*[-1,1]; ylm=(ymin+ymax)/2+ddxy*[-1,1];

psm=(pos(5,1:end-1)+pos(5,2:end))/2;
```

```
dthdt1=diff(pos(5,:))./diff(pos(1,:)).*cos(psm);
xmax=max(max(dthdt1),max(dthdt2));
xmin=min(min(dthdt1),min(dthdt2));
ddx=max(5,(xmax-xmin)*0.52);
xlm2=(xmax+xmin)/2+ddx*[-1,1];


axes('position',[0.12,0.05,0.2,0.17],'xlim',xlm,'ylim',ylm,'box',...
   'on','fontsize',ftsz);
hold on; plot(xm11,ym11,'r-'); plot(xm11,ym11,'.');
xlabel('X (m)'); ylabel('Y (m)');
title('Mass center trail','fontweight','bold');

axes('position',[0.39,0.05,0.1,0.17],'xlim',xlm2,'ylim',...
   [bot-dd,0],'box','on','fontsize',ftsz); hold on;
zmh=(zm(1:end-1)+zm(2:end))/2;
plot(dthdt1,zmh); plot([0,0],[bot,0],'r-.');
xlabel('\omega_3'); ylabel('Depth (m)');
title('Yaw Velocity','fontweight','bold');

axes('position',[0.6,0.05,0.2,0.17],'xlim',xlm,'ylim',ylm,'box',...
   'on','fontsize',ftsz);
hold on; plot(pos1(1,:),pos1(2,:),'r-'); plot(pos1(1,:),...
   pos1(2,:),'.');
xlabel('X (m)');  ylabel('Y (m)');
title('Mass center trail','fontweight','bold');

axes('position',[0.88,0.05,0.1,0.17],'xlim',xlm2,'ylim',...
   [bot-dd,0],'box','on','fontsize',ftsz); hold on;
    plot(dthdt2,pos1(3,:)); plot([0,0],[bot,0],'r-.');
    xlabel('\omega_3'); ylabel('Depth (m)');
    title('Yaw Velocity','fontweight','bold');

% Plot a data card to annotate the final velocity components,impact
% angle time and horizontial movement for the respective mine drop
% 3-D model solutions.

xyPos = sqrt(Pos(1)^2 + Pos(2)^2);
ang2fm = Ang(2)*180/pi;
% Corrects the angle to display -180 to 180.
if ang2fm > 180
   ang2fm = ang2fm - 360;
end

axes('position',[0.77,0.75,0.20,0.24],'fontsize',ftsz);
axis off;
hold on;

dx=1; x1=0; x2=1;
ddy=1/2; y2=1;
x3=x1+0.08*dx; x4=x3+0.3*dx; xm1=(x1+x2)/2;

y=y2-.008*ddy;
text(xm1,y,'Final Model','HorizontalAlignment','center','fontsize',...
      ftsz,'fontweight','bold');
```

```
y=y-.01*ddy; text(xm1,y,'Parameters','HorizontalAlignment','center',...
      'fontsize',ftsz,'fontweight','bold')
y=y-.01*ddy; text(x3,y,'time:','fontsize',ftsz);
text(x4,y,[num2str((time),3),' (s)'],'fontsize',ftsz);
y=y-.01*ddy; text(x3,y,'xy_f_m:','fontsize',ftsz);
text(x4,y,[num2str(xyPos,3),' (m)'],'fontsize',ftsz);
y=y-.01*ddy; text(x3,y,'V_x_f_m:','fontsize',ftsz);
text(x4,y,[num2str(Vo(1),3),' (m/s)'],'fontsize',ftsz);
y=y-.01*ddy; text(x3,y,'V_y_f_m:','fontsize',ftsz);
text(x4,y,[num2str(Vo(2),3),' (m/s)'],'fontsize',ftsz);
y=y-.01*ddy; text(x3,y,'V_z_f_m:','fontsize',ftsz);
text(x4,y,[num2str(Vo(3),3),' (m/s)'],'fontsize',ftsz);
y=y-.01*ddy; text(x3,y,'\psi_2_f_m:','fontsize',ftsz);
text(x4,y,[num2str(ang2fm,3),'^o'],'fontsize',ftsz);
y1=y-.01*ddy;

set(gca,'ylim',[y1,y2],'xlim',[x1,x2]);
plot([x1,x2,x2,x1,x1],[y1,y1,y2,y2,y1]);
hold off

% prints the figure using filename to the current data directory
% for later analysis and use for presentation as apost script file
% and jpeg format for powerpoint presentation.

eval(['print -tiff -depsc carderockplts/',flnmp,'.eps;'])
eval(['print -djpeg carderockplts/',flnmp,'.jpg;'])

% This section prints out the final velocities, transverse
displacement,
% and sediment impact angles to file for both the data and the model.

Vcfm=sqrt(Vo(1)^2+Vo(2)^2);
Vcfe=sqrt(Vxf^2+Vyf^2);
Vfile = [Vcfm;Vcfe;abs(Vo(3));...
abs(Vzf);ang2fm;angf;xyPos;xyf];
fid=fopen(['velocity.txt'],'a+');
fseek(fid,0,'eof');
fprintf(fid,'%s\t',flnmp);
for k=1:length(Vfile)
   fprintf(fid,'%6.3f\t',Vfile(k));
end
fprintf(fid,'\n');
fclose(fid);

% This section creates the initial output case file to use as input
% to IMPACT28. The angles are converted to the correct format to
% input directly to IMPACT28.

Vco=sqrt(Vxo^2+Vyo^2);
Vfile1 = [(90-(ang2i*180/pi));abs(Vco);abs(Vzo);Omgmo];
fid=fopen(['initialpar.txt'],'a+');
fseek(fid,0,'eof');
fprintf(fid,'%s\t',flnmp);
for k=1:length(Vfile1)
   fprintf(fid,'%6.3f\t',Vfile1(k));
end
```

```
fprintf(fid,'\n');
fclose(fid);

% End of program.
```

B. MIDEX DATA CODE

```
% MIDEX.m, This program computes the position of MIDEX data for 230
% 1/15 scale drops and plots them to screen in an S (path) vs Z plot,
% x-y bottom plot and center of mass movement angle plot. The second
% part of the program uses the data initial conditions and runs the
% Mine Burial 3-D model and produces the same set of plots from the
% 3-D model for comparison.
%
% Chenwu Fan and Ashley D. Evans LCDR/USN
% Thesis Program 2002
% NOAP Lab for Peter Chu.
% August 2002

clear;

% Creates a relative pointer to the folder containing MIDEX data.

dr='tonydata/';

% MIDEX general mine shape model parameters.

Li=[0.152,0.121,0.0912]; mi=[0.3225,0.2542,0.2153];
voli=[191.0088,152.0531,114.6053]*1e-6; rmi=[1688.5,1671.7,1878.5];
chii=[0.0046,0.7411,1.4772;
0.0644,0.5307,0.9970;0.0029,0.2911,0.5796]/100;

%  chii(min#,case#) a 2-D array.

Ji=[0.33046,0.27132,0.23503,0.33046,0.27132,0.23503,0.33046,0.27132,...
      0.23503;6.0879, 3.4262, 1.6952, 5.7830, 3.2065, 1.5775,
6.2338,...
      3.3126, 1.5568;6.0879, 3.4262, 1.6952, 5.7830, 3.2065, 1.5775,...
      6.2338, 3.3126, 1.5568]*1e-4;

Ji=reshape(Ji,[3,3,3]);

%  Ji(:,min#,case#) a 3-D array.

% Sets a path marker to subroutines used within the main program.

minepath;

minen=[15,12,9];

rw=1028; Vwater=zeros(3,1); temp=20; sea_water=0;
d=0.04; d2r=pi/180; ftsz=8;

% Water density calculation.

rw=1028.17 – 0.0742*temp - 0.0048*(temp^2);

% Requests input for model size, center of mass position, and drop
% angle to access files.
```

```
mca=input...
   ('input mine#(9,12,15)  case#(-2,-1,0,1,2)  ang(15,30,45,60,75)
cc:',...
   's');

% This section of the code reads in the MIDEX data and stores it as the
% 't' array.

while(~isempty(mca))
  mca=str2num(mca); mine=mca(1); cas=mca(2); iag=mca(3);
  mca1=num2str(mine); mca2=num2str(cas); mca3=num2str(iag);
  if(length(mca) == 4)
     cc = mca(4)
  else
     cc = 0.05;
  end
  minn=find(minen==mine);
  casn=abs(cas)+1; sag=[int2str(iag),'/'];
  L=Li(minn); m=mi(minn); J=Ji(:,minn,casn); chi=chii(minn,casn);
  vol=voli(minn); rhomn=m/vol;

  fid=fopen([dr,sag,'flnm.dat']);
    dfnm=fscanf(fid,'%f',[4,inf]);
  fclose(fid);
  ii=find(dfnm(1,:)==mine & dfnm(4,:)==cas); dfnm=dfnm(:,ii);

  % This for loop looks in the open file folder 'dfnm'and reads files
  % until it reaches the end of file marker. Files are grouped by drop
  % angle first then com position and mine length.

  for i=1:size(dfnm,2)
    i2=num2str(i);
    flnm=[int2str(mine),'-',int2str(round(dfnm(2,i)*1000))];
    fid=fopen([dr,sag,flnm,'.dat']);
    fgetl(fid); fgetl(fid);

    % The t array contains all tony data for the given run.

    t=fscanf(fid,'%f',[11,inf]);
    fclose(fid);

    % Arrays are defined for use in generating plots. Also generated
    % are the initial condition vectors to be fed to the 3-D model.

   time=t(1,:)-t(1,1); % Time vector
   xm=t(2,:)-t(2,1); % x coordinate vector
   ym=t(3,:)-t(3,1); % y coordinate vector
   zm=t(4,:)-t(4,1); % z coordinate vector
   bot=zm(end); % Bottom

   % This sect calculates angle 3 and insures they are all
   % < 180 degrees.

   dag3=diff(t(6,:));
   ii=find(dag3>200);
```

```
   if(~isempty(ii));
      for k=1:length(ii);
         t(6,ii(k)+1:end)=t(6,ii(k)+1:end)-360;
      end
   end
   ii=find(dag3<-200);
   if(~isempty(ii))
      for k=1:length(ii)
         t(6,ii(k)+1:end)=t(6,ii(k)+1:end)+360
      end
   end

   ag2=(t(5,:)-90)*d2r; % angle about the y axis or pitch angle.
   ag3=t(6,:)*d2r; % angle around the z axis or yaw angle.
   dd=abs(bot)/30;
   Vo=t(7:9,1); % Initial linear velocity vector to feed to the
   % the 3-D model.
   Omgm=[0;t(5,3)-t(5,1);(t(6,3)-t(6,1))*cos(ag2(2);]*d2r/(t(1,3)-
t(1,1));
   % Initial Angular velocities in rad/sec
   Omgmo = Omgm;

% New figure defined.

    figure('units','inches','position',[1,0.4,8,7],'paperposition',...
       [1.5,1.6,5.5,8],'paperorientation','portrait');
    axes('position',[0.1,0.175,0.44,0.67],'xdir','reverse','ylim',...
       [bot-dd,0],'box','on','fontsize',ftsz); hold on;
    axis('equal'); ylabel('Depth (m)'); xlabel('Path Distance (m)');

    % A distance covered vector is created from the x-y data and
plotted
    % versus depth for the MIDEX data set.

    pt=sqrt(diff(ym).^2+diff(xm).^2);
    pt=[0,pt]; pt=cumsum(pt);
    % Plot of the MIDEX data for the given read case.
    plot(pt,zm);
    yy=dd*[1;-1]*cos(ag2)+[1;1]*pt; zz=dd*[-1;1]*sin(ag2)+[1;1]*zm;
    plot(yy,zz,'r-'); plot(yy(1,:),zz(1,:),'ro','markersize',3);
    title(['MIDEX Run ',mca1,'-',mca2,'-',mca3,', Run ',i2],...
       'fontweight','bold')

    % Creates a value containing the transverse distance covered
    % across the x-y plane for the given MIDEX data set.

    xyf=sqrt(xm(end)^2+ym(end)^2);

    % Model input and output to plot.

    axes('position',[0.55,0.175,0.44,0.67],'xdir','reverse','ylim',...
       [bot-dd,0],'box','on','fontsize',ftsz);
    hold on;
    axis('equal'); xlabel('Path Distance (m)');
    set(gca,'yticklabel',[]);
```

```
Pos=[xm(1);ym(1);zm(1)]; Ang=[0;ag2(1);ag3(1)];
eRm=ERM(Ang(2),Ang(3));
       dt=1/30;
    if(cas<0), chi=-chi; end

    % Creates empty arrays to stored the position , and angle
    % information from the subroutines.

    pos=Pos; ang=Ang; tim=0; dthdt2=Omgm(3);

    % Main subroutine marker feed for the 3-D model.

    for k=1:700
       [Pos,Ang,Vo,Omgm,eRm]=diag1step(m,J,d,L,chi,Pos,Ang,Vo,...
          Omgm,eRm,dt,rhomn,rw,Vwater,temp,sea_water,cc);
      pos=[pos,Pos]; ang=[ang,Ang]; dthdt2=[dthdt2,Omgm(3)];
      if(Pos(3)<bot), break; end
      % If the bottom is encountered
      % then the program break routine and default to end of program.
      tim=tim+dt;
    end
    angd=ang/d2r;

    % A distance covered vector is created from the x-y data and
    % plotted versus depth for the model output.

    ptt=sqrt(diff(pos(1,:)).^2+diff(pos(2,:)).^2);
    ptt=[0,ptt]; ptt=cumsum(ptt);
    plot(ptt,pos(3,:));
    xxx=dd*[1;-1]*cos(ang(2,:))+[1;1]*ptt;
    zzz=dd*[-1;1]*sin(ang(2,:))+[1;1]*pos(3,:);

       plot(xxx,zzz,'r-'); plot(xxx(1,:),zzz(1,:),'ro','markersize',3);
    title(['3-D Model Output ',mca1,'-',mca2,'-',mca3,...
          ', Run ',i2],'fontweight','bold')

    % A value is created containing the xy plane horizontal chord
    % distance covered data from the 3-D model results.

    xyPosf=sqrt(Pos(1)^2+Pos(2)^2);

    xlm=get(gca,'xlim'); ylm=get(gca,'ylim');

% Prints the card for the initial parameters for the model inside
% the axes of the model figure on the output page.

       dx=diff(xlm); dy=diff(ylm);
       x1=xlm(2); y1=ylm(2)-0.02*dy;
       ddy=0.08*dy;
    x3=x1-.05*dx; x4=x3 - .09*dx; y = y1; y=y-.2*ddy;
    text(x1-.025,y,'Model Initial','fontsize',ftsz,...
       'fontweight','bold');
       y=y-.75*ddy;
```

```
  text(x1-.025,y,'Parameters','fontsize',ftsz,...
   'fontweight','bold');
   y=y-.75*ddy; text(x3,y,'\psi_2_o:','fontsize',8);
   text(x4,y,[num2str(ag2(1)/d2r,2),'^o'],'fontsize',8);
   y=y-.75*ddy; text(x3,y,'\omega_2_o:','fontsize',8);
   text(x4,y,[num2str(Omgmo(2),2),' (r/s)'],'fontsize',8);
   y=y-.75*ddy; text(x3,y,'V_x_o:','fontsize',8);
   text(x4,y,[num2str(t(7,1),3),' (m/s)'],'fontsize',8);
   y=y-.75*ddy; text(x3,y,'V_y_o:','fontsize',8);
   text(x4,y,[num2str(t(8,1),3),' (m/s)'],'fontsize',8);
   y=y-.75*ddy; text(x3,y,'V_z_o:','fontsize',8);
   text(x4,y,[num2str(t(9,1),3),' (m/s)'],'fontsize',8);
   y=y-.75*ddy; text(x3,y,'dt:','fontsize',8);
   text(x4,y,['1/'num2str(1/dt,2),' (s)'],'fontsize',8);
   hold off

% Plots the xy plots and angle plots for both the MIDEX
% data and the model output.

% Computes themax and mins for the xy plot.

xmax=max(max(xm),max(pos(1,:)));
xmin=min(min(xm),min(pos(1,:)));
ymax=max(max(ym),max(pos(2,:)));
ymin=min(min(ym),min(pos(2,:)));
ddxy=max([5*L,(xmax-xmin),(ymax-ymin)])*0.52;
xlm=(xmin+xmax)/2+ddxy*[-1,1];
ylm=(ymin+ymax)/2+ddxy*[-1,1];

% Computes the max and mins for the angle 3 plots.

psm=(ag2(1:end-1)+ag2(2:end))/2;
dthdt1=diff(ag3)./diff(t(1,:)).*cos(psm);
xmax=max(max(dthdt1),max(dthdt2));
xmin=min(min(dthdt1),min(dthdt2));
ddx=max(5,(xmax-xmin)*0.52);
xlm2=(xmax+xmin)/2+ddx*[-1,1];

% MIDEX xy planer plot

   axes('position',[0.12,0.05,0.2,0.17],'xlim',xlm,'ylim',ylm,...
  'box','on','fontsize',ftsz);
hold on;
plot(xm,ym,'r-');
plot(xm,ym,'.');
xlabel('X (m)'); ylabel('Y (m)');
title('Mass center trail','fontweight','bold');

% MIDEX Yaw Velocity plot.

axes('position',[0.39,0.05,0.1,0.17],'xlim',xlm2,...
   'ylim',[bot-dd,0],'box','on','fontsize',ftsz); hold on;
zmh=(zm(1:end-1)+zm(2:end))/2;
plot(dthdt1,zmh);
plot([0,0],[bot,0],'r-.');
xlabel('\omega_3'); ylabel('Depth (m)');
```

```
    title('Yaw Velocity','fontweight','bold');

    % 3-D model xy planer plot


       axes('position',[0.6,0.05,0.22,0.17],'xlim',xlm,'ylim',...
       ylm,'box','on','fontsize',ftsz);
       hold on;
       plot(pos(1,:),pos(2,:),'r-'); plot(pos(1,:),pos(2,:),'.');
    xlabel('X (m)');  ylabel('Y (m)');
    title('Mass center trail','fontweight','bold');

    % 3-D model Yaw Velocity plot.

    axes('position',[0.88,0.05,0.1,0.17],'xlim',xlm2,...
       'ylim',[bot-dd,0],'box','on','fontsize',ftsz); hold on;
    plot(dthdt2,pos(3,:));
    plot([0,0],[bot,0],'r-.');
    xlabel('\omega_3'); ylabel('Depth (m)');
    title('Yaw Velocity','fontweight','bold');

    %Plots the parameter boxes for the final MIBEX position data
    % and the final model data.

    % Plot of the general mine parameters table for the given
    % data set and run.

    axes('position',[0.42,0.75,0.25,0.24],'xlim',[-1,21],...
       'ylim',[0,11]);
    hold on; axis('off');
    plot([-1,21,21,-1,-1],[0,0,11,11,0]);
    text(10,9.8,['Mine Shape'],'horizontalalignment',...
       'center','fontsize',ftsz,'fontweight','bold');
    text(10,8.6,['Parameters (',sag,flnm,')'],'horizontalalignment',...
       'center','fontsize',ftsz,'fontweight','bold');
    text(1.5,7.6,'d: ','fontsize',ftsz);
    text(6,7.6,[num2str(d,3),'(m)'],'fontsize',ftsz);
    text(1.5,6.6,'L: ','fontsize',ftsz);
    text(6,6.6,[num2str(L,3),'(m)'],'fontsize',ftsz);
    text(1.5,5.6,'m: ','fontsize',ftsz);
    text(6,5.6,[num2str(m,3),'(m)'],'fontsize',ftsz);
    text(1.5,4.6,'J_1: ','fontsize',ftsz);
    text(6,4.6,[num2str(J(1),3),'(kg*m^2)'],'fontsize',ftsz);
    text(1.5,3.6,'J_2: ','fontsize',ftsz);
       text(6,3.6,[num2str(J(2),3),'(kg*m^2)'],'fontsize',ftsz);
       text(1.5,2.6,'J_3: ','fontsize',ftsz);
    text(6,2.6,[num2str(J(3),3),'(kg*m^2)'],'fontsize',ftsz);
    text(1.5,1.6,'\chi: ','fontsize',ftsz);
    text(6,1.6,[num2str(chi,4),'(m)'],'fontsize',ftsz);

% Final Drop Parameters

axes('position',[0.11,0.75,0.25,0.24],'xlim',[-1,21],...
   'ylim',[0,11]);
    axis('off'); hold on;
    plot([-1,21,21,-1,-1],[0,0,11,11,0]);
```

```
    text(10,9.8,['Final Drop'],'horizontalalignment',...
       'center','fontsize',ftsz,'fontweight','bold');
    text(10,8.6,['Parameters (',sag,flnm,')'],'horizontalalignment',...
       'center','fontsize',ftsz,'fontweight','bold');
    text(1.5,7.6,'time: ','fontsize',ftsz);
    text(7,7.6,[num2str(time(end),3),'(m)'],'fontsize',ftsz);
    text(1.5,6.6,'xy_f_e: ','fontsize',ftsz);
    text(7,6.6,[num2str(xyf,3),'(m)'],'fontsize',ftsz);
    text(1.5,5.6,'V_x_f_e: ','fontsize',ftsz);
    text(7,5.6,[num2str(t(7,end),3),'(m/s)'],'fontsize',ftsz);
    text(1.5,4.6,'V_y_f_e: ','fontsize',ftsz);
    text(7,4.6,[num2str(t(8,end),3),'(m/s)'],'fontsize',ftsz);
    text(1.5,3.6,'V_z_f_e: ','fontsize',ftsz);
       text(7,3.6,[num2str(t(9,end),3),'(m/s)'],'fontsize',ftsz);
       text(1.5,2.6,'\psi_f_e: ','fontsize',ftsz);
    text(7,2.6,[num2str(ag2(end)/d2r,4),'^o'],'fontsize',ftsz);
    text(1.5,1.6,'depth: ','fontsize',ftsz);
    text(7,1.6,[num2str(-zm(end),3),'(m)'],'fontsize',ftsz);

% Final Model Parameters.



Angf=Ang(2)/d2r;

if 180 < Angf <= 359
   Angf = Angf - 360
else
   Angf = Angf
end

   %if(Angf>200);
   %  Angf=Angf-360;
   %end
   %if(Angf<-200);
   %   Angf=Angf+360
   %end

axes('position',[0.73,0.75,0.25,0.24],'xlim',[-1,21],...
   'ylim',[0,11]);
    axis('off'); hold on;
    plot([-1,21,21,-1,-1],[0,0,11,11,0]);

    text(10,9.8,['Final Model'],'horizontalalignment',...
       'center','fontsize',ftsz,'fontweight','bold');
    text(10,8.6,['Parameters (',sag,flnm,')'],'horizontalalignment',...
       'center','fontsize',ftsz,'fontweight','bold');
    text(1.5,7.6,'time: ','fontsize',ftsz);
    text(7,7.6,[num2str(tim,3),'(m)'],'fontsize',ftsz);
    text(1.5,6.6,'xy_f_m: ','fontsize',ftsz);
    text(7,6.6,[num2str(xyPosf,3),'(m)'],'fontsize',ftsz);
    text(1.5,5.6,'V_x_f_m: ','fontsize',ftsz);
    text(7,5.6,[num2str(-Vo(2),3),'(m/s)'],'fontsize',ftsz);
    text(1.5,4.6,'V_y_f_m: ','fontsize',ftsz);
```

```
      text(7,4.6,[num2str(-Vo(1),3),'(m/s)'],'fontsize',ftsz);
      text(1.5,3.6,'V_z_f_m: ','fontsize',ftsz);
       text(7,3.6,[num2str(Vo(3),3),'(m/s)'],'fontsize',ftsz);
       text(1.5,2.6,'\psi_f_m: ','fontsize',ftsz);
    text(7,2.6,[num2str(Angf,4),'^o'],'fontsize',ftsz);
    text(1.5,1.6,'depth: ','fontsize',ftsz);
    text(7,1.6,[num2str(-Pos(3),3),'(m)'],'fontsize',ftsz);

    % prnt(flnm);

% prints the figure using filename to the current data directory
% for later analysis and use for presentation as apost script file
% and jpeg format for powerpoint presentation.
flnmp = [mca1,'-',mca2,'-',mca3,'-',i2];
      eval(['print -tiff -depsc carderockplts/',flnmp,'.eps;'])
      eval(['print -djpeg carderockplts/',flnmp,'.jpg;'])

% This section prints out the final velocities, transverse
% displacement, and sediment impact angles to file for both
% the data and the model.

Vce=sqrt(t(7,end)^2+t(8,end)^2);
Vcm=sqrt(Vo(1)^2+Vo(2)^2);
       Vfile = [Vcm;Vce;abs(Vo(3));abs(t(9,end));...
             Ang(2)/d2r;ag2(end)/d2r;xyPosf;xyf];
       fid=fopen(['velocitytd.txt'],'a+');
       fseek(fid,0,'eof');
       fprintf(fid,'%s\t',flnmp);
       for k=1:length(Vfile)
          fprintf(fid,'%5.3f\t',Vfile(k));
       end
       fprintf(fid,'\n');
       fclose(fid);

% This section creates the initial output case file to use as input
% to IMPACT28.
       Vco = sqrt(t(8,1)^2+t(7,1)^2);
    Vfile1 = [(90-(ag2(1)*180/pi));Vco;abs(t(9,1));Omgmo(2)];
       fid=fopen(['initialpartd.txt'],'a+');
       fseek(fid,0,'eof');
       fprintf(fid,'%s\t',flnmp);
       for k=1:length(Vfile1)
          fprintf(fid,'%5.3f\t',Vfile1(k));
       end
       fprintf(fid,'\n');
       fclose(fid);
       % close (gcf)
  end
  % This ends the central for loop and then asks if you have more files
  % to process, a total of 230 plots will be generated in this program
  % and write to file 230 lines of final positions and initial
  % condition data used to initialize IMPACT28.
  mca=input...
  ('input mine#(9,12,15) case#(-2,-1,0,1,2) ang(15,30,45,60,75): ,'s');
  close all; end
```

APPENDIX D. NUMERICAL PROCEDURE OUTLINE

A. NUMERICAL PROCEDURE (DIMENSIONAL)

1. Initialize the variables $(x,y,z,u,v,w,\ \psi_2,\ \psi_3,\ \Omega,\ \omega_2,\ \omega_3)$ and the earth fixed coordinate reference frame to body-fixed coordinate reference frame rotational matrix $({}^{E}_{M}R)$.

2. Get mine axis director $\vec{i}_M = {}^{M}_{E}R(:,1)$, and rotation matrix between the earth fixed coordinate reference frame, body-fixed coordinate reference frame and drag-lift force coordinate reference frame.

3. Convert angular velocity components (ω_2, ω_3) from body-fixed coordinate reference frame to drag-lift force coordinate reference frame $(\omega_2',\ \omega_3')$.

$$\begin{bmatrix} \Omega \\ \omega_2' \\ \omega_3' \end{bmatrix} = {}^{D}_{M}R \cdot \begin{bmatrix} \Omega \\ \omega_2 \\ \omega_3 \end{bmatrix} \tag{157}$$

$${}^{D}_{M}R = {}^{D}_{E}R \square {}^{E}_{M}R \tag{158}$$

4. Transfer body-fixed coordinate frame velocity components $\vec{V} = f(u_M, v_M, w_M)$ to the drag-lift force coordinate frame velocity components (u_F, v_F, w_F), then calculate the Reynolds number and the drag and lift coefficients $(C_{d1},\ C_{d2},\ C_{d3,}\ C_l)$.

5. Calculate the drag-lift force coordinate reference frame components of drag and lift force, $\vec{F}(\vec{i}_F,\ \vec{j}_F,\ \vec{k}_F)$. Then rotate to the earth fixed coordinate reference frame. Compute the float force term. There are three component

momentum equations in the earth fixed coordinate reference frame where $\frac{d\vec{V}}{dt}$ is computed.

6. Transfer body-fixed coordinate reference frame angular velocity components $\vec{\omega} = f(\Omega_M, \omega_1, \omega_2)$ to the drag-lift force coordinate reference frame angular velocity components $f\left(\Omega_F, \omega_1', \omega_2'\right)$. Calculate the Reynolds number and the drag and lift moment coefficients $\left(C_{m1}, C_{m2}, C_{m3,}\ C_{ml}\right)$.

7. Calculate the drag-lift force coordinate reference frame torque components, $\vec{M}\left(\vec{i}_F, \vec{j}_F, \vec{k}_F\right)$. Now convert to the body fixed coordinate reference frame. Calculate the buoyancy moment term. There are three moment of momentum equations in the body-fixed coordinate reference frame where $d\vec{\omega}/dt$ is computed.

8. Get analytical solution for each component of the system of linear ordinary differential equations, and update $(u, v, w, \Omega, \omega_2, \omega_3)$.

9. Integrate to get the new position (x, y, z) and the increment $(d\psi_2, d\psi_3)$ in the earth fixed reference frame.

$$x^{n+1} = x^n + \int_0^{dt} u\,dt \tag{159}$$

$$y^{n+1} = y^n + \int_0^{dt} v\,dt \tag{160}$$

$$z^{n+1} = z^n + \int_0^{dt} w\,dt \tag{161}$$

$$d\psi_2 = \int_0^{dt} \omega_2 dt \tag{162}$$

$$d\psi_3 = \int_0^{dt} \omega_3 dt \tag{163}$$

10. Update rotation matrix (${}^{E}_{M}R$) by rotating ($d\psi_3$) around ($\bar{e}_3$) and ($d\psi_2$) around ($\bar{e}_2$).

$${}^{E}_{M}R^{n+1} = {}^{E}_{M}R^{n} \begin{bmatrix} \cos(d\psi_3) & -\sin(d\psi_3) & 0 \\ \sin(d\psi_3) & \cos(d\psi_3) & 0 \\ 0 & 0 & 1 \end{bmatrix} \begin{bmatrix} \cos(d\psi_2) & 0 & \sin(d\psi_2) \\ 0 & 1 & 0 \\ -\sin(d\psi_2) & 0 & \cos(d\psi_2) \end{bmatrix} \tag{164}$$

11. Update (ψ_2^{n+1}) and (ψ_3^{n+1}) from rotation matrix (${}^{E}_{M}R^{n+1}$) as:

$$\begin{aligned} {}^{E}_{M}R^{n+1} &= \begin{bmatrix} \cos\psi_3 & -\sin\psi_3 & 0 \\ \sin\psi_3 & \cos\psi_3 & 0 \\ 0 & 0 & 1 \end{bmatrix} \begin{bmatrix} \cos\psi_2 & 0 & \sin\psi_2 \\ 0 & 1 & 0 \\ -\sin\psi_2 & 0 & \cos\psi_2 \end{bmatrix} \\ &= \begin{bmatrix} \cos\psi_3 \cdot \cos\psi_2 & -\sin\psi_3 & \cos\psi_3 \cdot \sin\psi_2 \\ \sin\psi_3 \cdot \cos\psi_2 & \cos\psi_3 & \sin\psi_3 \cdot \sin\psi_2 \\ -\sin\psi_2 & 0 & \cos\psi_2 \end{bmatrix} \end{aligned} \tag{165}$$

$$\psi_2^{n+1} = \arccos\left({}^{E}_{M}R^{n+1}(3,3) \right) \tag{166}$$

$$\psi_3^{n+1} = \arccos\left({}^{E}_{M}R^{n+1}(2,2) \right) \tag{167}$$

If ${}^{E}_{M}R^{n+1}(1,2) > 0$,

$$\psi_3^{n+1} = \psi_3^{n+1} + \Pi \tag{168}$$

If ${}^{E}_{M}R^{n+1}(3,1) > 0$,

$$\psi_3^{n+1} = \psi_3^{n+1} + \Pi \tag{169}$$

12. Return to step 2, until the end of the trajectory (bottom) is reached.

B. NUMERICAL PROCEDURE FLOWCHART

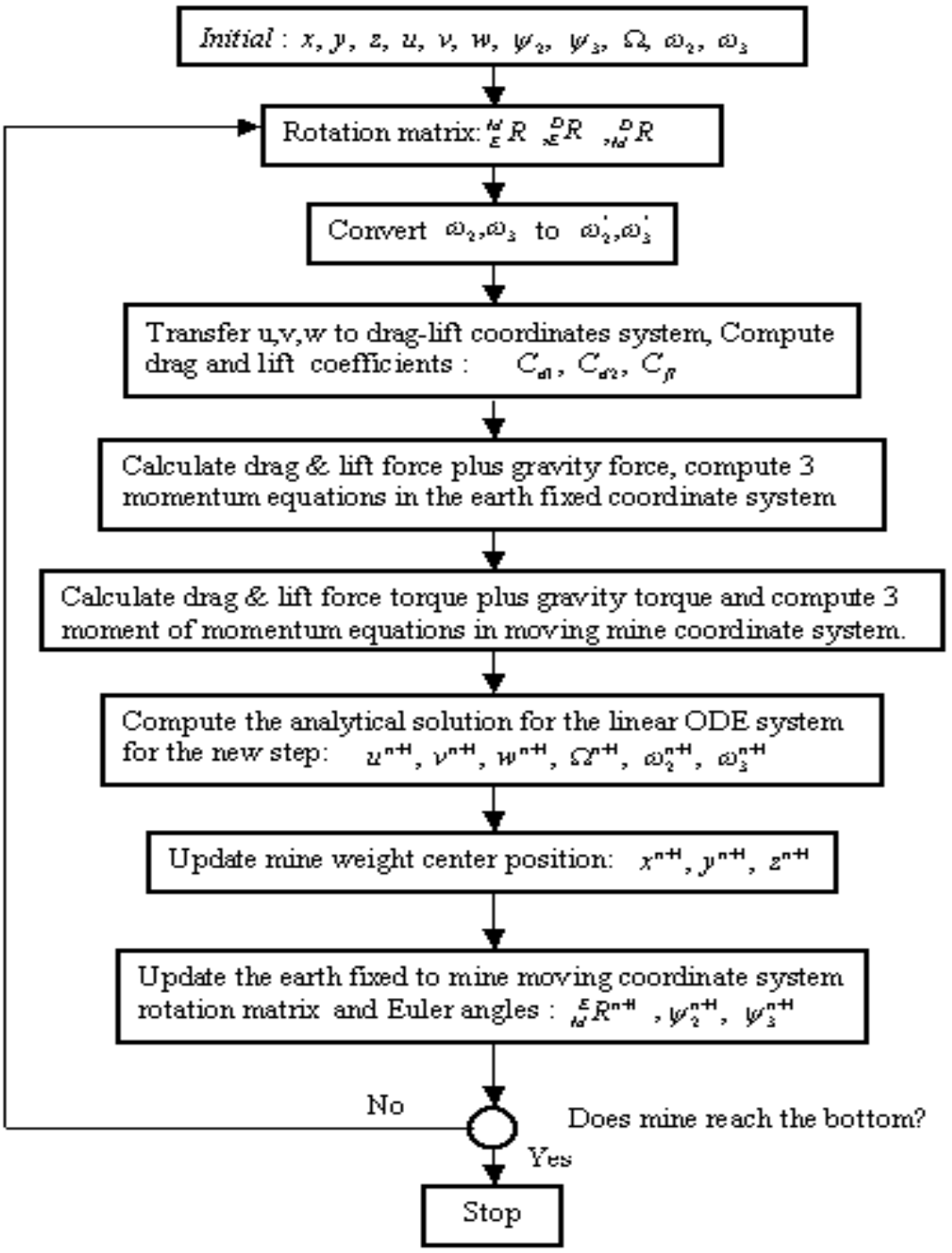

Figure 40. Flowchart of the Numerical Procedure Followed in the Source code Subroutines found in Appendix B.

THIS PAGE INTENTIONALLY LEFT BLANK

LIST OF REFERENCES

Aref, H and S.W. Jones, December 1993. “Chaotic Motion of a Solid Through Ideal Fluid.” American Institute of Physics, *Physics of Fluids,* A5 (12), 3026-3028.

Arnone, R. A., and L.E. Bowen, 1980. “Prediction Model of the Time History Penetration of a Cylinder Through the Air-Water-Sediment Phases.” NCSC Letter Report 734-36. *Naval Coastal Systems Cente*r, Panama City, FL.

Bennett, R.H., August 2000. “Mine Burial Prediction Workshop Report and Recommendations: Final Report.” SEAPROBE, Inc Technical Report SI-0000-02, 71 pp.

Boiffer, J.L., 1998. “The Dynamics of Flight, The Equations.” John Wiley & Sons, Chichester, 353 pp.

Boorda, J. M., December, 1995. "Mine Countermeasures - An Integral Part of our Strategy and our Forces.” White Paper, Office of the Chief of Naval Operations, Washington D.C., 4 pp.

Cannon, R.H., 1967. “Dynamics of Physical Systems.” McGraw-Hill Book Company, New York, 904 pp.

Chu, P.C., 2001. “Assessment and Reconstruct of Navy’s Mine Impact Burial Prediction Model.” Naval Postgraduate School, Monterey, CA, 8 pp.

Crowe, C.T., J.A. Roberson, and D.F. Elger, 2001. “Engineering Fluid Mechanics.” 7th edition. John Wiley & Sons Inc, New York, 714 pp.

Dolan, R., N. Langhorne, and C. Butler, November 1999. “Formation of a Working Group to Assess the Potential of Expert Systems Approach to Modeling Mine Burial Processes.” Office of Naval Research, International Field Office Report, London, 9 pp.

Garrald, T., 1998. “U.S. Navy MCM Update”. Surface Warfare Officers School. Powerpoint presentation, 26 slides. Retrieved 22 July, 2002 from Surface Warfare Officer School on the World Wide Web: (http://www.fas.org/man/dod-101/navy/docs/swos/cmd/fts/Fts10).

Gilless, A., 2001. “Hydrodynamic Features of Falling Mine Detected from Drop Experiment.” *Master Thesis*, Naval Postgraduate School, Monterey, CA.

Goff, J. A., 2002. “A Statistical Framework for Monte Carlo Mine Burial Modeling Experiments.” A Technical Report for the ONR Mine Burial Program. University of Texas Institute for Geophysics, Austin, TX, 5 pp.

Gottshall, E.L, 1997. “Environmental Effects on Warfare Simulations.” *Master Thesis*, Naval Postgraduate School, Monterey, CA.

Hoerner, S.F., 1951. “Aerodynamic Drag.” Hoerner Publications, Midland Park, N.J., 259 pp.

Hurst, R.B., and S. Murdoch, November 1991. “Measurements of Sediment Shear Strength for Mine Impact Burial Prediction.” Report of Meeting of the Technical Cooperation Program Panel, GTP-13.

Hurst, R.B., February 1992. “Mine Impact Burial Prediction Model - Technical Description of Recent Changes and Developments.” Defence Scientific Establishment, Auckland, New Zealand, Report 149.

Lamb, H., 1932. “Hydrodynamics.” Dover Publications, New York, 738 pp

Lehr, S.E., April 2000. “Mine Warfare: To Enable Maneuver.” Amphibious Warfare Conference, PowerPoint Presentation. Retrieved 15 July, 2002 from the Office of Chief of Naval Operations Expeditionary Warfare on the World Wide Web: (http://www.exwar.org/awcfinal/6th/n852mines.ppt).

Lluy, P. A., December 1995. “Mine Warfare: An Old Threat Presents New Challenges for NATO's Post-Cold War Navies.” *Master Thesis,* Naval Postgraduate School, Monterey, CA, 211p.

Lott, D.F., 2001. “Modeling Mine Burial Processes: A Review.” With Contributions by C. Friedrichs, M. Richardson, and P. Valent. Naval Research Laboratory, Stennis Space Center, MS.

Lugt, H.J., 1983. “Autorotation.” *Annual Review of Fluid Mechanics,* 15, 123-147.

“Mine Burial Prediction,” June 1999. NATO SG/31. Subgroup 31 Analysis and Final Report, 115p.

Montgomery, D.C., E.A. Peck and G.G Vining, 2001. “Introduction to Linear Regression Analysis.” Wiley Series in Probability and Statistics. Wiley & Sons, Inc, New York, 635 pp.

Mulhearn, P.J., July 1993. “Experiments on Mine Burial on Impact-Sydney Harbor.” *U.S. Navy Journal of Underwater Acoustics,* vol 43, no 3, pp 1271-1281.

Panton, R.L., 1996. “Incompressible Flow.” 2nd ed. John Wiley & Sons, New York, 837 pp.

Purday, H.F.P, 1949. “An Introduction to the Mechanics of Viscous Flow.” Dover Publications Inc, New York, 185 pp.

Rennie, S. and A Brandt, 2002. “An Expert Systems Approach for Predicting Mine Burial.” Fifth International Symposium on Technology and the Mine Problem. John Hopkins University Applied Physics Laboratory, Laurel, Md, 7 pp.

Richardson, M.D., P.J. Valent, K.B. Briggs, J. Bradley, and S. Griffin, 2001a. “ NRL Mine Burial Experiments.” Second Australian-American Joint Conference on the Technologies of Mine Countermeasures. Defence Science and Technology Organization, Sydney, Australia.

Richardson, M.D., P.J. Valent, T.K. Holland, K.B. Briggs and C.L. Vincent, 2001b. “Mine Burial Prediction: A Cooperative NRL/ONR Study.” Marine Geosciences Division, Naval Research Laboratory, Stennis Space Center, MS, 5 pp.

Rhodes, J.E., G. Holder, May 1998. “Concept for Future Naval Mine Countermeasures in Littoral Power Projection, A 21st Century Warfighting Concept.” Marine Corps Combat Development Command. Retrieved 20 July, 2002 from Marine Corps Combat Development Command on the World Wide Web (http:// 192.156.75.102/mcm.htm)

Rouse, H, 1938. “Fluid Mechanics for Hydraulic Engineers”. Mcgraw-Hill Book Company Inc, New York, 422 pp.

Rumball, E.I. and S. Kitchings, 1989. “Sensitivity Analysis of the Impact Burial Prediction Model.” DSE Technical Note 89/2 NR 1265, Defense Scientific Establishment, Auckland, New Zealand.
Satkowiak, L.J, 1987. “Users Guide for the Modified Impact Burial Prediction Model.” NCSC Technical Note 884-87. Naval Coastal Systems Center, Panama City, FL.

Satkowiak, L.J, 1988. “Sensitivity Study of the NCSC Modified Impact Burial Prediction Model.” NCSC Technical Note 934-88. Naval Coastal Systems Center, Panama City, FL.

Schlichting, H., 1979. “Boundary Layer Theory.” McGraw-Hill Book Company, New York, 806 pp.

Smith, T.B., 2000. “Validation of the Mine Impact Burial Model Using Experimental Data.” *Master Thesis*, Naval Postgraduate School, Monterey, CA.

Soulsby, R., 1997. “Dynamics of Marine Sands: A Manual for Practical Applications.” Thomas Telford Publications, London, United Kingdom, 249 pp.

Sumer, B.M. and J. Fredsøe, 1997. “Hydrodynamics Around Cylindrical Structures.” World Scientific, 530 pgs.

Taber, V.L, 1999. “Environmental Sensitivity Study on Mine Impact Burial Prediction Model.” *Master Thesis*, Naval Postgraduate School, Monterey, CA.

“U.S. Naval Mine Warfare Plan Fourth Edition, (NMWP), Programs for the Millennium,” January 2000. Department of the Navy, Washington, D.C.

“U.S. Navy Mine Countermeasures Familiarizer,(NMCF)” 1991. Naval Mine Warfare Engineering Activity (NMWEA), Naval Coastal Systems Center, Panama City, FL.

Valent, P.J., and K.T. Holland, September 2001. “Quick Look Report, Model Mine Hydrodynamic Test, serial number 7400/105.” NSWC-Carderock, 10-14 Sep 2001. Naval Research Laboratory, Stennis Space Center, MS, 18 pp.

Valent, P.J., K.T. Holland, A.W. Green, S. Theophanis, C. King, M.D. Richardson, G.R. Bower, P. Congedo, and W. Lewis, January 2002. “Observations of Velocities and Orientation of Cylindrical Bodies at Terminal Condition in the Water.” Fifth International Symposium on Technology and the Mine Problem. Naval Research Laboratory, Stennis Space Center, MS, 9 pp.

Von Mises, R, 1959. “Theory of Flight.” Dover Publications, New York, 629 pp.

Wettern, D., 1991. “Coping with the Hidden Threat: The Neglected Art of Mine Warfare.” *Sea Power*, Mar 1991, pp 36-40.

White, F.M., 1974. “Viscous Fluid Flow.” McGraw-Hill Book Company, New York, 725 pp.

White, F.M., 1979. “Fluid Mechanics.” McGraw-Hill Book Company, New York, 701 pp.

THIS PAGE INTENTIONALLY LEFT BLANK

BIBLIOGRAPHY

Chu, P.C., E. Gottshall, and T.E. Halwachs, 1998. "Environmental Effects on Naval Warfare Simulations." *Institute of Joint Warfare Analysis, Naval Postgraduate Schoo*l, Technical Report, NPS-IJWA-98-006, 33 pp.

Chu, P.C., V.I. Taber, and S.D. Haeger, 2000a. "A Mine Impact Burial Model Sensitivity Study." *Institute of Joint Warfare Analysis, Naval Postgraduate Schoo*l, Technical Report, NPS-IJWA-00-003, 48 pp.

Chu, P.C., V.I. Taber, and S.D. Haeger, 2000b. "Environmental Sensitivity Study on Mine Impact Burial Prediction Model." *Proceedings on the Fourth International Symposium on Technology and the Mine Problem,* 10 pp.

Chu, P.C., T. B. Smith, S.D. Haeger, 2001. "Mine Burial Impact Prediction Experiment." *Institute of Joint Warfare Analysis, Naval Postgraduate Schoo***l,** Technical Report, NPS-IJWA-01-007, pp.161.

Chu, P.C., A.F. Gilless, C. Fan, and P. Fleischer, January 2002a. "Hydrodynamics of a Falling Mine in the Water Column." *Journal of Counter-Ordnance Technology. Fifth International Symposium on Technology and the Mine Problem*, 9 pp.

Chu, P.C., A.F. Gilless, C. Fan, and P. Fleischer, 2002b. "Hydrodynamical Characteristics of a Falling Cylinder in the Water Column." *Advances in Fluid Mechanics IV*, vol 32, C.A. Brebbia, M. Rahman, and R. Verhoeven, 19 pp.

Clark, V. and J.L. Jones, 2002. "Naval Transformation Roadmap, Power and Access… From the Sea: Sea Strike, Sea Shield, Sea Basing. Department of the Navy, Washington D.C.

Goff, J.A., 2001. "Building a Statistical Framework for Mine Burial Predictions." University of Texas Institute for Geophysics, Austin, TX, 4 pp.

Kroo, I., 1983. "Drag Due to Lift: Concepts for Prediction and Reduction." *Annual Review of Fluid Mechanics,* 33, 587-617.

"Minehunting for the 1990s," 1989. *Naval Forces,* Vol X, No. I, pp 63-68.

"Naval Mine Warfare: Operational and Technical Challenges for Naval Forces," 2001. Committee for Mine Warfare Assessment, Naval Studies Board, Division on Engineering and Physical Sciences, National Research Council. National Academy Press, Washington D.C.

Prandtl, L. and O.G. Tietjens, 1934. "Applied Hydro- and Aerodynamics." Engineering Society Monographs. McGraw-Hill Book Company Inc, New York, 311 pp.

Richardson, M.D. and S.G. Tooma, July 1993. "Environmental Requirements to Support Mine Countermeasures Operations in Shallow Water." *U.S. Navy Journal of Underwater Acoustics*, Vol 43, no 3, pp 977-991, (Restricted).

Rodholm, B., 1990. "Advances in Mine Warfare." *Naval Forces* Vol XI, No. VI, pp 49-53.

Soulsby, R.L. and R.J.S. Whitehouse, 1997. "Threshold of Sediment Motion in Coastal Environments." Presented at Pacific Coasts and Ports '97, 13th Australasian Coastal and Ocean Engineering Conference and 6th Australasian Port and Harbor Conference, 7-11, September, Christchurch, New Zealand.

Tokumaru, P.T. and P. Dimotakis, 1993. "The Lift of a Cylinder Executing Rotary Motions in a Uniform Flow." *Journal of Fluid Dynamics*, vol 255, pp 1-10.

Tubridy, L. and B. Blumenthal, 1998. "Tactical Oceanography in Mine Countermeasures." *U.S. Navy Journal of Underwater Acoustics*, Vol. 48, No. 3, pp 529-538.

INITIAL DISTRIBUTION LIST

1. Defense Technical Information Center
   Ft. Belvoir, VA

2. Dudley Knox Library
   Naval Postgraduate School
   Monterey, CA

3. Dr. Brian Almquist
   Office of Naval Research
   Arlington, VA

4. Dr. Richard Bennett
   SEAPROBE, Inc.
   Picayune, MS

5. CDR Jim Berdeguez
   Chief of Naval Operations, N96
   Washington, D.C.

6. Dr. Thomas Drake
   Office of Naval Research
   Arlington, VA

7. CDR Bob Kiser
   Commander Naval Meteorology and Oceanography
   Stennis Space Center, MS

8. Dr. Wayne Dunlap
   Off Shore Technology Research Center
   College Station, TX

9. Dr. Peter Fleischer
   Naval Oceanographic Office
   Stennis Space Center, MS

10. CDR Eric Gottshall
    SPAWAR
    San Diego, CA

11. Dr. Steve Haeger
    Naval Oceanographic Office
    Stennis Space Center, MS

12. CDR Eric Long
Chief of Naval Operations, N75
Washington, D.C.

13. Mr. Mark Null
Mine Warfare Liaison
Naval Oceanographic Office
Stennis Space Center, MS

14. Dr. Mike Richardson
Naval Research Laboratory
Stennis Space Center, MS

15. Dr. Richard Spinrad
Chief of Naval Operations N96
Washington, D.C.

16. Dr. Robert Stoll
Columbia University
Palisades, N.Y.

17. Dr. Philip Valent
Naval Research Laboratory
Stennis Space Center, MS

18. Dr. Linwood Vincent
Office of Naval Research
Arlington, VA

19. Dr. Roy Wilkins
Hawaii Institute of Geophysics
University of Hawaii
Honolulu, HI.

20. Ms. Sarah Rennie
Applied Physics Laboratory
John Hopkins University
Laural, MD